Contrast-Enhanced Ultrasound

From Simple to Complex

Alexander N. Sencha
Yury N. Patrunov
Editors

MOREMEDIA

Springer

Contrast-Enhanced Ultrasound

Alexander N. Sencha • Yury N. Patrunov
Editors

Contrast-Enhanced Ultrasound

From Simple to Complex

Springer

Editors
Alexander N. Sencha
Department of Visual and Functional Diagnostics
Federal State Budget Institution
National Medical Research Center for Obstetrics
Moscow, Russia

Yury N. Patrunov
Department of Ultrasound Diagnostics
Clinical Hospital "RZD-Medicina"
Yaroslavl, Russia

ISBN 978-3-030-91763-0 ISBN 978-3-030-91764-7 (eBook)
https://doi.org/10.1007/978-3-030-91764-7

This Springer imprint is published by the registered company Springer Nature Switzerland AG
The registered company address is: Gewerbestrasse 11, 6330 Cham, Switzerland

Foreword

Current imaging techniques suggest great opportunities. New diagnostic modalities demonstrate fantastic capabilities. Now, the diagnostic aims may be achieved with simpler and safer methods. Modern ultrasound options make the diagnosis more efficient and cost-effective. Contrast-enhanced ultrasound (CEUS) is a young, rapidly developing entity. It not only provides accurate real-time noninvasive assessment of the body anatomy but also supplies physiologic data on blood supply and perfusion. It has already proven its efficiency and has further prospects for development and improvement. Many aspects of CEUS are still not completely studied, some issues are debatable, and some data are ambiguous or contradictory. It still undergoes verification, systemic analysis, and general recognition by radiologists.

CEUS attracts the attention of not only radiologists but practitioners of other fields of medicine due to its availability and simple performance on an outpatient basis.

This book is created by a team of highly qualified doctors from the leading Russian clinics, who have implemented CEUS in their routine practice. They accurately demonstrate the current value of CEUS for early and differential diagnosis of a wide range of abnormalities in surgery, therapy, and gynecology. They share their extensive experience and offer tips and tricks that make the study smooth and reliable.

The original material, large number of own observations, and substantial analysis of related publications allowed the authors to create a book for practical use in the diagnosis of the pathology of the liver, pancreas, kidneys, thyroid, parathyroids, mammary glands, uterus, ovaries, bladder, prostate, and other organs. Extravascular applications of ultrasound contrast agents, hystero-salpingo-contrast sonography in particular, are also well discussed. This application has recently been introduced into practice and is increasingly being used to assess the patency of the fallopian tubes, analyze the state of the uterine cavity, and differentiate defects and anomalies of the female reproductive system. The unique images and video material illustrate the text that enables a clear understanding of the numerous visual features detected with CEUS in normal and pathological conditions.

The book gives a full understanding of the possibilities of CEUS and motivates the reader to start its practical use or continue the professional way of perfection.

Peter M. Kotlyarov

Scientific-Research Department of New Technologies and Imaging Semiotics of the Diseases of Organs and Tissues
Federal State Budgetary Institution
"Russian Scientific Center of Rentgenoradiology"
of the Ministry of Healthcare of the Russian Federation
Moscow Russia

Russian Federation
Moscow Russia

Preface

Dear colleagues, dear friends! It is a great honor for us to introduce this new book on ultrasound diagnostics. We consider that studying ultrasound step by step from simple to complex is a pleasure. Now we publish a work dedicated to modern sophisticated ultrasound technology based on ultrasound contrast enhancement. You, our friends, who are keen on your profession, who sincerely and selflessly devote yourself to diagnostic ultrasound, which is quite young but extremely effective and promising, those professionals who are just mastering the aces of multiparametric ultrasound or already are perfect in it, this book is dedicated to …

This book is based on the original studies of our large team that obtained substantial experience in contrast-enhanced ultrasound (CEUS). We aimed to analyze our knowledge in association with widely recognized best practices for the diagnosis of a wide variety of diseases. Meanwhile, we tried to cover as many aspects of CEUS as possible and felt competent to create a kind of guidebook for practical use.

We are grateful to our colleagues for their practical assistance in the preparation of this book. Indeed, this publication would be impossible and the content incomplete without the close collaboration and guidance of our friends. Wise suggestions and recommendations of these professionals of diagnostic and clinical medicine granted additional illustrations and ideas were of great benefit and are highly appreciated.

The book starts with the basics of CEUS that necessarily include physical principles and technology of application in various organs. We discuss the variants of contrast enhancement in normal conditions and decisive features for early and differential diagnosis of different diseases and illustrate them with our ultrasound images. The analysis of vascularity of affected organs provides great opportunities. However, its advantages in practice are sometimes accompanied by a range of drawbacks that limit the capabilities of the method. We share the tips and tricks to get the best of the examination.

Wide application of contrast agents helped us to assess and describe in detail the technology, indications and contraindications, data of qualitative and quantitative analysis, the efficiency (with SonoVue®) in the early and differential diagnosis of neoplasms, their role in the evaluation of neoangiogenesis in tumors, and the place in diagnostic algorithms. Specific features for the use in pediatric practice with a special focus on its safety, indications, and monitoring are presented in detail.

Along with intravenous administration of ultrasound contrast agents, intracavitary and rare ways of use are described. A separate chapter is devoted to sonohysterosalpingography with various ultrasound contrast agents and their role in the assessment of endometrium and fallopian tubes.

The book will be a helpful tool for both residents and practitioners approaching ultrasound diagnostics, as well as for more experienced radiologists and other professionals. It is created to promote CEUS as a simple and efficient way for oncologists, surgeons, therapists, gynecologists, and other practitioners to make complex early and differential diagnosis of various diseases even better.

Moscow, Russia — Alexander N. Sencha
Yaroslavl, Russia — Yury N. Patrunov

Contents

Abbreviations

3D	Three-dimensional image reconstruction
AASLD	American Association for the Study of Liver Diseases
ACR	American College of Radiology
AML	Angiomyolipoma
BI-RADS	Breast imaging reporting and data system
BPH	Benign prostate hyperplasia
CDI	Color Doppler imaging
CE-CT	Contrast-enhanced computed tomography
CE-TRUS	Contrast-enhanced transrectal ultrasound
CEUS	Contrast-enhanced ultrasound
CEVUS	Contrast-enhanced voiding urosonography
CI	Confidence interval
CT	Computed tomography
DNA	Deoxyribonucleic acid
DV	Descending velocity
EASL	European Association for the Study of the Liver
EFSUMB	European Federation for Ultrasound in Medicine and Biology
FLL	Focal liver lesion
FNH	Focal nodular hyperplasia
HCA	Hepatocellular adenoma
HCC	Hepatocellular carcinoma
HIFU	High intensity focused ultrasound
HSG	Hysterosalpingography
HVAT	Hepatic vein arrival time
HVPG	Hepatic venous pressure gradient
HyCoSy	Hystero-salpingo-contrast sonography
IBD	Inflammatory bowel disease
IPMN	Intraductal papillary mucinous neoplasm
ITT	Intrahepatic transit time
IVC	Inferior vena cava
IVF	In vitro fertilization
LI-RADS	Liver imaging reporting and data system
LN	Lymph node
MI	Mechanical index
MRI	Magnetic resonance imaging
NPV	Negative predictive value
OLT	Orthotopic liver transplantation

PDI	Power Doppler imaging
PET	Positron emission tomography
PI	Peak intensity
PPV	Positive predictive value
PSA	Prostate-specific antigen
ROI	Region of interest
SHAPE	Subharmonic-aided pressure estimation
TIC	Time-intensity curve
TIPS	Transjugular intrahepatic portosystemic shunt
TRUS	Transrectal ultrasonography
UCA	Ultrasound contrast agent
US	Ultrasound (echography)
VUR	Vesicoureteral reflux

Introduction

Ultrasound has always been important for the correct diagnosis and treatment. Issues of improving methods and technologies of ultrasound diagnosis for diseases of various organs and systems are constantly reviewed in connection with the development of science and technology, the emergence of new techniques, and diagnostic equipment, expanding its functionality and coverage. Its role has expanded greatly due to the introduction of ultrasound contrast agents to routine practice and the increasing knowledge of the experts in this field.

Modern imaging in many cases requires contrast enhancement, especially in oncology patients. Contrast agents are different for each modality but all of them aim to increase contrast resolution. In classical X-ray plain films and computed tomography, they contain iodine, MRI—paramagnetic, and ultrasound—gas bubbles. Intravenously administered contrast media are distributed with the blood flow throughout the body. In cases of X-ray-based imaging techniques, they improve image quality by selectively increasing the radiodensity of organs and tissues, as for MRI—by changing the magnetic properties. Contrast-enhanced ultrasound (CEUS) is quite different. Microbubbles of most contrast agents remain within the blood vessel's lumen, demonstrate vascularity, and do not affect the tissues. CEUS is a new expert technology. It is an important component of multiparametric ultrasound.

The book is prepared by a team of scientists and practitioners, who are well known in their disciplines. They are respected professionals of national centers and medical institutions of several regions of the Russian Federation. Based on their own experience and the analysis of publications they attempted to summarize and analyze all issues of CEUS application for diagnosis of various diseases, demonstrate its value, and identify its place in the diagnostic flow.

While creating the book the authors analyzed CEUS exams of more than 2000 patients with different surgical, therapeutic, or gynecological problems, such as diseases of abdominal organs, retroperitoneal space, small pelvis, superficial organs, and vessels of various locations. More than 500 sonohysterosalpingography contrast studies were performed for fallopian tube evaluation. This extensive experience permitted us to form a well-grounded opinion about the possibilities of CEUS in the assessment of vascularity in normal and pathological conditions.

The book also reveals the current difficulties and problems of CEUS and suggests ways to overcome them. It discusses the modern trends and prospects of the method. Many problems of CEUS remain unsolved. As always, the

reader is left with the opportunity for analysis, remarks, comments, further scientific search, and practical verification. We hope for the deliberated reader's comments and suggestions, which will be gratefully accepted and taken into consideration in further practical work and scientific research.

Thank you, dear reader, for your attention and credit. Continuously increasing professional knowledge, skills, and experience determine better healthcare and chance for our patients.

1 General Aspects of the Use of Contrast Agents in Diagnostic Ultrasound. History and Current State of the Technology. Review of Contrast Agents

Alexander N. Sencha, Ella I. Peniaeva, Munir G. Tukhbatullin, Elena A. Zubareva, Liubov A. Timofeyeva, Yury N. Patrunov, Roman A. Barmin, and Polina G. Rudakovskaya

Modern medical imaging is impossible without contrast agents. X-ray-based methods (e.g. computed tomography) use iodine-containing media, magnetic resonance imaging (MRI) utilize paramagnetic agents. A contrast agent is a drug introduced into a blood vessel, cavity, or hollow organ that provides contrast enhancement during radiological (including ultrasound) studies. It improves image quality by selectively increasing the radiodensity of organs and tissues with X-ray-based methods, increasing the signal with MRI and ultrasound (US). It results in higher contrast resolution and signal-to-noise ratio that expands the diagnostic value of the study.

Depending on the examination, contrast agents differ in their composition, the mechanism of action, and the method of administration.

A. N. Sencha (✉)
Department of Visual and Functional Diagnostics, Federal State Budget Institution "National Medical Research Center for Obstetrics, Gynecology and Perinatology n.a. V.I.Kulakov", Moscow, Russian Federation

E. I. Peniaeva
Department of Ultrasound Diagnostics of the Center for Radiological Diagnostics, Private Healthcare Institution, "Clinical Hospital "RZD-Medicina" of Yaroslavl City", Yaroslavl, Russian Federation

M. G. Tukhbatullin
Department of Ultrasound Diagnosis, Kazan State Medical Academy, Kazan, Russian Federation

E. A. Zubareva
Department of Ultrasound Diagnosis of the Postgraduate Education Division, Russian National Medical Research University n.a. N.I.Pirogov, Moscow, Russian Federation

L. A. Timofeyeva
Department of Propaedeutics of Internal Diseases with Radiation Diagnostics Course, I. N. Ulianov Chuvash State University, Cheboksary, Chuvash Republic, Russian Federation

Y. N. Patrunov
Department of Ultrasound Diagnostics of the Center for Radiological Diagnostics, Private Healthcare Institution "Clinical Hospital "RZD-Medicina" of Yaroslavl City", Yaroslavl, Russian Federation

R. A. Barmin · P. G. Rudakovskaya
Center for Photonics and Quantum Materials, Skolkovo Institute of Science and Technology, Moscow, Russian Federation

A. N. Sencha, Y. N. Patrunov (eds.), *Contrast-Enhanced Ultrasound*,
https://doi.org/10.1007/978-3-030-91764-7_1

Accordingly, the following groups can be allocated:

1. Contrast agents for intravenous administration
   (a) intravascular
   (b) extracellular
   (c) organ-specific
2. Contrast agents with other types of administration
   (a) oral
   (b) retrograde
   (c) intraluminal
   (d) intrathecal

Contrast-enhanced ultrasound examination (CEUS) is a type of US study that utilizes contrast media administered intravenously or some other way to provide additional information on the organ condition.

The development of ultrasound contrast agents (UCAs) began in the 1960s when Raymond Gramak and Pravin Shah [1] described the effect of contrast enhancement at the administration of indocyanine green in the left atrium when performing M-mode echography. Similar effects were registered with saline and dextrose solution. By analogy with contrast angiography, this study was named "contrast echography." Shortly before this publication, the cardiologist Cloude Joyner at the First International Conference on Diagnostic Ultrasound announced his observations of echo signal enhancement during angiography after the administration of radiocontrast substances, but these results were not published [2].

Later, the same effect was reported during the introduction of any fluid, especially when mixing it with the patient's blood in the syringe. Dr. Steve Feinberg reported that this phenomenon resulted from the presence in the solution of air microbubbles stabilized with serum albumin. He also noticed that the pressure increase in the syringe destroys microbubbles [3]. The identification of this effect enabled to apply "shaken saline" to improve the visualization of the left to right shunts with echocardiography.

About 20 years from the discovery of this phenomenon to the first commercially available UCAs, short-lived unstandardized handmade substances were used for contrast enhancement. Attempts to use barium sulfate, collagen and gelatin microspheres, lipid emulsion, perfluorates, biliary radiocontrast media, sonificated glucose solution, vitamins solutions with CO_2, shaken plasma, sonificated albumin, and other substances [4–9] were undertaken. However, instability in the bloodstream with the destruction within a few seconds limited their application.

In 1991, Echovist (Schering AG, Berlin, Germany) was introduced in Europe as the first commercially available UCA. Its galactose-stabilized gas bubbles had a short lifetime due to destruction in lung capillaries. Attempts to use it to examine intracardial shunts, myocardial structure, vessels, eyes, orbits, for contrast hysterosalpingography, fistulography were reported [7, 9–11]. The first stable UCA capable of passing through pulmonary capillaries and cardiac valves was introduced in 1984 by S.B. Feinshtain et al. [12]. They used sonificated albumin solution and demonstrated the presence of microbubbles in the left heart chambers after the injection into the peripheral vein. This UCA was presented in 1994 in the USA with the commercial name Albunex® (Mallinckrodt Medical, Inc., St. Louis, Missouri, USA).

The next commercially available UCA was Levovist (1996, Schering AG, Berlin, Germany) that contained gas microbubbles stabilized with galactose and palmitic acid. It was also able to pass small lung capillaries, but the ultrasound exposure induced fast destruction of microbubbles. As a result, the study time was limited to 2 min. Levovist was used for studies of the heart, aorta, carotid arteries, inferior vena cava, portal vein, peripheral vessels, small arteries, for differential diagnosis of malignant neoplasms of the breast, liver, thyroid gland, eyes, orbits, diagnosis of pancreatic diseases, prostate gland, ultrasound studies in gynecology [5, 13–26].

US studies were carried out with color Doppler mode. Later, specific contrast compatible modes were suggested. One important feature of Levovist was absorption by reticuloendothelial cells of the liver and spleen. It led to its wide use for the differential diagnosis of liver tumors and the search for metastases free of Kupffer cells. Currently, the drug is out of production [11].

Second-generation UCAs show greater microbubbles stability with ultrasound exposure due to the incorporation of poorly soluble gases (e.g. perfluorocarbons). Today, their application is approved in more than 70 countries of the world. The most popular are the following: SonoVue® (Bracco, Italy), Optison (Mallinckrodt, USA), SonoGen (Sonus Pharmaceuticals, USA), Sonazoid (Nycomed Imagent Alliance/Schering, USA), Definity (Lantheus Medical Imaging, USA).

One second-generation UCA EchoGen (Sonus Pharmaceuticals, Inc., Bothell, USA) was introduced in 1996. It contained dodecafluoropentane fluid in the dispersed phase, which after administration to blood flow immediately turn into microbubbles. It was used to diagnose the pathology of the heart, small vessels, liver, breast, prostate gland, etc. [27–29].

Optison (1998, Molecular Biosystems, San Diego, CA, USA) is currently produced by GE Healthcare AS, Oslo, Norway. It contains microspheres of 3.0–4.5 μm in size filled with gas perflutren and human serum albumin sheath. It is used to study heart chambers, differential diagnosis of focal liver and pancreatic lesions, breast diseases [30–33].

The UCA Definity/Luminity (Laantheus Medical Imaging, Boston, USA) is composed of octafluoropropane microbubbles in a lipid shell with a diameter of 1.1–3.3 μm. It is a fairly stable preparation, effective to enhance the echoes even at low doses (0.2–0.4 ml for liver study). It is used to diagnose the diseases of the cardiovascular system.

Organ-specific UCA Sonazoid (Daiichi Sankyo, Tokyo, Japan) contains microbubbles of perfluorobutane stabilized with a monomolecular membrane of hydrogenated egg phosphatidylserine built into amorphous sucrose with a diameter of 2.6 μm. Its distinctive feature is the ability to be absorbed by Kupffer cells. It interacts with the reticuloendothelial system and enhances the US signal not only within the vessel lumen. This feature provides the late phase of the enhancement of the liver and splenic parenchyma after absorbing from the vascular system that permits detection of malignant neoplasms, which lack Kupffer cells. Hence, Sonazoid is widely used for liver studies. It is also recommended for the evaluation of breast lesions [11, 34].

The use of UCAs for the diagnosis of the diseases of the liver, kidneys, pancreas, prostate, thyroid gland, breast, vessels, and heart is not only of scientific but also of practical interest (Table 1.1).

The basic requirements for modern UCAs are listed as follows [11]:

- availability and economic advantage, incl. in comparison with other imaging methods,
- possibility of intravenous administration,
- preservation of stability for a period required to obtain diagnostic information,
- low or absent toxic effect,
- ability to change one or more acoustic properties of organs and tissues, which can be detected with the diagnostic US.

The most common use of the UCAs is liver study. The European Federation of Societies for Ultrasound in Medicine and Biology (EFSUMB) in 2004 published Guidelines for the Use of Contrast Agents in Ultrasound, which was entirely devoted to the liver application [36]. Individual Guidelines and Good Clinical Practice Recommendations for Contrast-Enhanced Ultrasound (CEUS) in the Liver were revised several times and last time updated in 2020 [37]. This document was created in cooperation with the European Federation of Societies for Ultrasound in Medicine and Biology (EFSUMB), Asian Federation of Societies for Ultrasound in Medicine and Biology (AFSUMB), American Institute of Ultrasound in Medicine (AIUM), and Latin American Federation of Societies for Ultrasound in Medicine and Biology (FLAUS) and is internationally appreciated.

Studies on the use of UCAs in the diagnosis of various pathologies of other internal organs in gastroenterology, nephrology, urology, gynecology, pulmonology, angiology, arthrology, traumatology, etc. resulted in sufficient experience, which was summarized in The EFSUMB Guidelines and Recommendations on the Clinical Practice of Contrast-Enhanced Ultrasound (CEUS): Update

Table 1.1 Basic information on UCAs [35]

UCA	Manufacturer and year of registration	Composition	Areas of use	Registration countries/notes
Echovist	Schering, Germany, 1991	Galactose with air	Heart	Currently out of use
Albunex	Molecular Biosystems, USA, 1995	Albumin with air	Heart	Currently out of use
Levovist	Schering, Germany, 1997	Galactose with palmitic acid and air	Heart, liver, vesicoureteral reflux	Currently out of use
Optison	GE Healthcare, Norway, 2008	Perfluoropropane in albumin shell	Heart, vessels	Austria, Belgium, Brazil, Bulgaria, Cyprus, Czech Republic, Estonia, Germany, Holland, Ireland, Latvia, Lithuania, Luxembourg, Malta, Norway, Poland, Portugal, Romania, Slovakia, Slovenia, Spain, Sweden, UK, USA
SonoVue/*Lumason	Bracco, Italy, 2001/2014*	Sulfur hexafluoride in phospholipid shell	Heart, liver, breast, vessels, vesicoureteral reflux*	Austria, Belgium, Brazil, Bulgaria, China, Cyprus, Czech Republic, Estonia, Finland, France, Germany, Greece, Holland, Hong Kong, Hungary, Iceland, India, Ireland, Italy, Japan, Latvia, Lithuania, Luxembourg, Malta, Norway, Poland, Portugal, Romania, Russia, Singapore, Switzerland, Slovakia, Slovenia, South Korea, Spain, Sweden, UK, USA*
Sonazoid	GE Healthcare, Japan, 2007/2012	Perfluorobutan in phospholipid shell	Liver, breast	Japan, Norway, North Korea
Definity	Lantheus MI, USA, 2001	Perfluoropropane in phospholipid shell	Heart, liver, kidney	Australia, Brazil, Canada, India, Israel, Mexico, New Zealand, Singapore, South Korea, UAE, USA
Optison	GE Healthcare, Norway 2008/Mallinckrodt, USA,1998	Perfluoropropane in albumin shell	Heart, vessels	Japan, Norway, South Korea

2011 on non-hepatic applications in 2011 [38], which were updated in 2017 [39].

The second-generation UCA SonoVue® (2001, Bracco Swiss CA, Italy) is now well recognized in many countries. It is one most popular and most commonly used UCA approved by the European Medicines Agency in 2001 with further updates [40]. In 2014, SonoVue® was approved in the USA under the trade name Lumason for echocardiography, in 2016 - for liver studies in adult and pediatric practice, in 2017 - for intracavitary use for the study of vesicoureteral reflux in pediatric patients.

SonoVue® is represented with a heterogeneous phospholipid system containing sulfur hexafluoride microbubbles stabilized with palmitic acid (Fig. 1.1). One milliliter of the preparation contains about 8 μl of sulfur hexafluoride incorporated in 200 million microbubbles. The bubbles are smaller than 10 μm in size that is comparable to erythrocyte dimensions. This permits them to pass with the bloodstream through small capillaries (Fig. 1.2). They do not penetrate the vascular wall and always remain within the vessel lumen. SonoVue® is a solely intravascular UCA that differs from radiocontrast and paramagnetic, which spread into intercellular fluid [11].

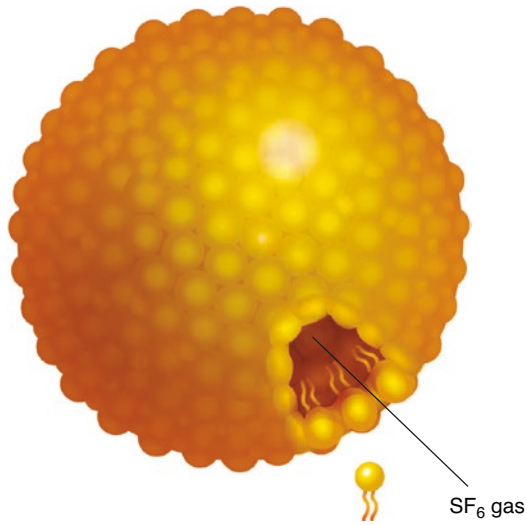

Fig. 1.1 SonoVue® microbubble. Phospholipid shell. Scheme

SonoVue® allows confident CEUS examination for 5–6 min, which enables evaluation of micro- and macrovascular features within the area of interest in all vascular phases. The half-life period is about 12 min (ranges from 2 to 33 min). After degradation, sulfur hexafluoride is eliminated with breathing, and the components of phospholipid shell are metabolized in the liver.

SonoVue® has a good safety profile. Substantial retrospective studies reported the incidence of severe adverse reactions between 0.0086% and 0.9% [41, 42]. The publication [42] based on 34,478 examinations indicated that the overall incidence of adverse effects was 0.12%. SonoVue® does not demonstrate any cardio-, hepato-, or nephrotoxic effect, thus there is no need for liver and/or kidney function assessment before the examination. The rate of severe hypersensitivity reactions to UCA components is lower than to iodine-containing contrast media.

Following the manufacturer's instruction, CEUS with SonoVue® has the below-listed principal indications:

- echocardiography (in patients with suspected cardiovascular diseases for enhancement of heart chambers and precise delineation of left ventricle endocardial margin),
- study of large blood vessels (diagnosis of anomalies, pathologies of the aorta, carotids, peripheral arteries, portal, and other veins based on echo enhancement and improved signal-to-noise ratio),
- study of the microvasculature of organs (imaging of tissue perfusion for assessment of the vascularization of focal lesions).

Currently, in clinical practice, the SonoVue® is applied for the following studies [37–39]:

- heart and large blood vessels
- liver and gallbladder
- kidneys
- bladder and vesicoureteral reflux
- scrotum
- pancreas
- spleen

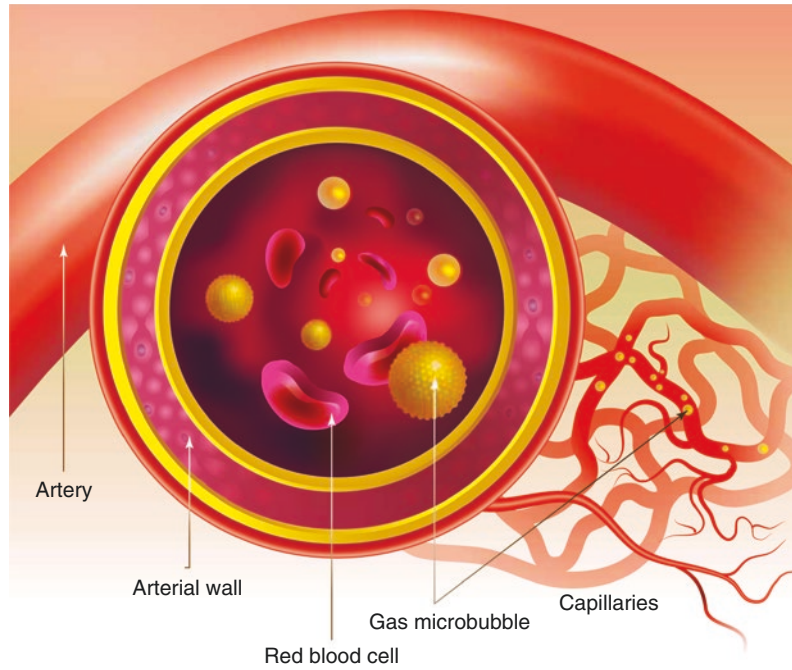

Fig. 1.2 Schematic representation of SonoVue® microbubbles in the vascular bed. The microbubbles cannot leave the intact vascular bed because of their size and thus enhance exclusively the intravascular compartment

- gastrointestinal tract
- abdominal trauma
- in association with interventions and minimally invasive ablative manipulations, for monitoring the response to treatment
- intracavitary use, inclusive of contrast-enhanced hystero-salpingo-contrast-sonography.

Despite active research and some promising results, at the moment, the clinical application of CEUS in the below-listed organs remains disputable:

- prostate
- thyroid gland
- breast
- salivary glands
- lymph nodes
- gynecological studies.

Contraindications for CEUS with SonoVue® that are mentioned by the manufacturer include the following conditions:

- hypersensitivity to the components of the UCAs
- patients known to have right-to-left shunts
- severe pulmonary hypertension (pulmonary arterial pressure >90 mm Hg),
- uncontrolled systemic hypertension
- adult respiratory distress syndrome
- ventilated patients
- unstable neurological diseases
- age below 18 years.

It is preferable to avoid the use of SonoVue® during pregnancy. In breastfeeding mothers, it is considered that breastfeeding can be resumed 2–3 h after administration of SonoVue®. Caution is needed at CEUS in patients with acute endocarditis, artificial heart valves, acute systemic inflammation with/without sepsis, blood hypercoagulation with/without recent thromboembolism, terminal renal or hepatic disease.

SonoVue® should not be used in combination with dobutamine in patients with conditions suggesting cardiovascular instability where dobutamine is contraindicated.

It is recommended to keep the patient under close medical supervision during and for at least 30 minutes following the administration of SonoVue®.

Side effects or adverse reactions are rare and mild. Uncommon conditions confer headache, paraesthesia, dizziness, dysgeusia, flushing, pharyngitis, nausea, abdominal pain, pruritus, rash, back pain, chest discomfort, injection site reaction, feeling hot, hyperglycemia. Rare side effects (≥1/10,000 to <1/1000) may include Hypersensitivity (associated with skin erythema, bradycardia, hypotension, dyspnea, loss of consciousness, cardiac/cardiorespiratory arrest, anaphylactic reaction, anaphylactoid reaction, or anaphylactic shock), sinus headache, vision blurred, hypotension, chest pain, fatigue. There are single fatal cases associated with SonoVue® [43]. All of them occurred in patients with the underlying severe cardiac disease after contrast-enhanced echocardiography. However, in the majority of cases, the autopsies failed to relate the deaths with the administration of SonoVue®. Regarding interaction, there was no apparent relationship concerning the occurrence of adverse events in the clinical studies for patients receiving various categories of the most common concomitant medications.

References

1. Gramiak R, Shah PM. Echocardiography of the aortic root. Investig Radiol. 1968;3(5):356–66. https://doi.org/10.1097/00004424-196809000-00011.
2. Shah PM. Contrast echocardiography - a historical perspective. In: Nanda NC, Schlief R, editors. Advances in echo imaging using contrast enhancement. Dordrecht: Springer; 1993. https://doi.org/10.1007/978-94-015-8126-4_1.
3. Lencioni R. Enhancing the role of ultrasound with contrast agents. Springer; 2006.
4. Chiang CW, Lin FC, Fu M, Fang BR, Hsu TS, Lee YS. Importance of adequate gas-mixing in contrast echocardiography. Chest. 1986;89(5):723–6. https://doi.org/10.1378/chest.89.5.723.
5. Cosgrove D, Eckersley R. Contrast-enhanced ultrasound: basic physics and technology overview. In: Lencioni R, editor. Enhancing the role of ultrasound with contrast agents. Milano: Springer; 2006.
6. Leopold GR, Asher WM. Deleterious effects of gastrointestinal contrast material on abdominal echography. Radiology. 1971;98(3):637–40. https://doi.org/10.1148/98.3.637.
7. Mattrey RF, Leopold GR, vanSonnenberg E, Gosink BB, Scheible FW, Long DM. Perfluorochemicals as liver- and spleen-seeking ultrasound contrast agents. J Ultrasound Med. 1983;2(4):173–6. https://doi.org/10.7863/jum.1983.2.4.173.
8. Ophir J, Parker KJ. Contrast agents in diagnostic ultrasound. Ultrasound Med Biol. 1990;16(2):209. https://doi.org/10.1016/0301-5629(90)90151-2.
9. Tuthill TA, Baggs RB, Violante MR, Parker KJ. Ultrasound properties of liver with and without particulate contrast agents. Ultrasound Med Biol. 1991;17(3):231–7. https://doi.org/10.1016/0301-5629(91)90044-w.
10. Rovai D, Lombardi M, Distante A, L'Abbate A. Myocardial perfusion by contrast echocardiography. From off-line processing to radio frequency analysis. Circulation. 1991;83(5 Suppl):III97–III103.
11. Weskott HP. Contrast-enhanced ultrasound. 2nd ed. London: Uni-Med Science; 2013.
12. Feinstein SB, Shah PM, Bing RJ, Meerbaum S, Corday E, Chang BL, et al. Microbubble dynamics visualized in the intact capillary circulation. J Am Coll Cardiol. 1984;4(3):595–600. https://doi.org/10.1016/s0735-1097(84)80107-2.
13. De Castro S, Agati L, Cartoni D. Harmonic imaging with Levovist for transthoracic echocardiographic reconstruction of left ventricle in patients with post-ischemic left ventricular dysfunction and suboptimal acoustic windows. J Am Soc Echocardiogr. 2000;13(2):139–45.
14. Drelich-Zbroja A, Jargiełło T, Szymańska A, Krzyzanowski W, Szczerbo-Trojanowska M. Can Levovist-enhanced Doppler ultrasound replace angiography in renal arteries imaging? Med Sci Monit. 2004;10(3):36–41.
15. Ernst H, Hahn EG, Balzer T, et al. Color Doppler ultrasound of liver lesion signal enhancement after intravenous injection of the ultrasound contrast agent Levovist. J Clin Ultrasound. 1996;24(1):31–5.
16. Frauscher F, Klauser A, Halpern EJ, Horninger W, Bartsch G. Detection of prostate cancer with a microbubble ultrasound contrast agent. Lancet. 2001;357(9271):1849–50. https://doi.org/10.1016/s0140-6736(00)04970-9.
17. Kahl A, Venz S, Keske U, Bechstein WO, Berweck S, Felix R, et al. Magnetic resonance imaging and Levovist-enhanced color and power Doppler imaging in the follow-up of pancreas transplants in patients after combined pancreas and kidney transplantation. Transplant Proc. 1998;30(2):246–7. https://doi.org/10.1016/s0041-1345(97)01244-x.
18. Kedar RP, Cosgrove D, McCready VR, Bamber JC, Carter ER. Microbubble contrast agent for color Doppler US: effect on breast masses. Work Progr Radiol. 1996;198(3):679–86. https://doi.org/10.1148/radiology.198.3.8628854.
19. Kratzer W, Reuter S, Hirschbuehl K, Ehrhardt AR, Mason RA, Haenle MM, et al. Comparison of contrast-enhanced power Doppler ultrasound (Levovist) and computed tomography in alveolar echinococcosis. Abdom Imaging. 2005;30(3):286–90. https://doi.org/10.1007/s00261-004-0263-7.

20. Sidhu PS, Marshall MM, Ryan SM, Ellis SM. Clinical use of Levovist, an ultrasound contrast agent, in the imaging of liver transplantation: assessment of the pre- and post-transplant patient. Eur Radiol. 2000;10(7):1114–26. https://doi.org/10.1007/s003309900117.
21. Spiezia S, Farina R, Cerbone G. Analysis of color Doppler signal intensity variation after levovist injection: a new approach to the diagnosis of thyroid nodules. J Ultrasound Med. 2001;20(3):223–31.
22. Stuhrmann M, Schwarz T, Schietzel M. Mammakarzinom-Rezidiv versus postoperative Narbe. Sonographische Differenzierung unter Einsatz des Ultraschall-Kontrastmittels Levovist [Breast cancer recurrence versus scar. Ultrasonographic differentiation using Levovist as the contrast medium]. Ultraschall Med. 2001;22(1):2–6. https://doi.org/10.1055/s-2001-11245.
23. Sviridov NK, Napolov IK. Klinicheskoe primenenie ul'trazvukovogo kontrastnogo sredstva levovista dlia vizualizatsii transplantata pecheni [Clinical use of the ultrasound contrast Levovist for hepatic graft visualization]. Vestn Rentgenol Radiol. 2003;(1):61–2.
24. Gazhonova VE, Zubarev AV, Kislyakova MV. Ekhokontrastnaya angiografiya predstatel'noj zhelezy s Levovistom dlya uluchsheniya vizualizacii krovotoka [Echocontrast angiography of the prostate with Levovist to improve the visualization of blood flow]. In: Sandrikov VA, editor. Diagnostika – novye metody [Diagnostics – new methods]. Moscow: AirArt; 1998. p. 151–6. Russian.
25. Zubarev AV. 3-dementional and contrast-enhanced angiography. Meditsinskaya Vizualizatsiya. 1997;4:3–8. Russian.
26. Kamalov YR, Sandrikov VA, Gavrilov AV. Ispol'zovanie ul'trazvukovogo kontrasta Levovist pri obsledovanii bol'nyh opuholyami pecheni, portal'noj gipertenziej i pri ortotopicheskoj transplantacii pecheni [The use of Levovist ultrasound contrast agent in the examination of patients with liver tumors, portal hypertension, and orthotopic liver transplantation]. In: Sandrikov VA, editor. Diagnostika – novye metody [Diagnostics – new methods]. Moscow: AirArt; 1998. Russian.
27. Grayburn PA, Weiss JL, Hack TC, et al. Phase III multicenter trial comparing the efficacy of 2% dodecafluoropentane emulsion (EchoGen) and sonicated 5% human albumin (Albunex) as ultrasound contrast agents in patients with suboptimal echocardiograms. J Am Coll Cardiol. 1998;32(1):230–6. https://doi.org/10.1016/s0735-1097(98)00219-8.
28. Ragde H, Kenny GM, Murphy GP, Landin K. Transrectal ultrasound microbubble contrast angiography of the prostate. Prostate. 1997;32(4):279–83. https://doi.org/10.1002/(sici)1097-0045(19970901)32:4<279::aid-pros8>3.0.co;2-e.
29. Robbin ML, Eisenfeld AJ. Perflenapent emulsion: a US contrast agent for diagnostic radiology – multicenter, double-blind comparison with a placebo. EchoGen Contrst Ultrasound Study Group. Radiology. 1998;207(3):717–22. https://doi.org/10.1148/radiology.207.3.9609895.
30. Bernatik T, Becker D, Neureiter D, et al. Hepatic transit time of an echo enhancer: an indicator of metastatic spread to the liver. Eur J Gastroenterol Hepatol. 2004;16(3):313–7. https://doi.org/10.1097/00042737-200403000-00011.
31. Clark LN, Dittrich HC. Cardiac imaging using Optison. Am J Cardiol. 2000;86(4A):14G–8G. https://doi.org/10.1016/s0002-9149(00)00984-x.
32. Jung EM, Clevert DA, Rupp N. Erste Erfahrungen mit der kontrastmittelverstärkten Sonographie mit Optison bei der perkutanen Thermoablation von Lebertumoren [Contrast-enhanced ultrasound with Optison in percutaneous thermoablation of liver tumors]. Rofo. 2003;175(10):1403–12. https://doi.org/10.1055/s-2003-42882.
33. Jung EM, Jungius KP, Rupp N, et al. Contrast enhanced harmonic ultrasound for differentiating breast tumors - first results. Clin Hemorheol Microcirc. 2005;33(2):109–20.
34. Sontum PC. Physicochemical characteristics of Sonazoid, a new contrast agent for ultrasound imaging. Ultrasound Med Biol. 2008;34(5):824–33. https://doi.org/10.1016/j.ultrasmedbio.2007.11.006.
35. Ignee A, Atkinson NS, Schuessler G, Dietrich CF. Ultrasound contrast agents. Endosc Ultrasound. 2016;5(6):355–62. https://doi.org/10.4103/2303-9027.193594.
36. Albrecht T, Blomley M, Bolondi L, et al. Guidelines for the use of contrast agents in ultrasound. Ultraschall Med. 2004;25:249–56.
37. Dietrich CF, Nolsøe CP, Barr RG, Berzigotti A, Burns PN, Cantisani V, et al. Guidelines and good clinical practice recommendations for contrast enhanced ultrasound (CEUS) in the liver - update 2020 - WFUMB in cooperation with EFSUMB, AFSUMB, AIUM, and FLAUS. Ultraschall Med. 2020;41(5):562–85. https://doi.org/10.1055/a-1177-0530.
38. Piscaglia F, Nolsøe C, Dietrich CF, et al. The EFSUMB guidelines and recommendations on the clinical practice of contrast enhanced ultrasound (CEUS). update 2011 on non-hepatic applications. Ultraschall Med. 2011;32:1–27.
39. Sidhu PS, Cantisani V, Dietrich CF, Gilja OH, Saftoiu A, Bartels E, et al. The EFSUMB guidelines and recommendations for the clinical practice of contrast-enhanced ultrasound (CEUS) in non-hepatic applications: update 2017 (long version). Ultraschall Med. 2018;39(2):e2–e44. https://doi.org/10.1055/a-0586-1107.
40. Summary of product characteristics. SonoVue 8 microlitres/ml powder and solvent for dispersion for injection. https://ec.europa.eu/health/documents/community-register/2015/20150619132105/anx_132105_en.pdf. Accessed 15 Feb 2021.
41. Piscaglia F, Bolondi L. Italian Society for Ultrasound in Medicine and Biology (SIUMB) Study Group on Ultrasound Contrast Agents. The safety of SonoVue

in abdominal applications: retrospective analysis of 23188 investigations. Ultrasound Med Biol. 2006;32:1369–75.
42. Hu C, Feng Y, Huang P, Jin J. Adverse reactions after the use of SonoVue contrast agent. Characteristics and nursing care experience. Medicine (Baltimore). 2019;98(44):e17745.
43. Assessment report. SonoVue committee for medicinal products for human use (CHMP). 2 May 2014 EMA/454283/2014. https://www.ema.europa.eu/en/documents/variation-report/sonovue-h-c-303-ii-0025-epar-assessment-report-variation_en.pdf. Accessed 15 Feb 2021.

2 Physical Principles and Technical Aspects of CEUS

Ella I. Peniaeva, Alexander N. Sencha, Yuly R. Kamalov, Yury N. Patrunov, Elena P. Fisenko, Natalia N. Vetsheva, Roman A. Barmin, and Polina G. Rudakovskaya

CEUS aims to assess tissue microvascularization, which is practically impossible with other US methods [1]. With conventional ultrasound, the echoes of the surrounding tissues are significantly stronger, and blind the echo from blood in small vessels. In addition to enhancing the blood echoes with UCAs, special modes to amplify blood echoes and suppress tissue echoes are applied. This is possible due to the specific mechanism of interaction of US waves with microbubbles and differences in its scattering depending on the amplitude and frequency.

In the initially provided contrast-specific modes at low acoustic power, the reverse linear dispersion from microbubbles was higher, which led to an increase in blood echo. With power increase to ultrasound pressure of 50–100 kPa, microbubbles start to vibrate and reflect the US wave with harmonic components, which is used in modern harmonic and pulse inversion imaging modes. When acoustic pressure approaches the values of standard scanning modes, the microbubbles are destroyed with the release of the incorporated gas. To avoid premature destruction of microbubbles, scanners use modes with a low mechanical index (MI), which demonstrate an approximate pressure for the average tissue in the focus of the US beam [1]. The index itself has an estimated value and, taking into account the complex calculation procedure, the indices displayed on various devices are not exactly equal. Therefore, recommendations for one equipment settings cannot be appropriate to the equipment of other manufacturers.

When using harmonic imaging modes, the system filters all signals except those close to the

E. I. Peniaeva (✉) · Y. N. Patrunov
Department of Ultrasound Diagnostics of the Center for Radiological Diagnostics, Private Healthcare Institution "Clinical Hospital "RZD-Medicina" of Yaroslavl City", Yaroslavl, Russian Federation

A. N. Sencha
Department of Visual and Functional Diagnostics, Federal State Budget Institution "National Medical Research Center for Obstetrics, Gynecology and Perinatology n.a. V.I.Kulakov", Moscow, Russian Federation

Y. R. Kamalov
Petrovsky National Research Centre of Surgery, Moscow, Russian Federation

E. P. Fisenko
Ultrasound Diagnostics Laboratory, Department of Clinical Physiology, Instrumental and Radiology Diagnostics, B.V. Petrovsky Russian Research Surgery Center, Moscow, Russian Federation

N. N. Vetsheva
Ultrasound Diagnostics Department, State Budgetary Healthcare Institution of Moscow Area "Moscow Regional Research Clinical Institute n.a. M.F. Vladimirskiy", Moscow, Russian Federation

R. A. Barmin · P. G. Rudakovskaya
Center for Photonics and Quantum Materials, Skolkovo Institute of Science and Technology, Moscow, Russian Federation

A. N. Sencha, Y. N. Patrunov (eds.), *Contrast-Enhanced Ultrasound*,
https://doi.org/10.1007/978-3-030-91764-7_2

second harmonic sorting out a double frequency reflected echo. This way of signal processing leads to a low spatial resolution.

Pulse inversion imaging technique permitted to overcome the limitations of harmonic modes. This technology is now applied in the majority of contrast-specific US modes in the equipment of various manufacturers [2]. The scanner generates two consecutive pulses that are mirror mapping each other (the change in phase by 180°). The sum of the reflected echo in the case of a linear response (reflection from the tissue) will amount to zero. In the case of nonlinear behavior (reflection from microbubbles), the reflected echo signals will not be a mirror mapping of each other due to the change in the diameter of the resonating microbubble, and accordingly, their amount will differ from zero. In this case, there is no limitation of the bandwidth, and utilization of the full range of frequencies with the reconstruction of a high-resolution broadband image is possible (Fig. 2.1).

Each manufacturer develops its own techniques for CEUS. The adequate subtraction of the tissue results in the fact that parenchyma becomes practically invisible (colored with black) on the contrast-enhanced image. Nevertheless, good reflectors, such as vascular structures and the diaphragm, may remain slightly visible. Accordingly, CEUS should be performed only with a specialized contrast-specific mode [1, 3–5].

For best results, the correct configuration of the scanning mode is important. In most cases, the manufacturer's configuration preset is used, but some adjustments may be appropriate.

Low MI helps to avoid microbubble destruction with the US exposure but leads to a decrease in penetration and intensity of the echo signal. Consequently, the contrast resolution is lower with depth. Penetrating ability can be improved

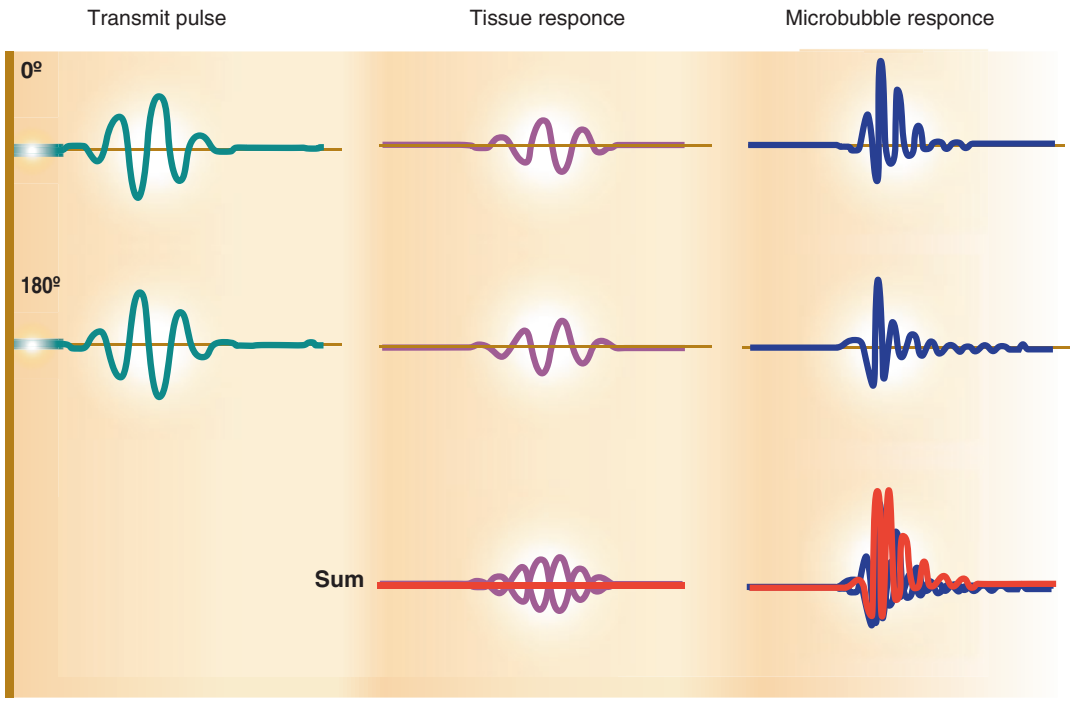

Fig. 2.1 Schematic representation of the separation of tissue echo signals from microbubbles. Two pulses are transmitted one by one. They are different in shape (amplitude modulation and phase inversion). When scattered back from tissues, the pulses accurately correspond to the shape of the initial pulse (linear response). Due to oscillations with individual resonance frequency, microbubbles generate their own signal (blue), which is different from the initial pulse (nonlinear response). Mathematical processing of the resulting echoes subtracts linear responses of the tissue, and nonlinear signals from microbubbles are displayed as a final contrast image (red)

by decreasing the scanning frequency. That does not influence bubble destruction but deteriorates spatial resolution [4].

Maximum bubble destruction occurs within the US focus zone. It may have a "washout" appearance. Alternatively, the too deep position of the focus can lead to the "loss" of the near field. The optimal focus location is behind the lower boundary of the zone of interest [1, 3–5].

For adequate imaging, analysis, and recording of contrast enhancement, the screen frame rate of 10 Hz and higher is recommended, because some hypervascular lesions exhibit very fast filling, which may be completed in a second. Hence, the repeated analysis of the slow motion cine loop is always necessary (Fig. 2.2). A high frame rate is also beneficial for focal lesion detection while scanning the entire organ [5]. However, an increase in frame rate can accelerate bubble destruction. The decrease in frame rate during the late venous phase can prolong the time of contrast enhancement [3, 4].

Correct setting of the dynamic range is also a key point in CEUS. It determines the range of the intensities of displayed echo signals (Fig. 2.3). A wide dynamic range increases the number of signal grades ("shades of gray") that works for better differentiation of variable intensities of contrast enhancement [3, 5–7]. Narrow dynamic range decreases the number of "shades" in the image and increases the visual contrast. A narrow dynamic range may be preferable to visualize areas or lesions with low perfusion. A too narrow dynamic range reduces the distinction between the zones with different contrast enhancement. For example, peripheral ring-shaped hyperenhancement, which is characteristic for liver metastases, may be missed, as it appears the same color as the entire lesion.

The gain setting corresponds to the amplification of the received echo signal. For CEUS, the initial gain is usually set slightly higher than the noise level, so that before bubbles appear the image is dark with slightly visible hyperechoic structures. In the case of too low gain, CEUS lacks the reflections from microbubbles in small vessels, and only large vessels can be observed. Too high gain results in excessive saturation of the image.

Currently, almost all manufacturers of US scanners offer a wide choice of probes, which are optimized for CEUS. In most cases, convex probes are considered optimal for the study of internal organs, and linear probes are used for superficial and small parts. The higher is the probe's frequency, the higher dose of the UCA is necessary [1, 3, 5].

One important aspect of CEUS is the choice of UCA dose. Too high dosage causes artifacts, especially in the early arterial phase. These can be acoustic shadows, the excessive enhancement of small structures, and oversaturation of the echo signal, which will limit further quantitative analysis [3, 5]. On the other hand, a too low dose of UCA may lead to inadequate diagnosis related to weak contrast enhancement, especially in the far field, and difficulties in washout assessment (Fig. 2.4).

At liver CEUS, if the unchanged liver parenchyma demonstrates strong and fast washout, regard that the dose was probably too small. In complex imaging conditions (liver cirrhosis, steatosis, obesity, etc.), the attenuation is often significantly increased, which prevents echo propagation. To compensate for attenuation, it is possible to use a higher MI. Meanwhile, the focal liver lesion sustains nearly the same acoustic pressure as in the normal liver with low MI. In some cases, this may require an increase in the UCA dose.

If the contrast enhancement (bubble appearance) in the target organ is not registered within 30–60 s after contrast medium introduction, consider an incorrect injection. In this case, bubbles cannot be detected in large vessels (e.g. carotids) either. Contrast media at the injection site can be observed in soft tissues adjacent to cubital (or other) vein as an amorphous heterogenous area easily detected in "contrast" mode (Fig. 2.5). This infiltration typically causes neither pain nor other significant discomforts, and completely disappears within 3–5 days.

The literature data report on cases of pseudoenhancement in avascular echogenic tissues,

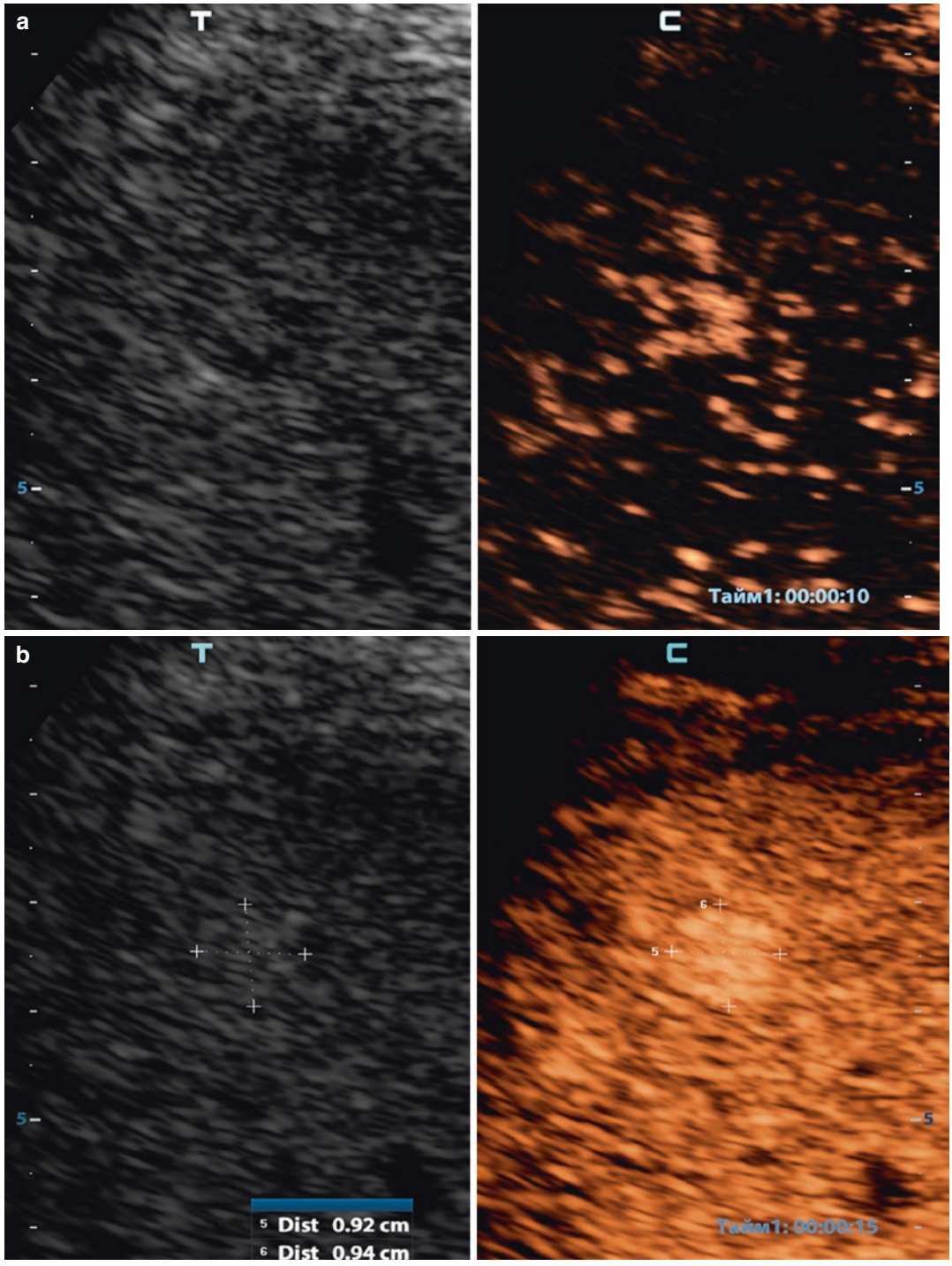

Fig. 2.2 Fast contrast enhancement of liver hemangioma. CEUS images. (**a**) Peripheral nodular enhancement, characteristic of liver hemangioma, 10 s. (**b**) Complete enhancement of the same lesion, 15 s

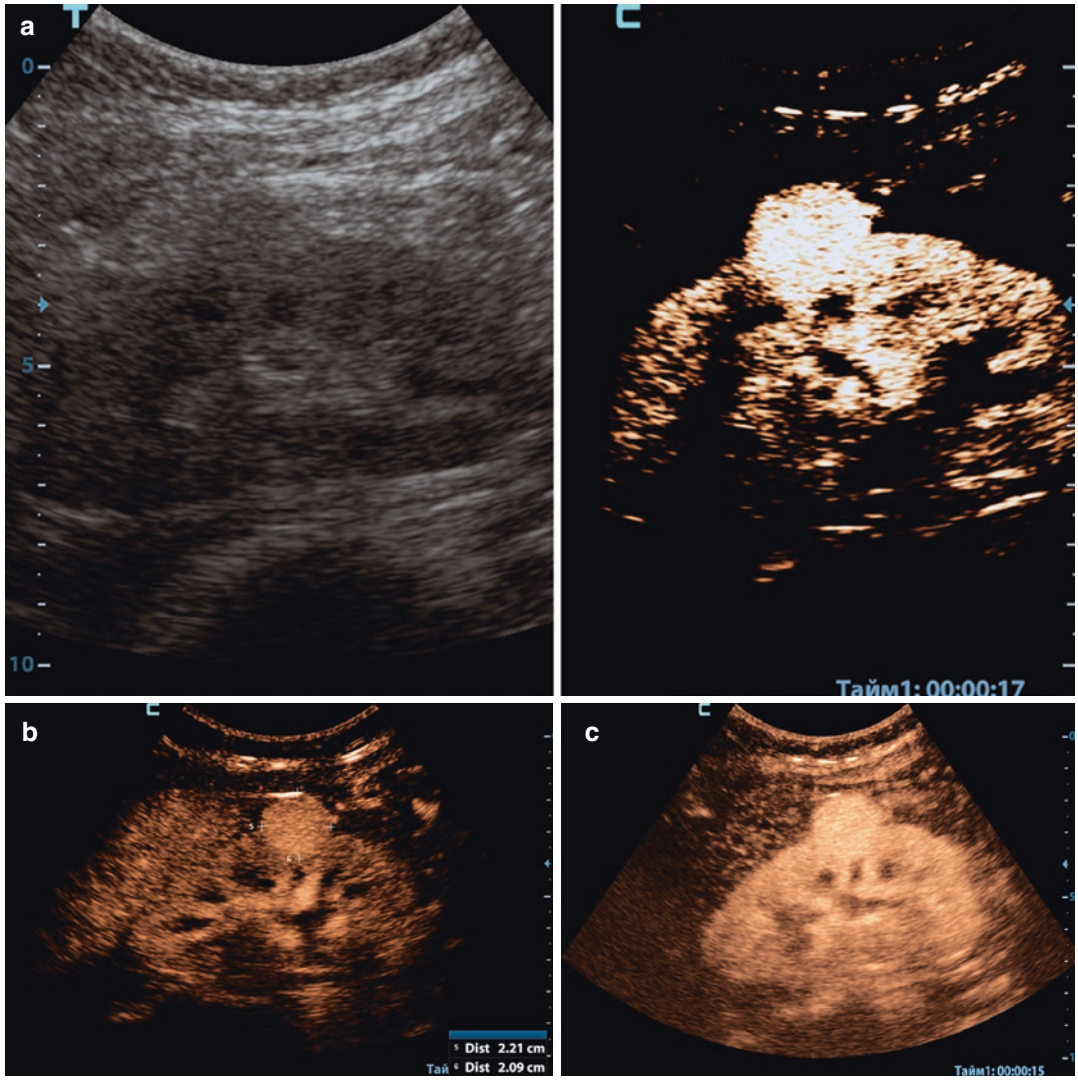

Fig. 2.3 Dynamic range settings. CEUS images. (**a**) Narrow. (**b**) Medium. (**c**) Wide

when the reflections from tissues are displayed as signals from microbubbles [3, 5]. Such a pseudoenhancement is a consequence of the presence of microbubbles in the way of the US beam between the ultrasound probe and the pseudoenhancing zone that leads to nonlinear propagation of the US and, accordingly, to nonlinear echoes from linear reflectors. This, in turn, leads to the distortion of the image, especially in deep areas, due to the US beam passing through the large volume of microbubbles. To reduce this artifact, one should avoid excessive doses of contrast media, deep location of the zone of interest, and large vessels in the way of the US beam near the studied are [5].

Subtraction of echo signals from the tissue is effective for the assessment of lesions in parenchymatous organs. However, phase aber-

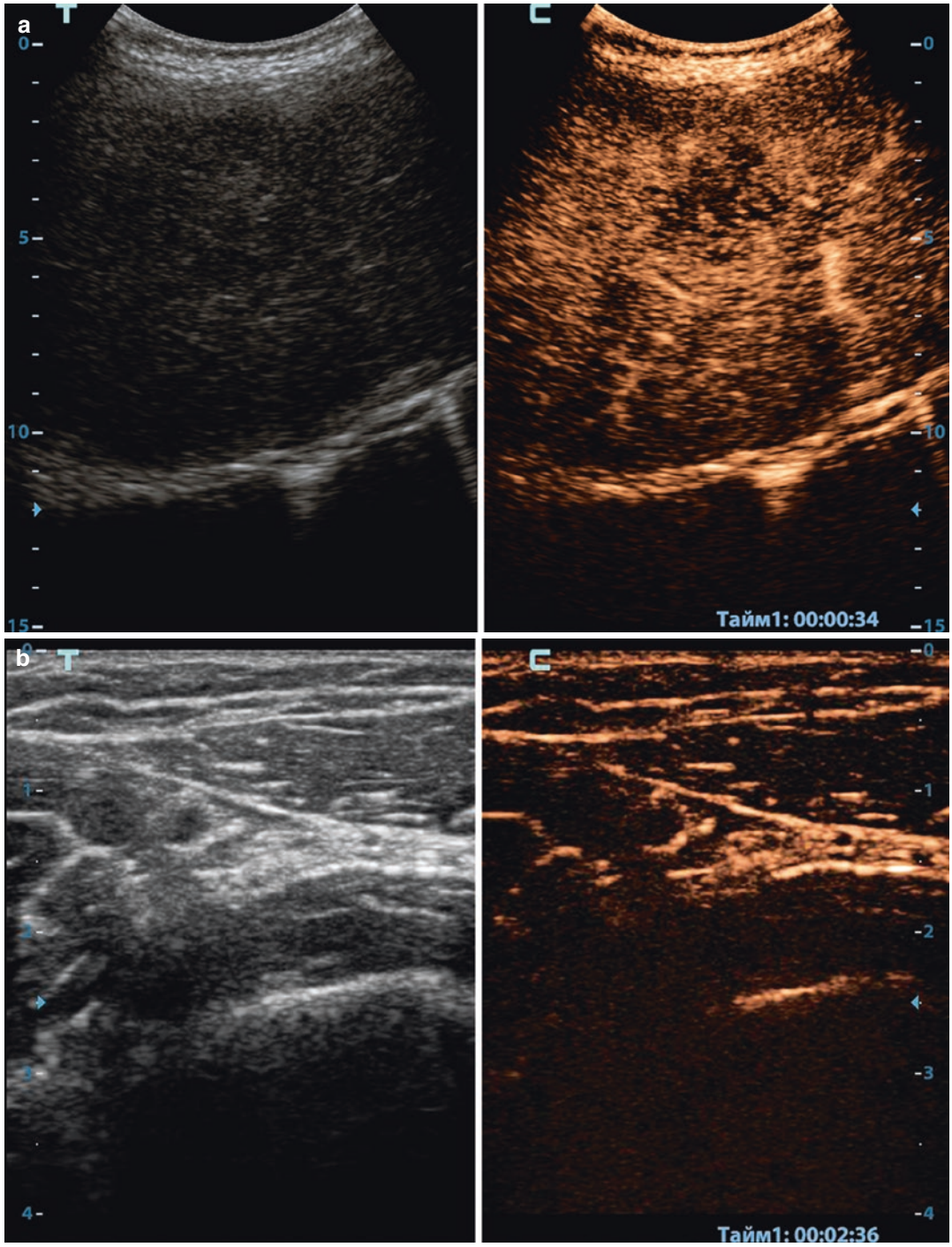

Fig. 2.4 Example of poor quality CEUS images due to the lack of UCA resulted from misadministration. (**a**) Insufficient contrast enhancement of the liver lesion and parenchyma. (**b**) Some UCA in the tissues near the cubital vein

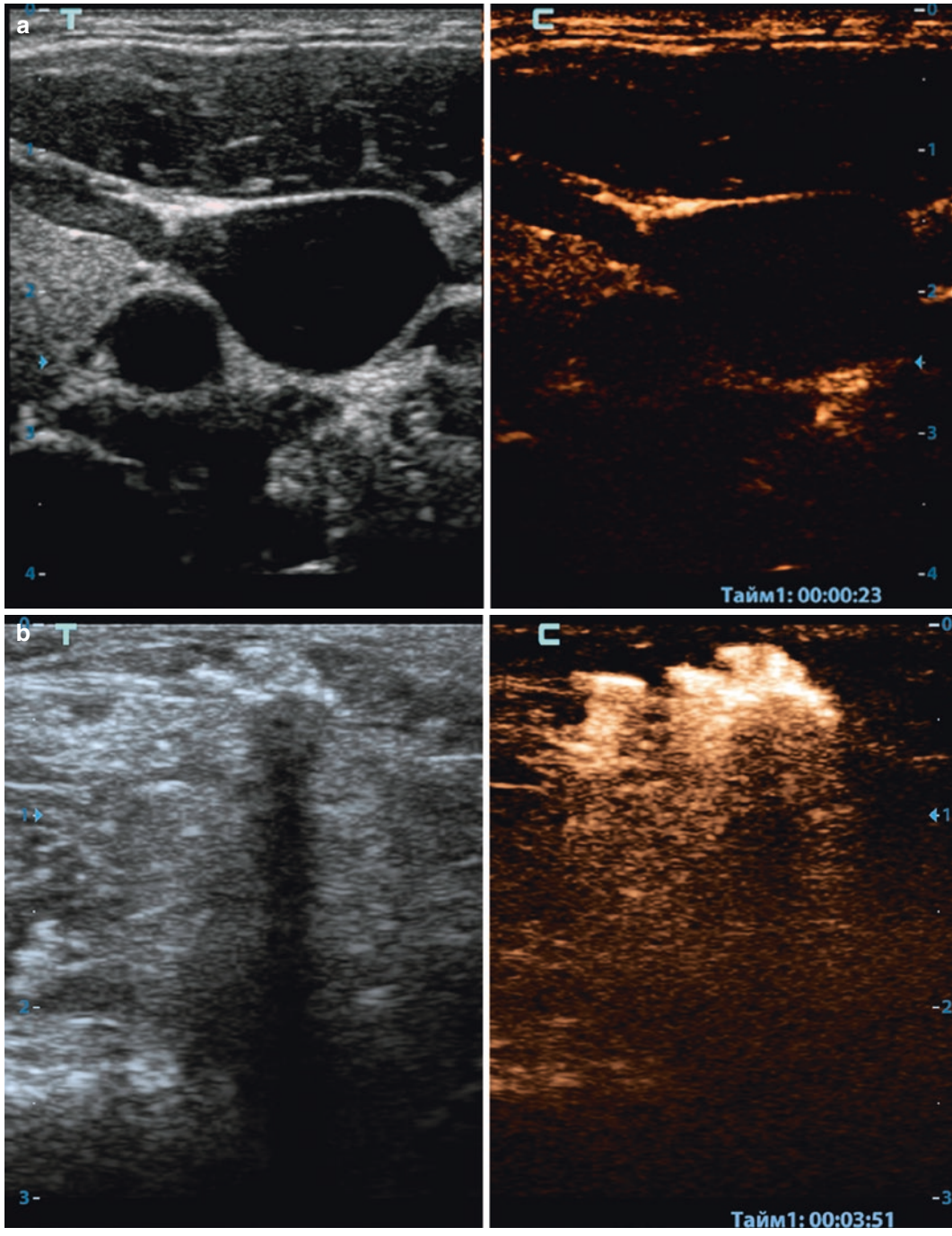

Fig. 2.5 Example of CEUS images in a patient with improper UCA administration. (**a**) No UCA in the common carotid artery lumen longer than 20 s after the injection. (**b**) Contrast agent in the subcutaneous soft tissues of the elbow fold

rations that occur in some tissues lead to a less effective subtraction. It is usually observed in the subcutaneous adipose layer and liver steatosis. Additionally, if one gradually amplifies the acoustic power to improve the signal from a deeper area or to increase the signal from bubbles in the late phase of contrast enhancement, the signal from nonlinear harmonics, created by the background tissues, may be non-proportionally amplified, which leads to pseudoenhancement. These artifacts can be minimized by choosing the appropriate power and amplification settings before UCA introduction. To differentiate true and false enhancement, the "Flash" function is of benefit. In the case of true enhancement, Flash induces bubble destruction with their subsequent reaccumulation. False enhancement remains the same before and after Flash.

The background noise may result from too high MI with insufficient subtraction of echo signals from tissues or high gain. In those cases, this artifact is present before the UCA introduction and cannot be eliminated with a high MI pulse (Flash). Gain-dependent noise is evenly distributed across the ultrasound field of view or correlates with gain/depth adjustment settings. Meanwhile, the MI-dependent noise occurs in hyperechoic tissues [3, 5]. Background noise deteriorates the differentiation of enhancing and non-enhancing areas. Gain and MI adjustment eliminate these artifacts.

Acoustic shadow is one most common artifact related to reflection, absorption, and refraction of the US beam. In CEUS, most of the ultrasound energy is reflected by good reflectors (microbubbles) or absorbed by high attenuation structures [3]. After passing through such structures, ultrasound energy significantly decreases. It leads to an acoustic shadow behind the bubble collection. As the bubbles subside with time, it becomes less prominent along with the decrease in the contrast enhancement [5].

Pseudo-washout is associated with the incidental destruction of contrast medium microbubbles in tissue with abnormal perfusion, e.g. in liver hemangioma with low-velocity blood flow. In the case of slow motion of microbubbles within the scan zone, the risk of their destruction is higher due to longer US exposure. It may lead to a faster decrease in contrast enhancement of the corresponding area. Considering that washout features are important for the diagnosis of liver malignancies, the appearance of such an artifact may significantly influence the conclusion, tending to false-positive reports [3–5].

Bubble destruction in the near field may incidentally occur because the acoustic pressure in the scan area is inhomogeneous with peak values in the near zone and in-focus zone. This starts with the progressive loss of echo in the near field and results in a dark strip with low or absent enhancement in tissue adjacent to the probe surface [3, 5]. With higher MI values, US frequency, and frame rate, it gets worse up to the "burnout" effect in the near field due to faster bubble destruction (Fig. 2.6).

CEUS requires special attention to the correct settings of the scanner, UCA dose along with the way and place of its administration, and considering probable ultrasound effects during the study.

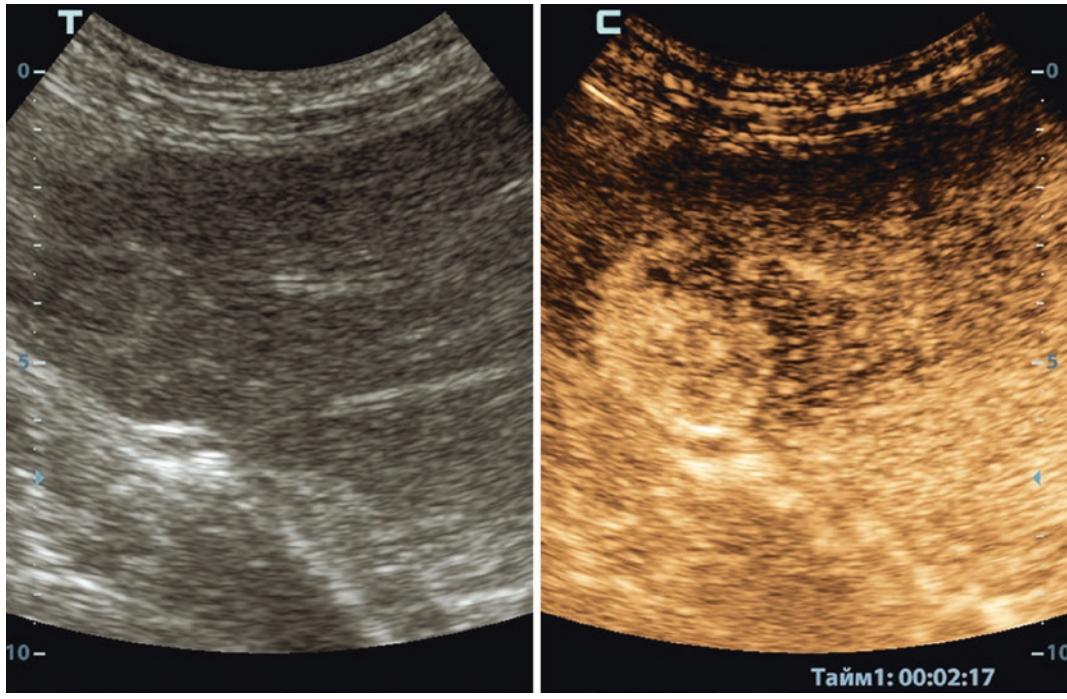

Fig. 2.6 Example CEUS image with bubble destruction in the near field

References

1. Weskott HP. Contrast-enhanced ultrasound. 2nd ed. London: Uni-Med Science; 2013.
2. Greis C. Technische Grundlagen der Kontrastsonographie im Überblick und Ausblick in die Zukunft [Summary of technical principles of contrast sonography and future perspectives]. Radiologe. 2011;51(6):456–61. German. https://doi.org/10.1007/s00117-010-2099-1.
3. Dietrich CF, Ignee A, Greis C, Cui XW, Schreiber-Dietrich DG, Hocke M. Artifacts and pitfalls in contrast-enhanced ultrasound of the liver. Ultraschall Med. 2014;35(2):108–25.; Quiz 126–7. https://doi.org/10.1055/s-0033-1355872.
4. Dietrich CF, Averkiou M, Nielsen MB, et al. How to perform contrast-enhanced ultrasound (CEUS). Ultrasound Int Open. 2018;4(1):E2–E15. https://doi.org/10.1055/s-0043-123931.
5. Fetzer DT, Rafailidis V, Peterson C, Grant EG, Sidhu P, Barr RG. Artifacts in contrast-enhanced ultrasound: a pictorial essay. Abdom Radiol (NY). 2018;43(4):977–97. https://doi.org/10.1007/s00261-017-1417-8.
6. Claudon M, Dietrich CF, Choi BI, Cosgrove DO, Kudo M, Nolsøe CP, et al. Guidelines and good clinical practice recommendations for contrast enhanced ultrasound (CEUS) in the liver--update 2012: a WFUMB-EFSUMB initiative in cooperation with representatives of AFSUMB, AIUM, ASUM, FLAUS and ICUS. Ultraschall Med. 2013;34(1):11–29. https://doi.org/10.1055/s-0032-1325499.
7. Cosgrove D, Eckersley R. Contrast-enhanced ultrasound: basic physics and technology overview. In: Lencioni R, editor. Enhancing the role of ultrasound with contrast agents. Milano: Springer; 2006.

Technique of CEUS and Data Analysis

3

Ella I. Peniaeva, Alexander N. Sencha, Alexey V. Pomortsev, Liubov A. Timofeyeva, Yury N. Patrunov, and Ekaterina A. Sencha

SEUS is performed in aseptic conditions applicable to minimally invasive manipulations, preferably in a clean dressing room. The room should necessarily have medicines for the treatment of possible anaphylactic reactions that does not exclude the patient's possible transportation to the intensive care unit and further follow-up. CEUS is possible only with those ultrasound scanners, which incorporate specialized modes intended for contrasting imaging.

CEUS confers the following stages:

1. Preliminary stage
   (a) review of the patient's clinical history, laboratory data, prior imaging findings, and obtaining the informed consent for the procedure,
   (b) choice of the optomal arrangement, which is convenient for the patient and ensures unlimited access to the patient and the equipment
   (c) general survey with the conventional US of the target area, the definition of the zones of interest, lesions, and so on, assessment of imaging conditions,
   (d) pre-configuration of ultrasound equipment, adjustment of the contrast mode settings,
   (e) preparation of the UCAs: the opening of the package, dissolving the drug according to the instructions, gaining the required volume of contrast medium in the syringe ready for intravenous administration.

Supplementary Information The online version contains supplementary material available at [https://doi.org/10.1007/978-3-030-91764-7_3].

E. I. Peniaeva (✉) · Y. N. Patrunov
Department of Ultrasound Diagnostics of the Center for Radiological Diagnostics, Private Healthcare Institution "Clinical Hospital "RZD-Medicina" of Yaroslavl City", Yaroslavl, Russian Federation

A. N. Sencha
Department of Visual and Functional Diagnostics, Federal State Budget Institution "National Medical Research Center for Obstetrics, Gynecology and Perinatology n.a. V.I.Kulakov", Moscow, Russian Federation

A. V. Pomortsev
Department of Radiation Diagnostics, Federal State Budgetary Educational Institution of Higher Education "Kuban State Medical University", Krasnodar, Russian Federation

L. A. Timofeyeva
Department of Propaedeutics of Internal Diseases with Radiation Diagnostics Course, I. N. Ulianov Chuvash State University, Cheboksary, the Chuvash Republic, Russian Federation

E. A. Sencha
Ultrasound Diagnostics Department, Federal State Budget Institution "Medical Diagnostic Center No. 9" of the Ministry of Defence of the Russian Federation, Moscow, Russian Federation

A. N. Sencha, Y. N. Patrunov (eds.), *Contrast-Enhanced Ultrasound*,
https://doi.org/10.1007/978-3-030-91764-7_3

2. Actual CEUS examination
   (a) introduction of the UCA to the peripheral vein along with the start of the cine loop record,
   (b) simultaneous ultrasound study in specialized mode with a low mechanical index, visual spotting of the beginning of contrast enhancement, monitoring washin and washout, flushing, etc. while recording single cine loop,
   (c) assessment of the need for additional contrast medium administration,
   (d) CEUS procedure finishes for the patient with a tight sterile bandage application at the injection site.
3. Postprocessing
   (a) a thorough reassessment of the recorded cine loop in slow-motion and quantitative analysis,
   (b) discussion of obtained results and creation of the study summary,
   (c) completion of the study report, giving out further recommendations for the patient.

Before CEUS, it is necessary to evaluate the indications and benefits of the modality for the individual patient, and estimate contraindications. The patient should be properly informed about the study and possible side effects and give a signed voluntary informed consent. The preparation of the patient for CEUS is the same as for conventional US study.

Before UCA injection, the standard US is of much help to decide on the value of CEUS for the diagnosis in an individual patient. It clarifies the current imaging conditions related to anatomical features, the location of the target area, and temporary aspects. The actual presence, number, and size of lesions can be easily specified to facilitate optimal scanning plane selection. The target area should be clearly visible and remain within the scanning range throughout the study, preferably with as little motion as possible. Acoustic shadows and other artifacts that deteriorate imaging should be avoided.

If CEUS is considered appropriate, the contrast medium is prepared according to the manufacturer's manual.

Fig. 3.1 Photo of items in the SonoVue® set. (1) Dry substance sulfur hexafluoride. (2) Minispike transfer system. (3) Syringe body filled with 0.9% normal saline. (4) Syringe plunger rod

The SonovVue set includes the following items (Fig. 3.1):

- vial with sulfur hexafluoride dry substance,
- a syringe filled with 0.9% sodium chloride,
- minispike transfer system—the adapter for dissolving the vial contents,
- paper product manual.

The SonoVue® microbubble suspension is prepared immediately before use by injecting the solvent (5 mL 0.9% sodium chloride for injections in the supplied syringe) into the vial through minispike transfer system. After that, the vial is shaken until the substance is completely dissolved. The chemical and physical stability of the microbubble dispersion has been demonstrated for 6 h. The desired amount is obtained with a syringe and immediately introduced

intravenously. If some suspension is left in the vial to be used in the next study, the vial should be shaken before filling the next syringe to regenerate the bubble suspension.

The process of preparing the SonoVue® suspension is demonstrated in Fig. 3.2.

SonoVue® dose depends on the studied organ, scanning conditions, equipment, and probe frequency. Manufacturer recommended dose for the cardiac chambers at rest or with stress is 2.0 mL, vascular Doppler imaging—2.4 mL. However, now, the dose in adults ranges from 0.8 to 5.0 mL

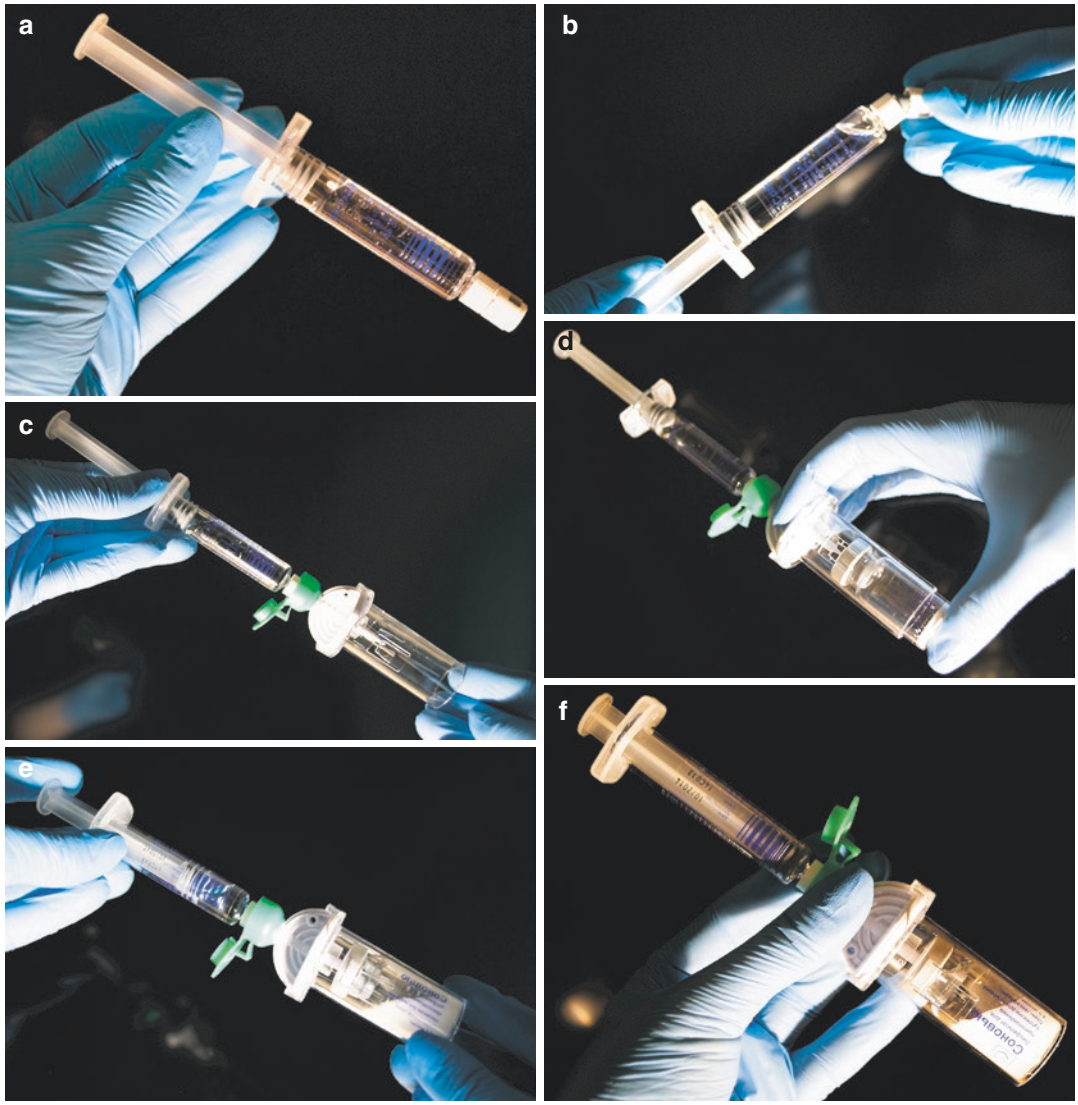

Fig. 3.2 Consecutive photo of SonoVue® preparation. (**a**) Connect the plunger rod by screwing it clockwise into the syringe. (**b**) Break off the protective cap from the syringe hub and open the minispike transfer system blister. (**c**) Open the transfer system cap and connect the syringe to the transfer system by screwing it in clockwise. (**d**). Remove the protective plastic disk cap from the vial stopper. Slide the vial into the transparent sleeve of the transfer system and press firmly to lock the vial in place. (**e**) Inject the saline from the syringe into the vial by pushing on the plunger rod. (**f**) Shake vigorously for 20 s to mix all the contents in the vial to obtain a white milky homogeneous liquid. (**g**) Invert the system and carefully withdraw the necessary dose of SonoVue® into the syringe. (**h**) Unscrew the syringe from the transfer system. It is ready for use

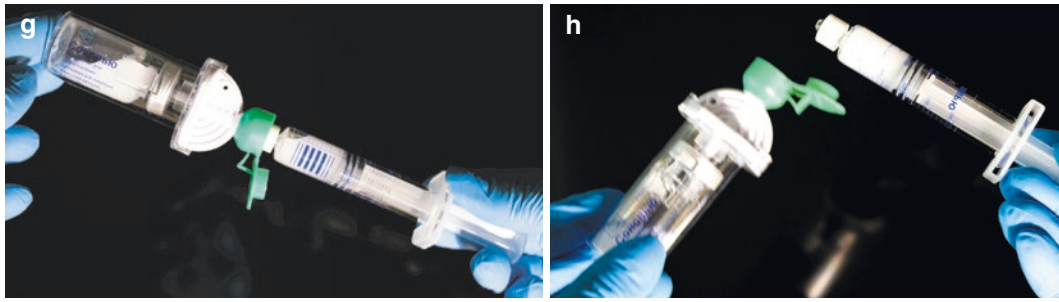

Fig. 3.2 (continued)

Fig. 3.3 The photo of SonoVue® bubble destruction in the syringe when exposed to overpressure by pushing the plunger rod. The suspension becomes more transparent

depending on the study. The dose for individual organs is discussed in the corresponding chapters of this book.

Bubble suspension is introduced intravenously, with a velocity of approximately 1–2 mL/s avoiding the increased pressure on the syringe plunger. Excessive pressure may lead to unwanted bubble destruction (Fig. 3.3). Every injection should be followed by a flush with 5–10 mL of 0.9% sodium chloride solution for injection with the velocity of about 2 mL/s.

The peripheral venous catheter of 20 G or larger is advised for UCA administration (Fig. 3.4), which minimizes bubble destruction during their passage through the narrow needle lumen. Preinstalled catheters should be checked for passability before the introduction of the contrast medium. Central venous catheter and special venous ports can be used if contain no filter. The UCA travel time to the right atrium, and therefore, to the target area depends on the injection site and decreases when using central access.

In some cases, like the ones listed below, the second injection of the UCA may be necessary:

- presence of other lesions in different locations.
- the first injection failed to supply the expected diagnostic information due to some technical fault.
- CUES data does not correspond to other studies, e.g. presence of washout areas, which were not detected with the grayscale US.

In the first two cases, the second injection is recommended after a 10–15 min pause, depending on the patient's age and constitution, to achieve a complete or significant decrease in contrast enhancement. However, to assess the arterial phase in the washout area, which is not differentiated with B-mode, it is recommended to re-inject the contrast medium before the decrease in contrast enhancement to preserve the appropriate image quality. United States Food and Drug Administration (US FDA) admits the repeated introduction of a contrast medium in a total dose that does not exceed one vial for the study.

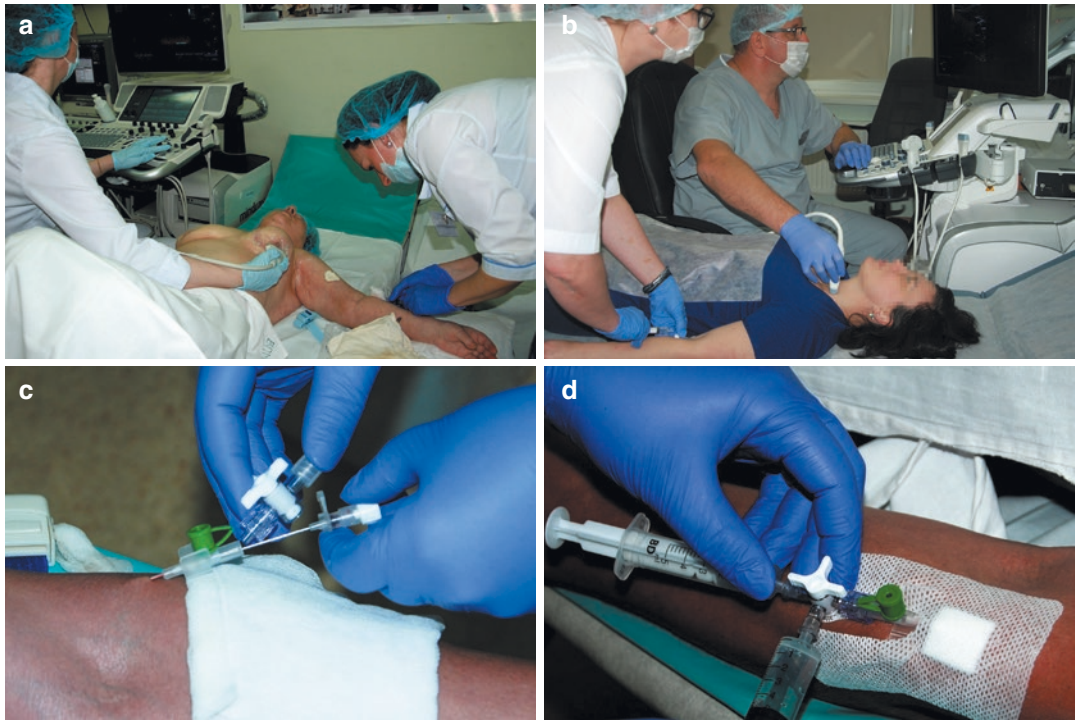

Fig. 3.4 Photo of typical CEUS study. (**a**, **b**) Location of medical staff around the patient. (**c**) Installation of a three-way stop cock. (**d**) Utilization of a three-way stop cock for convenient saline flush. The syringe with SonoVue® is connected to the opposite port, saline flush follows through the extra hub

In cases of arterial hyperperfusion of the target area or lesion, the repeated slow-motion analysis of the cine loop may be beneficial. Therefore, the timely start of the cine recording is very important. Additionally, the cine loop permits a quantitative analysis, which facilitates the evaluation of time-related data, such as arrival time, time to peak, washout half-time, etc.

Most experts advise starting a prospective cine loop record at the moment of the introduction of the UCA. Some authors suggest starting the recording at the time of the detection of the first microbubbles within the target area. However, in the last case, regarding highly hypervascular lesions, the initial moment of contrast enhancement may be easily skipped due to fast washin flash.

For liver CUES, continuous scanning and cine loop recording from the moment of contrast medium injection up to 60 s followed with intermittent short clip recordings with an interval of 30–60 s for reliable washout registration is recommended. This scanning method aims to decrease bubble destruction associated with long US exposure. However, current guidelines recommend the continuous recording/assessment of the arterial and portal venous phases and consider interval scanning for the late phase.

When performing CEUS, the field of view split into two equal parts that correspond to B-mode and the contrast-specific mode permits efficient monitoring of the position of the target lesion within the scanning range.

The conclusion on the CEUS study is often based on further analysis of the recorded cine with the specification of qualitative and quantitative data of contrast enhancement.

3.1 Qualitative Analysis of CEUS Data

Currently, CEUS is based mainly on the analysis of qualitative parameters of contrast enhancement, which accurately demonstrate microvascularization within the target area. Microvascularization features contribute to the differential diagnosis of various pathologies with all contrast-based imaging modalities.

Qualitative parameters of CEUS imply a visual assessment of the washin, accumulation, distribution, and subsequent washout of the UCAs in the area of interest as compared with the surrounding normal parenchyma.

When describing contrast enhancement, it is necessary to use standard terms. That decreases the inter- and intraobserver variability for more objective follow-up in subsequent studies.

WFSUMB experts utilize the following terms [1]:

1. Contrast enhancement of the lesion implicates its signal intensity relative to the signal of the adjacent parenchyma. It may be described with the attributes, such as
   (a) isoenhancing—the same intensity
   (b) hyperenhancing—higher intensity
   (c) hypoenhancing—lower intensity
   (d) nonenhancing—a complete absence of enhancement.
2. Persistent contrast enhancement means the uninterrupted presence of the UCAs in the target area for a long time.
3. Enhancement defect—the nonenhancing area on the enhanced background in the post-vascular phase of organ-specific UCA.
4. Washin is a period of progressive UCA arrival in the target area from the moment of the appearance of the first microbubbles to the peak of contrast enhancement.
5. Washout is a period of decrease in contract enhancement, which follows the peak.

Contrast enhancement of most organs, except for the liver and spleen, confers the two below listed vascular phases [2]:

- Arterial phase, which starts from the moment of UCA arrival (usually 10–20 s after the administration in the peripheral vein) and lasts until the 30–45th second with the increase in contrast enhancement.
- Venous phase, which usually begins at the 30–45th second after UCA injection and lasts until the complete disappearance of microbubbles.

The liver has a dual blood supply with the liver artery and portal vein. Hence, with liver CEUS, the diagnosis is based on the dynamic assessment in the following three vascular phases [3]:

- The arterial phase usually begins 10–20 s after the intravenous UCA injection and continues up to the 30–45th second.
- Portal venous phase typically lasts from 30th to 45th second to 120th second.
- The late venous phase follows the portal venous phase.

With CEUS, the following main time-related and spatial features of contrast enhancement should be estimated:

- the appearance of actual contrast enhancement, which proves vascularization of the target zone
- dynamics of UCA arrival (early or late)
- contrast enhancement of the lesion relative to the adjacent parenchyma in different vascular phases
- distribution of UCA within the area of interest
  - fast or slow
  - typical patterns in the early arterial phase, such as spoke-wheel, basketball basket,

peripheral nodular, or rim-like enhancement, etc.
  - enhancement spreading (diffuse, centripetal, centrifugal, or other)
- enhancement uniformity (perfusion defects or hyperenhancing areas)
- UCA washout
  - time-related features (fast or slow)
  - severity (prominent or mild).

The diagnostic value and visual perception of CEUS may be improved with 3D image reconstruction. It is useful for real-time image monitoring in various phases of contrast enhancement, mapping anatomical structures, spatial orientation in large-sized lesions, and conducting ultrasound-guided interventions [4].

3.2 Quantitative Analysis of CEUS Data

Quantitative analysis of CEUS, which implies the analysis of time-intensity curves (TICs), is appropriate for the objective estimation of the obtained data, comparison of several imaging methods, quantitative evaluation of the perfusion of tumors for differential diagnosis, and follow-up the response to therapy [5].

As for the tumor response assessment, CEUS quantitative analysis permits registration of the changes in tumor perfusion that is analogous to the Modified response evaluation criteria in solid tumors (mRECIST), in contrast to generally accepted size-based criteria (RECIST) [6, 7].

Quantitative and semi-quantitative analysis was initially used for early response assessment of gastrointestinal stromal tumors, renal-cell cancer, hepatocellular carcinoma, and colorectal cancer metastases. Currently, it is expected to be useful for the diagnosis of inflammatory diseases and other tumors [5].

Quantitative analysis is based on the relation between time and intensity of contrast enhancement in the target lesion, which quantitatively characterizes blood perfusion. Digitally recorded cine loop with the target area is necessary.

Incorporated scanner software or independent specialized software applications, such as VueBox™ (Bracco), Sonoliver® (TomTec Imaging Systems), and others, can be used. The box of the region of interest (ROI) is positioned manually within the target lesion and/or reference zone. Usually, simultaneous analysis in several ROI is possible. The obtained digital data is automatically displayed as a TIC for each ROI. The time of enhancement is plotted on the X-axis of the graph and its intensity on *Y*-axis.

There are two ways to conduct quantitative CEUS, as follows.

1. Evaluation of washin and washout with standard intravenous bolus introduction of UCA while keeping to one still scanning plane in contrast (low MI) mode throughout the study. The intensity of the echo signal in the ROI is calculated in linear units and displayed as a TIC (Fig. 3.5a). Placing ROI in various areas enables the objective comparison of the dynamics of UCA washin and washout.
2. Evaluation of perfusion with a disruption-replenishment protocol. It uses flash mode, which is a special function of the scanner to send an US impulse of increased MI to destroy microbubbles in the condition of permanent UCA level in the blood. In this case, slow intravenous infusion of UCA is maintained for 5–20 min with a special infusomat that supports the bubble resuspension or a dropper system (for Definity contrast agent). After the beginning of UCA infusion, the scan is acquired in standard low MI contrast mode, then bubbles are destroyed with flash, and subsequent scan registers the arrival of new bubbles. The TIC demonstrates the accumulation of bubbles and gradual contrast enhancement within the target zone (Fig. 3.5b).

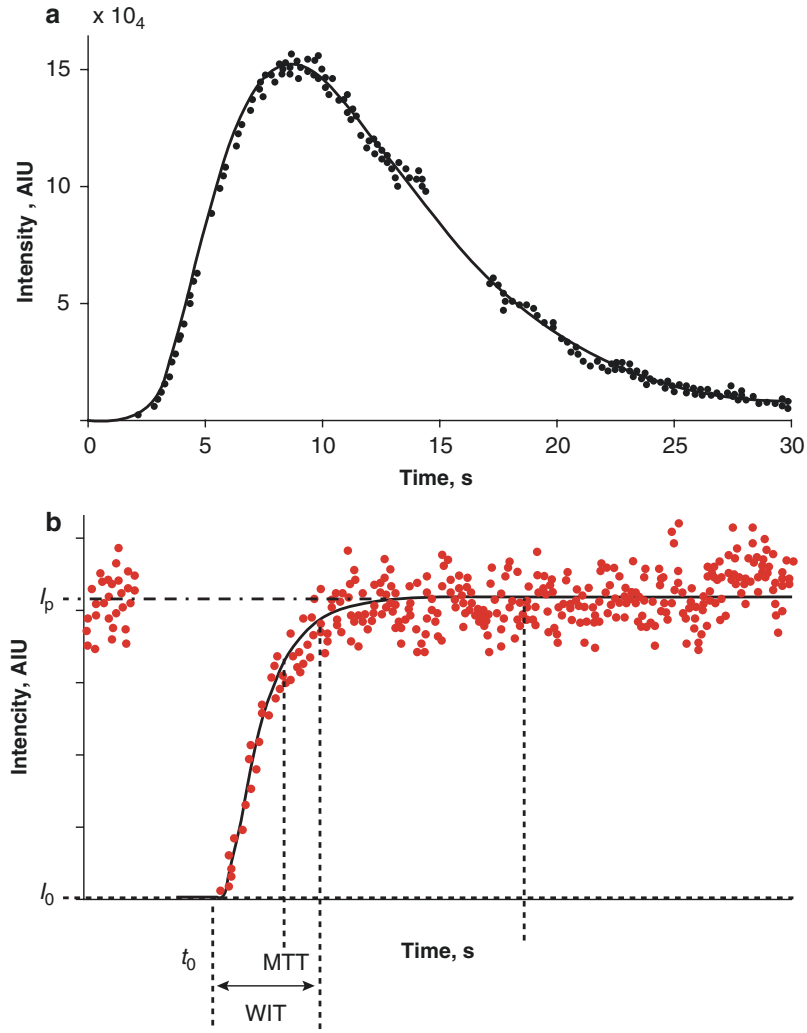

Fig. 3.5 Example TICs of contrast enhancement in two protocols of UCAs administration. (**a**) Bolus method. (**b**) Infusion method

Currently, the bolus UCA technique is commonly used for quantitative analysis. It can be used as an additional stage to complement the qualitative analysis of contrast enhancement without the need for the second UCA injection. Additionally, it permits quantitative monitoring of UCA washout, which is valuable for tumor differentiation but impossible with infusion technique.

Quantitative data are calculated based on the TIC, but not directly derived from raw data [5]. To build a curve, unprocessed linearized data is optimal due to significant difference between the intensities of the accepted native echo and output video signal. The dynamic range of the raw signal (~60 dB) exceeds the capabilities of the display and visual perception. Hence, the logarithmic compression, which is embedded in signal processing results in TIC distortion. Curves, which are based on linear data, are more accurate in presenting raw data. However, some authors suppose that the use of logarithmic data is more convenient. Logarithmic data is measured in decibel (dB) and linear intensity—in conventional units.

All data can be conditionally divided into the parameters of time/velocity and volume of blood flow. Currently, there are no standard designations of quantitative parameters and the way of their presentation in the scanners [5] (Table 3.1,

Table 3.1 The list of main quantitative parameters of the TIC

Parameter name	Synonym	Definition
Time-related parameters		
Time zero offset	Arrival time (AT), Time of arrival (TOA), (t_0)	Time from the UCA injection to the first appearance of any UCA signal within the ROI, corresponding to the point on the abscissa, where the TIC curve starts the uprise
Time to peak	Time to peak intensity (TTP, TPI, t_p)	Time to achieve the maximum intensity. It corresponds to the projection of the highest curve point on the abscissa
Washin time	WIT	Time from UCA appearance to maximum intensity time[a] [1]
Rise time	RT	Time from 5% intensity to 95% intensity. Sometimes is determined as the time from 10% intensity to 90% intensity. Some manufacturers mark as WIT [4]
Mean transit time	MTT	The mean time taken by the bubbles to pass through the ROI. Mathematically it is the first moment of the fitted curve
Washin rate	WIR, ascending slope (AS)	Characterizes the rate of UCA accumulation in the zone of interest. WIR is calculated as the maximum tangent of the angle formed between the curve and the abscissa at the accumulation slope, or as a ratio of the increase in the intensity to the increase in time between two points of the curve
Washout time	WOT	Time from maximum intensity to zero intensity during the washout phase
Half-time of washout	HTWo	Analog to WOR that estimates the time between the peak value and half-maximum value in the washout phase
	Descending time/2 (DT/2)	
Washout rate	WOR, descending slope (DS)	Characterizes the rate of UCA washout in the ROI. WOR is calculated as the maximum tangent of the angle between the curve and the abscissa at the washout slope, or as a ratio of the decrease in the intensity to the increase in time between two points of the curve.
Full width at half-maximum	FWHM	The time between the values of half amplitude on each side of the maximum. As MTT, it also reflects the average flow velocity in the ROI
Parameters that characterize volume blood flow		
Peak intensity	PI, peak of enhancement (PE)	The maximum value of the intensity in arbitrary units
Area under the curve	AUC	Allows to estimate the relative blood volume regardless of the time of arrival and flow velocity of the bubbles in ROI. This is important in lesions with irregular contrast enhancement. It is calculated as the area under the curve between the UCA arrival time and full washout.
Area under the washin curve	AUWI	
Area under the washout curve	AUWO	

[a] The definition of WIT and RT can vary depending on the software

Fig. 3.6). A schematic representation of the TIC parameters is supplied in Fig. 3.7.

The most often used parameters are the arrival time (AT, TOA), time to peak (TTP), peak intensity (PI, PE), washin rate (WIR, AS), washout rate (WOR, DS), washout time (WOT) or half-time of washout (HTWo, DT/2), and area under the curve (AUC). Many aspects can influence CEUS findings. To obtain reliable quantitative data, it is necessary to strictly follow the protocol.

Quantitative analysis decreases the operator dependence of the results, nevertheless, the procedure flow is a subject for standardization. For example, for comparison of AUC in the same patient or the sample, it is necessary to ensure the same duration of the analyzed cine loops, since the value directly depends on the record duration.

The TIC is based on the average value of the contrast enhancement intensity within the actual ROI box, so the size and location of the ROI are

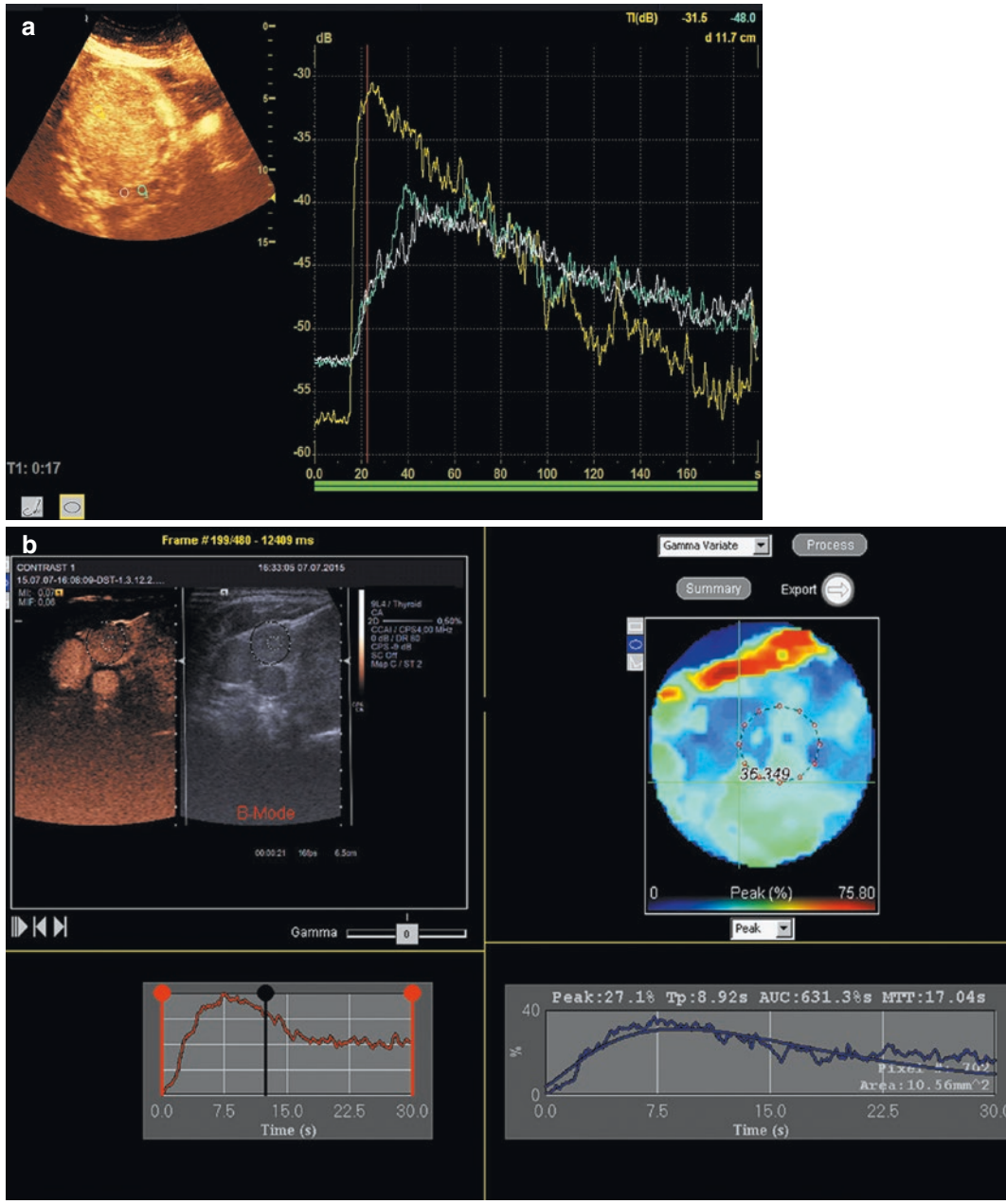

Fig. 3.6 Examples of TIC presentation in the scanners of various manufacturers. (**a**) General Electric. (**b**) Siemens. (**c**) Hitachi. (**d**) Mindray

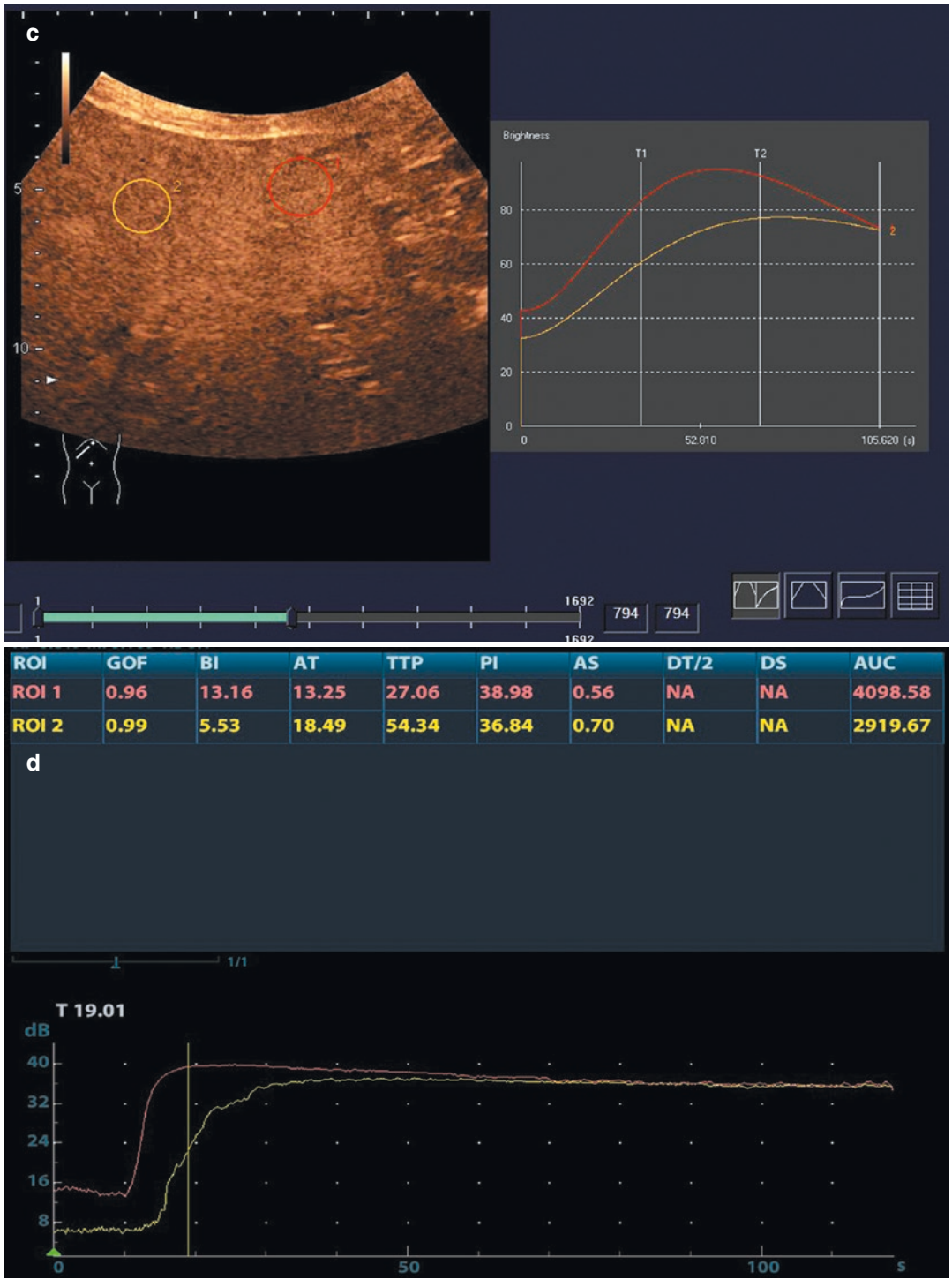

Fig. 3.6 (continued)

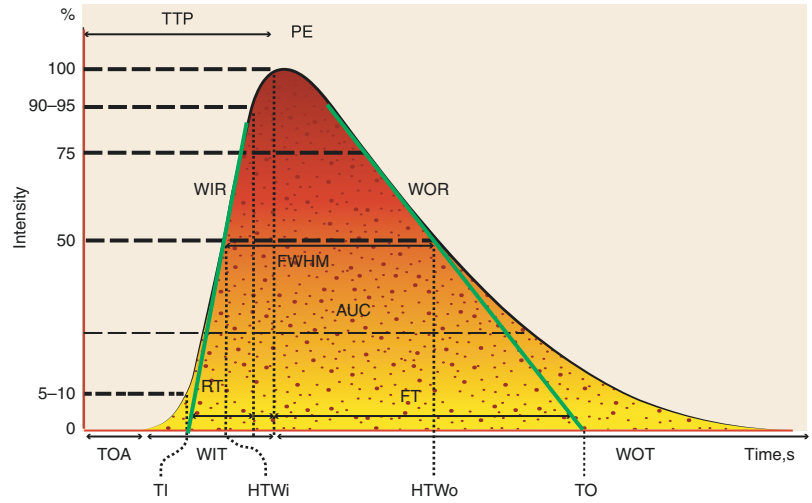

Fig. 3.7 The graph with common TIC parameters. See the text and Table 3.1 for explanations

to be carefully considered. Small ROI in the most enhanced area does not reflect the true perfusion of the entire studied area and does not provide reproducibility with the dynamic study. Excessively large ROI may accidentally include the adjacent structures, which can also affect the measurement results. The motion of the studied object is also a challenge. To compensate for the movements, the incorporated software offers the tracking function, which provides an automatic ROI shift corresponding to the movements of the studied area.

According to some authors [4], an important issue when measuring peak intensity is the need to subtract basic intensity if it is not zero. Subtraction should only be done when working with linear data because in the case of a logarithmic format this will lead to a false low peak intensity value.

Comparison of quantitative data from different ROI to estimate perfusion in various areas should be carried out with caution, because the intensity values in different depths and side positions demonstrate the variations of 85% and 62%, respectively. An adequate dose of UCA, the correct position of the focus zone and gain settings can minimize the dispersion in the intensity values between different ROIs [8].

Some software offers conversion of quantitative data of individual pixels to a parametric color map, which permits visual identification of the zones of various perfusion. The encoding is usually carried out according to the time or intensity of the contrast enhancement (Fig. 3.8, Video 3.1).

CEUS quantitative analysis is recommended for monitoring the response to therapy of malignant neoplasms, the examination of patients with inflammatory bowel diseases, and so on. Recently, several publications report on its value for differential diagnosis of benign and malignant lesions of various locations.

The main stumbling block for the further development of this option may be unstandardized procedure protocol. The quantitative parameters presented in various scanner manufacturers are not unified. Even the intensity of contrast enhancement may be measured in dB, %, or conditional units. It leads to the fact that reproducing the study on different scanners is impossible. Currently, the analysis of TICs is mostly of scientific interest. However, taking into account the prospects of tissue perfusion quantification, some already obtained quantitative data should be considered for implementation.

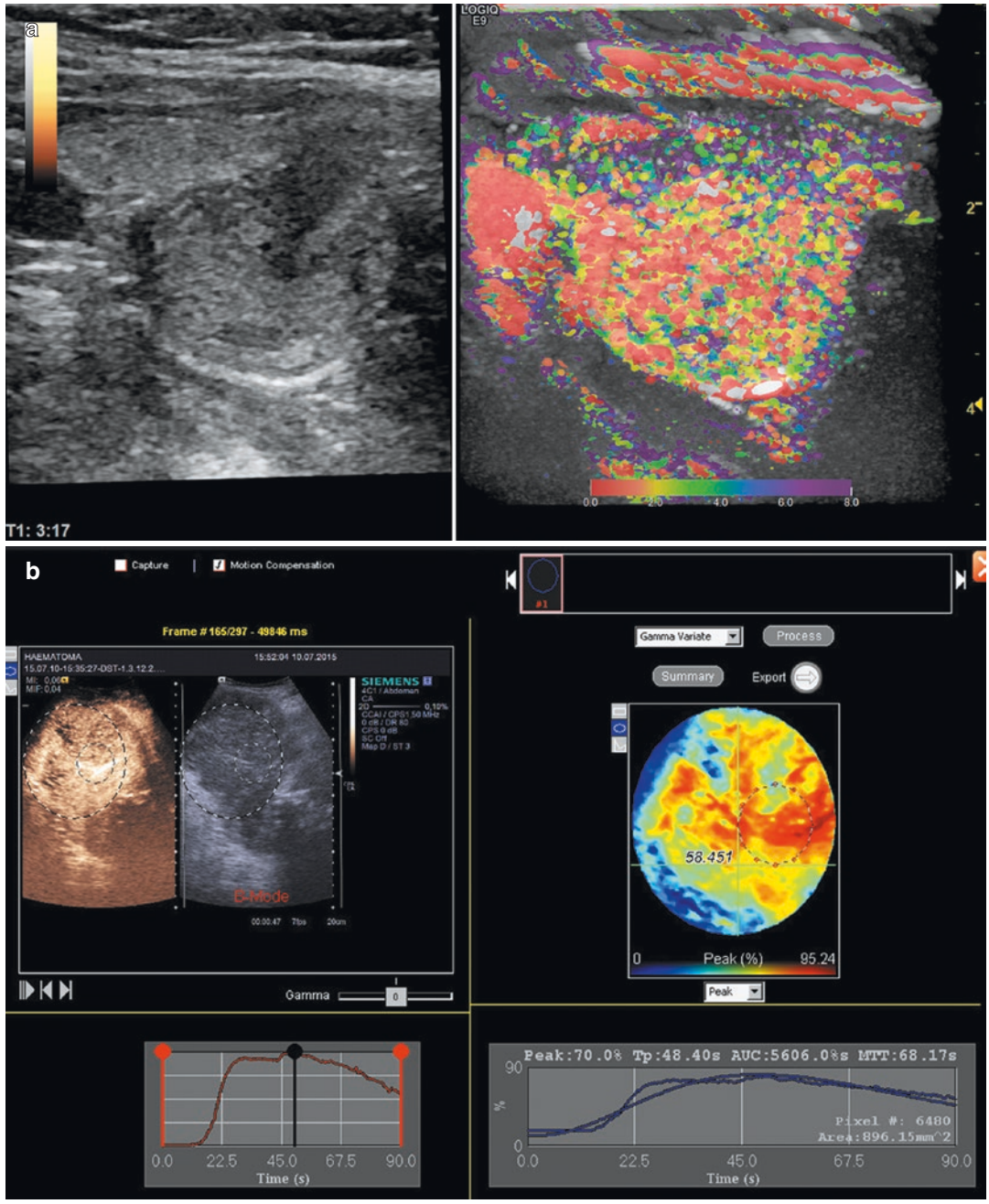

Fig. 3.8 Example images of the color maps of dynamic CEUS data in the scanners of various manufacturers. (**a**) General Electric. (**b**) Siemens. (**c**) Hitachi

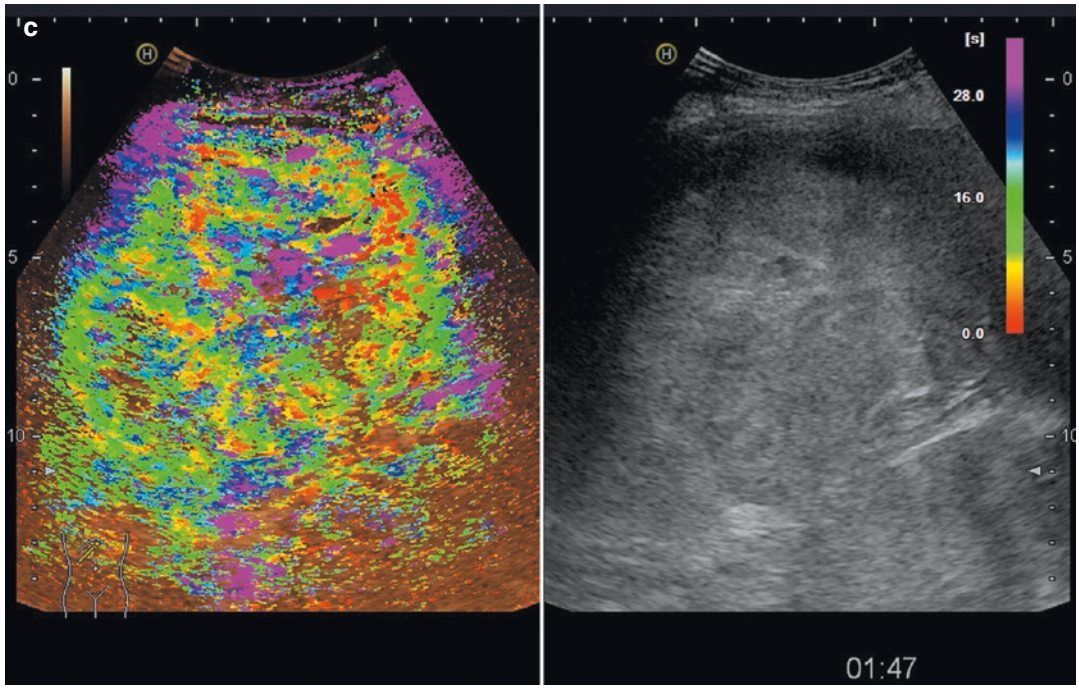

Fig. 3.8 (continued)

References

1. Claudon M, Dietrich CF, Choi BI, Cosgrove DO, Kudo M, Nolsøe CP, et al. Guidelines and good clinical practice recommendations for contrast enhanced ultrasound (CEUS) in the liver--update 2012: a WFUMB-EFSUMB initiative in cooperation with representatives of AFSUMB, AIUM, ASUM, FLAUS and ICUS. Ultraschall Med. 2013;34(1):11–29. https://doi.org/10.1055/s-0032-1325499.
2. Sidhu PS, Cantisani V, Dietrich CF, Gilja OH, Saftoiu A, Bartels E, et al. The EFSUMB guidelines and recommendations for the clinical practice of contrast-enhanced ultrasound (CEUS) in non-hepatic applications: update 2017 (long version). Ultraschall Med. 2018;39(2):e2–e44. https://doi.org/10.1055/a-0586-1107.
3. Dietrich CF, Nolsøe CP, Barr RG, Berzigotti A, Burns PN, Cantisani V, et al. Guidelines and good clinical practice recommendations for contrast enhanced ultrasound (CEUS) in the liver - update 2020 - WFUMB in cooperation with EFSUMB, AFSUMB, AIUM, and FLAUS. Ultraschall Med. 2020;41(5):562–85. https://doi.org/10.1055/a-1177-0530.
4. Weskott HP. Contrast-enhanced ultrasound. 2nd ed. London: Uni-Med Science; 2013.
5. Dietrich CF, Averkiou MA, Correas JM, Lassau N, Leen E, Piscaglia F. An EFSUMB introduction into dynamic contrast-enhanced ultrasound (DCE-US) for quantification of tumour perfusion. Ultraschall Med. 2012;33(4):344–51. https://doi.org/10.1055/s-0032-1313026.
6. Eisenhauer EA, Therasse P, Bogaerts J, Schwartz LH, Sargent D, Ford R, et al. New response evaluation criteria in solid tumours: revised RECIST guideline (version 1.1). Eur J Cancer. 2009;45(2):228–47. https://doi.org/10.1016/j.ejca.2008.10.026.
7. Lencioni R, Llovet JM. Modified RECIST (mRECIST) assessment for hepatocellular carcinoma. Semin Liver Dis. 2010;30(1):52–60. https://doi.org/10.1055/s-0030-1247132.
8. Greis C. Quantitative evaluation of microvascular blood flow by contrast-enhanced ultrasound (CEUS). Clin Hemorheol Microcirc. 2011;49(1–4):137–49. https://doi.org/10.3233/CH-2011-1464.

Liver

4

Ella I. Peniaeva and Yuly R. Kamalov

Liver CEUS is the most common ultrasound examination among all that utilize UCAs. It was proven a precise method for differential diagnosis of focal liver lesions (FLL), detection of metastases, monitoring the FLL response to therapy, and guidance of minimally invasive manipulations. The continuous improvement of CEUS protocols, evaluation of new differential diagnostic criteria for liver pathology, as well as successful CEUS implementation, led to the development of regularly revised individual guidelines and recommendations for liver CEUS in the clinical practice [1–4]. Liver CEUS is currently approved in the USA for the use in pediatric practice with UCA Lumason (the trade name of UCA SonoVue® in the USA).

The last revision of WFUMB Guidelines and Good Clinical Practice Recommendations for CEUS in the Liver was updated in 2020. It advises using liver CEUS for the following pathologies [4]:

1. to identify liver metastases as a part of a multimodal imaging,
2. for the differential diagnosis of uncertain FLL, incidentally detected with US in the non-cirrhotic liver:
   (a) as the first-line method in patients without any history or clinical suspicion of malignant disease,
   (b) as the first-line imaging method in patients with a history or clinical suspicion of malignant disease,
   (c) in patients with inconclusive findings at CT or MR imaging,
   (d) in patients with contraindications to both CT and MRI,
   (e) for characterization of hepatic abscess in the appropriate clinical setting,
   (f) if CEUS has definitively characterized a benign FLL, further investigations are not recommended to confirm the diagnosis.
3. for characterization of FLLs in liver cirrhosis:
   (a) as the first-line method to establish a diagnosis of malignancy (CEUS LR-M) or specifically of HCC (CEUS LR-5), but CT or MR imaging remain required for accurate staging unless contraindicated,
   (b) to assess the probability of a lesion to be an HCC, when CT or MR imaging is

Supplementary Information The online version contains supplementary material available at [https://doi.org/10.1007/978-3-030-91764-7_4].

E. I. Peniaeva (✉)
Department of Ultrasound Diagnostics of the Center for Radiological Diagnostics, Private Healthcare Institution "Clinical Hospital "RZD-Medicina" of Yaroslavl City", Yaroslavl, Russian Federation

Y. R. Kamalov
Petrovsky National Research Centre of Surgery, Moscow, Russian Federation

A. N. Sencha, Y. N. Patrunov (eds.), *Contrast-Enhanced Ultrasound*,
https://doi.org/10.1007/978-3-030-91764-7_4

inconclusive, especially in FLL not suitable for biopsy,
   (c) for the selection of FLL(s) to be biopsied when they are multiple or have different contrast patterns,
   (d) for monitoring changes in enhancement patterns in FLL requiring follow-up.
4. to differentiate between benign and malignant portal vein thrombosis,
5. for the biopsy of FLLs that are invisible or inconspicuous at B-mode imaging, in FLLs with potential necrotic areas, or if the previous biopsy resulted in necrotic material,
6. for the quantitative assessment of response to targeted therapies in patients with malignant tumors of the liver,
7. for the planning, guidance, and the evaluation of the treatment effect after ablative methods, judging on immediate US-guided retreatment of residual tumor, and in the follow-up after ablation treatment to identify residual or recurrent tumor at appropriate time intervals,
8. for delineation of the liver abscess cavity, identification of correct drain position and communication with other structures, and the guidance of transhepatic biliary interventions.

CEUS is performed only under the condition of satisfactory image quality, after pre-scanning at B-mode and Doppler modes. Patient preparation for the study does not differ from the preparation for the US of other abdominal organs. Currently, many experts agree that for the liver study, the optimal dosage of SonoVue® is 1.2 mL, an increase in the dose up to 2.4 mL may be required in cases of diffuse parenchymatous changes, for high-frequency probes, or mid-class US scanners [5, 6].

At the assessment of the qualitative parameters of contrast enhancement, three vascular phases that reflect the dual liver blood supply with the portal vein (up to 70–75%) and the hepatic artery (up to 25–30%) are distinguished [4], as follows:

- the arterial phase begins 10–20 s after the UCA introduction and continues to the 35–45 s,
- the portal venous phase begins 35–45 s from the moment of UCA introduction and lasts up to the end of the second minute,
- the late phase begins 2 min from the moment of UCA introduction and continues until the UCA is completely washed out of the liver parenchyma (on average up to 4–6 min),
- the post-vascular phase is only observed when using hepatic specific UCAs (like Sonazoid), due to the absorption of the UCA with Kupffer cells (starts 8 min after the UCA introduction and continues up to the 30th minute).

UCA after introduction to the peripheral vein passes the right heart chambers, the small circle of blood circulation, the left heart chambers, and the aorta and reaches the hepatic arteries with subsequent uniform contrast enhancement of the liver parenchyma. After 35–45 s from the moment of administration, UCA appears in the portal vein system, and the unchanged parenchyma of the liver exhibits a further homogeneous increase in the intensity of contrast enhancement. The late venous phase is associated with a gradual uniform decrease in contrast enhancement to the noise level (Fig. 4.1).

The possibility of continuous real-time imaging of the liver permits registration of the contrast enhancement patterns of various FLLs that are outside of the standard scanning protocol of contrast-enhanced CT or MRI, such as of hypervascular metastases with rapid washout or hemangiomas with fast enhancement in the arterial phase. Due to the exclusively intravascular circulation of the UCA, CEUS has certain advantages in the identification of washout as compared with CT and MRI [7]. Contrast agents in CT and MRI penetrate endothelium into the interstitium of the lesion that reduces the prominence of the washout effect.

4.1 Liver Tumors

The accurate timely differential diagnosis of liver tumors is an important issue in oncohepatology since the approach to the treatment of FLL depends on the tumor type. Increased availability

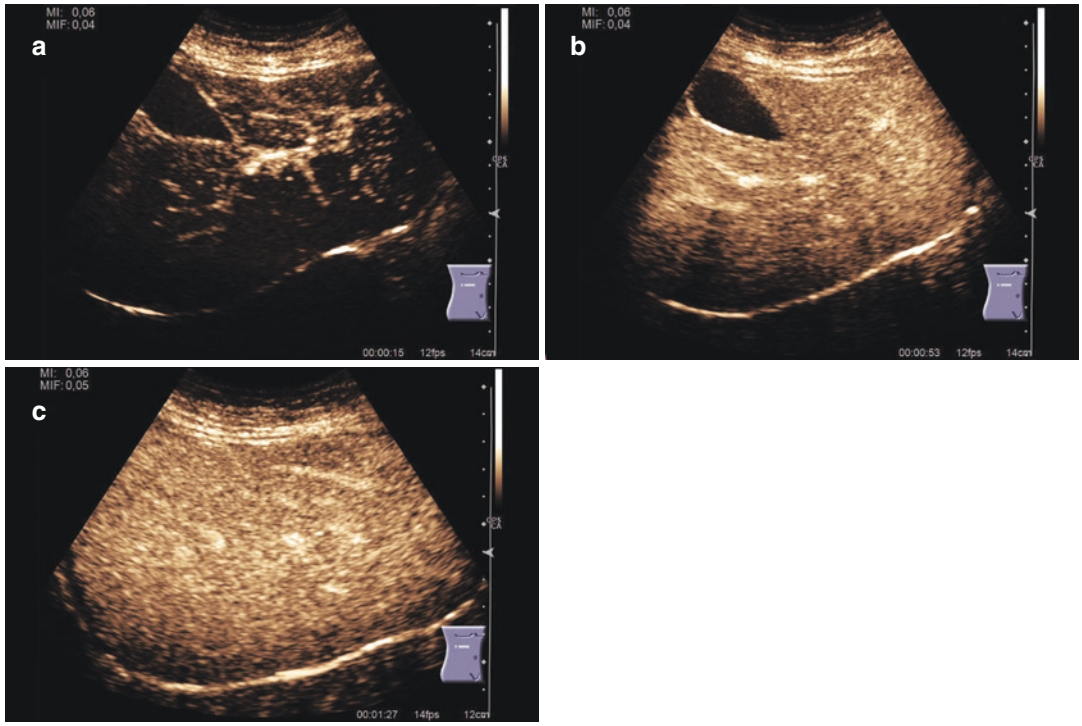

Fig. 4.1 CEUS images of the normal liver parenchyma in different vascular phases. (**a**) arterial phase. (**b**) portal venous phase. (**c**) late phase

of diagnostic imaging and the introduction of high-resolution diagnostic equipment to clinical practice led to an increase in the number of incidentally detected FLL. Most FLL, identified with ultrasound screening, are benign [8]. Conventional liver ultrasound has high sensitivity in the detection of FLL but exhibits low specificity [9]. CEUS in most cases permits the fast differential diagnosis of various FLLs with the sensitivity of 85–98%, the specificity of 86–97%, and accuracy of 88–99%, and minimization of the use of imaging methods with iodine-containing contrast media [10–15].

The last update on the classification of liver tumors of the World Health Organization (WHO) was published in 2019 [16]. In the new version, liver tumors are not a separate volume. They are included in the combined edition of digestive system tumors. In addition, the tumors with a not strictly specific structure (mesenchymal and hematolymphoid) are moved to separate chapters common to all parts of the digestive tract.

WHO classification of tumors of the liver and intrahepatic bile ducts, based on histologic appearance, is provided below.

Benign hepatocellular tumors, ICD-O codes

- Hepatocellular adenoma, 8170/0
  - HNF1A inactivated hepatocellular adenoma.
  - Inflammatory hepatocellular adenoma.
  - B-catenin activated hepatocellular adenoma.
  - B-catenin activated inflammatory hepatocellular adenoma.

Malignant hepatocellular tumors and precursors, ICD-O codes

- Hepatocellular carcinoma, NOS, 8170/3
  - Hepatocellular carcinoma, fibrolamellar, 8171/3.
  - Hepatocellular carcinoma, scirrhous, 8172/3.
  - Hepatocellular carcinoma, clear cell type, 8174/3.
  - Hepatocellular carcinoma, steatohepatitic.

  - Hepatocellular carcinoma, macrotrabecular massive.
  - Hepatocellular carcinoma, chromophobe.
  - Hepatocellular carcinoma, neutrophil rich.
  - Hepatocellular carcinoma, lymphocyte rich.
- Hepatoblastoma, NOS8970/3.

Benign biliary tumors and precursors, ICD-O codes
- Bile duct adenoma, 8160/0.
- Adenofibroma, NOS, 9013/0.
- Biliary intraepithelial neoplasia, low grade, 8148/0.
- Biliary intraepithelial neoplasia, high grade, 8148/2.
- Intraductal papillary neoplasm with low grade intraepithelial neoplasia, 8503/0.
- Intraductal papillary neoplasm with high grade intraepithelial neoplasia, 8503/2.
- Intraductal papillary neoplasm with associated invasive carcinoma, 8503/3.
- Mucinous cystic neoplasm with low grade intraepithelial neoplasia, 8470/0.
- Mucinous cystic neoplasm with high grade intraepithelial neoplasia, 8470/2.
- Mucinous cystic neoplasm with associated invasive carcinoma, 8470/3.

Malignant biliary tumors, ICD-O codes
- Cholangiocarcinoma, 8160/3
  - Large duct intrahepatic cholangiocarcinoma.
  - Small duct intrahepatic cholangiocarcinoma.
- Carcinoma, undifferentiated, NOS, 8020/3.
- Combined hepatocellular carcinoma and cholangiocarcinoma, 8180/3.
- Neuroendocrine tumor, NOS, 8240/3
  - Neuroendocrine tumor, grade, 18240/3.
  - Neuroendocrine tumor, grade, 28249/3.
  - Neuroendocrine tumor, grade, 38249/3.
- Neuroendocrine carcinoma, NOS, 8246/3
  - Large cell neuroendocrine carcinoma, 8013/3.
  - Small cell neuroendocrine carcinoma, 8041/3.
- Mixed neuroendocrine—nonneuroendocrine neoplasm (MiNEN), 8154/3.

WHO classification of mesenchymal tumors of the digestive system is provided below.

Gastrointestinal stromal tumor, CD-O codes
- Gastrointestinal stromal tumor, 8936/3
  - Succinate dehydrogenase deficient gastrointestinal stromal tumor.

Adipose tissue and (myo)fibroblastic tumors, ICD-O codes
- Inflammatory myofibroblastic tumor, 8825/1
  - Epithelioid inflammatory myofibroblastic sarcoma.
- Desmoid type fibromatosis, 8821/1.
- Abdominal fibromatosis, 8815/1.
- Solitary fibrous tumor, NOS, 8815/3.
- Solitary fibrous tumor, malignant
  - Lipomatous solitary fibrous tumor.
  - Giant cell angiofibroma, 9160/0.
- Lipoma, NOS, 8850/0.
- Angiolipoma, NOS, 8861/0.
- Plexiform fibromyxoma, 8811/0.

Smooth muscle and skeletal muscle tumors, ICD-O codes
- Leiomyoma, NOS, 8890/0
  - Seedling leiomyomas.
  - Leiomyomatosis, NOS, 8890/1.
- Leiomyosarcoma, NOS, 8890/3.
- Embryonal rhabdomyosarcoma, NOS, 8910/3.
- Rhabdomyosarcoma, spindle cell/sclerosing type, 8912/3.
- Alveolar rhabdomyosarcoma, 8920/3.

Vascular and perivascular tumors, ICD-O codes
- Hemangioma, NOS, 9120/0
  - Dieulafoy lesion.
  - Gastric antral vascular ectasia (GAVE).
  - Angiodysplasia.
  - Anastomosing hemangioma.
  - Infantile hemangioma.
  - Diffuse hepatic hemangiomatosis.
  - Hepatic small vessel neoplasm.
- Epithelioid hemangioendothelioma, NOS, 9133/3.
- Kaposi sarcoma, 9140/3.
- Angiosarcoma, 9120/3
  - Epithelioid angiosarcoma.
- Glomus tumor, NOS, 8711/0.
- Glomangiomatosis, 8711/1.

- Glomus tumor of uncertain malignant potential, 8711/1.
- Glomus tumor, malignant, 8711/3.
- Lymphangioma, NOS, 9170/0.

Neural tumors, ICD-O codes
- Schwannoma, NOS, 9560/0
  - Microcystic/reticular schwannoma.
  - Mucosal Schwann cell hamartoma.
- Granular cell tumor, NOS, 9580/0.
- Granular cell tumor, malignant, 9580/3.
- Perineurioma, NOS, 9571/0.
- Ganglioneuroma, 9490/0.
- Ganglioneuromatosis, 9491/0.

Tumors of uncertain differentiation, ICD-O codes
- PEComa, benign, 8714/0
  - Sclerosing PEComa.
- Angiomyolipoma, 8860/0
  - Inflammatory subtype of angiomyolipoma.
- PEComa, malignant, 8714/3.
- Calcifying nested stromal epithelial tumor, 8975/1.
- Synovial sarcoma, NOS, 9040/3
  - Synovial sarcoma, monophasic fibrous, 9041/3.
  - Synovial sarcoma, biphasic, 9043/3.
- Clear cell sarcoma, NOS, 9044/3.
- Embryonal sarcoma, 8991/3.

In the previous classification of liver tumors and intrahepatic bile ducts (Lyon, 2010) [17] the focal nodular hyperplasia (FNH) was assigned to the group of benign hepatocellular epithelial tumors, while in the present classification, the FNH is mentioned only in the text and does not have a code due to being not a true tumor but a secondary hyperplastic reaction of hepatocytes to vascular disorders [18].

4.1.1 Benign Liver Lesions

CEUS-based differential diagnosis of benign and malignant liver tumors mostly implicates the assessment of their enhancement in the portal venous and late phases as compared to normal liver parenchyma. Benign FLLs almost in all cases demonstrate steady contrast iso- or hyperenhancement in the portal venous and late phase while being different in the arterial phase [1, 9, 19–22]. CEUS enables the final diagnosis in 90% of patients with benign FLL [6, 13, 23].

Liver hemangioma is the most common benign liver tumor. It is often incidentally detected when the patient is examined for other reasons. If the lesion demonstrates typical ultrasound signs of a hemangioma in a patient with no risk factors of hepatocellular carcinoma (HCC) and oncology history, the US is considered conclusive [24]. The value of conventional US is lower in lesions with atypical ultrasound signs, heterogeneous echostructure, large size, calcifications, hyalinized areas, multilocular composition, etc. [3, 9, 24, 25].

Hemangioma is a lesion composed of vascular cavities with flat endothelium lining and fibrous septa [24]. In most cases, they demonstrate slow blood flow and arterial blood supply. Hemangiomas with high blood flow velocities or arteriovenous shunts are rare [26]. A specific pattern for a liver hemangioma is peripheral globular contrast enhancement in the arterial phase with gradual centripetal filling in the portal venous and late phases (Figs. 4.2, 4.3, and 4.4, Videos 4.1 and 4.2).

Depending on the presence of necrotic or fibrotic areas, the hemangioma enhancement may be complete or incomplete with practically no washout in the portal and late phases [3, 11]. Publications [6, 25, 27, 28] report this type of contrast enhancement in 68–98% of histopathologically verified hemangiomas. A hemangioma may lack the characteristic contrast pattern in the cases of small (<15 mm) or large (>4 cm) size with high blood flow velocity and the presence of arteriovenous shunts, which facilitate the rapid enhancement of the lesion in the arterial phase [6, 15, 29] (Figs. 4.5 and 4.6, Video 4.3). In some cases, slow-motion analysis of the cine loop reveals a short-term typical peripheral globular enhancement. If this typical pattern is missed, the

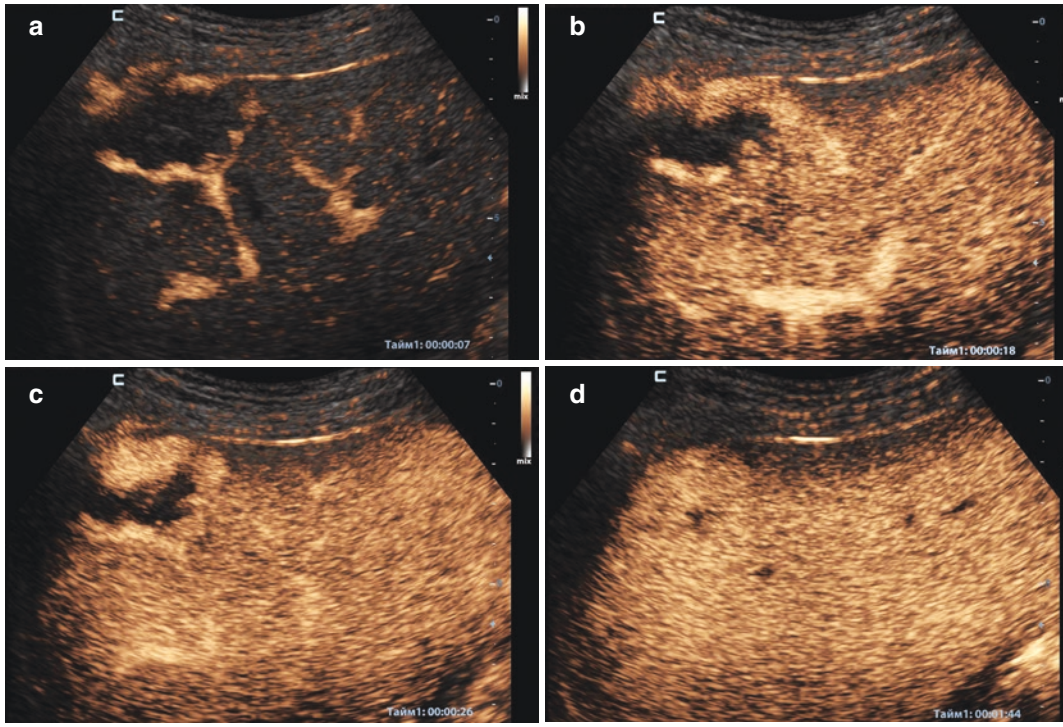

Fig. 4.2 Liver hemangioma. Typical peripheral globular contrast enhancement. (**a**) Early arterial phase CEUS image. (**b**) Arterial phase CEUS image. (**c**) Portal venous phase CEUS image. (**d**) Late phase CEUS image

differential diagnosis with focal nodular hyperplasia, liver adenoma, and HCC without washout becomes a challenge [29].

Some publications report about the cases of washout in the late phase, which significantly complicates differential diagnosis with malignant neoplasms. Washout in such cases may be the consequence of bubble destruction due to long US exposure, which is not compensated due to progressive dilution of the UCA and low blood flow velocity within the lesion [30–32].

Noticeable late phase washout in a combination with a typical for hemangioma peripheral globular contrast enhancement may indicate a rare vascular neoplasm with intermediate malignant potential—epithelioid hemangioendothelioma [33]. Hence, in FLL with registered washout, other imaging methods or histopathology verification are indicated. Additionally, differential diagnosis is difficult in the cases of nonenhancing hemangiomas with a subtle hyperenhancing peripheral rim that can be mistaken for malignant FLLs, especially for hypovascular metastases. Such a pattern is often associated with hyalinosis, fibrosis, cystic degeneration, or thrombosis [32].

The European Association for the Study of the Liver (EASL) included CEUS in Clinical Practice Guidelines on the management of benign liver tumors and approved it for the differential diagnosis of liver hemangioma with other tumors [24]. The diagnostic accuracy of CEUS in the differential diagnosis of liver hemangioma is close to MRI and CT. It demonstrates the sensitivity of 85.7–90.4%, specificity—97.2–98.8%, accuracy—94.1–96.9% [11, 27].

Focal nodular hyperplasia (FNH) is the second common benign liver lesion, which is a secondary hyperplastic reaction of hepatocytes for vascular disorders. FNH is supplied with

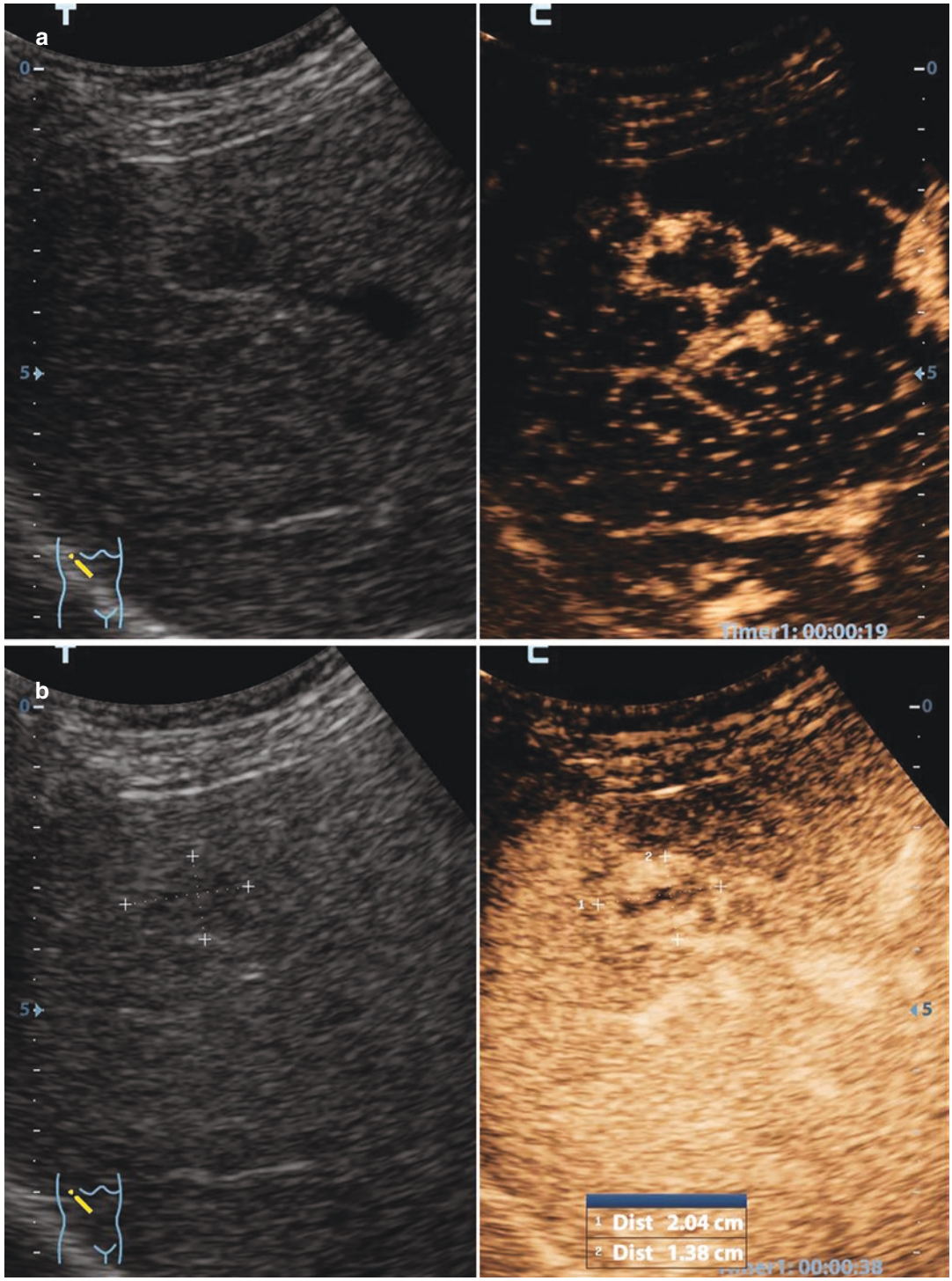

Fig. 4.3 Liver hemangioma. Typical peripheral globular contrast enhancement in (**a**) early arterial, (**b**) arterial, and (**c**) portal venous phase. CEUS images. (**d**) contrast-enhanced CT portal venous phase

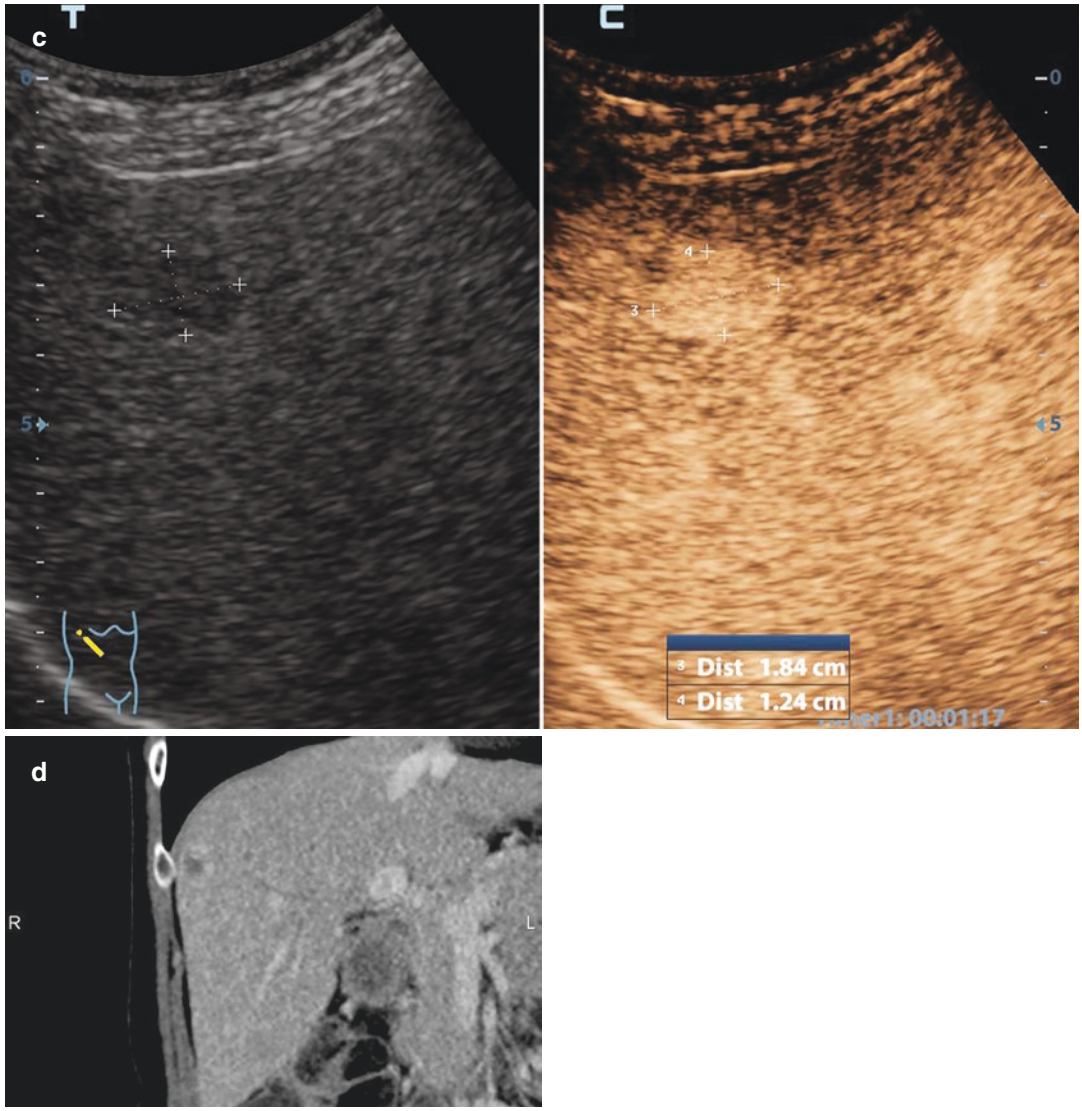

Fig. 4.3 (continued)

blood exclusively with the branches of the hepatic artery that pass in the central scar and fibrous septa [34]. This feature demonstrates the characteristic "spoke wheel" vascular pattern, which can be detected with CDI and PDI, but is more obvious with [3, 6, 35, 36]. FNH exhibits rapid fill-in from the center outwards with prominent hyperenhancement in the early arterial phase when the enhancement of the liver parenchyma is still low resulting in the sign of "light bulb." The enhancement of the FNH is so fast that the characteristic vascular pattern with centrifugal fill-in type can be easily missed, which often requires repeated slow-motion cine loop revision. In the eccentric FNH, the divergence of the vessels and the corresponding distribution of microbubbles

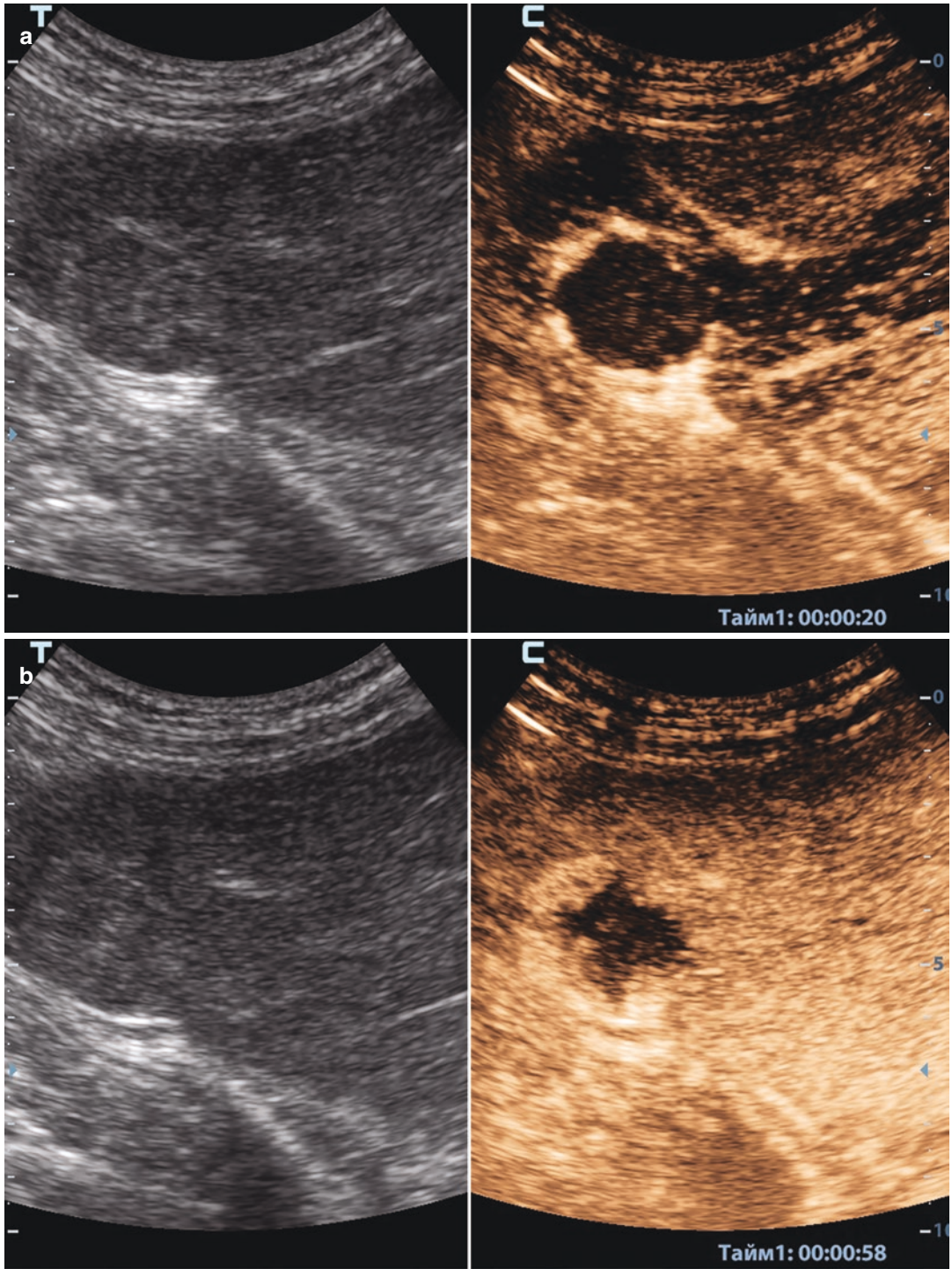

Fig. 4.4 Liver hemangioma. Typical peripheral globular contrast enhancement. (**a**) Arterial phase CEUS image. (**b**) Portal venous phase CEUS image. (**c**) Late portal venous phase CEUS image

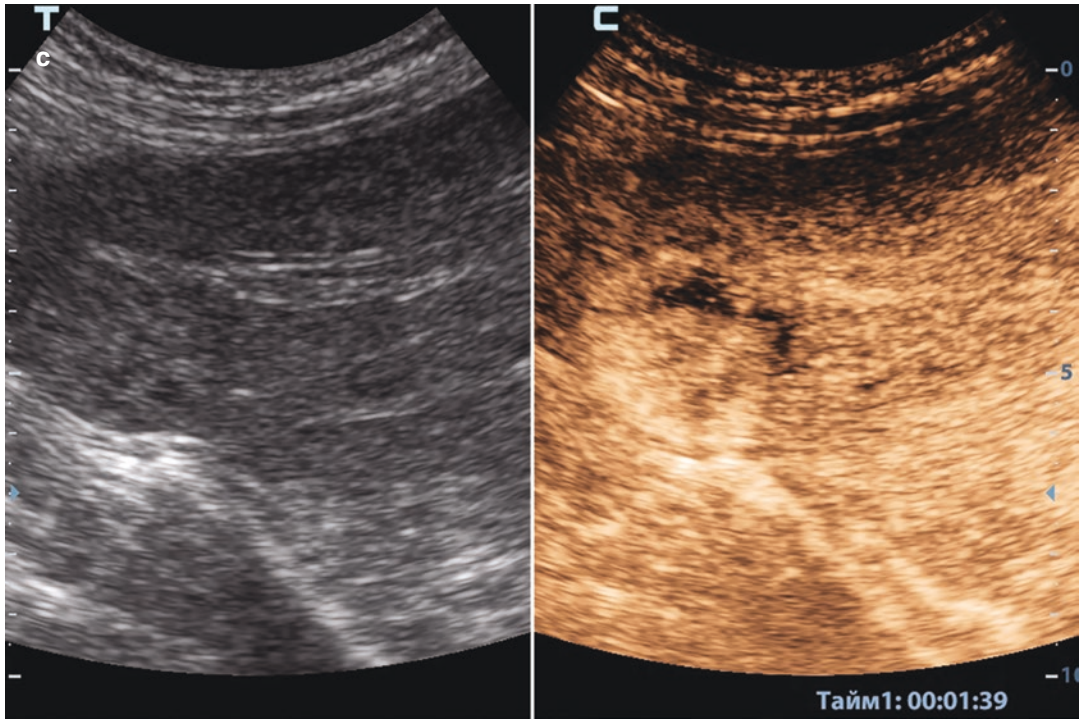

Fig. 4.4 (continued)

starts from the point on the periphery of the lesion [3, 6, 35, 36]. True lesion size and margins are most clearly defined in the arterial phase (Fig. 4.7, Videos 4.4 and 4.5). FMH in the portal venous and late phase can be slightly hyperenhanced or isoenhanced. The central scar can be identified as a hypoenhanced area in the late phase.

In some cases, a slight late phase washout can be registered due to bubble destruction under long US exposure or degenerative changes that may prevent confident differential diagnosis with malignant FLL [6, 36–39]. CEUS is reported preferable to MRI for the examination of FLL smaller than 3 cm, and the combination of MRI and CEUS increases the diagnostic accuracy in the diagnosis of FNH in the absence of characteristic MR signs [40]. The sensitivity and specificity of CEUS in the diagnosis of FNH were reported 80–82.5% and 94.3–95.6%, respectively [14, 27]. In the EASL Clinical Practice Guidelines on the management of benign liver tumors, CEUS is a part of the flowchart for the management of FNH [24] (Fig. 4.8).

Hepatocellular adenoma (HCA) is approximately 10 times less common than FNH. As etiological factors, oral contraceptives in women, anabolic steroids and androgens in men, tyrosinemia, diabetes, Fanconi anemia, glycogenolysis, and other conditions are considered. The lesion is usually presented with a single mass, but the cases of multiple HCAs are reported [24]. Its accurate and timely diagnosis is important due to the high risk of complications, such as bleeding and malignant transformation.

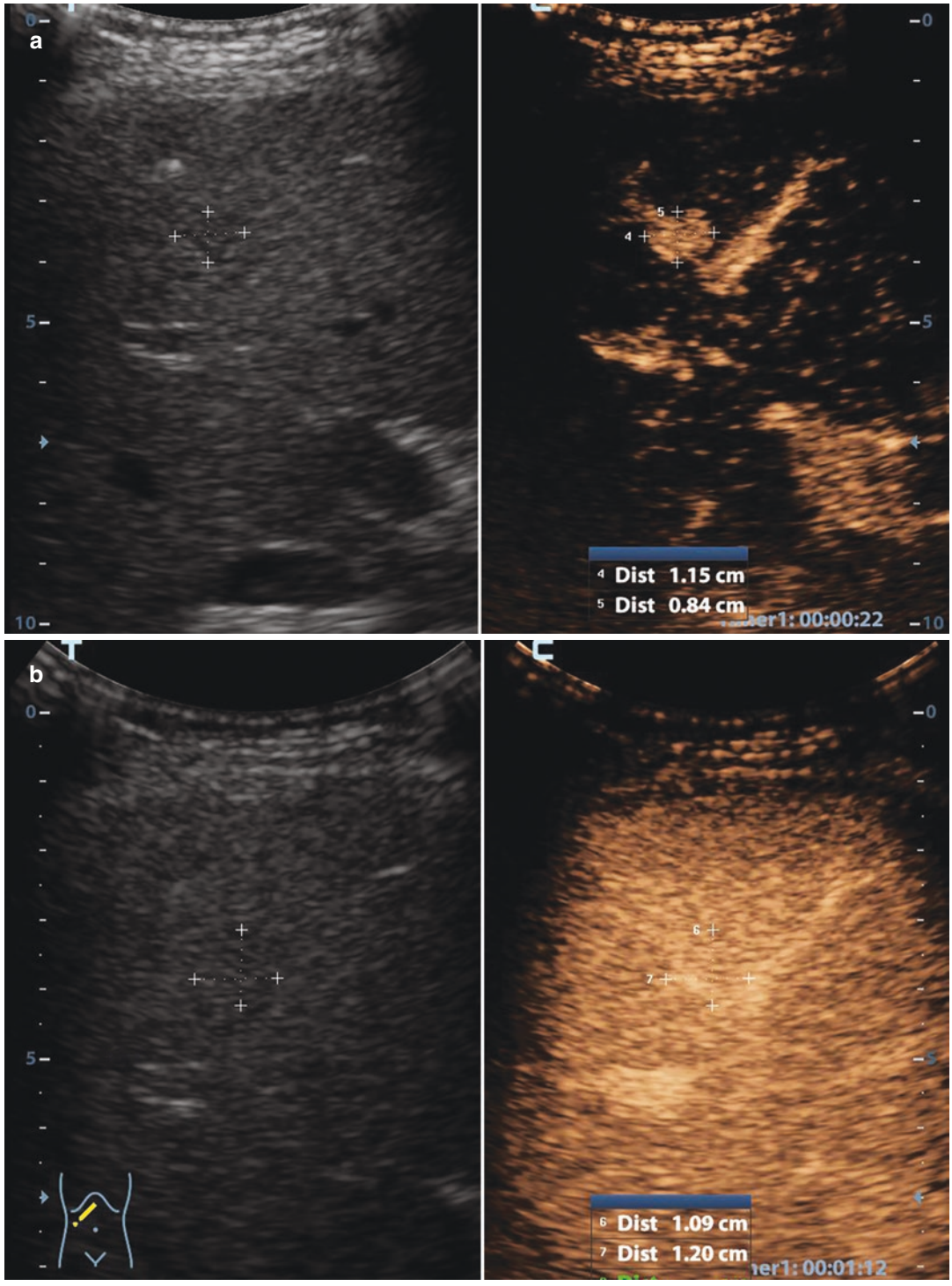

Fig. 4.5 Liver hemangioma. Rapid contrast enhancement. (**a**) arterial phase CEUS. (**b**) portal venous phase CEUS

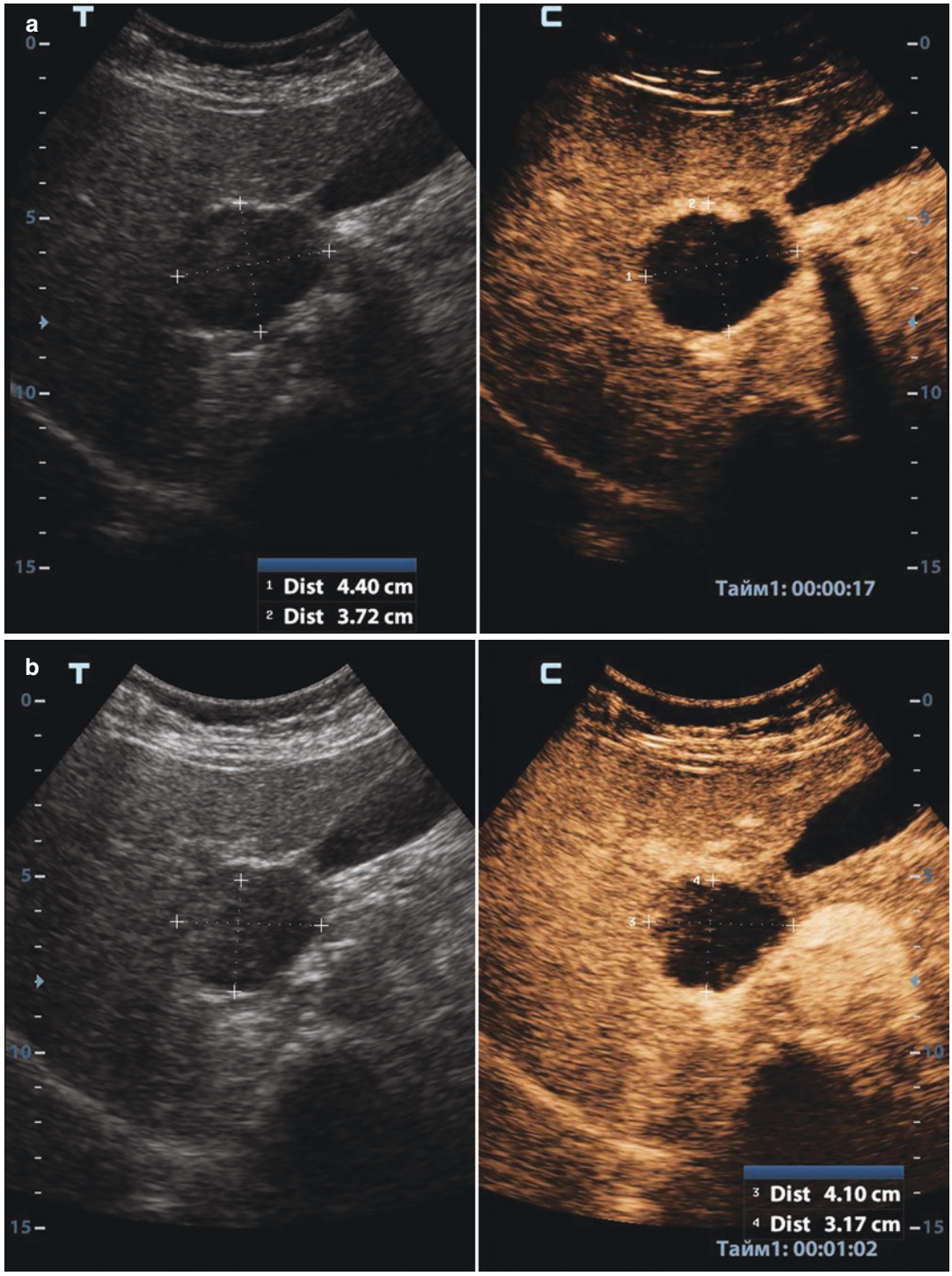

Fig. 4.6 Contrast enhancement of a liver hemangioma as a thin rim on the periphery of the lesion. (**a**) Arterial phase CEUS image. (**b**) Portal venous phase CEUS image

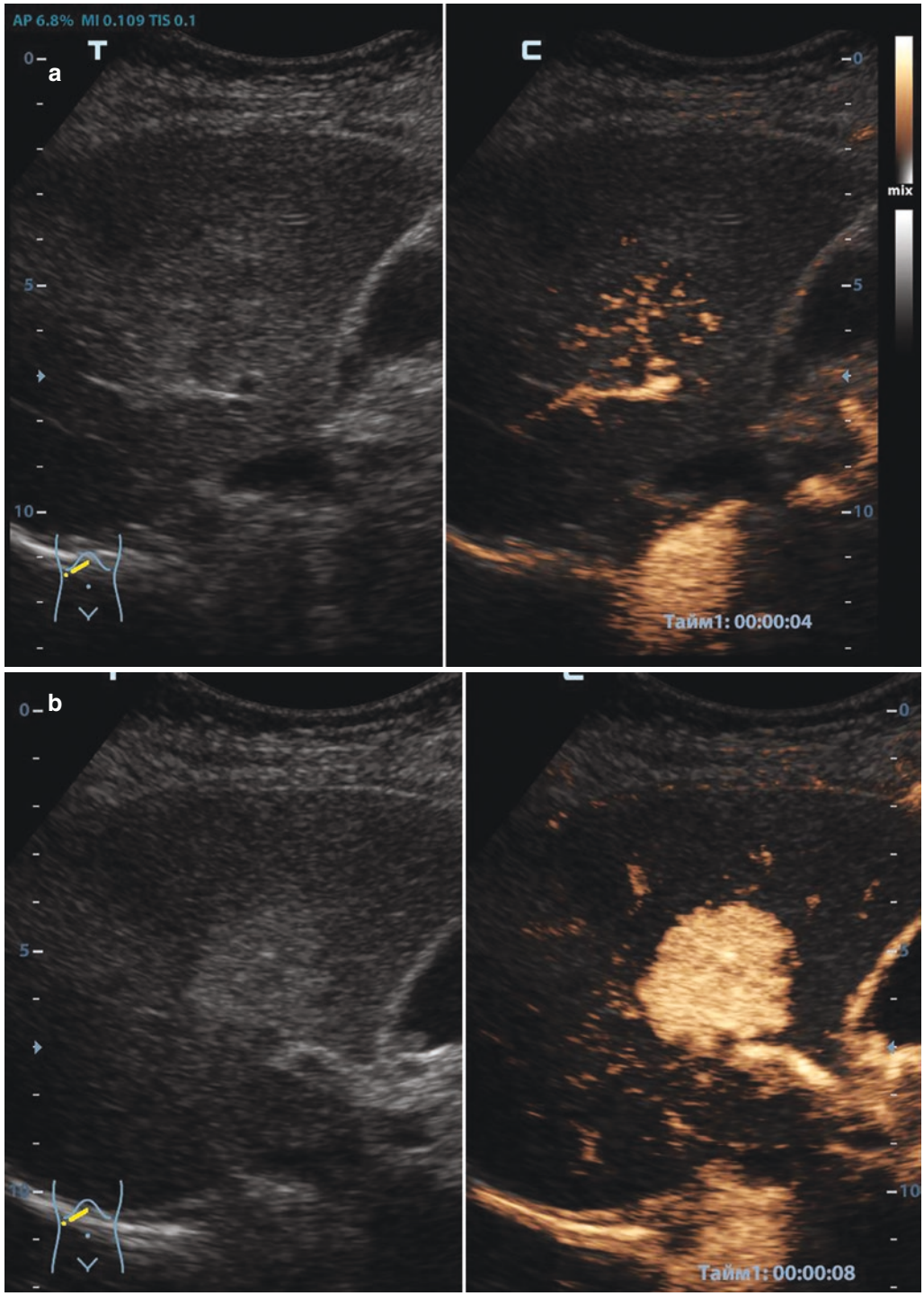

Fig. 4.7 Focal nodular hyperplasia. CEUS images. (**a**) Patient A. The spoke-wheel pattern of enhancement in the early arterial phase. (**b**) Patient A. Prominent hyperperfusion in the arterial phase, light-bulb sign. (**c**) Patient A. Persisting contrast enhancement in the late phase. (**d**) Patient A. 3D reconstruction of arterial phase CE-CT demonstrates the large feeding artery and hyperdense FNH. (**e**) Patient B. The spoke-wheel pattern of enhancement in the early arterial phase. (**f**) Patient B. Prominent hyperperfusion in the arterial phase, light-bulb sign. (**g**) Patient B. Persisting contrast enhancement in the late phase

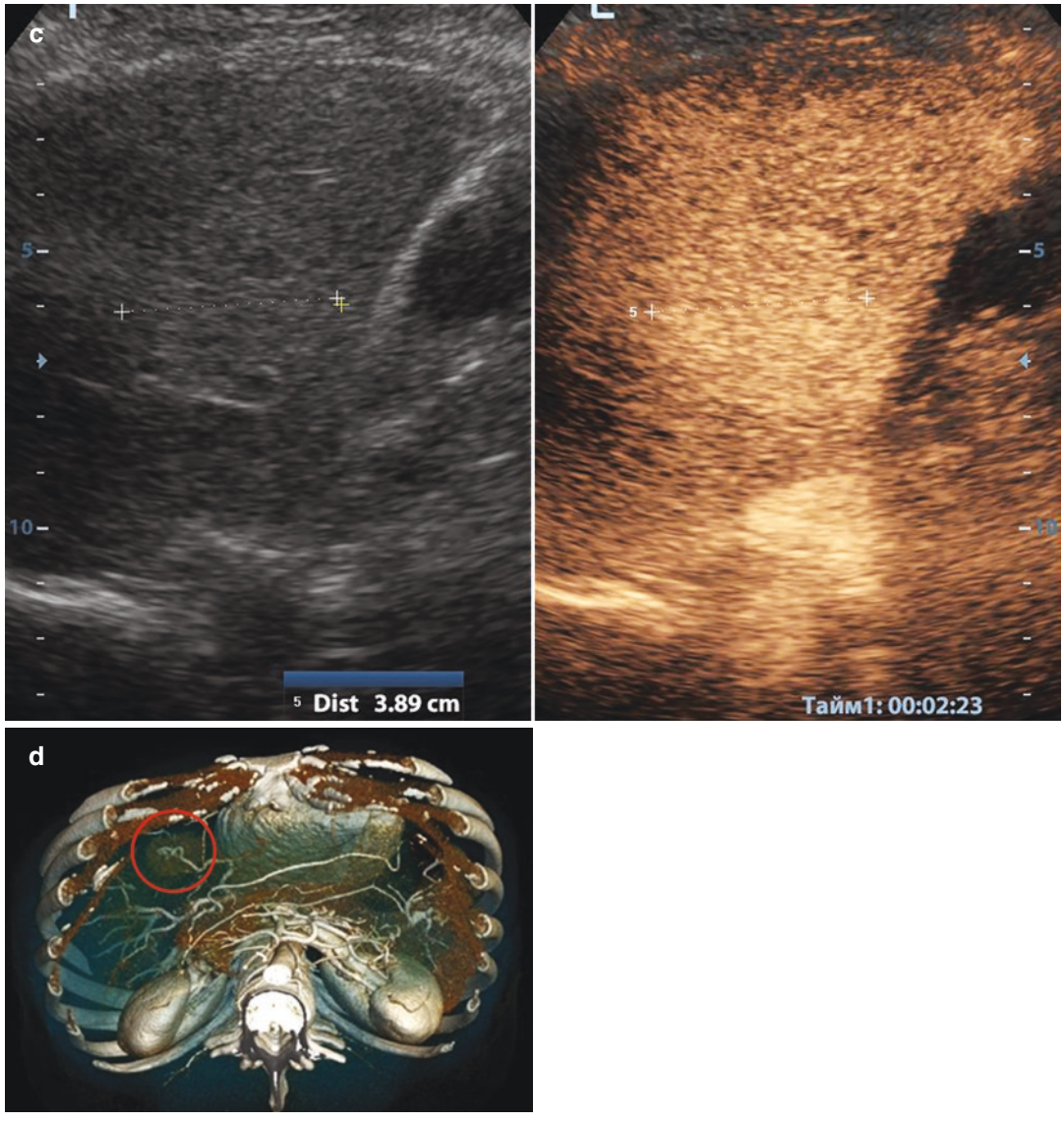

Fig. 4.7 (continued)

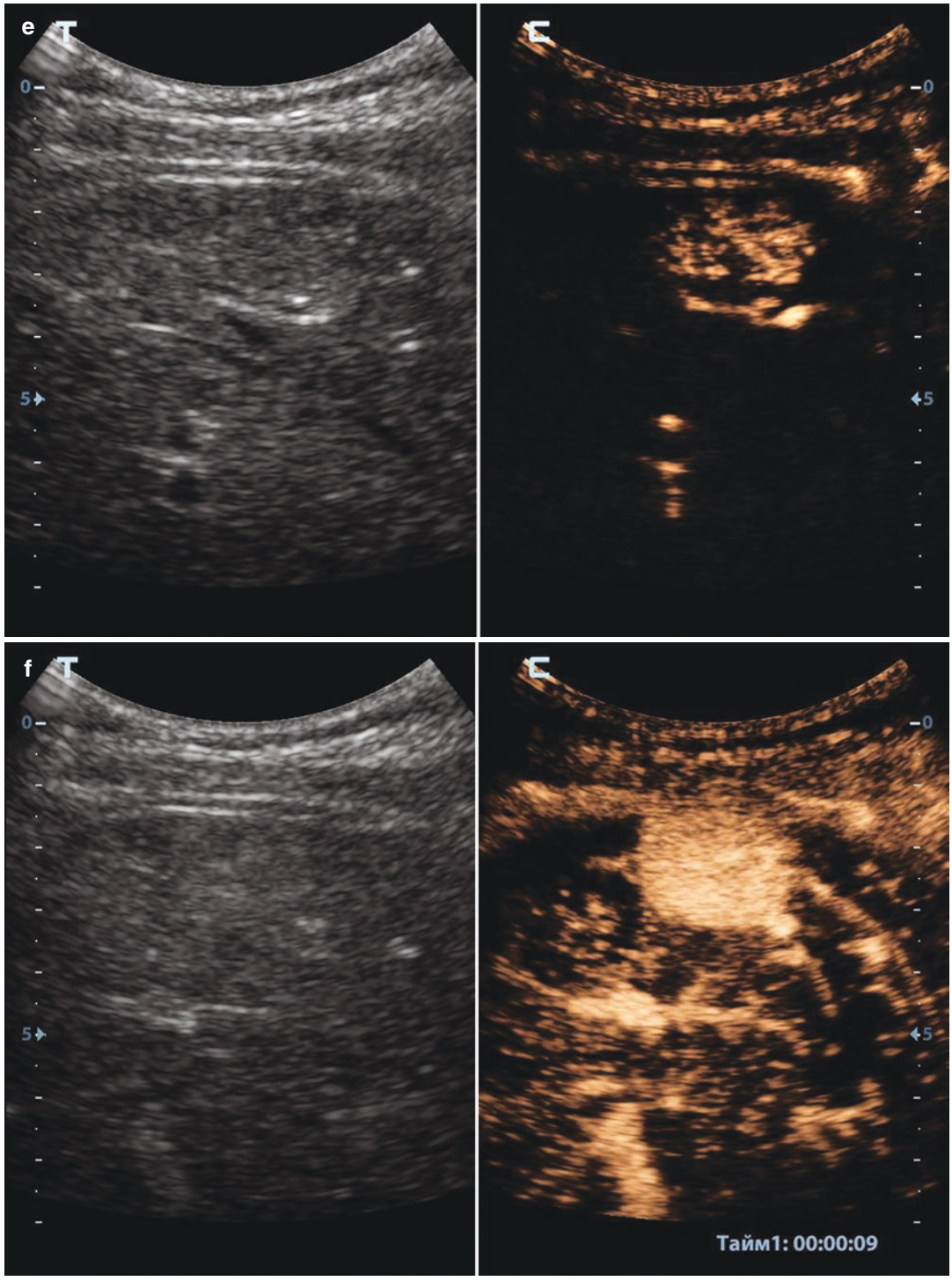

Fig. 4.7 (continued)

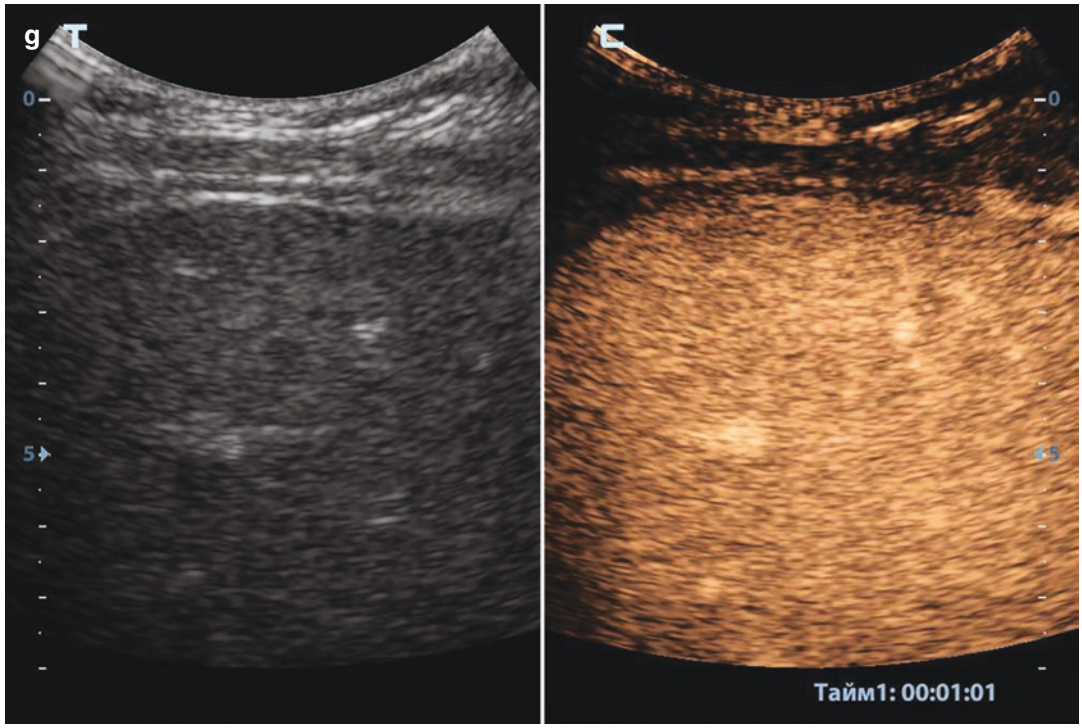

Fig. 4.7 (continued)

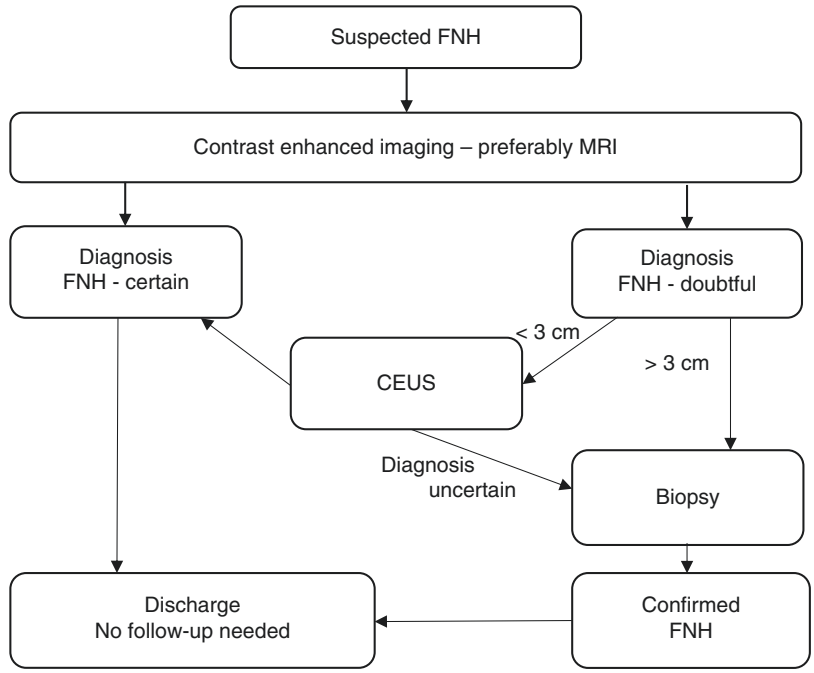

Fig. 4.8 Flow chart for the management of FNH

The following main subtypes based on gene mutations and the risk of malignant transformation are recognized [41]:

- HNF1α mutated hepatocellular adenoma (HA-H, ~35%).
- β catenin mutated hepatocellular adenoma (HA-B, ~10%).
- Inflammatory hepatocellular adenoma (HA-I, ~35%).
- Sonic hedgehog (SHH) hepatocellular adenoma (HA-sh, ~5%).
- Hepatocellular adenoma, not otherwise specified (HA-U, ~7%).

Hepatic adenoma is also supplied with blood from the liver artery system [6]. Histopathology reveals large subcapsular vessels with a large number of thin-walled capillaries that spread in the tumor, as well as wide sinusoids. With CEUS, it causes arterial phase hyperenhancement with a rapid fill-in from the periphery to the center. This phenomenon can also be easily missed, which requires repeated cine loop assessment. Visual perception of enhancement may benefit from parametric mapping (Fig. 4.9c, Videos 4.6 and 4.7).

Centripetal type of contrast enhancement permits differentiation of HCA from FNH. Both of them being hyperenhancing lesions, FNH is associated with the centrifugal type of fill-in [3]. Hepatic adenoma typically demonstrates homogeneous contrast enhancement. Heterogeneity may occur if areas of hemorrhage or necrosis are present, especially in large-sized HCA. In the portal venous phase, the HCA becomes isoenhanced (Fig. 4.9). The late phase may reveal slight hypoenhancement due to the absence of blood inflow from the portal vein system. Alternatively, or isoenhancement may preserve due to the retention of bubbles in sinusoids. In the case of a significant washout, the differential diagnosis with hepatic carcinoma is practically impossible.

Molecular classification of HCA contributed to the understanding of their malignant transformation. The highest risk of malignancy is observed in β-catenin HCA exon 3, which is typically detected in men. Accordingly, regardless of the size of the lesion, all men with HCA are advised hepatic resection or other treatment, while in women with smaller than 5 cm size HCA conservative management is possible [24].

The determination of HCA subtypes led to the search for their characteristic signs with CEUS, analogous to MRI. A reliable difference in contrast enhancement of HNF1A-inactivated and inflammatory HCAs was reported [42]. HNF1A-inactivated HCAs exhibit hyperenhancement in the arterial phase with a mixed type of fill-in and no washout in the portal venous and late phases. Inflammatory HCAs are also characterized by arterial phase hyperenhancement but accompanied by slight central hypoenhancement and peripheral isoenhancement in the late phase.

HNF1α mutated (HA-H) and inflammatory (HA-I) hepatic adenomas, as a rule, have no washout, whereas β-catenin inactivated (HA-B) and non-classified adenomas (HA-U) often exhibit late phase washout [43]. HA-H and HA-I in most cases do not exhibit washout and no reliable differential criteria between them are identified [44]. Currently, CEUS-based differential diagnosis of HCA subtypes is a subject of scientific research and is not recommended for clinical practice. If HCA demonstrates obvious washout effect and lack the reliable differential diagnostic features from malignant FLL, these cases are subject for histological verification.

Other rare benign liver tumors are inflammatory pseudotumor and angiomyolipoma. The publications on the patterns of contrast enhancement of these lesions are sporadic.

Hepatic inflammatory pseudotumor is a rare benign disease, which can be misdiagnosed as a malignant primary or secondary tumor. Individual CEUS literature data characterize it with rapid hyperenhancement in the arterial phase and washout in the portal venous and late phases that do not allow their differentiation from malignant FLLs [45–48]. In this lesion, CEUS is only capable to differentiate it from other benign FLL that have characteristic features.

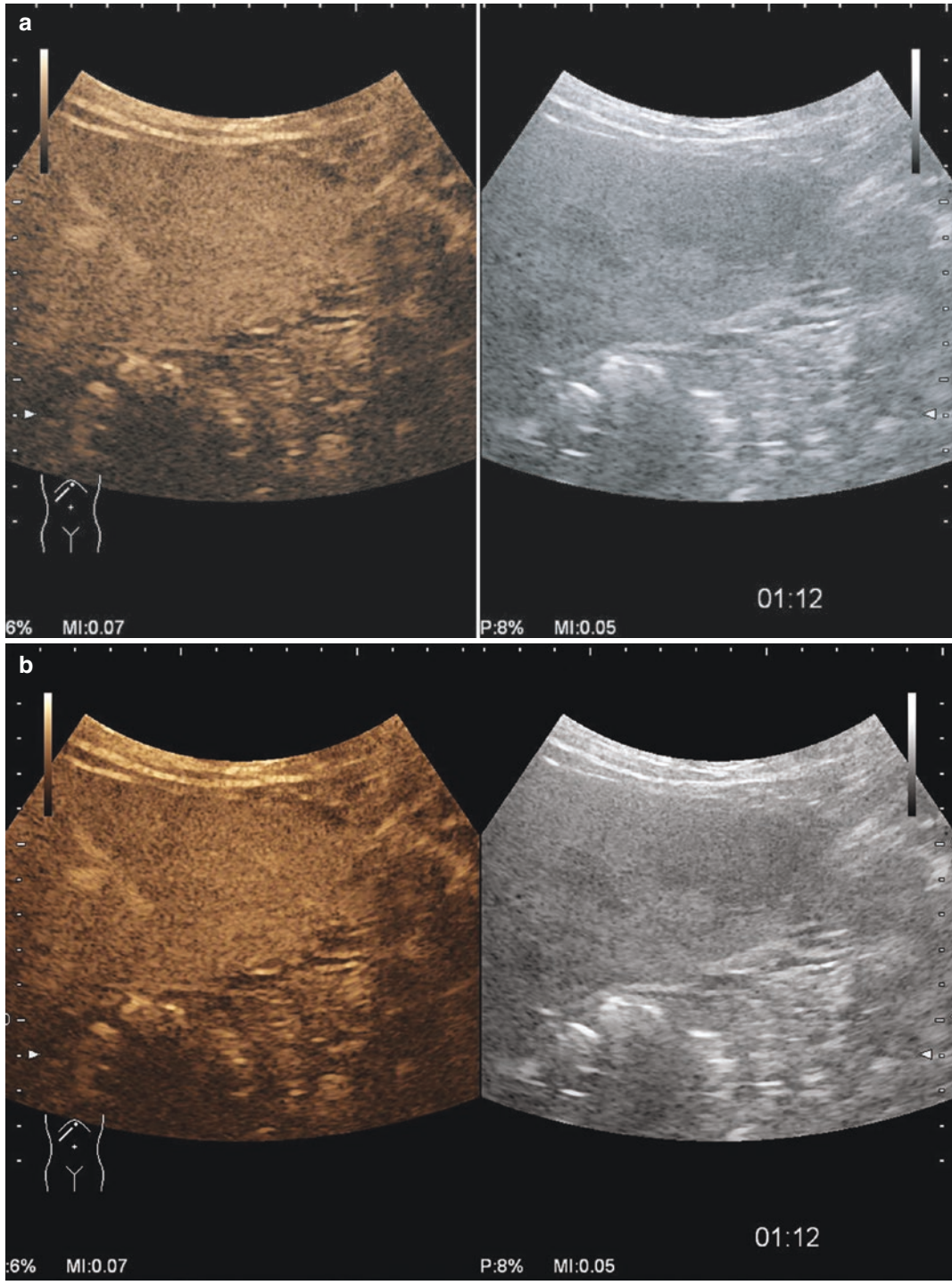

Fig. 4.9 Hepatic adenoma. (**a**) Rapid diffuse hyperenhancement in the arterial phase, CEUS image. (**b**) Isoenhancement in the portal venous phase makes adenoma invisible on the isoenhanced background liver parenchyma. CEUS image. (**c**) Parametric map of enhancement. (**d**) CE-CT

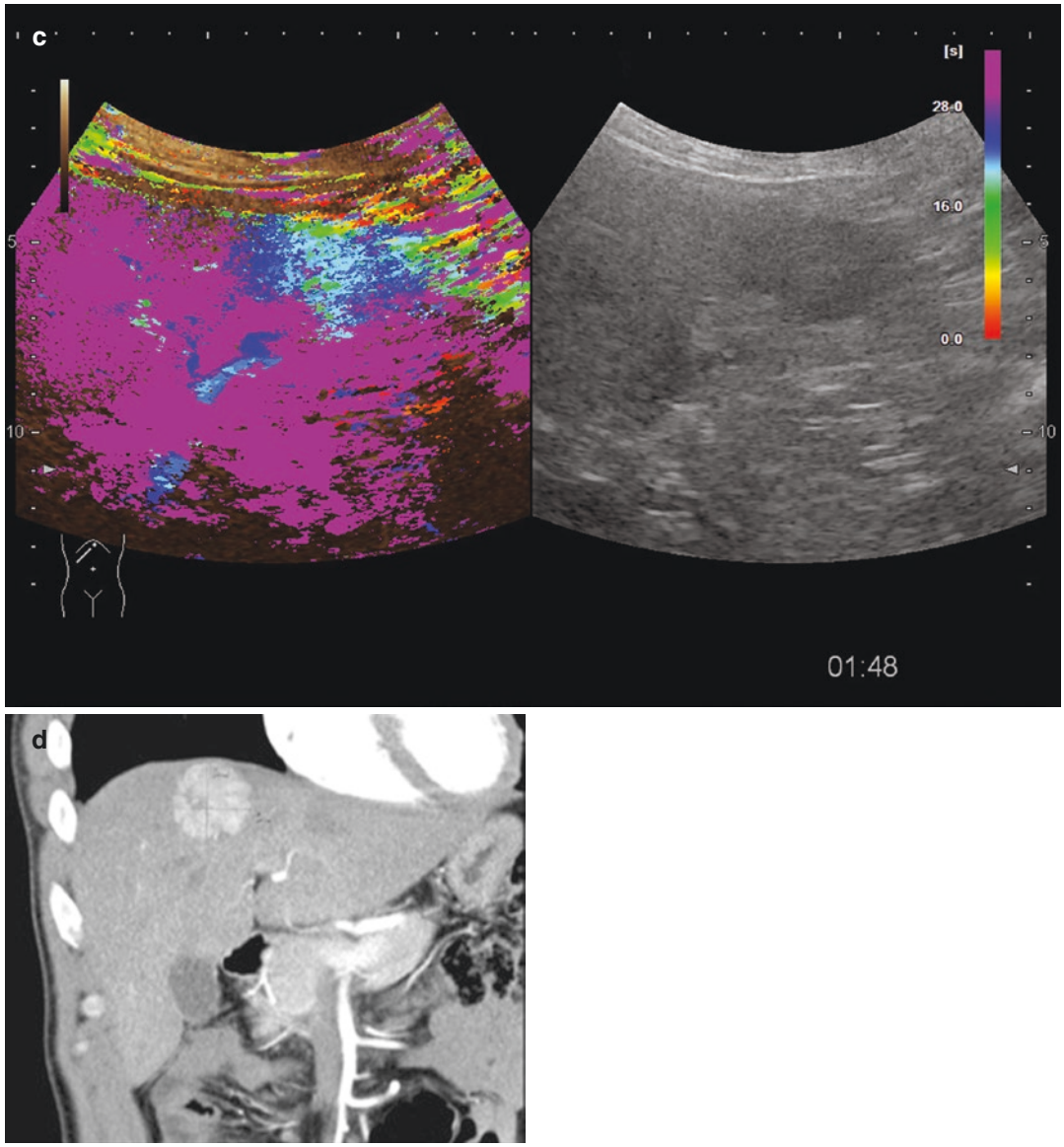

Fig. 4.9 (continued)

Cholangiocellular adenoma (bile duct adenoma) is a rare benign FLL of small size, usually smaller than 1 cm, which has exceptionally arterial blood supply. This tumor can also be misdiagnosed for malignancy due to arterial phase hyperenhancement and early washout [49].

Hepatic angiomyolipoma is a rare benign mesenchymal tumor represented with histopathology by three components in various proportions: proliferating thick-walled blood vessels, smooth muscles, and mature adipose cells [50, 51]. Although hepatic angiolipomas are considered benign, it is believed that they may have some malignant potential. Several patients there reported to have histopathological signs similar to malignant tumors and developed extrahepatic metastases [52, 53]. Typical benign angiomyolipoma is hyperenhancing in the arterial phase and remains moderately hyper- or isoenhanced in the

portal venous and late phases. Late phase washout in angiomyolipoma was reported in about 25% of cases, and a case of hypoenhancing angiomyolipoma in all vascular phases was published [52, 54]. Additionally, CEUS is better than CE-CT for the assessment of contrast agent washout [54]. CT in the cases of angiomyolipoma determined washout in 42.6% and false-positively declared the malignant FLL, while CEUS—only in 18.5% of cases.

4.1.2 Malignant Liver Lesions and Metastases

The specific feature of malignant liver tumors is hypoenhancement in the late phase and post-vascular phase (for Sonazoid) that corresponds to the washout of the UCA. It is registered in all cases of liver metastases regardless of contrast enhancement in the arterial phase [3]. The exceptions to this rule are quite rare.

Liver metastases are the most common malignant FLL. They are detected in 30–50% of oncological patients and occur 20–30 times more often than primary liver carcinoma [55]. The principal cause for liver metastasis is colorectal, esophageal, lung, duodenal, or pancreatic cancer.

Metastases in the liver have arterial blood supply without any inflow from the portal vein system [6]. With CEUS, they are characterized with pronounced hypoenhancement in the portal venous and late phases, looking like well-defined dark foci in the homogeneously enhanced normal liver parenchyma [3, 14, 15, 56–58] (Fig. 4.10). Washout usually starts within 60 s after UCA injection. However, in rare cases with small-sized lesions (<2 cm), washout may not be observed in the portal venous phase and begins in the late phase after 120 s [59].

In the arterial phase, various contrast enhancement of metastases are possible. Hypovascular metastases, which have a relatively low arterial perfusion, are hypoenhanced, sometimes with slight enhancement on the periphery. This pattern is often observed in the metastases of the gastrointestinal tract, lung, or breast adenocarcinoma [30, 60–63]. Hypervascular metastases are most often found in the cases of neuroendocrine tumors, carcinoid, melanoma, sarcoma, urothelial carcinoma, choriocarcinoma, breast, thyroid gland, or ovarian cancer. They have a very high arterial perfusion and exhibit diffuse hyperenhancement often with a peripheral rim in the arterial phase and washout in the portal venous and late phases [30, 60–63]. The beginning of contrast enhancement and the peak intensity in hypervascular metastases develop earlier and washout starts later than in hypovascular ones [62]. In rare cases, they observed isoenhancing metastases in the portal venous and late phases. The authors suppose that this pattern can be explained by an increase in arterial blood flow, which partially compensates for the reduced portal blood flow. It may be the cause of the erroneous interpretation of such masses as a well-differentiated hepatocellular carcinoma or benign lesions.

However, the pattern of arterial contrast enhancement has a limited diagnostic value. It may help to guess the probable location of the primary tumor and is often used for monitoring patients during anti-angiogenic therapy [6]. The arterial phase, which is associated with minimal enhancement of liver parenchyma, is most appropriate for evaluation of the vascular structure of the metastases and the detection of their feeding vessels. The differential diagnosis of cystic metastases from complex non-tumor cysts is feasible with the assessment of the peripheral rim-shaped contrast enhancement and the enhancement of the septal and mural components (Fig. 4.11, Video 4.8).

CEUS demonstrates excellent diagnostic accuracy in liver metastasis with the sensitivity of 94.4%, specificity—93.7%, and accuracy—94.11% [27]. The DEGUM multicenter trial reported the accuracy of 91.4% [23]. However, CEUS is limited with the assessment of the metastases located in one scanning plane. It fails to detect remote metastases and simultaneously evaluate the lesions within the whole liver volume.

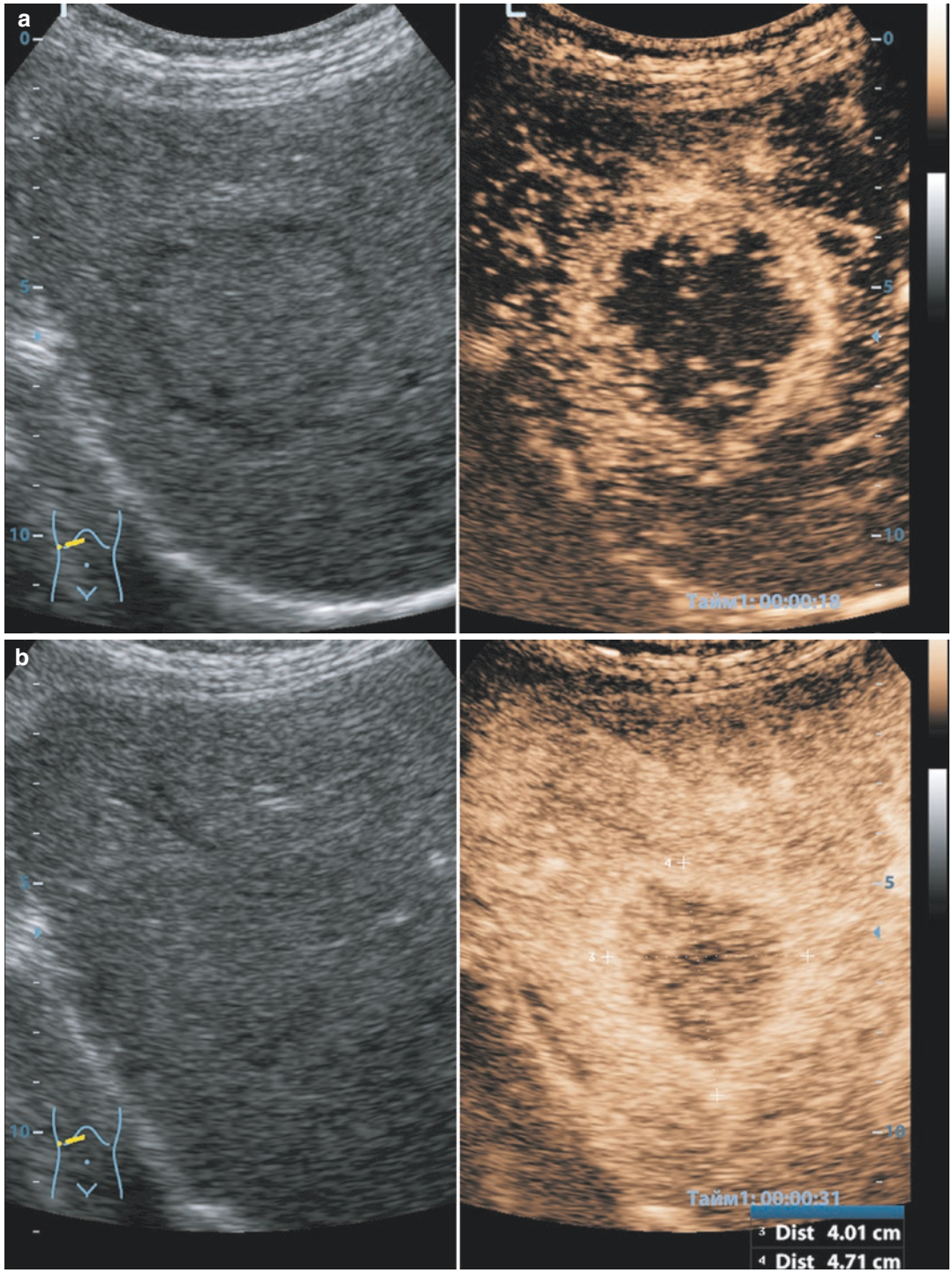

Fig. 4.10 Colorectal metastasis. CEUS images. (**a**) Early arterial phase. (**b**) Arterial phase. (**c**) Portal venous phase. (**d**) Late phase

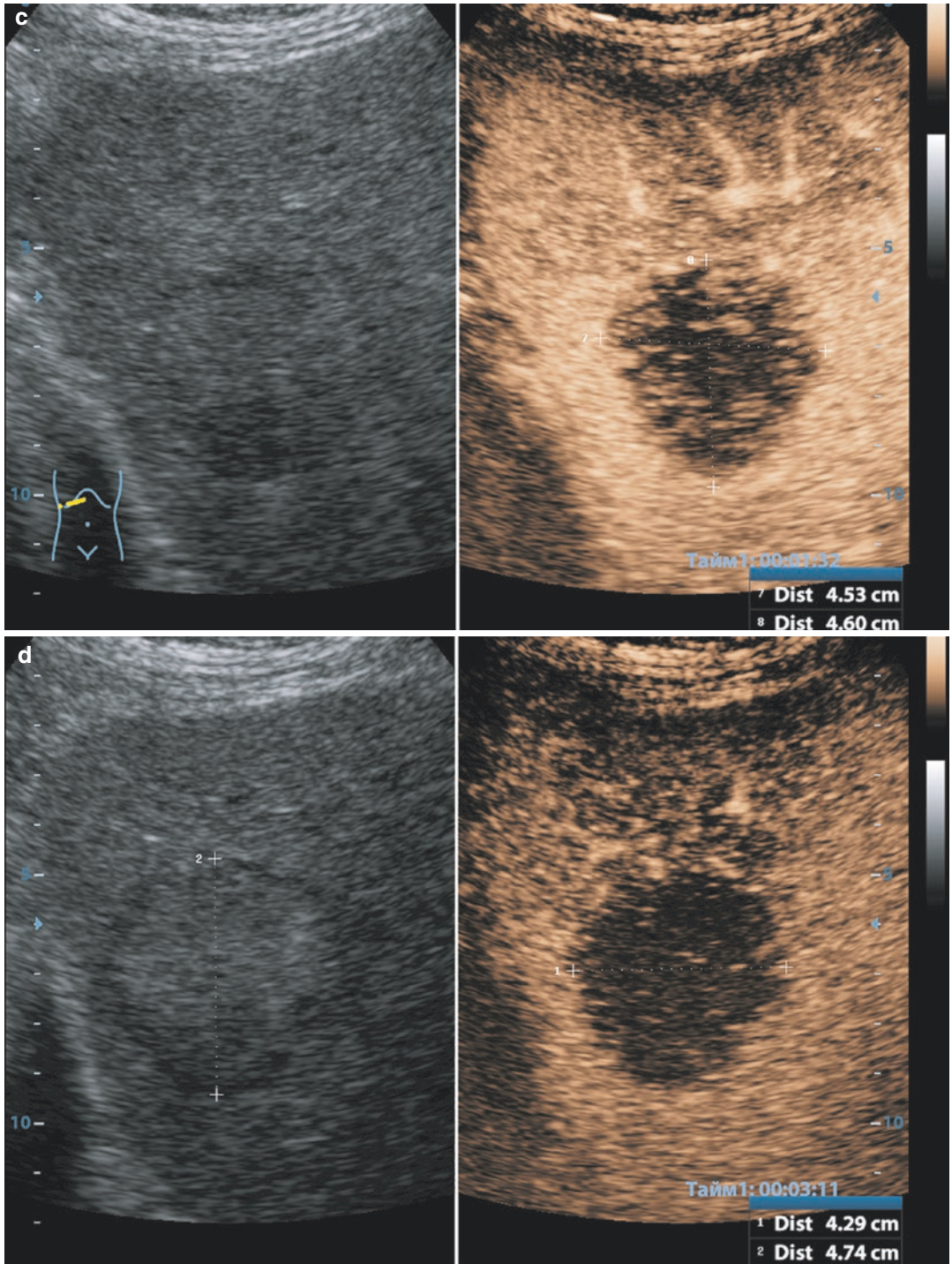

Fig. 4.10 (continued)

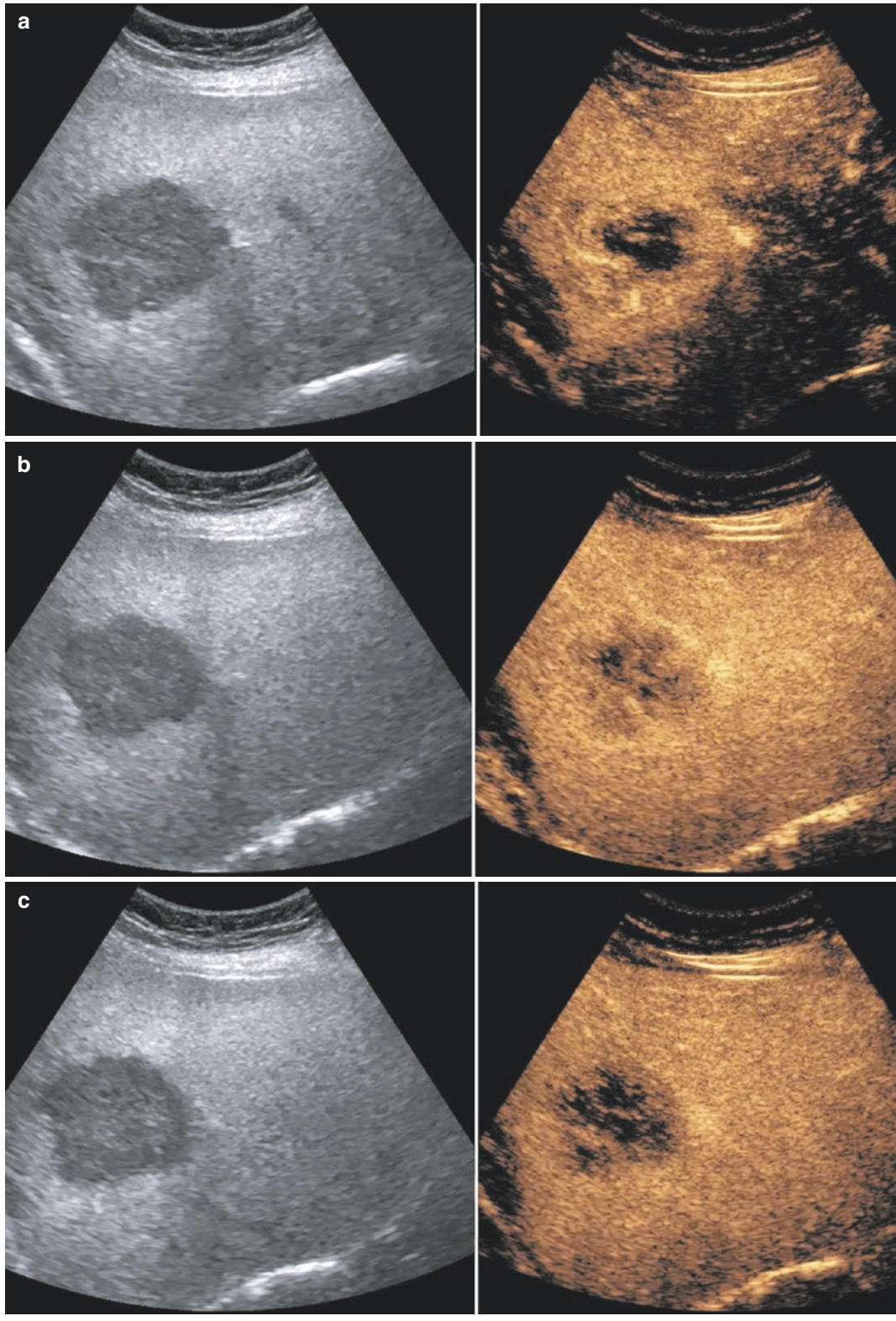

Fig. 4.11 Metastasis of breast carcinoma in the liver. CEUS images. (**a**) Early arterial phase. (**b**) Arterial phase. (**c**) Portal venous phase

Hepatocellular carcinoma (HCC) is a primary liver tumor accounting for 80% of all liver cancers. It takes the sixth place by prevalence and the second among the causes of mortality from cancer [64]. HCC often develops in the cirrhotic liver. However, liver cirrhosis is not considered a precancerous state. Approximately 20% of the HCCs develop in non-cirrhotic liver and is often associated with metabolic syndrome ar chronic hepatitis B. There are other risk factors, such as aflatoxin exposure, chronic alcoholism, non-alcoholic fatty liver disease, hereditary hemochromatosis, deficiency of α1-antitrypsin, Wilson disease, etc. [65, 66].

In the majority of cases (about 90%), HCC develops as a multi-stage process with gradual cellular and molecular dedifferentiation of hepatocytes.

The developing HCC passes the following stages [67] (Fig. 4.12):

- Regenerative macronodule, which is histopathologically identical to the liver parenchyma.
- Low-grade dysplastic nodule (LGDN). Its blood supply has practically no difference from the blood supply of the liver (about 80% of the portal and 20% arterial inflow).
- High-grade dysplastic nodule (HGDN). It exhibits active vascular restructuring with sinusoidal capillarization and development of unpaired arteries but preserved portal blood inflow and venous outflow.
- Early HCC, highly differentiated. Portal blood supply switches to arterial with the increase in the number of unpaired arteries and the disappearance of paired arteries.
- Progressive HCC, moderately or poorly differentiated. It may demonstrate invasive growth and metastasis. At this stage, there appears a fundamental change in the type of blood supply with the retrograde evacuation of blood from intra-tumor arteries to intratumor portal vessels and the sinusoids of the peritumoral space. As the tumor progreses is completely switches to arterial blood supply with full disappearance of the portal blood supply

An exception is HCC in the non-cirrhotic liver, which has no intermediate stages and histological precursors, and is defined as hepatic carcinogenesis de novo. For example, in chronic hepatitis B, the integration of the viral genome to the patient's DNA directly leads to the activation of the genes responsible for the development of HCC [67].

Ultrasound signs of HCC are nonspecific and largely depend on the tumor type: diffuse or nodular with the latter subdivided into a solitary nodule, solitary nodule with proliferation, multiple nodules, and merging multiple nodules [9]. The key point in the diagnosis of HCC is the understanding of the process of neoangiogenesis in the tumor and, consequently, the dynamics of arrival, accumulation, distribution, and washout of UCAs.

In the non-cirrhotic liver, HCC exhibits arterial phase hyperenhancement, as a rule with chaotic vascular pattern and fill-in from the periphery. If necrotic areas are present in the tumor, the enhancement is heterogeneous [3]. Iso- and hypoenhancing patterns in the arterial phase may be observed less often. The portal and late phases demonstrate slow and poor washout, which is less prominent than in other primary liver tumors or metastases. Washout often starts later than 60 s after the UCA introduction and in 25% of cases—later than 180 s [68].

Any FLL in the cirrhotic liver background without confidence in its benign nature is an indication for a contrast-enhanced study. The principal feature of HCC in the cirrhotic liver is hyperenhancement in the arterial phase followed by washout in the late phase, which is characteristic for more than 97% of HCCs [3, 68]. As a rule, in the arterial phase, the enhancement is homogeneous. Heterogeneous enhancement is rare and observed in lesions larger than 5 cm in size. Peripheral rim-shaped enhancement is not typical HCC. The UCA washout usually starts later and is mild that differs HCC from other liver malignancies (Figs. 4.13 and 4.14, Video 4.9).

The appearance and severity of the washout effect depend on tumor differentiation and size. It is less characteristic of well-differentiated HCC. If the lesion size is smaller than 2 cm,

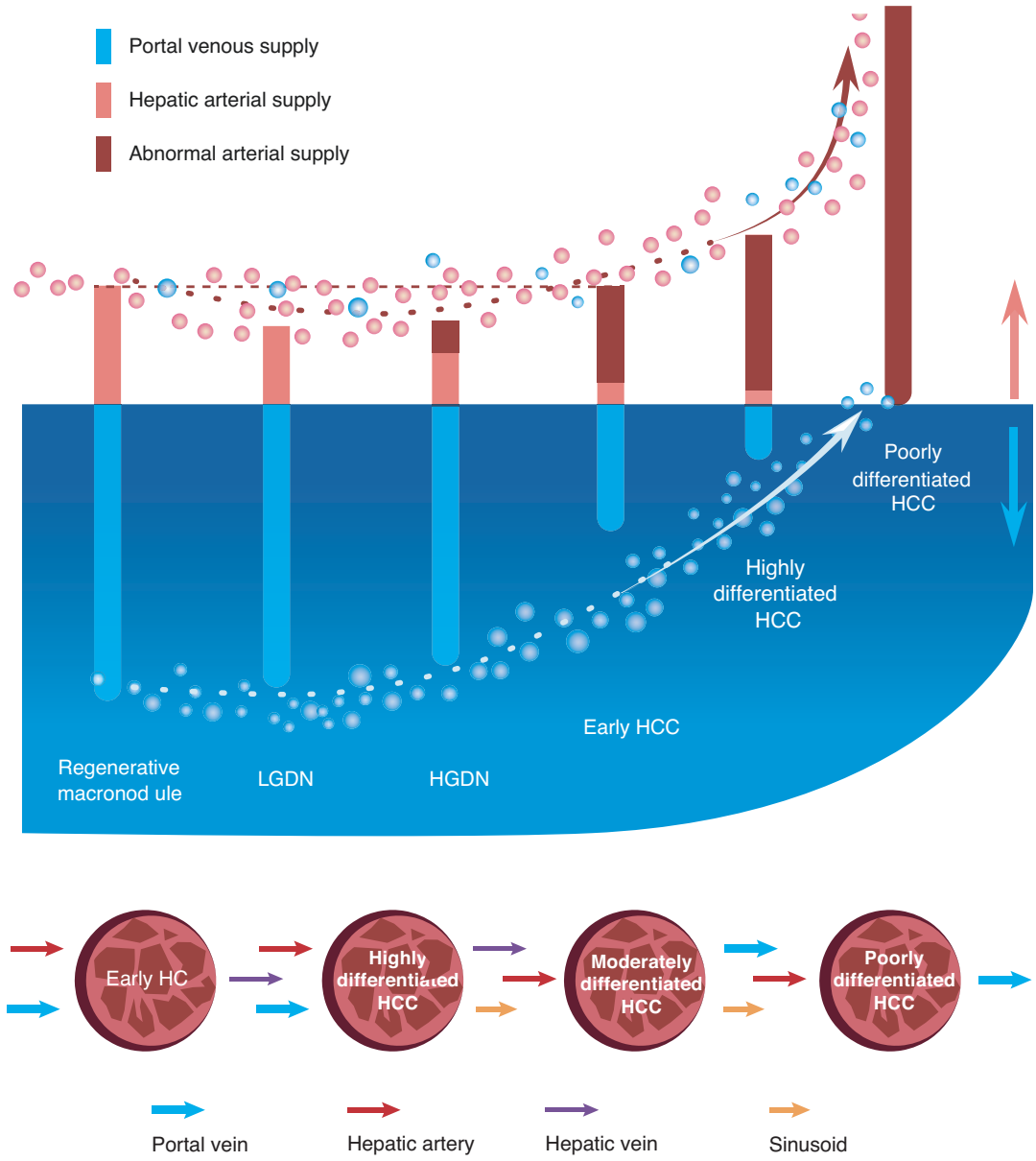

Fig. 4.12 Multistage development of HCC with the changes in blood flow

washout is registered in 20–30% of cases, and in 2–3 cm size lesions—in 40–60% [3, 65, 66] (Fig. 4.15).

Therefore, arterial phase hyperenhancement of FLL in the cirrhotic liver even without subsequent washout is highly suspicious for HCC. Rare cases of iso- and hypoenhancing HCC in the arterial phase and rapid washout in the portal venous phase were reported. The meta-analysis [69] demonstrated that CEUS in the diagnosis of HCC is characterized by the sensitivity of 85%, specificity—91%, and AUC—0.943. Our study demonstrated the sensitivity of 83.3%, specificity—95.7%, and accuracy—94.2% [27]. However, CEUS is not recommended for staging HCC.

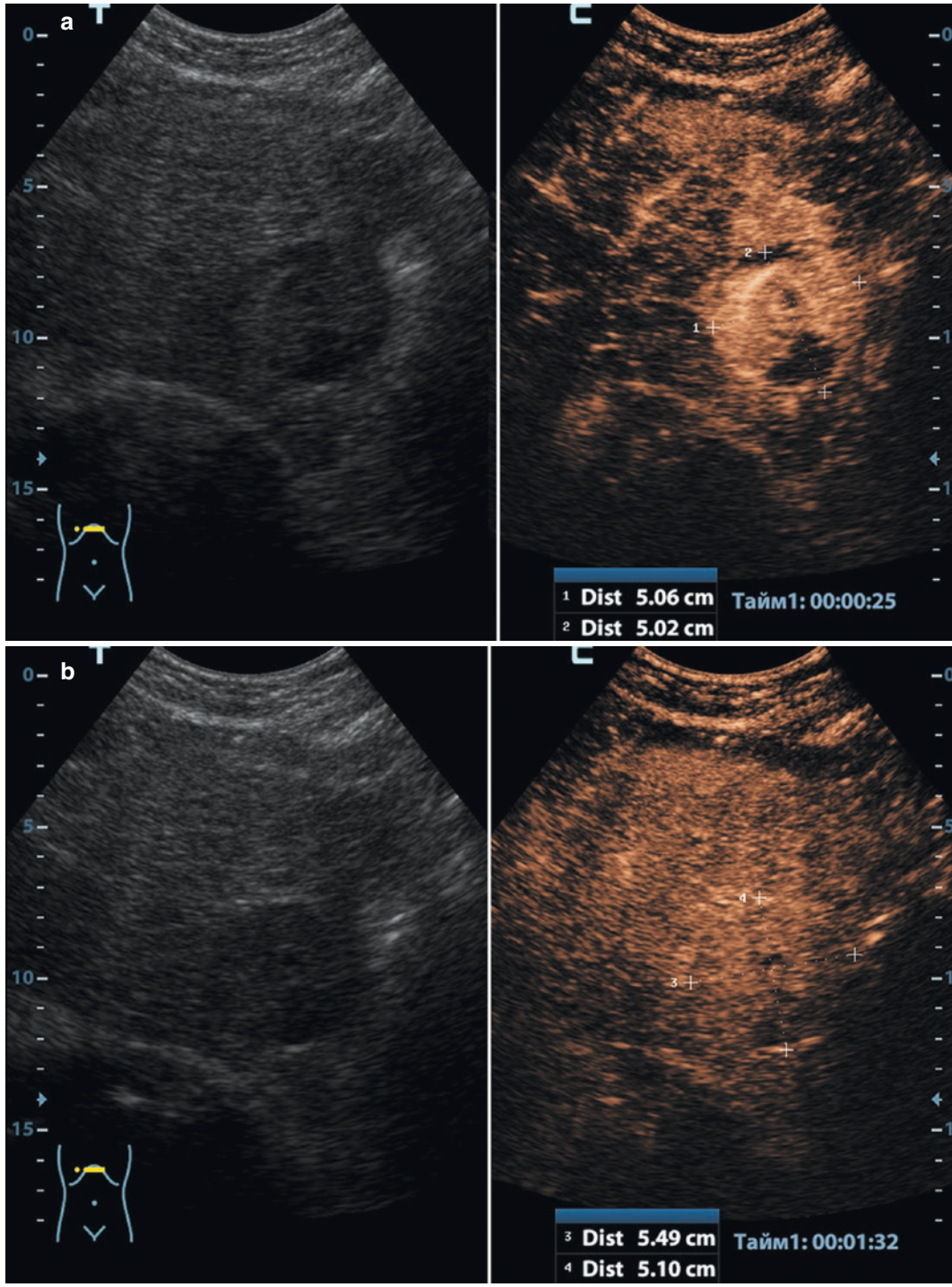

Fig. 4.13 HCC CEUS images. (**a**) Hyperenhancement in the arterial phase. (**b**) Isoenhancement in the portal venous phase. (**c**) Late hypoenhancement in the late phase

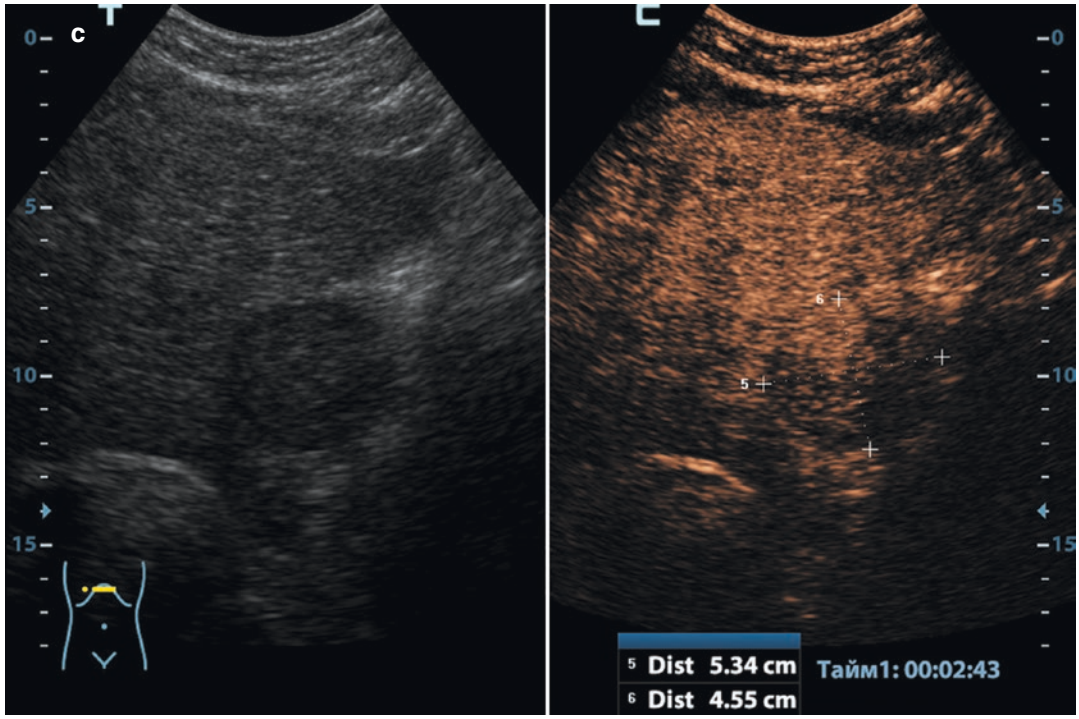

Fig. 4.13 (continued)

Tumor thrombosis of the portal vein is one sign that affects the definition of the HCC stage. CEUS permits confident differentiation of malignant and benign thrombus with the sensitivity of 0.94 (95% confidence interval 0.89–0.97) and specificity of 0.99 (95% CI 0.80–1.00), which makes CEUS the ideal method of study of the portal vein in patients with HCC [70].

Malignant thrombus exhibits the typical signs of HCC with rapid enhancement in the arterial phase, sometimes with linear or disorganized feeding vessels [71, 72]. Alternatively, benign thrombus does not accumulate UCAs. In patients with diffuse HCC, the presence of tumor thrombus of the portal vein may be the first sign of liver malignancy. In such a case, the detection of the washout phenomenon in the liver parenchyma adjacent to the affected portal vein and re-evaluation of the arterial phase in the search for the hyperenhanced lesion is beneficial for the diagnosis of HCC [6].

CEUS Liver Imaging Reporting and Data System (LI-RADS) algorithm was designed by the American College of Radiology (ACR) and revised in 2017 to ensure the non-invasive diagnosis of HCC in patients at high-risk. It aims to improve the consistency of diagnostic parameters, data interpretation, and reporting aspects of the liver CEUS studies [73] (Fig. 4.16). FLLs are categorized from CEUS LR-1 (definitely benign) to CEUS LR-5 (definitely HCC). Additionally, the categories of malignant neoplasms of non-hepatocellular nature (CEUS LR-M) and tumor-in-vein (CEUS LR-TIV) are specified.

- CEUS LR-1 category (definitely benign) includes FLLs with characteristic CEUS signs of a simple cyst, hemangioma, and hepatic fat deposition/sparing in a characteristic location around the gallbladder fossa and anterior to the right portal vein in segment 4 with isoenhancement in all phases.

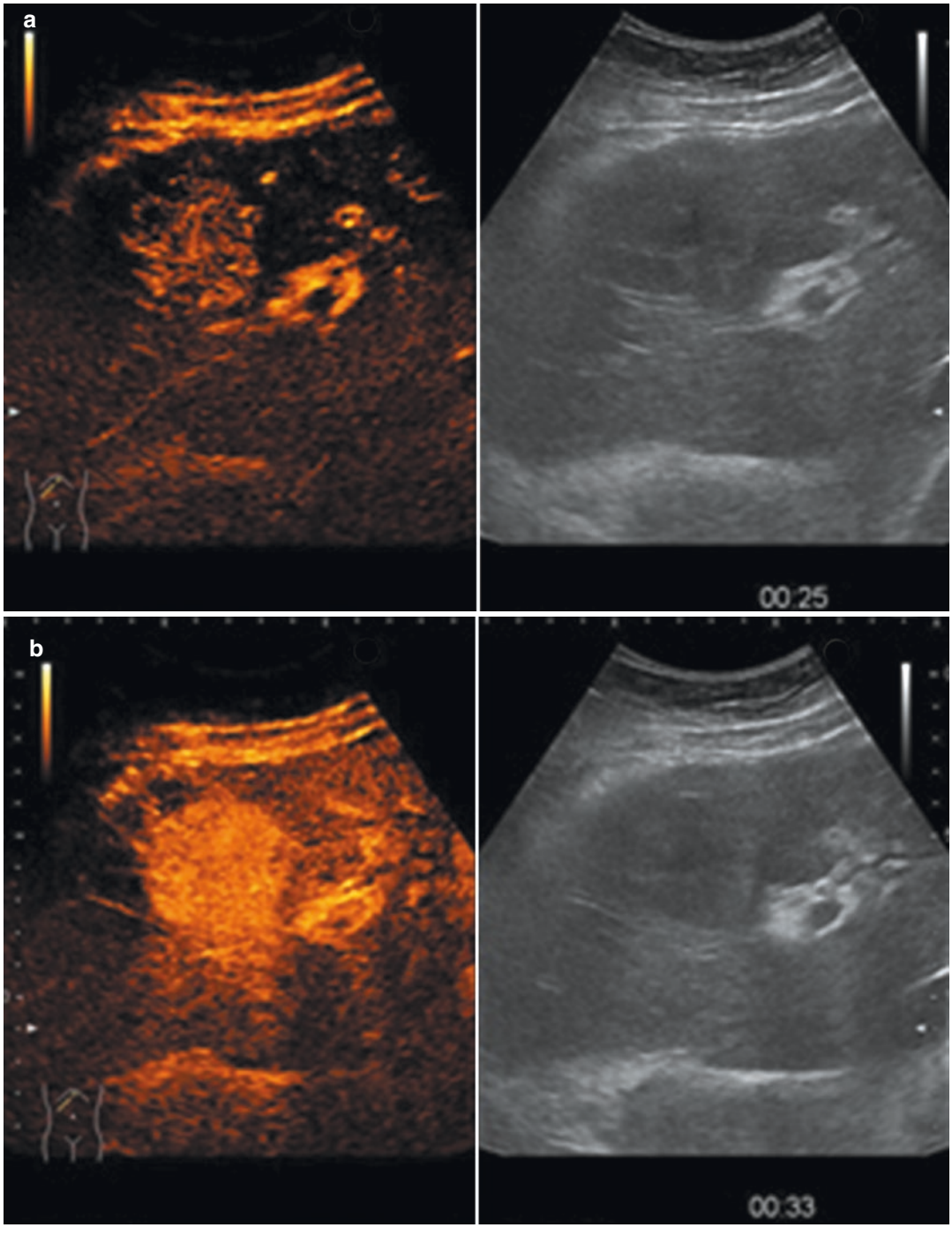

Fig. 4.14 HCC CEUS images. (**a**) Hyperenhancement in the early arterial phase. (**b**) Hyperenhancement in the arterial phase. (**c**) Isoenhancement in the portal venous phase. (**d**) Late hypoenhancement in the late phase

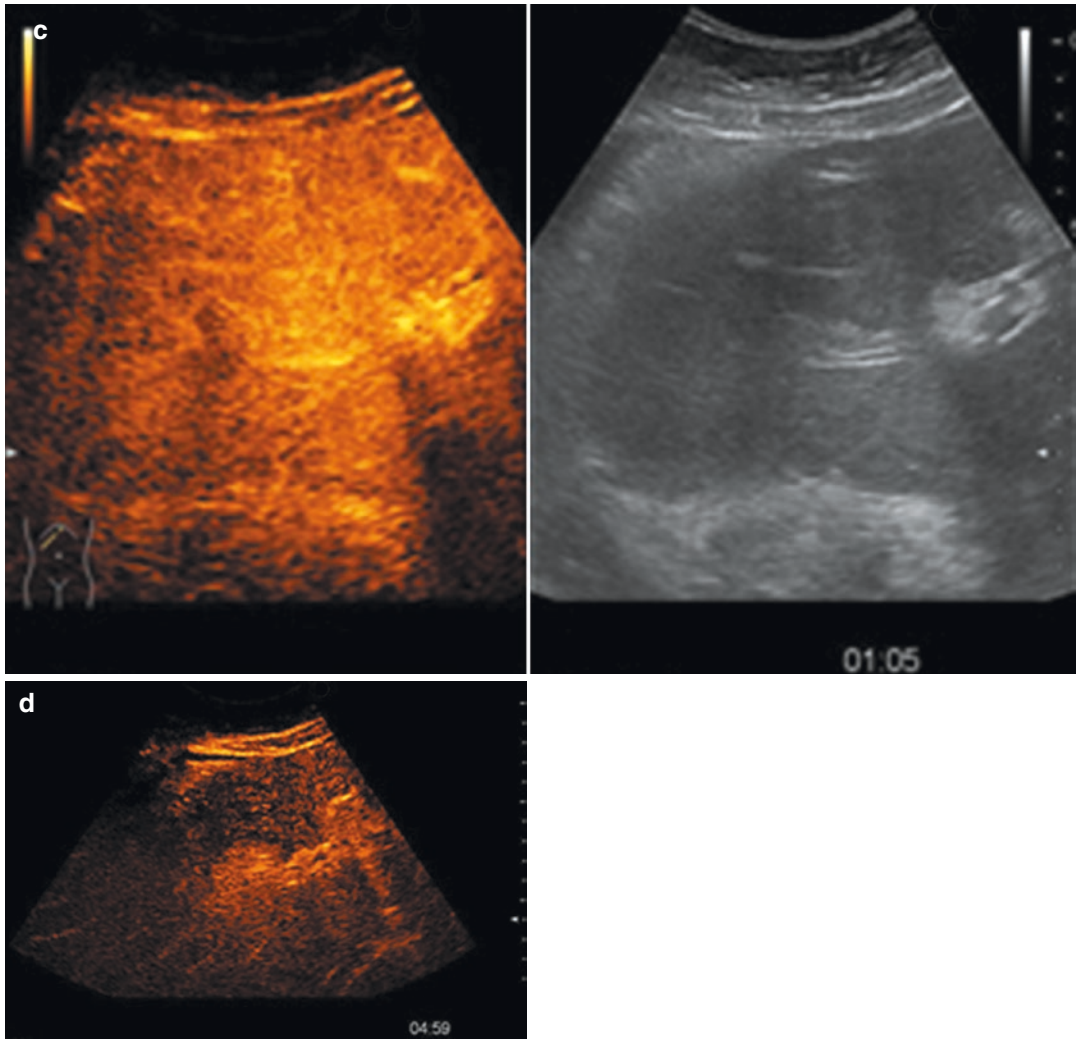

Fig. 4.14 (continued)

- CEUS LR-2 category (probably benign) includes hepatic fat deposition/sparing not in a characteristic location, distinct isoenhancing solid nodule <10 mm in size and CEUS LR-3 nodules with interval size stability for ≥2 years.
- CEUS LR-3, LR-4, and LR-5 categories reflect the progression from dysplastic nodules (>4 mm) to HCC. They are accompanied by the changes in vascularization and are estimated following the table (Fig. 4.16).
  - CEUS LR-5 (definitely HCC) category is assigned if the FLL is ≥10 mm in size with hyperenhancement of the entire nodule or its part in the arterial phase followed by late (≥60 s) and mild washout. ACR reports that these criteria practically exclude incorrect HCC diagnosis.
  - CEUS LR-4 (probably HCC) category confers FLL ≥ 20 mm in size without arterial phase hyperenhancement and FLL ≤ 10 mm with arterial phase hyperenhancement both

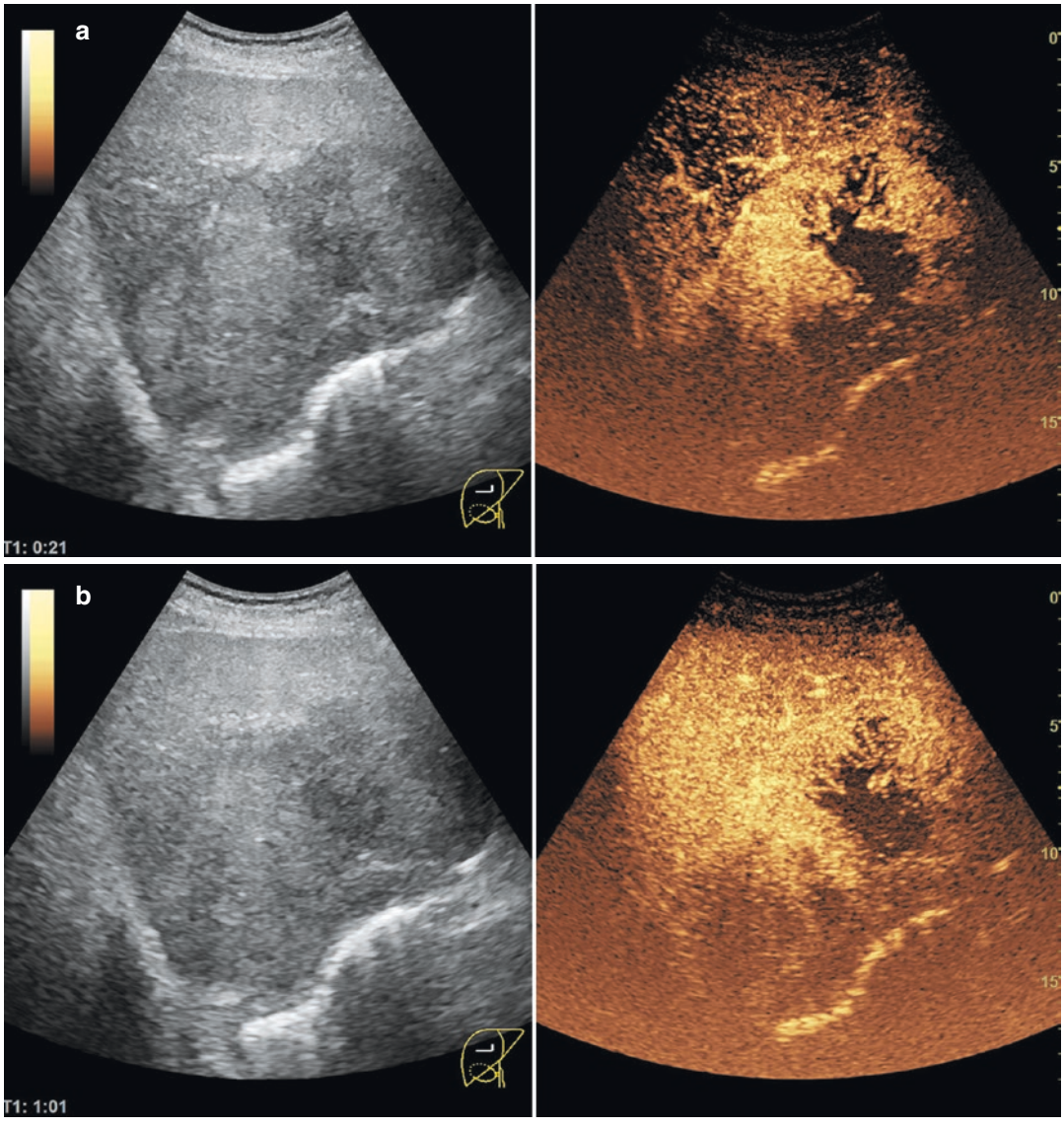

Fig. 4.15 HCC. CEUS images. (**a**) Hyperenhancement in the arterial phase. (**b**) Portal venous phase. (**c**) Prominent washout in the late phase. (**d**) CE-CT

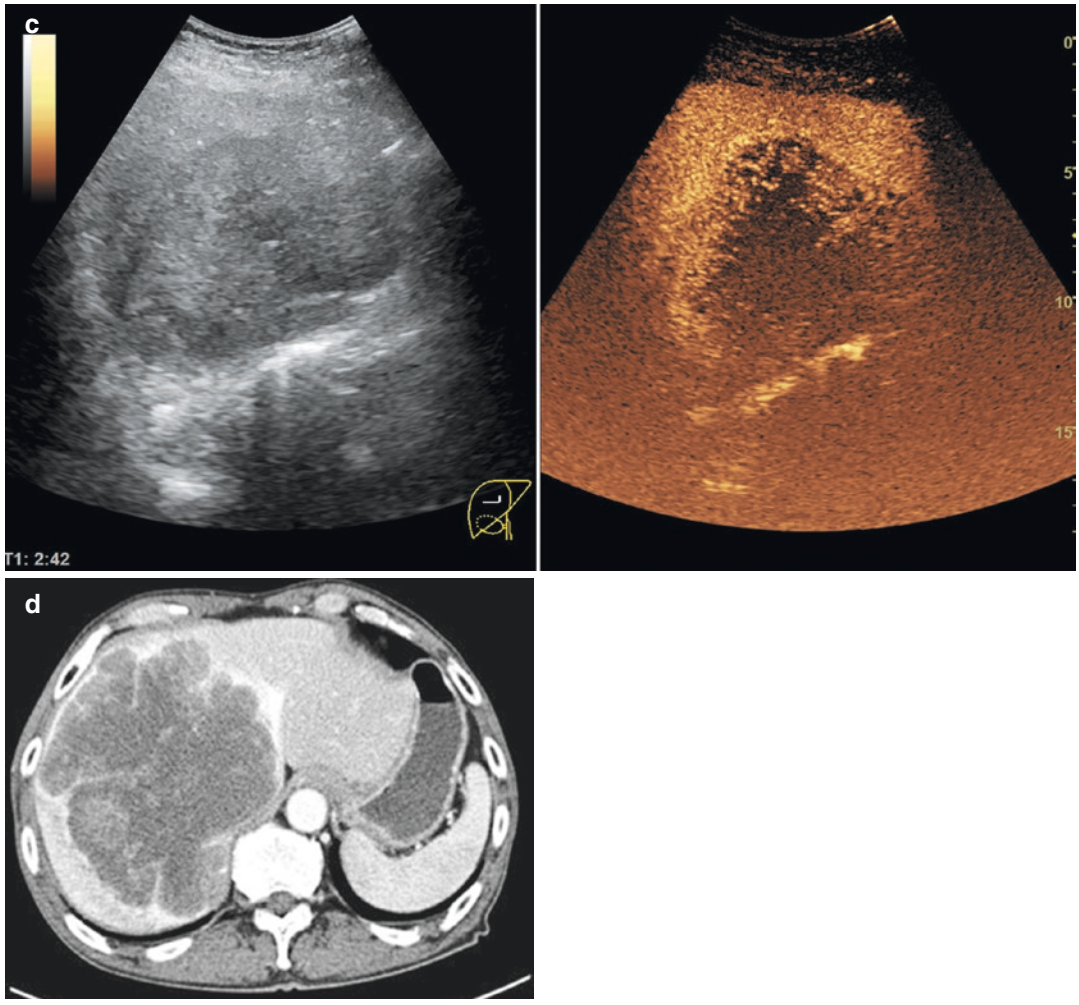

Fig. 4.15 (continued)

with mild and late (after 60 s) washout, and FLLs of ≥10 mm in size with arterial phase hyperenhancement and no washout of any type.

– CEUS LR-3 (intermediate probability of malignancy) category include any FLL without arterial phase hyperenhancement and no washout of any type; FLL smaller than 20 mm in size without arterial phase hyperenhancement with late and mild washout; small FLL (<10 mm) with arterial phase hyperenhancement and no washout of any type.

• CEUS LR-M (malignant FLL, not HCC) category includes the lesions with peripheral rim-shaped arterial phase hyperenhancement, or early (<60 s), or marked washout [73–75].

The CEUS LI-RADS algorithm has the sensitivity of 86%, specificity—96%, positive predictive value—98%, and negative predictive—73% [73, 76].

Cholangiocarcinoma represents the second most common primary liver tumor after hepatocellular carcinoma. Depending on the site of the tumor,

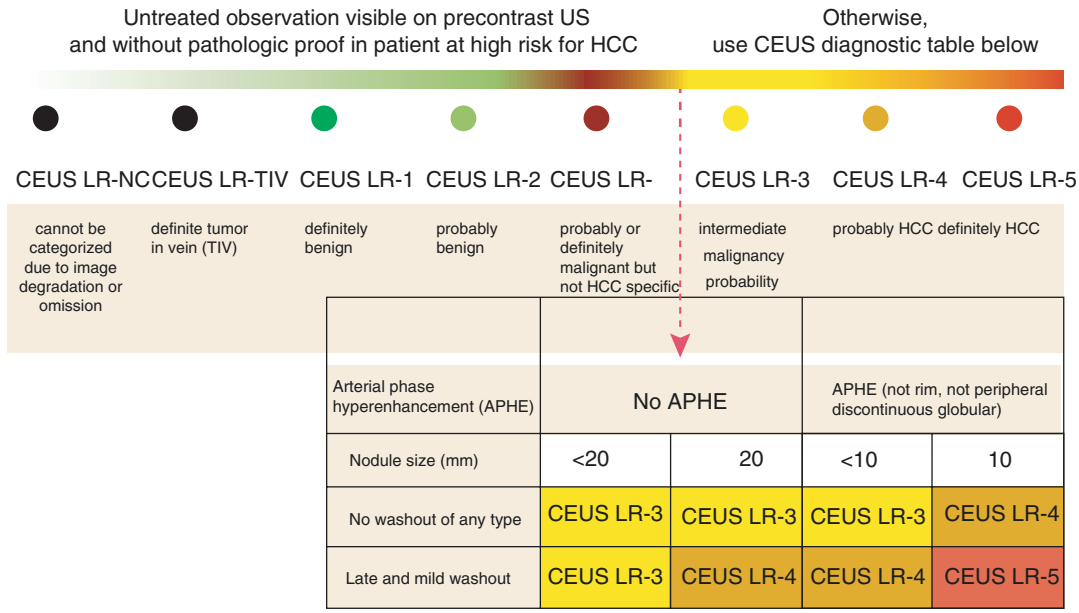

Fig. 4.16 CEUS-LIRADS algorithm. Scheme

intrahepatic (peripheral) and extrahepatic cholangiocarcinoma are specified, the latter subdivided into distal extrahepatic and perihilar (Klatskin tumor) [19]. Its imaging depends on the macroscopic type of the tumor, which in the case of intrahepatic cholangiocarcinoma can be mass-forming exophytic, periductal-infiltrating, or intraductal-polypoid, and mixed; and in the case of extrahepatic cholangiocarcinoma—sclerosing, periductal-infiltrating, nodular, and papillary [6, 77–79].

Cholangiocarcinoma of the nodular type often demonstrates heterogeneous peripheral rim-shaped hyperenhancement, less often—heterogeneous diffuse hyperenhancement, rarely—uniform hyperenhancement, sporadically—heterogeneous hypoenhancement [77, 80]. Infiltrating type cholangiocarcinoma usually exhibits heterogeneous arterial phase enhancement [79]. Intraductal-polypoid type is visualized as a mass with clear margins, local dilatation of bile ducts, and homogeneous hyperenhancement in the arterial phase [79]. Heterogeneity of contrast enhancement of cholangiocarcinoma depends on the prevalence of necrotic and fibrous areas within the tumor.

Cholangiocarcinoma has characteristic UCA washout in the portal venous and late phase, which usually starts earlier and is more expressed than in HCC [77–79] (Fig. 4.17). The degree of invasion in the periductal tissue and the true volume of the tumor is best determined in the portal venous and late phases. CEUS in the diagnosis of cholangiocarcinoma is not inferior to contrast-enhanced CT or MRI. UCAs are exclusively intravascular, which benefits for excellent identification of the washout effect. Contrast media for CT and MRI propagate into the fibrous stroma and accumulate in the extracellular interstitium of the tumor that makes washout less prominent [79].

Epithelioid hemangioendothelioma are rare liver vascular tumors of endothelial origin with intermediate malignant potential. The conventional US detects no specific features. Publications on CEUS in patients with these tumors are very rare and yet yielded to reveal no specific patterns of enhancement. However, being aware of possible patterns in hemangioendothelioma makes to expand the differential diagnostic row and avoid possible errors. Most hemangioendotheliomas

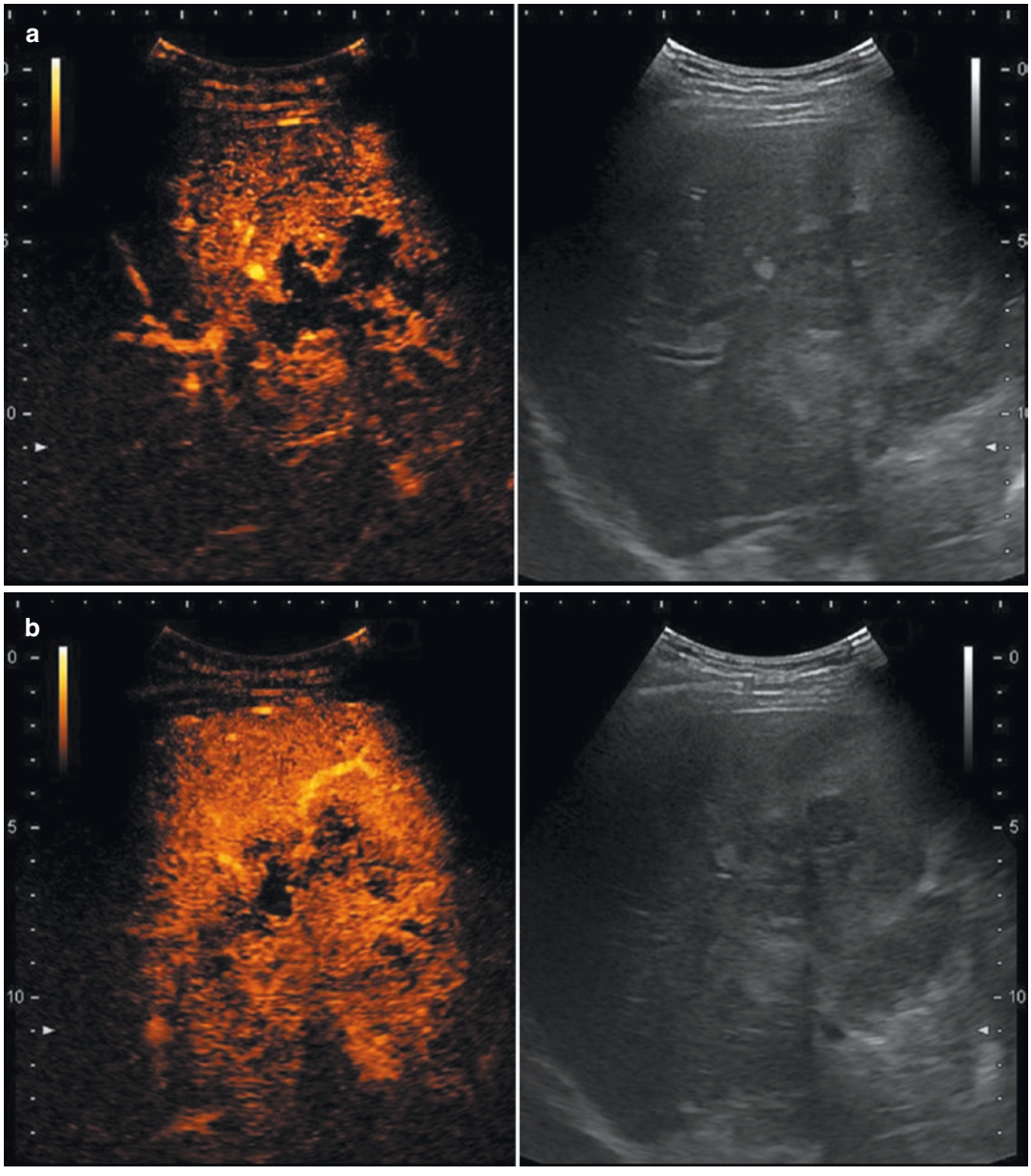

Fig. 4.17 Intrahepatic cholangiocarcinoma. CEUS images. (**a**) Heterogeneous contrast enhancement in the arterial phase. (**b**–**d**) Hypoenhancement in the portal venous and late phases

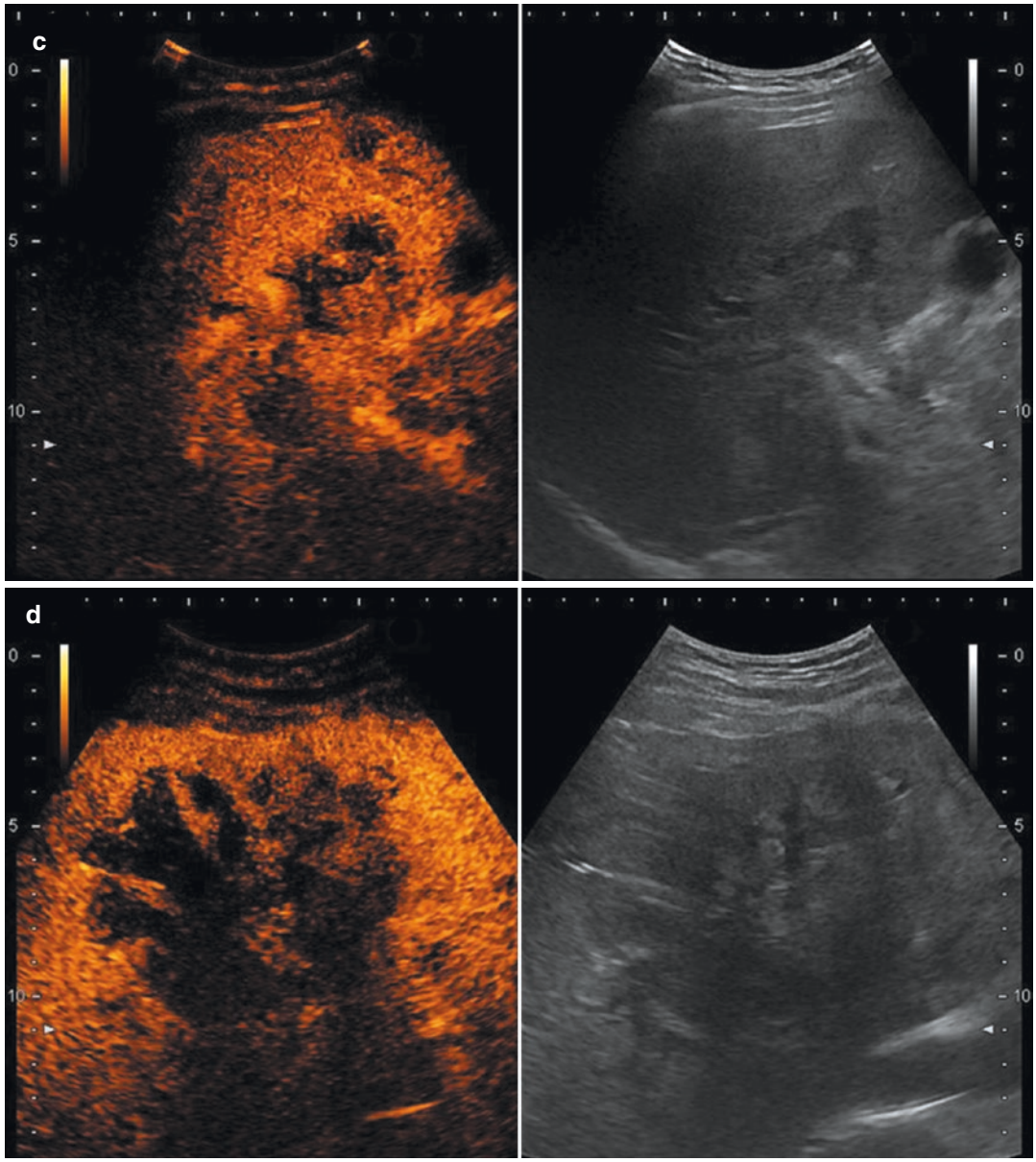

Fig. 4.17 (continued)

are characterized by peripheral rim-shaped contrast enhancement in the arterial phase that is similar to liver metastasis. The less common finding is heterogeneous hyperenhancement. All cases typically show rapid washout in the portal venous and late phase. Some studies report on individual cases of peripheral nodular contrast enhancement, which is typical for liver hemangioma. Possible malignant potential in these cases is suspected due to the above-mentioned washout features [81].

Liver lymphoma may have variable contrast enhancement in the arterial phase, but the characteristic washout in the portal venous and late phase suggests a malignant neoplasm [82].

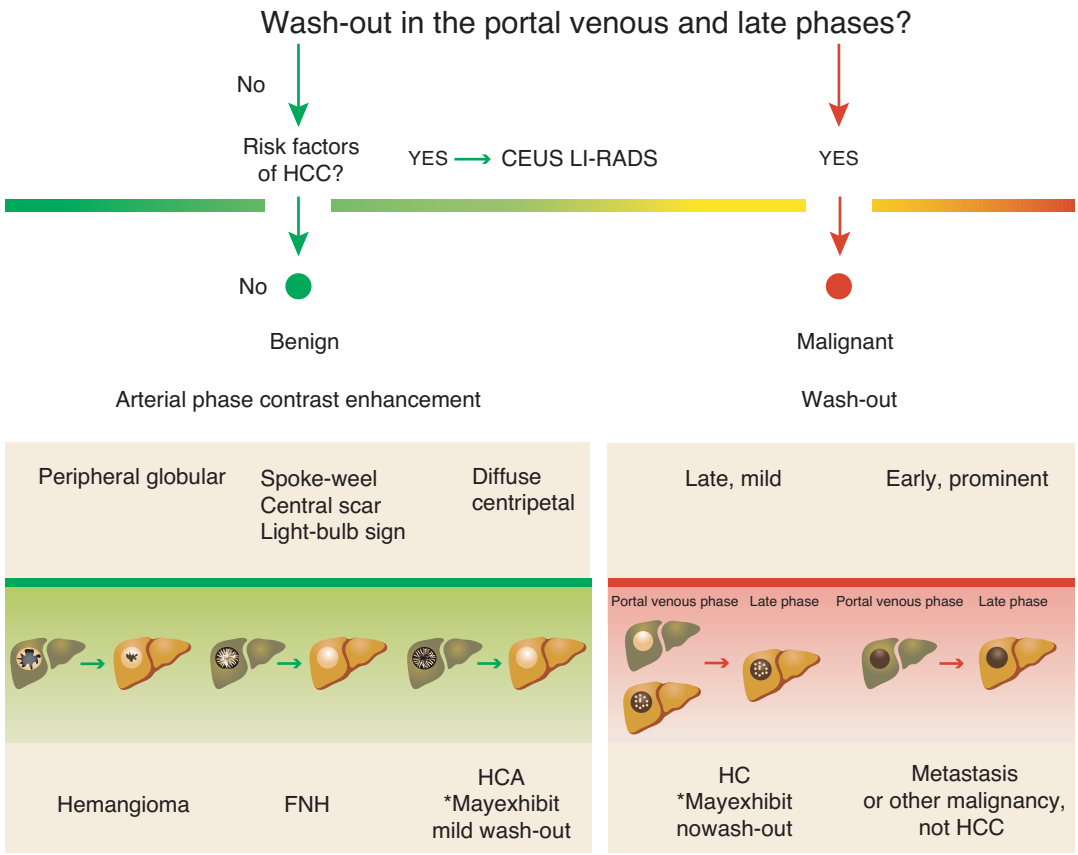

Fig. 4.18 Flowchart for evaluation of the qualitative parameters of CEUS for the most common FLL

Summarizing the written above, we offer the following flowchart for the differential diagnosis of the most common liver tumors (Fig. 4.18).

The use of the liver-specific UCA Sonazoid® in some cases increases the diagnostic accuracy of CEUS due to the evaluation of the post-vascular phase, which starts 10 min after the injection of UCA. Sonazoid interacts with the reticuloendothelial system and is absorbed by the Kupffer cells. Malignant FLLs lack Kupffer cells, so exhibit the enhancement defect in the post-vascular phase that differs them from liver parenchyma and most benign FLLs. To avoid unwanted destruction of UCA bubbles, it is recommended to scan for the first 30–60 s to assess the arterial and early portal venous phases, make a pause, and after 10 min start the scan again. This skips the late phase, which is considered less significant with Sonazoid. The duration of the post-vascular phase allows the careful examination of the entire volume of the liver. In the arterial, portal venous, and late phases, CEUS parameters are estimated the same way as with other second-generation UCAs. In the post-vascular phase, liver hemangioma is characterized by iso- or mild hypoenhancement, FNH—iso- or hyperenhancement, HCA—heterogeneous hypoenhancement. Malignant FLLs are usually nonenhancing or hypoenhancing as compared with the enhanced liver parenchyma background. The exceptions can be well-differentiated HCC and infiltrative type HCC [3, 29].

Screening CEUS can be used for liver metastases detection as part of a multimodality imaging approach in patients with a known malignant

neoplasm. Early detection of liver metastases is important for the specification of the stage of the disease and further management, which is crucial for the patient's survival. One drawback of conventional US is low sensitivity in the identification of small and isoechoic metastases, especially in deep location or diffuse liver changes [9]. The pronounced and early washout in the portal venous phase is characteristic of liver metastases and permits utilization of CEUS for their detection.

The study should begin with B-mode for preliminary assessment of the liver with possible detection of suspicious lesions, cysts, hemangiomas, fat deposits, etc. [61]. To detect liver metastases, follow the standard CEUS protocol. The most informative phase is the portal venous phase. The metastases appear prominently hypoenhanced on the background of the hyperenhanced liver parenchyma that resembles the perforation phenomenon [83] (Figs. 4.19 and 4.20, Videos 4.10, 4.11, and 4.12).

All liver segments are sequentially scanned and cine loop recorded in the portal venous phase. About half of all metastases are located within 1 cm from the capsule, therefore, careful scanning of the peripheral and subcapsular liver areas is important [6]. A thorough study of the entire liver is best achieved in the patient's position on the left side [21]. The left liver lobe is better scanned when the patient is lying on the back. However, taking into account the study time, which is limited by the circulation of UCA in the bloodstream (about 5 min), changing position may be inappropriate in immobile patients. The scanning of the entire volume of the liver is also necessary when the assigned for differential diagnosis FLL exhibits washout. It permits the detection of additional foci at one UCA introduction.

In some dubious cases, the detection of a perfusion defect may require re-administration of UCA for re-assessment of the arterial phase. In particular, if the lesion appeared undetected with the grayscale US, it is necessary to re-introduce the UCA without waiting for the elimination of all microbubbles in the scanning range. However, in our experience, UCA re-administration is appropriate only in the late phase when the liver parenchyma enhancement decreases, but the lesion remains visible.

Many authors reported that CEUS significantly increases the sensitivity of ultrasound in the detection of liver metastases. Piscaglia et al. [84] using intraoperative US, CT, and MRI as reference methods demonstrated the increase in sensitivity of conventional US from 77% to 95% if contrast enhancement is used. Cantisani et al. [85] reported the corresponding increase from 71.6% to 95.8% if referred to CT and MRI.

Difficulties in the detection of FLL are often caused by diffuse liver changes. Several publications show that contrast enhancement is not able to compensate for the attenuation of the echo signal in the fatty liver. However, there was a study by Bartolotta et al. [60] that included 37 patients with focal fatty liver and no lesions detected with the routine US. CEUS revealed liver metastases of 5–10 mm in size in 10.8% of these patients. They used CE-MRI as a reference method and reported the sensitivity of CEUS of 100%. The possibilities of identification of benign FLL and HCC are limited to the duration of the arterial phase and the isoenhancement of tumors in the portal venous and late phases.

4.2 Non-neoplastic Liver Lesions

In some cases, routine US experiences difficulties in the diagnosis of non-neoplastic FLLs, such as various cysts, focal fatty liver deposition or sparing, etc.

Most liver cysts are asymptomatic and incidentally detected. Conditionally, liver cysts can be classified into simple and complex, as well as true and false. True cysts have epithelial lining and are congenital. They confer simple, retention, dermoid cysts, multi-chamber cystadenoma, and so on. False cysts arise as a result of operations, injuries, or inflammation. Their walls consist of fibrous connective tissue. Primary cystic liver tumors (cystadenoma and cystadenocarcinoma) are rare entities. Parasitic cysts within the liver are considered separately.

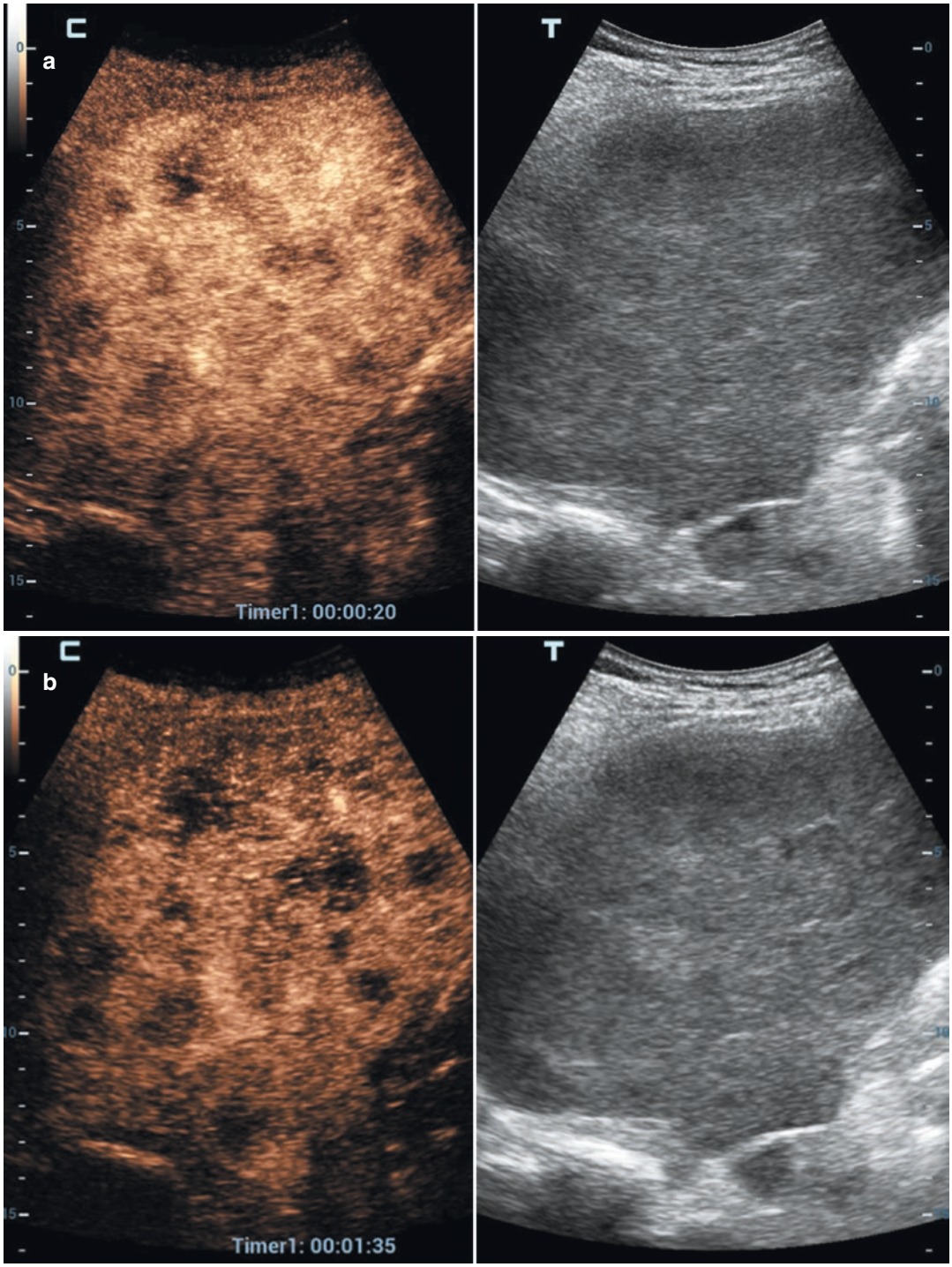

Fig. 4.19 Multiple liver metastases. (**a**) Patient A. Arterial phase CEUS image. (**b**) Patient A. Portal venous phase image. (**c**) Patient B. Portal venous phase image. (**d**) Patient B. Late phase image

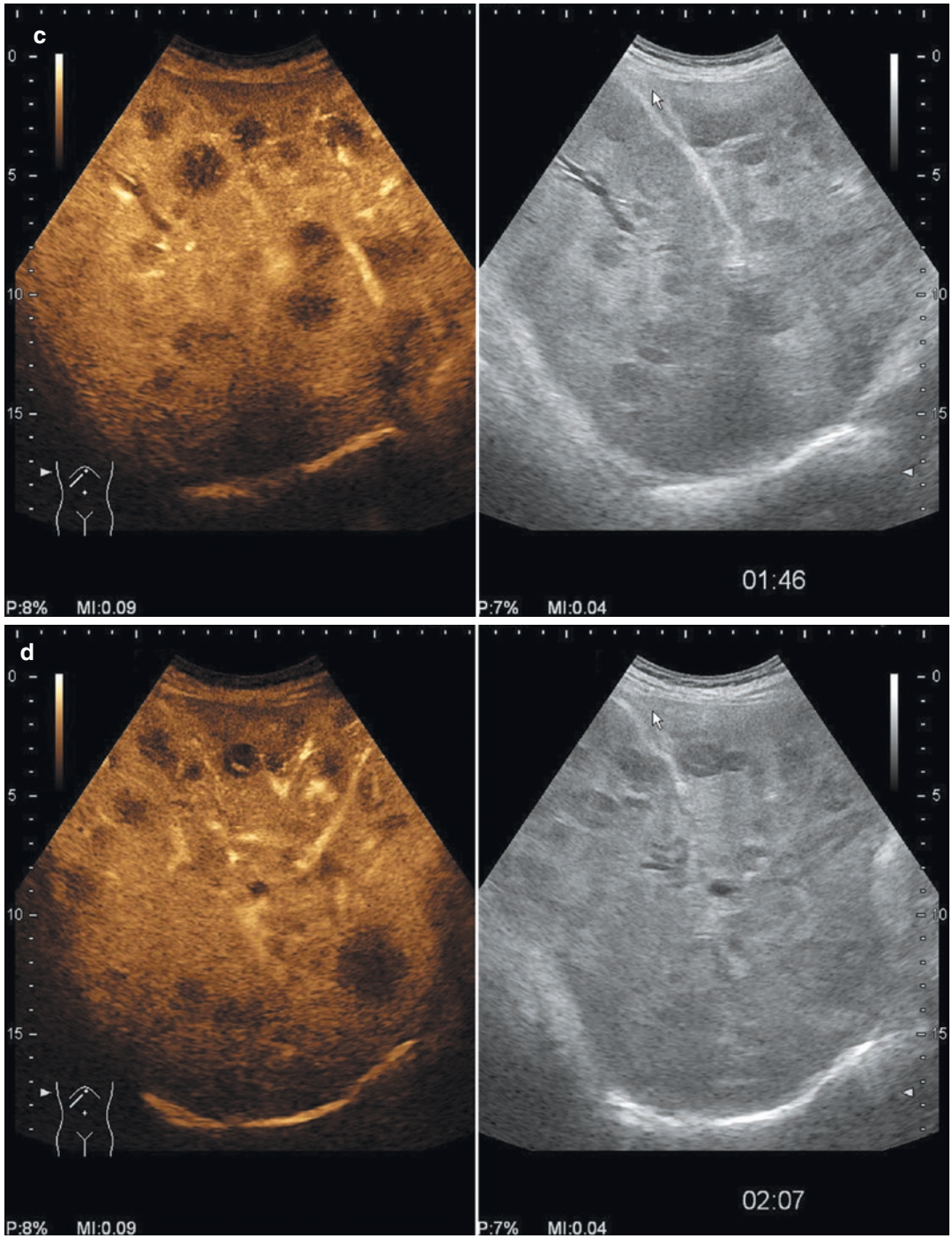

Fig. 4.19 (continued)

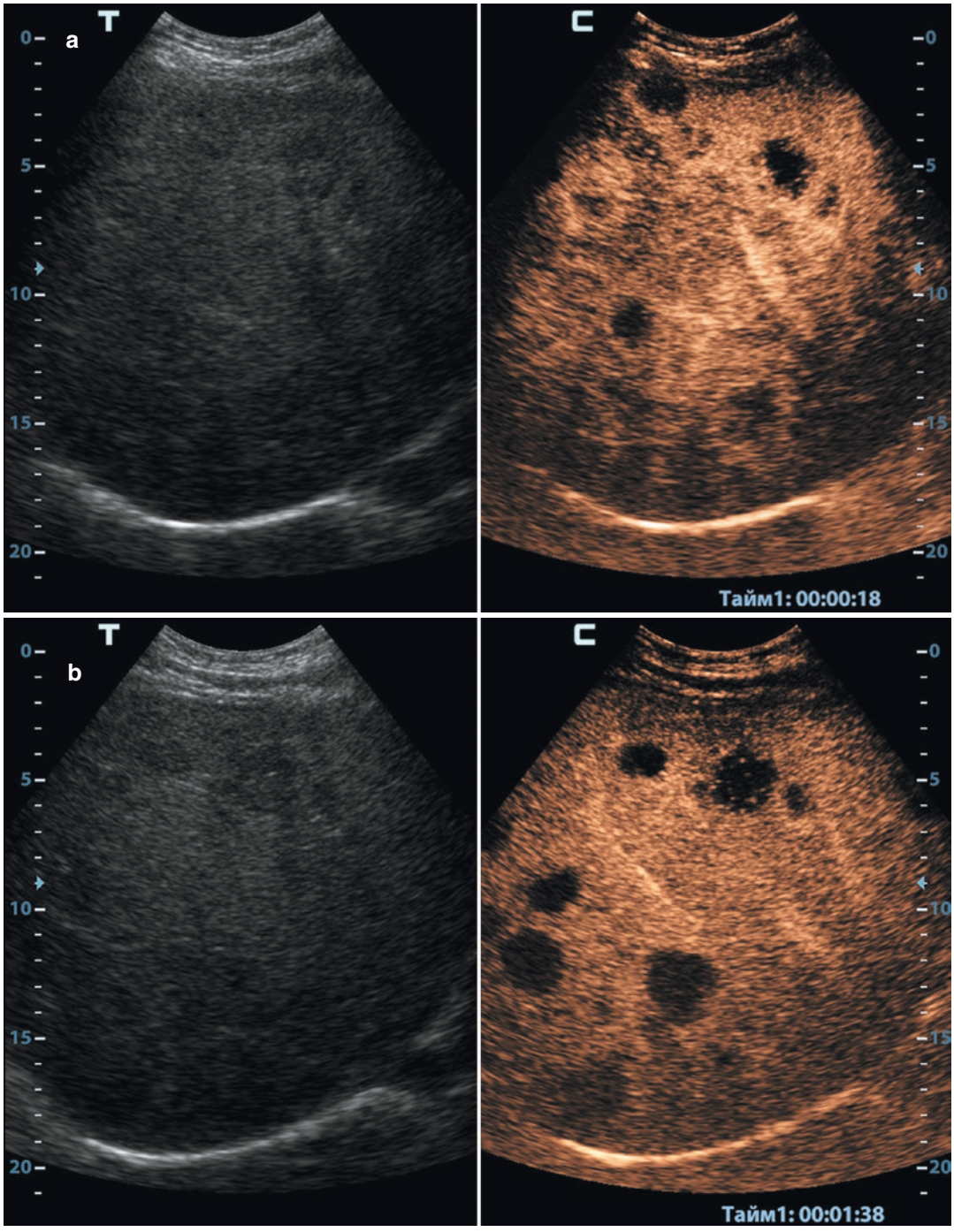

Fig. 4.20 Multiple liver metastases. (**a**) Arterial phase CEUS image. (**b**) Portal venous phase CEUS image

Liver cysts with CEUS are visualized as nonenhancing areas in all vascular phases with clear smooth boundaries. There is no contrast enhancement of internal septations or inner echogenic contents, which is often a consequence of hemorrhage [27] (Fig. 4.21).

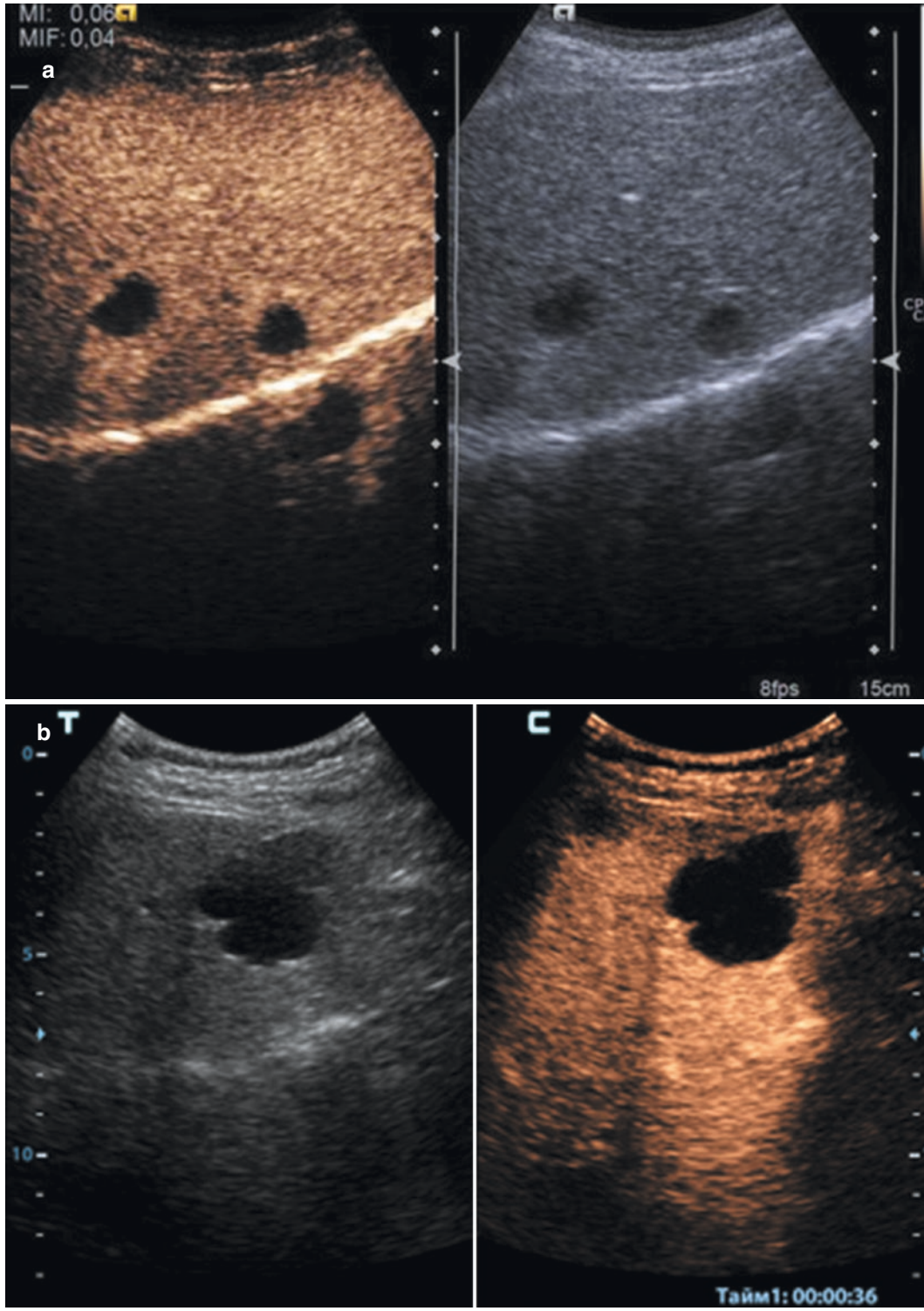

Fig. 4.21 Simple liver cysts. No contrast enhancement of inner contents, septations, or walls is registered. (**a**) Patient A. CEUS image. (**b**) Patient B. CEUS image. (**c**) Patient B. CE-CT. (**d**) Patient C. CEUS image. (**e**) Patient C. CE-CT

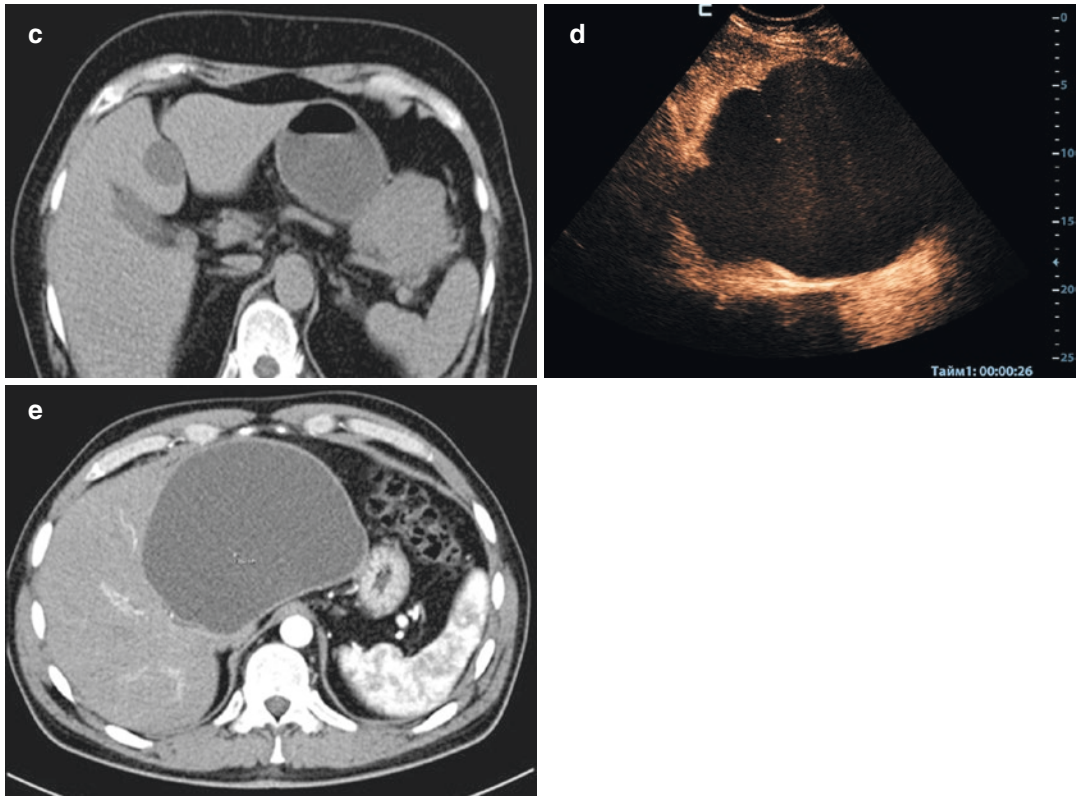

Fig. 4.21 (continued)

Differential diagnosis of cystadenoma and cystadenocarcinoma is based on the detection of contrast enhancement of septa or mural components. The sensitivity of CEUS in the detection of septal perfusion is reported higher than of CT or MRI. The washout phenomenon in the solid component of such cysts is thought more characteristic of malignant lesions [86]. However, the reliable criteria for the differential diagnosis of cystadenoma and cystadenocarcinoma with CEUS are not reported [87, 88].

Regenerative and dysplastic nodules exhibit simultaneous or slightly slowish contrast enhancement in the arterial phase remaining the same intensity as the liver parenchyma with no washout. Sometimes it is possible to note minimal arterial phase hypoenhancement followed by the persistent isoenhancing status. However, hyperenhancing areas in a dysplastic nodule may be the sign of emerging HCC. Approximately one-third of dysplastic nodules demonstrate mild washout, which significantly complicates the differential diagnosis.

Focal fatty liver does not change liver perfusion and CEUS reveals that these lesions are identical to the surrounding normal liver parenchyma in all vascular phases.

Liver abscess image with CEUS depends on the process stage. UCAs permit easy identification of any avascular areas, which correspond to necrosis or fluid collections. Therefore, CEUS is utilized to specify the abscess structure when the conventional US fails to differentiate the abscess components.

CEUS at the initial stage of liver abscess demonstrates a hyperenhanced area of inflammation. The appearance of small nonenhancing inclusions in hyperenhanced parenchyma a sign of the further progression of the disease

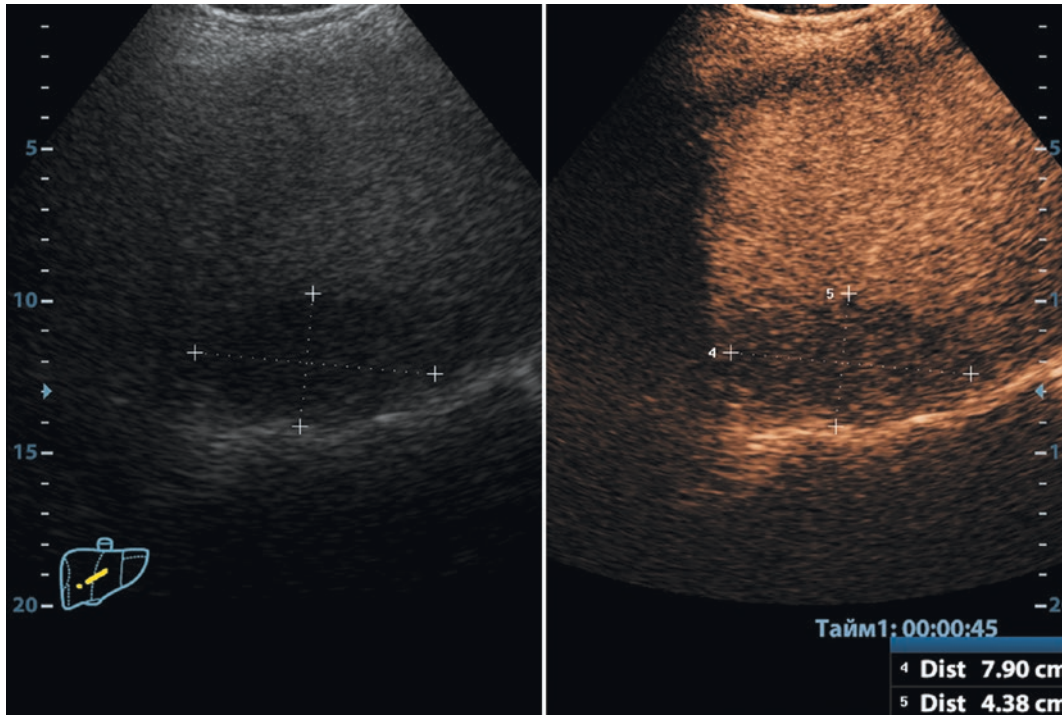

Fig. 4.22 Local liver changes as the outcome of the liver abscesses. Hypoenhancing area in the portal venous phase. CEUS image

and corresponds to focal necrosis. The abscess at this stage may resemble a honeycomb pattern. The layers of the parenchyma between such areas are usually hyperenhanced in the arterial phase. In some cases, washout in the late phase may be registered due to inflammatory hyperemia and possible thrombosis of small branches of the portal and/or hepatic veins. With further abscess development, non-enhancing necrotic areas increase in volume, and the intensity of contrast enhancement of viable tissues reduces. There remains the peripheral rim-shape hyperenhancement, which corresponds to the circumscribing zone of inflammatory hyperemia. The washout phenomenon complicates the differential diagnosis of the liver abscess and malignant FLL with necrosis [89, 90].

Effective treatment leads to local fibrous changes of liver parenchyma in the place of the former abscess, which arise in 1–2 months after the disease onset (Fig. 4.22). These areas are hypoenhancing in all vascular phases.

Parasitic liver lesions are commonly represented by echinococcosis. The two main types of the disease are cystic (unilocular) echinococcosis and alveolar echinococcosis. The single parasitic cyst is usually large, contains multiple septa and chambers with echogenic content, which demands differential diagnosis with a liver tumor. CEUS demonstrates the avascularity of the cystic content (Fig. 4.23). However, hyperenhancement of the liver parenchyma around the cyst is often observed, which is a consequence of inflammatory hyperemia [91].

Alveolar (multilocular) echinococcosis with conventional B-mode US looks like a solid lesion of different echogenicities. CEUS can determine peripheral rim-shaped contrast enhancement with the absent central enhancement that is typical for lesions smaller than 3 cm in size. Alternatively, hypoenhancement in all phases with washout in the late phase may be registered, which may resemble a malignant tumor. The image of alveolar echinococcosis with CEUS depends on the lesion size [29].

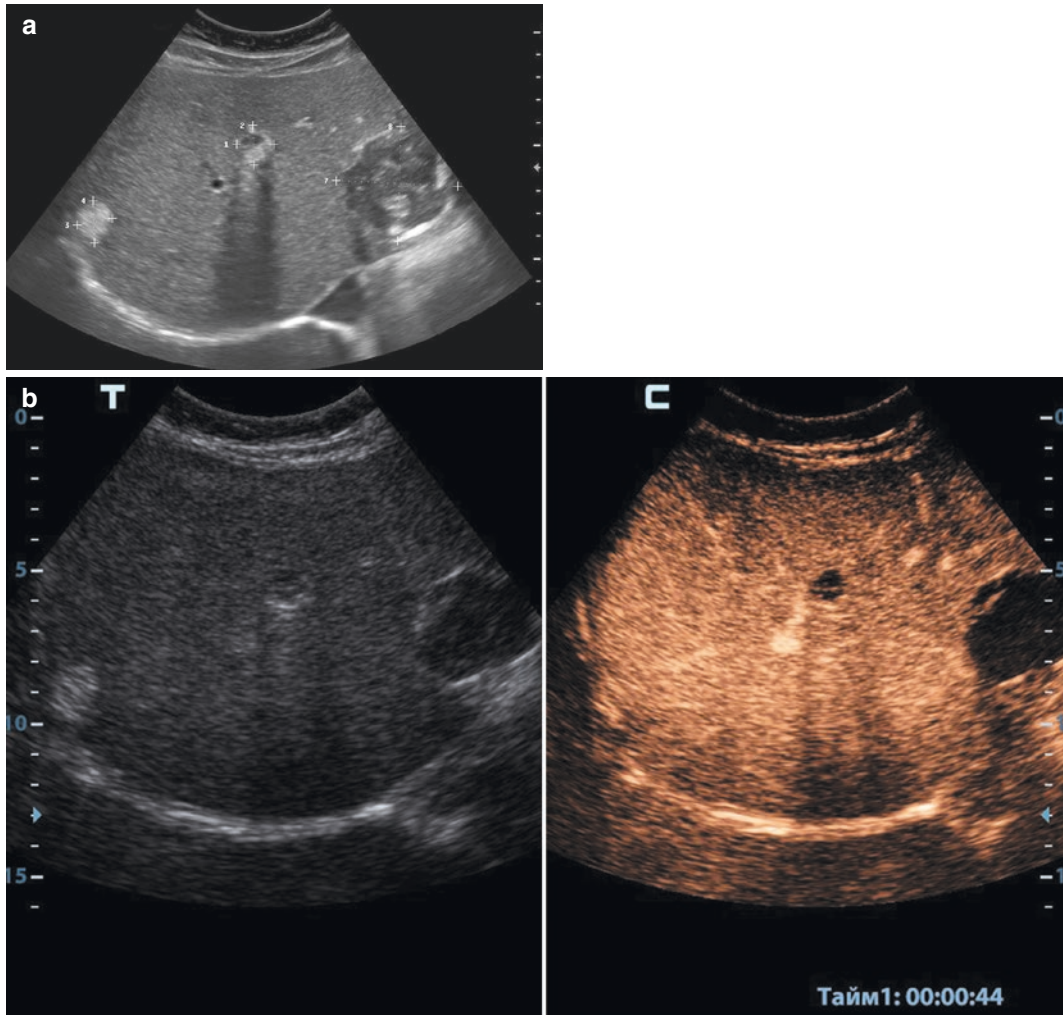

Fig. 4.23 Cystic echinococcosis of the liver. (**a**) Echogenic cystic contents with the grayscale US. (**b**) No contrast enhancement of the cyst with CEUS

4.3 Quantitative Analysis of CEUS Data in Differential Diagnosis of Focal Liver Lesions

CEUS demonstrates excellent diagnostic accuracy if typical enhancement patterns of FLL are detected. In their absence, the sensitivity and specificity of the study decrease. Therefore, the search for additional differential diagnostic criteria continues [27]. The use of quantitative analysis demonstrates a certain potential, allowing objective characterization of the washin, distribution, and washout of UCAs. Currently, there are no recommendations on the threshold values for the diagnosis of various types of liver tumors. This is primarily due to the small number of studies, lack of standardization of the quantitative analysis, and differences in processing and displaying the analyzed data on scanners of different manufacturers. However, the existing studies report some indicators characteristic of various types of tumors.

In a dubious case of a liver cyst, quantitative analysis of CEUS data permits reliable confirmation of the absence of contrast enhancement of the walls and contents of the cystic cavity.

Table 4.1 Quantitative values of TIC for groups and various types of FLL

Type of lesion	AT, s	TTP, s	PI, dB	AS, dB/s	DT/2, s	DS, dB/s
Malignant FLLs[a]	12.68 ± 2.95	24.32 ± 5.67	33.38 ± 2.57	0.95 ± 0.38	79.76 ± 25.84	0.64 ± 0.13
	7.2–19.2	15.1–37.4	27.2–36.6	0.35–1.94	50.69–145.30	0.04–0.31
Benign FLLs[a]	12.32 ± 3.14	35.91 ± 17.86	35.11 ± 3.55	0.71 ± 0.36	180.20 ± 24.44	0.02 ± 0.01
	6.82–21.15	15.17–69.25	24.2–39.2	0.18–1.37	127.44–230.7	0.01–0.04
HCC[b]	14.4 ± 3.1	27.20 ± 3.41	34.22 ± 1.93	0.67 ± 0.17	107.36 ± 17.38	0.07 ± 0.08
	10.39–18.63	22.32–31.58	31.48–36.46	0.39–0.84	90.54–133.76	0.05–0.09
Metastases[b]	11.57 ± 2.34	23.18 ± 6.36	33.15 ± 2.95	1.13 ± 0.38	62.19 ± 8.83	0.16 ± 0.06
	8.06–14.29	15.68–29.34	28.27–36.19	0.73–1.65	52.15–76.71	0.1–0.22
Hemangioma[b]	13.7 ± 3.4	54.61 ± 12.05	32.94 ± 4.17	0.41 ± 16.3	188.42 ± 20.11	0.02 ± 0.01
	10.1–17.6	37.8–68.7	27.10–37.54	0.21–0.66	161.61–209.57	0.01–0.03
FNH[b]	10.8 ± 2.53	23.4 ± 4.3	37.77 ± 1.70	0.84 ± 0.27	186.40 ± 28.95	0.02 ± 0.01
	7.2–13.4	16.39–27.52	34.93–39.18	0.57–1.27	163.22–230.70	0.01–0.03
HCA[b]	11.6 ± 2.5	22.07 ± 2.28	35.23 ± 1.78	0.97 ± 0.35	163.74 ± 18.91	0.03 ± 0.02
	8.8–15.7	18.95–25.40	33.37–38.06	0.49–1.37	5.91–186.11	0.01–0.05

AT arrival time, *TTP* time to peak, *PI* peak intensity, *AS* ascending slope (washin rate), *DT/2* descending time/2 (half-time of washout), *DS* descending slope (washout rate)
[a] Represented as Mean ± SD and 2.5–97.5 percentile
[b] Represented as Mean ± SD and 10–90 percentile

Benign liver tumors are characterized by stable contrast enhancement in the portal venous and late phase, which is distinctive from malignant tumors and can be confirmed quantitatively.

Malignant tumors show faster washout (M ± sd 65.1 ± 36.7 s) as compared with benign FLL (87.0 ± 36.1 s) [92]. In our study [20], malignant tumors demonstrated a smaller half washout time and a higher washout rate (Table 4.1). The threshold values obtained for malignant FLLs were characterized by sensitivity, specificity, and AUC for DT/2 ≤ 147.97—100%, 93.1%, and 0.996, and for washout rate (DS) ≤−0.060 dB/s—95.7%, 96.6%, and 0.997, respectively. HCC exhibited a later washout than compared with the liver metastases (Table 4.1). For the diagnosis of liver metastases, the DT/2 threshold value of ≤82.34 demonstrated the sensitivity and specificity of 100%, AUC 1.000; DS > 0.090 dB/s—the sensitivity of 94.7% and specificity of 100%, AUC 0.992.

Liver hemangiomas typically demonstrate gradual fill-in with UCA. This fact leads to elongated time to peak intensity (TTP) and lower washin rate (AS), which distinguishes hemangioma from other liver tumors with faster fill-in. For liver hemangioma, the threshold value of TTP ≥ 32.62 s yields the sensitivity of 97.5%, specificity of 100%, AUC—0.998; and in AS < 0.670 dB/s the sensitivity was 77.5%, specificity—100%, AUC—0,934. The threshold value of TTP 27.6 s enabled differentiation of hemangioma from other benign liver tumors with the sensitivity of 100%, specificity of 100%, AUC—1,000. Additionally, liver hemangiomas have lower peak intensity (PI) and longer half-time of washout (DT/2) as compared to FNH and HCA but the diagnostic value of these indicators is quite low. In the study [93] hemangiomas were associated with TTP > 37.75 s, and the minimum TTP values were registered in FNH and HCC.

Hepatic FNH is characterized by the pronounced arterial phase hyperenhancement that quantitatively corresponds to high peak intensity. Higher intensity maximum values (IMAX) in FNH ($p < 0.014$) as compared with HCC were reported [94]. With the threshold value of IMAX > 103.55%, the sensitivity was 90.9%, specificity—43.5%, AUC—0,680. We also obtained reliable differences of FNH based on this parameter, but the greatest differences were registered between FNH and other benign liver tumors. The threshold value of PI ≥ 36.280 dB demonstrated the sensitivity of 81.80%, specificity—87.50%, AUC—0.895 [20].

The greatest difficulties are caused by a hepatocellular adenoma, which exhibits arterial phase hyperenhancement and can demonstrate mild late washout in the late phase. Quantitative analysis revealed that HCA has the smallest figures of the half-time of washout (DT/2) in the group of benign liver tumors. This parameter is also significantly different from HCC, the latter having the reliably lower DT/2 (Table 4.1, Fig. 4.24).

Experimental data obtained in some studies suggest the diagnostic potential of quantitative analysis of CEUS data in the differential diagnostics of FLL. It supplies more objective and reproducible data, quantitatively evaluates tumor perfusion, which is successfully used in the assessment of the response to therapy. Some authors report the possible application of quantitative analysis for the prediction of the tumor response. Although the quantitative analysis of CEUS is not included in official guidelines and recommendations, the literature data created the background for further research and standardization of the protocols.

4.4 Diffuse Liver Disorders

Chronic diffuse liver diseases along with FLL are reported to benefit from CEUS. Depending on the stage, some of them are associated with characteristic changes in hepatic blood flow. Hemodynamic disturbances were assessed with Doppler imaging, studied in early publications with Levovist [95], and may be verified with quantitative analysis of CEUS.

Liver cirrhosis may be accompanied by the increased cardiac output, reduced peripheral vascular resistance, pulmonary arteriovenous shunts, portosystemic venous shunts, intrahepatic shunts between hepatic artery, portal, or hepatic veins, and arterialization of the hepatic capillary bed. It leads to the earlier arrival of the UCA bolus introduced into a peripheral vein [96].

In clinical practice, for the non-invasive diagnosis of liver cirrhosis, the definition of the time necessary for the UCA to arrive in hepatic veins (HVAT, Hepatic Vein Arrival Time) is most widely used. The study is typically conducted after night starvation with the position of the abdominal convex probe in the right intercostal spaces to visualize the right or middle hepatic vein. The original image of the hepatic vein is recorded for 10 s, then 2.4 mL of SonoVue® is introduced into the peripheral vein followed by 5 mL saline flush. The cine loop of the hepatic vein is recorded for 60 s after the UCA injection. In 5 s after UCA administration, the patient is asked to exhale and hold the breath for 20 s. To obtain the necessary TICs, position ROI in the hepatic vein of the first or second generation at the distance of 3–5 cm from the inferior vena cava (IVC). The highest TIC value during the first 10 s before the introduction of UCA is accepted for the original intensity. The HVAT is defined as the interval between the UCA administration and the moment of a 10% increase in the intensity on the TIC [97, 98].

Kim et al. [99] published the data of meta-analysis of 12 studies with 844 patients. They compared HVAT with the histopathology of the liver biopsy and reported the total sensitivity of HVAT for the diagnosis of liver cirrhosis of 0.83 (95%CI 0.77–0.89), specificity—0.75 (95%CI 0.69–0.79), PPV—3.45 (95%CI 1.60–7.43), and NPV—0.28 (95%CI 0.10–0.74). Additionally, they revealed a significant decrease in the HVAT ($p < 0.05$) in patients with liver fibrosis (Mean ± SD—25.01 ± 5.46 s) and cirrhosis (17.62 ± 3.57 s) compared with the group of healthy persons (34.63 ± 10.27 s). However, it should be noted that the studies in meta-analysis used different techniques (Doppler and contrast-specific) and different UCAs (Levovist and SonoVue®). The study [100] revealed the decrease in HVAT in patients with chronic hepatitis C that corresponded with the severity of liver fibrosis in both Levovist and SonoVue®. Mean HVTTs with SonoVue® in control, mild hepatitis, moderate or severe hepatitis, and cirrhosis groups were 38.3 s, 47.5 s, 29.5 s, and 17.6 s, respectively, with Levovist and 29.4 s, 27.4 s, 22.9 s, and 16.4 s, respectively. There was no significant difference in HVTT between mild and moderate hepatitis groups with SonoVue®; however, there were sig-

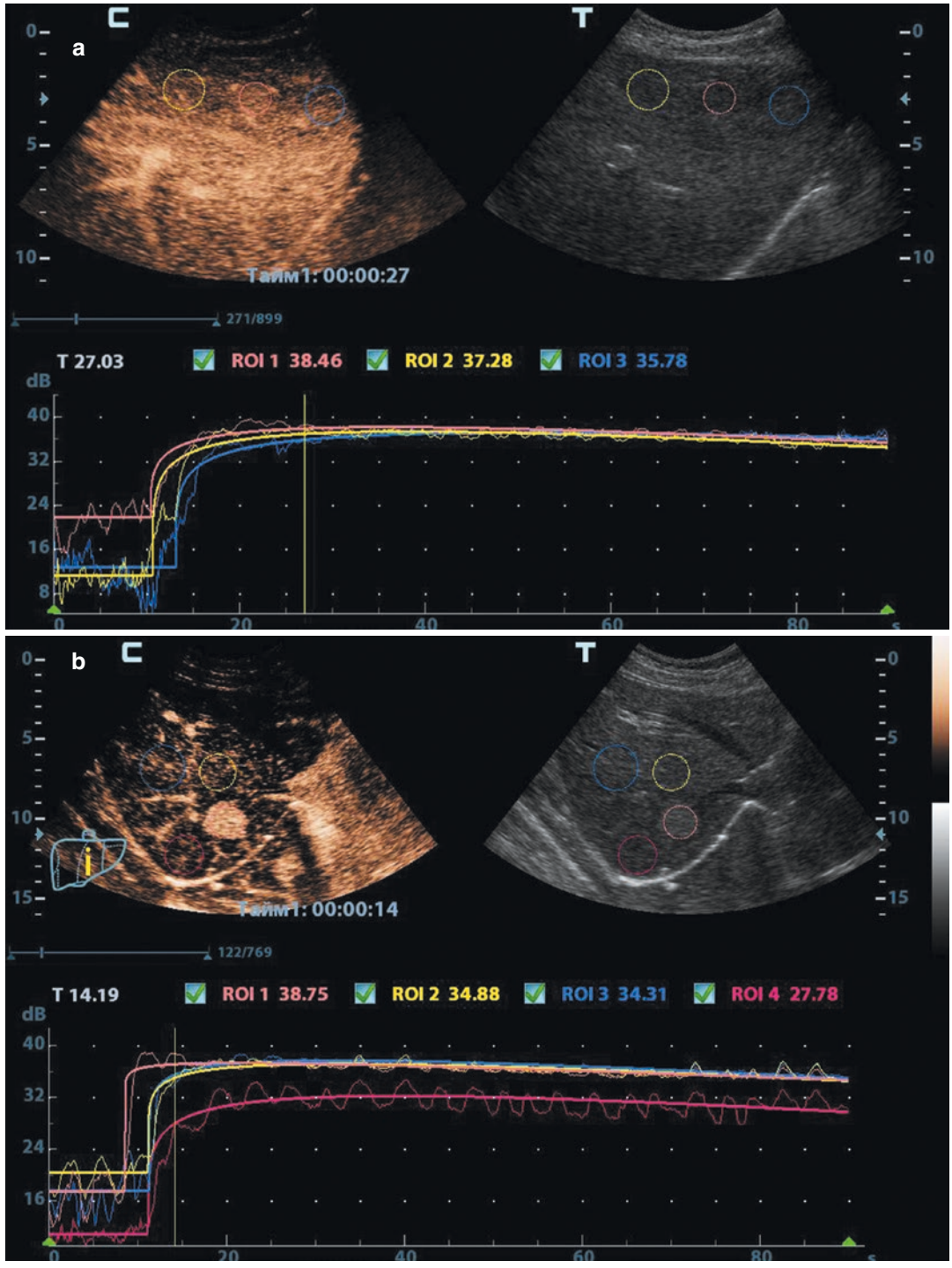

Fig. 4.24 Quantitative analysis of CEUS TICs. (**a**) Normal liver parenchyma, all ROIs. (**b**) FNH, ROI 1. (**c**) HCC, ROI 1. (**d**) Liver metastasis. (**e**) Liver cyst, ROI 1. (**f**) Hemangioma, ROI 1. In all images ROI 2, 3, and 4 correspond to the surrounding normal liver parenchyma

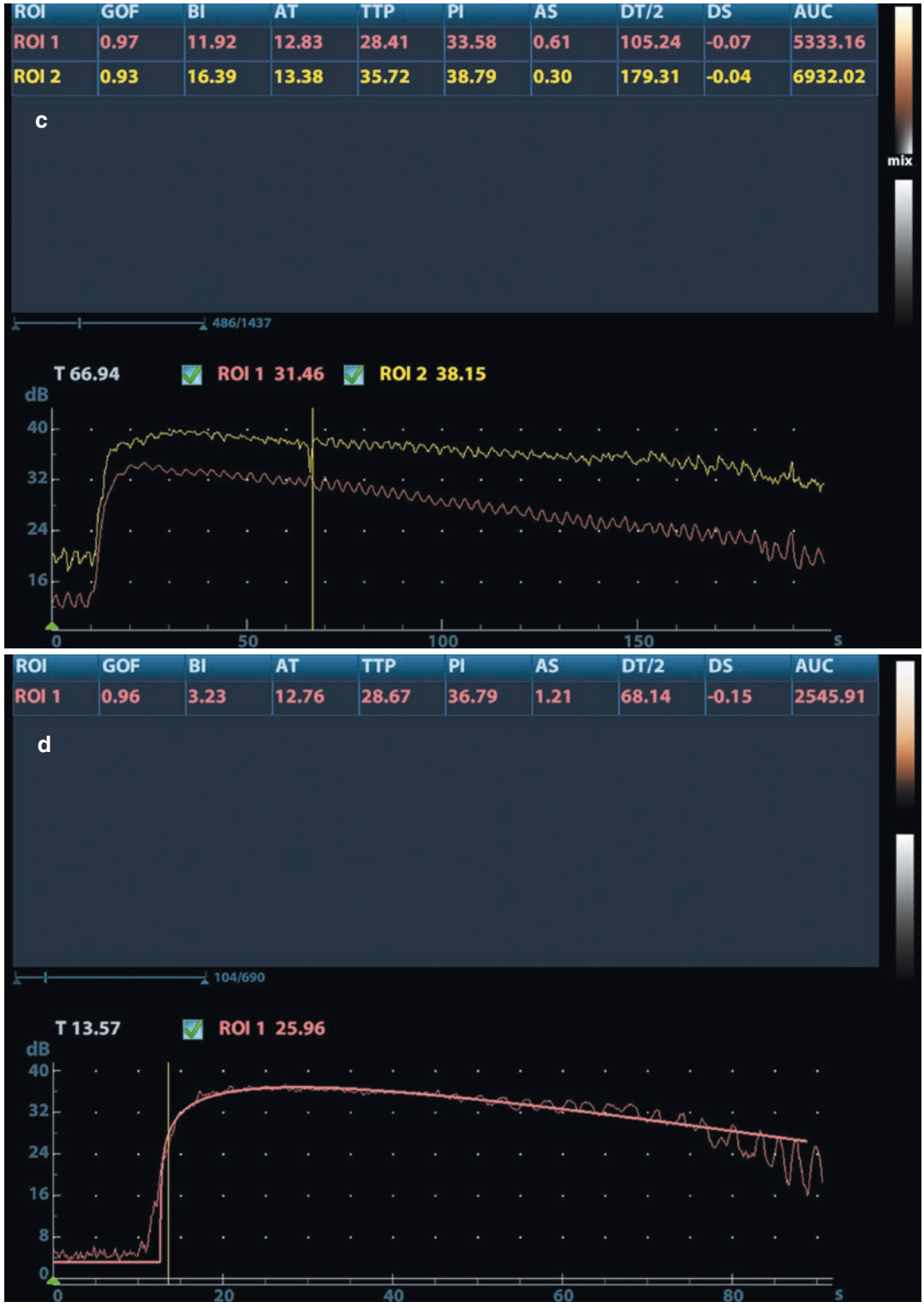

Fig. 4.24 (continued)

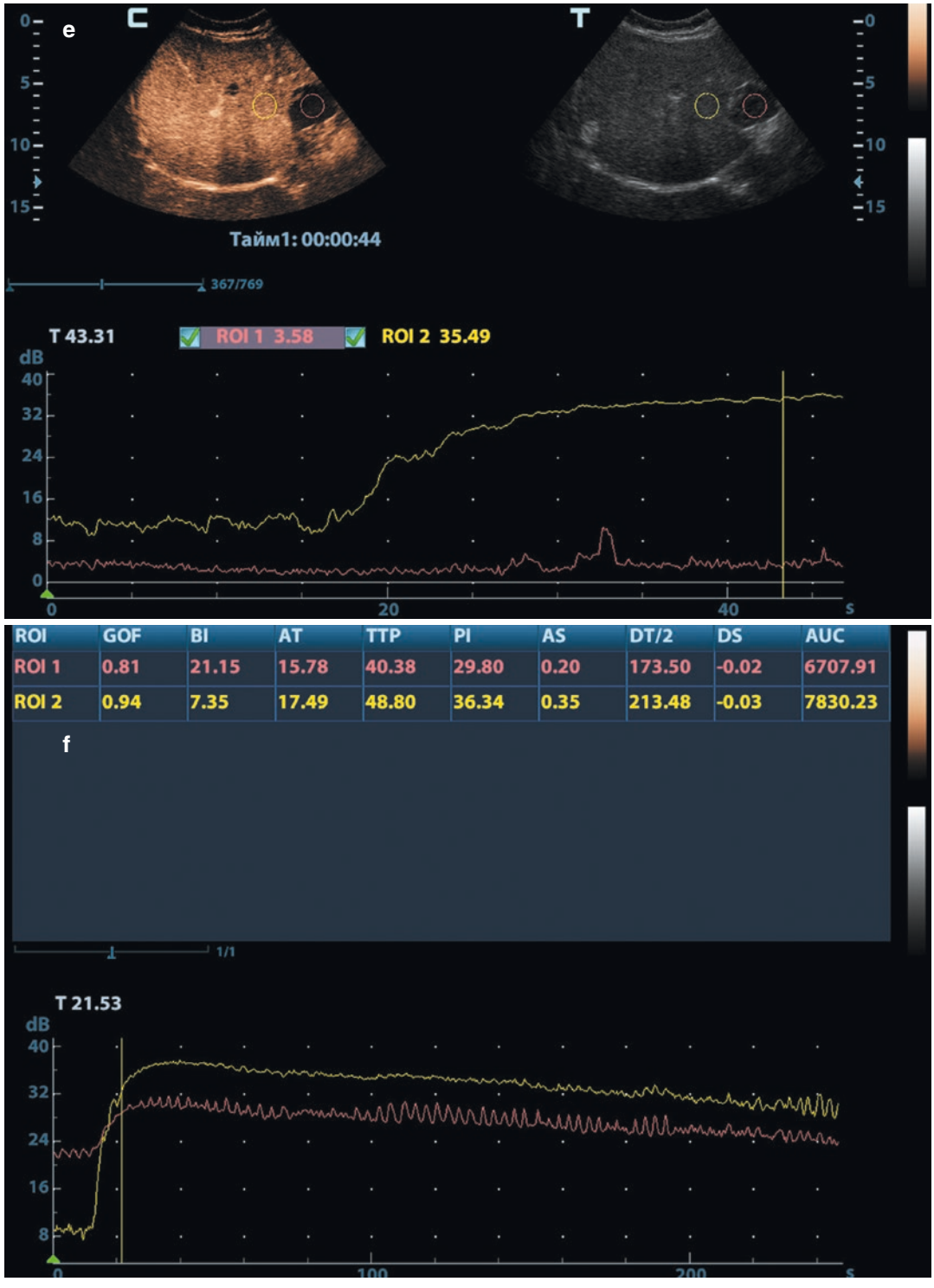

Fig. 4.24 (continued)

Table 4.2 HVAT values at various stages of liver fibrosis in different studies

Author, study	UCA	No fibrosis	Mild or moderate fibrosis	Cirrhosis
Abbattista et al. (2008) [102]	SonoVue	24.9 ± 4.4	21.7 ± 3.5	14.0 ± 2.5
Albrecht et al. (1999) [95]	Levovist	49.8 ± 22.6	35.8 ± 9.9	18.3 ± 3.0
Lim et al. (2006) [100]	Levovist	38.3 ± 2.4	47.5 ± 6.5/29.5 ± 10.8	17.6 ± 5.0
Lim et al. (2011) [103]	Levovist	33.8 ± 3.8	29.7 ± 2.2	15.8 ± 0.9
Lim et al. (2006) [100]	SonoVue	29.4 ± 6.9	27.4 ± 9.3/25.2 ± 7.0	16.4 ± 4.9
Ridolfi et al. (2007) [101]	SonoVue	24.8 ± 4.4	22.1 ± 3.4	14.3 ± 2.1

nificant differences in HVTT between all patient groups with Levovist.

The values of HVAT ≤ 17 s were reported to correspond to liver cirrhosis, while healthy individuals and patients with chronic liver diseases without cirrhosis exhibit HVAT > 18 s [101]. In the group of patients with chronic hepatitis C, the severity of liver fibrosis (METAVIR fibrosis stage 0–3) and necrotic/inflammatory changes did not significantly affect the HVAT. The authors suggest that HVAT can be a simple and reliable method to exclude liver cirrhosis with portal hypertension, but is not capable to assess the severity of liver fibrosis.

Table 4.2 confers the data of some publications, which demonstrate that HVAT values below 14–17 s were specific for liver cirrhosis [99].

Several studies demonstrated that HVAT increases in patients with liver metastases. This fact limits the use of HVAT for the specification of liver cirrhosis due to similar hemodynamic changes [104, 105].

Attempts were also made to use the intensity of contrast enhancement of the liver parenchyma to diagnose the liver cirrhosis based on the theory of degradation of Kupffer cells function in cirrhotic liver. However, these studies utilized Levovist, which is capable of interacting with the reticuloendothelial system.

The study [106] compared the intensity of contrast enhancement of the liver parenchyma and the right kidney in patients with alcohol and other diffuse liver diseases on the 20th, 90th seconds, and fifth minute after the introduction of Levovist and specified the following three types of contrast enhancement:

- Type A—on the 20th second, the contrast enhancement is observed only in the kidney, on the 90th—in the kidney and liver, on the fifth minute—only in the liver.
- Type B—on the 20th and 90th seconds contrasting enhancement is registered in the liver and kidney, but on the fifth minute—only in the liver.
- Type C—on the 20th and 90th seconds contrasting enhancement is registered in the liver and kidney, on the fifth minute—a low contrast enhancement of both organs.

Type A has been revealed in 83% of healthy people, type B—in 60–80% of patients with chronic diffuse liver diseases, and type C—in almost all patients with alcoholic liver disease. The authors associate the low contrast enhancement of the liver parenchyma in type C with the Kupffer cells dysfunction in cirrhotic liver, which causes the slow clearance of UCA [106].

A significant decrease in the liver parenchyma enhancement in the late phase (7 min after the administration of Levovist) in patients with liver cirrhosis stage A ($p < 0.05$) and C ($p < 0.001$) as compared to healthy people was reported [107]. Besides, the statistically significant ($p < 0.01$) decrease in the intensity of the contrast enhancement was determined in patients with liver cirrhosis stage C as compared to stage A. The authors explained it with the decrease in UCA absorption by the reticuloendothelial system resulted from the impaired functionality of the Kupffer cells due to portosystemic shunts (Figs. 4.25 and 4.26).

The study [108] with Levovist and inversed tissue harmonic revealed a significant reverse correlation between the brightness of the image of the liver parenchyma in the shades of gray and the fibrosis index ($r = -0.809$, $p < 0.01$). The average signal intensity was 144.5 in normal

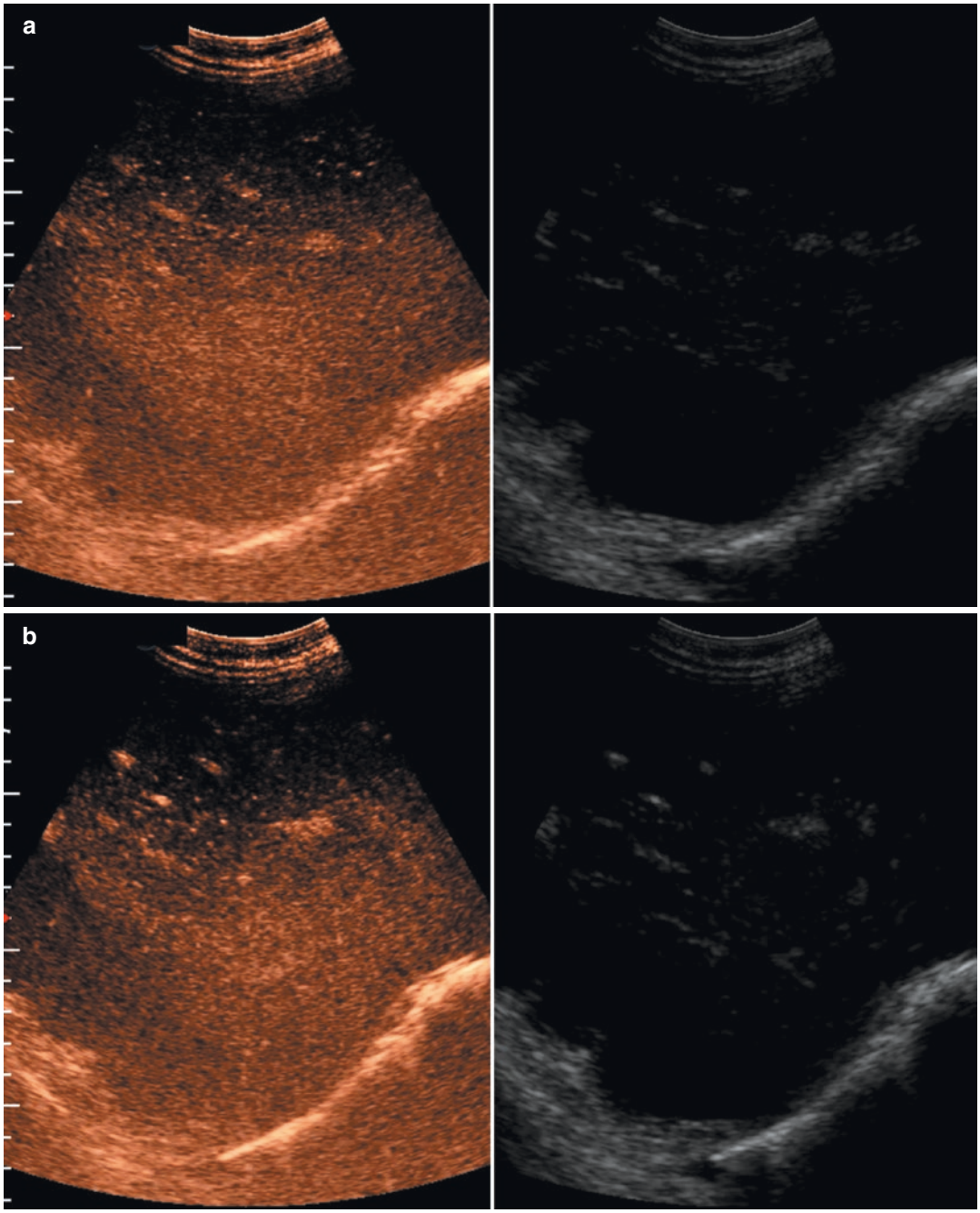

Fig. 4.25 Liver fibrosis. Reduced vascularization of the liver parenchyma. CEUS images. (**a**) Early portal venous phase. (**b**) The beginning of the late phase

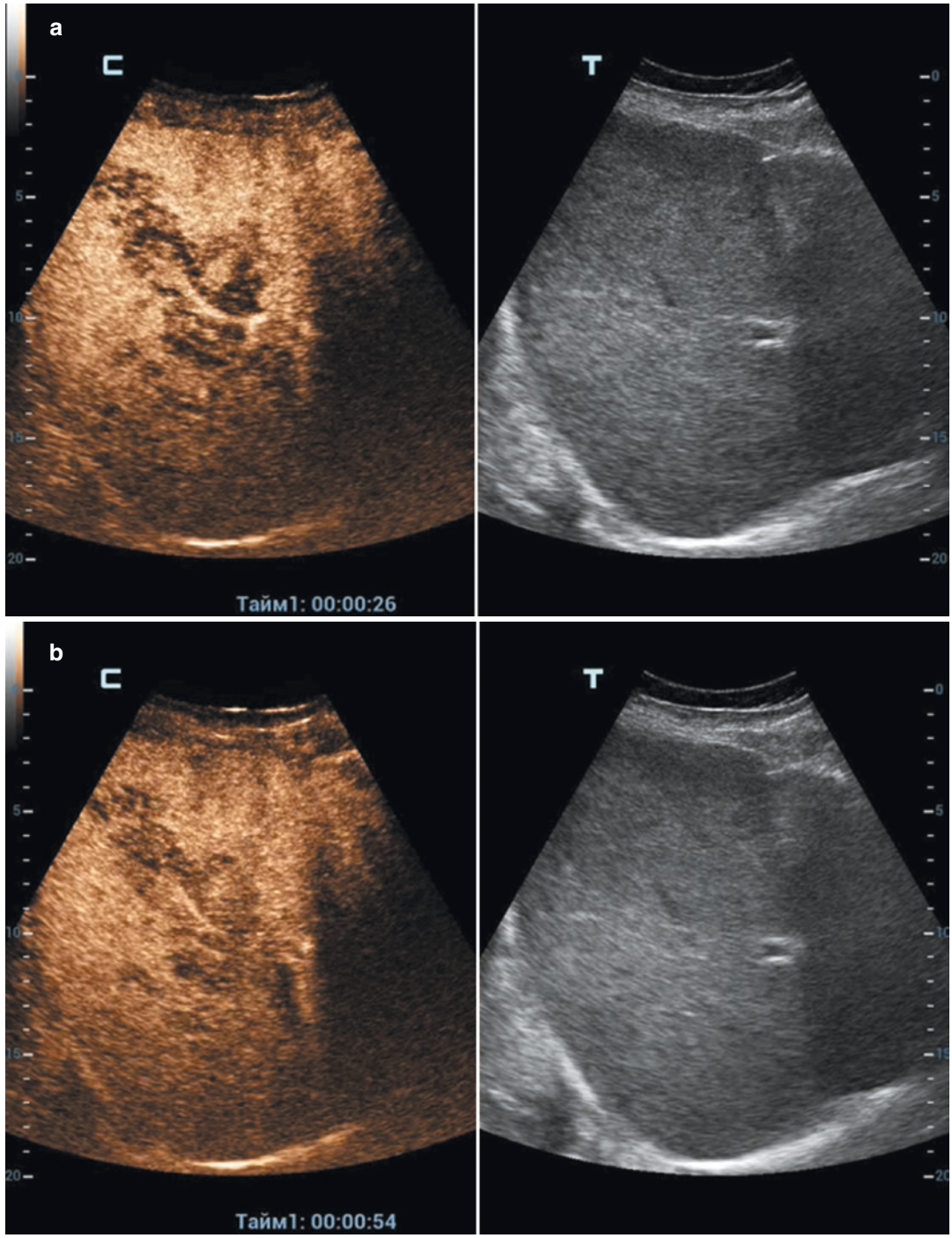

Fig. 4.26 Micronodular liver cirrhosis. CEUS images. Irregular non-intensive contrast enhancement of the liver parenchyma. (**a**) Arterial phase. (**b**) Portal venous phase. (**c**) Late phase. (**d**) Quantitative analysis

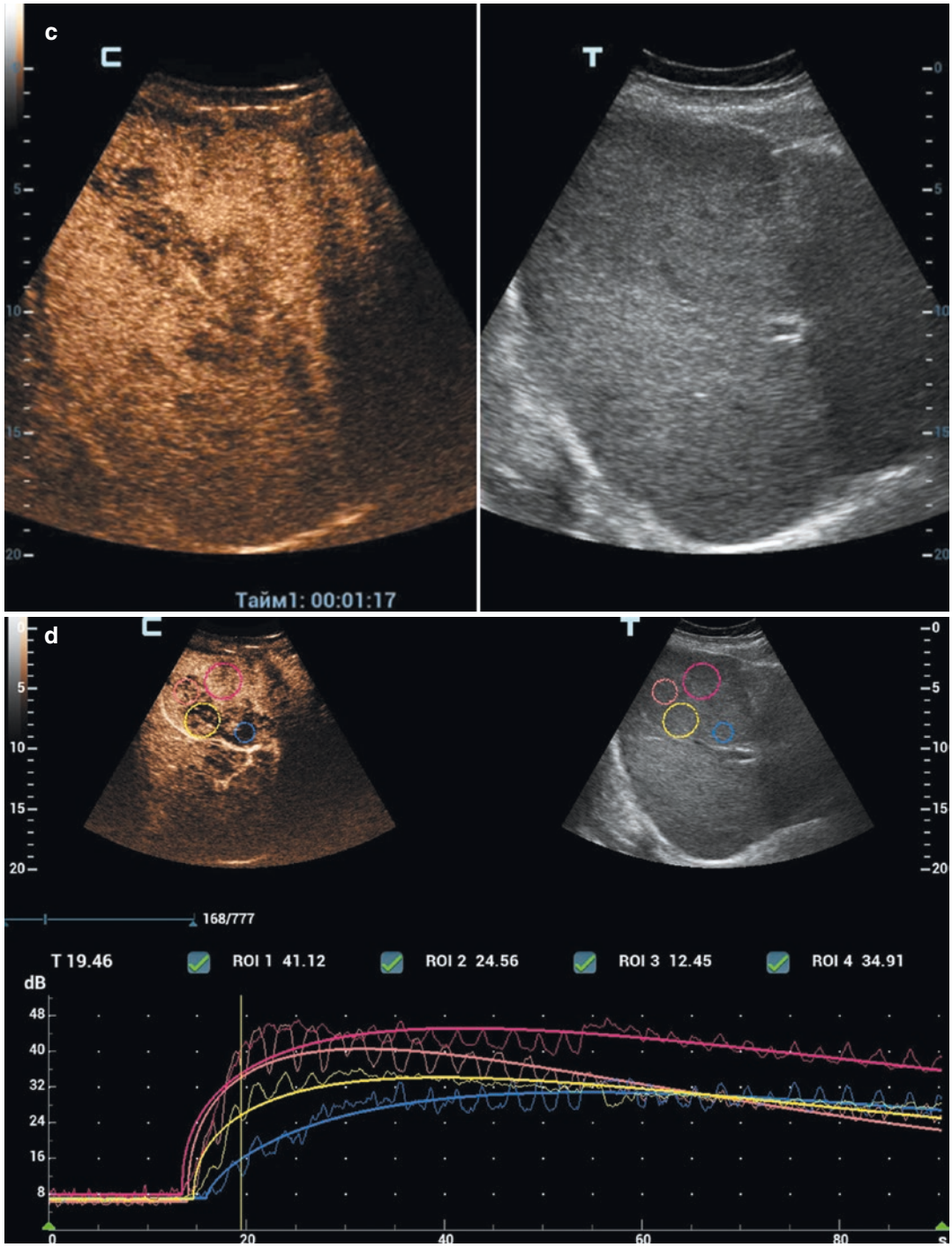

Fig. 4.26 (continued)

Table 4.3 Histopathological, hemodynamic, and clinical stages of liver fibrosis [112]

Classification	Stages				
METAVIR	F1–F3	F4	F4	F4	F4
HVPG (mmHg)		>6	>10	>12	>16
					>20
Clinical class	No cirrhosis	Stage 1	Stage 2	Stage 3	Stage 4
		Compensated	Compensated	Decompensated	Decompensated
			Varices	Variceal bleeding	Variceal bleeding
				Ascites	Ascites
				Encephalopathy	Encephalopathy
					Bacterial infection
					Hepatorenal syndrome
1-year mortality (%)		1	3	10–30	60–100

liver, 133.6—in chronic hepatitis, and 102.6—in cirrhotic liver with reliable difference between the groups of the normal and cirrhotic liver ($p < 0.01$). They suggested that the extent of the bubble destruction in the late phase with Levovist can correspond to the degree of liver fibrosis.

There are almost no publications on the diagnosis of chronic diffuse liver diseases with CEUS in recent years. This fact shows the decrease in the interest to this CEUS application. This is probably the result of the implementation of ultrasound elastometry, which has better diagnostic value for staging liver fibrosis and cirrhosis. Currently, CEUS is used to detect the liver cirrhosis complications, such as portal vein thrombosis and the development of HCC, as well as for the assessment of the transjugular intrahepatic portosystemic shunt.

Portal hypertension is a clinical syndrome, which results from the increase in hepatic venous pressure gradient (HVPG) >5 mmHg, due to high hepatic resistance [109]. Portal hypertension develops in patients with liver fibrosis and is one cause of serious complications of liver cirrhosis (esophageal or gastric variceal bleeding, ascites, peritonitis, and hepatic encephalopathy), which are associated with high mortality [110].

HVPG is usually measured by cannulation of the liver vein with a balloon catheter. It is defined as the difference between the wedged and free hepatic venous pressures. It is assumed that serial HVPG measurements contribute to the determination of the liver fibrosis stage and liver cirrhosis regardless of their etiology [111, 112]. HVPG measurement is also used for risk stratification, preoperative screening before liver resection, monitoring the response to drug therapy, and specification of the prognosis of liver cirrhosis [113].

A new classification of liver cirrhosis, which combines histopathological, clinical, hemodynamic, and prognostic signs was proposed [112] (Table 4.3). This system classifies liver fibrosis depending on compensation or decompensation, which are determined by clinical manifestations [114].

Endoscopic examination is the "gold standard" for the identification and staging of esophageal and gastric varices. However, both the definition of HVPG and endoscopic examination are invasive techniques with some possible complications. Therefore, new alternative tests for non-invasive diagnosis, including CEUS, are developing in recent years [115].

The correlation between the regional liver perfusion, HVPG ($r = 0.279$, $p = 0.041$), and the hyperdynamic syndrome markers was demonstrated by the study [116] with SonoVue® and a disruption-replenishment protocol described in Sect. 3.2. Regional hepatic perfusion was calculated as microbubbles velocity multiplied by their concentration.

Compared to healthy people, in patients with liver cirrhosis, regional hepatic perfusion

increases (3.4 ± 0.7 and 5.1 ± 3.7, respectively) and correlates with the model of the terminal stage of the disease. The inverse correlation of the quantitative TIC parameters with portal venous pressure with a bolus administration of SonoVue® is reported [117]. Portal venous pressure was inversely correlated with the area under the portal vein/hepatic artery time-intensity curve ratio (Qp/Qa), portal vein/hepatic artery strength ratio (Ip/Ia), and portal vein/hepatic artery washin perfusion slope ratio (βp/βa), with correlation coefficients of −0.701, −0.625, and −0.494, respectively. The specified values in patients with portal hypertension and normal liver are presented in Table 4.4.

In a later experiment on dogs, the following results were obtained: with the threshold of ≥18 cm H_2O for Qp/Qa AUC—0.866, the sensitivity was 76%, specificity—84%; for Ip/Ia AUC—0.895, the sensitivity was 85% and specificity—89% [118].

Table 4.5 shows the data regarding the diagnostic value of HVAT and intrahepatic transit time (ITT, i.e. the difference between the time of the UCA arrival in the hepatic vein and hepatic artery).

Table 4.4 The TIC ratios in the diagnosis of portal hypertension [117]

Ratio	Portal hypertension	Normal liver	*p*
Qp/Qa	2.57 ± 1.20	4.93 ± 2.0	0.001
Ip/Ia	0.35 ± 0.18	1.91 ± 0.75	0.001
βp/βa	0.23 ± 0.21	0.63 ± 0.53	0.006

Shimada et al. [121] suggested using not hepatic, but splenic hemodynamics to assess HVPG, determining the difference between the arrival time of Sonazoid in the splenic artery and the peak intensity time in the splenic vein. They reported a positive correlation of this parameter with HVPG. At HVPG ≥ 10 mmHg and the threshold of 13.5 s, it had AUC—0.76, sensitivity—71%, and specificity—68%; at HVPG ≥ 12 mmHg and the threshold of 14.5 s it had AUC—0.76, sensitivity—60%, and specificity—80%, which indicate the relatively satisfactory capabilities of this technique to determine HVPG.

Eisenbrey et al. [122] based on the fact that the pressure of the fluid surrounding microbubbles can be evaluated when determining the subharmonic amplitude (subharmonic-aided pressure estimation—SHAPE) with the appropriate mathematical modeling, demonstrated that SHAPE gradient between the portal and hepatic veins has a good correlation with HVPG (r = 0.82). They report the SHAPE sensitivity of 89% and the specificity of 88% in the detection of HVPG ≥ 10 mmHg; and the sensitivity and specificity of 100% and 81%, respectively, in HVPG ≥ 12 mmHg.

Amat-Roldan et al. [22] showed that the clustering coefficient of the vascular connectome, created with computer graphic analysis of ultra-

Table 4.5 Diagnostic values of HVAT and ITT in the determination of HVPG with SonoVue®

Study	Number of patients	Parameter (threshold)	Severity of portal hypertension	Se/Sp/PPV/NPV/Ac/PLR/NLR	AUC
Kim et al. (2013) [119]	71	HVAT (14 s)	Clinically significant (HVPG ≥ 10 mmHg)	93/87/91/90/–/6.95/0.08	0.973
Jeong et al. (2015) [120]	53	HVAT (19 s)	Pronounced (HVPG ≥ 12 mmHg)	56/89/95/35/63/–/–	0.72
				R1	
				50/89/94/32/58/–/–	0.71
				R2	
		ITT (6 s)	Pronounced (HVPG ≥ 12 mmHg)	91/89/97/73/91/–/–	0.94
				R1	
				85/78/94/58/84/–/–	0.90
				R2	

Se/Sp/PPV/NPV/Ac/PLR/NLR/—sensitivity/specificity/positive predictive value/negative predictive value/diagnostic accuracy/positive likelihood ratio/negative likelihood ratio
R1 researcher 1, *R2* researcher 2

sound CEUS images with SonoVue, was lower in patients with HVPG > 10 mmHg than in patients with HVPG < 10 mmHg ($p = 0.006$). The use of this technique enabled to reach AUC 0.889 (95% CI 0.810–0.967, $p < 0.001$) at HVPG ≥ 10 mmHg, AUC 0.887 (95% CI 0.826–0.968, $p < 0.001$) at HVPG ≥ 12 mmHg, and AUC 0.911 (95% CI 0.848–0.974, $p < 0.001$) at HVPG ≥ 16 mmHg. However, the authors studied the data of only 45 patients with liver cirrhosis, and further research is required to confirm their results.

CEUS in the diagnosis of esophageal varices A negative correlation is observed between the HVAT and developing esophageal varices ($r = -0.589$, $p < 0.001$). HVAT is a good predictor of esophageal varices and a high risk of bleeding (AUROC 0.833 and 0.840) at threshold values of 22 s and 20.8 s, respectively [123].

According to some researchers, as compared to HVAT, the interval between the arrival time of UCA to the hepatic vein and the hepatic artery permits a more reliable prediction of esophageal varices (AUROC 0.883) and esophageal varices with a high risk of bleeding (AUROC 0.915).

The number of time-related parameters, such as hepatic artery arrival time, hepatic vein arrival time, portal vein arrival time, the time interval between injection and liver parenchyma peak time, the difference between hepatic vein arrival time and hepatic artery arrival time, the difference between portal vein arrival time and hepatic artery arrival time, the rise time from 10% to 90% of liver parenchyma peak signal intensity, and the quantitative parameter of enhancement—the difference between the peak signal intensity in the liver parenchyma and baseline intensity may be analyzed [124]. The diagnostic efficiency of these parameters in predicting the presence of esophageal varices and the risk assessment of bleeding from esophageal varices is shown in Table 4.6. The most effective parameter for predicting the presence of esophageal varices and bleeding risk assessment was the difference between hepatic vein arrival time and hepatic artery arrival time.

Another way to predict esophageal varices with CEUS used the measurement of the thickness of the double layer of the mucosa and submucosa, the anterior–posterior distance, and the time to the peak intensity of the lower third of the esophagus after the administration of the UCA [125]. The best diagnostic value for the pronounced esophageal varices was demonstrated by the measurement of the thickness of the mucosa and submucosa in the lower third of the esophagus (with cut-off >8.15 mm AUROC is 0.987, sensitivity—93.8%, specificity—95.0%).

Portal vein thrombosis is also reliably diagnosed with CEUS. It is detected in 0.6–11% of patients with liver cirrhosis and may be either a blood clot resulted from a complication of inflammatory or infectious diseases of the liver, pancreas, intestines, hypercoagulability syndrome, endoscopic sclerotherapy of esophageal varices, percutaneous ablative techniques, etc., or tumor thrombus, which is often a manifestation of HCC [72, 126]. In the latter case, the main advantage of CEUS is the possibility to detect vascularization in the thrombus, which indicates its neoplastic character [127]. The contrast enhancement of such a thrombus can be reliably registered in all vascular phases even with fast and intensive washout. The diagnostic accuracy of CEUS is superior to CE-CT in the detection of the portal vein thrombus (100% vs. 68%) and differential diagnosis (98% vs. 68%, respectively) [71]. Also, CEUS is applicable to evaluate the effectiveness of anticoagulant therapy.

Transjugular intrahepatic portosystemic shunt (TIPS) is an endovascular method of the treatment of portal hypertension. It is a minimally invasive technique used in recent years for portal vein decompression. This procedure creates a communication between the portal and hepatic veins (usually the right hepatic vein) with the subsequent installation of the stent. Endovascular surgeons use the catheter, which is introduced through the inner jugular vein, passes in the lumen of the superior vena cava, right atrium, and inferior vena cava to hepatic veins. In patients with TIPS, CEUS is applied in contrast-specific modes with high MI to identify TIPS abnormalities. It exhibits a sensitivity of 94.4%, specific-

Table 4.6 Diagnostic performance of contrast-enhanced ultrasonography in assessing the presence of esophageal varices and high-risk esophageal varices

Feature	AUC (95% confidence interval)	Cut-off value	Sensitivity (%)	Specificity (%)	+LR	−LR	PPV (%)	NPV (%)	Accuracy (%)
Presence of esophageal varices									
Hepatic vein arrival time	0.838 (0.718–0.922)	≤22 s	85.00	72.22	3.06	0.21	87.18	68.42	81.03
HV–HA	0.883 (0.771–0.952)	≤8.2 s	85.00	77.78	3.83	0.19	89.48	70.00	82.76
PV–HA	0.726 (0.593–0.835)	≥5.4 s	60.00	77.78	2.70	0.51	85.72	46.66	48.28
PSI	0.710 (0.516–0.821)	≤67.5	95.00	38.89	1.55	0.13	77.56	77.77	77.59
High-risk esophageal varices									
Hepatic vein arrival time	0.840 (0.720–0.923)	≤20.8 s	82.14	80.00	4.11	0.22	79.31	82.75	81.03
HV–HA	0.915 (0.812–0.972)	≤7.0 s	82.14	90.00	8.21	0.20	88.46	84.37	86.21
PV–HA	0.714 (0.581–0.825)	≥5.4 s	67.86	70.00	2.26	0.46	67.86	70.00	51.72
PSI	0.672 (0.536–0.790)	≤43	42.86	90.00	4.29	0.63	80.00	62.79	65.12

HV − HA—the difference between hepatic vein arrival time and hepatic artery arrival time, PV − HA—the difference between portal vein arrival time and hepatic artery arrival time, PSI—the difference between liver parenchyma peak signal intensity and baseline intensity
+LR positive likelihood ratio, *−LR* negative likelihood ratio, *PPV* positive predictive value, *NPV* negative predictive value

ity—93.8%, and AUC—0.94 in the detection of TIPS stenosis or occlusion [128]. The use of low MI modes slightly reduces the diagnostic accuracy of CEUS accounting for 70%, which, however, exceeds the diagnostic accuracy of CDI (50%) [128].

4.5 Liver Transplant

Up to now, orthotopic liver transplantation (OLT) is the only method of treatment of acute irreversible (terminal) and chronic liver failure. Over the past four decades, the OLT has become an almost routine operation with a good survival rate, which is relatively stable over the last 15 years and amounts to >80% for 1 year and 70% for 5 years after the OLT [119, 129].

Indications for OLT are diverse and confer terminal stages of chronic liver diseases, acute (fulminant) liver failure, and some benign and malignant liver tumors. The OLT should be considered as a treatment method for each patient when is expected to increase life expectancy or quality.

Currently, the below-listed types of OLT are usually used:

- whole liver transplantation from a deceased donor.
- split liver transplantation from a deceased donor.
- liver fragment transplantation from a living donor.

Preoperative imaging aims to choose the candidates for the OLT without contraindications (such as hepatic and extrahepatic non-HCC tumors) and to determine the patency and anatomical features of the hepatic vessels and biliary system. Most of these tasks can be successfully solved by CT, MRI, and MR cholangiography [130, 131].

At this stage, CEUS is mainly used for the differential diagnosis of the FLLs in cirrhotic liver and the detection of tumor thrombosis in the portal vein [132]. The AASLD and EASL guidelines recommend multi-phase CT and/or MRI to diagnose HCC or other malignant liver tumors and to determine the number and sizes of HCC nodules. Following the Milan criteria, OLT in patients with HCC is possible if there is a single lesion ≤5 cm, or up to three lesions, each ≤3 cm, no macrovascular invasion, regional, or remote metastases [24, 133, 134].

During the operation of the liver transplantation, US contrast-enhanced cholangiography (UCA is introduced into the bile ducts) can be performed to specify the biliary anatomy. Intraoperative 3D US contrast-enhanced cholangiography permits the creation of the entire biliary tree maps from the common hepatic duct to the fifth-order branches that contain all anatomical features to reduce the risk of bile duct damage during the operation. However, this method at the moment is under study, and there are no recommendations on its use in clinical practice [135, 136].

After the OLT, several possible complications may occur that require a fast and accurate diagnosis to preserve the liver transplant and ensure the patient's survival [130]. Indications for CEUS are still limited to its use as a specific method for solving individual issues with dubious results of CT and/or MRI and as a supplement to multiparametric ultrasound, which provides a safe first-line "all-in-one" study to detect complications. It also eliminates the risks associated with iodine-containing radiocontrast media and is easily performed at the bedside [132].

Abnormal blood supply after the OLT remains one critical complication. Severe and sometimes irreversible ischemic damage to the transplant induces massive necrosis of hepatocytes and biliary epithelium and initiates the development of multisystem organ failure and uncontrolled sepsis [137].

According to the WFUMB Guidelines and good clinical practice recommendations for CEUS in the liver [3], CEUS after the OLT can be used for the following purposes:

- Confirmation of occlusion of the intrahepatic hepatic arteries, portal veins, hepatic veins, or inferior vena cava after an inconclusive Doppler evaluation of the liver vasculature
- Confirmation of the presence and assessment of the nature of fluid collections and, in case

of recent hematomas, to search for active bleeding
- Exclusion of perfusion defects when infarction is suspected
- Monitoring the success of thrombolysis in the intensive care unit after interventions for hepatic artery occlusion

AS compared with CDI and PDI, CEUS provides more informative images similar to angiography that contributes to a more adequate analysis of the state of intra- and extrahepatic arteries and portal veins, hepatic veins, and IVC [138–141].

After the introduction of UCA according to the standard protocol, the hepatic arteries are enhanced first and are well visualized in the early arterial phase against the background of unenhanced liver parenchyma (Fig. 4.27). The portal vein and its branches enhance in the portal phase (Fig. 4.28), after which the liver can be scanned for parenchymal infarct.

Hepatic artery occlusion with thrombus is a severe complication after liver transplantation, which arises in 2.5–9% of cases [142]. To prevent the loss of the transplant and the patient's death, urgent revascularization is necessary. CEUS improves the visualization of blood flow in the hepatic artery and reduces the time for diagnosis [139, 143]. CEUS is characterized by high sensitivity (100%) and accuracy (97.8%) in the identification of the hepatic artery thrombus that enabled omitting invasive arteriography in 62.9% of cases [144].

The characteristic feature of the hepatic artery thrombosis is the absence of its contrast enhancement in the arterial phase of the study. The infarct of the liver transplant parenchyma is defined as the area of missing or significantly decreased arterial perfusion [29]. Collateralization around the hepatic artery is visualized with CEUS as contrast enhancement of intrahepatic arteries and the conglomeration of small vessels in the porta hepatis [142].

The hepatic artery stenosis complicates the postoperative period in 4–11% of patients [142]. Although CEUS permits direct imaging of the hepatic artery stenosis, no guidelines and recommendations are available at the moment [145].

Hepatic artery pseudoaneurysm is a rare condition but is considered a serious complication with a high risk of death from rupture and bleeding. A pseudoaneurysm can be intrahepatic or extrahepatic, the latter more often arising in the area of anastomosis or the ligation zone of the donor gastroduodenal artery. With CEUS, they are detected as a circular enhanced zone around the hepatic artery with a characteristic turbulent flow [146].

Splenic steal syndrome is a possible complication after liver transplantation. The blood flows preferentially from the celiac artery into the splenic artery. The hepatic artery is relatively hypoperfused, which leads to liver transplant ischemia. The successful use of CEUS to diagnose arterial splenic steal syndrome [142, 147]. The authors report slow weak contrast enhancement of the hepatic artery in combination with the rapid enhancement of portal veins, but these features may also be observed in the ischemia, which occurred for other reasons.

Stenosis or occlusion of the portal vein leads to a severe decrease in liver function due to the predominance of portal blood supply in the liver vasculature. With CEUS, the portal vein thrombosis demonstrates a complete absence of the portal vein lumen enhancement in the case of its occlusion or the narrowing of the lumen with nonenhancing masses in non-occlusive thrombosis. It detects the thrombosis of the portal vein with high diagnostic accuracy (97–100%) and reduces the study time as compared with traditional Doppler ultrasound [140]. One CEUS advantage is the high-quality delineation of the lumen of the portal vein, which enables precise estimation of the severity and length of the stenosis.

Thrombosis and stenosis of hepatic veins usually manifest in the early postoperative period but may occur a long time after OLT [137]. CEUS is a promising method for the diagnosis of the obstruction of the middle hepatic venous tributaries with the sensitivity of 91%, specificity—97%,

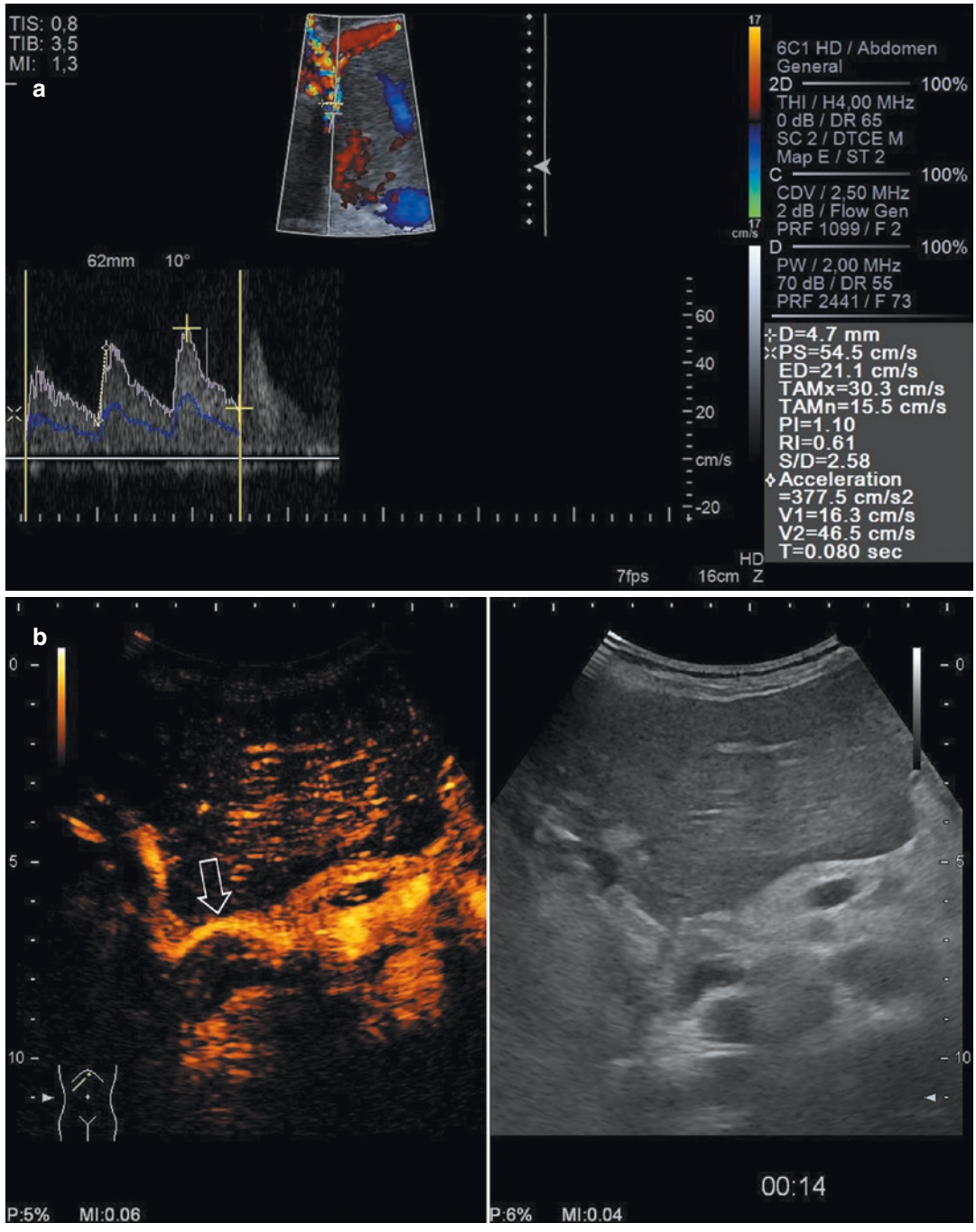

Fig. 4.27 Liver ultrasound in a patient after transplantation of the left lateral sector of the liver and stenting the portal vein for postoperative stenosis. The stent in the portal vein prevented CT to assess the extrahepatic segment of the hepatic artery. Oblique US scan under the left costal margin. (**a**) Normal blood flow values in the hepatic artery in the "hilum" of the liver transplant with pulsed-wave Doppler. (**b**) Normal passage of the hepatic artery with arterial phase CEUS (arrow). (**c**) Hepatic artery branch is well enhanced with arterial phase CEUS (arrow)

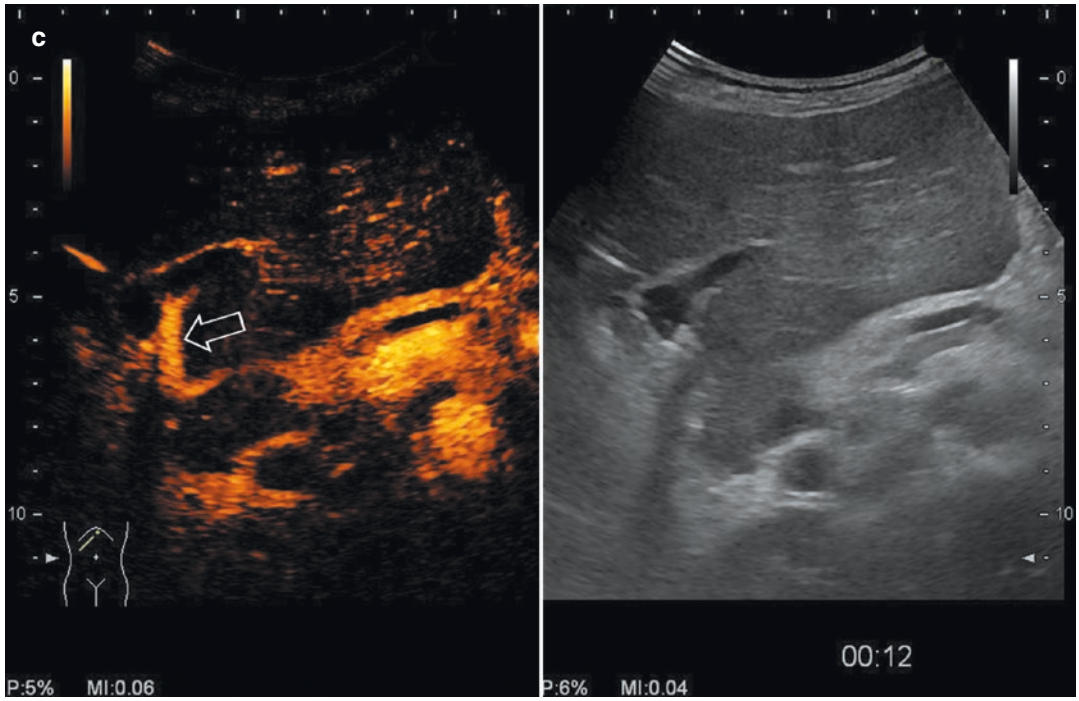

Fig. 4.27 (continued)

and accuracy—95% and allows to determine the decrease in the liver perfusion (the number of false-positive results reduced from 14% to 3%) [148]. The obstruction of the hepatic veins is accompanied by hyperenhancement of the liver parenchyma in the arterial phase with the decreased or average intensity of the enhancement in the portal venous phase. This fact may be the result of the sinusoidal stagnation followed by the decrease in both arterial and portal blood inflow, in some cases with the development of hepatofugal blood flow in portal veins [149] (Fig. 4.29).

Ultrasound contrast-enhanced cholangiography with the introduction of UCA through the drainage system enables accurate demonstration of the biliary tree anatomy and stenotic zones with the creation of 3D models similar to the preoperative study. CEUS can help to diagnose outflow disorders, such as stenosis and leaks of anastomosis. In these cases, CEUS detects the delay in the UCA outflow with the decrease in the contrast enhancement of the duodenum, and the persistence of the high-intensity enhancement of the biliary tree in 10 min after the intraductal administration of UCA. Anastomosis leakage is characterized by the spread of UCA beyond the lumen of the extrahepatic bile duct (Fig. 4.30). Anastomotic stricture is characterized by noncompliance of the extended biliary duct of the transplant and the conventional diameter of the duct of the recipient.

Another threatening complication is the ischemic changes of the biliary system, which has an exceptionally arterial blood supply. The decrease in the perfusion caused by the damage of the peribiliary vascular plexus is considered its morphological basis. With CEUS, such changes are characterized by the decrease or absence in the arterial phase enhancement of the bile duct walls,

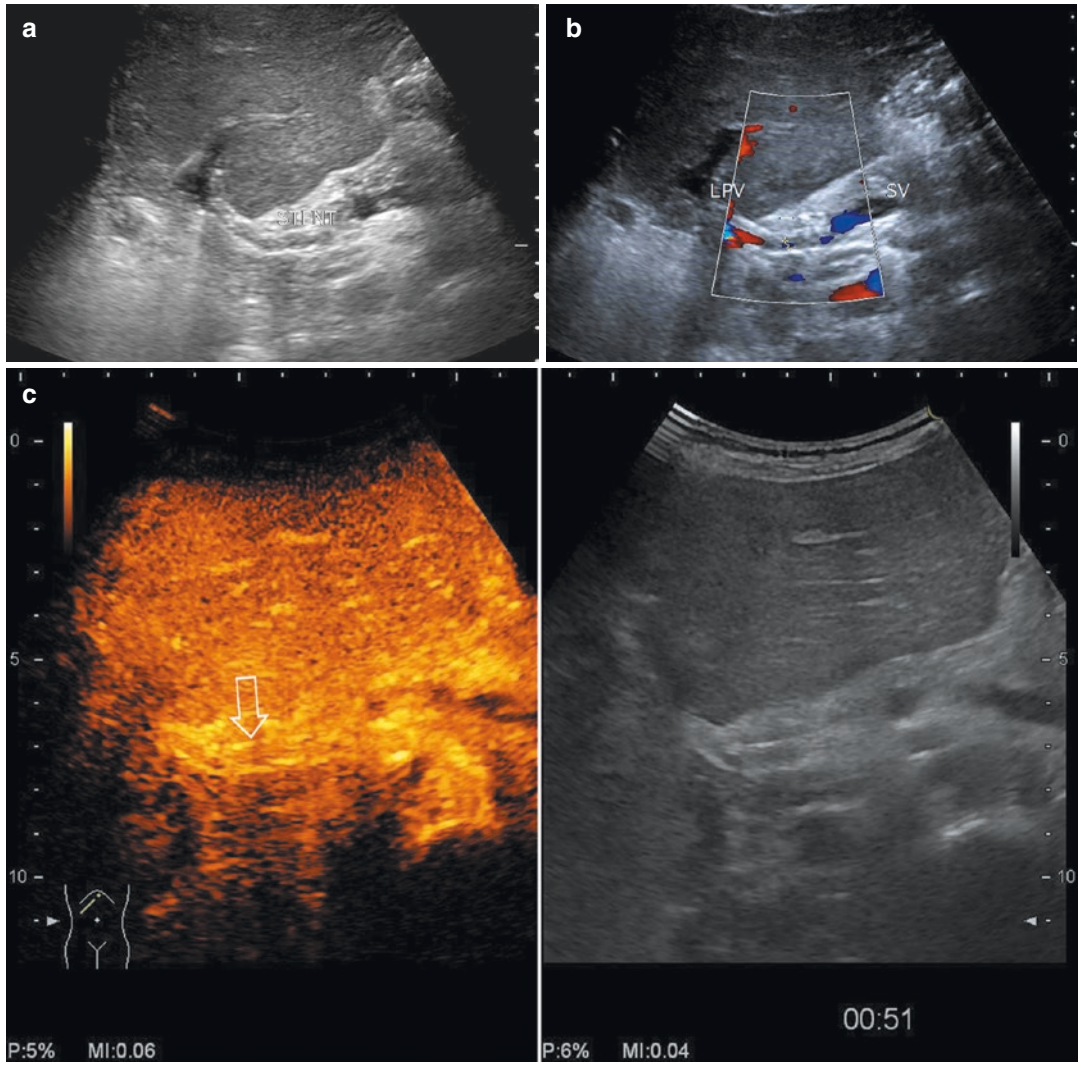

Fig. 4.28 The same patient as in Fig. 4.27 after transplantation of the left lateral sector of the liver and stenting the portal vein for postoperative stenosis. Oblique US scan under the left costal margin. (**a**) Grayscale US gives the impression of the echogenic masses in the lumen of the portal vein stent (arrow). (**b**) CDI also reveals single color spots of blood flow in the portal vein stent and suspects its narrowing and partial occlusion. (**c**) The portal vein stent is filled with the contrast agent in portal venous phase CEUS (arrow) that verifies its patency. *LPV* left portal vein, *SV* splenic vein

as opposed to their hyperenhancement in healthy volunteers. This fact enabled the diagnosis of ischemic changes in bile ducts with a sensitivity of 66.7%, specificity—88.9%, and accuracy—76.2% [142].

CEUS is beneficial at all stages of the OLT. The inclusion of this method into the diagnostic flowchart for the OLT depends on the operator's expertise, availability of UCA, and the choice of a multidisciplinary approach aimed at clinical needs.

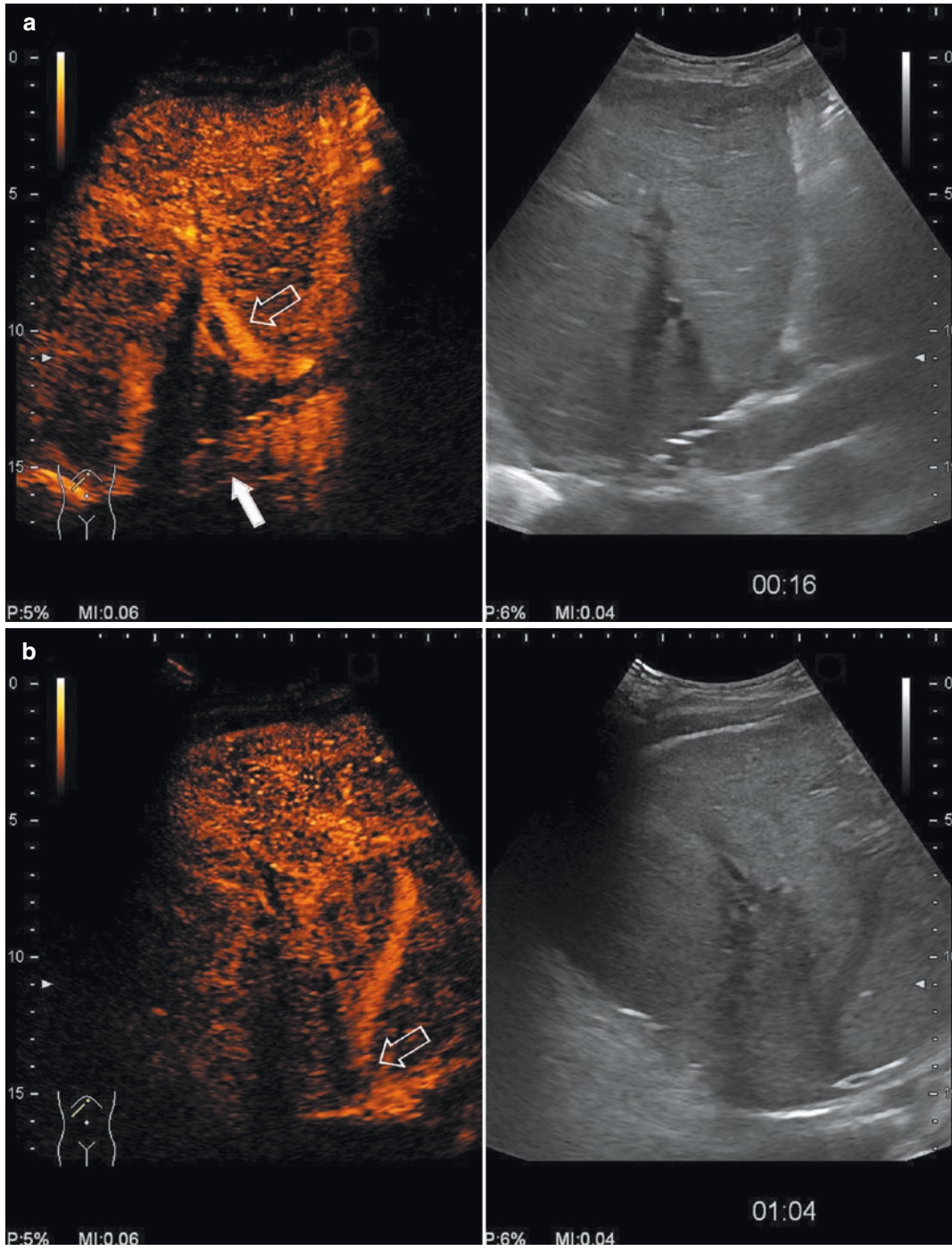

Fig. 4.29 Stenosis of the IVC after the transplantation of the left liver lobe. CEUS images. (**a**) The empty arrow indicates the left portal vein with uniform caliber. The solid arrow indicates the IVC with a narrowing in the area of hepatic caval anastomosis. (**b**) Late portal phase CEUS. The arrow indicates the narrowing of the hepatic caval anastomosis

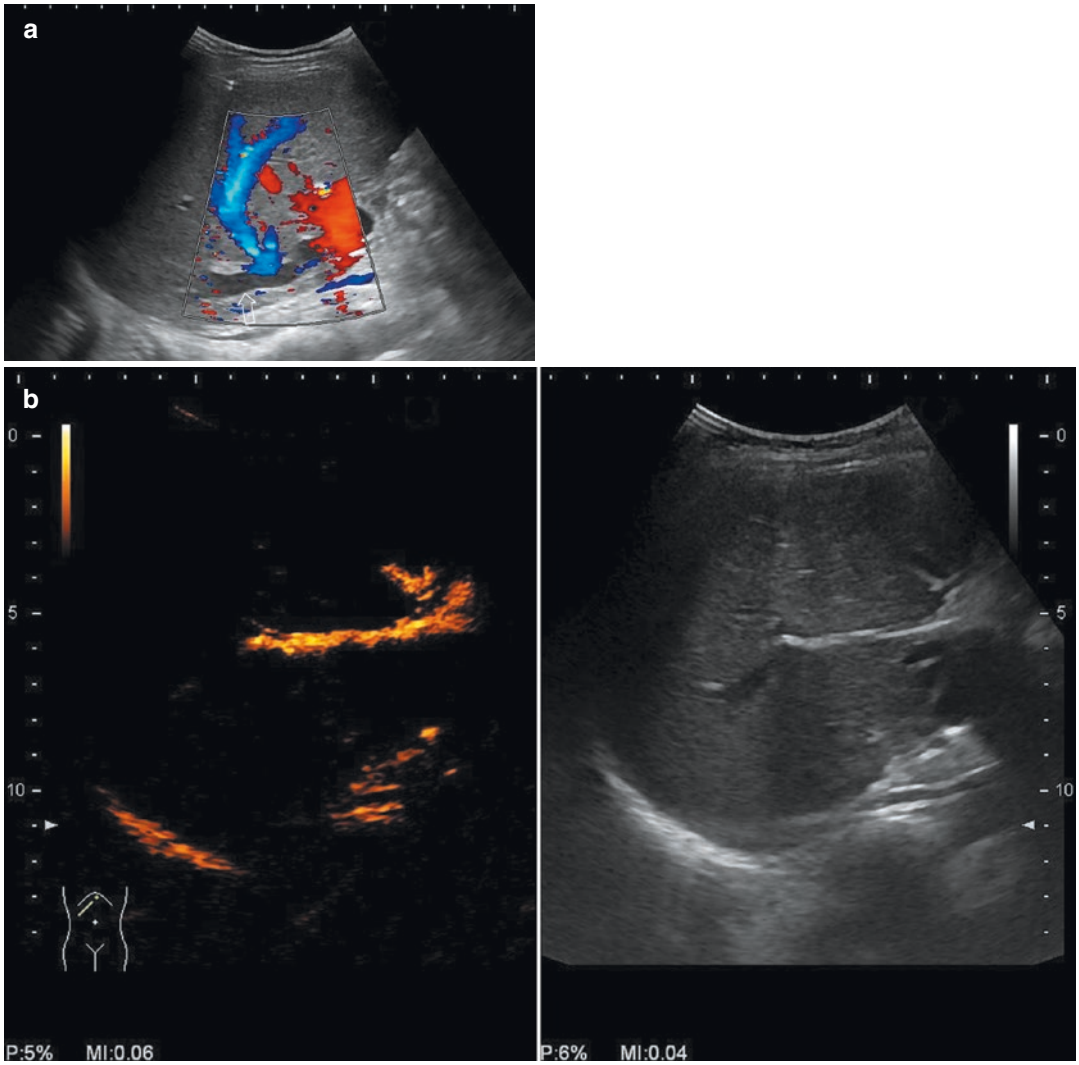

Fig. 4.30 Stricture of biliodigestive anastomosis after the transplantation of the right liver lobe. Percutaneous transhepatic cholangiostomy is also applied. (**a**) CDI demonstrates avascular tubular structure, which corresponds to the bile duct of the VI-VII liver segments (arrow). (**b**) After the introduction of UCA into the biliary drain, bile ducts of V-VIII liver segments are enhanced. UCA is also detected in the intestine that verifies the patency of the biliodigestive anastomosis. But the bile ducts of VI-VII segments are not enhanced, which indicates insufficient drainage

References

1. Albrecht T, Blomley M, Bolondi L, Claudon M, Correas JM, Cosgrove D, et al. Guidelines for the use of contrast agents in ultrasound. Ultraschall Med. 2004;25(4):249–56. https://doi.org/10.1055/s-2004-813245.
2. Claudon M, Cosgrove D, Albrecht T, Bolondi L, Bosio M, Calliada F, et al. Guidelines and good clinical practice recommendations for contrast enhanced ultrasound (CEUS) - update 2008. Ultraschall Med. 2008;29(1):28–44. https://doi.org/10.1055/s-2007-963785.
3. Claudon M, Dietrich CF, Choi BI, Cosgrove DO, Kudo M, Nolsøe CP, et al. Guidelines and good clinical practice recommendations for contrast enhanced ultrasound (CEUS) in the liver--update 2012: a WFUMB-EFSUMB initiative in cooperation with representatives of AFSUMB, AIUM, ASUM,

FLAUS and ICUS. Ultraschall Med. 2013;34(1):11–29. https://doi.org/10.1055/s-0032-1325499.
4. Dietrich CF, Nolsøe CP, Barr RG, Berzigotti A, Burns PN, Cantisani V, et al. Guidelines and good clinical practice recommendations for contrast enhanced ultrasound (CEUS) in the liver - update 2020 - WFUMB in cooperation with EFSUMB, AFSUMB, AIUM, and FLAUS. Ultraschall Med. 2020;41(5):562–85. https://doi.org/10.1055/a-1177-0530.
5. Dietrich CF, Averkiou M, Nielsen MB, Barr RG, Burns PN, Calliada F, et al. How to perform contrast-enhanced ultrasound (CEUS). Ultrasound Int Open. 2018;4(1):E2–E15. https://doi.org/10.1055/s-0043-123931.
6. Weskott HP. Contrast-enhanced ultrasound. 2nd ed. London: Uni-Med Science; 2013.
7. Wilson SR, Kim TK, Jang HJ, Burns PN. Enhancement patterns of focal liver masses: discordance between contrast-enhanced sonography and contrast-enhanced CT and MRI. AJR Am J Roentgenol. 2007;189(1):W7–W12. https://doi.org/10.2214/AJR.06.1060.
8. Koea JB. Hepatic incidentaloma: the rule of tens. HPB (Oxford). 2013;15(5):379–83. https://doi.org/10.1111/j.1477-2574.2012.00595.x.
9. Kamalov YR, Sandrikov VA, Gavrilov AV. Ispol'zovanie ul'trazvukovogo kontrasta Levovist pri obsledovanii bol'nyh opuholyami pecheni, portal'noj gipertenziej i pri ortotopicheskoj transplantacii pecheni. Klinicheskaya fiziologiya [The use of Levovist ultrasound contrast agent in the examination of patients with liver tumors, portal hypertension and orthotopic liver transplantation. Clinical physiology]. In: Sandrikov VA, editor. Diagnostika – novye metody. Moscow: Air-Art; 1998. p. 144–9. Russian.
10. Romanini L, Passamonti M, Aiani L, Cabassa P, Raieli G, Montermini I, et al. Economic assessment of contrast-enhanced ultrasonography for evaluation of focal liver lesions: a multicentre Italian experience. Eur Radiol. 2007;17(Suppl 6):F99–106. https://doi.org/10.1007/s10406-007-0234-5.
11. Sirli R, Sporea I, Săndulescu DL, Popescu A, Dănilă M, Săftoiu A, et al. Contrast enhanced ultrasound for the diagnosis of liver hemangiomas - results of a Romanian multicentre study. Med Ultrason. 2015;17(4):444–50. https://doi.org/10.11152/mu.2013.2066.174.csu.
12. Sporea I, Badea R, Popescu A, Spârchez Z, Sirli RL, Dănilă M, et al. Contrast-enhanced ultrasound (CEUS) for the evaluation of focal liver lesions - a prospective multicenter study of its usefulness in clinical practice. Ultraschall Med. 2014;35(3):259–66. https://doi.org/10.1055/s-0033-1355728.
13. Strobel D, Seitz K, Blank W, Schuler A, Dietrich CF, von Herbay A, et al. Tumor-specific vascularization pattern of liver metastasis, hepatocellular carcinoma, hemangioma and focal nodular hyperplasia in the differential diagnosis of 1,349 liver lesions in contrast-enhanced ultrasound (CEUS). Ultraschall Med. 2009;30(4):376–82. https://doi.org/10.1055/s-0028-1109672.
14. Tranquart F, Le Gouge A, Correas JM, Ladam Marcus V, Manzoni P, Vilgrain V, et al. Role of contrast-enhanced ultrasound in the blinded assessment of focal liver lesions in comparison with MDCT and CEMRI: results from a multicentre clinical trial. EJC Suppl. 2008;11(6):9–15. https://doi.org/10.1016/j.ejcsup.2008.06.003.
15. Trillaud H, Bruel JM, Valette PJ, Vilgrain V, Schmutz G, Oyen R, et al. Characterization of focal liver lesions with SonoVue-enhanced sonography: international multicenter-study in comparison to CT and MRI. World J Gastroenterol. 2009;15(30):3748–56. https://doi.org/10.3748/wjg.15.3748.
16. WHO Classification of Tumours Editorial Board. WHO classification of tumours. Digestive system tumours. 5th ed. Lyon: IARC Press; 2019.
17. Bosman F, Carneiro F, Hruban R, editors. WHO classification of tumours of the digestive system. 4th ed. Lyon: IARC; 2010.
18. Luk'yanchenko AB, Medvedeva BM, Karseladze AI, Romanova KA. Morfologicheskaya klassifikaciya opuholej pecheni (sravnitel'nye osobennosti klassifikacij VOZ 2010 i 2019 gg.) [Morphological classification of liver tumors (comparative features of the WHO classifications of 2010 and 2019)]. Medicinskaya Vizualizaciya. 2020;24(2):138–43. Russian.
19. Danzanova TY. Strategiya ul'trazvukovyh diagnosticheskih tekhnologij v hirurgicheskoj onkogepatologii [Strategy of ultrasonic diagnostic technologies in surgical oncohepatology]. Dissertation. Moscow. 2015. Russian.
20. Peniaeva EI, Kamalov JR, Sencha AN, Patrunov UN. Value of quantitative contrast-enhanced ultrasound in differential diagnosis of focal liver lesions. Ultrasound Funct Diagn. 2018;1:13–29. Russian. English abstract.
21. Albrecht T. Detection and characterisation of liver metastases. In: Lencioni R, editor. Enhancing the role of ultrasound with contrast agents. Pisa: Springer; 2006. p. 53–67.
22. Amat-Roldan I, Berzigotti A, Gilabert R, Bosch J. Assessment of hepatic vascular network connectivity with automated graph analysis of dynamic contrast-enhanced us to evaluate portal hypertension in patients with cirrhosis: a pilot study. Radiology. 2015;277(1):268–76. https://doi.org/10.1148/radiol.2015141941.
23. Seitz K, Strobel D, Bernatik T, Blank W, Friedrich-Rust M, Herbay AV, et al. Contrast-enhanced ultrasound (CEUS) for the characterization of focal liver lesions - prospective comparison in clinical practice: CEUS vs. CT (DEGUM multicenter trial). Parts of this manuscript were presented at the Ultrasound Dreiländertreffen 2008, Davos. Ultraschall Med. 2009;30(4):383–9. https://doi.org/10.1055/s-0028-1109673.

24. European Association for the Study of the Liver (EASL). EASL clinical practice guidelines on the management of benign liver tumours. J Hepatol. 2016;65(2):386–98. https://doi.org/10.1016/j.jhep.2016.04.001.
25. Dietrich CF, Mertens JC, Braden B, Schuessler G, Ott M, Ignee A. Contrast-enhanced ultrasound of histologically proven liver hemangiomas. Hepatology. 2007;45(5):1139–45. https://doi.org/10.1002/hep.21615.
26. Li GW, Chen QL, Jiang JT, Zhao ZR. The origin of blood supply for cavernous hemangioma of the liver. Hepatobiliary Pancreat Dis Int. 2003;2(3):367–70.
27. Peniaeva EI, Kamalov JR, Sencha AN, Patrunov UN, Sencha EA. Value of contrast-enhanced ultrasound in differential diagnosis of focal liver lesions. Med Visualiz. 2017;21(2):36–52. https://doi.org/10.24835/1607-0763-2017-2-36-52. Russian.
28. Fang L, Huang BJ, Ding H, Mao F, Li CL, Zeng MS, et al. Contrast-enhanced ultrasound (CEUS) for the diagnosis of hypoechoic hepatic hemangioma in clinical practice. Clin Hemorheol Microcirc. 2019;72(4):395–405. https://doi.org/10.3233/CH-190558.
29. Lyshchik A, editor. Specialty imaging: fundamentals of CEUS. 1st ed. Philadelphia, PA: Elsevier; 2019.
30. Bernatik T, Seitz K, Blank W, Schuler A, Dietrich CF, Strobel D. Unclear focal liver lesions in contrast-enhanced ultrasonography--lessons to be learned from the DEGUM multicenter study for the characterization of liver tumors. Ultraschall Med. 2010;31(6):577–81. https://doi.org/10.1055/s-0029-1245649.
31. Bhayana D, Kim TK, Jang HJ, Burns PN, Wilson SR. Hypervascular liver masses on contrast-enhanced ultrasound: the importance of washout. AJR Am J Roentgenol. 2010;194(4):977–83. https://doi.org/10.2214/AJR.09.3375.
32. Giannetti A, Franci L, Grechi C, Giangregorio F. Contrast-enhanced sonography in the diagnosis of hepatic hemangiomas: atypical appearance due to the washout of microbubbles. J Clin Ultrasound. 2013;41(6):361–5. https://doi.org/10.1002/jcu.21939.
33. Klinger C, Stuckmann G, Dietrich CF, Berzigotti A, Horger MS, Debove I, et al. Contrast-enhanced imaging in hepatic epithelioid hemangioendothelioma: retrospective study of 10 patients. Z Gastroenterol. 2019;57(6):753–66. https://doi.org/10.1055/a-0886-0081.
34. Tumanova UN, Karmazanovskij GG, Dubova EA, Shchegolev AI. Sravnitel'nyj analiz stepeni vaskulyarizacii gepatocellyulyarnogo raka i ochagovoj uzlovoj giperplazii pecheni po dannym komp'yuterno-tomograficheskogo i morfologicheskogo issledovanij [Comparative analysis of the degree of vascularization of hepatocellular carcinoma and liver focal nodular hyperplasia according to computer tomographic and morphological studies]. Vestn Ross Akad Med Nauk. 2013;68(12):9–15. Russian.
35. Dietrich CF, Schuessler G, Trojan J, Fellbaum C, Ignee A. Differentiation of focal nodular hyperplasia and hepatocellular adenoma by contrast-enhanced ultrasound. Br J Radiol. 2005;78(932):704–7. https://doi.org/10.1259/bjr/88181612.
36. Piscaglia F, Venturi A, Mancini M, Giangregorio F, Vidili G, Magnolfi F, et al. Diagnostic features of real-time contrast-enhanced ultrasound in focal nodular hyperplasia of the liver. Ultraschall Med. 2010;31(3):276–82. https://doi.org/10.1055/s-0028-1109852.
37. Bertin C, Egels S, Wagner M, Huynh-Charlier I, Vilgrain V, Lucidarme O. Contrast-enhanced ultrasound of focal nodular hyperplasia: a matter of size. Eur Radiol. 2014;24(10):2561–71. https://doi.org/10.1007/s00330-014-3280-0.
38. Jang JY, Kim MY, Jeong SW, Kim TY, Kim SU, Lee SH, et al. Current consensus and guidelines of contrast enhanced ultrasound for the characterization of focal liver lesions. Clin Mol Hepatol. 2013;19(1):1–16. https://doi.org/10.3350/cmh.2013.19.1.1.
39. Yen YH, Wang JH, Lu SN, Chen TY, Changchien CS, Chen CH, et al. Contrast-enhanced ultrasonographic spoke-wheel sign in hepatic focal nodular hyperplasia. Eur J Radiol. 2006;60(3):439–44. https://doi.org/10.1016/j.ejrad.2006.06.007.
40. Soussan M, Aubé C, Bahrami S, Boursier J, Valla DC, Vilgrain V. Incidental focal solid liver lesions: diagnostic performance of contrast-enhanced ultrasound and MR imaging. Eur Radiol. 2010;20(7):1715–25. https://doi.org/10.1007/s00330-009-1700-3.
41. Védie AL, Sutter O, Ziol M, Nault JC. Molecular classification of hepatocellular adenomas: impact on clinical practice. Hepat Oncol. 2018;5(1):HEP04. https://doi.org/10.2217/hep-2017-0023.
42. Laumonier H, Cailliez H, Balabaud C, Possenti L, Zucman-Rossi J, Bioulac-Sage P, Trillaud H. Role of contrast-enhanced sonography in differentiation of subtypes of hepatocellular adenoma: correlation with MRI findings. AJR Am J Roentgenol. 2012;199(2):341–8. https://doi.org/10.2214/AJR.11.7046.
43. Gregory J, Kiani A, Vernuccio F, Vernuccio F, Bertin C, Vullierme M-P, et al. Key points of US/CEUS/MR imaging of the different sub-types of hepatocellular adenomas: how to get closer to pathology. ECR 2017 poster C-1662. Vienna: European Society of Radiology. https://doi.org/10.1594/ecr2017/C-1662.
44. Gregory J, Paisant A, Paulatto L, Raynaud L, Bertin C, Kerbaol A, et al. Limited added value of contrast-enhanced ultrasound over B-mode for the subtyping of hepatocellular adenomas. Eur J Radiol. 2020;128:109027. https://doi.org/10.1016/j.ejrad.2020.109027.
45. Gesualdo A, Tamburrano R, Gentile A, Giannini A, Palasciano G, Palmieri VO. A diagnosis of inflammatory pseudotumor of the liver by contrast enhaced ultrasound and fine-needle biopsy: a case report. Eur J Case Rep Intern Med. 2017;4(2):000495. https://doi.org/10.12890/2016_000495.

46. Guarino B, Catalano O, Corvino A, Corvino F, Amore A, Petrillo A. Hepatic inflammatory pseudotumor: educational value of an incorrect diagnosis at contrast-enhanced ultrasound. J Med Ultrason. 2015;42(4):547–52. https://doi.org/10.1007/s10396-015-0624-6.
47. Kong WT, Wang WP, Cai H, Huang BJ, Ding H, Mao F. The analysis of enhancement pattern of hepatic inflammatory pseudotumor on contrast-enhanced ultrasound. Abdom Imaging. 2014;39(1):168–74. https://doi.org/10.1007/s00261-013-0051-3.
48. Shang J, Wang YY, Dang Y, Zhang XJ, Song Y, Ruan LT. An inflammatory myofibroblastic tumor in the transplanted liver displaying quick wash-in and wash-out on contrast-enhanced ultrasound: a case report. Medicine (Baltimore). 2017;96(49):e9024. https://doi.org/10.1097/MD.0000000000009024.
49. Ignee A, Piscaglia F, Ott M, Salvatore V, Dietrich CF. A benign tumour of the liver mimicking malignant liver disease--cholangiocellular adenoma. Scand J Gastroenterol. 2009;44(5):633–6. https://doi.org/10.1080/00365520802538229.
50. Bartolotta TV, Runza G, Minervini M, Midiri M. Hepatic angiomyolipoma: contrast-enhanced pulse inversion US in a case. Radiol Med. 2003;105(5–6):514–8. English, Italian.
51. Wang Z, Xu HX, Xie XY, Xie XH, Kuang M, Xu ZF, et al. Imaging features of hepatic angiomyolipomas on real-time contrast-enhanced ultrasound. Br J Radiol. 2010;83(989):411–8. https://doi.org/10.1259/bjr/81174247.
52. Dalle I, Sciot R, de Vos R, Aerts R, van Damme B, Desmet V, Roskams T. Malignant angiomyolipoma of the liver: a hitherto unreported variant. Histopathology. 2000;36(5):443–50. https://doi.org/10.1046/j.1365-2559.2000.00891.x.
53. Nguyen TT, Gorman B, Shields D, Goodman Z. Malignant hepatic angiomyolipoma: report of a case and review of literature. Am J Surg Pathol. 2008;32(5):793–8. https://doi.org/10.1097/PAS.0b013e3181607349.
54. Li R, Tang CL, Cai P, Ma KS, Zhang XH, Ding SY, et al. Comparison of CT and contrast-enhanced ultrasound findings in hepatic angiomyolipoma with pathological correlations. Abdom Radiol (NY). 2016;41(2):248–56. https://doi.org/10.1007/s00261-015-0571-0.
55. Vishlenkova EA. Elastometriya i elastografiya v kompleksnoj ocenke effektivnosti himioterapii metastazov kolorektal'nogo raka v pecheni [Elastometry and elastography in a comprehensive assessment of the effectiveness of chemotherapy for colorectal cancer metastases in the liver]. Dissertation. Moscow. 2015. Russian.
56. Mitina LA, Guc OV, Stepanov SO, et al. UZI pecheni s kontrastom pri metastazah kolorektal'nogo raka v pechen' [Ultrasound of the liver with contrast enhancement at metastases of colorectal cancer in the liver]. Koloproktologiya. 2017;60(S2):32–6. Russian.
57. Sidorov DV, Stepanov SO, Lozhkin MV, et al. Pervyj rossijskij opyt intraoperacionnoj ul'trazvukovoj navigacii s kontrastnym usileniem pri vypolnenii rezekcij pecheni po povodu zlokachestvennyh opuholej [The first Russian experience of intraoperative ultrasound navigation with contrast enhancement when performing liver resections for malignant tumors]. Issledovaniya i Praktika v Medicine. 2017;4(4):125–32. Russian.
58. Dănilă M, Popescu A, Sirli R, Sporea I, Martie A, Sendroiu M. Contrast enhanced ultrasound (CEUS) in the evaluation of liver metastases. Med Ultrason. 2010;12(3):233–7.
59. Dong Y, Zhang XL, Mao F, Huang BJ, Si Q, Wang WP. Contrast-enhanced ultrasound features of histologically proven small (≤20 mm) liver metastases. Scand J Gastroenterol. 2017;52(1):23–8. https://doi.org/10.1080/00365521.2016.1224380.
60. Bartolotta TV, Taibbi A, Picone D, Anastasi A, Midiri M, Lagalla R. Detection of liver metastases in cancer patients with geographic fatty infiltration of the liver: the added value of contrast-enhanced sonography. Ultrasonography. 2017;36(2):160–9. https://doi.org/10.14366/usg.16041.
61. Cantisani V, Grazhdani H, Fioravanti C, Rosignuolo M, Calliada F, Messineo D, et al. Liver metastases: contrast-enhanced ultrasound compared with computed tomography and magnetic resonance. World J Gastroenterol. 2014;20(29):9998–10007. https://doi.org/10.3748/wjg.v20.i29.9998.
62. Kong WT, Ji ZB, Wang WP, Cai H, Huang BJ, Ding H. Evaluation of liver metastases using contrast-enhanced ultrasound: enhancement patterns and influencing factors. Gut Liver. 2016;10(2):283–7. https://doi.org/10.5009/gnl14324.
63. Larsen LP, Rosenkilde M, Christensen H, Bang N, Bolvig L, Christiansen T, Laurberg S. The value of contrast enhanced ultrasonography in detection of liver metastases from colorectal cancer: a prospective double-blinded study. Eur J Radiol. 2007;62(2):302–7. https://doi.org/10.1016/j.ejrad.2006.11.033.
64. Ferlay J, Soerjomataram I, Dikshit R, Eser S, Mathers C, Rebelo M, et al. Cancer incidence and mortality worldwide: sources, methods and major patterns in GLOBOCAN 2012. Int J Cancer. 2015;136(5):E359–86. https://doi.org/10.1002/ijc.29210.
65. Schütte K, Schulz C, Poranzke J, Antweiler K, Bornschein J, Bretschneider T, et al. Characterization and prognosis of patients with hepatocellular carcinoma (HCC) in the non-cirrhotic liver. BMC Gastroenterol. 2014;14:117. https://doi.org/10.1186/1471-230X-14-117.
66. Stewart BW, Wild CP. World cancer report 2014. Geneva: WHO Press; 2014.
67. Matsui O, Kobayashi S, Sanada J, Kouda W, Ryu Y, Kozaka K, et al. Hepatocelluar nodules in liver cirrhosis: hemodynamic evaluation (angiography-assisted CT) with special reference to multi-step hepatocarcinogenesis. Abdom Imaging. 2011;36(3):264–72. https://doi.org/10.1007/s00261-011-9685-1.

68. Boozari B, Soudah B, Rifai K, Schneidewind S, Vogel A, Hecker H, et al. Grading of hypervascular hepatocellular carcinoma using late phase of contrast enhanced sonography - a prospective study. Dig Liver Dis. 2011;43(6):484–90. https://doi.org/10.1016/j.dld.2011.01.001.
69. Zhang J, Yu Y, Li Y, Wei L. Diagnostic value of contrast-enhanced ultrasound in hepatocellular carcinoma: a meta-analysis with evidence from 1998 to 2016. Oncotarget. 2017;8(43):75418–26. https://doi.org/10.18632/oncotarget.20049.
70. Chen J, Zhu J, Zhang C, Song Y, Huang P. Contrast-enhanced ultrasound for the characterization of portal vein thrombosis vs tumor-in-vein in HCC patients: a systematic review and meta-analysis. Eur Radiol. 2020;30(5):2871–80. https://doi.org/10.1007/s00330-019-06649-z.
71. Rossi S, Ghittoni G, Ravetta V, Torello Viera F, Rosa L, Serassi M, et al. Contrast-enhanced ultrasonography and spiral computed tomography in the detection and characterization of portal vein thrombosis complicating hepatocellular carcinoma. Eur Radiol. 2008;18(8):1749–56. https://doi.org/10.1007/s00330-008-0931-z.
72. Tarantino L, Francica G, Sordelli I, Esposito F, Giorgio A, Sorrentino P, et al. Diagnosis of benign and malignant portal vein thrombosis in cirrhotic patients with hepatocellular carcinoma: color Doppler US, contrast-enhanced US, and fine-needle biopsy. Abdom Imaging. 2006;31(5):537–44. https://doi.org/10.1007/s00261-005-0150-x.
73. Piscaglia F, Wilson SR, Lyshchik A, Cosgrove D, Dietrich CF, Jang HJ, et al. American College of Radiology contrast enhanced ultrasound liver imaging reporting and data system (CEUS LI-RADS) for the diagnosis of Hepatocellular Carcinoma: a pictorial essay. Ultraschall Med. 2017;38(3):320–4. https://doi.org/10.1055/s-0042-124661. English.
74. Bartolotta TV, Terranova MC, Gagliardo C, Taibbi A. CEUS LI-RADS: a pictorial review. Insights Imaging. 2020;11(1):9. https://doi.org/10.1186/s13244-019-0819-2.
75. Wilson SR, Lyshchik A, Piscaglia F, Cosgrove D, Jang HJ, Sirlin C, et al. CEUS LI-RADS: algorithm, implementation, and key differences from CT/MRI. Abdom Radiol (NY). 2018;43(1):127–42. https://doi.org/10.1007/s00261-017-1250-0.
76. Makoyeva A, Kim TK, Jang HJ, Medellin A, Wilson SR. Use of CEUS LI-RADS for the accurate diagnosis of nodules in patients at risk for hepatocellular carcinoma: a validation study. Radiol Imaging Cancer. 2020;2:2. https://doi.org/10.1148/rycan.2020190014.
77. Chen LD, Xu HX, Xie XY, Lu MD, Xu ZF, Liu GJ, et al. Enhancement patterns of intrahepatic cholangiocarcinoma: comparison between contrast-enhanced ultrasound and contrast-enhanced CT. Br J Radiol. 2008;81(971):881–9. https://doi.org/10.1259/bjr/22318475.
78. Li C, Wang W, Ding H, Huang B, Cao J, Mao F, Ji Z. Value of contrast-enhanced sonography in the diagnosis of peripheral intrahepatic cholangiocarcinoma. J Clin Ultrasound. 2011;39(8):447–53. https://doi.org/10.1002/jcu.20797.
79. Xu HX, Chen LD, Liu LN, Zhang YF, Guo LH, Liu C. Contrast-enhanced ultrasound of intrahepatic cholangiocarcinoma: correlation with pathological examination. Br J Radiol. 2012;85(1016):1029–37. https://doi.org/10.1259/bjr/21653786.
80. Chen LD, Xu HX, Xie XY, Xie XH, Xu ZF, Liu GJ, et al. Intrahepatic cholangiocarcinoma and hepatocellular carcinoma: differential diagnosis with contrast-enhanced ultrasound. Eur Radiol. 2010;20(3):743–53. https://doi.org/10.1007/s00330-009-1599-8.
81. Dong Y, Wang WP, Cantisani V, D'Onofrio M, Ignee A, Mulazzani L, et al. Contrast-enhanced ultrasound of histologically proven hepatic epithelioid hemangioendothelioma. World J Gastroenterol. 2016;22(19):4741–9. https://doi.org/10.3748/wjg.v22.i19.4741.
82. Foschi FG, Dall'Aglio AC, Marano G, Lanzi A, Savini P, Piscaglia F, et al. Role of contrast-enhanced ultrasonography in primary hepatic lymphoma. J Ultrasound Med. 2010;29(9):1353–6. https://doi.org/10.7863/jum.2010.29.9.1353.
83. Quaia E, Gennari AG. The most appropriate time delay after microbubble contrast agent intravenous injection to maximize liver metastasis conspicuity on contrast-enhanced ultrasound. J Med Ultrasound. 2018;26(3):128–33. https://doi.org/10.4103/JMU.JMU_12_17.
84. Piscaglia F, Corradi F, Mancini M, Giangregorio F, Tamberi S, Ugolini G, et al. Real time contrast enhanced ultrasonography in detection of liver metastases from gastrointestinal cancer. BMC Cancer. 2007;7:171. https://doi.org/10.1186/1471-2407-7-171.
85. Cantisani V, Ricci P, Erturk M, Pagliara E, Drudi F, Calliada F, et al. Detection of hepatic metastases from colorectal cancer: prospective evaluation of gray scale US versus SonoVue® low mechanical index real time-enhanced US as compared with multidetector-CT or Gd-BOPTA-MRI. Ultraschall Med. 2010;31(5):500–5. https://doi.org/10.1055/s-0028-1109751.
86. Dong Y, Wang WP, Mao F, Fan M, Ignee A, Serra C, et al. Contrast-enhanced ultrasound features of hepatic cystadenoma and hepatic cystadenocarcinoma. Scand J Gastroenterol. 2017;52(3):365–72. https://doi.org/10.1080/00365521.2016.1259652.
87. Corvino A, Catalano O, Setola SV, Sandomenico F, Corvino F, Petrillo A. Contrast-enhanced ultrasound in the characterization of complex cystic focal liver lesions. Ultrasound Med Biol. 2015;41(5):1301–10. https://doi.org/10.1016/j.ultrasmedbio.2014.12.667.
88. Xu HX, Lu MD, Liu LN, Zhang YF, Guo LH, Liu C, Wang S. Imaging features of intrahepatic biliary cystadenoma and cystadenocarcinoma

on B-mode and contrast-enhanced ultrasound. Ultraschall Med. 2012;33(7):E241–9. https://doi.org/10.1055/s-0031-1299276.
89. Kunze G, Staritz M, Köhler M. Contrast-enhanced ultrasound in different stages of pyogenic liver abscess. Ultrasound Med Biol. 2015;41(4):952–9. https://doi.org/10.1016/j.ultrasmedbio.2014.12.001.
90. Popescu A, Sporea I, Şirli R, Dănilă M, Mare R, Grădinaru Taşcău O, Moga T. Does contrast enhanced ultrasound improve the management of liver abscesses? A single centre experience. Med Ultrason. 2015;17(4):451–5. https://doi.org/10.11152/mu.2013.2066.174.deu.
91. Schwarze V, Mueller-Peltzer K, Negrão de Figueiredo G, Lindner F, Rübenthaler J, Clevert DA. The use of contrast-enhanced ultrasound (CEUS) for the diagnostic evaluation of hepatic echinococcosis. Clin Hemorheol Microcirc. 2018;70(4):449–55. https://doi.org/10.3233/CH-189310.
92. Shan QY, Chen LD, Zhou LY, Wang Z, Liu GJ, Huang Y, et al. Focal lesions in fatty liver: if quantitative analysis facilitates the differentiation of atypical benign from malignant lesions. Sci Rep. 2016;6:18640. https://doi.org/10.1038/srep18640.
93. Oliveira PB, Belo-Soares P, Magalhaes M, Andrade D, Pinto E, Caseiro Alves F. Value of time-intensity – based quantification of focal liver lesions on contrast enhanced ultrasound. ECR 2013 poster C-1036. Vienna: European Society of Radiology. https://doi.org/10.1594/ecr2013/C-1036.
94. Pei XQ, Liu LZ, Xiong YH, Zou RH, Chen MS, Li AH, Cai MY. Quantitative analysis of contrast-enhanced ultrasonography: differentiating focal nodular hyperplasia from hepatocellular carcinoma. Br J Radiol. 2013;86(1023):20120536. https://doi.org/10.1259/bjr.20120536.
95. Albrecht T, Blomley MJ, Cosgrove DO, Taylor-Robinson SD, Jayaram V, Eckersley R, et al. Non-invasive diagnosis of hepatic cirrhosis by transit-time analysis of an ultrasound contrast agent. Lancet. 1999;353(9164):1579–83. https://doi.org/10.1016/S0140-6736(98)06373-9.
96. Grier S, Lim AK, Patel N, Cobbold JF, Thomas HC, Cox IJ, Taylor-Robinson SD. Role of microbubble ultrasound contrast agents in the non-invasive assessment of chronic hepatitis C-related liver disease. World J Gastroenterol. 2006;12(22):3461–5. https://doi.org/10.3748/wjg.v12.i22.3461.
97. Blomley MJ, Lim AK, Harvey CJ, Patel N, Eckersley RJ, Basilico R, et al. Liver microbubble transit time compared with histology and Child-Pugh score in diffuse liver disease: a cross sectional study. Gut. 2003;52(8):1188–93. https://doi.org/10.1136/gut.52.8.1188.
98. Lim AK, Taylor-Robinson SD, Patel N, Eckersley RJ, Goldin RD, Hamilton G, et al. Hepatic vein transit times using a microbubble agent can predict disease severity non-invasively in patients with hepatitis C. Gut. 2005;54(1):128–33. https://doi.org/10.1136/gut.2003.030965.
99. Kim G, Shim KY, Baik SK. Diagnostic accuracy of hepatic vein arrival time performed with contrast-enhanced ultrasonography for cirrhosis: a systematic review and meta-analysis. Gut Liver. 2017;11(1):93–101. https://doi.org/10.5009/gnl16031.
100. Lim AK, Patel N, Eckersley RJ, Goldin RD, Thomas HC, Cosgrove DO, et al. Hepatic vein transit time of SonoVue: a comparative study with Levovist. Radiology. 2006;240(1):130–5. https://doi.org/10.1148/radiol.2401041517.
101. Ridolfi F, Abbattista T, Marini F, Vedovelli A, Quagliarini P, Busilacchi P, Brunelli E. Contrast-enhanced ultrasound to evaluate the severity of chronic hepatitis C. Dig Liver Dis. 2007;39(10):929–35. https://doi.org/10.1016/j.dld.2007.06.006.
102. Abbattista T, Ridolfi F, Ciabattoni E, Marini F, Bendia E, Brunelli E, Busilacchi P. Diagnosis of liver cirrhosis by transit-time analysis at contrast-enhanced ultrasonography. Radiol Med. 2008;113(6):860–74. https://doi.org/10.1007/s11547-008-0292-3. English, Italian.
103. Lim AK, Patel N, Eckersley RJ, Fitzpatrick J, Crossey MM, Hamilton G, et al. A comparison of 31P magnetic resonance spectroscopy and microbubble-enhanced ultrasound for characterizing hepatitis c-related liver disease. J Viral Hepat. 2011;18(10):e530–4. https://doi.org/10.1111/j.1365-2893.2011.01455.x.
104. Bernatik T, Strobel D, Häusler J, Hahn EG, Becker D. Hepatische Transitzeit eines Echosignalverstärkers als Indikator einer Lebermetastasierung - erste klinische Ergebnisse [Hepatic transit time of an ultrasound echo enhancer indicating the presence of liver metastases - first clinical results]. Ultraschall Med. 2002;23(2):91–5. https://doi.org/10.1055/s--2002-25196. German.
105. Zhang H, He Y, Du L, Wu Y. Shorter hepatic transit time can suggest coming metastases: through-monitoring by contrast-enhanced ultrasonography? J Ultrasound Med. 2010;29(5):719–26. https://doi.org/10.7863/jum.2010.29.5.719.
106. Fujita Y, Watanabe M, Sasao K, Wakui N, Shinohara M, Ishii K, Sumino Y. Investigation of liver parenchymal flow using contrast-enhanced ultrasound in patients with alcoholic liver disease. Alcohol Clin Exp Res. 2004;28(8 Suppl):169S–73S. https://doi.org/10.1097/01.alc.0000133546.24180.17. Proceedings.
107. Gasparini C, Bertolotto M, Crocè SL, Perrone R, Quaia E, Tiribelli C. Evaluation of liver parenchymal blood flow with contrast-enhanced US: preliminary results in healthy and cirrhotic patients. Acad Radiol. 2003;10(8):869–76. https://doi.org/10.1016/s1076-6332(03)00003-5.
108. Kaneko T, Teshigawara O, Sugimoto H, Hirota M, Inoue S, Takeda S, Nakao A. Signal intensity of the liver parenchyma in microbubble contrast agent in the late liver phase reflects advanced fibrosis of the liver. Liver Int. 2005;25(2):288–93. https://doi.org/10.1111/j.1478-3231.2005.01025.x.
109. Sanyal AJ, Bosch J, Blei A, Arroyo V. Portal hypertension and its complications. Gastroenterology.

2008;134(6):1715–28. https://doi.org/10.1053/j.gastro.2008.03.007.
110. de Franchis R, Primignani M. Natural history of portal hypertension in patients with cirrhosis. Clin Liver Dis. 2001;5(3):645–63. https://doi.org/10.1016/s1089-3261(05)70186-0.
111. Bosch J, Abraldes JG, Berzigotti A, García-Pagan JC. The clinical use of HVPG measurements in chronic liver disease. Nat Rev Gastroenterol Hepatol. 2009;6(10):573–82. https://doi.org/10.1038/nrgastro.2009.149.
112. Suk KT. Hepatic venous pressure gradient: clinical use in chronic liver disease. Clin Mol Hepatol. 2014;20(1):6–14. https://doi.org/10.3350/cmh.2014.20.1.6.
113. Merkel C, Montagnese S. Hepatic venous pressure gradient measurement in clinical hepatology. Dig Liver Dis. 2011;43(10):762–7. https://doi.org/10.1016/j.dld.2011.03.002.
114. Castera L, Pinzani M. Biopsy and non-invasive methods for the diagnosis of liver fibrosis: does it take two to tango? Gut. 2010;59(7):861–6. https://doi.org/10.1136/gut.2010.214650.
115. Maruyama H, Kato N. Contrast-enhanced ultrasonography for the diagnosis of portal hypertension. In: Berzigotti AA, Bosch JJ, editors. Diagnostic methods for cirrhosis and portal hypertension. New York, NY: Springer; 2018. p. 149–58.
116. Berzigotti A, Nicolau C, Bellot P, Abraldes JG, Gilabert R, García-Pagan JC, Bosch J. Evaluation of regional hepatic perfusion (RHP) by contrast-enhanced ultrasound in patients with cirrhosis. J Hepatol. 2011;55(2):307–14. https://doi.org/10.1016/j.jhep.2010.10.038.
117. Qu EZ, Zhang YC, Li ZY, Liu Y, Wang JR. Contrast-enhanced sonography for quantitative assessment of portal hypertension in patients with liver cirrhosis. J Ultrasound Med. 2014;33(11):1971–7. https://doi.org/10.7863/ultra.33.11.1971.
118. Zhai L, Qiu LY, Zu Y, Yan Y, Ren XZ, Zhao JF, et al. Contrast-enhanced ultrasound for quantitative assessment of portal pressure in canine liver fibrosis. World J Gastroenterol. 2015;21(15):4509–16. https://doi.org/10.3748/wjg.v21.i15.4509.
119. Kim WR, Stock PG, Smith JM, Heimbach JK, Skeans MA, Edwards EB, et al. OPTN/SRTR 2011 annual data report: liver. Am J Transplant. 2013;13(Suppl 1):73–102. https://doi.org/10.1111/ajt.12021.
120. Jeong WK, Kim TY, Sohn JH, Kim Y, Kim J. Severe portal hypertension in cirrhosis: evaluation of perfusion parameters with contrast-enhanced ultrasonography. PLoS One. 2015;10(3):e0121601. https://doi.org/10.1371/journal.pone.0121601.
121. Shimada T, Maruyama H, Kondo T, Sekimoto T, Takahashi M, Yokosuka O. Impact of splenic circulation: non-invasive microbubble-based assessment of portal hemodynamics. Eur Radiol. 2015;25(3):812–20. https://doi.org/10.1007/s00330-014-3476-3.
122. Eisenbrey JR, Dave JK, Halldorsdottir VG, Merton DA, Miller C, Gonzalez JM, et al. Chronic liver disease: noninvasive subharmonic aided pressure estimation of hepatic venous pressure gradient. Radiology. 2013;268(2):581–8. https://doi.org/10.1148/radiol.13121769.
123. Kim MY, Suk KT, Baik SK, Kim HA, Kim YJ, Cha SH, et al. Hepatic vein arrival time as assessed by contrast-enhanced ultrasonography is useful for the assessment of portal hypertension in compensated cirrhosis. Hepatology. 2012;56(3):1053–62. https://doi.org/10.1002/hep.25752.
124. Li J, Feng JC, Peng XY, Wu XW, Du TT, Wang JJ, et al. Usefulness of contrast-enhanced ultrasonography for predicting esophageal varices in patients with hepatitis B virus (HBV)-related cirrhosis. Med Sci Monit. 2017;23:2241–9. https://doi.org/10.12659/msm.904227.
125. Qiu L, Zhang X, Liu D, Qian L, Hu X. Contrast-enhanced ultrasonography diagnostic evaluation of esophageal varices in patients with cirrhosis. Ultrasound Q. 2016;32(2):136–43. https://doi.org/10.1097/RUQ.0000000000000173.
126. Raza SA, Jang HJ, Kim TK. Differentiating malignant from benign thrombosis in hepatocellular carcinoma: contrast-enhanced ultrasound. Abdom Imaging. 2014;39(1):153–61. https://doi.org/10.1007/s00261-013-0034-4.
127. Vilana R, Bru C, Bruix J, Castells A, Sole M, Rodes J. Fine-needle aspiration biopsy of portal vein thrombus: value in detecting malignant thrombosis. AJR Am J Roentgenol. 1993;160(6):1285–7. https://doi.org/10.2214/ajr.160.6.8388621.
128. Gao X, Wang HH, Zhang YZ, Liu XB, Qin XC. Contrast-enhanced ultrasound at high mechanical index: a new method for transjugular intrahepatic portosystemic shunt follow-up. Clin Radiol. 2020;75(4):302–7. https://doi.org/10.1016/j.crad.2019.10.011.
129. Jones PD, Hayashi PH, Barritt AS IV. Liver transplantation in 2013: challenges and controversies. Minerva Gastroenterol Dietol. 2013;59(2):117–31.
130. Girometti R, Pancot M, Como G, Zuiani C. Imaging of liver transplantation. Eur J Radiol. 2017;93:295–307. https://doi.org/10.1016/j.ejrad.2017.05.014.
131. Hackl C, Schlitt HJ, Kirchner GI, Knoppke B, Loss M. Liver transplantation for malignancy: current treatment strategies and future perspectives. World J Gastroenterol. 2014;20(18):5331–44. https://doi.org/10.3748/wjg.v20.i18.5331.
132. Como G, Montaldo L, Baccarani U, Lorenzin D, Zuiani C, Girometti R. Contrast-enhanced ultrasound applications in liver transplant imaging. Abdom Radiol (NY). 2021;46(1):84–95. https://doi.org/10.1007/s00261-020-02402-z.
133. Marrero JA, Kulik LM, Sirlin CB, Zhu AX, Finn RS, Abecassis MM, et al. Diagnosis, staging, and management of hepatocellular carcinoma: 2018 practice guidance by the American Association for the study of liver diseases. Hepatology. 2018;68(2):723–50. https://doi.org/10.1002/hep.29913.
134. Mazzaferro V, Regalia E, Doci R, Andreola S, Pulvirenti A, Bozzetti F, et al. Liver transplanta-

tion for the treatment of small hepatocellular carcinomas in patients with cirrhosis. N Engl J Med. 1996;334(11):693–9. https://doi.org/10.1056/NEJM199603143341104.
135. Xu EJ, Mao R, Zheng RQ, Lu MQ, Liao M, Ren J, Li K. Three-dimensional contrast-enhanced ultrasonic cholangiography: a new technique for delineation of the biliary tract in a liver donor. Liver Transpl. 2009;15(9):1154–6. https://doi.org/10.1002/lt.21783.
136. Zheng RQ, Chen GH, Xu EJ, Mao R, Lu MQ, Liao M, et al. Evaluating biliary anatomy and variations in living liver donors by a new technique: three-dimensional contrast-enhanced ultrasonic cholangiography. Ultrasound Med Biol. 2010;36(8):1282–7. https://doi.org/10.1016/j.ultrasmedbio.2010.05.001.
137. Novruzbekov MS, Olisov OD. Sosudistye oslozhneniya posle ortotopicheskoj transplantacii pecheni [Vascular complications after orthotopic liver transplantation]. Transplantologiya. 2017;9(1):35–50. https://doi.org/10.23873/2074-0506-2017-9-1-35-50. Russian.
138. Herold C, Reck T, Ott R, Schneider HT, Becker D, Schuppan D, Hahn EG. Contrast-enhanced ultrasound improves hepatic vessel visualization after orthotopic liver transplantation. Abdom Imaging. 2001;26(6):597–600. https://doi.org/10.1007/s00261-001-0064-1.
139. Hom BK, Shrestha R, Palmer SL, Katz MD, Selby RR, Asatryan Z, et al. Prospective evaluation of vascular complications after liver transplantation: comparison of conventional and microbubble contrast-enhanced US. Radiology. 2006;241(1):267–74. https://doi.org/10.1148/radiol.2411050597.
140. Ma L, Lu Q, Luo Y. Vascular complications after adult living donor liver transplantation: evaluation with ultrasonography. World J Gastroenterol. 2016;22(4):1617–26. https://doi.org/10.3748/wjg.v22.i4.1617.
141. Zheng RQ, Mao R, Ren J, Xu EJ, Liao M, Wang P, et al. Contrast-enhanced ultrasound for the evaluation of hepatic artery stenosis after liver transplantation: potential role in changing the clinical algorithm. Liver Transpl. 2010;16(6):729–35. https://doi.org/10.1002/lt.22054.
142. Ren J, Wu T, Zheng BW, Tan YY, Zheng RQ, Chen GH. Application of contrast-enhanced ultrasound after liver transplantation: current status and perspectives. World J Gastroenterol. 2016;22(4):1607–16. https://doi.org/10.3748/wjg.v22.i4.1607.
143. Luo Y, Fan YT, Lu Q, Li B, Wen TF, Zhang ZW. CEUS: a new imaging approach for postoperative vascular complications after right-lobe LDLT. World J Gastroenterol. 2009;15(29):3670–5. https://doi.org/10.3748/wjg.15.3670.
144. Sidhu PS, Shaw AS, Ellis SM, Karani JB, Ryan SM. Microbubble ultrasound contrast in the assessment of hepatic artery patency following liver transplantation: role in reducing frequency of hepatic artery arteriography. Eur Radiol. 2004;14(1):21–30. https://doi.org/10.1007/s00330-003-1981-x.
145. Huang DY, Yusuf GT, Daneshi M, Ramnarine R, Deganello A, Sellars ME, Sidhu PS. Contrast-enhanced ultrasound (CEUS) in abdominal intervention. Abdom Radiol (NY). 2018;43(4):960–76. https://doi.org/10.1007/s00261-018-1473-8.
146. Ren X, Luo Y, Gao N, Niu H, Tang J. Common ultrasound and contrast-enhanced ultrasonography in the diagnosis of hepatic artery pseudoaneurysm after liver transplantation. Exp Ther Med. 2016;12(2):1029–33. https://doi.org/10.3892/etm.2016.3343.
147. Zhu XS, Gao YH, Wang SS, Cheng Q, Ling Y, Fan L, et al. Contrast-enhanced ultrasound diagnosis of splenic artery steal syndrome after orthotopic liver transplantation. Liver Transpl. 2012;18(8):966–71. https://doi.org/10.1002/lt.23453.
148. Park YS, Kim KW, Kim SY, Lee SJ, Lee J, Kim JH, et al. Obstruction at middle hepatic venous tributaries in modified right lobe grafts after living-donor liver Transplantation: diagnosis with contrast-enhanced US. Radiology. 2012;265(2):617–26. https://doi.org/10.1148/radiol.12112042.
149. Hwang HJ, Kim KW, Jeong WK, Kim SY, Song GW, Hwang S, Lee SG. Hepatic outflow obstruction at middle hepatic vein tributaries or inferior right hepatic veins after living donor liver transplantation with modified right lobe graft: comparison of CT and Doppler ultrasound. AJR Am J Roentgenol. 2009;193(3):745–51. https://doi.org/10.2214/AJR.08.2145.

Gallbladder

5

Ella I. Peniaeva, Alexander N. Sencha, and Yury N. Patrunov

Traditionally, the examinations of the gallbladder in the clinical practice begin with an ultrasound study. This method demonstrates high sensitivity and specificity in the detection of stones. However, the capability of conventional US in the assessment of microvascularity is limited. CEUS overcomes these limitations and permits evaluation of the perfusion in both the gallbladder wall and intraluminal lesions.

The EFSUMB Guidelines and Recommendations on the Clinical Practice of CEUS on non-hepatic applications suggest using CEUS in the following conditions [1]:

- in acute cholecystitis to better detect local complications,
- to differentiate chronic cholecystitis from gallbladder carcinoma,
- to differentiate between a perfused gallbladder lesion and motionless biliary sludge.

E. I. Peniaeva (✉) · Y. N. Patrunov
Department of Ultrasound Diagnostics of the Center for Radiological Diagnostics, Private Healthcare Institution "Clinical Hospital "RZD-Medicina" of Yaroslavl City", Yaroslavl, Russian Federation

A. N. Sencha
Department of Visual and Functional Diagnostics, Federal State Budget Institution "National Medical Research Center for Obstetrics, Gynecology and Perinatology n.a. V.I.Kulakov", Moscow, Russian Federation

CEUS is considered necessary only in the cases of the indefinite results of conventional US. The study is held after 8 h of fasting and uses the standard protocol. For the study, 1.2–2.4 mL of SonoVue® is usually enough. A dose up to 4.8 mL is required if a high-frequency probe is used [2].

The dynamics of the gallbladder wall contrast enhancement differs from the liver because it has an exclusively arterial blood supply from the cystic artery without any participation of the portal vein system. Therefore, the gallbladder CEUS implicates only two phases: arterial (<30 s) and venous (>31 s). The washout of the UCA from the gallbladder wall starts earlier than from the liver parenchyma. CEUS of the gallbladder walls and lesions evaluates the perfusion, kinetics of the UCA, vascular architectonics, and the continuity of the gallbladder wall. The intensity of enhancement is compared with normal liver parenchyma [2]. The normal gallbladder wall is thin and enhances simultaneously with the arterial system of the liver (Fig. 5.1) with the beginning of washout in the late portal venous phase. In some cases, it is possible to visualize anatomic variations and separate branches.

Acute cholecystitis is often (in 85–90%) a consequence of gallstones and obstruction. The clinical signs are diverse and depend on the morphologic type of inflammation, its severity, the presence of peritonitis, and related changes in

A. N. Sencha, Y. N. Patrunov (eds.), *Contrast-Enhanced Ultrasound*,
https://doi.org/10.1007/978-3-030-91764-7_5

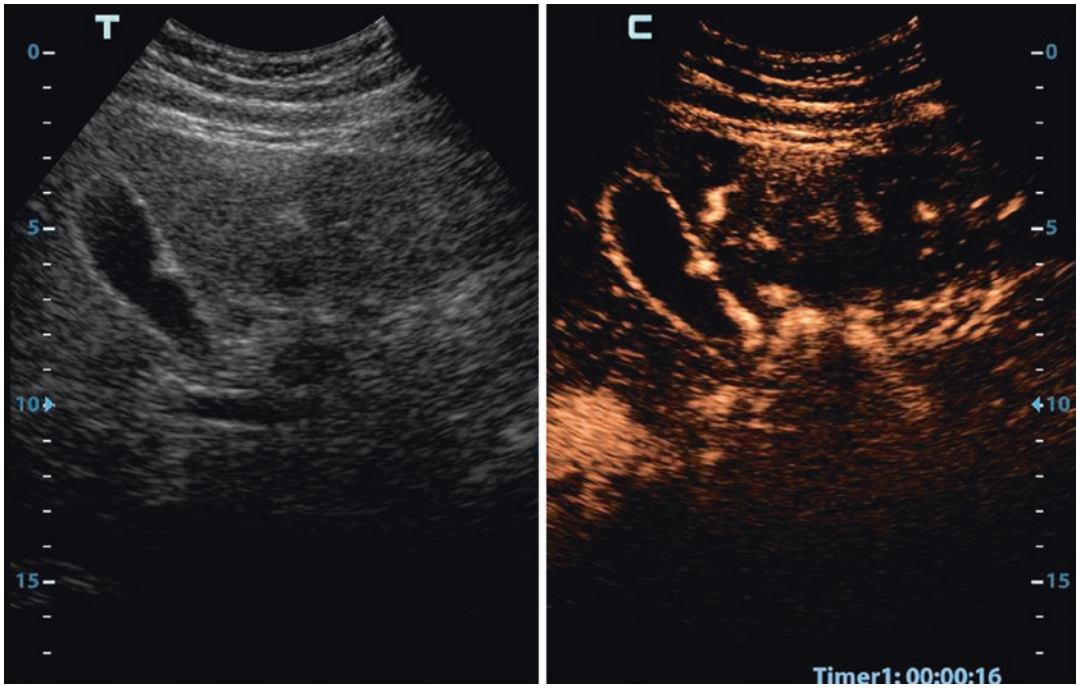

Fig. 5.1 Normal gallbladder. CEUS image. Obvious regular contrast enhancement of the gallbladder wall, no enhancement of the contents

the bile ducts. The early acute inflammation in the gallbladder wall exhibits hypervascularization [3]. CEUS reveals early arterial phase hyperenhancement of the thickened gallbladder wall with washout in the venous phase [2] (Fig. 5.2).

Without treatment, acute serous cholecystitis can progress to the destructive type with such serious local complications as empyema, gangrene, perforation, and perivesical abscess [4]. When the inflammation involves the adjacent liver parenchyma, there arises reactive hepatitis, which demonstrates local arterial phase hyperenhancement of liver parenchyma [1]. The gallbladder wall distension and swelling lead to impaired microcirculation. Gangrenous cholecystitis and

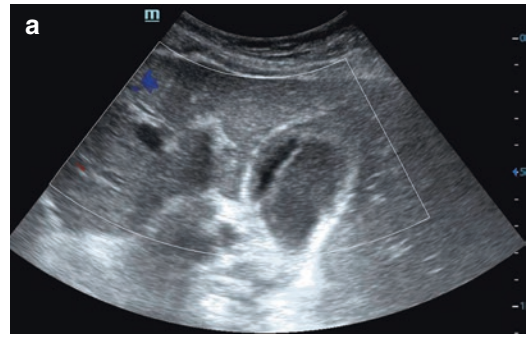

Fig. 5.2 Acute cholecystitis with local mural destruction. (**a**) Grayscale US and CDI image. (**b**) The arterial phase CEUS image. (**c**) The venous phase CEUS image. Note the hyperenhancing thickened gallbladder wall with a nonenhancing area; the echogenic content is also nonenhancing

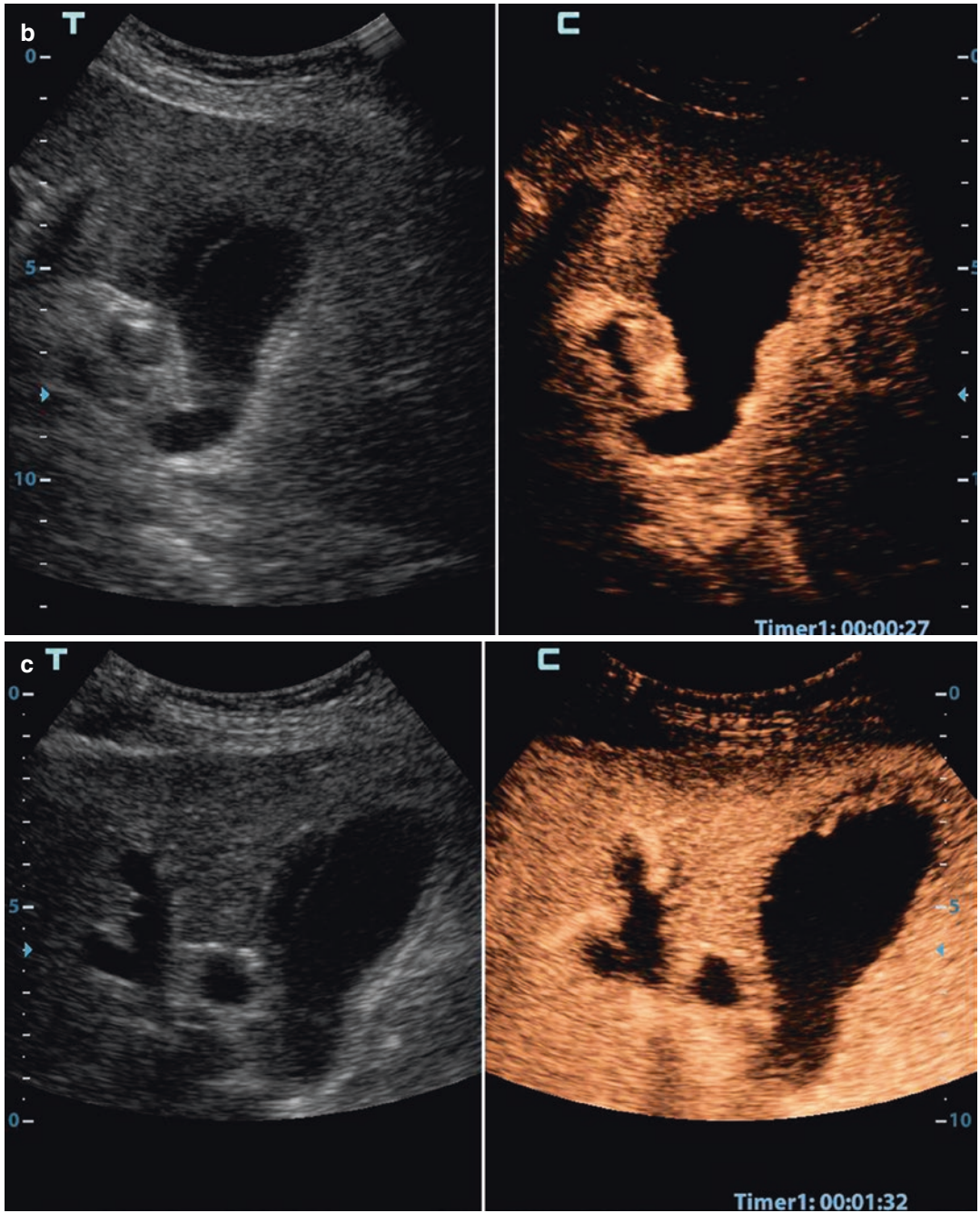

Fig. 5.2 (continued)

transmural necrosis are associated with heterogeneous enhancement of the wall with irregular discontinuous margins [5–7] (Fig. 5.2). The detection of a nonenhancing area (enhancement defect) within the gallbladder wall enabled diagnosis of the gangrene with a sensitivity of 85–91% and specificity of 67.5–84.8% [7]. A good interobserver agreement was also demonstrated (median *k* value 0.664, range 0.655–0.680).

The transmural necrosis with gallbladder wall perforation demonstrates the complete absence of contrast enhancement in this zone. In 1934, Niemeier [8] classified the condition into the following three types:

- type I, acute perforation into the free peritoneal cavity,
- type II, subacute perforation with abscess formation,
- type III, chronic perforation with fistula formation between the gallbladder and another viscus.

Intra- or extra-hepatic abscess associated with the gallbladder perforation is visualized as a mixed mass with heterogeneous contrast enhancement of honeycomb pattern [9].

Concerning the gallbladder cavity, the biliary sludge is usually easily differentiated by the conventional US as it moves when changing the patient's body position. It may cause diagnostic problems if fixed with no displacement within the cavity. In this case, the main criterion to differentiate the sludge from a lesion is vascularity. CDI is not always confident in the complete avascularity of the gallbladder mass, because its capabilities in the detection of microcirculation are limited. On the other hand, artifacts from dense inclusions within the aggregation may mimic blood flow. CEUS reliably demonstrates the absence of vascularization of biliary sludge providing high accuracy in differential diagnosis from the tumors of the gallbladder wall [2].

The value of CEUS for the differential diagnosis of polyp, adenoma, and non-invasive gallbladder carcinoma is currently not evaluated.

Gallbladder polyps are often an incidental US finding. More than 60–70% of them are represented by cholesterol polyps [10]. In primary sclerosing cholangitis and gastrointestinal polyposis syndromes, up to 60% of the gallbladder polyps are malignant [11]. Malignancy in gallbladder polyps between 6 and 10 mm is extremely rare, while polyps >10 mm are regarded as preinvasive adenomas and papillary neoplasms [1].

The gallbladder adenoma is a relatively rare entity. It is represented by a polypoid lesion with a smooth or tuberous surface, a relatively homogeneous internal structure without any infiltration of the underlying wall. CEUS reveals uniform hyperenhancement or isoenhancement in the arterial phase (Fig. 5.3) with subsequent iso- or hypoenhancement in the venous phase [2]. Polyps >10 mm which show an iso- and inhomogeneous enhancement pattern may be a criterion to differentiate adenomas from cholesterol polyps [1].

Adenomyomomatosis is a hyperplastic process of the gallbladder wall that does not have malignant potential and may occur in a focal, segmental, or diffuse type. It is characterized by wall hyperplasia with intramural diverticula of the mucous membrane (Rokitansky–Aschoff sinuses). Arterial phase CEUS demonstrates the characteristic enhancement of the "moth-eaten" pattern of the affected gallbladder wall with nonenhanced sinuses. An important feature is a clear

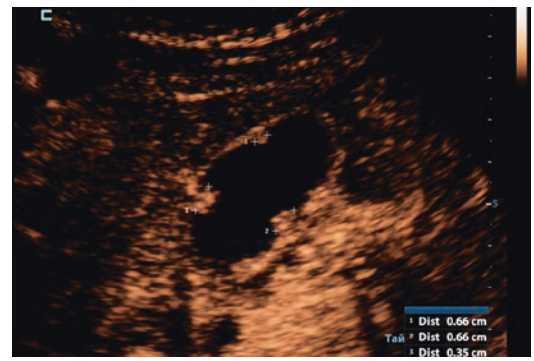

Fig. 5.3 Adenomatous polyps of the gallbladder. CEUS image. Contrast enhancement of polypoid lesions in the arterial phase

boundary with the surrounding tissues. Another feature is the isoenhancement of the thickened wall with a small non-enhanced rim surrounding the gallbladder [1, 2, 10].

Gallbladder carcinoma is a rare malignant tumor, which mostly affects elderly people with long-term gallstone disease. About 80% of the gallbladder malignancies are represented by adenocarcinoma. Gallbladder sarcoma and metastases are extremely rare. About 60% of carcinomas occur in the gallbladder fundus, 30% in the body, and 10% in the neck [12]. The early-stage tumor is difficult to differentiate from other abnormalities.

The detection of tortuous tumor vessels with irregular branching exhibited the sensitivity of 75%, specificity—100%, and diagnostic accuracy—91% [13]. Hyperenhancement of the tumor in the arterial phase cannot be a differential diagnostic sign, because is observed both in malignant (85%) and benign (70%) lesions [1, 13].

Adenocarcinoma of the gallbladder in 90.9% demonstrates hyper- or isoenhancement in the arterial phase with the beginning of washout and hypoenhancement within 35 s after the introduction of UCA [14]. Another important differential diagnostic sign is the destruction of the gallbladder wall and infiltration of the adjacent liver tissue, characterized by the sensitivity of 84.8% and specificity of 100%. Besides, in the case of liver infiltration, the hypoenhanced tumor is better differentiated in the portal phase against the background of homogeneous intense enhancement of liver parenchyma, which enables specification of the tumor size and severity of invasion [15].

Despite the above data, the practical application of CEUS for the differential diagnosis of benign and malignant lesions of the gallbladder remains the subject for discussion.

References

1. Sidhu PS, Cantisani V, Dietrich CF, Gilja OH, Saftoiu A, Bartels E, et al. The EFSUMB guidelines and recommendations for the clinical practice of contrast-enhanced ultrasound (CEUS) in non-hepatic applications: update 2017 (long version). Ultraschall Med. 2018;39(2):e2–e44. https://doi.org/10.1055/a-0586-1107.
2. Sparchez Z, Radu P. Role of CEUS in the diagnosis of gallbladder disease. Med Ultrason. 2012;14(4):326–30.
3. Karmazanovskij GG, Ternovoj SK, editors. Luchevaya diagnostika i terapiya v gastroenterologii: nacional'noe rukovodstvo [Radiation diagnostics and therapy in gastroenterology: national guidelines]. Moscow: Geotar-Media; 2014. Russian.
4. Smith EA, Dillman JR, Elsayes KM, Menias CO, Bude RO. Cross-sectional imaging of acute and chronic gallbladder inflammatory disease. AJR Am J Roentgenol. 2009;192(1):188–96. https://doi.org/10.2214/AJR.07.3803.
5. Kawai R, Hata J, Manabe N, Imamura H, Iida A, Nakatou R, et al. Contrast-enhanced ultrasonography with Sonazoid for diagnosis of gangrenous cholecystitis. J Med Ultrason. 2016;43(2):193–9. https://doi.org/10.1007/s10396-015-0677-6.
6. Revel L, Lubrano J, Badet N, Manzoni P, Degano SV, Delabrousse E. Preoperative diagnosis of gangrenous acute cholecystitis: usefulness of CEUS. Abdom Imaging. 2014;39(6):1175–81. https://doi.org/10.1007/s00261-014-0151-8.
7. Ripollés T, Martínez-Pérez MJ, Martin G, Vizuete J, Martínez-García R, Diez J, Martí E. Usefulness of contrast-enhanced US in the diagnosis of acute gangrenous cholecystitis: a comparative study with surgical and pathological findings. Eur J Radiol. 2016;85(1):31–8. https://doi.org/10.1016/j.ejrad.2015.10.010.
8. Niemeier OW. Acute free perforation of the gallbladder. Ann Surg. 1934;99(6):922–4.
9. Tang S, Wang Y, Wang Y. Contrast-enhanced ultrasonography to diagnose gallbladder perforation. Am J Emerg Med. 2013;31(8):1240–3. https://doi.org/10.1016/j.ajem.2013.04.034.
10. Weskott HP. Contrast-enhanced ultrasound. 2nd ed. London: Uni-Med Science; 2013.
11. Gallahan WC, Conway JD. Diagnosis and management of gallbladder polyps. Gastroenterol Clin N Am. 2010;39:359–67.
12. Associaciya onkologov Rossii. Rossijskoe obshchestvo klinicheskih onkologov. Rak zhelchevyvodyashchej sistemy. Klinicheskie rekomendacii. [Association of Oncologists of Russia. Russian Society of Clinical Oncologists. Cancer of the biliary system. Clinical recommendations]. Moscow: Associaciya onkologov Rossii; 2018. Russian. http://www.oncology.ru/association/clinical-guidelines/2018/rak_zhelchevyvodyashey_sistemy_pr2018.pdf. Accessed 15 Feb 2021.
13. Numata K, Oka H, Morimoto M, Sugimori K, Kunisaki R, Nihonmatsu H, et al. Differential diagnosis of gallbladder diseases with contrast-enhanced harmonic gray scale ultrasonography. J Ultrasound Med. 2007;26(6):763–74. https://doi.org/10.7863/jum.2007.26.6.763.

14. Xie XH, Xu HX, Xie XY, Lu MD, Kuang M, Xu ZF, et al. Differential diagnosis between benign and malignant gallbladder diseases with real-time contrast-enhanced ultrasound. Eur Radiol. 2010;20(1):239–48. https://doi.org/10.1007/s00330-009-1538-8.

15. Liu LN, Xu HX, Lu MD, Xie XY, Wang WP, Hu B, et al. Contrast-enhanced ultrasound in the diagnosis of gallbladder diseases: a multi-center experience. PLoS One. 2012;7(10):e48371. https://doi.org/10.1371/journal.pone.0048371.

Pancreas

6

Alexander N. Sencha, Elena P. Fisenko, Natalia N. Vetsheva, and Ella I. Peniaeva

The pancreas is supplied with blood with numerous branches of the common hepatic, splenic, and superior mesenteric arteries. Blood supply sources for the head, body, and tail are different. The head and uncinate process receive their blood supply from the superior (anterior and posterior) and inferior (anterior and posterior) pancreaticoduodenal arteries, which communicate and form anterior and posterior arterial arcades. These arteries are branches of the gastroduodenal and superior mesenteric arteries. The body and tail of the pancreas are predominantly supplied by the branches of the splenic artery and smaller branches that stem from the gastroduodenal and superior mesenteric arteries. Venous drainage of the pancreas is into the portal vein system mainly via splenic and superior mesenteric veins, which accompany the same arteries.

CEUS increased the diagnostic accuracy of ultrasound in the diagnosis of pancreatic diseases [1–5]. According to the EFSUMB Guidelines and Recommendations for the Clinical Practice of CEUS in Non-Hepatic Applications, Update 2017 [6], CEUS is applicable for the following purposes:

- to reliably characterize ductal adenocarcinoma in solid pancreatic lesions,
- to distinguish between pancreatic ductal adenocarcinoma and neuroendocrine tumors,
- to differentiate between cystic neoplasms and pseudocysts,
- to differentiate vascular (solid) from avascular (e.g., liquid or necrotic) components of a pancreatic lesion,
- to define the dimensions and margins of a pancreatic lesion and its vascular relationships,
- to diagnose and follow-up acute necrotizing pancreatitis,

Supplementary Information The online version contains supplementary material available at [https://doi.org/10.1007/978-3-030-91764-7_6].

A. N. Sencha (✉)
Department of Visual and Functional Diagnostics, Federal State Budget Institution "National Medical Research Center for Obstetrics, Gynecology and Perinatology n.a. V.I.Kulakov", Moscow, Russian Federation

E. P. Fisenko
Ultrasound Diagnostics Laboratory, Department of Clinical Physiology, Instrumental and Radiology Diagnostics, B.V. Petrovsky Russian Research Surgery Center, Moscow, Russian Federation

N. N. Vetsheva
Ultrasound Diagnostics Department, State Budgetary Healthcare Institution of Moscow Area "Moscow Regional Research Clinical Institute n.a. M.F. Vladimirskiy", Moscow, Russian Federation

E. I. Peniaeva
Department of Ultrasound Diagnostics of the Center for Radiological Diagnostics, Private Healthcare Institution "Clinical Hospital "RZD-Medicina" of Yaroslavl City", Yaroslavl, Russian Federation

A. N. Sencha, Y. N. Patrunov (eds.), *Contrast-Enhanced Ultrasound*,
https://doi.org/10.1007/978-3-030-91764-7_6

- to follow-up indeterminate cystic pancreatic lesions,
- to improve the accuracy of percutaneous ultrasound-guided pancreatic procedures,
- to assess pancreatic graft ischemia and other vascular disorders.

CEUS procedure for the diagnosis of pancreatic diseases is the same as for other abdominal or retroperitoneal organs. The study demands an initially good grayscale image of the target lesion. In patients with poor visualization with the B-mode US (e.g. tympanites, hypersthenic constitution), CEUS will not supply any additional diagnostic information [2].

In adult patients, a bolus introduction of 2.4 ml of SonoVue® is required when using a convex probe and 4.8 ml of SonoVue® with a linear probe. In some cases, the diagnosis of small-sized tumors is difficult with the standard CEUS technique. Endoscopic CEUS, which combines the advantages of high-resolution US and contrast enhancement may be of benefit [7].

The arterial contrast enhancement of the pancreas starts almost simultaneously with the enhancement of the aorta (10–30 s) followed by the venous phase (30–120 s), and the late venous phase (>120 s). The pancreas begins to enhance earlier than the liver and the enhancement lasts shorter due to solely arterial blood supply. The arterial phase enhancement is uniform and intense [5].

6.1 Pancreatic Tumors

If the conventional US detects a pancreatic lesion, it should be followed by CEUS to differentiate the findings [3]. CEUS implicates the comparison of the contrast enhancement of the lesion and normal pancreatic tissue. The sensitivity and specificity of CEUS in pancreatic neoplasms are 91% and 87%, respectively [8]. CEUS is not inferior to the CT in the identification of ductal carcinoma, and even exceeds CT in the lesions of smaller than 2 cm in size (the sensitivity of CEUS and CT were reported 100% and 73.3%, respectively) [9].

The endoscopic US is a method of choice to exclude pancreatic tumors, identify and differentiate small-sized solid lesions, and detect their connection with the ducts. Dietrich et al. [10] demonstrated that CT failed to identify 37% of small-sized pancreatic lesions (≤15 mm), which were imaged by CEUS and endoscopic CEUS. High value of endoscopic CEUS for differential diagnosis of the pancreatic masses is also reported by several publications [11, 12]. CEUS and endoscopic CEUS have similar enhancement patterns in the corresponding histopathological types of pancreatic tumors.

Ductal adenocarcinoma confers approximately 95% of all exocrine pancreatic neoplasms [13]. These tumors are very aggressive, and at the time of the diagnosis, only 10–20% of tumors remain resectable. The 5-year survival rate is less than 5% [13–15]. Ductal adenocarcinomas predominantly affect the pancreatic head, and only about 30% are located in the body or tail of the pancreas.

CEUS reveals ductal adenocarcinoma as a lesion with indistinct margins, which is hypoenhancing in all phases (Figs. 6.1 and 6.2, Video 6.1). A pancreatic multicenter ultrasound study (PAMUS) in 2012 demonstrated that this enhancement pattern is characteristic of 90% of ductal adenocarcinomas and is explained by the histopathological structure of the tumor with pronounced sclerosis, desmoplasia, and poor vascularity [16].

Besides, the severity of the tumor hypoenhancement in some cases is related to the degree of differentiation. The more pronounced is hypoenhancement, the less differentiated and more aggressive is the tumor [17]. Hypoenhancement of ductal adenocarcinoma in all vascular phases permits differential diagnosis with well vascularized neuroendocrine tumor and inflammatory pseudotumor, the latter demonstrating the isoenhancing pattern identical to the normal pancreatic parenchyma [10, 16].

Sporadic publications on quantitative analysis of CEUS [1, 18, 19] indicate its use for the differential diagnosis of ductal adenocarcinoma and inflammatory pseudotumor. All of them underline the differences in the peak intensity of the enhancement of the adenocarcinoma and pancre-

atic parenchyma, inclusive of inflammatory pseudotumor. The value of other TIC data remains disputable.

Askerova [1] reports that pancreatic ductal adenocarcinoma is characterized by longer arrival time and TTP intensity, lower peak intensity and the area under the curve, and earlier washout (Table 6.1). The study of D'Onofrio et al. [18] did not reveal any reliable difference in TTP but demonstrated the difference in peak intensity, which in all cases objectively confirms the hypoenhancement of the tumor.

Neuroendocrine tumor is the second most common solid pancreatic tumor. In most cases, it is less aggressive than ductal adenocarcinoma [20]. These tumors are divided into functional, the most common of which are insulinoma and gastrinoma, and non-functional, the latter having higher malignant potential. Both functional and non-functional neuroendocrine tumors have rich

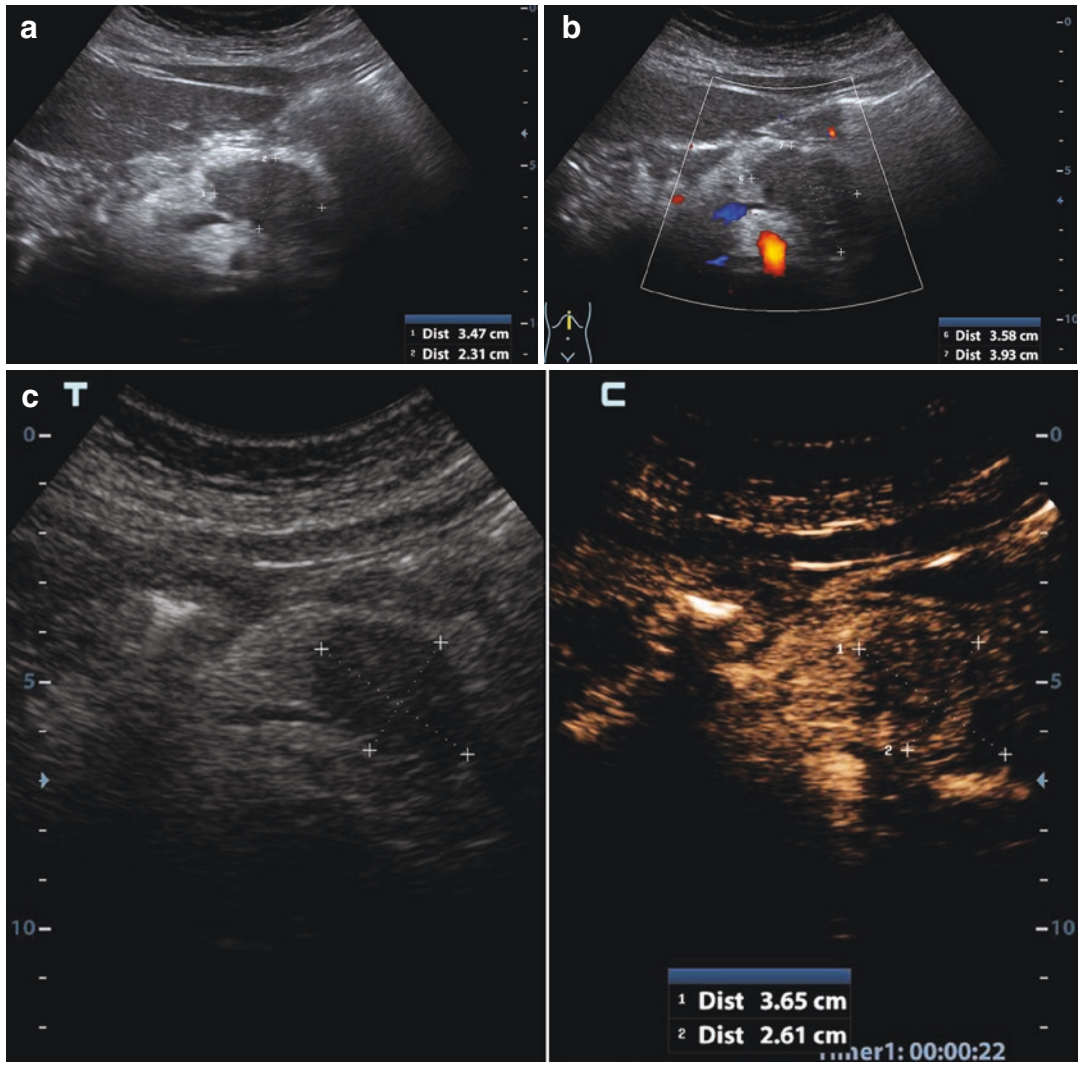

Fig. 6.1 Pancreatic adenocarcinoma. (**a**) The hypoechoic lesion in the pancreatic body. Grayscale US image. (**b**) CDI image. Hypovascularity of the lesion. (**c**) Hypoenhancement of the lesion in the early arterial phase with CEUS. (**d**) Hypoenhancement of the lesion in the arterial phase with CEUS. (**e**) TIC for the tumor (ROI1, pink) and normal parenchyma of the pancreas (ROI2, yellow). Rapid washout of the tumor. (**f**) TIC parameters for Fig. 6.1.e exhibit low enhancement (low PI) and fast washout (low DT/2) of the tumor

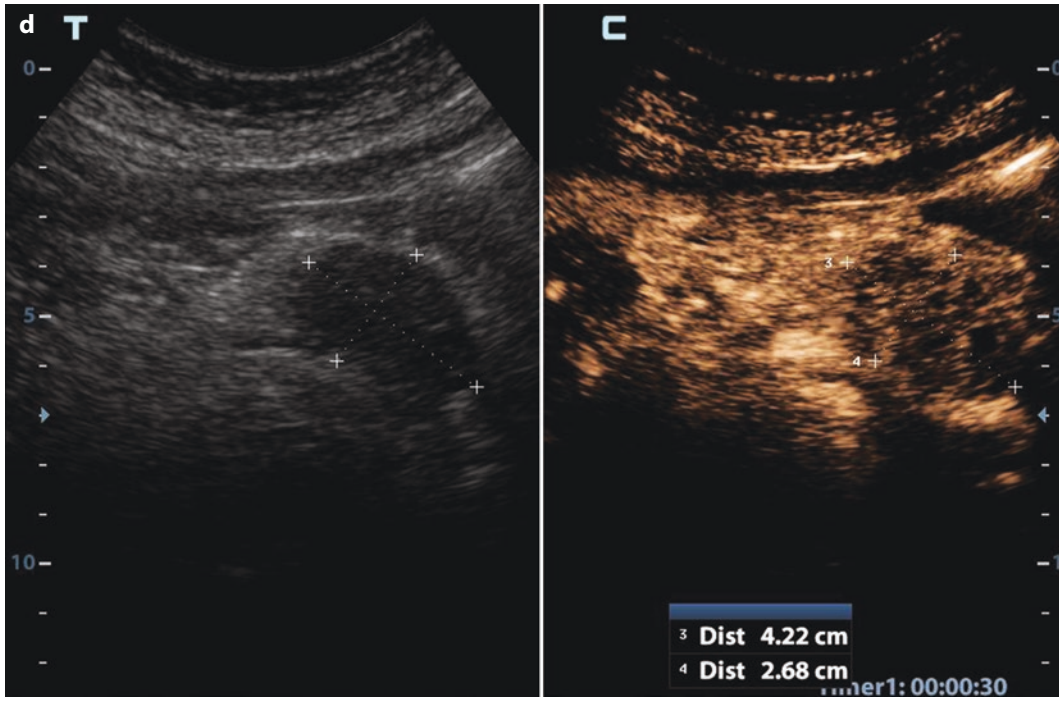

Fig. 6.1 (continued)

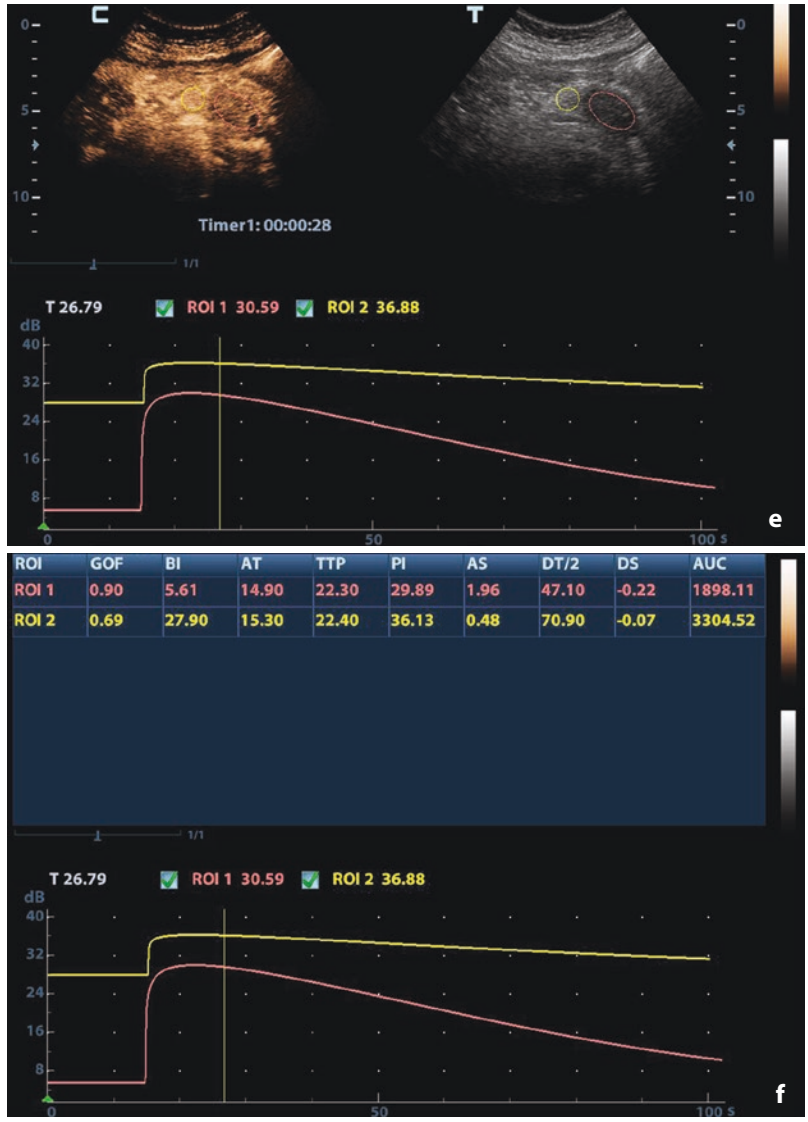

Fig. 6.1 (continued)

arterial vascular supply. Therefore, even when Doppler imaging does not detect hypervascularization, CEUS demonstrates hyperenhancement in the arterial phase [21] (Fig. 6.3, Video 6.2). Contrast enhancement of large or low-differentiated tumors may be heterogeneous due to necrotic areas. Late phase hypoenhancement is observed regardless of the tumor size [20]. Another characteristic feature of neuroendocrine tumors is the peripheral rim-shaped hyperenhancement. In rare cases, the tumor hypoenhancement may be observed due to dense hyalinized stroma.

There are just single publications, which quantitatively analyze CEUS of neuroendocrine tumors. They report a reliable difference ($p \leq 0.05$) in the corresponding TIC data in the tumors of various degrees of differentiation. G1 demonstrated a shorter arrival time, TTP, washin

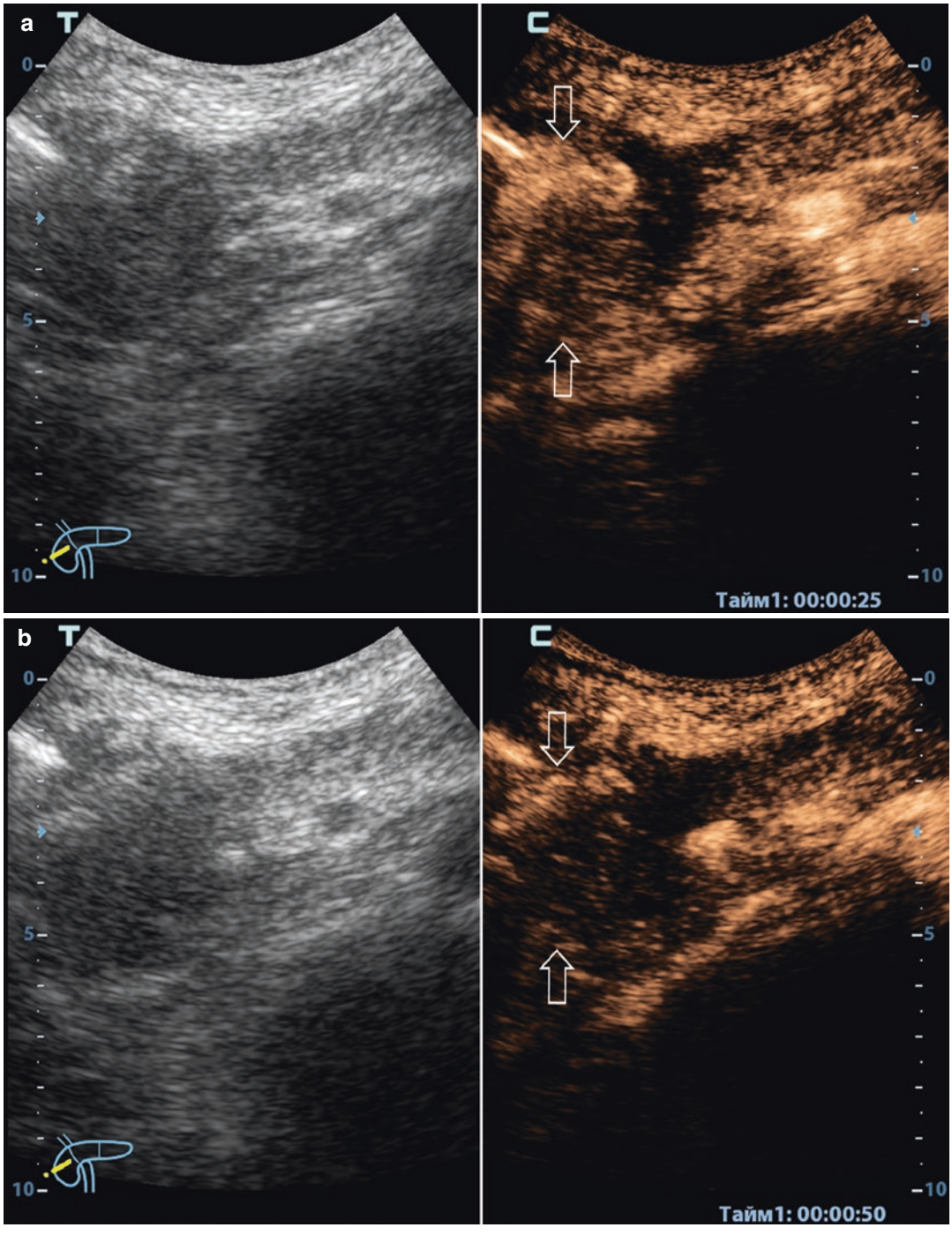

Fig. 6.2 Pancreatic adenocarcinoma of the pancreatic head. (**a**) Irregular enhancement of the lesion in the arterial phase CEUS image. (**b**) Rapid washout of the tumor in the venous phase CEUS image

Table 6.1 TIC data for pancreatic ductal adenocarcinoma, inflammatory pseudotumor, and normal pancreatic parenchyma

	Kersting et al. [19] Mean, 95% CI			D'Onofrio et al. [18]		Askerova [1] Mean ± SD		
Parameter	PDAC	IPT	Normal	PDAC	Normal	PDAC	IPT	Normal
AT, s	26.2 22.6–29.8	16.9 12.6–21.2	14.2 13.1–15.3			20.9 ± 4.5	12 ± 1.4	14.2 13.1–15.3
TTP, s	57.3 52.5–62.1	30.2 23.0–27.4	22.4 22.1–25.9	7.97	8.89	49.1 ± 2.4	29.4 ± 1.8	22.4 22.1–25.9
PI,	2.6 dB 2.2–3.1	3.5 dB 2.2–4.8	5.3 dB 4.9–5.7	17.19%	33.57%	13.2 ± 4.5 dB	19.6 ± 1.2 dB	5.3 dB 4.9–5.7
AUC, dB×s	179 143–214	171 116–226	413 378–449			617.1 ± 31.4	989 ± 45.7	413 378–449
Ascending curve				159.52%s	355.29%s			
Washin time, s						48 ± 6.2	48.9 ± 3.02	

PDAC pancreatic ductal adenocarcinoma, *IPT* inflammatory pseudotumor

time, higher peak intensity, and the area under the curve as compared with G2. However, no difference in washout time was revealed [1] (Table 6.2).

Due to the lack of data standardization and a small sample volume, quantitative analysis needs further studies and so far cannot be recommended for the use in routine practice.

Solid pseudopapillary tumor of the pancreas is a rare well-differentiated malignant neoplasm with a fairly favorable clinical course [20]. Traditional ultrasound demonstrates it as a hypovascular mass, which is heterogeneous due to necrotic areas, hemorrhagic components, and cystic degeneration. Small-sized lesions with CEUS exhibit the same enhancement pattern as neuroendocrine tumors. Large-sized lesions demonstrate heterogeneous enhancement of thick walls and solid components.

Metastases in the pancreas are rare. The majority of them are metastases or renal-cell carcinoma. They hyperenhance in the arterial phase of CEUS, which permits differential diagnosis with ductal adenocarcinoma. However, clear recommendations are not available yet due to the small number of studies.

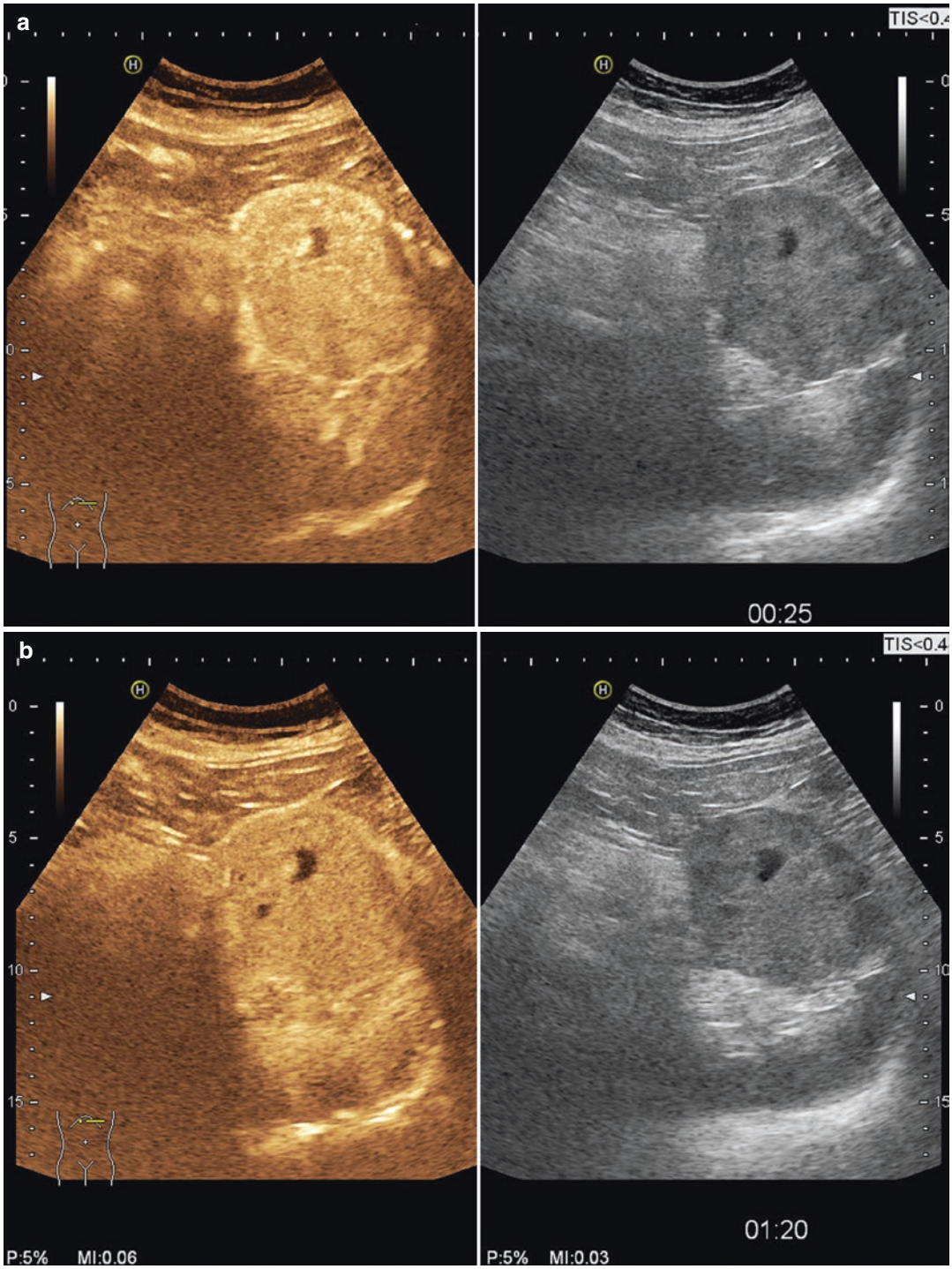

Fig. 6.3 Pancreatic neuroendocrine tumor of the pancreatic tail. CEUS. (**a**) Hyperenhancement in the arterial phase. Note peripheral rim-shaped enhancement. (**b**) Mild washout in the venous phase

Table 6.2 The TIC data in the low (G1) and intermediate (G2) grade neuroendocrine tumors

Parameter	AT, s	TTP, s	PI dB	AUC	Washin time, s	Washout time, s
Grade 1	10.1 ± 0.8	17.1 ± 2.6	35.7 ± 3.6	1315.9 ± 27.01	23.1 ± 1.4	73.4 ± 1.6
Grade 2	12.2 ± 0.5	23.4 ± 1.9	28.8 ± 2.2	1265.9 ± 51.1	25.9 ± 1.1	73.3 ± 1.6
P	≤0.05	≤0.05	≤0.05	≤0.05	≤0.05	>0.05
Normal pancreatic parenchyma	12.8 ± 1.3	22.6 ± 2.9	23.6 ± 1.6	1162.9 ± 43.1	43.9 ± 2.7	64 ± 2.6

6.2 Pancreatic Cystic Lesions

The cystic lesions of the pancreas may have various origins. Most of these cysts are diagnosed incidentally. They are usually benign or low-grade neoplasms.

Mucinous cystic neoplasms confer about 10% of all cystic pancreatic lesions. Although being a benign tumor, it has a high risk of malignant transformation to a mucinous cystadenocarcinoma. Therefore, surgical resection is indicative in all cases [22, 23].

With conventional ultrasound, it is visualized as a cystic lesion with thick irregular walls and partitions, mural echogenic component, or nodules. It contains dense fluid (mucin) and sometimes calcification at the periphery. CEUS reveals good enhancement of the walls and septa in all vascular phases, which is a reliable feature for differential diagnostics with pseudocyst.

Intraductal papillary mucinous neoplasm (IPMN) is a mucin secreting tumor, which originates from the main pancreatic duct or its branches. This group confers hyperplasia, adenoma, borderline tumors, in situ- or invasive carcinoma [24]. CEUS helps to identify a vascularized (enhancing) solid component of intramural nodules and nonenhancing mucin collections. However, it cannot identify the tumor connection with ducts, which is necessary for the diagnosis of IPMN. The study may benefit from the endoscopic US and endoscopic CEUS with high-resolution probes close to the pancreas. The combination of the endoscopic US and endoscopic CEUS demonstrates the sensitivity of 100%, specificity—97%, and accuracy—98% [25].

Serous cystic neoplasm is a benign lesion with a low risk of malignant transformation. It has a lobulated structure with microcystic honeycomb-like inclusions, central scar, and radial septa. It is not connected with the main pancreatic duct, but this fact is impossible to prove with transabdominal US and CEUS. As a rule, this tumor is hypervascular with hyperenhancing septa with CEUS [20, 26]. If the cystic cavities are very small in size, this serous microcystic adenoma can mimic a solid lesion.

Contrast agents improve the value of US not only for the diagnosis of pancreatic lesions but also for its diffuse diseases, especially in **acute necrotizing pancreatitis**. Early differential diagnosis of the edematous and necrotizing types of pancreatitis with the assessment of the severity of necrotic changes is critical for further patients management. CEUS successfully differentiates viable enhancing pancreatic tissue with preserved vascularity from the necrotic areas, which appear non-enhanced. CEUS demonstrates high diagnostic accuracy in the evaluation of the severity of acute pancreatitis with the sensitivity of 86–90.3%, specificity of 97–98.8%, and accuracy of 97.4% [26, 27].

Pseudocyst is the most common pancreatic cystic lesion. It is a cavity with fibrous walls without epithelial lining. It may cause diagnostic difficulties if contains heterogeneous debris. CEUS demonstrates no contrast enhancement that reflects its avascularity and reliably differentiates pseudocyst from pancreatic tumors (Fig. 6.4). In some cases, single vessels that cross the pseudocyst can be determined. Multiparametric US in a combination with CEUS has the sensitivity of

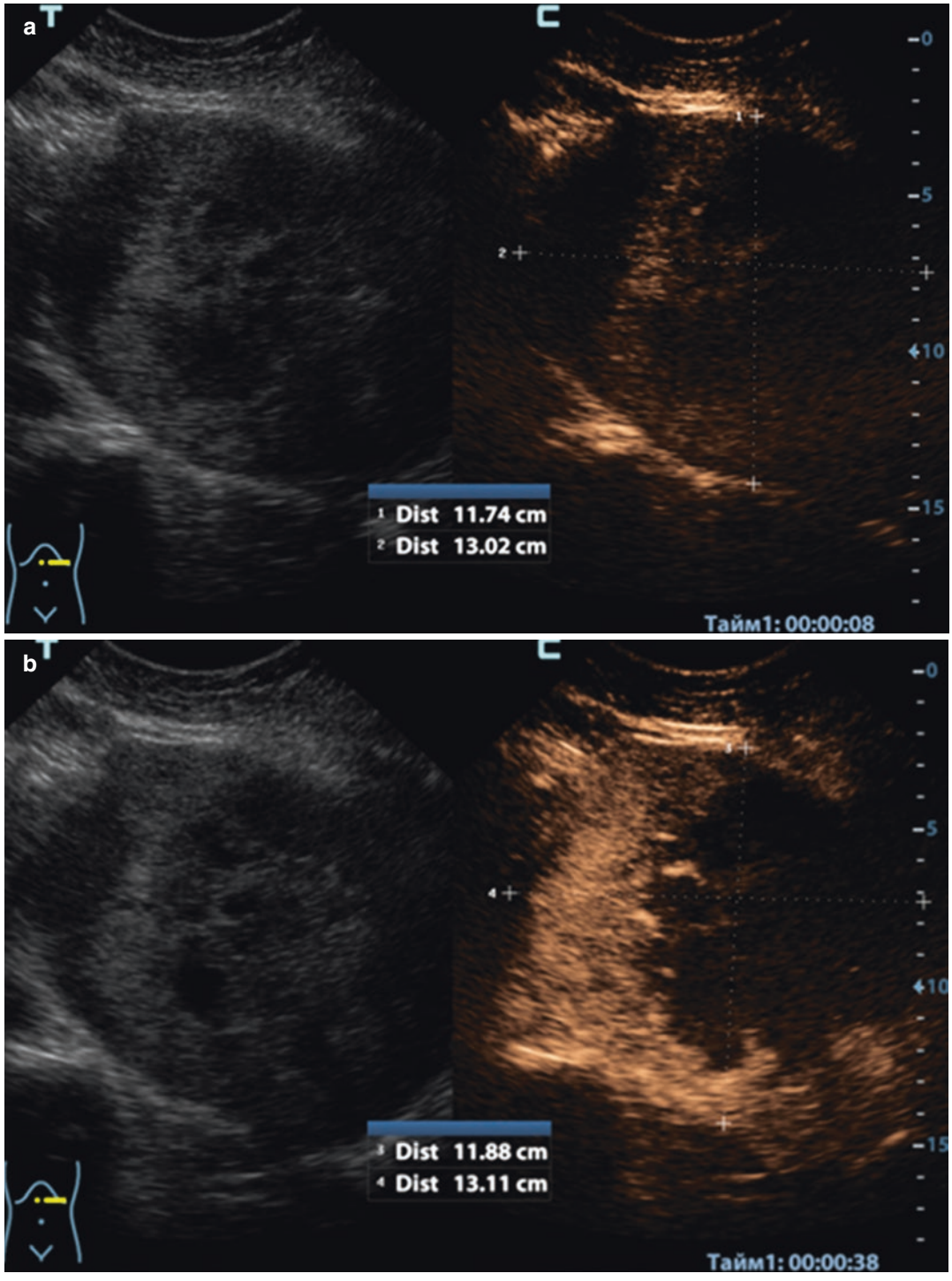

Fig. 6.4 Pancreatic pseudocyst. CEUS images. The nonenhancing area (perfusion defect) corresponds to the necrotic cavity. (**a**) Early arterial phase. (**b**) Early venous phase

94%, specificity—96.9%, PPV—95.9%, NPV—95.4%, and accuracy—96.6% [28].

CEUS can be used for the monitoring of acute pancreatitis after staging it with CT. It may serve as an alternative diagnostic method in patients with contraindications to CE-CT [4, 27]. Significant correlations between CEUS and CT data while staging acute pancreatitis with Baltazar score (r = 0.884), assessment of the necrosis (r = 0.893), and the severity index (r = 0.926) were reported [27]. It demonstrated that CEUS can evaluate inflammatory and necrotic changes and determine the severity of pancreatitis (Table 6.3).

During CEUS study in acute pancreatitis, limited visualization of various parts of the pancreas may enforce to repeat UCA injections to precisely evaluate the entire pancreas and retroperitoneal space.

Table 6.3 Balthazar CT scoring for the assessment of the severity of acute pancreatitis

1. Balthazar scale		
Grade A:	Normal pancreas	0 Point
Grade B:	Focal or diffuse enlargement of the pancreas	1 Point
Grade C:	Pancreatic inflammation and/or peripancreatic fat	2 Point
Grade D:	Single peripancreatic fluid collection	3 Point
Grade E:	Two or multiple fluid collections and/or retroperitoneal air	4 Point
2. Categorization of the extent of necrosis		
Necrosis absent	0 Points	
< 30% necrosis	2 Points	
30–50%	4 Points	
> 50% necrosis	6 Points	
3. Grading severity of acute pancreatitis		
Mild (interstitial) pancreatitis	Score 0–3 Balthazar B or C grade, without necrosis of the pancreas or peripancreatic fat	
Moderate (exudative) pancreatitis	Score 4–6 Balthazar D or E grade, without necrosis of the pancreas, peripancreatic fluid due to necrosis	
Severe (necrotizing) pancreatitis	Score 7–10 Necrosis of the pancreas (nonenhancing area in the pancreas)	

Autoimmune pancreatitis with CEUS demonstrates medium or pronounced contrast enhancement, which is heterogeneous due to focal fibrosis and lymphoid infiltration, followed by slow washout. CEUS can be particularly useful in patients with focal autoimmune chronic pancreatitis when differential diagnosis with ductal adenocarcinoma is crucial for further management.

Vascular features of the pancreas create the ideal conditions for CEUS in the assessment of vascular complications in the first days after **transplantation**. Such complications may include venous thrombosis, strictures of the anastomosis, arterial occlusion, or local perfusion deficiency. There is limited data on the use of CEUS in the diagnosis of post-transplant complications.

Kersting et al. [29] compared the results of CEUS in patients with acute transplant rejection with the same of patients without or successful treatment of transplant rejection. They reported a slower achievement and lower values of the maximum intensity of contrast enhancement in patients with transplant rejection proven with TIC analysis. After the resolution of the rejection episode, TICs almost returned to the initial values. The peak intensity during the rejection was lower than in the case of unchanged graft and after treatment (19.4 dB vs. 28.3 dB and 26.2 dB, respectively).

The intraoperative US is mandatory during surgical treatment of functional neuroendocrine tumors. However, in the cases of isoechogenic lesions, specification of the exact location of the tumor remains a challenge. CEUS is a simple option that enforces the intraoperative US and enables differentiation of these tumors due to their hyperenhancing pattern [1]. Additionally, CEUS clarifies the margins of the neoplasm and evaluates local spreading. Vetsheva [2] reported that the boundaries of malignant pancreatic masses are best delineated in the venous phase. Furthermore, hypoenhancing foci around extrapancreatic vessels in the peripancreatic fat indicate that the vascular walls are also affected by

the tumor. The obtained additional CEUS data permit specification of the margins and volume of the tumor resection.

References

1. Askerova NN. Ul'trazvukovoe issledovanie s kontrastnym usileniem v differencial'noj diagnostike opuholej podzheludochnoj zhelezy [Contrast-enhanced ultrasound in the differential diagnosis of pancreatic tumors]. Dissertation. Moscow. 2019. Russian.
2. Vetsheva NN. Instrumental'naya diagnostika solidnyh opuholej podzheludochnoj zhelezy [Instrumental diagnosis of solid pancreatic tumors]. Dissertation. Moscow. 2017. Russian.
3. D'Onofrio M, Canestrini S, De Robertis R, Crosara S, Demozzi E, Ciaravino V, Pozzi Mucelli R. CEUS of the pancreas: still research or the standard of care. Eur J Radiol. 2015;84(9):1644–9. https://doi.org/10.1016/j.ejrad.2015.02.021.
4. Rickes S, Uhle C, Kahl S, Kolfenbach S, Monkemuller K, Effenberger O, Malfertheiner P. Echo enhanced ultrasound: a new valid initial imaging approach for severe acute pancreatitis. Gut. 2006;55(1):74–8. https://doi.org/10.1136/gut.2005.070276.
5. Weskott HP. Contrast-enhanced ultrasound. 2nd ed. London: Uni-Med Science; 2013.
6. Sidhu PS, Cantisani V, Dietrich CF, Gilja OH, Saftoiu A, Bartels E, et al. The EFSUMB guidelines and recommendations for the clinical practice of contrast-enhanced ultrasound (CEUS) in non-hepatic applications: update 2017 (long version). Ultraschall Med. 2018;39(2):e2–e44. https://doi.org/10.1055/a-0586-1107.
7. Dietrich CF, Ignee A, Frey H. Contrast-enhanced endoscopic ultrasound with low mechanical index: a new technique. Z Gastroenterol. 2005;43(11):1219–23. https://doi.org/10.1055/s-2005-858662.
8. Li XZ, Song J, Sun ZX, Yang YY, Wang H. Diagnostic performance of contrast-enhanced ultrasound for pancreatic neoplasms: a systematic review and meta-analysis. Dig Liver Dis. 2018;50(2):132–8. https://doi.org/10.1016/j.dld.2017.10.012.
9. D'Onofrio M, Crosara S, Signorini M, De Robertis R, Canestrini S, Principe F, Pozzi Mucelli R. Comparison between CT and CEUS in the diagnosis of pancreatic adenocarcinoma. Ultraschall Med. 2013;34(4):377–81. https://doi.org/10.1055/s-0032-1325324.
10. Dietrich CF, Sahai AV, D'Onofrio M, Will U, Arcidiacono PG, Petrone MC, et al. Differential diagnosis of small solid pancreatic lesions. Gastrointest Endosc. 2016;84(6):933–40. https://doi.org/10.1016/j.gie.2016.04.034.
11. Bang JY, Varadarajulu S. Neoplasia in chronic pancreatitis: how to maximize the yield of endoscopic ultrasound-guided fine needle aspiration. Clin Endosc. 2014;47(5):420–4. https://doi.org/10.5946/ce.2014.47.5.420.
12. Kitano M, Sakamoto H, Kudo M. Contrast-enhanced endoscopic ultrasound. Dig Endosc. 2014;26(Suppl 1):79–85. https://doi.org/10.1111/den.12179.
13. Klinicheskie rekomendacii po diagnostike i lecheniyu zlokachestvennyh opuholej podzheludochnoj zhelezy [Clinical recommendations for the diagnosis and treatment of malignant tumors of the pancreas] Moscow; 2018. Russian. http://www.oncology.ru/association/clinical-guidelines/2018/rak_podzheludochnoy_zhelezy_pr2018.pdf. Accessed 22 Feb 2021.
14. Bouvet M, Binmoeller KF, Moossa AR. Diagnosis of adenocarcinoma of the pancreas. In: Cameron JL, editor. Atlas of clinical oncology. Pancreatic Cancer. London: BC Decker Inc Hamilton; 2001. p. 67–86.
15. Jamieson NB, Chan NI, Foulis AK, Dickson EJ, McKay CJ, Carter CR. The prognostic influence of resection margin clearance following pancreaticoduodenectomy for pancreatic ductal adenocarcinoma. J Gastrointest Surg. 2013;17(3):511–21. https://doi.org/10.1007/s11605-012-2131-z.
16. D'Onofrio M, Barbi E, Dietrich CF, Kitano M, Numata K, Sofuni A, Principe F, Gallotti A, Zamboni GA, Mucelli RP. Pancreatic multicenter ultrasound study (PAMUS). Eur J Radiol. 2012;81(4):630–8. https://doi.org/10.1016/j.ejrad.2011.01.053.
17. Saftoiu A, Sparches Z, Lyshchik A. Pancreas: solid lesions. In: Lyshchik A, editor. Specialty imaging: fundamentals of CEUS. 1st ed. Philadelphia: Elsevier; 2019. p. 186–90.
18. D'Onofrio M, Canestrini S, Crosara S, De Robertis R, Pozzi Mucelli R. Contrast enhanced ultrasound with quantitative perfusion analysis for objective characterization of pancreatic ductal adenocarcinoma: a feasibility study. World J Radiol. 2014;6(3):31–5. https://doi.org/10.4329/wjr.v6.i3.31.
19. Kersting S, Konopke R, Kersting F, Volk A, Distler M, Bergert H, et al. Quantitative perfusion analysis of transabdominal contrast-enhanced ultrasonography of pancreatic masses and carcinomas. Gastroenterology. 2009;137(6):1903–11. https://doi.org/10.1053/j.gastro.2009.08.049.
20. De Robertis R, D'Onofrio M, Crosara S, Dal Corso F, Barbi E, Canestrini S, Mucelli RP. Contrast-enhanced ultrasound of pancreatic tumours. Aust J Ultrasound Med. 2014;17(3):96–109. https://doi.org/10.1002/j.2205-0140.2014.tb00032.x.
21. D'Onofrio M, Mansueto G, Falconi M, Procacci C. Neuroendocrine pancreatic tumor: value of contrast enhanced ultrasonography. Abdom Imaging. 2004;29(2):246–58. https://doi.org/10.1007/s00261-003-0097-8.
22. Shchegolev AI, Skuba ND, Shchegoleva NN. Klassifikaciya i morfologicheskaya harakteristika opuholej podzheludochnoj zhelezy: dobrokachestvennye i pogranichnye opuholi ekzokrinnoj chasti. [Classification and morphological characteristics of pancreatic tumors: benign and borderline

tumors of the exocrine part]. Medicinskaya vizualizaciya. 2003;3:6–12. Russian.
23. Tedesco G, Sarno A, Rizzo G, Grecchi A, Testa I, Giannotti G, D'Onofrio M. Clinical use of contrast-enhanced ultrasound beyond the liver: a focus on renal, splenic, and pancreatic applications. Ultrasonography. 2019;38(4):278–88. https://doi.org/10.14366/usg.18061.
24. Ishida M, Egawa S, Aoki T, Sakata N, Mikami Y, Motoi F, Abe T, Fukuyama S, Sunamura M, Unno M, Moriya T, Horii A, Furukawa T. Characteristic clinicopathological features of the types of intraductal papillary-mucinous neoplasms of the pancreas. Pancreas. 2007;35(4):348–52. https://doi.org/10.1097/mpa.0b013e31806da090.
25. Harima H, Kaino S, Shinoda S, Kawano M, Suenaga S, Sakaida I. Differential diagnosis of benign and malignant branch duct intraductal papillary mucinous neoplasm using contrast-enhanced endoscopic ultrasonography. World J Gastroenterol. 2015;21(20):6252–60. https://doi.org/10.3748/wjg.v21.i20.6252.
26. Ardelean M, Şirli R, Sporea I, Bota S, Martie A, Popescu A, Dănila M, Timar B, Buzas R, Lighezan D. Contrast enhanced ultrasound in the pathology of the pancreas - a monocentric experience. Med Ultrason. 2014;16(4):325–31.
27. Ripollés T, Martínez MJ, López E, Castelló I, Delgado F. Contrast-enhanced ultrasound in the staging of acute pancreatitis. Eur Radiol. 2010;20(10):2518–23. https://doi.org/10.1007/s00330-010-1824-5.
28. Beyer-Enke SA, Hocke M, Ignee A, Braden B, Dietrich CF. Contrast enhanced transabdominal ultrasound in the characterisation of pancreatic lesions with cystic appearance. JOP. 2010;11(5):427–33.
29. Kersting S, Ludwig S, Ehehalt F, Volk A, Bunk A. Contrast-enhanced ultrasonography in pancreas transplantation. Transplantation. 2013;95(1):209–14. https://doi.org/10.1097/TP.0b013e31827864df.

Spleen

7

Alexander N. Sencha and Ella I. Peniaeva

Spleen is supplied with blood by the splenic artery, which is a branch of the celiac trunk. In some cases, the splenic artery may originate independently from the abdominal aorta or joint with the left gastric artery. The venous blood flows to the splenic vein, which joins the portal vein.

Although the pathology of the spleen has a lower incidence than the pathology of other abdominal organs, accurate noninvasive diagnosis is important due to high risk of bleeding if punctured. CEUS increases the value of US for the identification and differential diagnosis of splenic abnormalities [1–4].

According to the EFSUMB Guidelines and Recommendations for the Clinical Practice of CEUS in Non-Hepatic Applications: Update 2017 [4], CEUS of the spleen can be used in the following situations:

- to improve the detection of focal splenic abnormalities,
- to characterize suspected accessory spleens or splenosis,
- to diagnose splenic infarction,
- to identify benign focal splenic lesions by showing persistent enhancement in the late phase.

Splenic CEUS is carried out with the standard ultrasound access in the patient's position on the right side provided the grayscale US image of the spleen and target area has good quality. To study the spleen, 1.2–2.4 ml of SonoVue® is required. More often 1.2 ml is enough. CEUS of the spleen implicates the arterial (from the beginning of contrast enhancement up to 60 s) and parenchymal (60 s–5–7 min) phases.

The contrast enhancement of the spleen begins in 8–20 s from UCA introduction. In the arterial phase, the parenchyma enhances in a heterogeneous "zebra-striped" way and becomes homogeneous within 60 s. Probably, this type of enhancement is a consequence of the unique splenic blood circulation—open and closed system [5]. In closed circulation (10% of blood flow), the central artery supplies the white pulp, the blood passes through the marginal zone and drains to venous sinusoids. About 90% of the blood takes the open route of circulation. The central artery supplies the red pulp and branches to capillaries draining to the parenchyma. From

A. N. Sencha (✉)
Department of Visual and Functional Diagnostics, Federal State Budget Institution "National Medical Research Center for Obstetrics, Gynecology and Perinatology n.a. V.I.Kulakov", Moscow, Russian Federation

E. I. Peniaeva
Department of Ultrasound Diagnostics of the Center for Radiological Diagnostics, Private Healthcare Institution "Clinical Hospital "RZD-Medicina" of Yaroslavl City", Yaroslavl, Russian Federation

A. N. Sencha, Y. N. Patrunov (eds.), *Contrast-Enhanced Ultrasound*,
https://doi.org/10.1007/978-3-030-91764-7_7

there, blood travels to venous sinuses, which are assembled to trabecular veins and the splenic vein [6]. In the late parenchymal phase, the contrast enhancement persists for a long time (up to 5–7 min) due to the accumulation of UCA in sinusoids, which differs the spleen from other organs (Fig. 7.1).

Ultrasound is a fairly accurate method to diagnose microsplenia, which measures smaller than 7 × 2 cm [5]. CEUS does not determine the cause

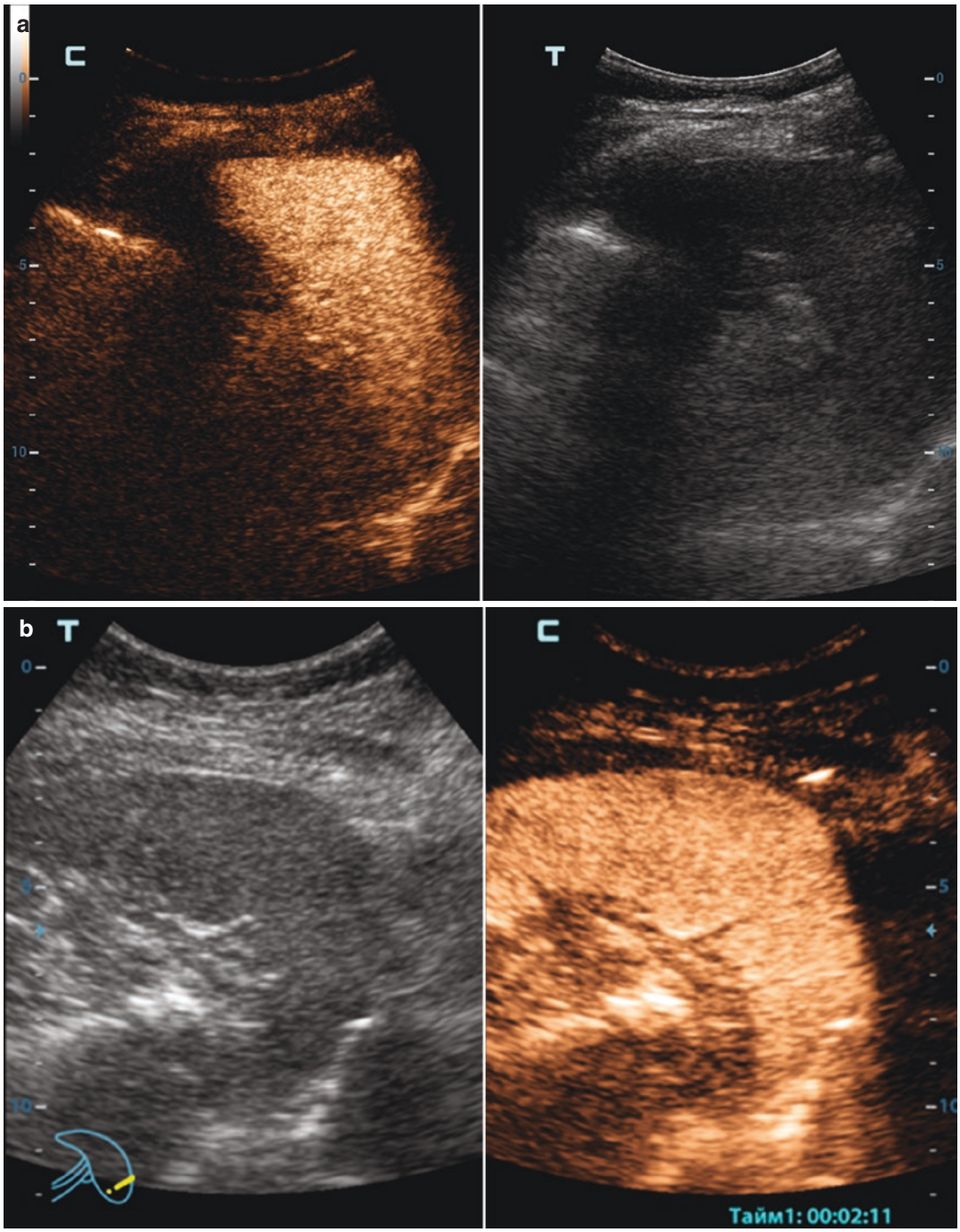

Fig. 7.1 Normal spleen. Uniform contrast enhancement. CEUS images. (**a**) Arterial phase. (**b**) Venous phase

of microsplenia. However, according to some publications [7], it may identify functional asplenia with pronounced decrease or absence of contrast enhancement.

Accessory spleen is a common finding with conventional US and is detected in 10–15% of patients. The diagnosis usually does not cause any difficulties. However, large-sized and atypically located accessory spleens sometimes demand differential diagnosis with a left adrenal lesion, enlarged lymph node, and neoplasms of the pancreatic tail, intestine, or stomach. It is not always possible with the traditional US [1, 3].

Similar difficulties may arise in the diagnosis of **splenosis**, which is the autotransplanted splenic tissue after trauma or surgery. The histological structure and vascularity of the ectopic tissue are identical to the normal spleen that permits successful diagnosis with CEUS. Accessory and ectopic spleens demonstrate the typical splenic contrast enhancement pattern in all vascular phases with CEUS. The most important diagnostic sign is persistent contrast enhancement of the splenic tissue in the late parenchymal phase due to the accumulation of the UCA in sinusoids. The masses of other origins demonstrate a slow decrease in contrast enhancement (Fig. 7.2) [1, 3].

In the cases of heterogeneous splenic parenchyma, CEUS improves the value of general ultrasound in the identification of the **focal splenic lesions**. CEUS exhibits the sensitivity of 90% and specificity of 100% in the evaluation of splenic masses in patients with lymphoma, with CE-CT as a reference method [8]. Some authors demonstrate [9] that the diagnostic accuracy of CEUS is higher than the same of CT. The EFSUMB recommendations in 2011 indicated that CEUS might be utilized to identify focal splenic lesions in oncological patients if CE-CT, MRI, or PET-CT were contraindicated or returned ambiguous results.

CEUS enables correct diagnosis in most cases of uncertain results of PET-CT [10]. CEUS detects 38% more lesions in addition to traditional ultrasound in patients with metastases in

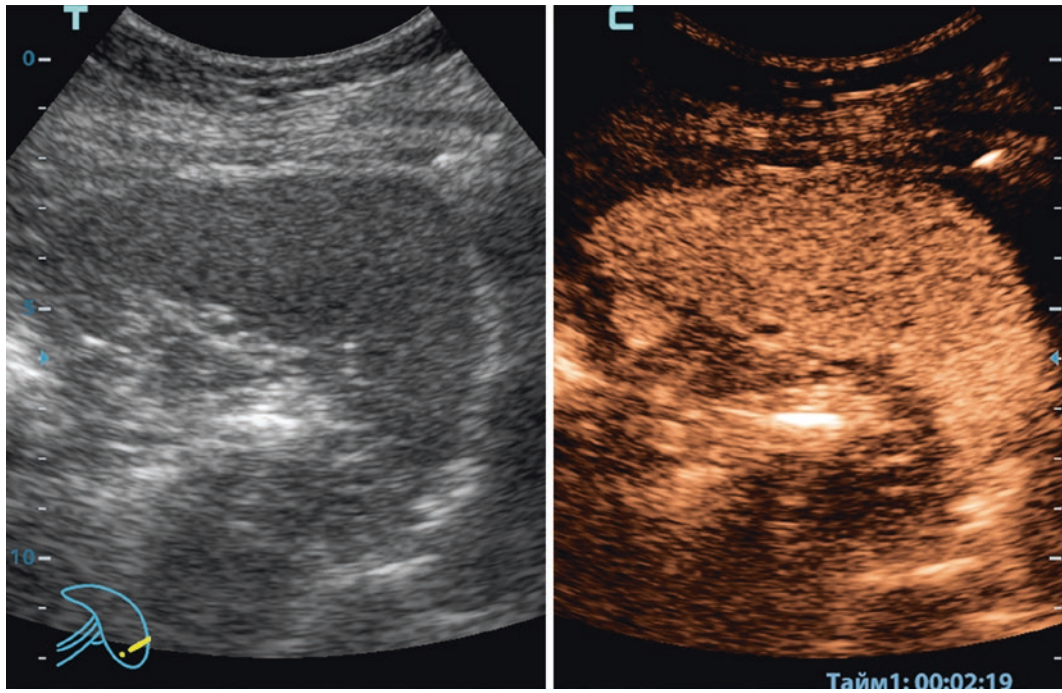

Fig. 7.2 The accessory spleen adjacent to the visceral surface near the upper pole of the normal spleen. CEUS image. Contrast enhancement of the accessory spleen in the parenchymal phase is identical to the normal splenic parenchyma

the spleen [11]. However, the metastases in the spleen are rare (below 1% of all visceral oncologic cases). Therefore, CEUS is not used in practice for the screening of the metastases in the spleen in oncological patients. Taking into account that the spleen is often affected with lymphoma (30–40% of cases), this pathology seems more promising for CEUS [12].

The malignant tumors of the spleen are mainly represented by lymphoma and metastases. As opposed to benign tumors, splenic malignancies are characterized by rapid wash-out with CEUS.

Lymphoma is the most common malignant splenic tumor. Primary splenic lymphoma is extremely rare. The spleen is usually involved by lymphomas as part of the systemic illness [8]. The spleen is affected in about one-third of patients with lymphoma. The imaging is variable and can be represented with diffuse infiltration, miliary nodules, solitary or multiple lesions. Large lesions may have cystic components associated with central necrosis [13].

Arterial phase CEUS demonstrates diffuse iso- or hypoenhancement of splenic lesions as compared with the surrounding normal parenchyma. The enhancement pattern is usually homogeneous. Peripheral rim-shaped enhancement may be registered in some cases. The parenchymal phase shows wash-out. Tumors become hypoenhanced and clearly depicted on the background of the intact parenchyma [8, 13].

In the arterial phase, irregular vessels within the tumor with microbubble circulation may be registered. The differential diagnosis with the splenic abscess is difficult. The enhancement pattern of diffuse infiltration with lymphoma is identical to congestive splenomegaly.

Metastases in the spleen are rare, usually asymptomatic, and indicate the far gone primary disease. The typical sources of metastasis are melanoma, breast, lung, ovarian, stomach, and colorectal carcinoma [2, 14]. Metastases are often represented by solid lesions but sometimes may have cystic structure, especially in ovarian cancer. Contrast enhancement of the metastases in the spleen is similar to the same in liver metastases. Arterial phase CEUS can demonstrate various patterns: hypoenhancement, peripheral rim-shaped, complete or incomplete heterogeneous contrast enhancement. The parenchymal phase is characterized by fast wash-out. Chaotically distributed vessels may be observed [3, 11, 13].

The capabilities of CEUS in the differential diagnosis of focal splenic lesions remain the subject for discussion. In the study [15], the sensitivity and specificity of CEUS in the diagnosis of malignant lesions were 91% and 92%, respectively, provided the radiologist was aware of the patient's clinical data. Similar data were obtained by other authors [16]. CEUS also demonstrates high accuracy in the diagnosis of **benign splenic lesions**.

Cysts are the most common lesions of the spleen. Depending on the structure and origin they confer the following types [13]:

- Primary (true) cysts: congenital epithelial, mesothelial, dermoid; parasitic; tumor (lymphangioma and cystic angioma).
- Secondary cysts (pseudocysts): post-traumatic, degenerative, inflammatory.

Simple epithelial cysts are always located within the parenchyma, have a typical US picture, and do not cause any diagnostic difficulties. Some questions occur if the cyst has echogenic contents or thick walls. Normally, CEUS demonstrates no enhancement of the cystic walls and contents. The margins of the cyst become clearly seen on the background of enhanced splenic parenchyma.

Lymphangioma is a benign tumor, which develops from lymphatic vessels and can arise in the skin, subcutaneous fat, mediastinum, retroperitoneal space, liver, spleen, kidneys, etc. It is often of cystic type. Splenic lymphangioma is visualized as a multicystic lesion with echogenic content and thin septations, sometimes with calcifications. CEUS reveals the enhancement of the walls and septa with unenhanced contents (Fig. 7.3). These tumors can be detected at any age but typically diagnosed in the first year of life, so the data on CEUS in their diagnosis is limited [13].

Hemangioma is the most common solid benign splenic lesion. Hemangioma, which

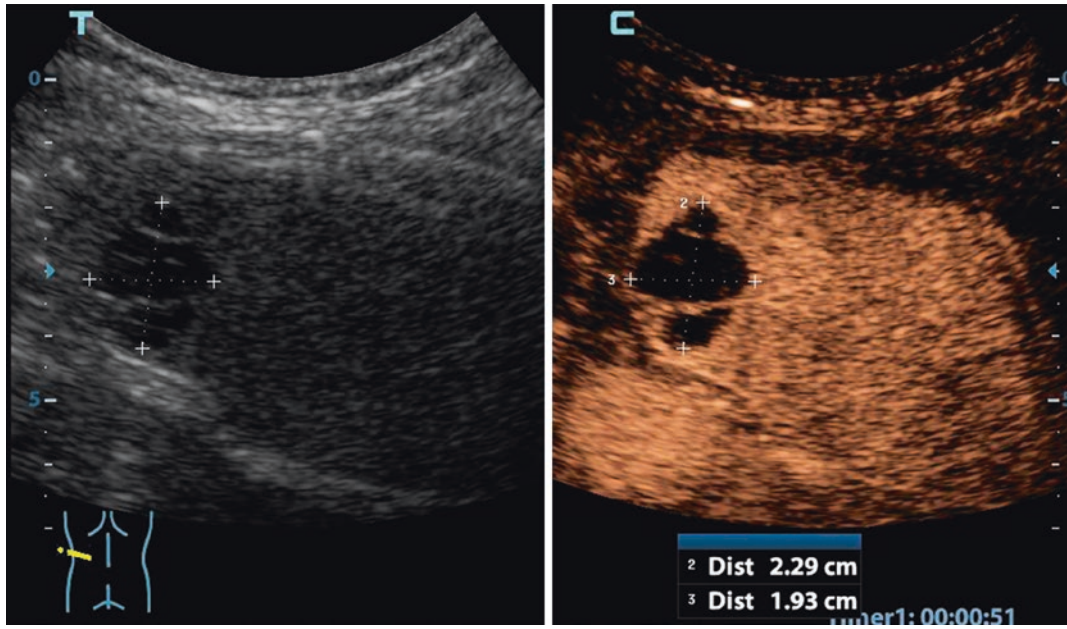

Fig. 7.3 Complex splenic cyst. CEUS image. Enhanced walls and nonenhanced contents of the cyst in the late arterial phase

exhibits typical signs with conventional US, is smaller than 2 cm in size, with no evidence of oncology in the patient's history requires no further diagnostic procedures. Atypical ultrasound signs, such as decreased echogenicity, cystic component, or calcifications implicit additional imaging. CEUS in these cases confirms the benign character of the mass with the steady contrast enhancement in the parenchymal phase (Fig. 7.4). However, peripheral globular enhancement, which is typical for liver hemangioma, is less common for splenic hemangioma [1, 5, 16]. In addition, difficulties may occur in the cases of moderate wash-out in the parenchymal phase. Still, in hemangioma, wash-out appears much later than in malignant neoplasm.

Hamartoma of the spleen, also known as splenoma or splenic adenoma, is a rare benign splenic lesion histopathologically represented by proliferating fibromuscular elements with epithelial inclusions, partial metaplasia, without signs of atypia. There are two subtypes of hamartoma: a white pulp lesion consisting of an aberrant lymphoid tissue and red pulp lesion consisting of an aberrant complex of sinusoids [17]. However, most hamartomas contain both types of elements.

Splenic hamartoma is typically a solid mass, which compresses the surrounding parenchyma. In some cases, the cystic component and calcifications may be observed. With CEUS, it demonstrates various degrees of contrast enhancement in the arterial phase maintaining permanently enhanced in the parenchymal phase, which is characteristic of benign lesions. The cystic component remains unenhanced in all vascular phases.

Sarcoidosis is a systemic inflammatory disease that affects various organs, mostly lungs and mediastinal lymph nodes. Spleen is affected in about 15% of patients with sarcoidosis [13]. There are individual publications [13, 18] on CEUS of the spleen in sarcoidosis. They report multiple fine nodules with either no enhancement or hypoenhancement in all vascular phases.

Splenic infarction is a consequence of the embolism or thrombosis of the splenic artery or its branches. It can lead to a total infarction but segmental damage is much more common. In the case of the thrombosis of the splenic or portal

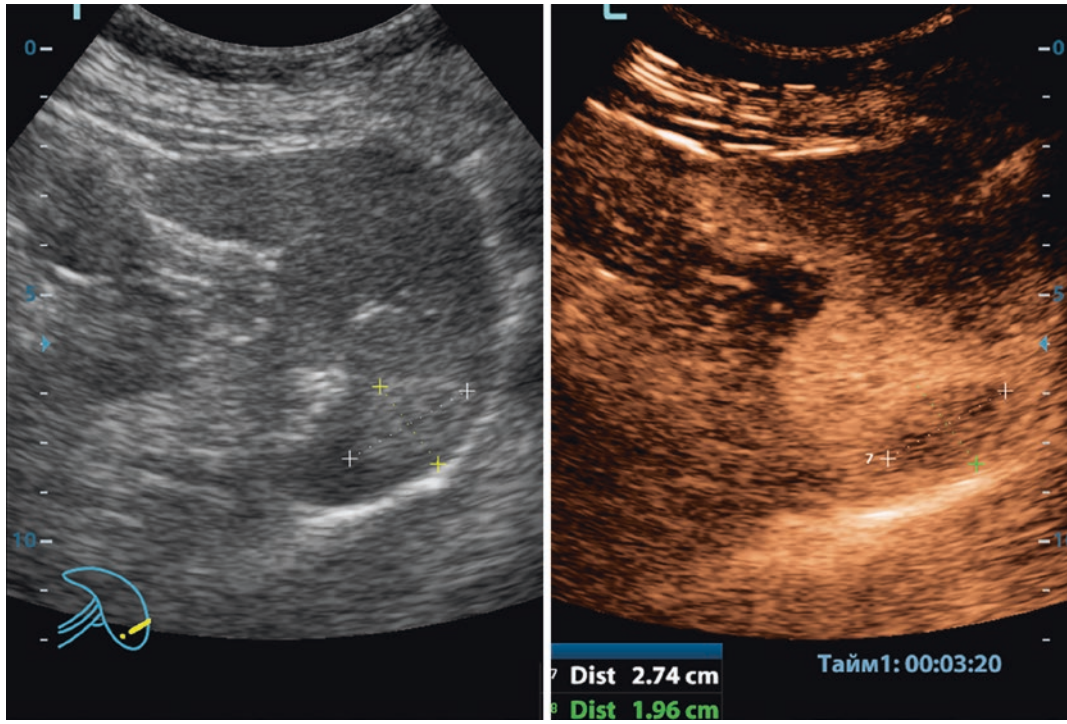

Fig. 7.4 Splenic hemangioma. CEUS image. Typical contrast enhancement of the lesion in the arterial phase

vein, venous infarction may develop. The infarction zone in the early stages is difficult to differentiate with traditional US due to its isoechoic structure. The decrease in echogenicity occurs with time. Splenic infarction margins are better delineated with CEUS. CEUS typically reveals a wedge-shaped nonenhancing region based on the splenic capsule with the apex pointed toward the hilum [1, 5, 13, 19]. The assessment is better in the late parenchymal phase. One extremely rare pathology is the torsion of the accessory spleen, which is characterized by the absence or pronounced decrease in contrast enhancement [20].

Other possible ways to use CEUS, which lack the official recommendations, are the diagnosis of an abscess and traumatic damage of the spleen.

Splenic abscess in about 70% of cases is the result of hematogenous dissemination from the foci of primary infection, such as endocardium, urinary system, postoperative or post-traumatic inflammation, appendix, etc. Splenic abscess with CEUS demonstrates the same "honeycomb" contrast enhancement pattern as in other parenchymatous organs with enhanced thick walls and septa and nonenhanced fluid components [3, 12].

The traumatic injury of the spleen is an urgent condition, which is often associated with abdominal trauma. Forty-six percent of cases are presented with isolated splenic damage. The spleen has high blood flow, which compounds up to 350 liters per day, so in the case of injury, the risk of massive bleeding is very high [21]. In severe injuries, the CT remains the method of choice. But in mild and moderate injuries, CEUS can be considered an alternative diagnostic method, which is confirmed by several studies [22–24].

CEUS seems particularly useful in monitoring the patient's status and in pediatric practice. The diagnosis of splenic damage is obvious if the free anechoic fluid is observed adjacent to the spleen. But the image of the fresh blood is isoechoic and appears similar to the splenic parenchyma. This fact makes the timely diagnosis with traditional US difficult. CEUS depicts perfused and nonperfused areas of the spleen and facilitates dif-

ferentiation of the hemorrhagic collections [25]. CEUS spleen injury diagnostic sensitivity was 96.9% and, according to the American Association for the Surgery of Trauma (AAST)—spleen injury scale (SIS), CEUS-CT concordance was 95.8% [26].

References

1. Görg C. The forgotten organ: contrast enhanced sonography of the spleen. Eur J Radiol. 2007;64(2):189–201. https://doi.org/10.1016/j.ejrad.2007.06.036.
2. Lam KY, Tang V. Metastatic tumors to the spleen: a 25-year clinicopathologic study. Arch Pathol Lab Med. 2000;124(4):526–30. https://doi.org/10.1043/0003-9985(2000)124<0526:MTTTS>2.0.CO;2.
3. Omar A, Freeman S. Contrast-enhanced ultrasound of the spleen. Ultrasound. 2016;24(1):41–9. https://doi.org/10.1177/1742271X15617214.
4. Sidhu PS, Cantisani V, Dietrich CF, Gilja OH, Saftoiu A, Bartels E, et al. The EFSUMB guidelines and recommendations for the clinical practice of contrast-enhanced ultrasound (CEUS) in non-hepatic applications: update 2017 (Long version). Ultraschall Med. 2018;39(2):e2–e44. https://doi.org/10.1055/a-0586-1107.
5. Weskott HP. Contrast-enhanced ultrasound. 2nd ed. London: Uni-Med Science; 2013.
6. Delyagin VM, Polyaev YA, Isaeva MV, Garbuzov RV. Ekhografiya selezenki u detej i podrostkov [Echography of the spleen in children and adolescents]. SonoAce Ultrasound. 2009;19:57–69. Russian.
7. Trenker C, May L, Librizzi D, Neesse A, Görg C. Contrast-enhanced sonography in patients with hyposplenia: a retrospective analysis in forty-three patients. Digestion. 2019;100(3):170–5. https://doi.org/10.1159/000494755.
8. Tafuto S, Catalano O, Barba G, Sandomenico F, Lobianco R, Tortoriello A, et al. Real-time contrast-enhanced specific ultrasound in staging and follow-up of splenic lymphomas. Front Biosci. 2006;11:2224–9. https://doi.org/10.2741/1965.
9. Picardi M, Soricelli A, Pane F, Zeppa P, Nicolai E, De Laurentiis M, Grimaldi F, Rotoli B. Contrast-enhanced harmonic compound US of the spleen to increase staging accuracy in patients with Hodgkin lymphoma: a prospective study. Radiology. 2009;251(2):574–82. https://doi.org/10.1148/radiol.2512081293.
10. Catalano O, Sandomenico F, Vallone P, Setola SV, Granata V, Fusco R, et al. Contrast-enhanced ultrasound in the assessment of patients with indeterminate abdominal findings at positron emission tomography imaging. Ultrasound Med Biol. 2016;42(11):2717–23. https://doi.org/10.1016/j.ultrasmedbio.2016.06.023.
11. Neesse A, Huth J, Kunsch S, Michl P, Bert T, Tebbe JJ, Gress TM, Görg C. Contrast-enhanced ultrasound pattern of splenic metastases - a retrospective study in 32 patients. Ultraschall Med. 2010;31(3):264–9. https://doi.org/10.1055/s-0028-1109812.
12. Sutherland T, Temple F, Galvin A, Hennessy O. Contrast-enhanced ultrasound of the spleen: an introduction and pictorial essay. Insights Imaging. 2011;2(5):515–24. https://doi.org/10.1007/s13244-011-0106-3.
13. Zavariz JD, Konstantatou E, Deganello A, Bosanac D, Huang DY, Sellars ME, Sidhu PS. Common and uncommon features of focal splenic lesions on contrast-enhanced ultrasound: a pictorial review. Radiol Bras. 2017;50(6):395–404. https://doi.org/10.1590/0100-3984.2015.0209.
14. Compérat E, Bardier-Dupas A, Camparo P, Capron F, Charlotte F. Splenic metastases: clinicopathologic presentation, differential diagnosis, and pathogenesis. Arch Pathol Lab Med. 2007;131(6):965–9. https://doi.org/10.5858/2007-131-965-SMCPDD.
15. Stang A, Keles H, Hentschke S, von Seydewitz CU, Dahlke J, Malzfeldt E, Braumann D. Differentiation of benign from malignant focal splenic lesions using sulfur hexafluoride-filled microbubble contrast-enhanced pulse-inversion sonography. AJR Am J Roentgenol. 2009;193(3):709–21. https://doi.org/10.2214/AJR.07.3988.
16. Yu X, Yu J, Liang P, Liu F. Real-time contrast-enhanced ultrasound in diagnosing of focal spleen lesions. Eur J Radiol. 2012;81(3):430–6. https://doi.org/10.1016/j.ejrad.2010.12.052.
17. Stepanova YA, Ionkin DA. Ul'trazvukovaya diagnostika gamartomy selezenki [Ultrasound diagnosis of spleen hamartoma]. SonoAce Ultrasound. 2012;24:60–5. Russian.
18. Pérez-Grueso MJ, Repiso A, Gómez R, Gonzalez C, de Artaza T, Valle J, García A, Carrobles JM. Splenic focal lesions as manifestation of sarcoidosis: characterization with contrast-enhanced sonography. J Clin Ultrasound. 2007;35(7):405–8. https://doi.org/10.1002/jcu.20322.
19. Zavariz J, Deganello A, Sidhu PS. Spleen: benign lesions. In: Lyshchik A, editor. Specialty imaging: fundamentals of CEUS. 1st ed. Philadelphia: Elsevier; 2019. p. 196–200.
20. Trinci M, Ianniello S, Galluzzo M, Giangregorio C, Palliola R, Briganti V, et al. A rare case of accessory spleen torsion in a child diagnosed by ultrasound (US) and contrast-enhanced ultrasound (CEUS). J Ultrasound. 2019;22(1):99–102. https://doi.org/10.1007/s40477-019-00359-4.
21. Piccolo CL, Trinci M, Pinto A, Brunese L, Miele V. Role of contrast-enhanced ultrasound (CEUS) in the diagnosis and management of traumatic splenic injuries. J Ultrasound. 2018;21(4):315–27. https://doi.org/10.1007/s40477-018-0327-0.
22. Manetta R, Pistoia ML, Bultrini C, Stavroulis E, Di Cesare E, Masciocchi C. Ultrasound enhanced with sulphur-hexafluoride-filled microbubbles agent

(SonoVue) in the follow-up of mild liver and spleen trauma. Radiol Med. 2009;114(5):771–9. English, Italian. https://doi.org/10.1007/s11547-009-0406-6.
23. Miele V, Piccolo CL, Trinci M, Galluzzo M, Ianniello S, Brunese L. Diagnostic imaging of blunt abdominal trauma in pediatric patients. Radiol Med. 2016;121(5):409–30. https://doi.org/10.1007/s11547-016-0637-2.
24. Pinto F, Valentino M, Romanini L, Basilico R, Miele V. The role of CEUS in the assessment of haemodynamically stable patients with blunt abdominal trauma. Radiol Med. 2015;120(1):3–11. https://doi.org/10.1007/s11547-014-0455-3.
25. Valentino M, Serra C, Zironi G, De Luca C, Pavlica P, Barozzi L. Blunt abdominal trauma: emergency contrast-enhanced sonography for detection of solid organ injuries. AJR Am J Roentgenol. 2006;186(5):1361–7. https://doi.org/10.2214/AJR.05.0027.
26. Tagliati C, Argalia G, Graziani B, Salmistraro D, Giuseppetti GM, Giovagnoni A. Contrast-enhanced ultrasound in the evaluation of splenic injury healing time and grade. Radiol Med. 2019;124(3):163–9. https://doi.org/10.1007/s11547-018-0954-8.

Kidneys and Adrenals

8

Yury N. Patrunov, Ella I. Peniaeva, Alexander N. Sencha, and Liubov A. Timofeyeva

The kidneys receive their blood supply from paired renal arteries, which originate from the abdominal aorta. The renal artery on each side typically branches to the larger anterior and smaller posterior division. Both of them split into segmental arteries, which pass the renal sinus and undergo further division to interlobar arteries. They enter the renal parenchyma and proceed in the columns adjacent to the sides of renal pyramids. At the border of the cortex and pyramid base, they form arcuate arteries. A further level of division, numerous interlobular arteries, arises from arcuate arteries perpendicularly and head to the renal periphery within the cortex. The last branching is to the afferent arterioles, which form a capillary network, the glomerulus, where filtration takes place. The capillaries come together to form the efferent arterioles and proceed to the capillary network of the nephrons in the cortex and pyramids.

The important aspect of arterial blood supply is that there is no communication between the arteries of the kidney in any level of branching. This results in a lack of compensation in the case of arterial occlusion. Therefore, any obstruction of the arterial branch leads to the ischemia of the whole distal tree pool.

The kidneys demonstrate a large number of congenital vascular anomalies. Accessory and aberrant arteries are common and registered in about every fourth patent.

Venous blood after filtration travels through the network of venules to interlobular veins and further to the larger veins, which accompany the same name arteries (arcuate and interlobar), converge to renal veins and drain to the inferior vena cava.

According to the EFSUMB guidelines and recommendations for the clinical practice of CEUS in non-hepatic applications, update 2017 [1], kidney CEUS is feasible for the following purposes:

Supplementary Information The online version contains supplementary material available at [https://doi.org/10.1007/978-3-030-91764-7_8].

Y. N. Patrunov (✉) · E. I. Peniaeva
Department of Ultrasound Diagnostics of the Center for Radiological Diagnostics, Private Healthcare Institution "Clinical Hospital "RZD-Medicina" of Yaroslavl City", Yaroslavl, Russian Federation

A. N. Sencha
Department of Visual and Functional Diagnostics, Federal State Budget Institution "National Medical Research Center for Obstetrics, Gynecology and Perinatology n.a. V.I.Kulakov", Moscow, Russian Federation

L. A. Timofeyeva
Department of Propaedeutics of Internal Diseases with Radiation Diagnostics Course, I. N. Ulianov Chuvash State University, Cheboksary, Russian Federation

A. N. Sencha, Y. N. Patrunov (eds.), *Contrast-Enhanced Ultrasound*,
https://doi.org/10.1007/978-3-030-91764-7_8

- to diagnose ischemic renal disorders, such as infarction,
- to differentiate between renal tumors and anatomical variants mimicking a renal tumor ("pseudotumors") when the conventional US is equivocal,
- to characterize complex cysts according to the Bosniak criteria,
- to characterize indeterminate renal lesions,
- to identify renal abscesses in complicated acute pyelonephritis,
- to follow-up non-surgical renal lesions.

The blood supply of the kidney is very high and is 50 times higher than the same in other internal organs. Therefore, the SonoVue® dose of 0.8–1.5 ml is sufficient for standard CEUS with a convex probe.

Kidney CEUS confers two vascular phases. The cortical phase starts after UCA injection and lasts about 25–30 s. It is followed by the parenchymatous phase [1]. Rapid and intense contrast enhancement begins 10–15 s after the injection of UCA. The renal artery and its branches enhance quickly and depict the macrovascular features of the kidney. The cortex enhances in a few seconds followed by the gradual enhancement of the pyramids from the base to the apex that shows renal perfusion [2] (Figs. 8.1 and 8.2, Videos 8.1 and 8.2). As the microbubbles collapse with time, and their amount in the blood pool decreases, the contrast enhancement of the kidney gradually fades, starting with pyramids.

Although the macrovascularity is well observed with CEUS, it is not beneficial for the detection of vascular anomalies as compared with Doppler imaging. However, CEUS is of much better value for the assessment of microvascularity that is superior to CDI and PDI. It provides a clear delineation of the pyramids and easily depicts the structure of the renal parenchyma.

Kidneys may exhibit many anatomical variants, such as embryonic lobulation, dromedary hump, segmental hypertrophy, Bertin column hypertrophy that look like tumors with the conventional US. With CEUS, the contrast enhancement of these pseudotumors is identical to the same of the normal renal parenchyma in all vascular phases. Alternatively, renal tumors and other abnormal lesions demonstrate the enhancement, which is different from the normal parenchyma in the pattern, time, or intensity [1–4] (Figs. 8.2 and 8.3, Videos 8.2 and 8.3).

As opposed to the radiocontrast agents, SonoVue® is an exclusively intravascular UCA. It is not excreted with urine, so, the renal calyces, pelvis, and ureter are always UCA-free and their lumen remains unenhanced in all vascular phases.

8.1 **Renal Ischemic Injury.** Kidney Transplant

The diagnostic value of CEUS in the detection of renal parenchymal ischemia is comparable with such of CE-CT and higher than Doppler studies. Considering that UCAs have no nephrotoxic effect, it makes CEUS the method of choice for the diagnosis of renal infarct or ischemia [5].

CEUS permits accurate delineation of the focal infarction [2, 5, 6], which is detected as a wedge-shaped unenhanced area stretched from the capsule to the sinus on the background of the normally enhanced other renal aspects. It is the result of the occlusion of a renal artery branch. The size of the infarction depends on the level of occlusion. The occlusion of the trunk of the renal artery leads to the total renal infarction, which exhibits the complete absence of contrast enhancement of the whole kidney.

Focal renal infarction and cortical necrosis may be also confidently differentiated with CEUS based on the shape and location of the nonenhanced area. Renal cortical necrosis results from the blockage of the small arteries that supply blood to the cortex followed by a significant decrease in cortical perfusion. It is usually associated with a catastrophic decrease in blood pressure and results in acute renal injury and failure. In such a case, CEUS reveals nonenhancing peripheral cortical areas with preserved hilar vascularity [1].

One important aspect of CEUS in patients with renal ischemia is the differential diagnosis

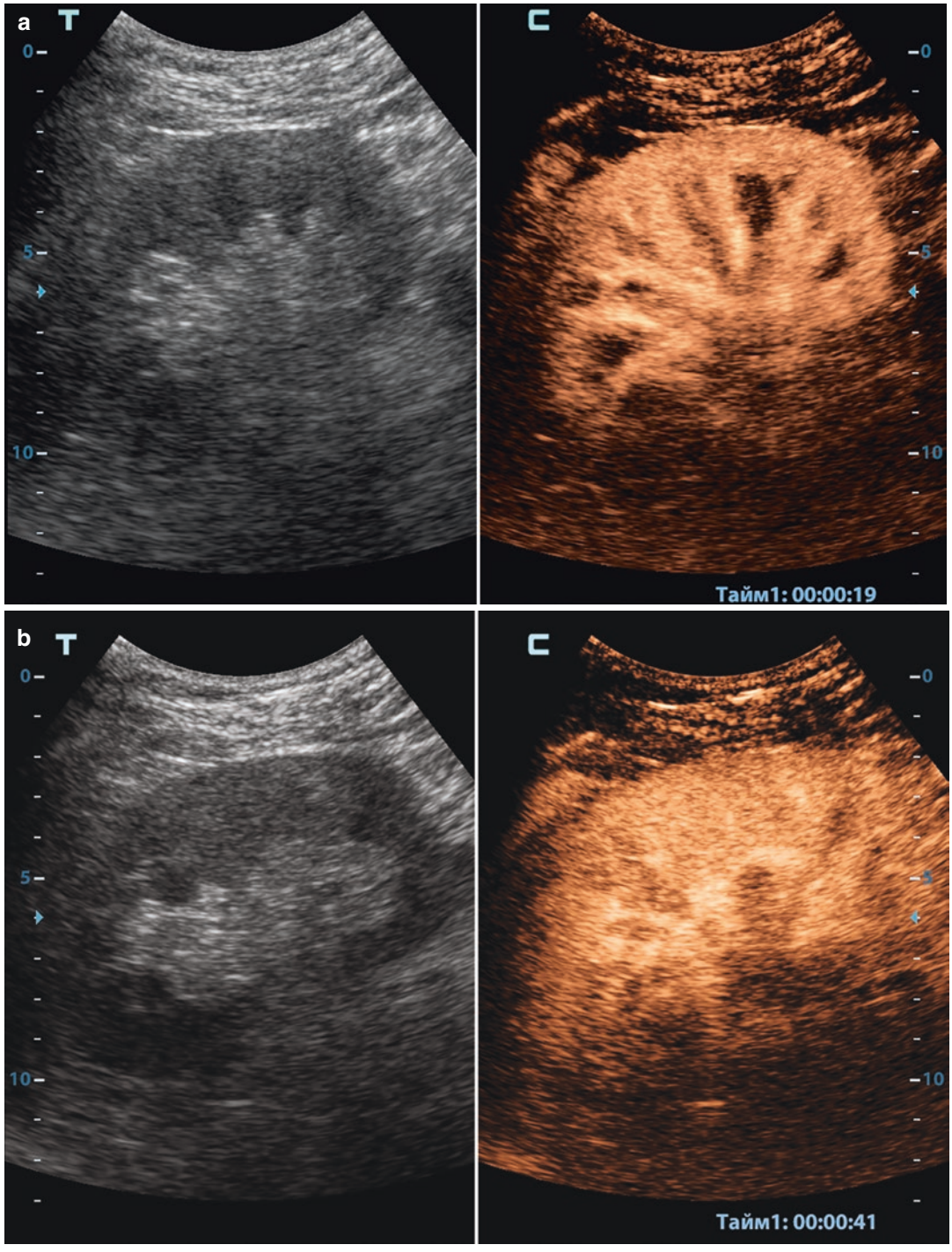

Fig. 8.1 Contrast enhancement pattern of the normal kidney. (**a**) Uniform contrast enhancement of the renal cortex in the cortical phase. CEUS image. (**b**) Contrast enhancement of the cortex and medulla in the parenchymatous phase. CEUS image

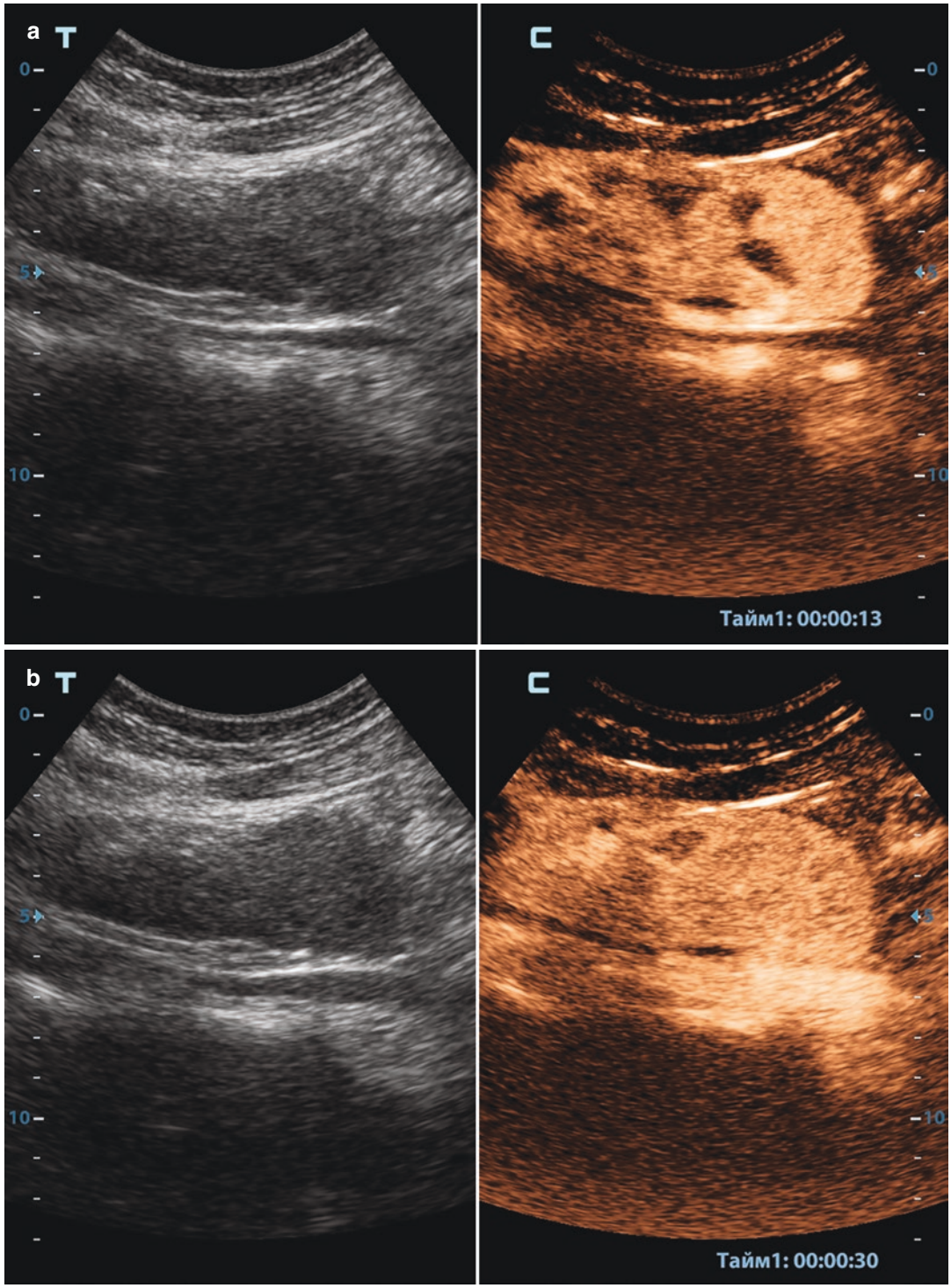

Fig. 8.2 Normal contrast enhancement of the dystopic kidney. The grayscale and Doppler US detected an ovoid hypoechoic mass in the small pelvis, which was suspicious for the dystopic kidney. (**a**) The arterial phase reveals a typical structure of renal parenchyma with clearly depicted cortex and medulla. CEUS image. (**b**) Parenchymatous phase. CEUS image

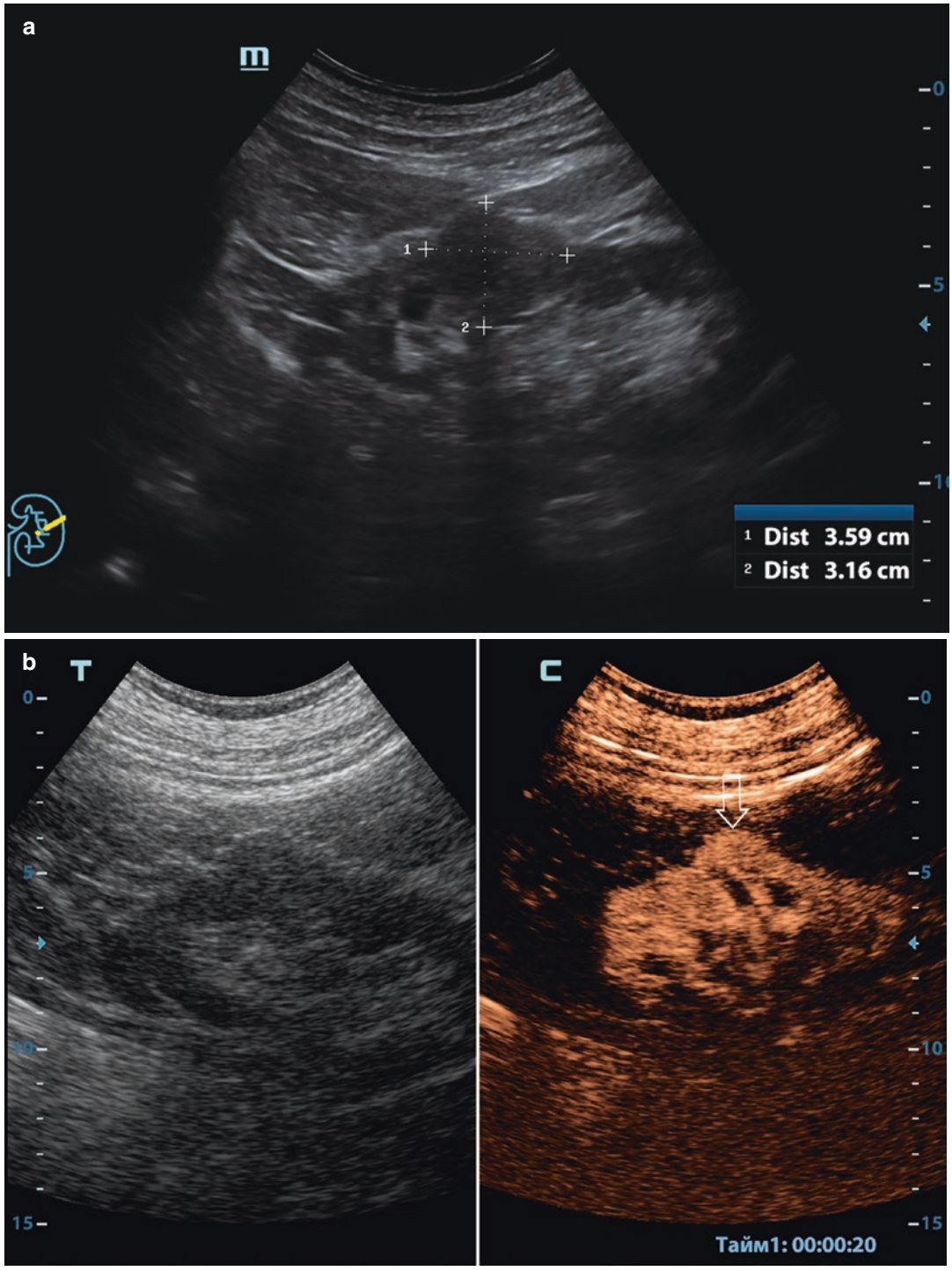

Fig. 8.3 Dromedary hump kidney. (**a**) Conventional grayscale US fails to reliably differentiate the anatomical variant from the lesion. CEUS image. (**b**) Contrast enhancement pattern in the suspicious area (arrow) corresponds to the normal renal parenchyma. Late cortical phase. CEUS image

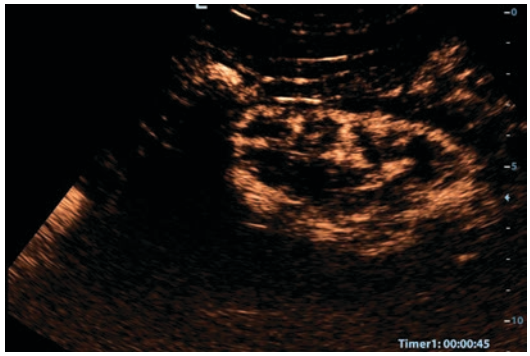

Fig. 8.4 Chronic renal failure. Decreased contrast enhancement throughout the whole kidney. CEUS image in the parenchymatous phase

of hypoperfused and non-perfused areas in both acute and chronic renal failure (Fig. 8.4, Video 8.4). In this connection, the quantitative analysis of CEUS is a promising modality for objective assessment of the ischemic damage severity.

An experimental study [7] on mice demonstrated that after 10–45 min compression of the vascular pedicle of the kidney, CEUS yielded to evaluate renal perfusion impairment associated with chronic kidney disease and predict the progression of renal fibrosis after acute ischemic renal damage. In diabetic nephropathy, CEUS identifies renal hyperperfusion at an early stage [8]. The authors report that area under the descending curve was significantly increased in early stage diabetic nephropathy compared to middle-stage ($p < 0.05$). Quantitative assessment of renal perfusion with CEUS revealed the decrease in renal perfusion in patients with acute and chronic renal failure in patients with chronic heart failure compared to healthy volunteers and patients with chronic heart failure without renal failure. However, reliable threshold values for the diagnosis of renal hypoperfusion are not proposed yet due to the limited number of publications and the lack of standardization.

Kidney transplantation is one radical method for the treatment of end-stage renal disease. It reduces the risk of cardiovascular mortality, ensures a high quality of life, and confidently increases the life expectancy in these patients [9].

CEUS can be successfully used to examine the kidney graft for early detection of perfusion disorders, stenosis, thrombosis, pseudoaneurysm, arteriovenous fistula, bleeding, and the assessment of pararenal tissue [10–12]. Although vascular complications in kidney transplantation are relatively seldom, with late diagnosis and treatment they rapidly cause renal transplant dysfunction and end up with graft removal [13].

The contrast enhancement of the renal graft occurs in the same time intervals and has the same vascular phases as in a normal kidney.

The diagnosis of acute **cortical necrosis** with CEUS was reported [14]. The study analyzed the CEUS image in patients, who subsequently had the kidney transplant removed due to acute cortical necrosis. CEUS revealed peripheral unenhanced rim-like subcapsular line and preserved enhancement of the renal vessels and medulla similar to the same in CE-CT and MRI. It appeared more sensitive as compared with the evaluation of peripheral resistance with spectral pulsed-wave Doppler.

Renal artery thrombosis is an urgent condition. CEUS supplies additional diagnostic information to CDI and pulsed-wave Doppler through accurate estimation of the decrease in renal perfusion. Complete occlusion of the renal artery with the absence of arterial blood supply is characterized by the absence of contrast enhancement of the entire kidney. Functioning accessory or aberrant arteries may maintain the blood perfusion in some areas of the kidney, which remain enhanced on the background of the otherwise unenhanced kidney.

Stenosis of the renal artery (both in own and transplanted kidney) exhibits slow contrast enhancement of the kidney cortex, which has the corresponding change in the time-intensity curve shape. Additionally, CEUS in many cases permits direct imaging of the stenotic segment. The study [15] reports that CEUS is superior to the color and pulsed-wave Doppler, and permits skipping the CT-angiography in some cases. The sensitivity, specificity, and AUC in the diagnosis of renal artery stenosis of the transplant were 92.3%, 87.5%, and 0.92, respectively.

Renal vein thrombosis occurs more rarely as compared to arterial thrombosis. Doppler modes reveal no blood flow in the renal vein and reversed diastolic blood flow in the renal artery. CEUS additionally determines slow heterogeneous contrast enhancement of the renal cortex and unenhanced renal veins. Sometimes in the first seconds of UCA arrival, the pulsed character of washin may be registered, which is probably associated with an increase in peripheral resistance in the renal artery system with congestion.

Renal transplant rejection is diagnosed with a combination of several methods. Imaging is not enough, and histopathology is necessary for the final diagnosis. Currently, there are no recommendations for the use of CEUS in the diagnosis of renal transplant rejection, but publications [10, 11, 16–18] indicate the prospects of quantitative analysis.

Transplanted kidneys with acute tubular necrosis and rejection crisis demonstrate the increased resistivity index and reduced peak enhancement and regional blood flow [16]. As compared to normal posttransplantation evolution, cortical to medullary ratios of regional blood flow and mean transit time were lower among acute tubular necrosis cases, while TTP was higher in acute rejection episodes. Additionally, mean transit time on the fifth day after grafting was significantly related to creatinine at follow-up. The possibility of using CEUS for monitoring the kidney during the treatment of graft rejection by assessing the perfusion of the parenchyma was reported [19].

In patients with **kidney injury**, CEUS is used to evaluate the renal perfusion and the severity of contusion, detect retroperitoneal bleeding and damage of the renal arteries, determine the true size of the kidneys, the location and size of hematoma. CEUS is performed individually for each kidney with the separate introduction of UCAs. The traumatic damage can be represented by perfusion defects with the otherwise preserved kidney perfusion (Fig. 8.5). The renal artery rupture or thrombosis is characterized by the complete absence or pronounced decrease in kidney contrast enhancement. In the active bleeding, extravasation of the UCA is registered.

8.2 Renal Inflammatory Diseases

In **acute pyelonephritis**, imaging methods detect possible complications. CEUS is indicative if the fever persists for more than 3 days from the beginning of treatment. Focal pyelonephritis exhibits hypoenhanced round or wedge-shaped areas located in the cortex or spreading to the medulla, which are better observed in the parenchymal phase on the background of homogeneously enhanced renal parenchyma [1].

These areas can demonstrate hypoenhancement throughout the entire study, but in some cases, they may appear isoenhanced in the early parenchymal phase with a subsequent decrease in enhancement. Locally thickened renal parenchyma, which is a consequence of the local inflammatory edema, can form hypoenhancing tumor-like lesions.

If the acute pyelonephritis is complicated by a **renal abscess,** CEUS detects the nonenhancing lesion of irregular shape, sometimes with the peripheral hyperenhanced rim or/and septa. These lesions can be observed both in the areas of focal changes in acute pyelonephritis and on the background of normal parenchyma (Fig. 8.6).

Merging abscesses look like a single lesion of irregular bizarre shape with multiple thick enhanced septa. The abscesses, which are treated with external drainage, can be additionally assessed with intraluminal UCA administration to specify its construction, septations, size, shape, location, relation to other retroperitoneal and abdominal structures, and detect fistula. CEUS increases the sensitivity of conventional US in the identification of pyelonephritis and small abscesses. The study [20] reports that normal US fails to recognize 22% of focal pyelonephritis, 42% of focal pyelonephritis with small abscesses, and 31% of renal abscesses detected with CEUS.

Additionally, CEUS may be used to follow-up the resolution of abscesses after treatment. After acute pyelonephritis, especially if complicated, the fibrous structures can be observed within the parenchyma. They are associated with focal cortical atrophy or defect and do not enhance with CEUS. However, recently after pyelonephritis, they may exhibit delayed enhancement due to

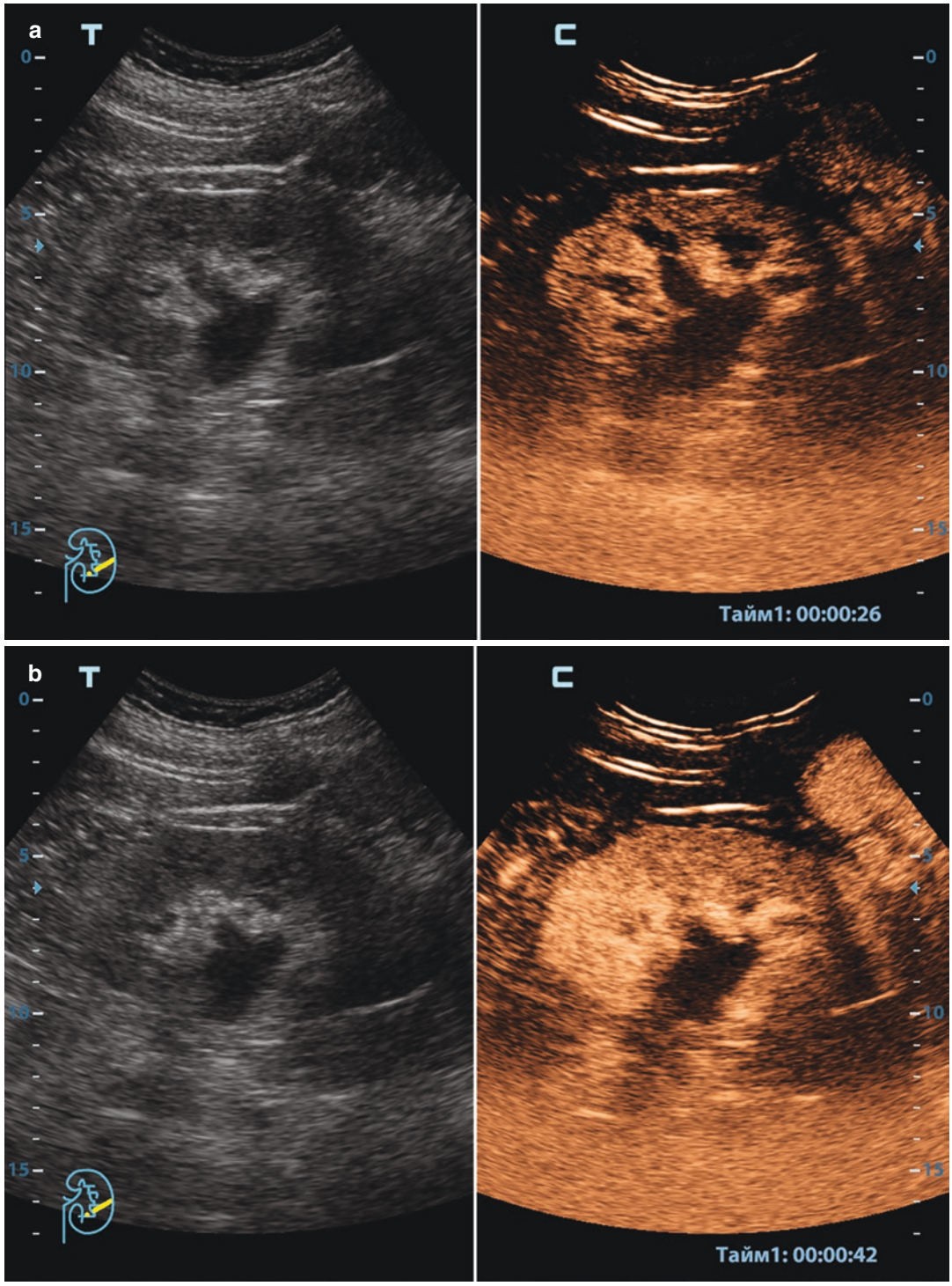

Fig. 8.5 Kidney contusion. Slow and mild contrast enhancement of the parenchyma. Unenhanced hypoechoic mass in the dilated pelvis corresponds to a blood clot. CEUS images. (**a**) Arterial phase. (**b**) Parenchymatous phase

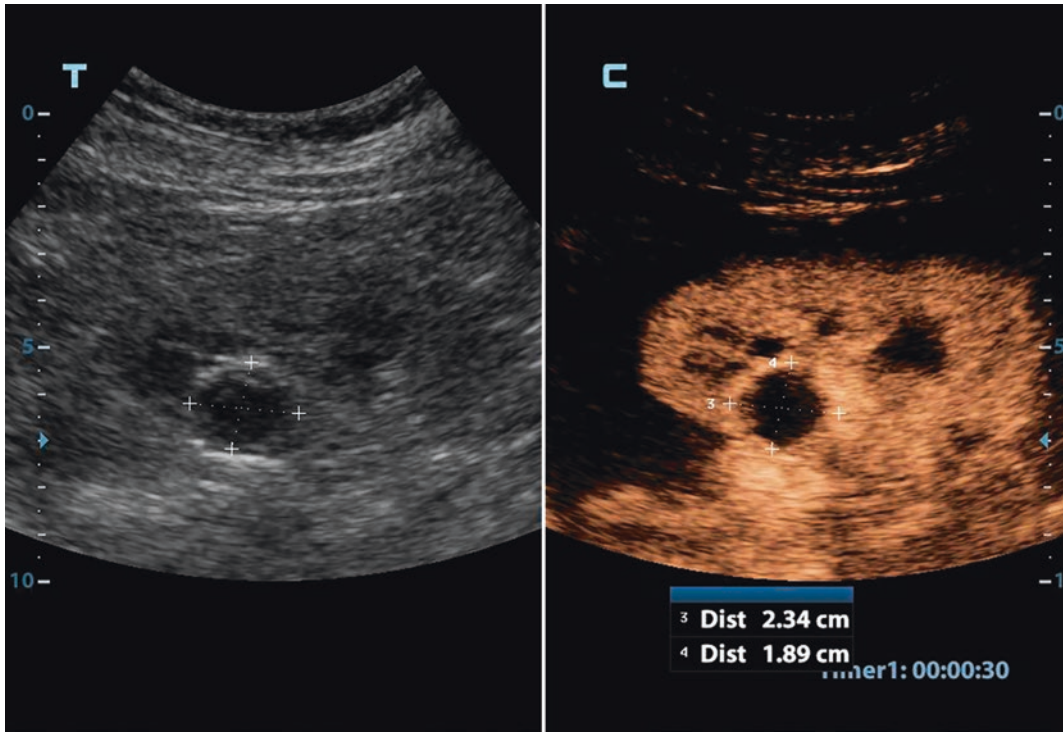

Fig. 8.6 Renal abscess. Rim-shaped peripheral hyperenhancement and no contrast enhancement of the internal echogenic component. CEUS image

granulation tissue [21]. The above-mentioned features are also appropriate for the inflammatory process in a renal transplant.

8.3 Renal Cysts

The classification of complex renal cysts was proposed in 1986 by M. Bosniak to stratify the risk of malignancy with CE-CT data and later was adapted to CEUS. It also suggests five categories, as follows [22–25] (Fig. 8.7):

- Category I. Benign simple cyst. Malignancy incidence of 0%. No follow-up is required. Thin wall with no septa, calcification, or solid components. No enhancement with CEUS (Fig. 8.8, Video 8.5).
- Category II. Benign minimally complex cyst. Malignancy incidence of 0%. No follow-up is required. A few thin <1 mm septa with a few microbubbles seen in them. Fine calcifications may be present in the wall or septa. Uniform high-attenuation lesions <3 cm in diameter that are well defined and do not enhance with contrast agent.
- Category IIF. Probably benign minimally complex cyst, require follow-up ("F" means "follow"). Malignancy incidence of about 5%. Multiple hairline-thin septa that show a few microbubbles traveling along them. Minimal thickening of wall or septa, which may contain some calcification but no enhancement with contrast agent. No enhancing soft-tissue components. Nonenhancing intrarenal lesions >3 cm in diameter.
- Category III. Indeterminate cyst. Malignancy incidence of about 50%. This group includes hemorrhagic or infected cysts and cystic neoplasms. Need surgical intervention. Cysts with thickened irregular walls or septa that show enhancement at CT and CEUS.
- Category IV. Clearly malignant cyst. Malignancy incidence of about 95–100%.

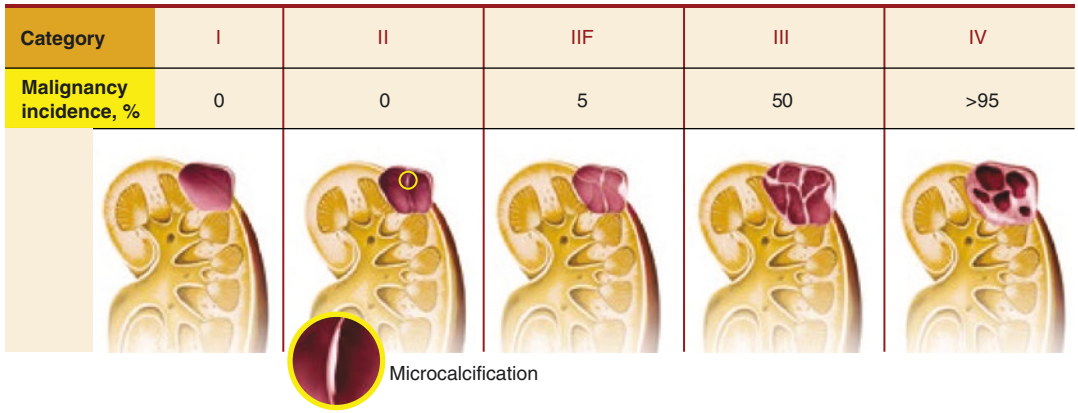

Fig. 8.7 Bosniak classification of renal cysts. Scheme

Require surgical resection. Cysts with distinct enhancing solid masses separate from the wall or septa in addition to the features in category III (Fig. 8.9, Video 8.6).

Some studies demonstrated that CEUS is superior to CE-CT in classifying complex renal cysts [26]. In the study [27], in 7/37 lesions (19%) the CE-CT and CEUS scores were different, while in 30/37 (81%) they were equivalent. CEUS depicted more thin septa or upgraded wall thickness, resulting in a Bosniak score upgrade from category II to IIF in 5 lesions. Two cystic renal masses could not be clearly assigned by CE-CT but were considered malignant due to the additional information from CEUS, which was confirmed by surgical removal [26].

CEUS is proposed for every renal mass with a complex cystic appearance [28]. CE-CT is a method of choice for the staging of those that reveal a malignant enhancement pattern at CEUS. Meanwhile, CEUS is considered an alternative to CT in the follow-up of complex renal cysts and for patients with renal insufficiency and/or contraindications to CE-CT or MRI [28].

8.4 Renal Tumors

Both renal cysts and solid tumors are often initially detected with ultrasound, but the diagnostic possibilities of traditional sonography in the differential diagnosis of benign and malignant lesions are limited. Several publications indicate the value of CEUS for differentiation of solid renal masses. CEUS surpasses MRI and CT in the identification of vascularity in hypovascular tumors [29]. A meta-analysis [30] conferred a total of 567 cases of histologically verified renal cell carcinoma and 313 patients with benign renal tumors. It reports the sensitivity of CEUS 88% and the specificity of 80%. The study of Barr et al. [31] on 1018 indeterminate renal masses demonstrated CEUS sensitivity of 100%, specificity of 95%, PPV of 94.7%, and NPV of 100%.

WHO classification of kidney tumors based on histologic appearance is provided below [32].

Renal cell tumors

- Clear cell renal cell carcinoma.
- Multilocular cystic renal neoplasm of low malignant potential.
- Papillary renal cell carcinoma.
- Hereditary leiomyomatosis and renal cell carcinoma associated renal cell carcinoma.
- Chromophobe renal cell carcinoma.
- Collecting duct carcinoma.
- Renal medullary carcinoma.
- MiT family translocation renal cell carcinomas.
- Succinate dehydrogenase deficient renal cell carcinoma.
- Mucinous tubular and spindle cell carcinoma.
- Tubulocystic renal cell carcinoma.
- Acquired cystic disease associated renal cell carcinoma.

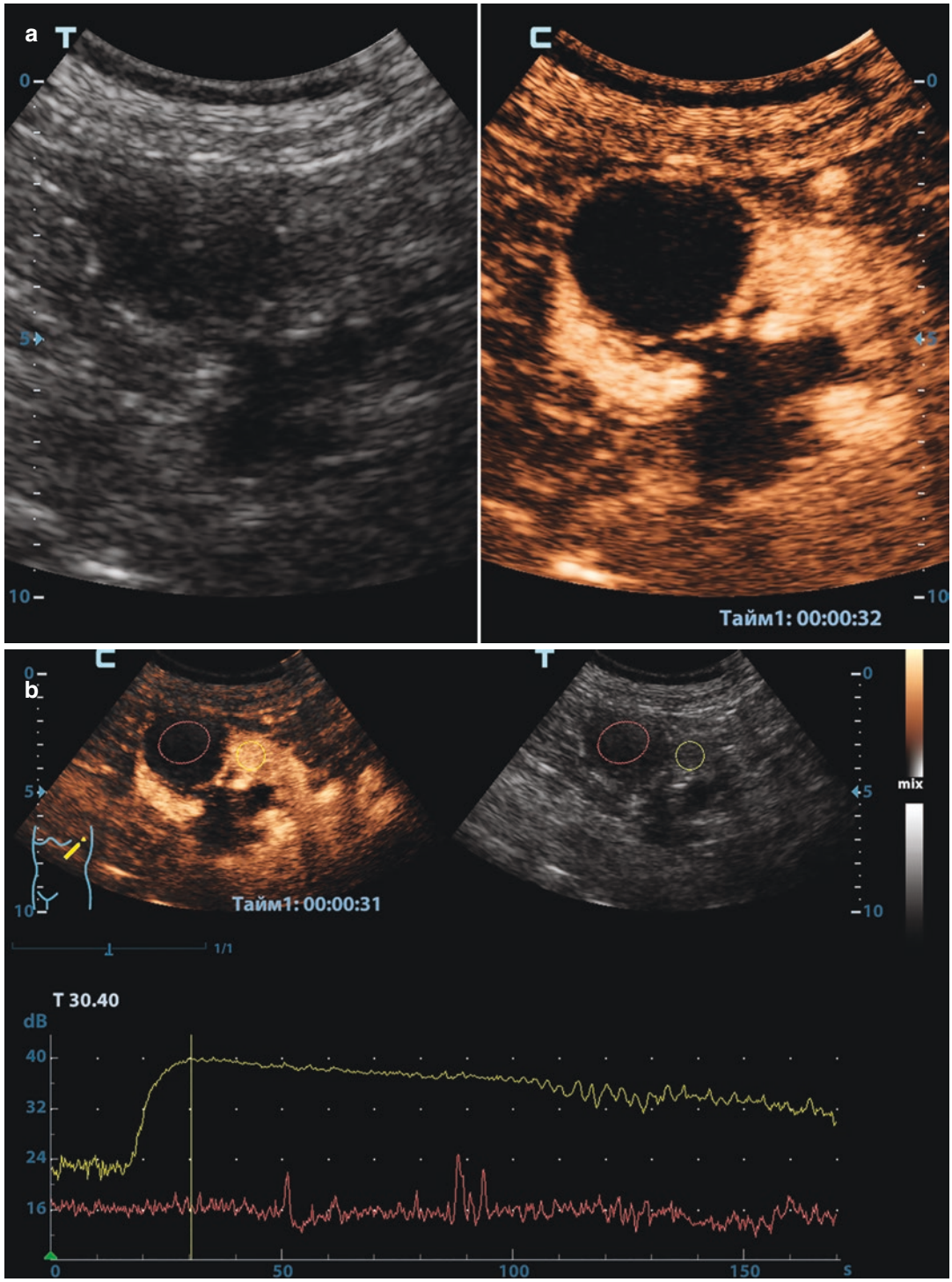

Fig. 8.8 Simple renal cyst, Bosniak category I. Thin walls, no septa, and no contrast enhancement (perfusion defect). (**a**) CEUS image. (**b**) Quantitative analysis with TIC demonstrates no contrast enhancement in the cyst (pink ROI) as opposed to renal parenchyma (yellow ROI). (**c**) CE-CT

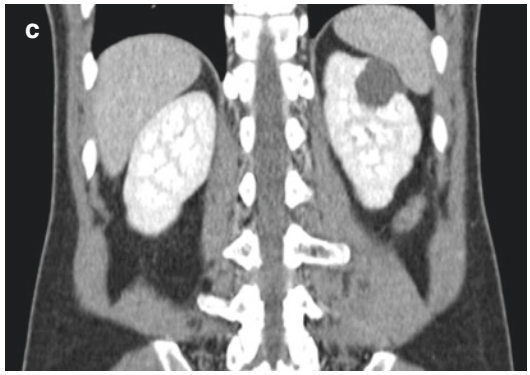

Fig. 8.8 (continued)

- Clear cell papillary renal cell carcinoma.
- Renal cell carcinoma, unclassified.
- Papillary adenoma.
- Oncocytoma.

Metanephric tumors
- Metanephric adenoma.
- Metanephric adenofibroma.
- Metanephric stromal tumor.

Nephroblastic and cystic tumors occurring mainly in children
- Nephrogenic rests.
- Nephroblastoma.
- Cystic partially differentiated nephroblastoma.
- Pediatric cystic nephroma.

Mesenchymal tumors
Mesenchymal tumors occurring mainly in children
- Clear cell sarcoma.
- Rhabdoid tumor.
- Congenital mesoblastic nephroma.
- Ossifying renal tumor of infancy.

Mesenchymal tumors occurring mainly in adults
- Leiomyosarcoma (including renal vein leiomyosarcoma).
- Angiosarcoma.
- Rhabdomyosarcoma.
- Osteosarcoma.
- Synovial sarcoma.
- Ewing sarcoma.
- Angiomyolipoma.
- Epithelioid angiomyolipoma.
- Leiomyoma.
- Hemangioma.
- Lymphangioma.
- Hemangioblastoma.
- Juxtaglomerular cell tumor.
- Renomedullary interstitial cell tumor.
- Schwannoma.
- Solitary fibrous tumor.

Mixed epithelial and stromal tumor family
- Adult cystic nephroma.
- Mixed epithelial and stromal tumor.

Neuroendocrine tumors
- Well differentiated neuroendocrine tumor.
- Large cell neuroendocrine carcinoma.
- Small cell neuroendocrine carcinoma.
- Paraganglioma.

Renal hematopoietic neoplasms.
Germ cell tumors.
Metastatic tumors.

Renal malignant tumors are mostly represented with renal cell carcinoma. Approximately 70% of them are clear cell carcinoma, 10–15% - papillary carcinoma, 5%—chromophobe carcinoma, and even rarer are collecting (Bellini) duct carcinoma and other types. Clear cell carcinoma has the greatest metastatic potential.

Renal cell carcinoma with histopathology exhibits numerous thin-walled vessels with active blood flow. Intratumoral necrosis, hemorrhage, and calcifications arise with growing and are often observed in large-sized tumors.

The enhancement pattern depends on the lesion size. Renal cell carcinoma smaller than 3 cm typically exhibits diffuse uniform hyperenhancement in the cortical phase (Fig. 8.10, Video 8.7) and lesions larger than 3 cm enhance heterogeneously [29] (Figs. 8.11, 8.12, and 8.13, Videos 8.8, 8.9, and 8.10). However, avascular areas, such as cystic components, etc., result in nonenhanced areas in the lesions regardless of the size (Fig. 8.14, Videos 8.11 and 8.12).

Heterogenous hypoenhancing pattern correlates with the tumor size [33]. Besides, malignant tumors of larger size washout earlier.

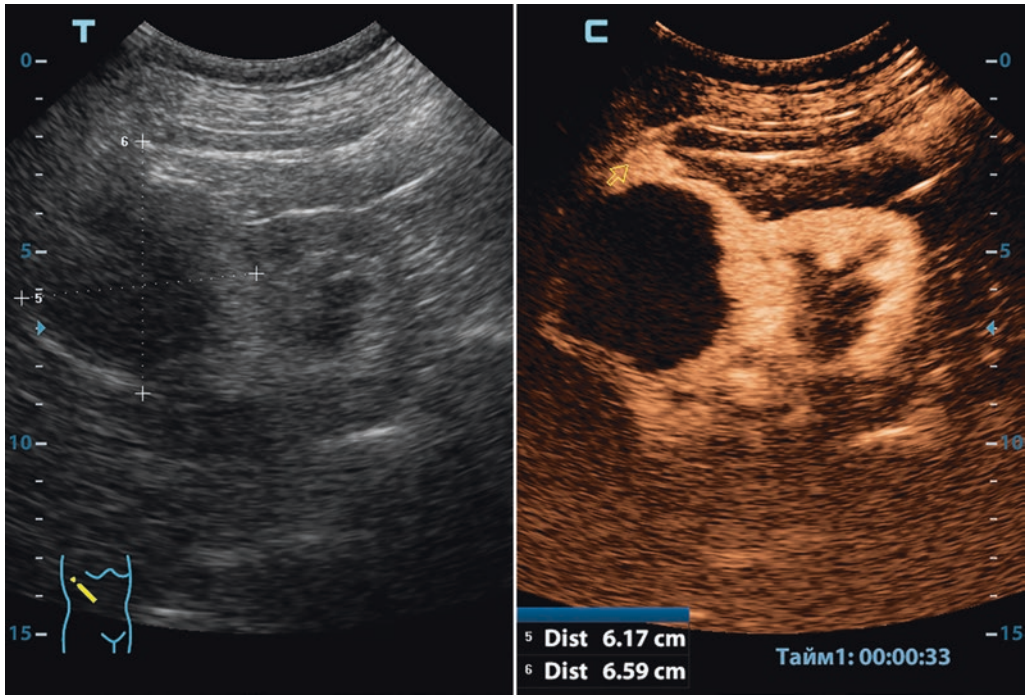

Fig. 8.9 Complex renal cyst (verified renal cell carcinoma) corresponds to Bosniak category IV. The contrast enhancement of the thickened irregular walls and mural nodules (arrow) protruding to the perirenal fat. CEUS image

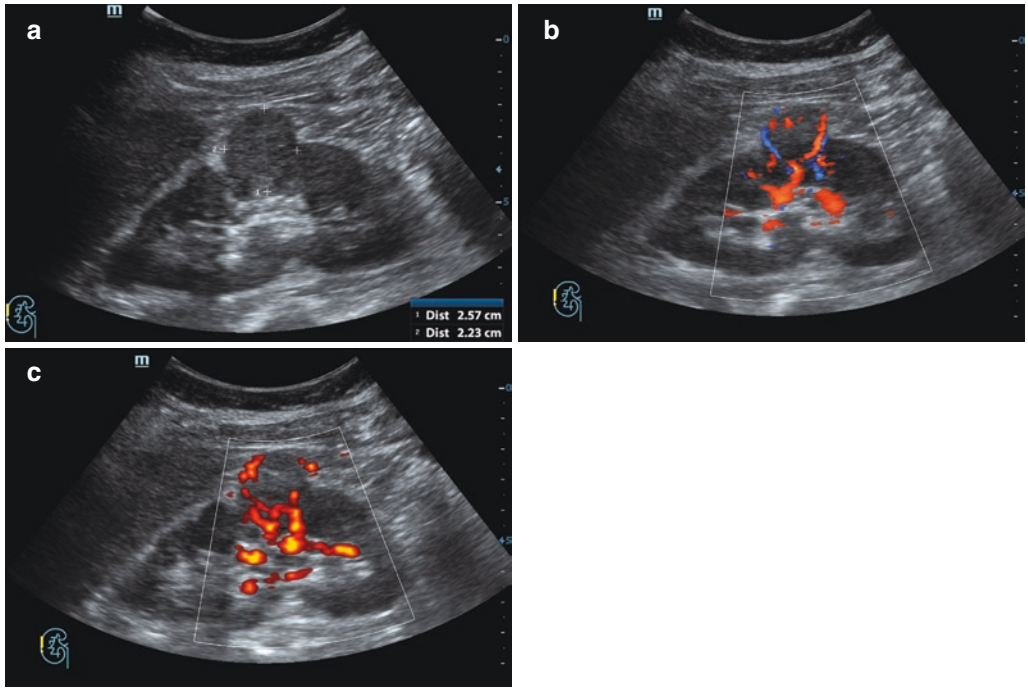

Fig. 8.10 Renal cell carcinoma of 2.5 cm in size. (**a**) The grayscale US demonstrates a homogeneous isoechoic lesion with a partially extrarenal location. (**b**) CDI exhibits good vascularity of predominantly peripheral pattern. (**c**) PDI exhibits good vascularity in the peripheral aspects of the lesion. (**d**) Arterial phase CEUS demonstrates early intense uniform contrast enhancement

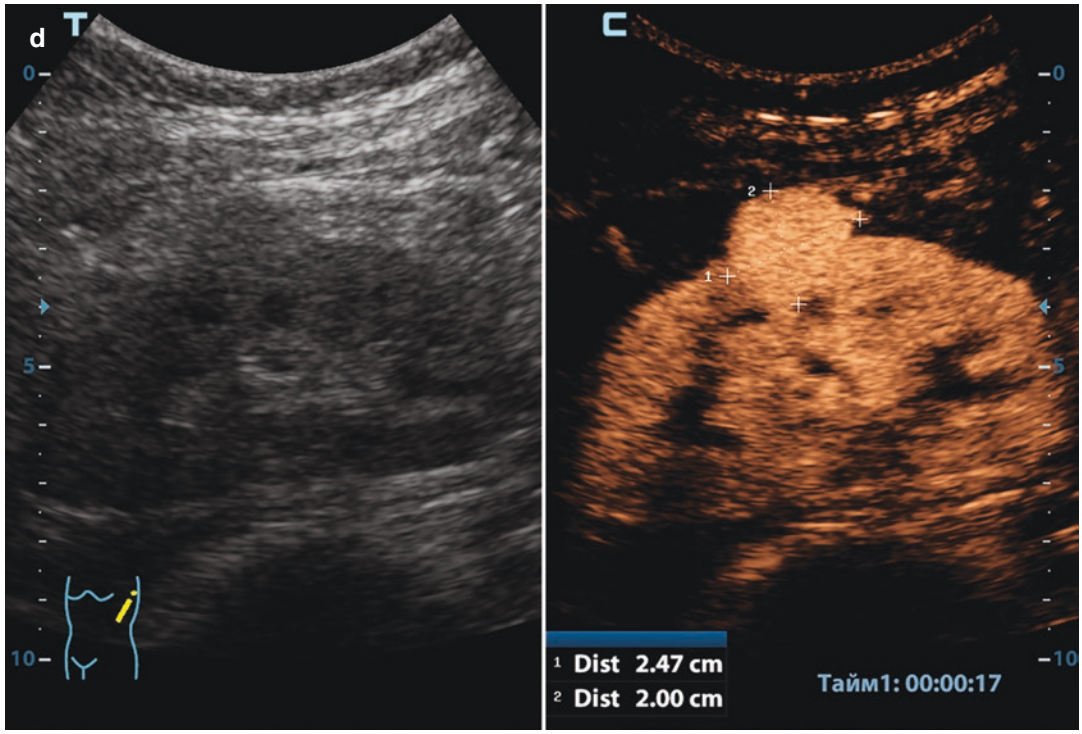

Fig. 8.10 (continued)

Some publications [34, 35] demonstrate the dependence of the contrast enhancement of renal cell carcinoma from the histological subtype. Clear cell carcinoma often exhibits hyperenhancement, while papillary carcinoma demonstrates inhomogeneous hypoenhancement in the cortical phase, which hampers differential diagnosis with angiomyolipoma. In the parenchymal phase, renal cell carcinoma is usually hypoenhanced, but about 19% of them can maintain isoenhancement [36].

The following types of contrast enhancement of clear cell carcinoma with respect to the surrounding kidney parenchyma may be observed [37]:

- quick washin—quick washout.
- quick washin—slow washout (Fig. 8.11, Video 8.8).
- identical to the renal parenchyma (Fig. 8.12, Video 8.9).

Regardless of the histological subtype, renal cell carcinoma may demonstrate pseudocapsule, which is represented by a hyperenhancing rim probably due to the compressed surrounding renal parenchyma [38, 39]. CEUS can also detect the zones of tumor invasion to the surrounding tissues or vessels, which lack pseudocapsule (Fig. 8.13, Video 8.10).

Urothelial carcinoma arises from the urothelial cells of the excretory system and in 7% of cases affects the renal pelvis. CEUS detects the microvascularity of the tumor and reliably differentiates them from blood clots, which are avascular. They are characterized by rapid hyperenhancement with fast washout. If located in the ureter, these tumors also hyperenhance and can cause hydronephrosis, spread local deposits, and invade the surrounding tissues.

Benign kidney tumors are typically represented by angiomyolipoma and oncocytoma. In the studies [40, 41], angiomyolipoma and oncocytoma were the causes for kidney surgery in 10–38% and 34–58%, respectively.

Angiomyolipoma (AML) usually includes three components: thick-walled blood vessels (angio-), smooth muscle fibers (myo-), and adi-

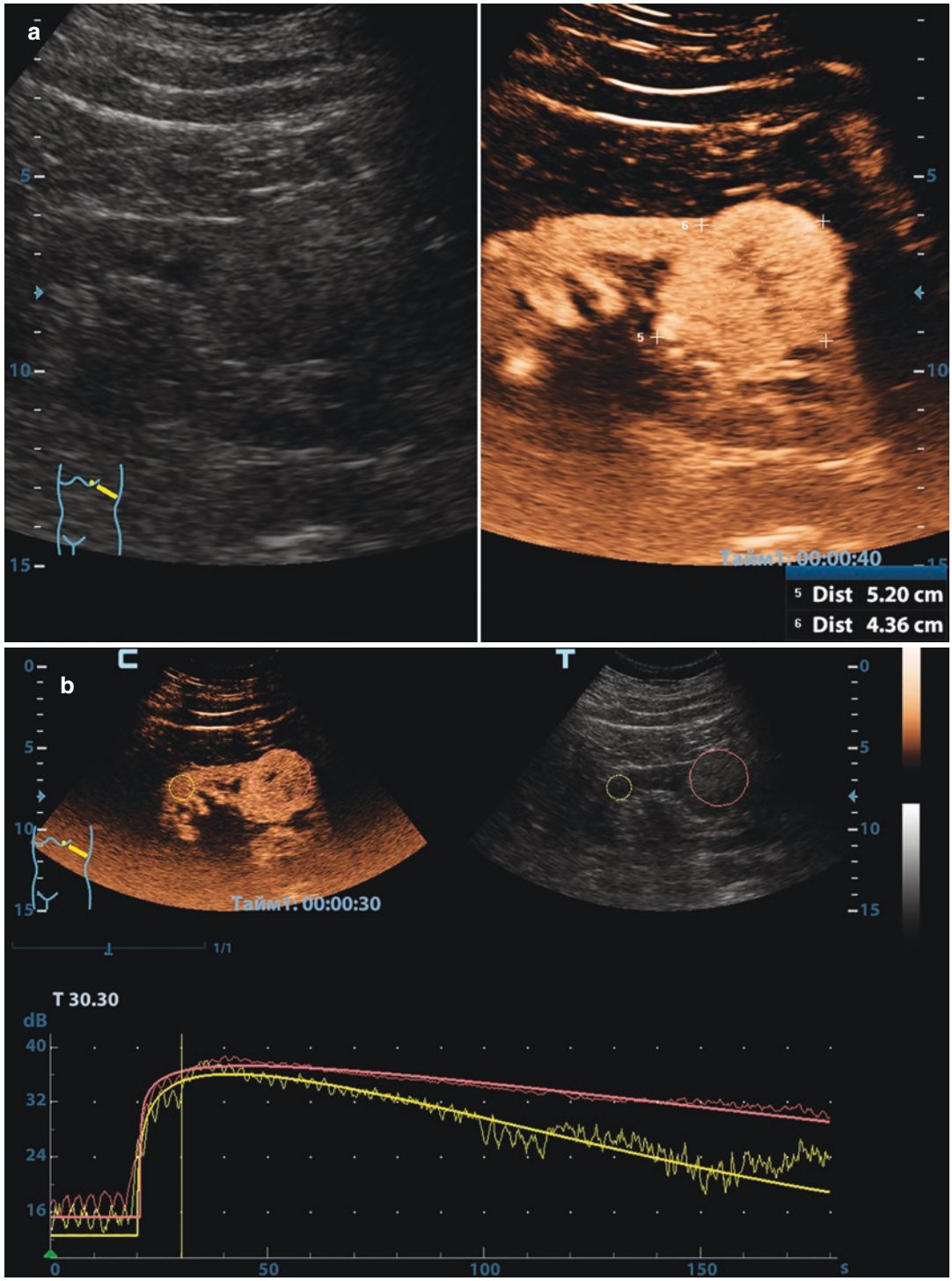

Fig. 8.11 Renal cell carcinoma of 5 cm in size. (**a**) CEUS image. The lesion exhibits heterogeneous enhancement, which is intense and uniform at the periphery and moderate in the central aspects with small perfusion defects. (**b**) TIC shape of the lesion enhancement (pink ROI) demonstrates slow washout as compared with the normal renal parenchyma (yellow ROI). (**c**) Arterial phase CE-CT

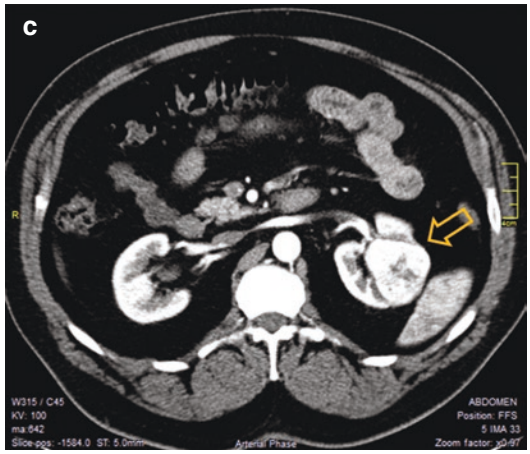

Fig. 8.11 (continued)

pose tissue (lipoma). The etiology and pathogenesis of these tumors remain unclear. They can arise sporadically or be a part of several diseases, such as tuberous sclerosis [42].

AMLs exhibit typical signs with the standard US. They appear uniform, hyperechoic with clear smooth margins, and avascular. However, in several cases, they demand differential diagnosis [4, 12].

With CEUS, a typical AML demonstrates centripetal hypoenhancement in relation to the surrounding renal parenchyma in the cortical phase, which is followed by homogeneous isoenhancement in the parenchymal phase without washout (Fig. 8.15, Video 8.13). Several AMLs may remain hypoenhanced in all vascular phases (Fig. 8.16, Video 8.14). Additionally, CEUS enables reliable identification of vascular aneurysms in large AMLs, the risk of which increases in AML larger than 4 cm in size [12, 43].

Classic three-component AML is a clearly benign tumor. However, epithelioid AML demonstrates the risk of malignant transformation. These tumors consist mainly of proliferating epithelioid cells with a small amount of adipose tissue. Occasional publications describe their enhancement features. In the study [44], epithelioid AMLs were characterized with hyperenhancement in the cortical phase. The hypervascularity of these tumors is also emphasized by [45]. The study analyzed the TICs and revealed significantly higher peak intensity in epithelioid AMLs than in three-component AMLs, which did not differ from renal cell carcinoma.

Oncocytoma is a common epithelial renal tumor, which is usually detected by chance and does not have any clinical signs. This tumor does not metastasize, but sometimes invasive growth with the infiltration of the renal capsule may occur. There are no reliable imaging, cytological, and histological criteria for differential diagnosis. Therefore, the final diagnosis bases on the histopathological study of the excised tumor.

The data on the CEUS features of oncocytoma are ambiguous. Some authors report early hyperenhancement and slow washout [30, 46]. The centripetal character of enhancement and the characteristic spoke-wheel pattern similar to that of the liver FNH are also reported [29].

CEUS is more sensitive than CT for detecting blood flow in hypovascular lesions and can be used in uncertain CT results [29]. In a significant number of cases, it is an alternative to CE-CT free from such drawbacks as nephrotoxicity of iodine-containing contrast agents and ionizing radiation. In each case, it is necessary to consider CEUS before appointing CE-CT. In many patients, CT will appear unnecessary or the study protocol will be changed.

Besides, CEUS is an efficient tool for monitoring the kidney condition and the change in structure and vascularity of renal lesions during and after minimally invasive ablative techniques, such as percutaneous radiofrequency ablation and others.

Quantitative analysis of CEUS for the diagnosis of kidney diseases seems more objective to estimate renal perfusion, but it is currently more applicable for scientific research and clinical trials [12].

The value of CEUS for evaluating renal perfusion was demonstrated in the experiment [37]. CEUS was able to detect changes in human renal cortical microcirculation as induced by angiotensin II infusion and/or captopril administration. The study used a disruption-replenishment protocol with a slow intravenous infusion of SonoVue® at a dose of 0.5 ml/min. After achieving constant concentration of UCA in the blood pool and TIC

plateau, angiotensin II at consecutive doses of 1 ng/kg/min and 3 ng/kg/min was infused followed by oral administration of captopril. US scanner software calculated the mean transit time (MTT), regional blood volume (RBV), and perfusion index (PI; PI = RBV/MTT), which is considered proportional to blood flow. These parameters are related to the peak intensity of contrast enhancement and TTP after microbubble destruction [47]. Quantitative CEUS registered an authentic decrease in renal perfusion after the introduction of angiotensin II and the increase in perfusion with captopril.

Changes in renal perfusion may be also evaluated with the common bolus administration of UCA. Patients with moderate and severe chronic renal failure due to diabetic nephropathy demonstrated a decrease in the area under the curve (AUC), increase in arrival time (AT) and time to peak (TTP) as compared with the control group

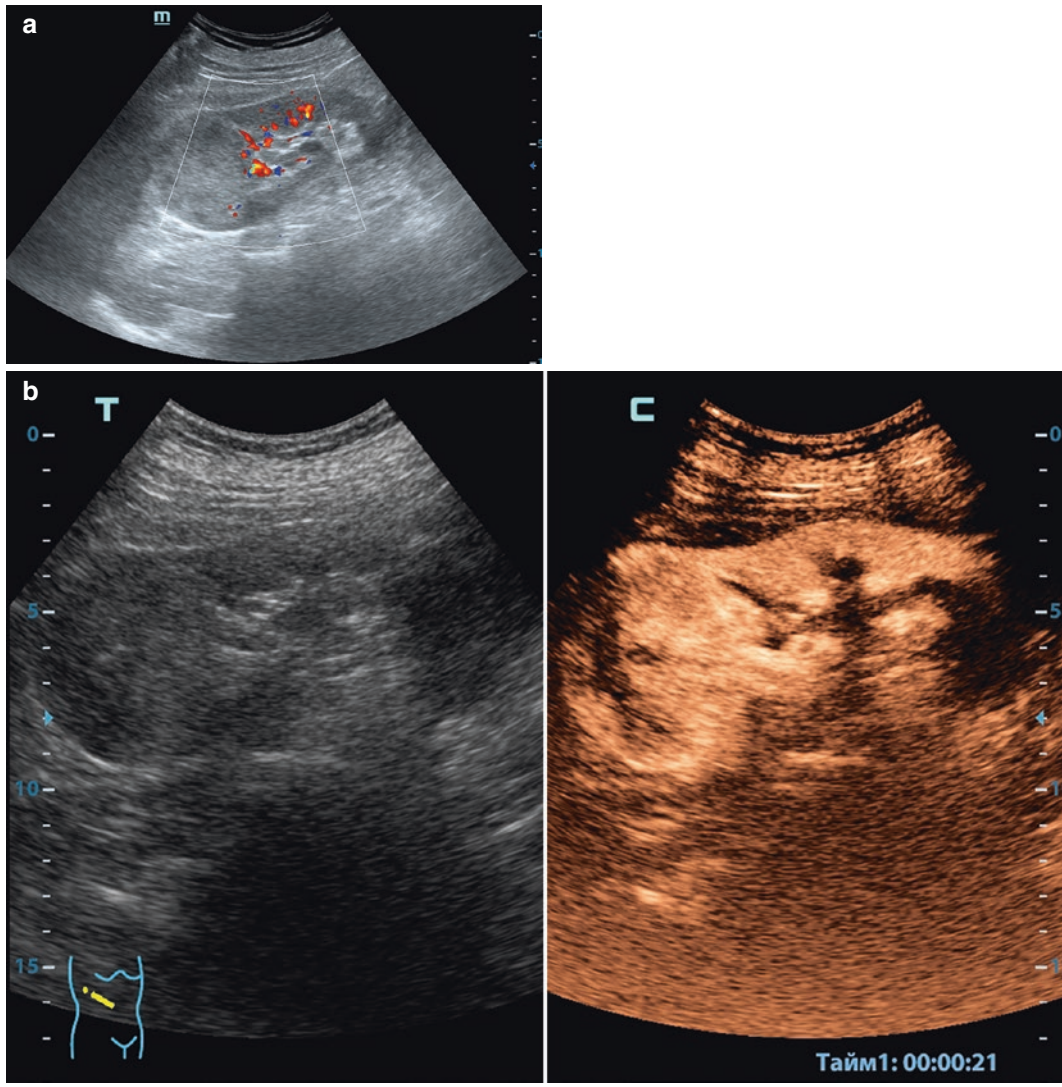

Fig. 8.12 Renal cell carcinoma of 6 cm in size. (**a**) Color Doppler image detects poor lesion vascularity. (**b**) CEUS image. The lesion exhibits heterogeneous enhancement, which is predominantly intense. (**c**) TIC of the lesion enhancement (pink ROI) is almost equal to the normal renal parenchyma (yellow ROI). (**d**) Venous phase CE-CT, the lesion is marked with an arrow. (**e**) Delayed phase CE-CT

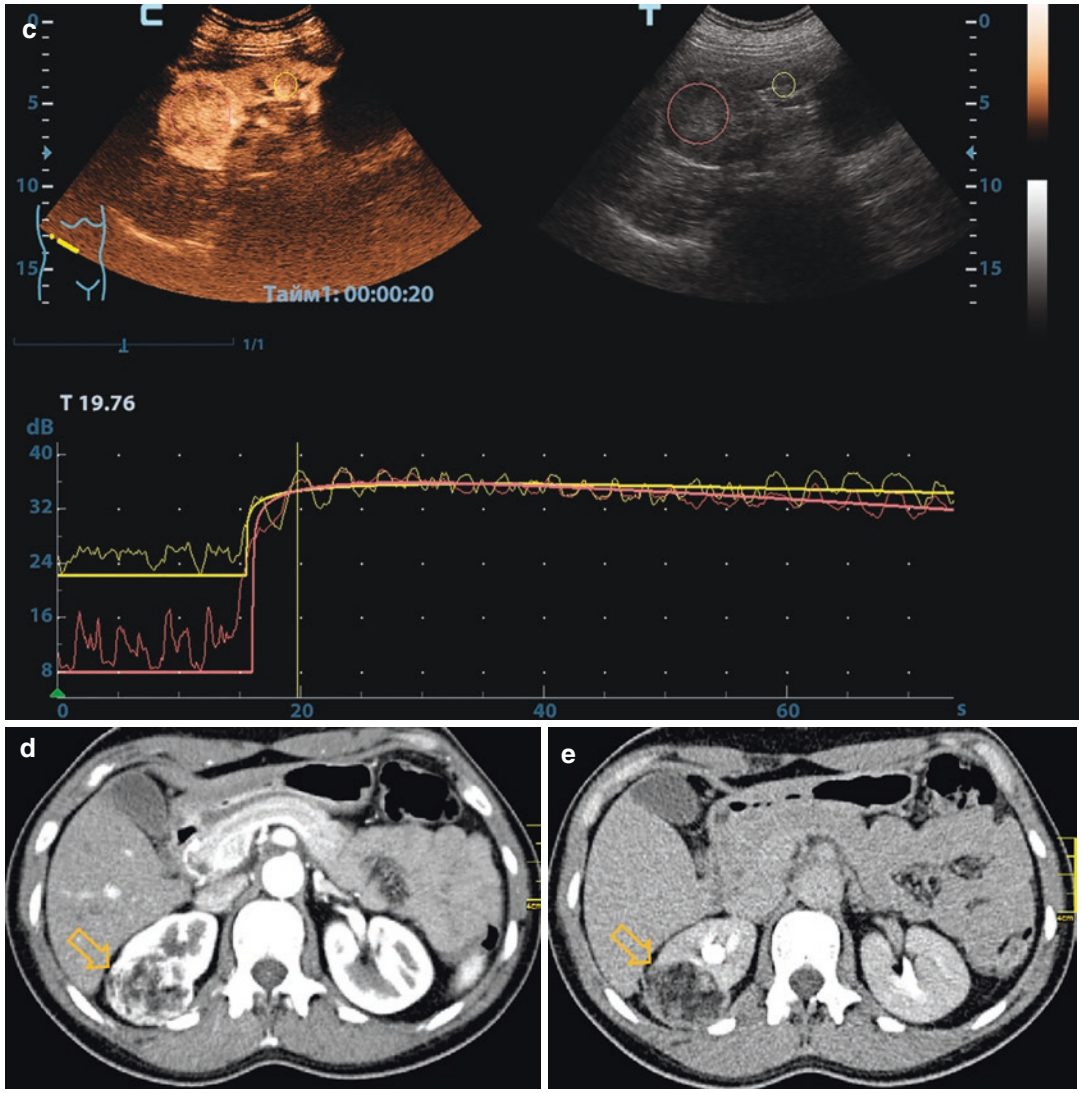

Fig. 8.12 (continued)

[48]. Besides, the changes were more prominent in the group of patients with severe chronic renal failure than in the group with moderate renal failure.

The data of publications on the quantitative analysis of CEUS for the differential diagnosis of benign and malignant renal tumors are contradictory. Probably, it is a consequence of the lack of protocol standardization, the difference in equipment, or the small study sample. The washin rate in malignant tumors exceeded the same parameter of benign lesions and also correlated with the degree of differentiation [33]. Peak intensity and time-to-80% on wash-out were also reported to provide significant differences between clear cell, papillary, and chromophobe renal cell carcinoma subtypes [49]. In small-sized renal cell carcinomas and AMLs, higher values of enhancement intensity, washout in the late phase, and perilesional rim-like enhancement were reported [50].

However, currently, the quantitative analysis of renal CEUS remains the subject of scientific study. It is rarely used in clinical practice except for the assessment of the tumor response to therapy.

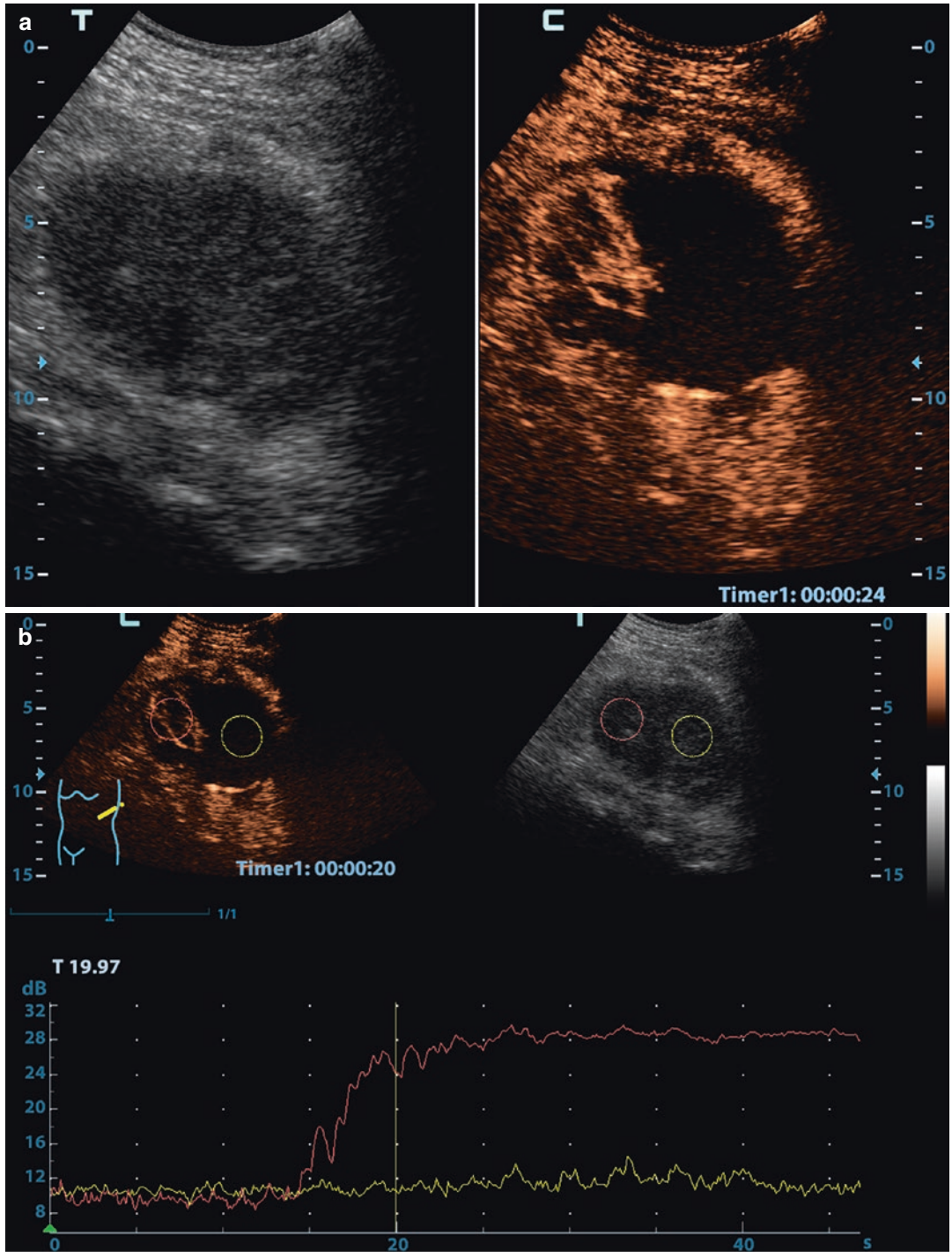

Fig. 8.13 Large renal cell carcinoma, which substitutes 2/3 of the kidney with penetration to retroperitoneal fat. (**a**) CEUS image. The lesion demonstrates poor enhancement with large avascular areas. Some normal parenchyma remains in the upper segment of the kidney. (**b**) TIC shows no enhancement of the lesion (yellow ROI) and typical enhancement of the remaining renal parenchyma (pink ROI). (**c**) Venous phase CE-CT

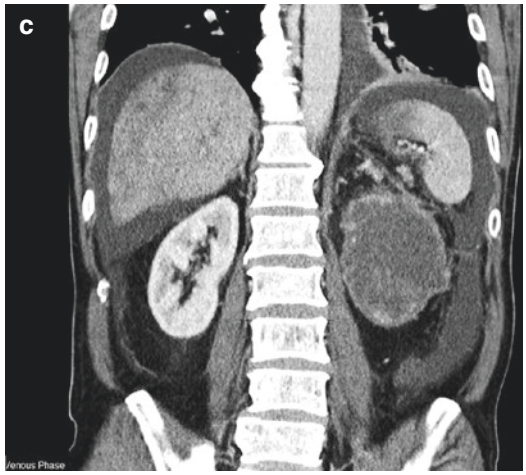

Fig. 8.13 (continued)

8.5 Adrenals

The adrenal glands are situated near the medial aspect of the upper poles of each kidney. They are richly supplied with blood via the superior, middle, and inferior suprarenal arteries, which arise from the inferior phrenic artery, abdominal aorta, and renal artery respectively. These vessels form a plexus within the capsule of the adrenal gland and form small arteries that descend through the cortex and medulla. These arteries compose a capillary network around the medullary secretory cells. The medullary veins merge to a single adrenal vein, which drains to the inferior vena cava on the right side and the left renal vein on the left.

Adrenals are normally examined together with the kidneys due to the anatomical intimacy. Therefore, most adrenal lesions are detected by chance and called incidentalomas. Imaging methods detect them in 2–4% of the general population and up to 9–10% in elderly people. The main two tasks with such a lesion are the evaluation of its hormonal activity and the risk of malignancy.

Adrenal adenoma is a dominating lesion, which accounts for about 80% of all incidentalomas. Pheochromocytoma, carcinoma, myelolipoma, cyst, metastasis, etc. exhibit significantly lower incidence.

CT confidently differentiates adrenal adenoma. A typical adenoma with a native CT scan has a density from −5 HU to +15 HU. In such cases, which make more than half of all adrenal scans, the introduction of the contrast medium is not required. In other cases, contrast-enhanced CT is necessary with the calculation of relative and absolute washout. Adenomas with high specificity demonstrate the values of >40% and >60%, respectively. All lesions that have lower washout values with CE-CT are considered not adenomas, and the specificity of CE-CT in this group is low. MR has similar diagnostic accuracy to CT allowing characterizing adenomas regardless of their CT enhancement.

With sonography, a similar approach is impossible. First of all, the features of the visualization of adrenal glands limit both grayscale and contrast-enhanced ultrasound. Adrenals are located deeply in the retroperitoneal space. Normal adrenals are flat and comparable on echogenicity with the surrounding fat. Therefore, conventional US is capable to detect only considerably large adrenal lesions. The left adrenal gland is surrounded by gas-containing organs, and the US often fails to determine its masses. The right adrenal lesions are well visualized with the grayscale US through the liver, but during CEUS, the liver enhancement negatively affects the imaging quality of the right adrenal lesions. Secondly, the microbubbles after bolus injection persist in the blood pool for less than 10 min due to their self-destruction, which has a non-linear character. This fact does not permit the interpolation of the CE-CT washout calculation method to CEUS.

EFSUMB guidelines and recommendations for the clinical practice of CEUS in non-hepatic applications (update 2017) devoted only two paragraphs to adrenal diseases [1]. No CEUS criteria were reported to reliably differentiate between benign and malignant adrenal gland tumors.

However, simple benign cysts, regardless of the origin, appear nonenhanced in all vascular phases (Fig. 8.17, Video 8.15). CEUS identifies adrenal cyst, abscess, and hematoma as avascular lesions [51].

Most adrenal adenomas are hypoenhancing in comparison with the liver without any typical vascular pattern [52] (Fig. 8.18, Video 8.16).

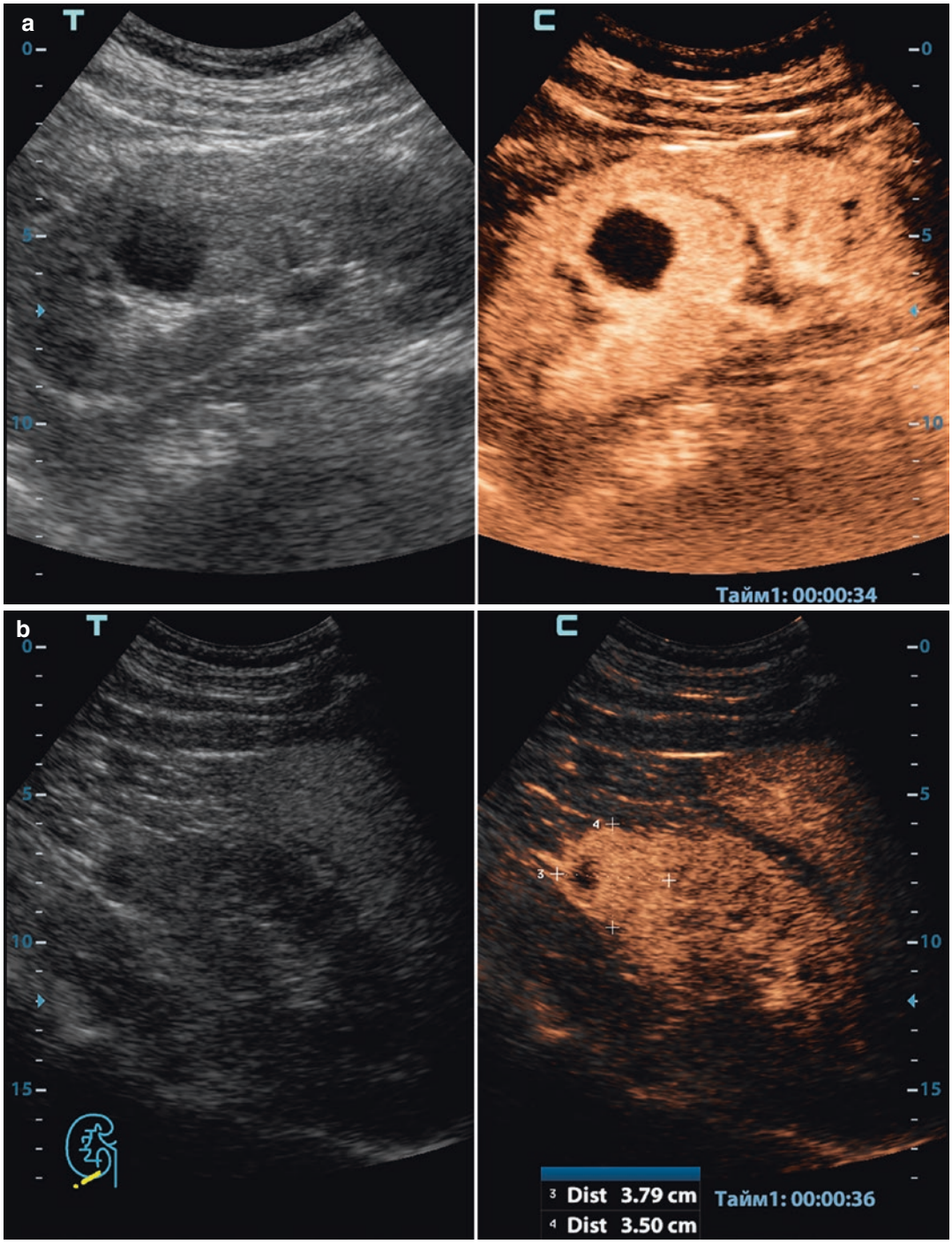

Fig. 8.14 Renal cell carcinoma. (**a**) CEUS image. The intrarenal lesion of about 5 cm in size with a single nonenhancing fluid collection and the otherwise uniform enhancement. (**b**) CEUS image. The lesion of 3 cm in size with a small nonenhancing area. (**c**) TIC shape of the lesion enhancement (pink ROI) is similar to the same of the normal renal parenchyma (yellow ROI)

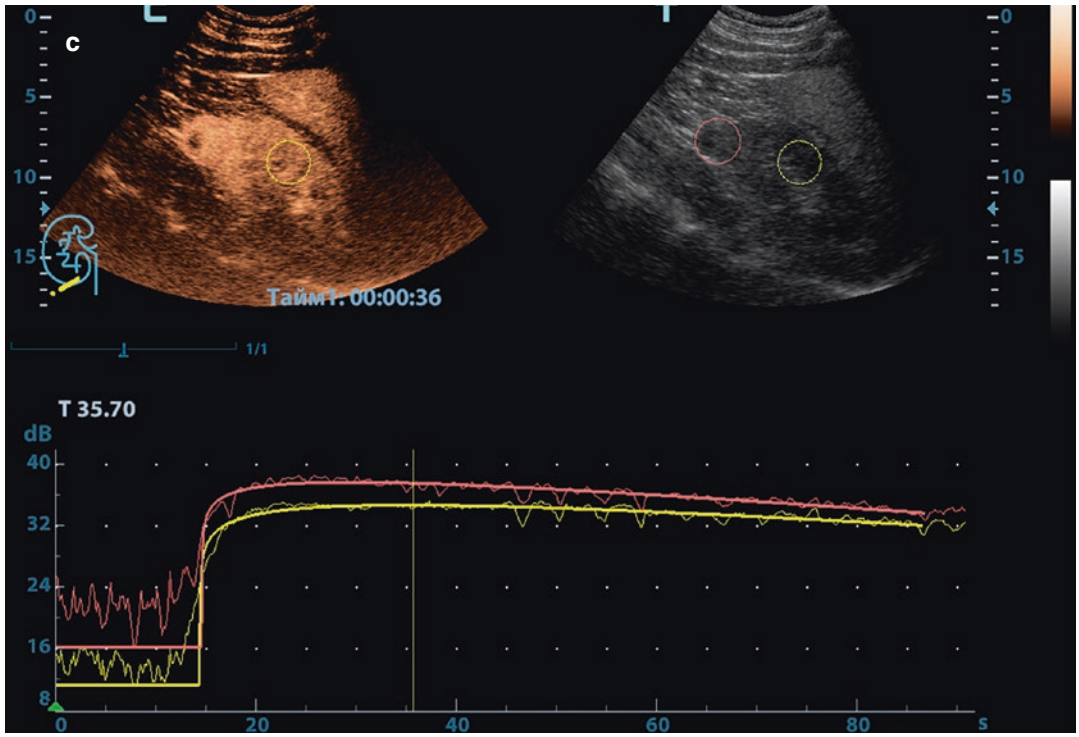

Fig. 8.14 (continued)

Other adrenal lesions, such as pheochromocytoma, cancer, and metastasis can demonstrate various enhancement patterns and do not have specific signs. CEUS may demonstrate characteristic hypervascularity of some adrenal gland tumors, e.g., pheochromocytoma, which typically also have necrotic regions with no contrast enhancement [1, 52, 53] (Fig. 8.19, Video 8.17).

In the adrenal gland, the size of the lesion is important. While the majority of benign masses are smaller than 3 cm, the malignant neoplasms and pheochromocytoma by the time of their detection are larger than 3 cm. Additionally, the larger the lesion, the more heterogeneously it enhances (Fig. 8.20, Video 8.18).

The same principle applies to the metastases in adrenal glands (Fig. 8.21, Video 8.19). Increased and irregular enhancement practically excludes adenoma and is an unfavorable prognostic sign. A single metastasis in the adrenal gland is a rare entity, it is usually accompanied by metastases in the other adrenal gland or other organs. The correlation of US findings with the patient's history, clinical, and laboratory data also facilitates the correct conclusion.

The adrenal tumors, which exhibit specific symptoms and were suspected based on clinical and laboratory data, require only precise localization. Since CEUS is not a method for the detection of the adrenal mass and can only characterize the already identified lesion, its utilization for the targeted examination of patients with adrenal gland hormone disorders is pointless.

Currently, CEUS of adrenal masses does not reach the diagnostic value of CE-CT and MRI. Moreover, in many cases, it does not provide additional clinically significant information to standard sonography with Doppler. However, individual cases may benefit from adrenal CEUS. For example, CEUS could easily confirm the absence of contrast enhancement in adrenal hematoma in children and follow them up without risks associated with iodine contrast agents and ionizing radiation of repeated CE-CT examinations [54].

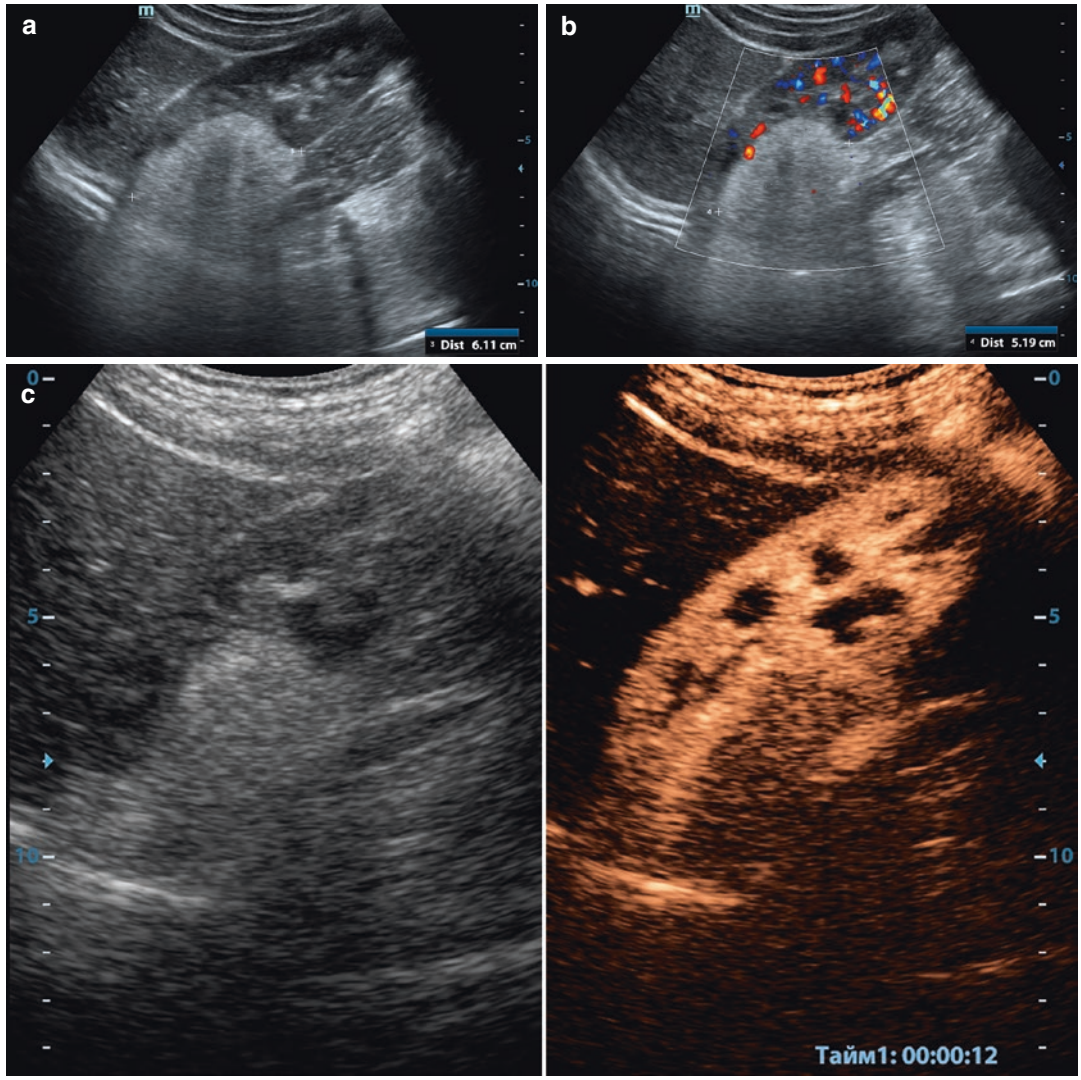

Fig. 8.15 Renal angiomyolipoma. (**a**) Grayscale US image reveals a hyperechoic lesion with smooth clear margins. (**b**) Color Doppler demonstrates the hypovascularity of the lesion. (**c**) Early cortical phase CEUS image demonstrates the beginning of the enhancement of the lesion at the periphery. (**d**) The late cortical phase CEUS image demonstrates the gradual uniform enhancement of the lesion from the periphery to the central aspects. (**e**) Parenchymal phase CEUS shows further enhancement of the lesion. (**f**) TIC of the lesion enhancement (pink ROI) is flattened as compared to the same of the normal renal parenchyma (yellow ROI)

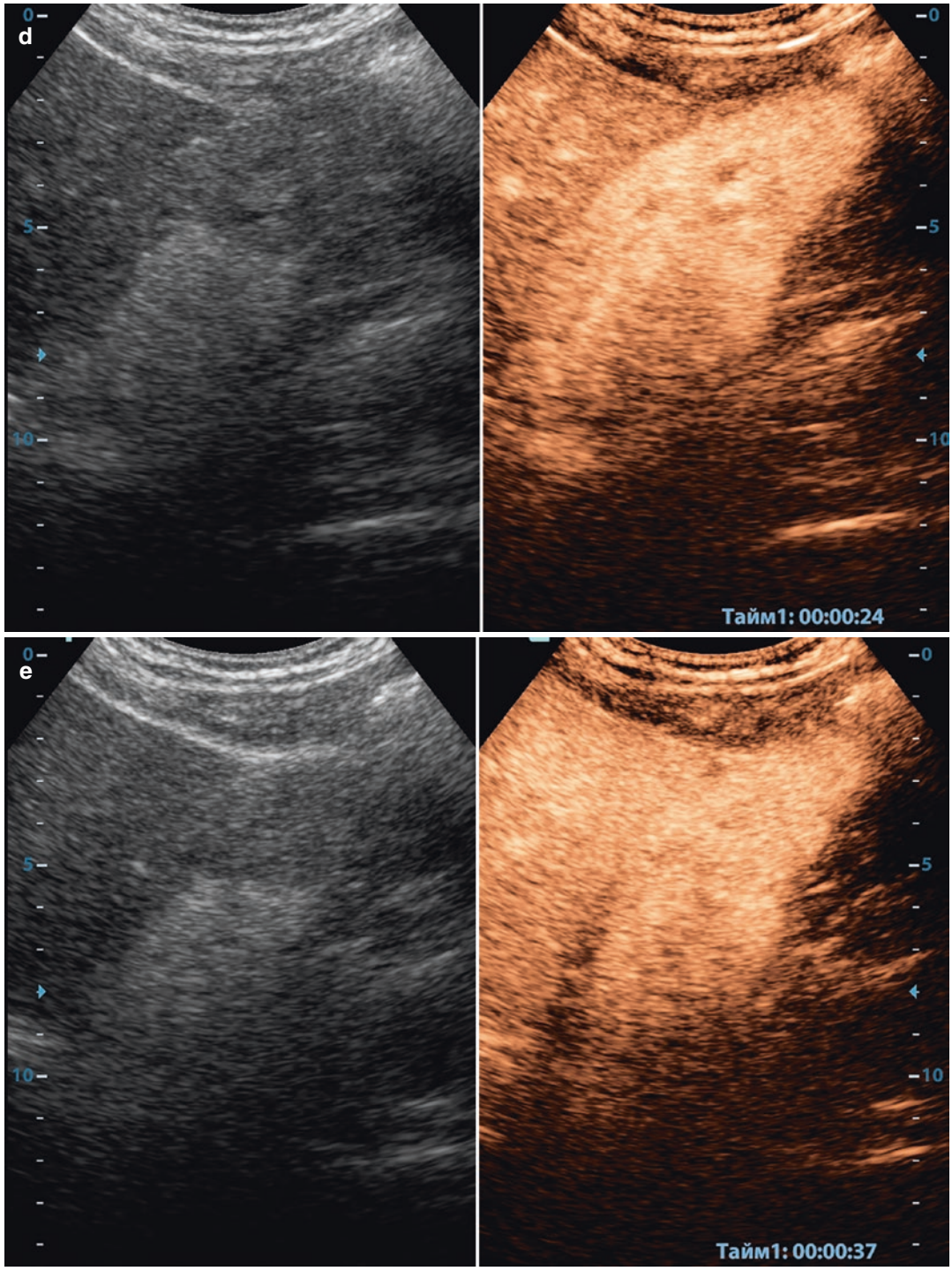

Fig. 8.15 (continued)

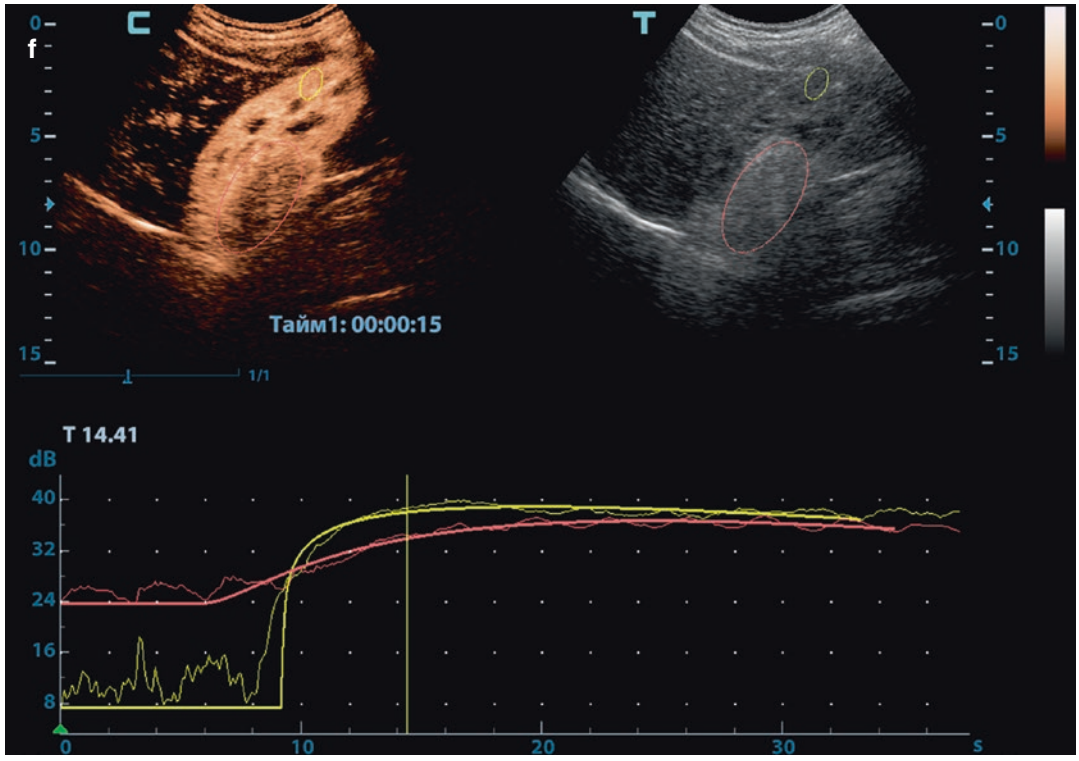

Fig. 8.15 (continued)

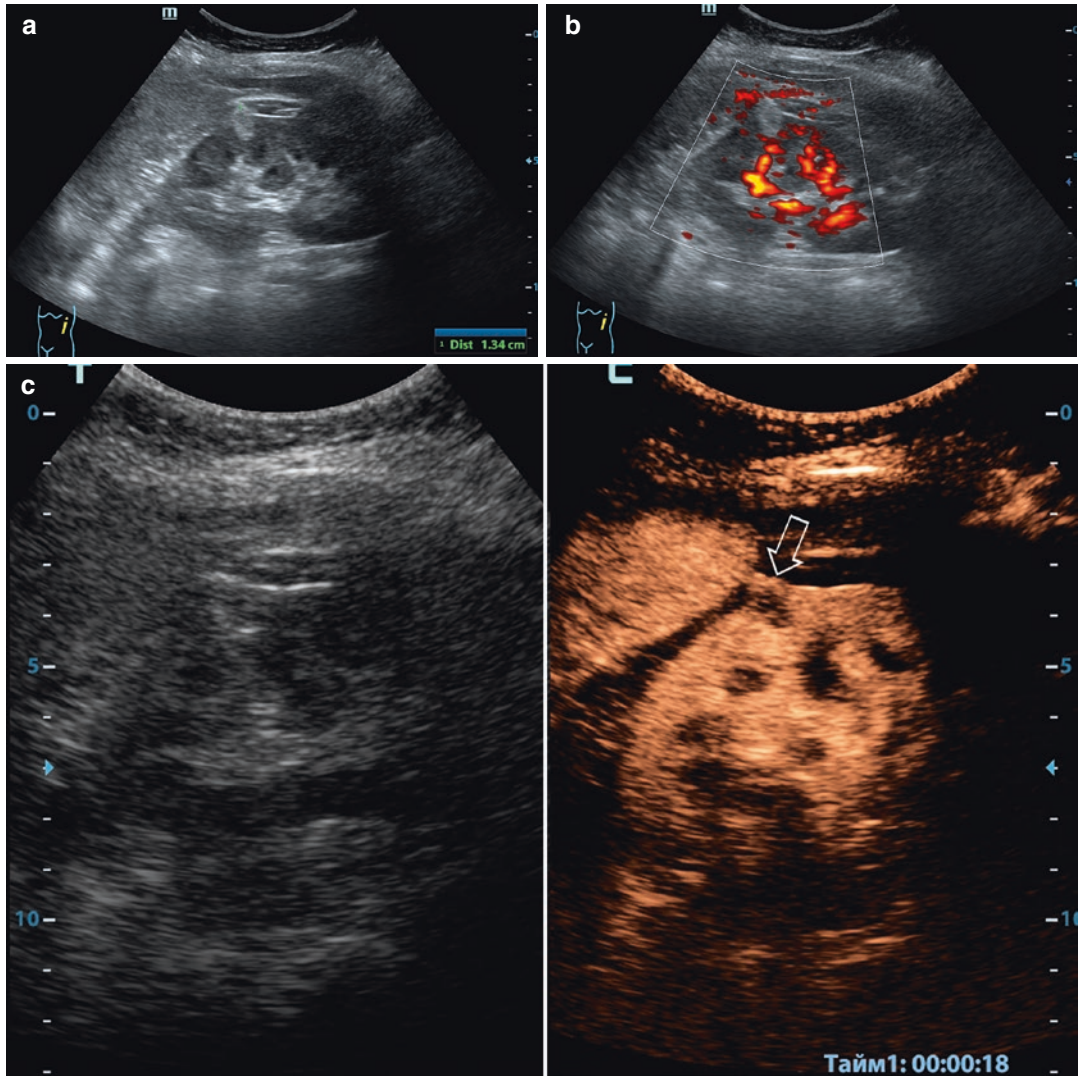

Fig. 8.16 Small renal angiomyolipoma. (**a**) Grayscale US image reveals typical signs of a renal AML. (**b**) Color Doppler demonstrates the hypovascularity of the lesion. (**c**) Cortical phase CEUS image demonstrates poor peripheral enhancement of the lesion. (**d**) Parenchymal phase CEUS shows persisting hypoenhancement. (**e**) TIC of the lesion enhancement (pink ROI) is low as compared to the same of the normal renal parenchyma (yellow ROI). (**f**) Native CT demonstrates typical AML with the density of -116HU

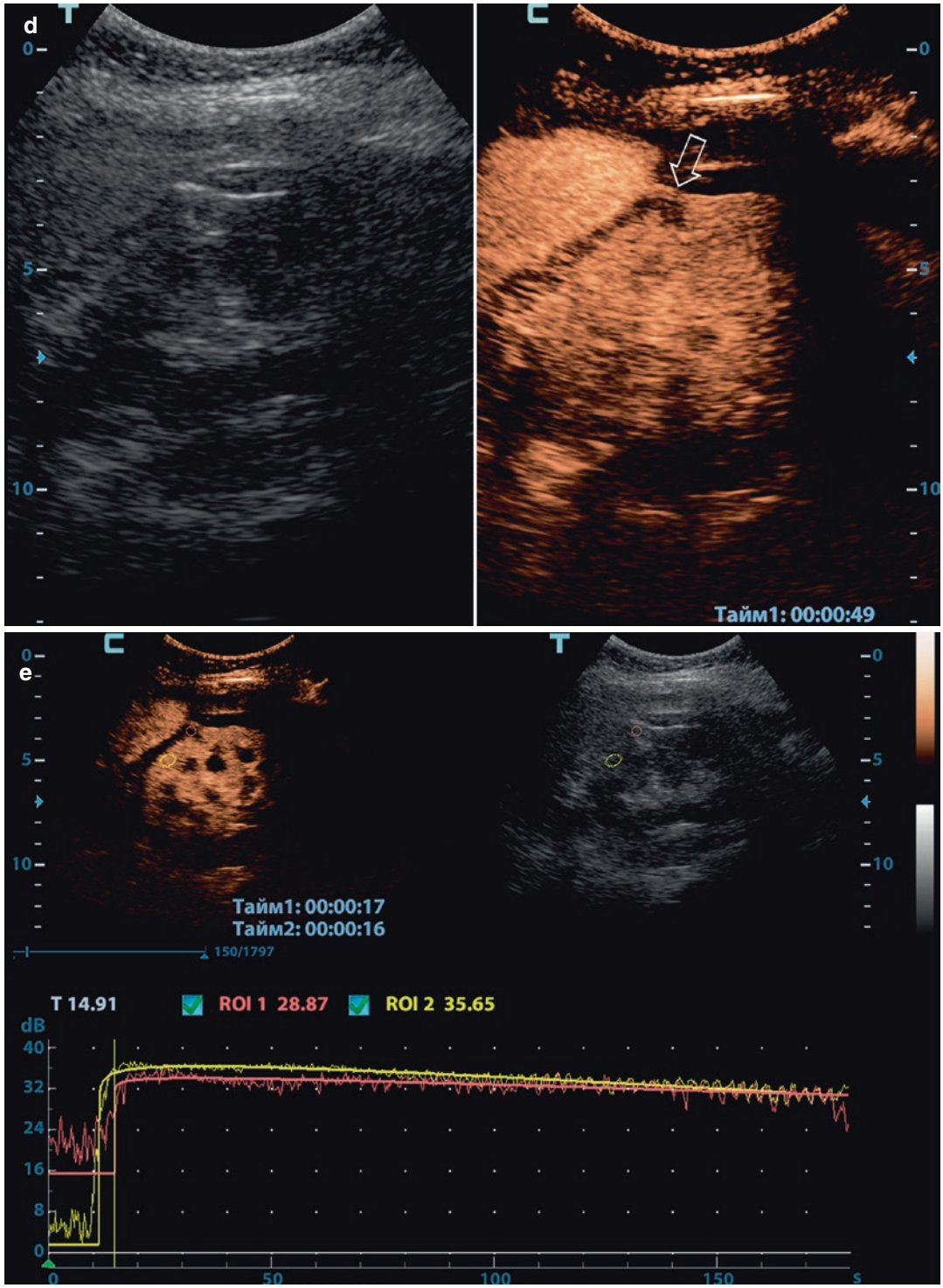

Fig. 8.16 (continued)

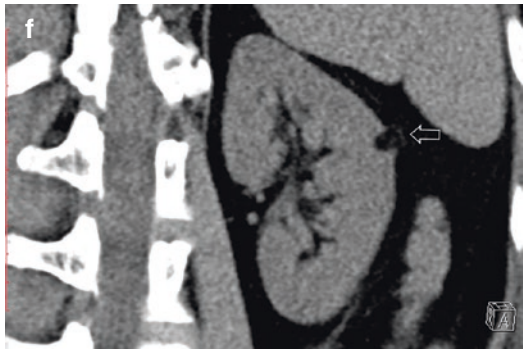

Fig. 8.16 (continued)

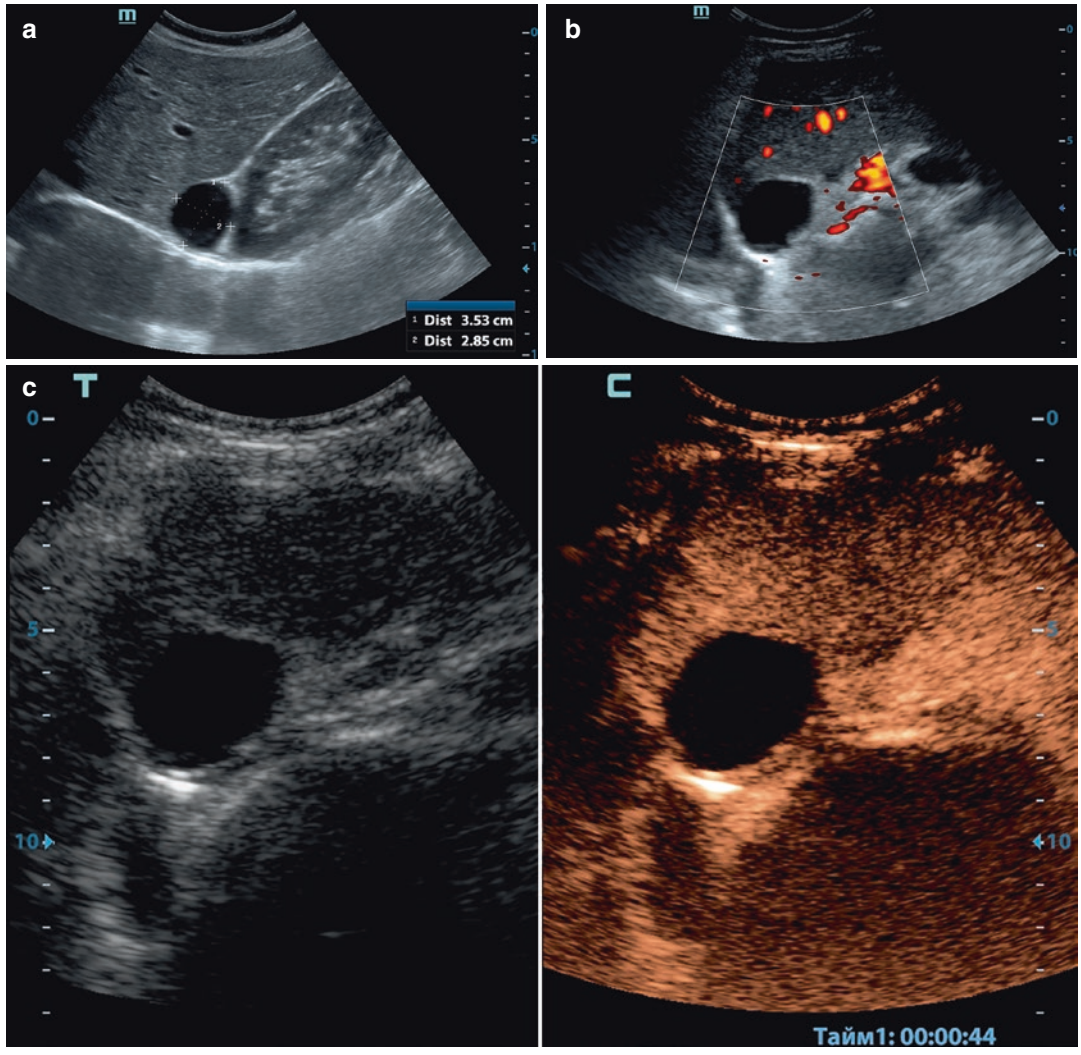

Fig. 8.17 Right adrenal gland cyst. (**a**) The grayscale US reveals a roundish anechoic lesion in the place of the right adrenal gland. (**b**) PDI detects no vascularity. (**c**) The lesion demonstrates no contrast enhancement (perfusion defect) with CEUS. (**d**) TIC proves no lesion enhancement (pink ROI), the normal liver parenchyma (yellow ROI) is supplied for reference

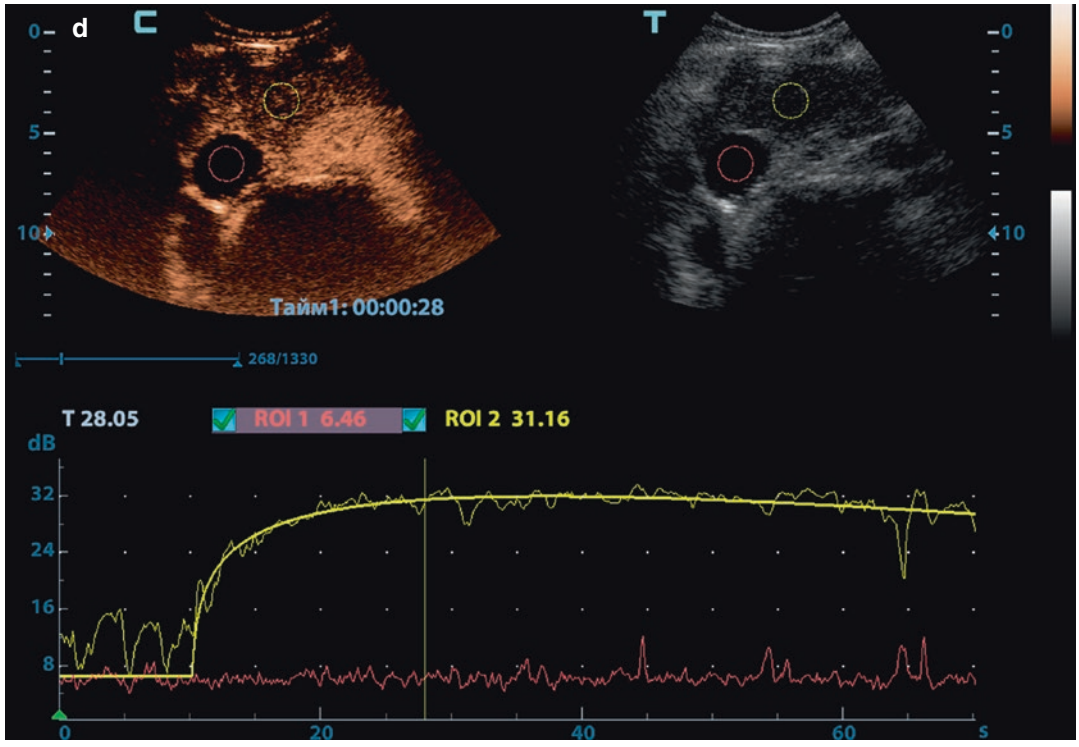

Fig. 8.17 (continued)

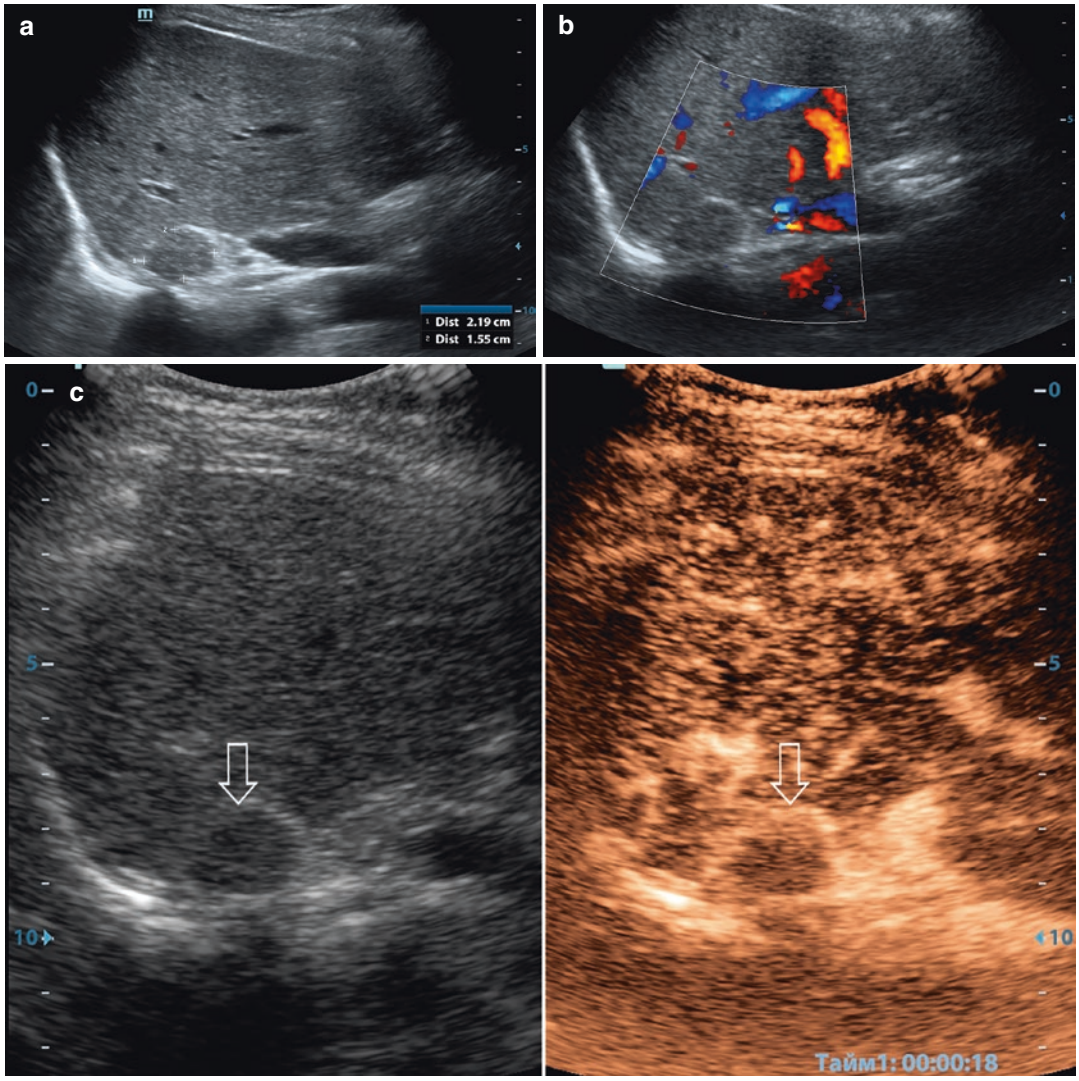

Fig. 8.18 Right adrenal adenoma. (**a**) The grayscale US demonstrates a homogeneous isoechoic lesion with regular margins in the place of the right adrenal gland. (**b**) CDI detects no vascularity. (**c**) Early arterial phase CEUS image demonstrates peripheral rim-like enhancement. (**d**) Venous phase CEUS image demonstrates poor homogeneous enhancement, which is well seen on the background of the enhanced liver parenchyma. (**e**) Late phase CEUS image after 4 min demonstrates homogeneous hypoenhancement. (**f**) TIC reveals general poor enhancement of the lesion with a peak in the arterial phase (pink ROI), the normal liver parenchyma (yellow ROI) is supplied for reference

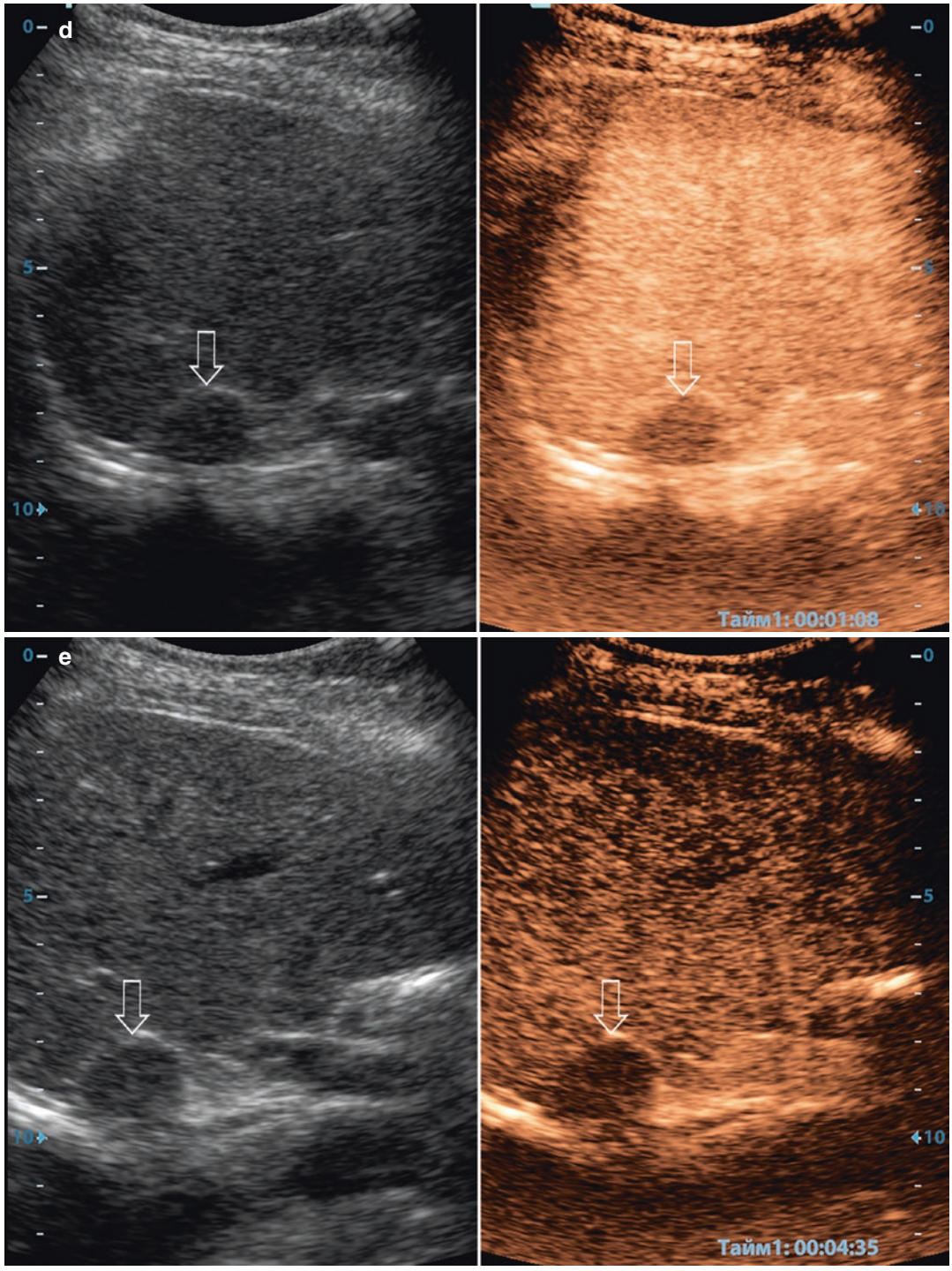

Fig. 8.18 (continued)

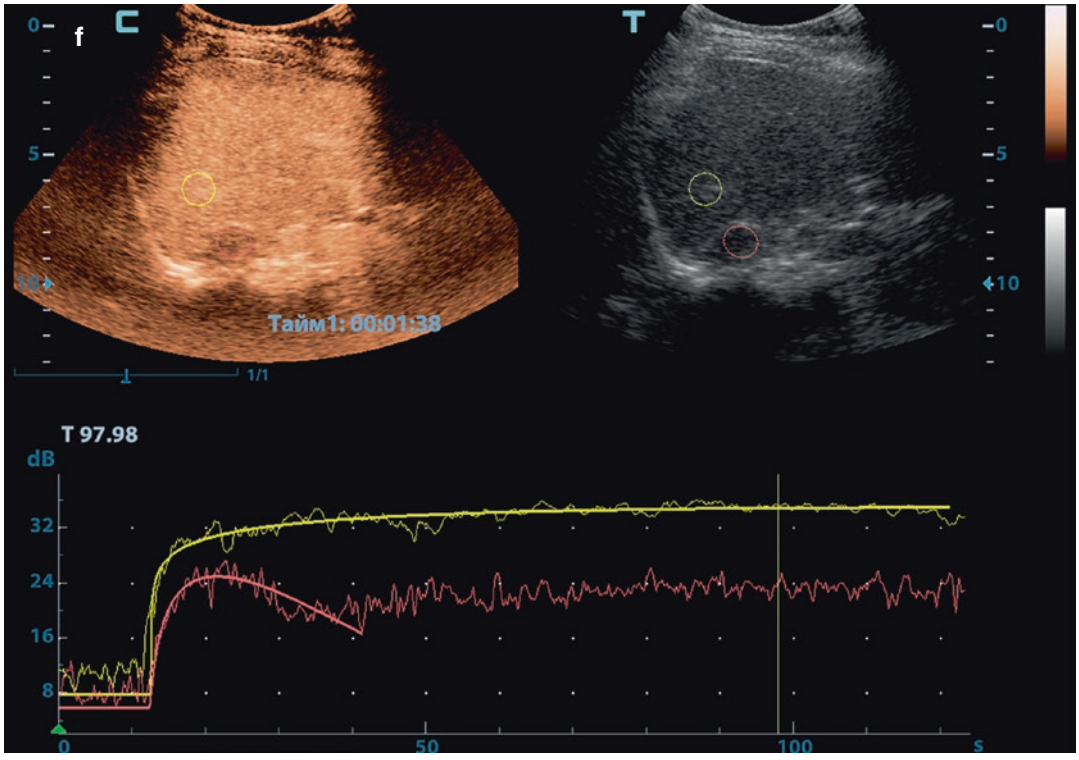

Fig. 8.18 (continued)

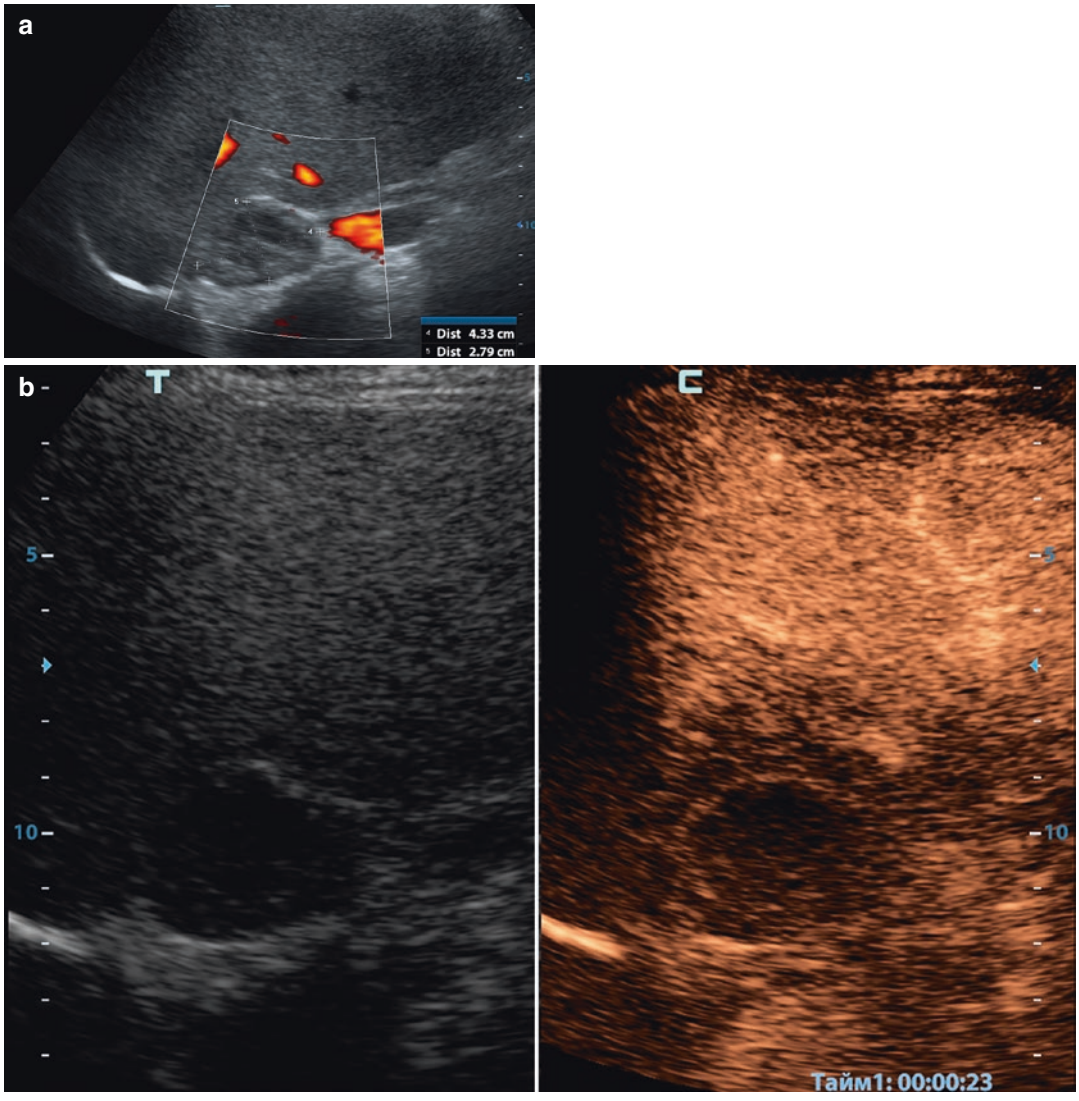

Fig. 8.19 Right adrenal pheochromocytoma. (**a**) PDI fails to detect any vascularity in the heterogeneous right adrenal lesion. Note the hypoechoic area within the lesion. (**b**) Arterial phase CEUS image demonstrates nonspecific moderate irregular enhancement with the nonenhanced area, which corresponds to the hypoechoic area. (**c**) Venous phase CEUS image shows almost the same enhancement pattern as in the arterial phase with moderate enhancement on the periphery and nonenhanced area in the central aspect. The enhancement pattern correlates with the same in CE-CT. (**d**) Native CT. (**e**) Venous phase CE-CT. (**f**) Delayed phase CE-CT

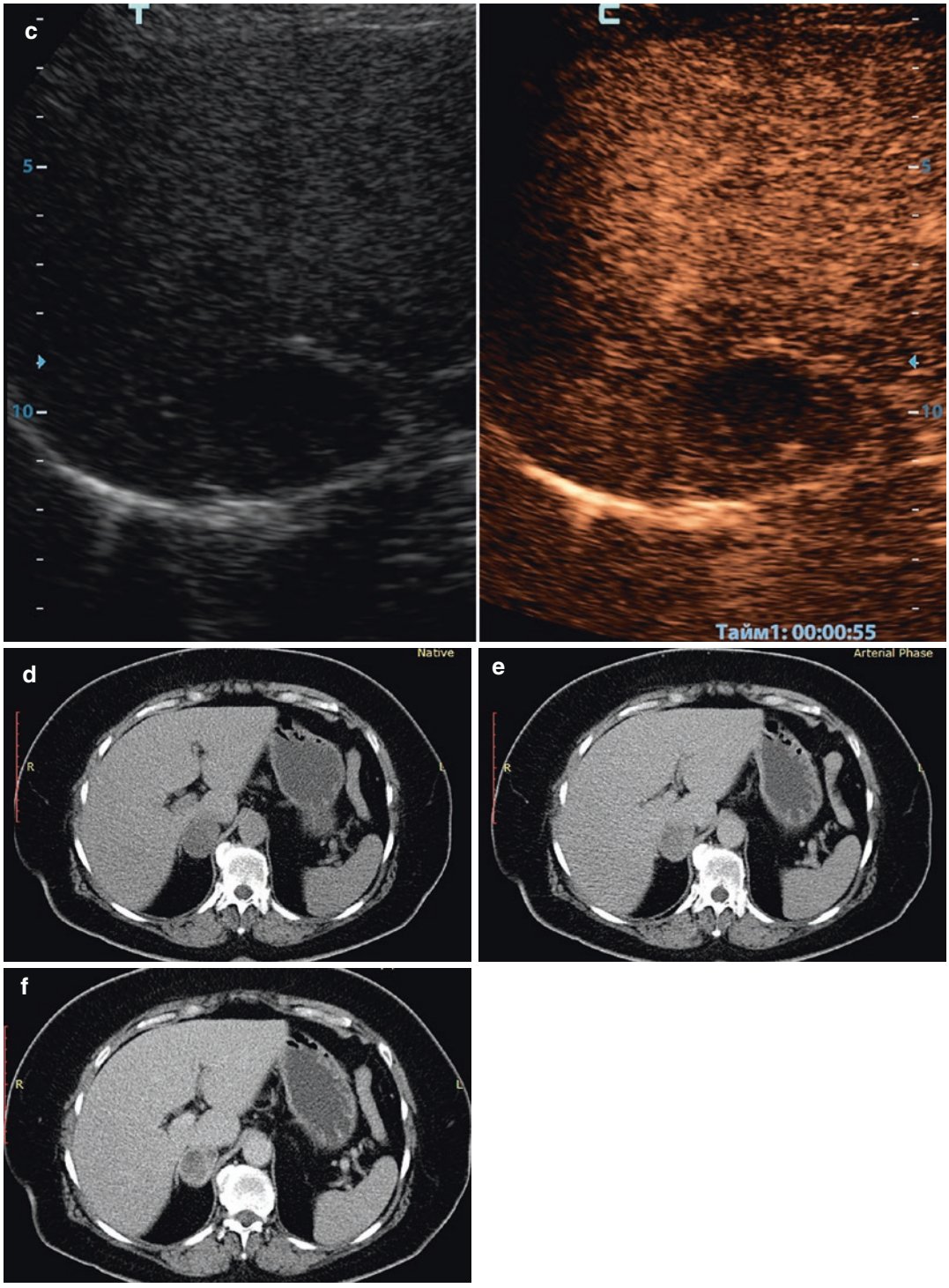

Fig. 8.19 (continued)

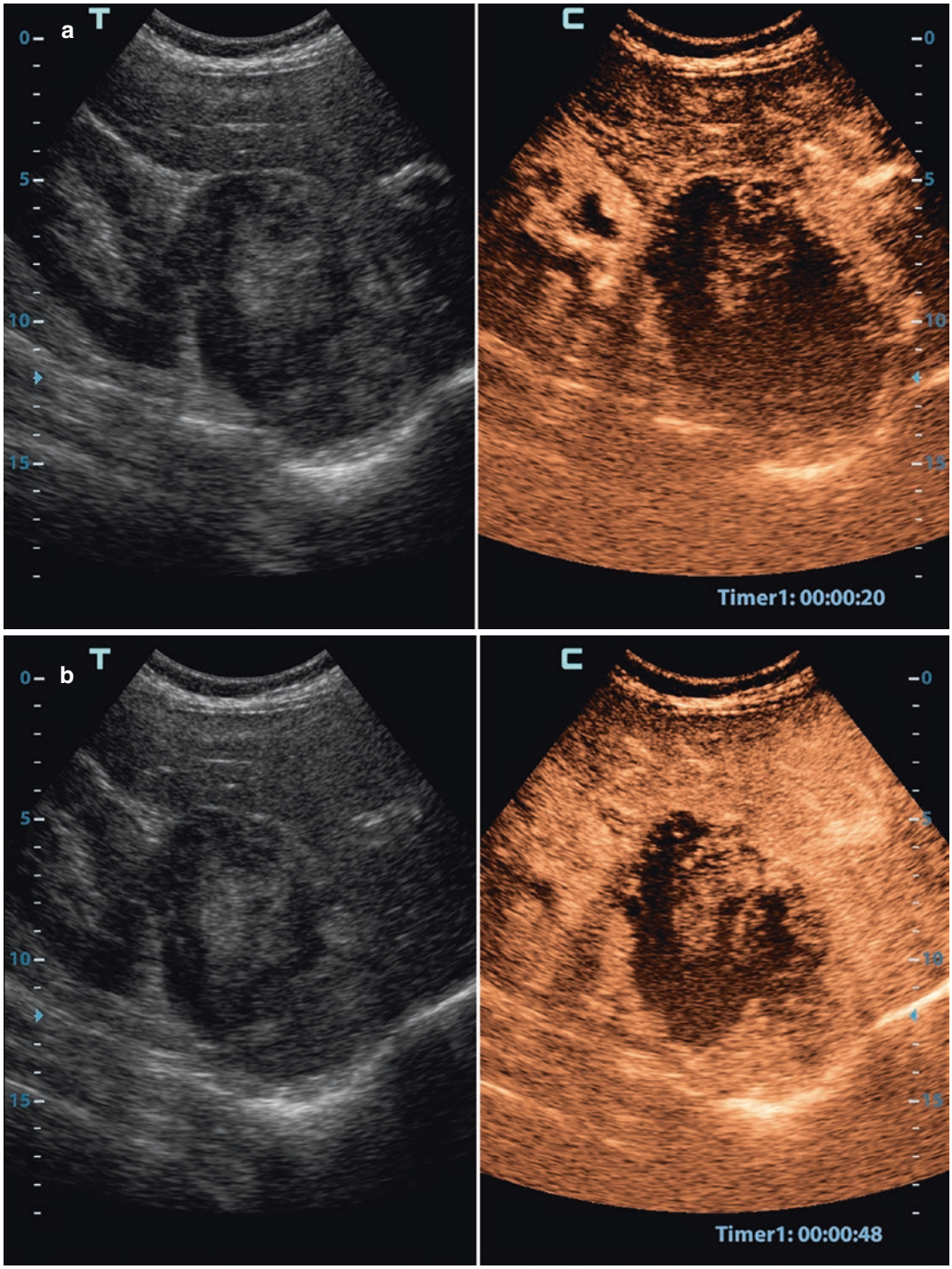

Fig. 8.20 Right adrenal sarcoma of large size. (**a**) The arterial phase CEUS image demonstrates slow irregular enhancement with a large nonenhanced area in the central part of the lesion. (**b**) Venous phase CEUS image shows gradual enhancement, which spreads from the periphery. There remains the central nonenhanced area of irregular shape. (**c**) TIC reveals overall poor enhancement of the lesion with (pink ROI) as compared to the kidney (yellow ROI) and liver (blue ROI) parenchyma

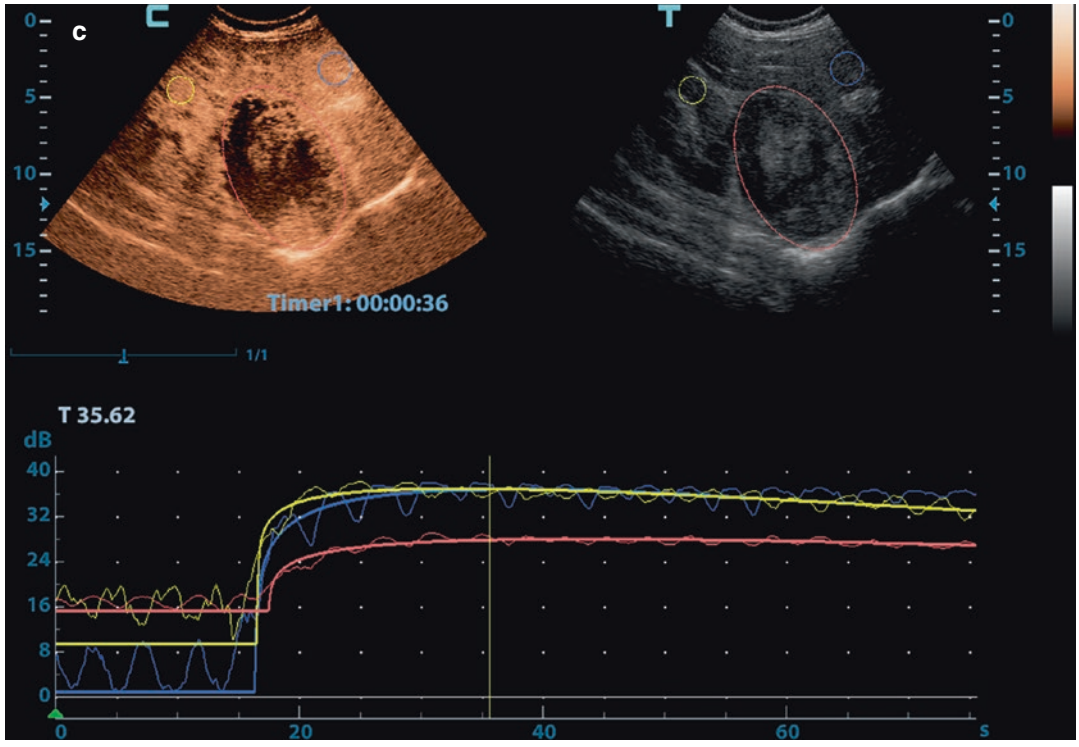

Fig. 8.20 (continued)

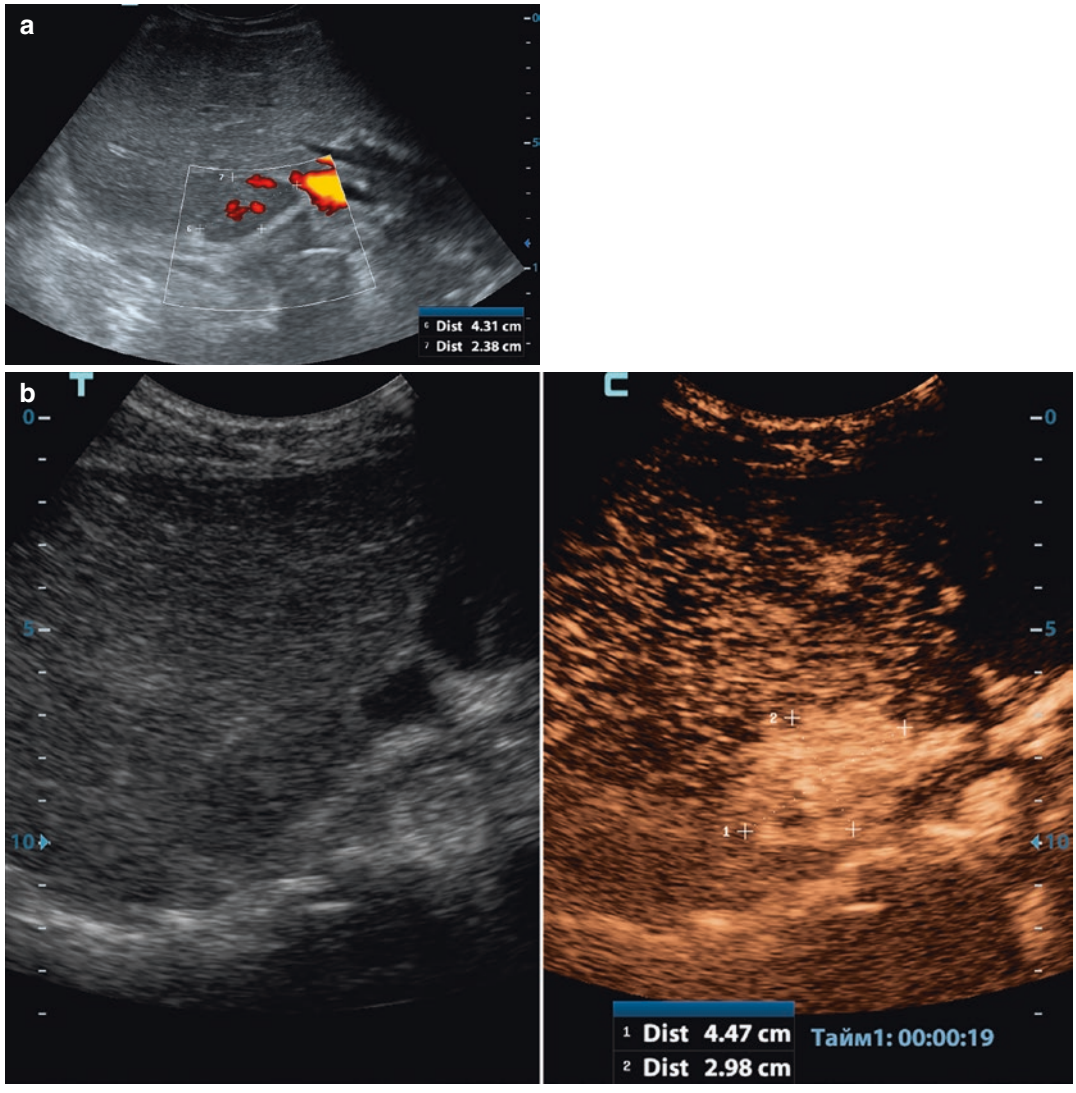

Fig. 8.21 Right adrenal metastasis. (**a**) PDI detects increased central and peripheral vascularity in the right adrenal mass. (**b**) Early arterial phase CEUS image demonstrates fast hyperenhancement of the adrenal lesion. (**c**) The arterial phase CEUS image shows significant hyperenhancement. (**d**) The venous phase CEUS demonstrates fast washout, which is prominent on the background of the persisting enhancement of the adjacent kidney and liver

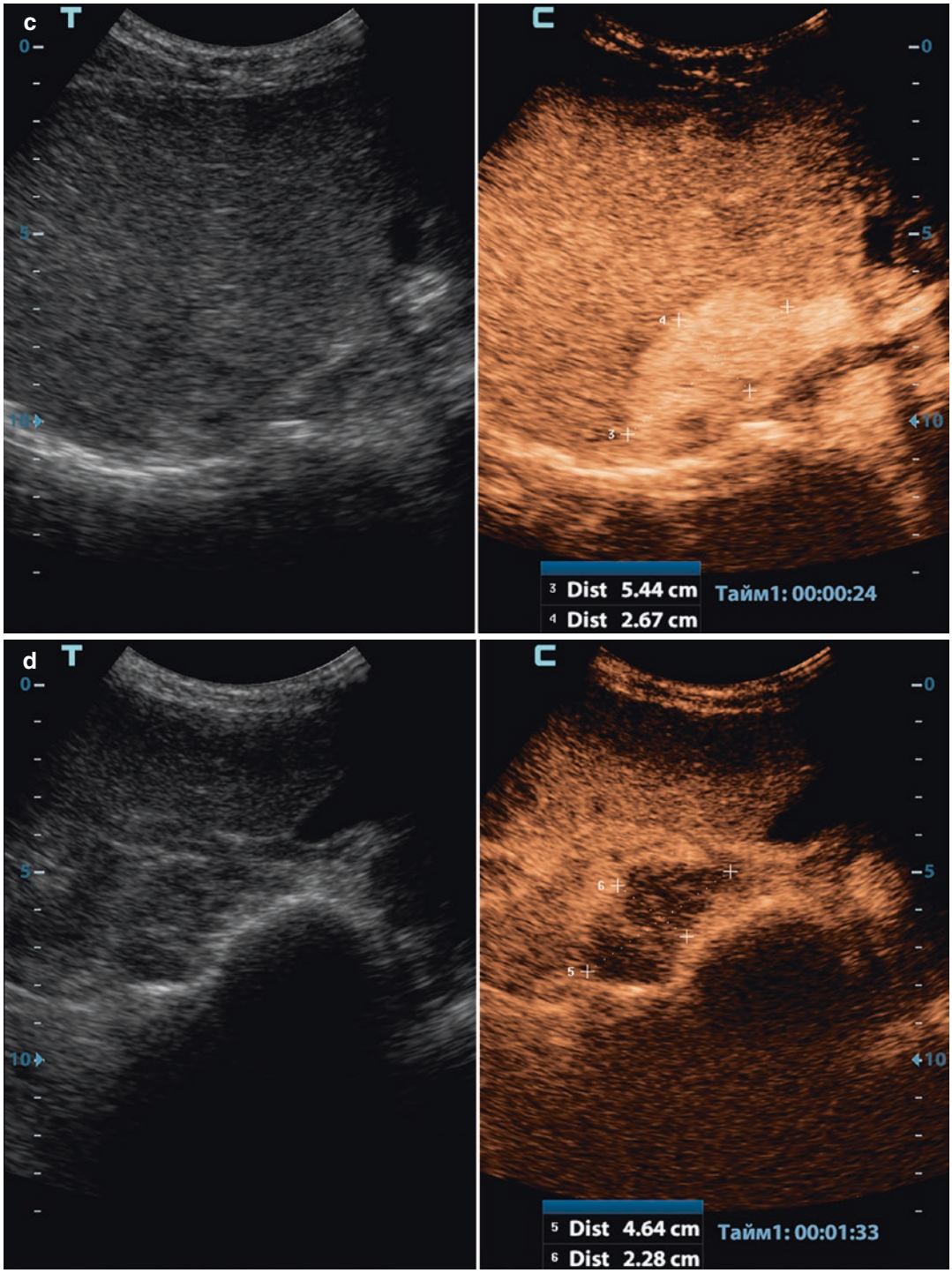

Fig. 8.21 (continued)

References

1. Sidhu PS, Cantisani V, Dietrich CF, Gilja OH, Saftoiu A, Bartels E, et al. The EFSUMB guidelines and recommendations for the clinical practice of contrast-enhanced ultrasound (CEUS) in non-hepatic applications: update 2017 (long version). Ultraschall Med. 2018;39(2):e2–e44. https://doi.org/10.1055/a-0586-1107.
2. Correas JM, Claudon M, Tranquart F, Hélénon AO. The kidney: imaging with microbubble contrast agents. Ultrasound Q. 2006;22(1):53–66.
3. Mazziotti S, Zimbaro F, Pandolfo A, Racchiusa S, Settineri N, Ascenti G. Usefulness of contrast-enhanced ultrasonography in the diagnosis of renal pseudotumors. Abdom Imaging. 2010;35(2):241–5. https://doi.org/10.1007/s00261-008-9499-y.
4. Stock K, Kübler H, Maurer T, Slotta-Huspenina J, Holzapfel K. CEUS – Diagnostik solider Nierentumoren [CEUS-diagnosis of solid renal tumors]. Radiologe. 2018;58(6):553–62. German. https://doi.org/10.1007/s00117-018-0392-6.
5. Girometti R, Stocca T, Serena E, Granata A, Bertolotto M. Impact of contrast-enhanced ultrasound in patients with renal function impairment. World J Radiol. 2017;9(1):10–6. https://doi.org/10.4329/wjr.v9.i1.10.
6. Bertolotto M, Martegani A, Aiani L, Zappetti R, Cernic S, Cova MA. Value of contrast-enhanced ultrasonography for detecting renal infarcts proven by contrast enhanced CT. A feasibility study. Eur Radiol. 2008;18(2):376–83. https://doi.org/10.1007/s00330-007-0747-2.
7. Cao W, Cui S, Yang L, Wu C, Liu J, Yang F, et al. Contrast-enhanced ultrasound for assessing renal perfusion impairment and predicting acute kidney injury to chronic kidney disease progression. Antioxid Redox Signal. 2017;27(17):1397–411. https://doi.org/10.1089/ars.2017.7006.
8. Wang L, Wu J, Cheng JF, Liu XY, Ma F, Guo LH, et al. Diagnostic value of quantitative contrast-enhanced ultrasound (CEUS) for early detection of renal hyperperfusion in diabetic kidney disease. J Nephrol. 2015;28(6):669–78. https://doi.org/10.1007/s40620-015-0183-3.
9. Tuhbatullin MG, Garifullina LI, Galeev SR. Sovremennaya ul'trazvukovaya diagnostika v ocenke sostoyaniya pochechnogo transplantata [Modern ultrasound diagnostics in the assessment of the state of renal transplant]. Prakticheskaya medicina. 2016;96(4–2):115–9. Russian.
10. Álvarez Rodríguez S, Hevia Palacios V, Sanz Mayayo E, Gómez Dos Santos V, Díez Nicolás V, Sánchez Gallego MD, et al. The usefulness of contrast-enhanced ultrasound in the assessment of early kidney transplant function and complications. Diagnostics (Basel). 2017;7(3):53. https://doi.org/10.3390/diagnostics7030053.
11. Schwenger V, Korosoglou G, Hinkel UP, Morath C, Hansen A, Sommerer C, et al. Real-time contrast-enhanced sonography of renal transplant recipients predicts chronic allograft nephropathy. Am J Transplant. 2006;6(3):609–15. https://doi.org/10.1111/j.1600-6143.2005.01224.x.
12. Weskott HP. Contrast-enhanced ultrasound. 2nd ed. London: Uni-Med Science; 2013.
13. Krajnik NA. Ul'trazvukovaya diagnostika sosudistyh oslozhnenij pochechnyh allotransplantatov v intraoperacionnom i rannem posleoperacionnom periodah [Ultrasound diagnostics of vascular complications of renal allografts in the intraoperative and early postoperative periods]. Dissertation. Moscow. Russian.
14. Fernandez CP, Ripolles T, Martinez MJ, Blay J, Pallardó L, Gavela E. Diagnosis of acute cortical necrosis in renal transplantation by contrast-enhanced ultrasound: a preliminary experience. Ultraschall Med. 2013;34(4):340–4. https://doi.org/10.1055/s-0032-1313007.
15. Pan FS, Liu M, Luo J, Tian WS, Liang JY, Xu M, et al. Transplant renal artery stenosis: evaluation with contrast-enhanced ultrasound. Eur J Radiol. 2017;90:42–9. https://doi.org/10.1016/j.ejrad.2017.02.031.
16. Benozzi L, Cappelli G, Granito M, Davoli D, Favali D, Montecchi MG, et al. Contrast-enhanced sonography in early kidney graft dysfunction. Transplant Proc. 2009;41(4):1214–5. https://doi.org/10.1016/j.transproceed.2009.03.029.
17. Grzelak P, Szymczyk K, Strzelczyk J, Kurnatowska I, Sapieha M, Nowicki M, Stefanczyk L. Perfusion of kidney graft pyramids and cortex in contrast-enhanced ultrasonography in the determination of the cause of delayed graft function. Ann Transplant. 2011;16(1):48–53.
18. Jin Y, Yang C, Wu S, Zhou S, Ji Z, Zhu T, He W. A novel simple noninvasive index to predict renal transplant acute rejection by contrast-enhanced ultrasonography. Transplantation. 2015;99(3):636–41. https://doi.org/10.1097/TP.0000000000000382.
19. Barozzi L, Capannelli D, Imbriani M. Contrast enhanced ultrasound in the assessment of urogenital pathology. Arch Ital Urol Androl. 2014;86(4):319–24. https://doi.org/10.4081/aiua.2014.4.319.
20. Fontanilla T, Minaya J, Cortés C, Hernando CG, Arangüena RP, Arriaga J, et al. Acute complicated pyelonephritis: contrast-enhanced ultrasound. Abdom Imaging. 2012;37(4):639–46. https://doi.org/10.1007/s00261-011-9781-2.
21. Tedesco G, Sarno A, Rizzo G, Grecchi A, Testa I, Giannotti G, D'Onofrio M. Clinical use of contrast-enhanced ultrasound beyond the liver: a focus on renal, splenic, and pancreatic applications. Ultrasonography. 2019;38(4):278–88. https://doi.org/10.14366/usg.18061.
22. Bosniak MA. The current radiological approach to renal cysts. Radiology. 1986;158(1):1–10. https://doi.org/10.1148/radiology.158.1.3510019.
23. Harvey CJ, Alsafi A, Kuzmich S, Ngo A, Papadopoulou I, Lakhani A, et al. Role of US contrast agents in the assessment of indeterminate solid

and cystic lesions in native and transplant kidneys. Radiographics. 2015;35(5):1419–30. https://doi.org/10.1148/rg.2015140222.
24. Rübenthaler J, Wilson S, Clevert DA. Multislice computed tomography/contrast-enhanced ultrasound image fusion as a tool for evaluating unclear renal cysts. Ultrasonography. 2019;38(2):181–7. https://doi.org/10.14366/usg.18024.
25. Ascenti G, Mazziotti S, Zimbaro G, Settineri N, Magno C, Melloni D, et al. Complex cystic renal masses: characterization with contrast-enhanced US. Radiology. 2007;243(1):158–65. https://doi.org/10.1148/radiol.2431051924.
26. Bertolotto M, Bucci S, Valentino M, Currò F, Sachs C, Cova MA. Contrast-enhanced ultrasound for characterizing renal masses. Eur J Radiol. 2018;105:41–8. https://doi.org/10.1016/j.ejrad.2018.05.015.
27. Clevert DA, Minaifar N, Weckbach S, Jung EM, Stock K, Reiser M, Staehler M. Multislice computed tomography versus contrast-enhanced ultrasound in evaluation of complex cystic renal masses using the Bosniak classification system. Clin Hemorheol Microcirc. 2008;39(1–4):171–8.
28. Quaia E, Bertolotto M, Cioffi V, Rossi A, Baratella E, Pizzolato R, Cov MA. Comparison of contrast-enhanced sonography with unenhanced sonography and contrast-enhanced CT in the diagnosis of malignancy in complex cystic renal masses. AJR Am J Roentgenol. 2008;191(4):1239–49. https://doi.org/10.2214/AJR.07.3546.
29. Tamai H, Takiguchi Y, Oka M, Shingaki N, Enomoto S, Shiraki T, et al. Contrast-enhanced ultrasonography in the diagnosis of solid renal tumors. J Ultrasound Med. 2005;24(12):1635–40. https://doi.org/10.7863/jum.2005.24.12.1635.
30. Wang C, Yu C, Yang F, Yang G. Diagnostic accuracy of contrast-enhanced ultrasound for renal cell carcinoma: a meta-analysis. Tumour Biol. 2014;35(7):6343–50. https://doi.org/10.1007/s13277-014-1815-2.
31. Barr RG, Peterson C, Hindi A. Evaluation of indeterminate renal masses with contrast-enhanced US: a diagnostic performance study. Radiology. 2014;271(1):133–42. https://doi.org/10.1148/radiol.13130161.
32. Moch H, Cubilla AL, Humphrey PA, Reuter VE, Ulbright TM. The 2016 WHO classification of tumours of the urinary system and male genital organs-Part A: renal, penile, and testicular tumours. Eur Urol. 2016;70(1):93–105. https://doi.org/10.1016/j.eururo.2016.02.029.
33. Solovev YA, Mitina LA, Mitkova MD. Contrast-enhanced ultrasound (CEUS) in differential diagnosis of benign and malignant renal tumors. Ultras Funct Diagnost. 2018;4:46–64. Russian.
34. Jiang J, Chen Y, Zhou Y, Zhang H. Clear cell renal cell carcinoma: contrast-enhanced ultrasound features relation to tumor size. Eur J Radiol. 2010;73(1):162–7. https://doi.org/10.1016/j.ejrad.2008.09.030.
35. Robbin ML, Lockhart ME, Barr RG. Renal imaging with ultrasound contrast: current status. Radiol Clin N Am. 2003;41(5):963–78. https://doi.org/10.1016/s0033-8389(03)00070-8.
36. Xu ZF, Xu HX, Xie XY, Liu GJ, Zheng YL, Liang JY, Lu MD. Renal cell carcinoma: real-time contrast-enhanced ultrasound findings. Abdom Imaging. 2010;35(6):750–6. https://doi.org/10.1007/s00261-009-9583-y.
37. Dong XQ, Shen Y, Xu LW, Xu CM, Bi W, Wang XM. Contrast-enhanced ultrasound for detection and diagnosis of renal clear cell carcinoma. Chin Med J. 2009;122(10):1179–83.
38. Ascenti G, Gaeta M, Magno C, Mazziotti S, Blandino A, Melloni D, Zimbaro G. Contrast-enhanced second-harmonic sonography in the detection of pseudocapsule in renal cell carcinoma. AJR Am J Roentgenol. 2004;182:1525–30.
39. Xu ZF, Xu HX, Xie XY, Liu GJ, Zheng YL, Lu MD. Renal cell carcinoma and renal angiomyolipoma: differential diagnosis with real-time contrast-enhanced ultrasonography. J Ultrasound Med. 2010;29(5):709–17. https://doi.org/10.7863/jum.2010.29.5.709.
40. Golan S, Eggener S, Subotic S, Barret E, Cormio L, Naito S, et al. Prediction of renal mass aggressiveness using clinical and radiographic features: a global, multicentre prospective study. BJU Int. 2016;117(6):914–22. https://doi.org/10.1111/bju.13331.
41. Bauman TM, Potretzke AM, Wright AJ, Knight BA, Vetter JM, Figenshau RS. Partial nephrectomy for presumed renal-cell carcinoma: incidence, predictors, and perioperative outcomes of benign lesions. J Endourol. 2017;31(4):412–7. https://doi.org/10.1089/end.2016.0667.
42. Vorob'ev AV. Morfologicheskaya klassifikaciya opuholej pochki. Dobrokachestvennye novoobrazovaniya (osobennosti diagnostiki i lecheniya) [morphological classification of kidney tumors. Benign neoplasms (features of diagnosis and treatment)]. Prakticheskaya onkologiya. 2005;6(3):141–7. Russian.
43. Harwey C. Kidney: benign lesions. In: Lyshchik A, editor. Specialty imaging: fundamentals of CEUS. 1st ed. Philadelphia: Elsevier; 2019. p. 138–44.
44. Yao D-W, Liu C, Liu X-J, Liu D, Zhang Q, Wang W, et al. Epithelioid angiomyolipoma of the kidney: CT and CEUS characteristics and clinical outcomes. Int J Clin Exp Med. 2016;9(7):14096–104.
45. Lu Q, Li CX, Huang BJ, Xue LY, Wang WP. Triphasic and epithelioid minimal fat renal angiomyolipoma and clear cell renal cell carcinoma: qualitative and quantitative CEUS characteristics and distinguishing features. Abdom Imaging. 2015;40(2):333–42. https://doi.org/10.1007/s00261-014-0221-y.
46. Gulati M, King KG, Gill IS, Pham V, Grant E, Duddalwar VA. Contrast-enhanced ultrasound (CEUS) of cystic and solid renal lesions: a review. Abdom Imaging. 2015;40(6):1982–96. https://doi.org/10.1007/s00261-015-0348-5.
47. Schneider AG, Hofmann L, Wuerzner G, Glatz N, Maillard M, Meuwly JY, et al. Renal perfusion

evaluation with contrast-enhanced ultrasonography. Nephrol Dial Transplant. 2012;27(2):674–81. https://doi.org/10.1093/ndt/gfr345.
48. Ma F, Cang Y, Zhao B, Liu Y, Wang C, Liu B, et al. Contrast-enhanced ultrasound with SonoVue could accurately assess the renal microvascular perfusion in diabetic kidney damage. Nephrol Dial Transplant. 2012;27(7):2891–8. https://doi.org/10.1093/ndt/gfr789.
49. Kasoji SK, Chang EH, Mullin LB, Chong WK, Rathmell WK, Dayton PA. A pilot clinical study in characterization of malignant renal-cell carcinoma subtype with contrast-enhanced ultrasound. Ultrason Imaging. 2017;39(2):126–36. https://doi.org/10.1177/0161734616666383.
50. Chen L, Wang L, Diao X, Qian W, Fang L, Pang Y, et al. The diagnostic value of contrast-enhanced ultrasound in differentiating small renal carcinoma and angiomyolipoma. Biosci Trends. 2015;9(4):252–8. https://doi.org/10.5582/bst.2015.01080.
51. Dietrich CF, Ignee A, Barreiros AP, Schreiber-Dietrich D, Sienz M, Bojunga J, Braden B. Contrast-enhanced ultrasound for imaging of adrenal masses. Ultraschall Med. 2010;31(2):163–8. https://doi.org/10.1055/s-0028-1109357.
52. Friedrich-Rust M, Glasemann T, Polta A, Eichler K, Holzer K, Kriener S, et al. Differentiation between benign and malignant adrenal mass using contrast-enhanced ultrasound. Ultraschall Med. 2011;32(5):460–71. https://doi.org/10.1055/s-0031-1273408.
53. Al Bunni F, Deganello A, Sellars ME, Schulte KM, Al-Adnani M, Sidhu PS. Contrast-enhanced ultrasound (CEUS) appearances of an adrenal phaeochromocytoma in a child with Von Hippel-Lindau disease. J Ultrasound. 2014;17(4):307–11. https://doi.org/10.1007/s40477-014-0083-8.
54. Rafailidis V, Deganello A, Sellars ME, Makin E, Sidhu PS. Pediatric adrenal trauma: evaluation and follow-up with contrast-enhanced ultrasound (CEUS). J Ultrasound. 2016;20(4):325–31. https://doi.org/10.1007/s40477-016-0220-7.

Small Intestine and Colon

9

Ella I. Peniaeva, Munir G. Tukhbatullin, Alexander N. Sencha, and Elena E. Fomina

The human digestive tract has a length of 8–10 m and is divided into the following departments: oral cavity, throat, esophagus, stomach, small and large intestines. The small intestine is typically 3–5 m long and is divided into duodenum, jejunum, and ileum. Jejunum and ileum, unlike the duodenum, are completely covered with peritoneum and suspended by the mesentery. Despite the lack of a clear anatomical border, there are some anatomical differences between the jejunum and ileum. The wall of the jejunum is thicker and better vascularized and the loops are located predominantly in the left meso- and hypogastric areas, while the loops of the ileum—on the right side. The large intestine has a length of about 1–1.5 m and confers cecum with the appendix, ascending colon, transverse colon, descending colon, sigmoid colon, rectum, and anal canal.

E. I. Peniaeva (✉)
Department of Ultrasound Diagnostics of the Center for Radiological Diagnostics, Private Healthcare Institution "Clinical Hospital "RZD-Medicina" of Yaroslavl City", Yaroslavl, Russian Federation

M. G. Tukhbatullin · E. E. Fomina
Department of Ultrasound Diagnosis, Kazan State Medical Academy, Kazan, Russian Federation

A. N. Sencha
Department of Visual and Functional Diagnostics, Federal State Budget Institution "National Medical Research Center for Obstetrics, Gynecology and Perinatology n.a. V.I.Kulakov", Moscow, Russian Federation

The jejunum and ileum receive blood supply from the superior mesenteric artery, which is the branch of the aorta. They form arterial arcades within the mesentery. Straight blood vessels travel from the arcades to the intestines. Venous blood outflows to the portal vein system. The colon is supplied with blood from the superior and inferior mesenteric arteries. Additionally, the middle and lower segments of the rectum get their arterial blood from the branches of the internal iliac artery. The venous outflow from the colon is carried out through the superior and inferior mesenteric veins. The middle and lower aspects of the rectum drain to the internal iliac vein [1].

Inflammatory bowel disease (IBD) includes nonspecific ulcerative colitis, which affects the mucous membrane of the colon, and Crohn's disease, characterized by transmural inflammation and the possible involvement of the entire digestive tract with the favorite localization in the terminal ileum [2]. Technological achievements and accumulated knowledge led to the increase in the value of traditional US for the diagnosis of IBD [3]. Noninvasive assessment of the disease activity in patients with IBD is important due to the necessity for monitoring the natural flow of the bowel inflammation and evaluation of the therapy effect. The thickness of the intestinal wall correlates with the activity of the inflammatory process, but in some cases, the wall thickening can persist in remission [4].

A. N. Sencha, Y. N. Patrunov (eds.), *Contrast-Enhanced Ultrasound*,
https://doi.org/10.1007/978-3-030-91764-7_9

Sonography identifies the following five layers of the intestinal wall, which correspond to the histological structure [5, 6]:

- External hyperechogenic layer—serous membrane.
- External hypoechogenic layer—muscular membrane.
- Medium hyperechogenic layer—submucosa.
- Internal hypoechogenic layer—mucosa.
- Internal hyperechogenic layer—the surface of the mucosa.

Altered stratification of bowel layers is a sign of the active inflammatory process and is common in patients with intestinal fistulae [7]. Inflammation is associated with microvascular dysfunction and neoangiogenesis [2]. Histopathological studies demonstrated that neovascularization of the intestinal wall with new capillaries in lamina propria and submucosa is an early sign of active IBD [8]. Doppler imaging is capable to register the changes in the vascularization of the bowel wall but its sensitivity in the detection of low-velocity blood flow is limited [4]. CEUS is free of this limitation.

According to the EFSUMB guidelines and recommendations for the clinical practice of CEUS in non-hepatic applications (update 2017) [9], intestinal CEUS is feasible for the following purposes:

- to evaluate the vascularity of the gastrointestinal wall and gastrointestinal tumors,
- to estimate disease activity in inflammatory bowel disease and to discern between fibrous and inflammatory strictures in Crohn's disease,
- to monitor the effectiveness of treatment in Crohn's disease,
- to detect abscesses and to confirm and track the route of fistulae,
- to evaluate perfusion and vascular complications after intestinal transplantation.

Intestinal CEUS utilizes the probes with the frequency of ≥7.5 MHz that require a higher dose of UCA—4.8 ml of SonoVue® for intravenous administration according to the standard technique. The study is conducted after the patient fasts, in the supine position, with free breathing. Before CEUS, it is necessary to identify the target area with normal transabdominal US of the bowel based on characteristic echographic signs of inflammation. The small intestine wall thicker than 3 mm, colon wall thicker than 5 mm, increased vascularity with CDI, inflammatory infiltration of the surrounding fat, and reactive lymph nodes indicate bowel inflammation. Besides, it is important to ensure good quality of general visualization and minimal peristaltic movements [4].

CEUS of the intestine includes two phases. The arterial phase (0—30 s) is followed by a venous phase [9]. After the intravenous introduction of the UCA, the selected intestinal segment is continuously scanned for 2 min at a fixed position of the probe. The sagittal scanning plane is optimal to avoid displacement of the target area outside the scanning range with respiratory movements. The first microbubbles in the bowel wall can be detected in 10–20 s after the UCA injection. The maximum enhancement is achieved after 30–40 s [9]. The enhancement intensity is proportional to the severity of inflammation. In the venous phase, the enhancement fades.

According to the EFSUMB recommendations and clinical guidelines for intestinal ultrasound in IBD [10], the enhancement parameters are divided into qualitative, semi-quantitative, and quantitative. The main qualitative and semi-quantitative parameters include different patterns of contrast enhancement, based on variations of bowel wall layer perfusion.

The inflammation activity evaluated with qualitative CEUS better correlates with the real activity of the inflammatory process than the thickening of the bowel wall. The enhancement patterns are different depending on the severity of the inflammation. The highest activity of Crohn's disease is associated with the transmural contrast enhancement of the bowel wall in the arterial phase or the enhancement of both the mucous membrane and submucosa layer [11]. Low inflammation activity demonstrates the

enhancement of only the submucosa layer. The absence of active disease results in no contrast enhancement.

The sensitivity and specificity of CEUS in the diagnosis of active disease were 81% and 63%, respectively [11]. With similar criteria, another study [12] demonstrated the sensitivity of 93.5% and specificity of 93.7%. A semi-quantitative method for evaluating the inflammation severity is suggested [11]. The ratio of the enhanced layer thickness to the total bowel wall thickness correlates with the index of Crohn's disease activity.

The intensity of the wall enhancement in low disease activity is lower with a faster decrease in the intensity after the peak. High disease activity is associated with prominent contrast enhancement and slow washout. Additionally, the active inflammatory process exhibits the comb sign due to the increased number of adjacent mesenteric vessels combined with transmural enhancement of the bowel wall [2, 4, 8].

Local hypo- or nonenhancing areas within the otherwise enhanced bowel wall may correspond to intramural abscesses. Extraintestinal complications in IBD include phlegmon and abscess formation. Traditional echography hardly differentiates inflammatory infiltrates from abscesses if gas, fluid, or clear signals of color Doppler in their interior are missing. CEUS is extremely useful in distinguishing these two entities since phlegmons show intra-lesional enhancement, while abscesses show enhancement only in the wall [4, 8]. In patients with IBD, CEUS is equal to MRI in the detection of active inflammation. The study [13] reported the CEUS sensitivity of 100% with MRI as a reference method.

The inflammation activity evaluated with quantitative CEUS is more objective. It utilizes time-intensity curves and reduces both inter- and intraobserver variability [14]. Quantitative parameters of TICs are based on the blood perfusion on the capillary level that enables registration of the change in vascularity associated with the decrease in the disease activity after therapy.

For correct TIC construction, ROI is positioned in the area of the maximum contrast enhancement of the bowel wall. If gas is present in the intestinal lumen, the optimal location for the ROI is the superficial wall. Several (typically, three) separate ROIs ensure reliable data and help to avoid movement artifacts [4]. Patients with excessive peristaltic activity benefit from peristalsis inhibition.

Although linearized processing most accurately assesses the perfusion, the logarithmically processed data provide the best reproducibility with standard settings. The reproducibility is important for the dynamic assessment of the inflammation activity change with treatment.

Among all quantitative parameters, the relative peak intensity (PI) and the area under the curve (AUC) are the most reliable and reproducible. They are used to determine disease activity [9]. Peak intensity directly depends on the concentration of microbubbles and correlates with the severity of inflammation [11]. The values of PI with intestine CEUS range from 10 to 30 dB. In no active inflammation PI is less than 15 dB, in mild—15.0–18.2 dB, moderate—18.2–23.0 dB, and in pronounced inflammation—more than 23 dB [4].

CEUS is feasible for the evaluation of the treatment efficacy. It permits noninvasive monitoring of the bowel inflammation activity in IBD. The bowel wall enhancement with CEUS correlates with the change in vascularity and inflammation activity with therapy. It facilitates the identification of patients with full, partial, and no response to treatment.

The enhancement intensity decreases along with the decrease in the activity of the bowel wall inflammation. The study [15] demonstrated the reliable difference in the values of TICs in patients with a good response and no response to therapy. They calculated the percentage of the increase in the corresponding parameter before and after therapy in each group (Table 9.1).

The limitations in quantitative analysis associated with different software of different scanners do not apply when monitoring patients' treatment on the same scanner with standard settings. After the remission is achieved, follow-up with CEUS and detection of the residual intestinal wall enhancement enables to identify the patients with incomplete histological remission and a tendency to recurrence [16].

Table 9.1 The percentage ratio of TIC parameters to their initial values in the groups of patients with present or absent response to treatment [15]

	Responders		Nonresponders	
Parameter	Mean ± SD	95% CI	Mean ± SD	95% CI
Peak enhancement	−40.78 ± 62.85	−63.83, −17.72	53.21 ± 72.5	18.26, 88.15
Washin rate	−34.8 ± 67.72	−59.64, −9.95	89.44 ± 145.32	19.39, 159.48
Washout rate	−5.64 ± 130.71	−53.59, −42.3	166.83 ± 204.44	68.29, 265.37
Washin perfusion index	−42.29 ± 59.21	−76.42, −46.72	50.96 ± 71.13	16.68, 85.25
AUC	−46.17 ± 48.42	−63.93, −28.41	41.78 ± 87.64	−0.45, 84.02
AUC during washin	−43.93 ± 54.29	−63.86, 24.03	39.79 ± 70.85	5.64, 73.94
AUC during washout	−49.36 ± 47.42	−66.75, −31.97	42.65 ± 97.09	−4.14, 89.45

Bowel stenosis is one complication of IBD, which significantly lowers the quality of life and the course of the disease. The differentiation of the inflammatory and fibrous components is important since the approaches to their treatment are different. When the stenotic zone is located in the small intestine, it is not always achievable with the endoscopic study. Inflammatory stenosis exhibits hyperenhancement of the bowel wall with CEUS. Alternatively, fibrous stenosis is characterized by hypoenhancement. The differentiation is difficult in the cases of the combination of inflammatory and fibrous components in one region.

Tumors of the gastrointestinal tract confer malignant and benign lesions. Primary malignant tumors are typically represented by adenocarcinoma, gastrointestinal stromal tumors, carcinoid, and lymphoma. Benign lesions include inflammatory polyps, inflammatory wall thickening, and tuberculosis.

CEUS in bowel lesions aims to identify its vascularization features, which may indicate its possible malignancy. It is always necessary to consider the location of the lesion relative to the bowel wall, such as intraluminal, intramural, subserous, exophytic, as well as the signs of an invasion. Unlike IBD, which affects long segments of the intestinal wall, the intestinal tumors occupy a sort wall range and destroy wall layer stratification.

Gastrointestinal stromal tumors implicate a group of subepithelial neoplasms of the stomach, duodenum, and small intestine. They are rare entities in the esophagus and the colon. Preliminary data suggest that CEUS and endoscopic CEUS may differentiate them from benign lesions since they appear hypervascular in all cases with slow washout. Additionally, gastrointestinal stromal tumors often contain cystic or necrotic components, which can be identified with CEUS as nonenhancing areas [4, 17]. Quantitative analysis of CEUS permits monitoring the response to antiangiogenic therapy by estimating the change in tumor perfusion.

Carcinoid and neuroendocrine tumors are represented with CEUS by roundish lesions, which hyperenhance in the arterial phase. The intensity and velocity of washout in these tumors correlate with their malignant potential.

Adenocarcinoma is the most common tumor that mainly occurs in the colon. It usually enhances with possible washout. Endoscopic, transrectal, or transvaginal CEUS in some cases can supply additional diagnostic information [4].

References

1. Prives MG, Lysenkov NK, Bushkovich VI. Anatomiya cheloveka [Human anatomy]. 12th ed. Hyppokrat: Saint Petersburg; 2017. Russian.
2. Weskott HP. Contrast-enhanced ultrasound. 2nd ed. London: Uni-Med Science; 2013.
3. Dietrich C, Chiorean L, Cui XW, Schreiber-Dietrich D, Braden B. Conventional and new ultrasound techniques in inflammatory bowel disease – update 2014. Koloproktologiya. 2014;3:4–21. Russian.
4. Medellin A, Merrill C, Wilson SR. Role of contrast-enhanced ultrasound in evaluation of the bowel. Abdom Radiol (NY). 2018r;43(4):918–33. https://doi.org/10.1007/s00261-017-1399-6.
5. Dietrich CF, editor. EFSUMB course book. http://www.efsumb-archive.org/ecb/ecb-01.asp. Accessed 22 Feb 2021.

6. Mit'kov VV, editor. Prakticheskoe rukovodstvo po ul'trazvukovoj diagnostike [Practical guide to ultrasound diagnostics]. 3rd ed. Moscow: Vidar; 2019. Russian.
7. Hirche TO, Russler J, Schröder O, Schuessler G, Kappeser P, Caspary WF, Dietrich CF. The value of routinely performed ultrasonography in patients with Crohn disease. Scand J Gastroenterol. 2002;37(10):1178–83. https://doi.org/10.1080/003655202760373399.
8. Ripollés T, Martínez-Pérez MJ, Blanc E, Delgado F, Vizuete J, Paredes JM, Vilar J. Contrast-enhanced ultrasound (CEUS) in Crohn's disease: technique, image interpretation and clinical applications. Insights Imaging. 2011;2(6):639–52. https://doi.org/10.1007/s13244-011-0124-1.
9. Sidhu PS, Cantisani V, Dietrich CF, Gilja OH, Saftoiu A, Bartels E, et al. The EFSUMB guidelines and recommendations for the clinical practice of contrast-enhanced ultrasound (CEUS) in non-hepatic applications: update 2017 (long version). Ultraschall Med. 2018;39(2):e2–e44. https://doi.org/10.1055/a-0586-1107.
10. Maconi G, Nylund K, Ripolles T, Calabrese E, Dirks K, Dietrich CF, et al. EFSUMB recommendations and clinical guidelines for intestinal ultrasound (GIUS) in inflammatory bowel diseases. Ultraschall Med. 2018;39(3):304–17. English. https://doi.org/10.1055/s-0043-125329.
11. Serra C, Menozzi G, Labate AM, Giangregorio F, Gionchetti P, Beltrami M, et al. Ultrasound assessment of vascularization of the thickened terminal ileum wall in Crohn's disease patients using a low-mechanical index real-time scanning technique with a second generation ultrasound contrast agent. Eur J Radiol. 2007;62(1):114–21. https://doi.org/10.1016/j.ejrad.2006.11.027.
12. Migaleddu V, Scanu AM, Quaia E, Rocca PC, Dore MP, Scanu D, Azzali L, Virgilio G. Contrast-enhanced ultrasonographic evaluation of inflammatory activity in Crohn's disease. Gastroenterology. 2009;137(1):43–52. https://doi.org/10.1053/j.gastro.2009.03.062.
13. Mudambi K, Sandberg J, Bass D, Rubesova E. Contrast enhanced ultrasound: comparing a novel modality to MRI to assess for bowel disease in pediatric Crohn's patients. Transl Gastroenterol Hepatol. 2020;5:13. https://doi.org/10.21037/tgh.2019.11.02.
14. Greis C. Quantitative evaluation of microvascular blood flow by contrast-enhanced ultrasound (CEUS). Clin Hemorheol Microcirc. 2011;49(1–4):137–49. https://doi.org/10.3233/CH-2011-1464.
15. Quaia E, Sozzi M, Angileri R, Gennari AG, Cova MA. Time-intensity curves obtained after microbubble injection can be used to differentiate responders from nonresponders among patients with clinically active crohn disease after 6 weeks of pharmacologic treatment. Radiology. 2016;281(2):606–16. https://doi.org/10.1148/radiol.2016152461.
16. Ripollés T, Martinez MJ, Barrachina M. Crohn's disease and color Doppler sonography: response to treatment and its relationship with long-term prognosis. J Clin Ultrasound. 2008;36:267–72. https://doi.org/10.1002/jcu.20423.
17. Ignee A, Jenssen C, Hocke M, Dong Y, Wang WP, Cui XW, et al. Contrast-enhanced (endoscopic) ultrasound and endoscopic ultrasound elastography in gastrointestinal stromal tumors. Endosc Ultrasound. 2017;6(1):55–60. https://doi.org/10.4103/2303-9027.200216.

Bladder

10

Alexander N. Sencha, Munir G. Tukhbatullin, Ella I. Peniaeva, and Marat Z. Khasanov

The bladder receives its blood supply from the internal iliac arteries via superior and inferior vesical arteries and the branches of the middle rectal, internal pudendal, and obturator arteries. The veins of the bladder form an extensive venous plexus, which communicates with prostatic and pudendal plexuses and the veins of the rectum and drains to the internal iliac veins.

According to the EFSUMB guidelines and recommendations, CEUS is most appropriate for the differential diagnosis of bladder cancer from a hematoma in patients with hematuria when the diagnosis is equivocal on conventional B-mode and Doppler US [1–4].

A. N. Sencha (✉)
Department of Visual and Functional Diagnostics, Federal State Budget Institution "National Medical Research Center for Obstetrics, Gynecology and Perinatology n.a. V.I.Kulakov", Moscow, Russian Federation

M. G. Tukhbatullin
Department of Ultrasound Diagnosis, Kazan State Medical Academy, Kazan, Russian Federation

E. I. Peniaeva
Department of Ultrasound Diagnostics, Center for Radiological Diagnostics, Private Healthcare Institution "Clinical Hospital "RZD-Medicina" of Yaroslavl City", Yaroslavl, Russian Federation

M. Z. Khasanov
Department of Ultrasound Diagnostics, Republican Clinical Oncological Dispensary of the Ministry of Healthcare of the Republic of Tatarstan, Kazan, Russian Federation

The following additional indications for the bladder CEUS may be considered:

- bladder wall lesions that require differential diagnosis (tumor, hematoma, dense precipitate, ureterocele, ureteral stones, etc.),
- specification of the tumoral invasion in the bladder wall,
- specification of the tumor volume and the changes in the adjacent organs.

Solid lesions enhance with CEUS, while the blood clots, precipitates, and stones do not enhance. CEUS exceeds the possibilities of traditional US in assessing the bladder wall invasion, but MRI and CT remain the methods of choice for staging bladder tumors [5–7] (Fig. 10.1).

Differential diagnosis of the bladder lesions with CEUS is an issue for debates. Normal bladder wall demonstrates regular stratification. The mucosa and submucosa layers enhance early, while the muscular (detrusor) layer demonstrates hypoenhancement. The bladder tumors typically exhibit fast hyperenhancement in the arterial phase followed by rapid washout in the venous phase [8] (Figs. 10.2 and 10.3). Malignant bladder tumors along with hypervascularization and fast washout exhibit heterogeneous structure and enhancement patterns (Fig. 10.3).

The character and dynamics of enhancement are different depending on the degree of differentiation of the bladder tumor [6]. Fast enhancement

A. N. Sencha, Y. N. Patrunov (eds.), *Contrast-Enhanced Ultrasound*,
https://doi.org/10.1007/978-3-030-91764-7_10

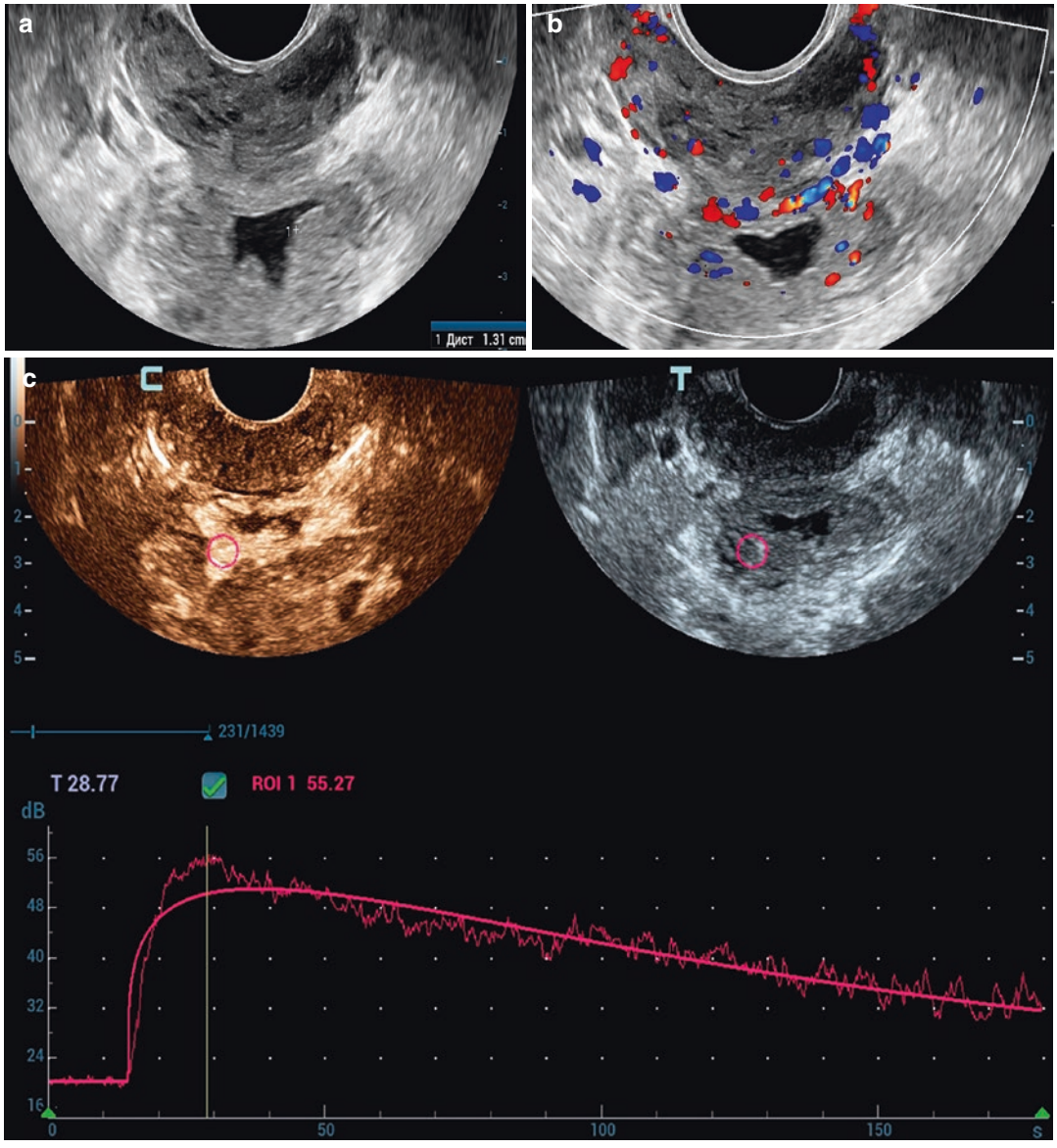

Fig. 10.1 Cystitis. (**a**) Grayscale US transvaginal image. The wall of the bladder is thickened. (**b**) CDI transvaginal image demonstrates the bladder wall hypervascularity. (**c**) CEUS image with TIC. Fast hyperenhancement of the bladder wall with slow washout

with fast washout is more characteristic of poorly differentiated urothelial carcinoma (PPV 90%), and fast enhancement with slow washout—of well-differentiated (PPV 92%). This conclusion is also obtained from the analysis of TICs [9]. The sensitivity of CEUS in the detection of bladder carcinoma of the size larger than 5 mm reaches 95%, but in lesions smaller than 5 mm it is only 20% [4].

Some publications [10] attempted to differentiate benign bladder wall changes from malignant neoplasms and well-differentiated tumors from poorly differentiated ones with quantitative analysis of CEUS. In the study, the normal bladder wall was characterized by time to peak >40 s, signal intensity <45%, and washout time >80 s. Poorly differentiated carcinoma demonstrated TTP < 28 s, signal intensity <45%, and washout time about 40 s. Well-

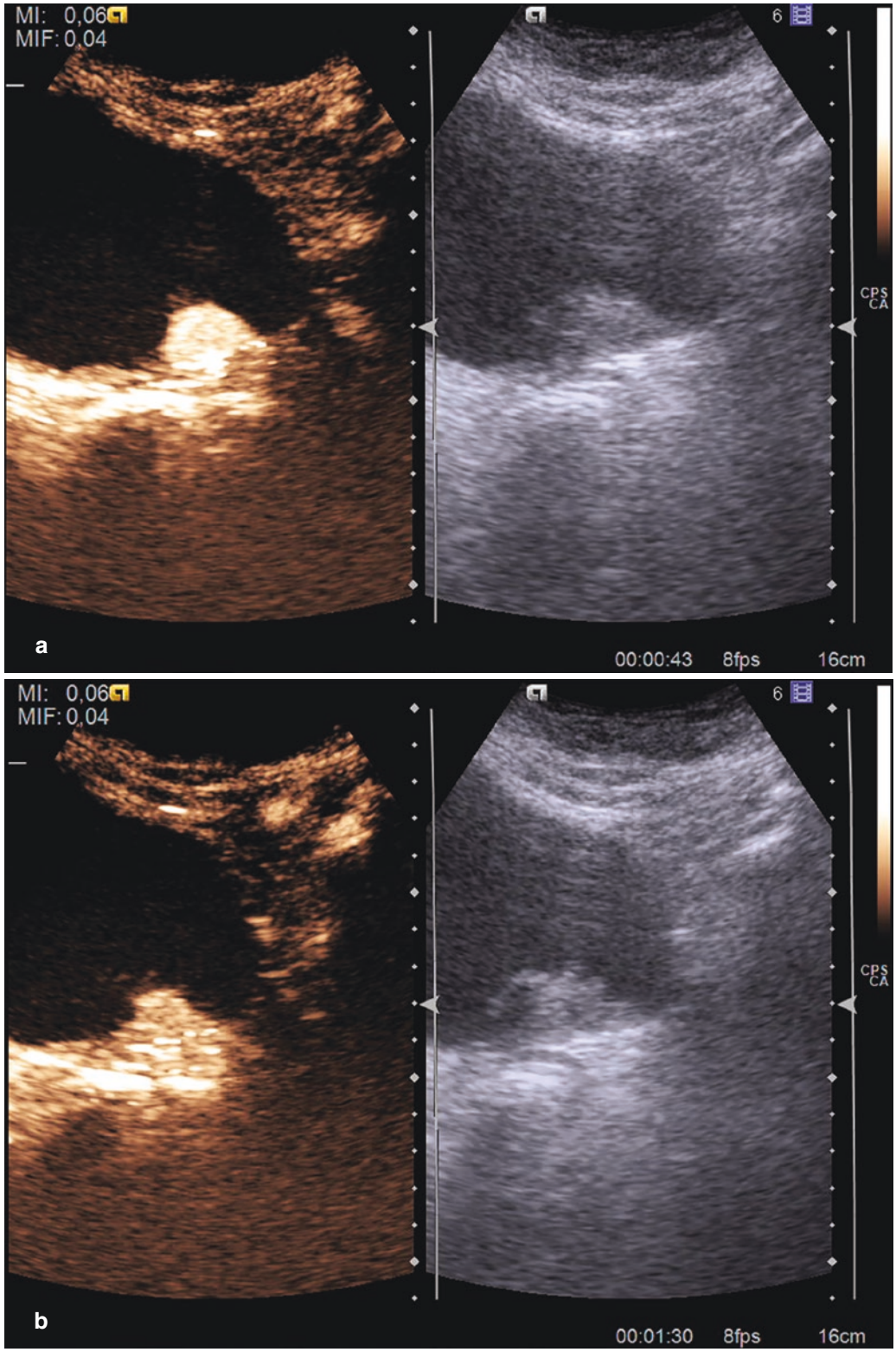

Fig. 10.2 The bladder papilloma. Hyperenhancement of the lesion in the arterial phase (**a**) and venous phase (**b**). CEUS images

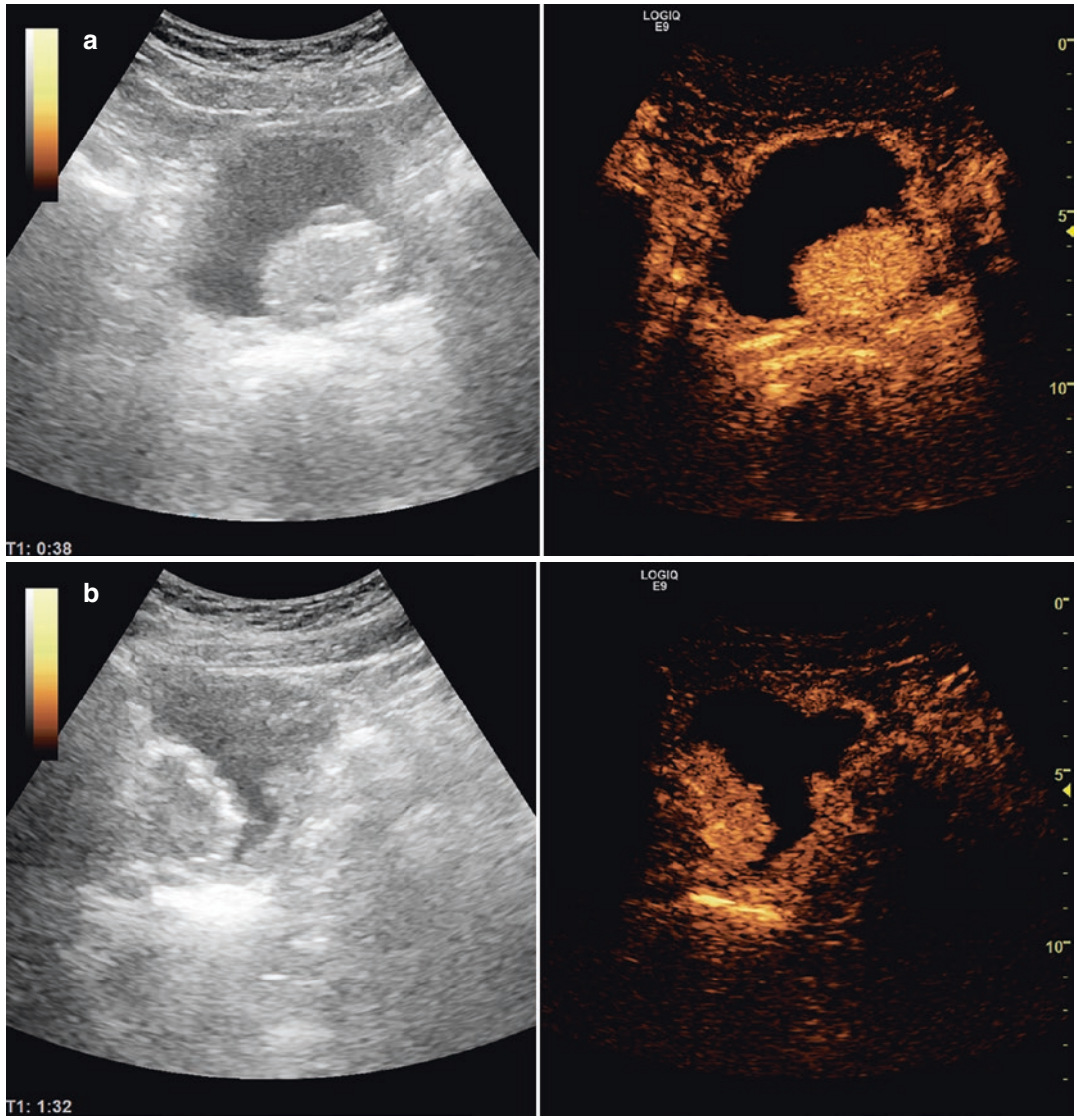

Fig. 10.3 Bladder cancer with multifocal growth. Hyperenhancement of the lesion in the arterial phase (**a**) and venous phase (**b**). CEUS images

differentiated carcinoma exhibited TTP > 28 s, signal intensity >50%, and washout time about 58 s.

References

1. Sidhu PS, Cantisani V, Dietrich CF, Gilja OH, Saftoiu A, Bartels E, et al. The EFSUMB guidelines and recommendations for the clinical practice of contrast-enhanced ultrasound (CEUS) in Non-Hepatic applications: update 2017. Ultraschall Med. 2018;39(2):e2–e44. https://doi.org/10.1055/a-0586-1107.
2. Drudi FM, Cantisani V, Liberatore M, Iori F, Erturk SM, Cristini C, Di Pierro G, D'Ambrosio U, Malpassini F, De Felice C, Di Leo N. Role of low-mechanical index CEUS in the differentiation between low and high grade bladder carcinoma: a pilot study. Ultraschall Med. 2010;31(6):589–95. https://doi.org/10.1055/s-0029-1245397.
3. Nicolau C, Bunesch L, Sebastia C, Salvador R. Diagnosis of bladder cancer: contrast-enhanced ultrasound. Abdom Imaging. 2010;35(4):494–503. https://doi.org/10.1007/s00261-009-9540-9.

4. Nicolau C, Bunesch L, Peri L, Salvador R, Corral JM, Mallofre C, Sebastia C. Accuracy of contrast-enhanced ultrasound in the detection of bladder cancer. Br J Radiol. 2011;84(1008):1091–9. https://doi.org/10.1259/bjr/43400531.
5. Caruso G, Salvaggio G, Campisi A, Melloni D, Midiri M, Bertolotto M, Lagalla R. Bladder tumor staging: comparison of contrast-enhanced and gray-scale ultrasound. AJR Am J Roentgenol. 2010;194(1):151–6. https://doi.org/10.2214/AJR.09.2741.
6. Li QY, Tang J, He EH, Zhou Y, Li YM, Fei X, Zhang Y. Role of contrast-enhanced ultrasound in the differentiation of high- and low-grade urothelial carcinoma. Zhongguo Yi Xue Ke Xue Yuan Xue Bao. 2012;34(4):364–8. https://doi.org/10.3881/j.issn.1000-503X.2012.04.010.
7. Wang XH, Wang YJ, Lei CG. Evaluating the perfusion of occupying lesions of kidney and bladder with contrast-enhanced ultrasound. Clin Imaging. 2011;35(6):447–51. https://doi.org/10.1016/j.clinimag.2010.11.001.
8. Zhang M, Niu C, Zhang M, Peng Q, Ouyang M. Contrast-enhanced ultrasound of small cell carcinoma in urinary bladder: a case report and review of literature. BMC Cancer. 2017;17(1):746. https://doi.org/10.1186/s12885-017-3692-8.
9. Drudi FM, Di Leo N, Malpassini F, Antonini F, Corongiu E, Iori F. CEUS in the differentiation between low and high-grade bladder carcinoma. J Ultrasound. 2012;15(4):247–51. https://doi.org/10.1016/j.jus.2012.09.002.
10. Drudi FM, Di Leo N, Maghella F, Malpassini F, Iera J, Rubini A, et al. CEUS in the study of bladder, method, administration and evaluation, a technical note. J Ultrasound. 2013;17(1):57–63. https://doi.org/10.1007/s40477-013-0032-y.

Prostate

11

Munir G. Tukhbatullin, Marat Z. Khasanov, Elena E. Fomina, and Natalya I. Bayazova

The prostate is supplied with blood by the main and additional arteries. The main arteries include paired inferior vesical and middle rectal arteries, which are the branches of the internal iliac arteries. The inferior vesical artery at the level of the bladder bottom proceeds to the prostatic artery, which branches to ureteral and capsular arteries. The urethral arteries enter the bladder/prostate conjunction, pass through the prostatic parenchyma to the urethra, and supply mainly the transition zone. Capsular arteries give rise to numerous small branches and supply the gland capsule. The middle rectal artery also gives the branches to the prostate capsule and seminal vesicles. The additional arteries of the prostate include the branches of the internal pudendal artery, obturator artery, and the artery of the ductus deferens. The branches from the main and additional arteries compose a pronounced vascular plexus on the surface of the prostate, which is more developed in the basal and lateral surfaces of the gland [1].

Numerous prostate veins form a periprostatic venous plexus. Its wide veins are located mainly along the lateral and posterior aspects of the gland, have multiple connections with the deep dorsal vein of the penis, veins of the bladder, seminal vesicles, ductus deferens, rectum, and perineum and drain to the internal iliac vein [2].

As the prostate perfusion is concerned, the blood supply of the inner and outer aspects of the gland is considered separately [3]. The inner part is prone to benign hyperplasia and the peripheral areas tend to malignant transformation [4, 5].

Currently, the standard method of prostate imaging is transrectal ultrasound (TRUS) with Doppler. It permits measurement of the prostate volume, evaluation of margins, structure, vascularity of the whole gland and its lesions, and assess hemodynamic data [6, 7]. Modern high-frequency rectal probes (5–16 MHz) enable a detailed image of the examined structures. However, the obtained data exhibit low specificity. For example, a hypoechogenic lesion in the peripheral zone is typical for prostate cancer [8]. But this feature can be detected in various benign changes, such as inflammatory process, hyperplasia, peripheral zone vessels, extended acini, etc. [9]. The literature data indicate that only 40% of hypoechogenic foci of the peripheral zone of the prostate are verified malignant [10].

M. G. Tukhbatullin (✉)
Department of Ultrasound Diagnosis, Kazan State Medical Academy, Kazan, Russian Federation
e-mail: munir.tuhbatullin@tatar.ru

M. Z. Khasanov
Department of Ultrasound Diagnostics, Republican Clinical Oncological Dispensary of the Ministry of Healthcare of the Republic of Tatarstan, Kazan, Russian Federation

E. E. Fomina · N. I. Bayazova
Department of Ultrasound Diagnosis, Kazan State Medical Academy, Kazan, Russian Federation

A. N. Sencha, Y. N. Patrunov (eds.), *Contrast-Enhanced Ultrasound*,
https://doi.org/10.1007/978-3-030-91764-7_11

The development of prostate carcinoma is associated with neoangiogenesis, and an increase in the density of the microvessels correlates with more aggressive tumors and a poor prognosis [10]. Increased vascularization of prostatic malignancies can be revealed with Doppler imaging. However, the increase in blood flow is a feature, which accompanies not only prostate cancer. A significant drawback of CDI is poor imaging of the slow-velocity microcirculation [11, 12]. Doppler modes identify vessels up to 1 mm in size, while the size of tumor vessels ranges from 10 to 50 μm [13]. Increased tumor vascularization, which is identified with Doppler, results from the detection of large feeding vessels but not from true microvascular neoangiogenesis [14].

Contrast-enhanced TRUS can be of benefit in the following situations:

- prostate lesions detected with the grayscale US that require differential diagnosis,
- rigid prostatic areas with per rectal examination,
- serum prostate-specific antigen (PSA) higher than 4 ng/ml and the free-to-total PSA ratio smaller than 15%,
- negative primary biopsy in patients with persistent suspicions for prostate malignancy,
- patients with prostate cancer suspicion, when MRI is impossible,
- assessment of the prostate after ablative techniques.

Publications often indicate the value of CEUS for the diagnosis of prostatic cancer. However, according to the clinical recommendations of EFSUMB (2017) [15], CEUS for the improvement of the prostate cancer detection rate is an active research field, it currently cannot be recommended for clinical use.

Typically, 2.4 ml of SonoVue® is used for the prostate CEUS. Two phases that are characteristic of most internal organs are recognized. The arterial phase lasts up to 30–45 s from the moment of intravenous UCA administration, and the venous phase follows immediately after it (Fig. 11.1).

Prostate CEUS usually aims to diagnose prostate cancer and determines the areas for the targeted biopsy. The most characteristic feature is fast asymmetric hyperenhancement followed by fast washout [16] (Fig. 11.2).

CEUS precisely demonstrates the prostatic perfusion and contributes to the determination of the biopsy areas. The density of the microvessels is associated with prostate carcinoma, which enabled correct diagnosis of prostatic cancer in 86% out of 70 patients subject to radical prostatectomy with CEUS and PDI [17]. The study [18] compared the efficacy of CEUS guided biopsy from five points and the blind systemic biopsy from ten points. It demonstrated a significant advantage of CEUS targeted biopsy. Many studies [19–22] have demonstrated the potential of CE-TRUS to increase the sensitivity of the targeted prostate biopsy for the diagnosis of carcinoma.

Qualitative CEUS in our study exhibited higher diagnostic value in the detection of prostate cancer, as compared with Doppler imaging (Table 11.1).

Quantitative assessment of CEUS is capable to improve the study accuracy and reduce the operator dependency [23] (Figs. 11.3 and 11.4). In this regard, the quantitative parameters, which characterize the accumulation of UCA in the prostate parenchyma and facilitate differential diagnosis of focal lesions, are studied.

Neovascularization in prostate carcinoma is characterized by an increase in the peak intensity, which was significantly higher than in benign hyperplasia (9.82 ± 3.73 vs. 7.51 ± 2.97, respectively) [24]. The tumor location and Gleason score also influence the value of peak intensity.

The values of peak intensity in cancer and the intact peripheral zone of the prostate significantly differ (17.2 and 12.6, respectively) [25]. Area under the curve (dB/s), mean transit time (s), and half time of washout (s) were also significantly higher in carcinoma than with benign lesions (1055.3/37.0/52.3 vs. 685.1/32.3/46.5, respectively). The study [25] used the regression model and calculated the diagnostic values of PI and AUC of the lesion considering the values of the intact peripheral zone of the prostate, which

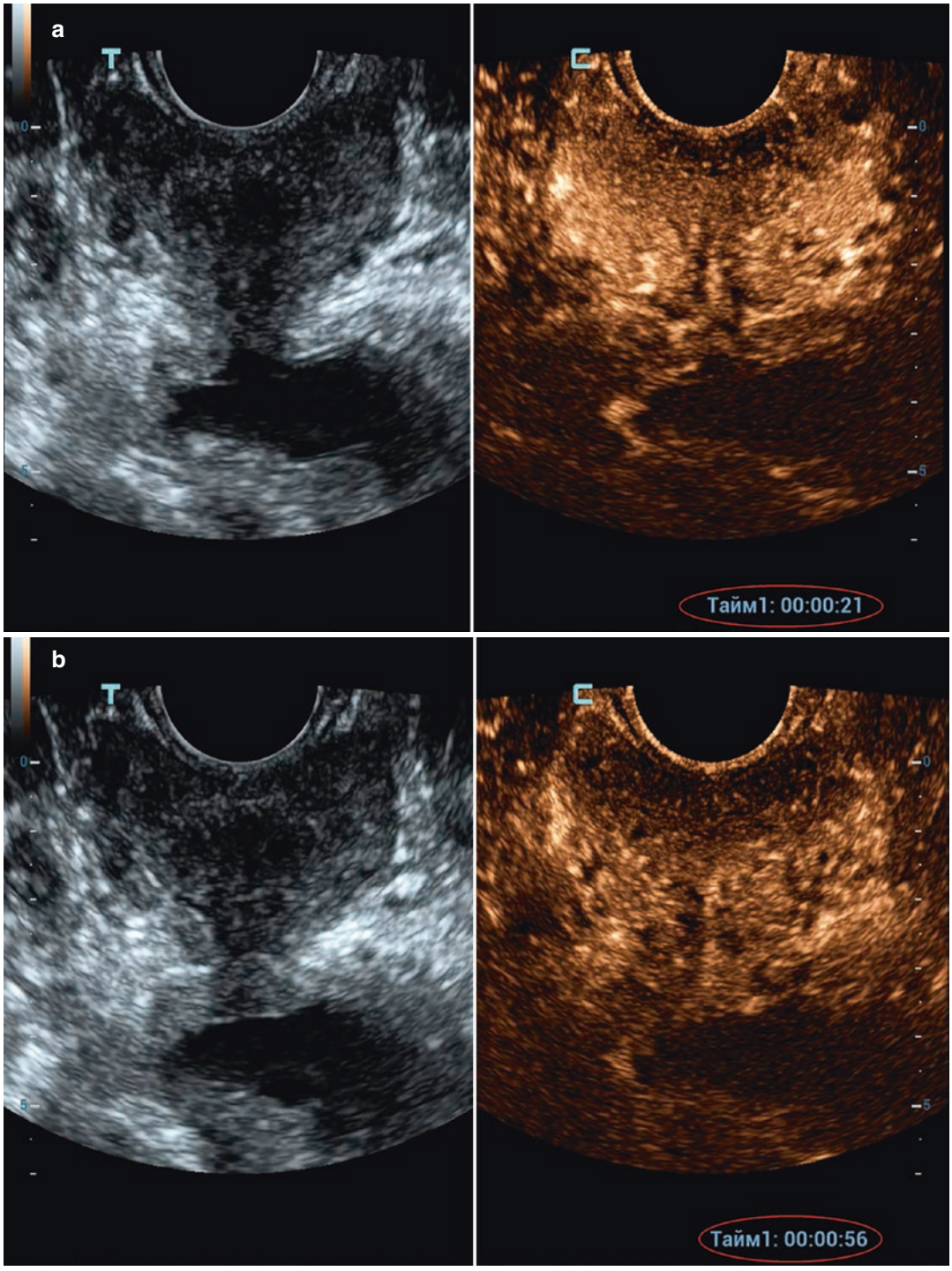

Fig. 11.1 Normal prostate CE-TRUS images. (**a**) The arterial phase. (**b**) Venous phase

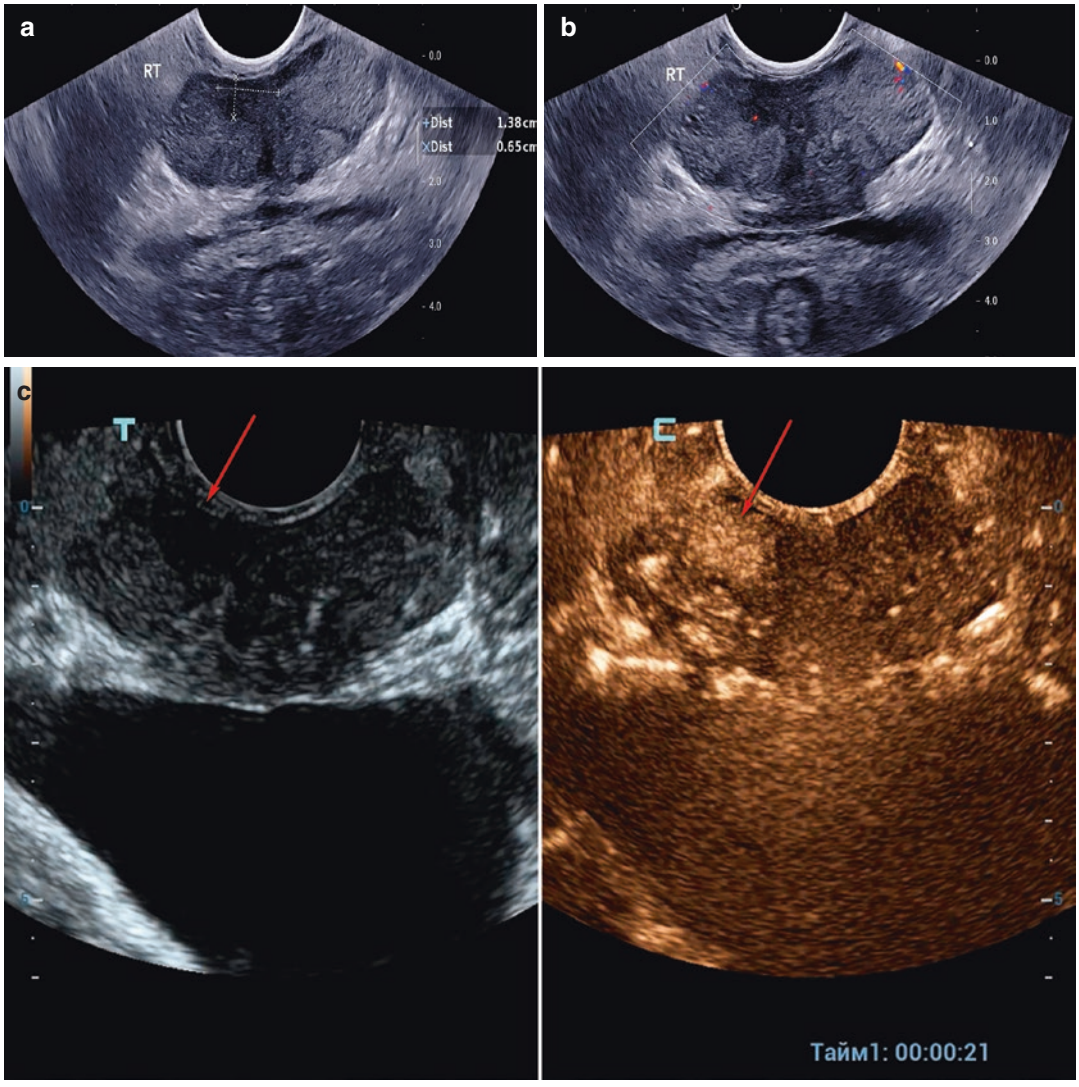

Fig. 11.2 Prostate acinar adenocarcinoma in the right lobe. (**a**) Grayscale TRUS image detects a hypoechogenic lesion with indistinct margins in the peripheral zone of the right prostatic lobe. (**b**) CDI image depicts sporadic vessels within the lesion. (**c**) Fast hyperenhancement in the arterial phase, CE-TRUS image. The lesion is marked with an arrow. (**d**) Fast washout in the early venous phase, CE-TRUS image

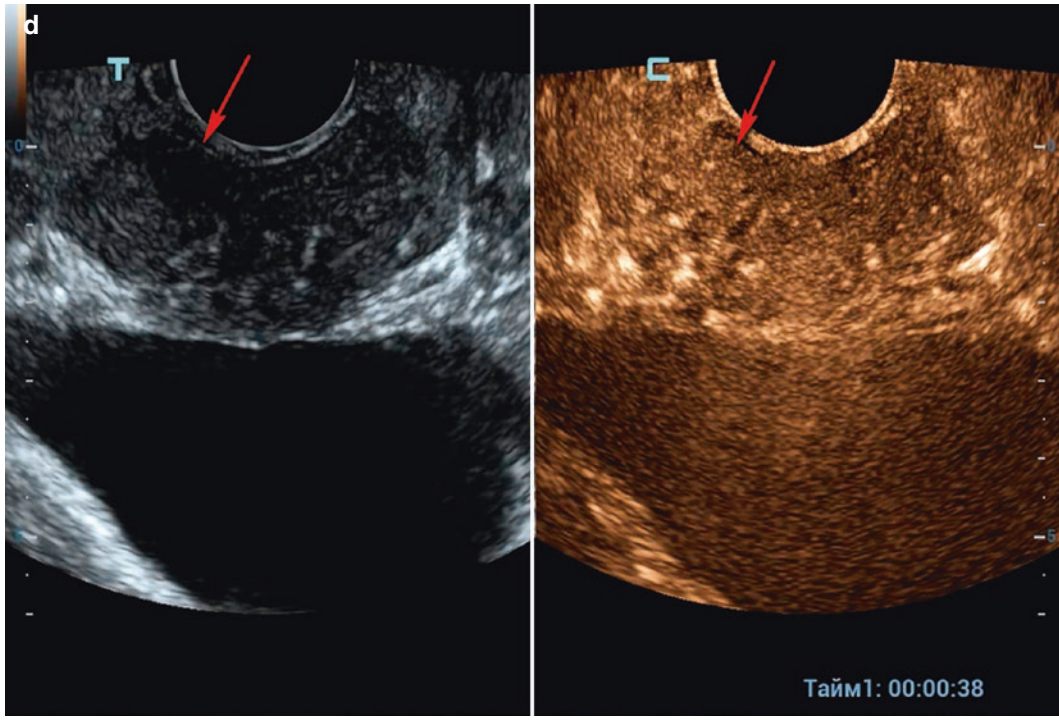

Fig. 11.2 (continued)

Table 11.1 The value of qualitative CEUS in the diagnosis of prostatic carcinoma

CEUS parameter	Sensitivity (%)	Specificity (%)	Diagnostic accuracy (%)	PPV (%)	NPV (%)
Hyperenhancement	58	69	62	74	51
Heterogeneous enhancement pattern	48	96	67	95	54
Fast washin and higher enhancement in the arterial phase as compared to the intact parenchyma	82	78	54	81	54
Faster washout as compared to the intact parenchyma	58	96	73	96	60
Three and more vascular spots in the lesion with CDI	35	77	52	70	43

significantly improved the diagnosis of prostate carcinoma and prediction of its aggressiveness. For PI/AUC of the lesion, the specificity, sensitivity, positive predictive value, and negative predictive value amounted to 73.7%/81.6%, 66.7%/53.7%, 64.3%/67.4%, and 75.7%/71.3%, respectively. When the analysis considered PI/AUC data of the intact parenchyma of the peripheral zone, these values increased to 90.8%/92.1%, 79.6%/72.2%, 86.0%/86.7%, and 86.3%/82.4%, respectively. However, any threshold values were not suggested.

Benign prostate hyperplasia (BPH) is the most common disease of the prostate gland in men of middle age and older. The disease prevalence increases with age. Thus, BPH in men of 31–40 years accounts for 8%, 51–60 years – 40–50%, and over 80 years exceeds 80% [26].

BPH is characterized by the increase in the volume of the inner aspects of the gland and the external part decreases due to compression [27]. CEUS enables visualization of the difference between the normal and hyperplastic tissues [28]. In BPH, the inner part of the prostate exhibits hyperenhancement, which spreads from the surgical capsule and the periurethral zone toward the inner part of the nodules with slow washout and the clear margin between the

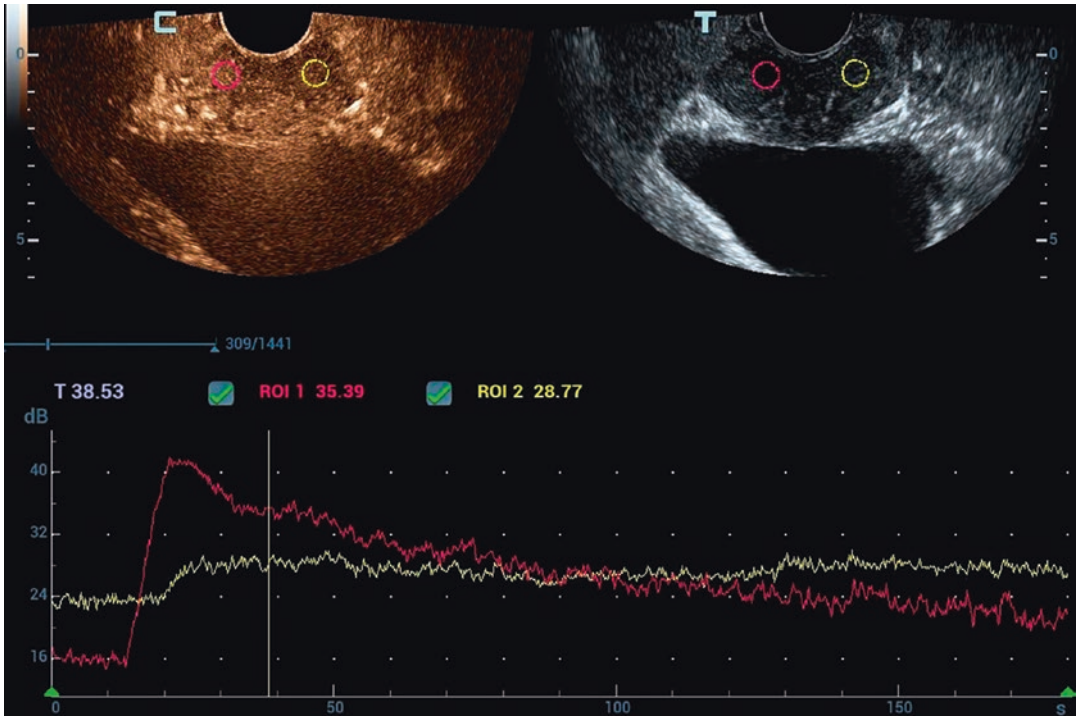

Fig. 11.3 Prostate acinar adenocarcinoma in the right lobe. CE-TRUS image. Quantitative analysis with TICs demonstrates hyperenhancement and fast washout of the prostate lesion (pink ROI) as compared to the intact parenchyma (yellow ROI)

inner and outer glands (Figs. 11.5, 11.6, 11.7, and 11.8).

In addition, CEUS of the prostate gland can be used as a tool to follow-up patients treated with ablative techniques, such as high-intensity focused ultrasound (HIFU). It may demonstrate perfusion defects after successful treatment and identify the suspicious areas with contrast enhancement in the ablation zone [29].

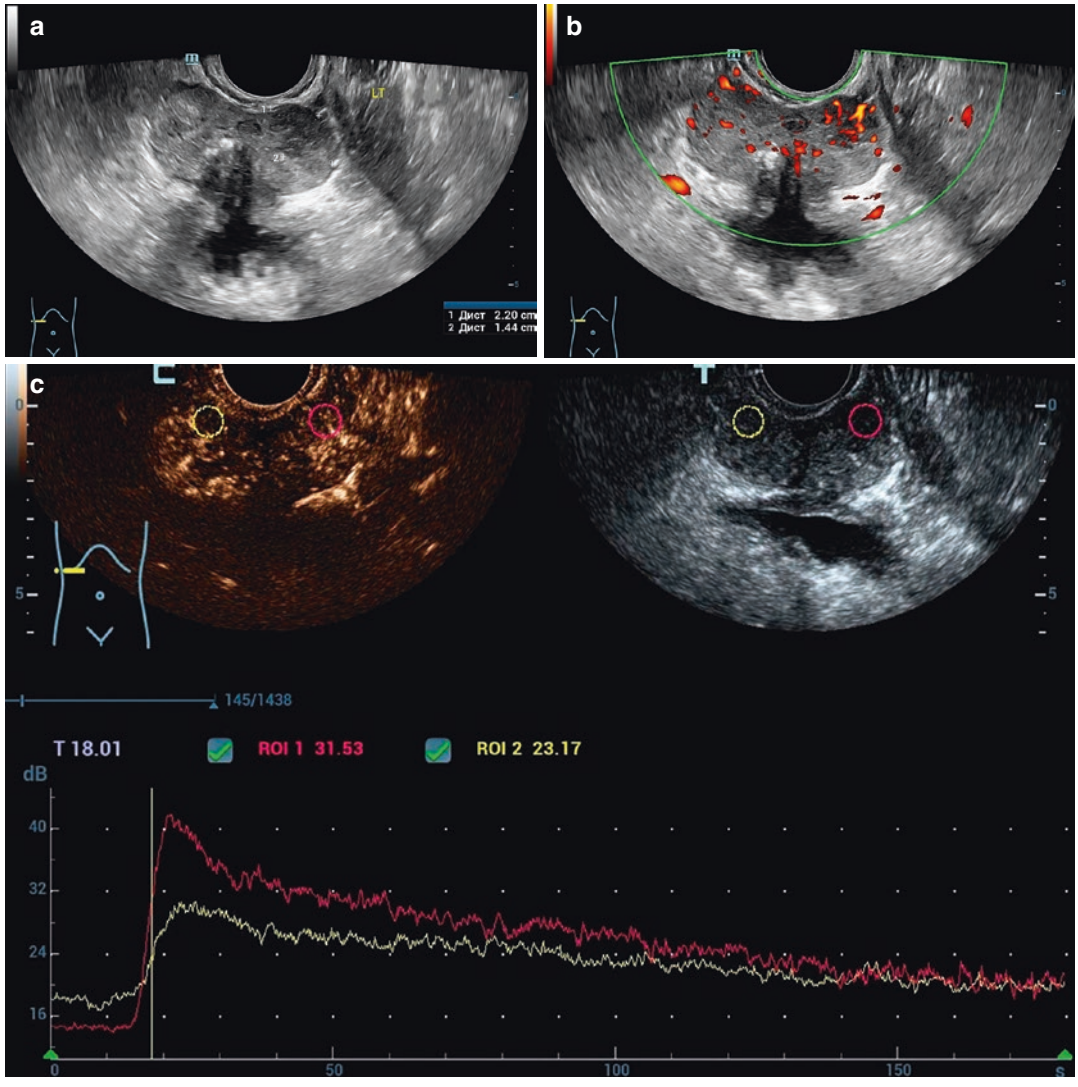

Fig. 11.4 Prostate adenocarcinoma. (**a**) Grayscale US image demonstrates a lesion (markers) of decreased echogenicity with indistinct margins in the peripheral zone of the left lobe of the prostate. (**b**) PDI detects increased vascularity of the lesion. (**c**) CEUS image quantitative analysis. The TICs demonstrate the differences in the contrast enhancement of the lesion (pink ROI) and the intact parenchyma of the right lobe (yellow ROI)

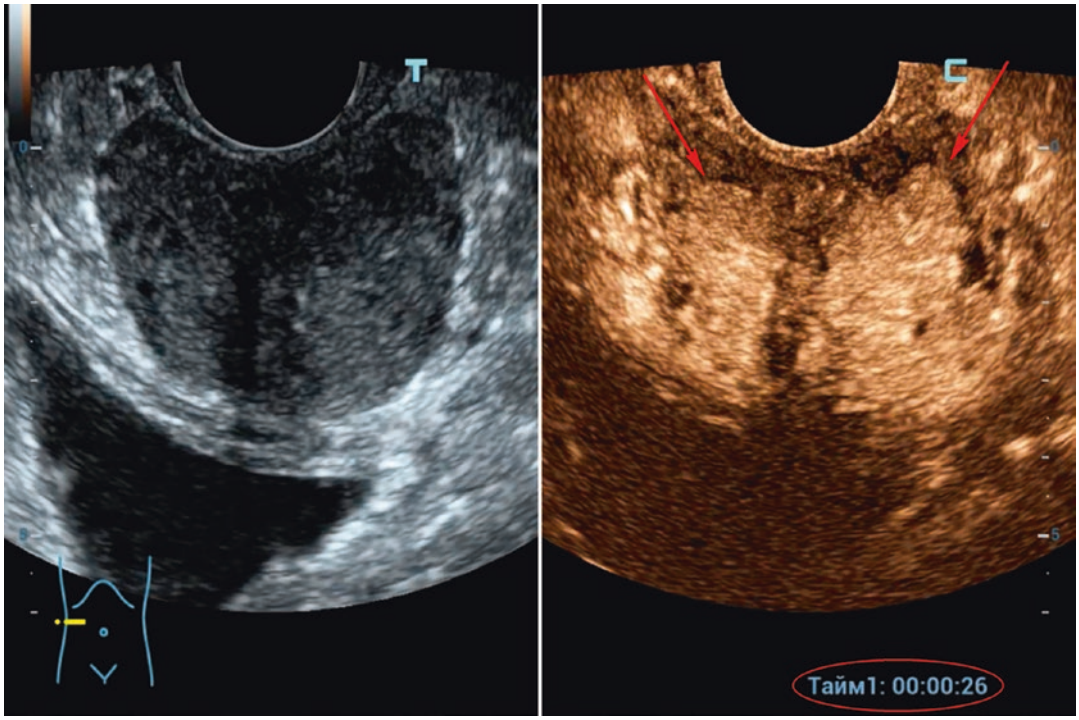

Fig. 11.5 BPH. CE-TRUS image, the arterial phase. Hyperenhanced inner aspects and isoenhanced peripheral zone of the prostate with a clear boundary between them (marked with arrows)

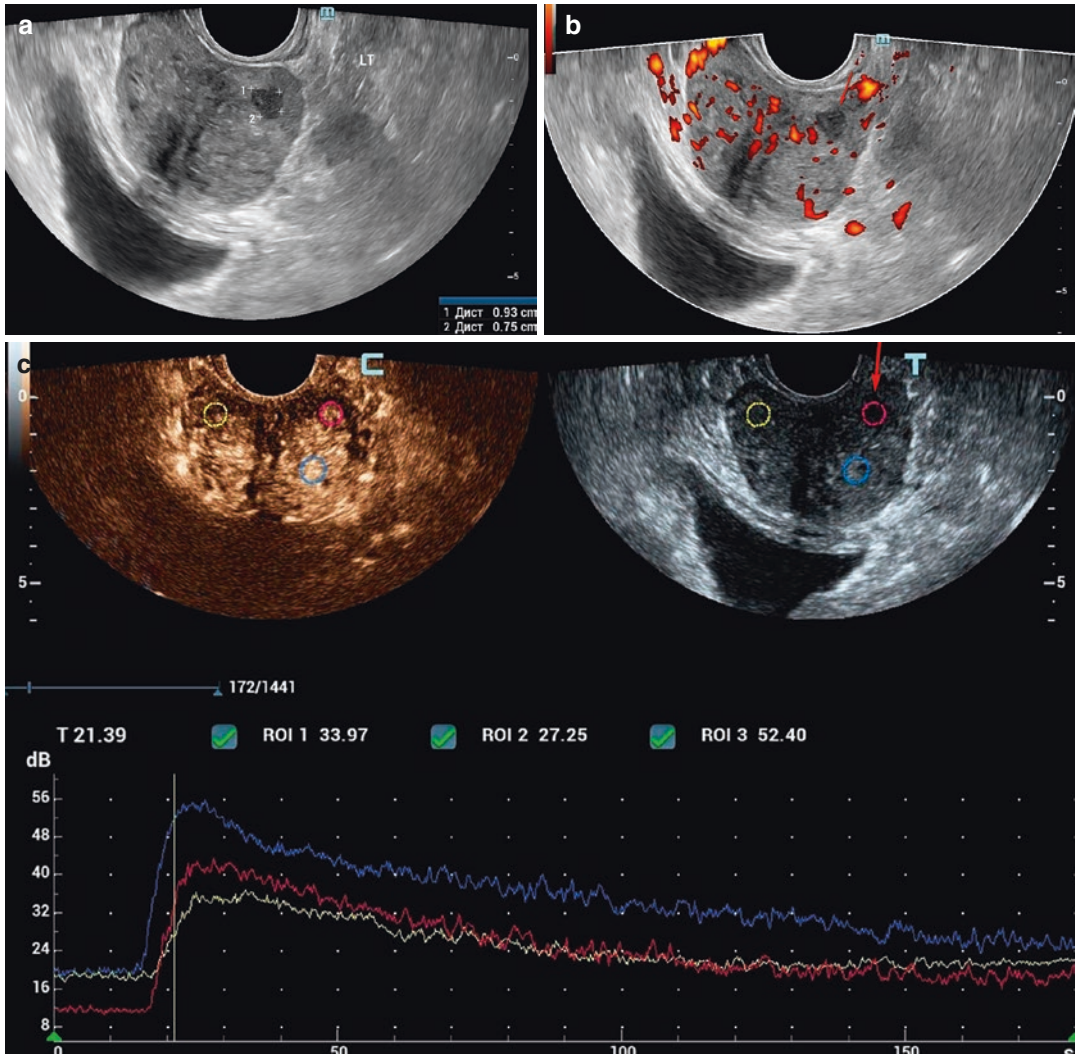

Fig. 11.6 BPH. (**a**) Grayscale TRUS detects a hypoechogenic lesion with clear margins in the left lobe (distance markers). (**b**) PDI demonstrates hypovascularity of the lesion (arrow). (**c**) CE-TRUS image, quantitative analysis. The lesion (pink ROI) exhibits slight hyperenhancement as compared with the contralateral peripheral zone (yellow ROI) and its enhancement does not exceed the same of the central part (blue ROI). (**d**) Numeric data of the enhancement for part (**c**)

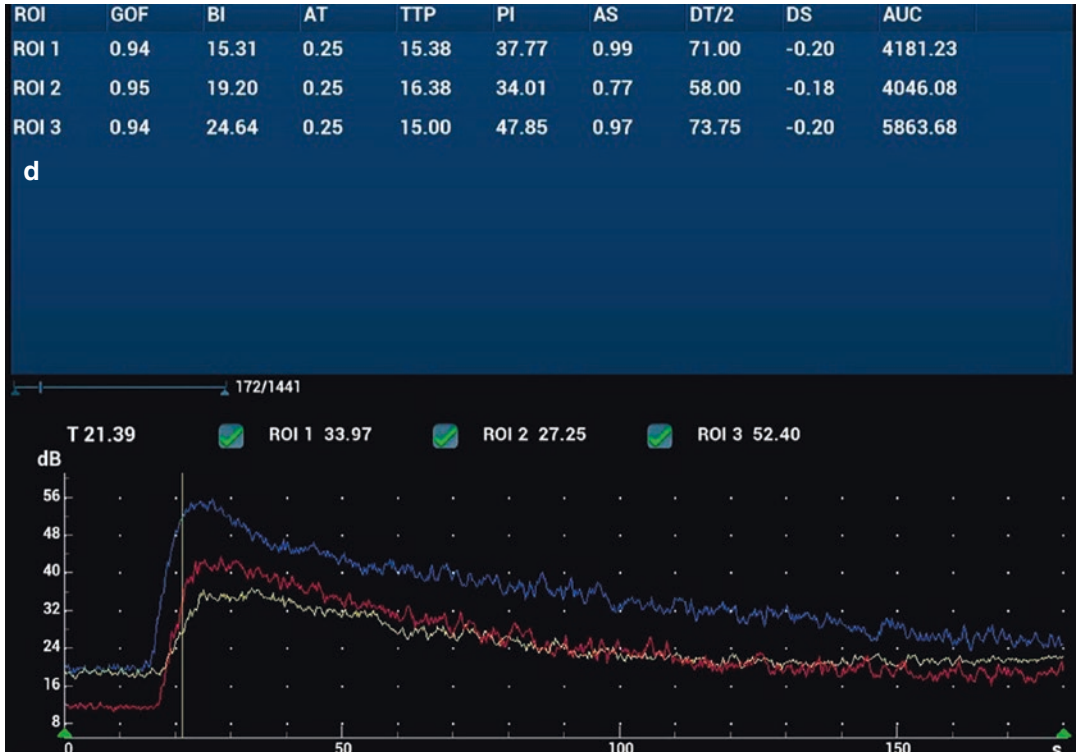

Fig. 11.6 (continued)

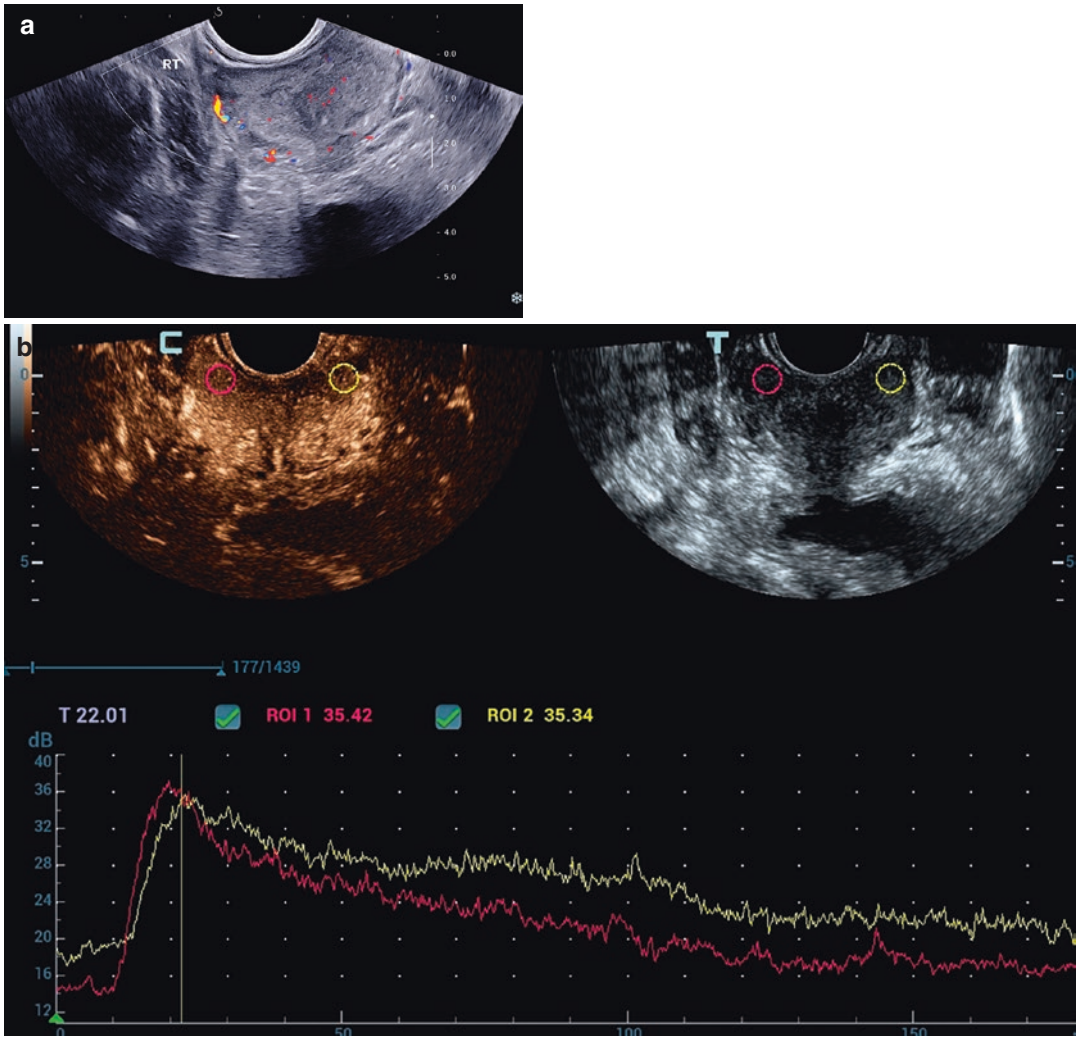

Fig. 11.7 BPH. (**a**) CDI demonstrates a hypoechogenic hypovascular lesion with blurred margins in the peripheral zone of the right lobe of the prostate. (**b**) CE-TRUS image. Quantitative analysis. The lesion in the right lobe is isoenhanced (pink ROI) with a moderately increased washin rate and a comparable washout rate as compared with the relatively intact peripheral zone of the left lobe (yellow ROI)

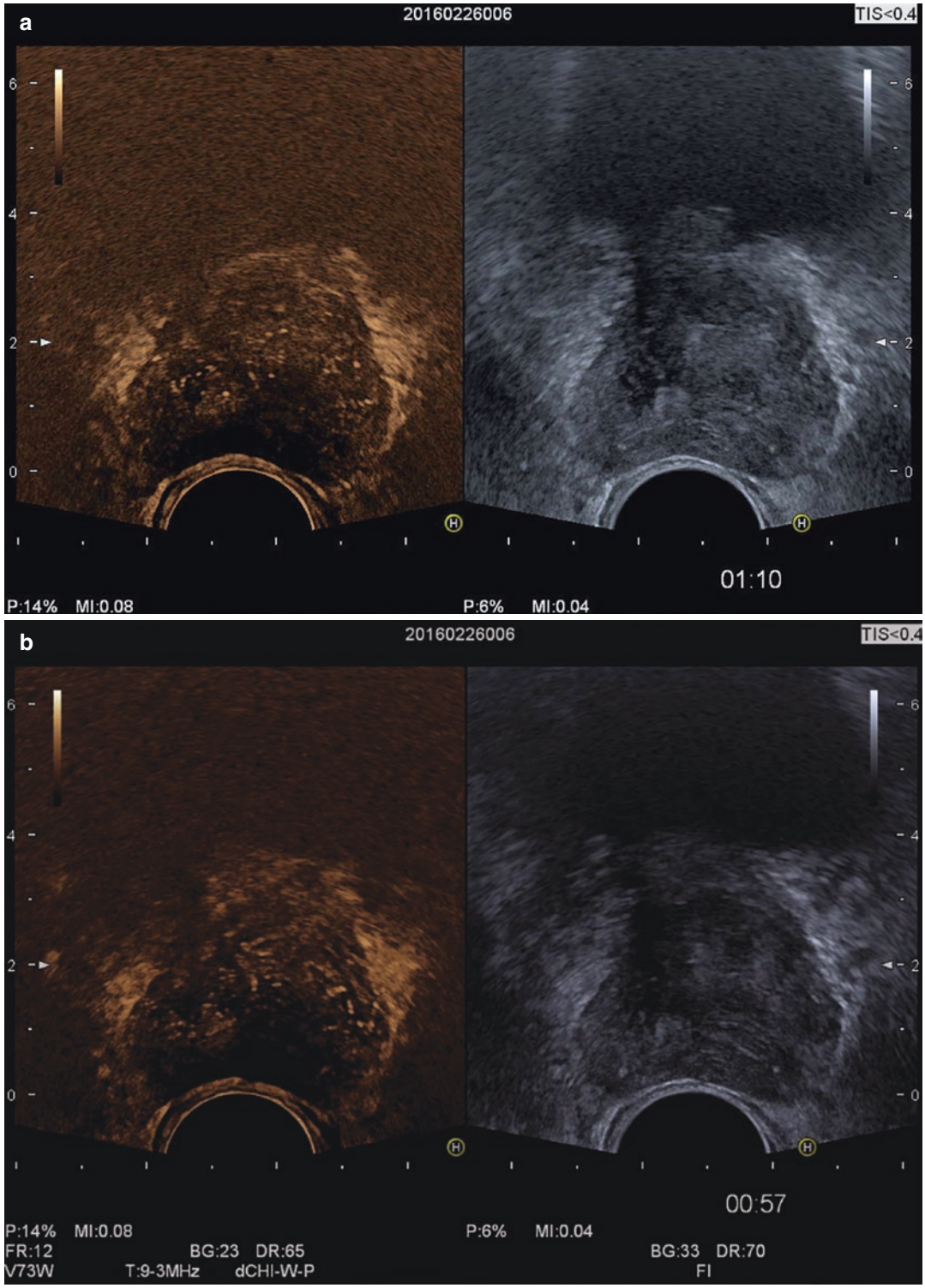

Fig. 11.8 BPH. (**a**) CE-TRUS image demonstrates regular symmetric enhancement in the transitional zone of the prostate. (**b**) CE-TRUS cine loop at ×1.5 speed exhibits regular distribution of microbubbles

References

1. Hnykin FN. Topografo-anatomicheskie osobennosti prostaty i eyo ekstraorgannyh sosudov u vzroslogo cheloveka [Topografo-anatomical features of the prostate and its extra-organ vessels in an adult]. Dissertation. Saint-Petersburg: Sankt-Peterburgskaya gosudarstvennaya pediatricheskaya medicinskaya akademiya. 2005.
2. Nazarenko GI, Hitrova AN. Ul'trazvukovaya diagnostika predstatel'noj zhelezy v sovremennoj urologicheskoj praktike [Ultrasound diagnostics of the prostate in modern urological practice]. Moscow: Vidar-M; 2012.
3. McNeal JE, Redwine EA, Freiha FS, Stamey TA. Zonal distribution of prostatic adenocarcinoma. Correlation with histologic pattern and direction of spread. Am J Surg Pathol. 1988;12(12):897–906. https://doi.org/10.1097/00000478-198812000-00001.
4. Ismail M, Gomella LG. Ultrasound for prostate imaging and biopsy. Curr Opin Urol. 2001;11(5):471–7. https://doi.org/10.1097/00042307-200109000-00004.
5. Bryusova PG, Zubaeva PN. Klinicheskaya onkologiya [Clinical oncology]. Saint Petersburg: Spetslit; 2012.
6. Pummer K, Rieken M, Augustin H, Gutschi T, Shariat SF. Innovations in diagnostic imaging of localized prostate cancer. World J Urol. 2014;32(4):881–90. https://doi.org/10.1007/s00345-013-1172-6.
7. Sholohov VN, Buharkin BV, Lepedatu PI. Ul'trazvukovaya tomografiya v diagnostike raka predstatel'noj zhelezy [Ultrasonic tomography in the diagnosis of prostate cancer]. Moscow; 2006.
8. Ellis WJ, Chetner MP, Preston SD, Brawer MK. Diagnosis of prostatic carcinoma: the yield of serum prostate specific antigen, digital rectal examination and transrectal ultrasonography. J Urol. 1994;152(1):1520–5. https://doi.org/10.1016/s0022-5347(17)32460-6.
9. Stecenko TN, et al. Vozmozhnosti ul'trazvukovogo metoda issledovaniya pri differencial'noj diagnostike raka predstatel'noj zhelezy i granulematoznogo prostatita [Possibilities of the ultrasound method in the differential diagnosis of prostate cancer and granulomatous prostatitis]. Luchevaya diagnostika i terapiya. 2013;3(4):77–82.
10. Russo G, Mischi M, Scheepens W, De la Rosette JJ, Wijkstra H. Angiogenesis in prostate cancer: onset, progression and imaging. BJU Int. 2012;110(11):794–808. https://doi.org/10.1111/j.1464-410X.2012.11444.x.
11. Karman AV, Dudarev VS, Leusik EA. Transrektal'noe ul'trazvukovoe issledovanie v diagnostike raka predstatel'noj zhelezy [Transrectal ultrasound examination in the diagnosis of prostate cancer]. Onkologicheskij zhurnal. 2013;7(3):66–74.
12. Catalona WJ, Richie JP, Ahmann FR, Hudson MA, Scardino PT, Flanigan RC, DeKernion JB, Ratliff TL, Kavoussi LR, Dalkin BL, Waters WB, MacFarlane MT, Southwick PC. Comparison of digital rectal examination and serum prostate specific antigen in the early detection of prostate cancer: results of a multicenter clinical trial of 6,630 men. J Urol. 1994;151(5):1283–90. https://doi.org/10.1016/s0022-5347(17)35233-3.
13. Eisenberg ML, Cowan JE, Carroll PR, Shinohara K. The adjunctive use of power Doppler imaging in the preoperative assessment of prostate cancer. BJU Int. 2010;105(9):1237–41. https://doi.org/10.1111/j.1464-410X.2009.08958.x.
14. Nelson ED, Slotoroff CB, Gomella LG, Halpern EJ. Targeted biopsy of the prostate: the impact of color Doppler imaging and elastography on prostate cancer detection and Gleason score. Urology. 2007;70(6):1136–40. https://doi.org/10.1016/j.urology.2007.07.067.
15. Sidhu PS, Cantisani V, Dietrich CF, Gilja OH, Saftoiu A, Bartels E, et al. The EFSUMB guidelines and recommendations for the clinical practice of contrast-enhanced ultrasound (CEUS) in Non-Hepatic applications: update 2017. Ultraschall Med. 2018;39(2):2–44. https://doi.org/10.1055/a-0586-1107.
16. Seitz M, Gratzke C, Schlenker B, Buchner A, Karl A, Roosen A, et al. Contrast-enhanced transrectal ultrasound (CE-TRUS) with cadence-contrast pulse sequence (CPS) technology for the identification of prostate cancer. Urol Oncol. 2011;29(3):295–301. https://doi.org/10.1016/j.urolonc.2009.03.032.
17. Sedelaar JP, van Leenders GJ, Goossen TE, Hulsbergen-van der Kaa CA, van Adrichem NP, Wijkstra H, de la Rosette JJ. Value of contrast ultrasonography in the detection of significant prostate cancer: correlation with radical prostatectomy specimens. Prostate. 2002;53(3):246–53. https://doi.org/10.1002/pros.10145.
18. Mitterberger MJ, Aigner F, Horninger W, Ulmer H, Cavuto S, Halpern EJ, Frauscher F. Comparative efficiency of contrast-enhanced colour Doppler ultrasound targeted versus systematic biopsy for prostate cancer detection. Eur Radiol. 2010;20(12):2791–6. https://doi.org/10.1007/s00330-010-1860-1.
19. Taverna G, Morandi G, Seveso M, Giusti G, Benetti A, Colombo P, et al. Colour Doppler and microbubble contrast agent ultrasonography do not improve cancer detection rate in transrectal systematic prostate biopsy sampling. BJU Int. 2011;108(11):1723–7. https://doi.org/10.1111/j.1464-410X.2011.10199.x.
20. Xie SW, Li HL, Du J, Xia JG, Guo YF, Xin M, Li FH. Contrast-enhanced ultrasonography with contrast-tuned imaging technology for the detection of prostate cancer: comparison with conventional ultrasonography. BJU Int. 2012;109(11):1620–6. https://doi.org/10.1111/j.1464-410X.2011.10577.x.
21. Uemura H, Sano F, Nomiya A, Yamamoto T, Nakamura M, Miyoshi Y, et al. Usefulness of perflubutane microbubble-enhanced ultrasound in imaging and detection of prostate cancer: phase II multicenter

clinical trial. World J Urol. 2013;31(5):1123–8. https://doi.org/10.1007/s00345-012-0833-1.
22. Zhao HX, Xia CX, Yin HX, Guo N, Zhu Q. The value and limitations of contrast-enhanced transrectal ultrasonography for the detection of prostate cancer. Eur J Radiol. 2013;82(11):641–7. https://doi.org/10.1016/j.ejrad.2013.07.004.
23. Smeenge M, Mischi M, Laguna Pes MP, de la Rosette JJ, Wijkstra H. Novel contrast-enhanced ultrasound imaging in prostate cancer. World J Urol. 2011;29(5):581–7. https://doi.org/10.1007/s00345-011-0747-3.
24. Jiang J, Chen YQ, Zhu YK, Yao XH, Qi J. Factors influencing the degree of enhancement of prostate cancer on contrast-enhanced transrectal ultrasonography: correlation with biopsy and radical prostatectomy specimens. Br J Radiol. 2012;85(1019):e979–86. https://doi.org/10.1259/bjr/63794331.
25. Huang H, Zhu ZQ, Zhou ZG, Chen LS, Zhao M, Zhang Y, et al. Contrast-enhanced transrectal ultrasound for prediction of prostate cancer aggressiveness: the role of normal peripheral zone time-intensity curves. Sci Rep. 2016;6:38643. https://doi.org/10.1038/srep38643.
26. Guess HA, Arrighi HM, Metter EJ, Fozard JL. Cumulative prevalence of prostatism matches the autopsy prevalence of benign prostatic hyperplasia. Prostate. 1990;17(3):241–6. https://doi.org/10.1002/pros.2990170308.
27. Halpern EJ. Contrast-enhanced ultrasound imaging of prostate cancer. Rev Urol. 2006;8(Suppl 1):29–37.
28. Salvatore V, Borghi A, Piscaglia F. Contrast-enhanced ultrasound for liver imaging: recent advances. Curr Pharm Des. 2012;18(15):2236–52. https://doi.org/10.2174/138161212800099892.
29. de Castro Abreu AL, Ashrafi AN, Gill IS, Oishi M, Winter MW, Park D, et al. Contrast-enhanced transrectal ultrasound for follow-up after focal HIFU ablation for prostate cancer. J Ultrasound Med. 2019;38(3):811–9. https://doi.org/10.1002/jum.14765.

CEUS in Gynecology

12

Elena P. Fedotkina, Alexander N. Sencha, Alexey V. Pomortsev, Munir G. Tukhbatullin, Anatoly G. Bykov, Yulia Y. Dyachenko, Elena E. Fomina, Natalya I. Bayazova, and Polina L. Sheshko

Ultrasound is a rapid and feasible method for primary imaging in women's health. Doppler assessment of tumor vascularity significantly contributed to modern oncogynecology with the possibility to identify tumor neovascularization [1]. CEUS is superior to Doppler imaging in the assessment of perfusion and microvascularity. It is successfully applied in some parenchymal organs. However, its role in the diagnosis of the diseases of the female reproductive system remains underestimated.

12.1 Uterus

The main blood supply to the uterus, broad and round ligaments, Fallopian tubes, ovaries, and vagina is provided by the uterine artery, which originates from the internal iliac artery. It runs down and medially at the base of the broad ligament, crosses the ureter, and supplies a vaginal branch to the uterine cervix and vagina. Then it turns up to the upper corner of the uterus and travels along the attachment line of the broad ligament. It anastomoses with the uterine branch of the ovarian artery and forms an arterial arch between the leaves of the broad ligament. The branches of the uterine artery after entering myometrium are arranged parallel to the uterine outer surface and form the arcuate arteries.

Supplementary Information The online version contains supplementary material available at [https://doi.org/10.1007/978-3-030-91764-7_12].

E. P. Fedotkina · A. N. Sencha (✉)
Department of Visual and Functional Diagnostics, Federal State Budget Institution "National Medical Research Center for Obstetrics, Gynecology and Perinatology n.a. V.I.Kulakov", Moscow, Russian Federation

A. V. Pomortsev · Y. Y. Dyachenko
Department of Radiation Diagnostics, Federal State Budgetary Educational Institution of Higher Education "Kuban State Medical University", Krasnodar, Russian Federation

M. G. Tukhbatullin · E. E. Fomina · N. I. Bayazova
Department of Ultrasound Diagnosis, Kazan State Medical Academy, Kazan, Russian Federation

A. G. Bykov
Department of Gynecology, Federal State Budget Institution "National Medical Research Center for Obstetrics, Gynecology and Perinatology n.a. V.I.Kulakov", Moscow, Russian Federation

P. L. Sheshko
Department of Innovative Oncology and Gynecology, Federal State Budget Institution "National Medical Research Center for Obstetrics, Gynecology and Perinatology n.a. V.I.Kulakov", Moscow, Russian Federation

A. N. Sencha, Y. N. Patrunov (eds.), *Contrast-Enhanced Ultrasound*,
https://doi.org/10.1007/978-3-030-91764-7_12

The largest arteries are located between the outer and middle muscle layers, forming the stratum vasculosum. They give rise to numerous smaller radial arteries that continue into the spiral arteries (anastomosing capillaries) of the inner muscle layer, which provide blood supply to the endometrium. There are two types of endometrial arterioles. The basal layer of the endometrium is supplied with blood by basal arterioles, and spiral arterioles feed the functional layer, which changes in different phases of the menstrual cycle. The outflow from the endometrium is provided by spiral veins, which continue to the radial and arcuate veins of the myometrium with further drainage to the uterine branch of the uterine vein. The latter vein is located along the lateral surface of the uterus and merges with the vaginal branches composing the uterovaginal venous plexus. The venous blood further drains through the uterine veins to the internal iliac veins [1–4].

CEUS of the uterus can be performed with either transabdominal or transvaginal access, depending on the size of the lesion. Transvaginal CEUS is preferable in most cases. SonoVue® in the dose of 1.5–2.4 ml is used. The arterial phase lasts up to 40 s from the moment of UCA administration. The uterus is enhanced from the periphery to the central aspects. The uterine arteries enhance first, followed by the enhancement of the outer layers of the myometrium, the inner layers of the myometrium, ending with the endometrium (Fig. 12.1). The venous phase follows the arterial phase and is characterized by a gradual decrease in the intensity of contrast enhancement.

Endometrial hyperplasia occurs under the influence of estrogen. It is a borderline condition between normal endometrium and invasive carcinoma [5] and an often cause of postmenopausal bleeding. The diagnosis requires histopathological study, which divides hyperplasia into simple and complex, with or without atypia. With traditional echography, the differential diagnosis of benign endometrial changes and endometrial cancer is difficult. CEUS permits detailed assessment of the perfusion of the thickened endometrium and identification of the invasion. Endometrial hyperplasia with CEUS demonstrates delayed hypoenhancement as compared with normal myometrium (Fig. 12.2, Video 12.1).

As opposed to hyperplasia, endometrial cancer typically exhibits early heterogeneous hyperenhancement and faster washout (67 s) as compared with normal myometrium (76 s). In combination with the assessment of the course of arcuate arteries, it enables assessment of the invasion of carcinoma into the myometrium [6–9].

Quantitative analysis confirms this data [5]. Endometrial cancer is characterized by a shorter arrival and rise time, shorter time to peak, higher average peak intensity and enhancement intensity, shorter half clearing time, and shorter washout half-time (Table 12.1). Average peak intensity and enhancement intensity demonstrate higher diagnostic accuracy with an AUC of 0.963 and 0.951, respectively.

One common finding with traditional echography is an endometrial polyp, which is associated with a low risk of malignancy. An important aspect in its diagnosis is the assessment of the stalk. CEUS depicts not only the vascular pedicle but also the perfusion of the entire polyp. Polyp exhibits rapid enhancement in the arterial phase with prolonged washout. However, histopathology is necessary for the final diagnosis [6] (Fig. 12.3).

Uterine fibroid is a common benign tumor of the myometrium. CDI usually identifies peripheral vessels with a basket-like pattern. Small fibroids and the periphery of large fibroids are more biologically active than the myometrium [7, 8]. The perfusion within the tumor cannot be assessed with CDI and PDI. It is traditionally studied with CE-MRI. Some researchers [9] report that CEUS is not inferior to MRI in detecting tumor microvascularization. After UCA injection, microbubbles first appear in the fibroid periphery with a characteristic basket vascular pattern, followed by centripetal filling of the whole mass. After that, the myometrium and endometrium enhance (Figs. 12.4, 12.5, and 12.6, Video 12.2).

The boundaries of the tumor with CEUS are clear and distinct. In the venous phase, homogeneous enhancement usually persists with gradual washout. Heterogeneous enhancement may result

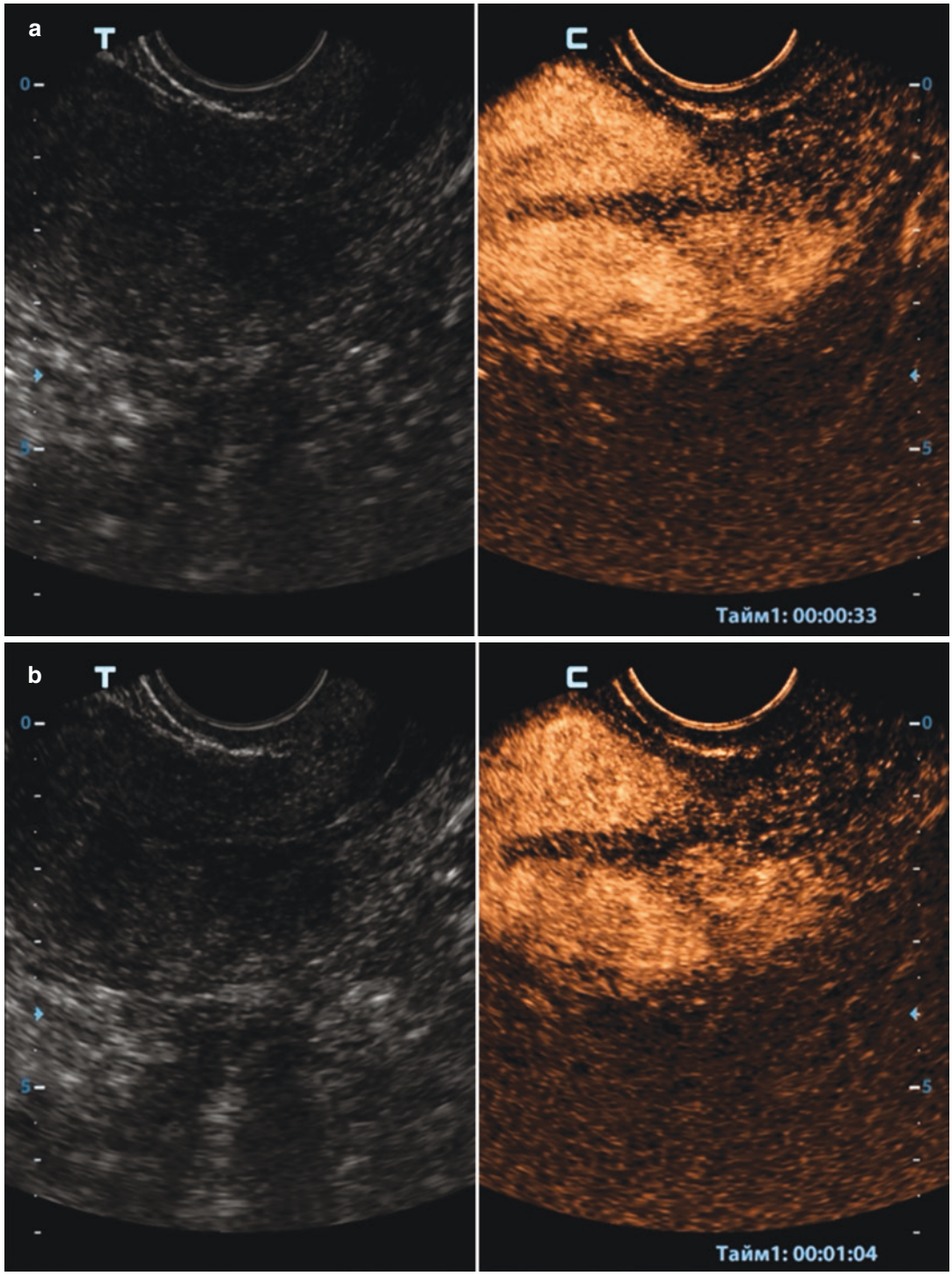

Fig. 12.1 Normal uterus. CEUS images. Intensive, symmetrical contrast enhancement of the myometrium and endometrium. (**a**) The arterial phase. (**b**) The venous phase. (**c**) Quantitative analysis of CEUS with TIC in different areas of the myometrium

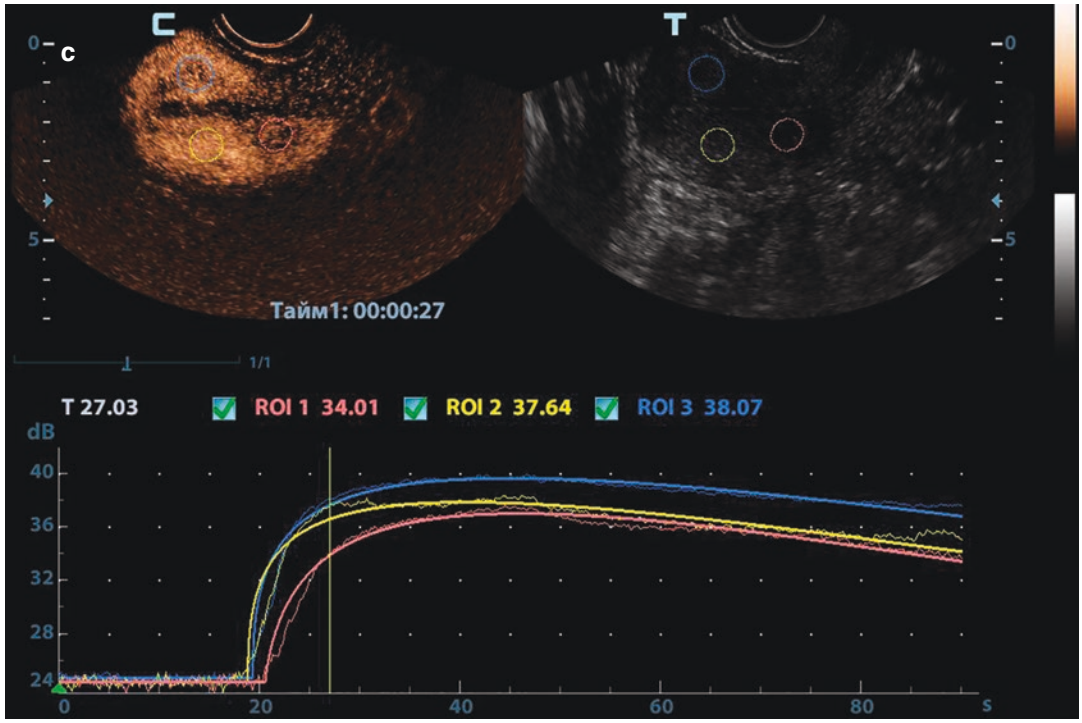

Fig. 12.1 (continued)

from the presence of avascular areas of degeneration or necrosis. In subserous and submucosal leiomyomas, the typical character of enhancement is preserved, and feeding arteries in the pedicle can be detected [10–12]. Leiomyoma sometimes demands differential diagnosis with leiomyosarcoma, which is a rare aggressive malignant tumor that develops from smooth muscle. Leiomyosarcoma is characterized by earlier and more intense contrast enhancement and lacks the typical basket vascular pattern.

Cervical cancer is a widespread malignancy and the fourth most common cause of cancer death among women worldwide. Active neoangiogenesis in the tumor serves as a poor prognostic factor for the recurrence and overall patients survival [13, 14]. In the initial stages, the arterial phase CEUS reveals a hyperenhancing lesion with further venous phase washout. As a result, in the venous phase, the tumor typically becomes hypoenhanced as compared to the myometrium (Fig. 12.7, Video 12.3).

The larger is the tumor, the more heterogeneous is the enhancement due to non-enhancing areas of necrosis [10]. With quantitative analysis, TIC in cervical cancer is characterized by higher peak intensity with shorter rise time and time to peak intensity than intact myometrium

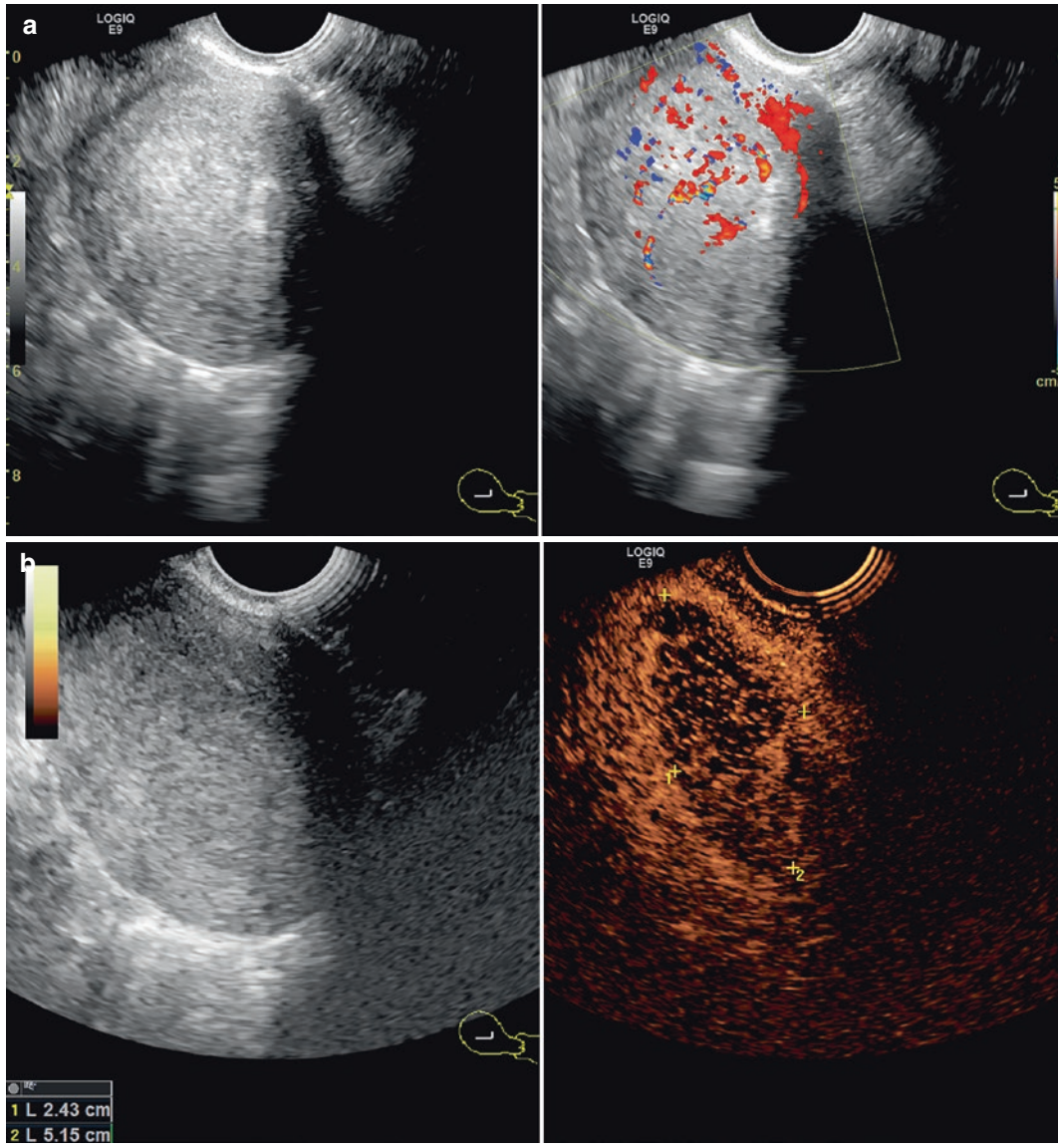

Fig. 12.2 Endometrial cancer. (**a**) CDI. (**b**) The venous phase CEUS image. Hypervascularization and indistinct contours of the thickened endometrium. (**c**) Quantitative analysis of CEUS with TIC in the endometrium (yellow and blue ROIs). (**d**) Coronal MRI. (**e**) Axial MRI

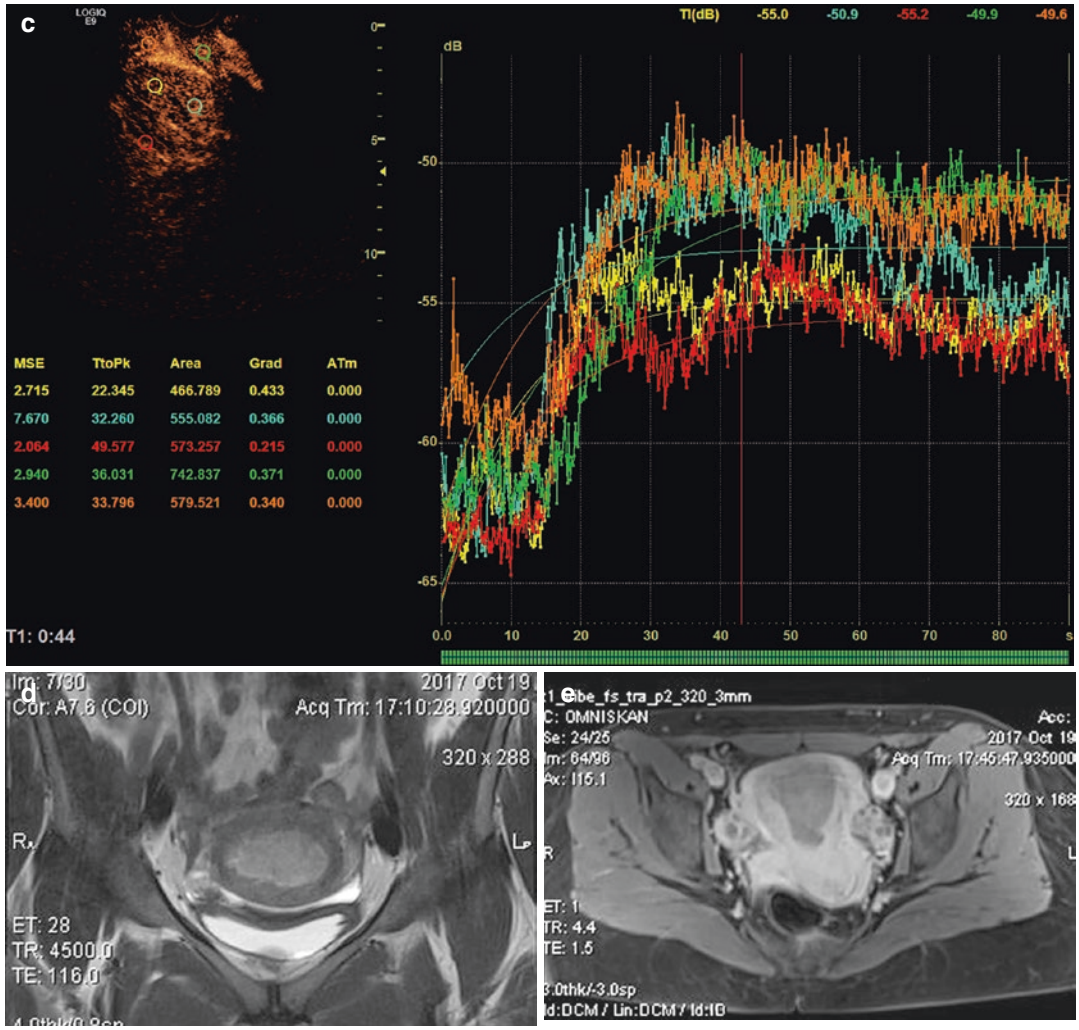

Fig. 12.2 (continued)

Table 12.1 The values of TIC in endometrial cancer and endometrial hyperplasia [5]

Parameter	Endometrial cancer	Endometrial hyperplasia	Sensitivity, specificity, AUC
PI (dB)	33.82 ± 3.17	26.80 ± 2.39	91.8%, 88.1%, 0.963
EI (dB)	25.05 ± 3.19	18.25 ± 2.57	85.7%, 92.9%, 0.951
AT (s)	11.79 ± 1.47	13.08 ± 1.24	64.3%, 75.5%, 0.741
TTP (s)	23.76 ± 2.39	28.56 ± 3.59	71.4%, 87.8%, 0.855
RT (s)	11.96 ± 2.76	15.48 ± 3.39	81.0%, 73.5%, 0.787
Was-out half-time (s)	71.26 ± 4.41	79.38 ± 6.27	71.4%, 81.6%, 0.848

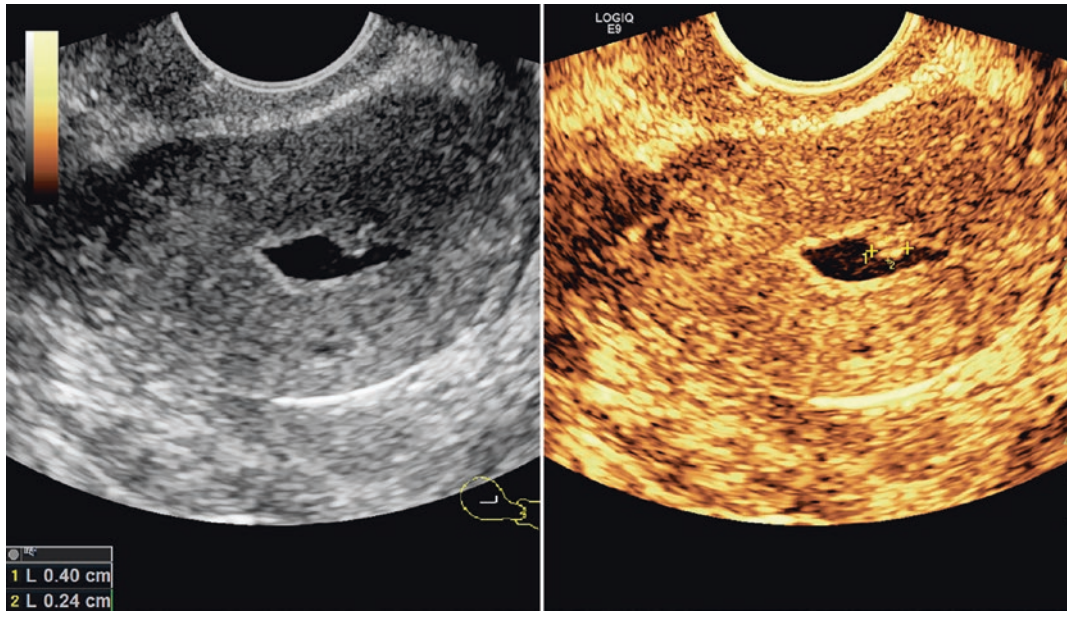

Fig. 12.3 Endometrial polyp. CEUS image

(Table 12.2). Besides, the intensity of tumor contrast enhancement correlates with the density of intratumoral vessels with the immunohistochemical study [15].

Focal and diffuse adenomyosis may cause pelvic pain, uterine bleeding, and implantation failures [16]. With CEUS, adenomyosis is characterized by a relatively rapid diffuse heterogeneous enhancement with hypoenhanced areas. This enhancement pattern is often referred to as "moth-eaten" [10] (Fig. 12.8, Video 12.4). It exhibits the sensitivity in the diagnosis of adenomyosis of 100% with the specificity of 83.3%. In the venous phase, adenomyosis exhibits diffuse contrast enhancement.

When analyzing the time-intensity curves, peak intensity and time to peak values showed the best accuracy. The peak intensity of contrast enhancement in adenomyosis is lower than in the intact myometrium (33.86 ± 1.89 dB vs. 37.39 ± 1.65 dB, respectively), which is probably due to the presence of hypoenhanced areas. The time to peak intensity in adenomyosis is longer than in the intact myometrium (22.30 ± 2.18 s vs.18.16 ± 2.67 s, respectively).

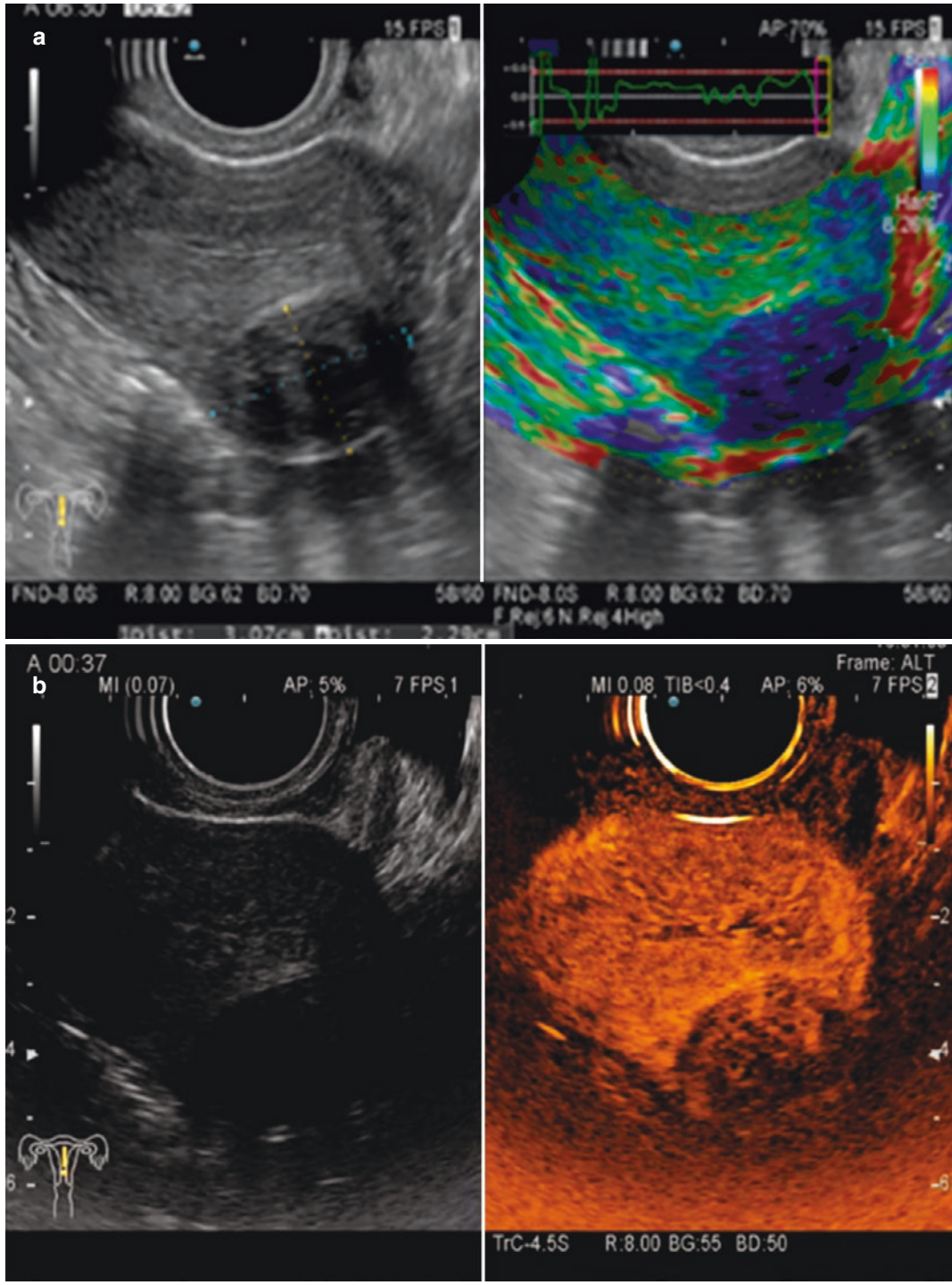

Fig. 12.4 Uterinefibroid. (**a**) Grayscale US and strain elastography. The hard pattern of the fibroid. (**b**) CEUS image in the arterial phase demonstrates vascularization of the lesion and its clear boundaries

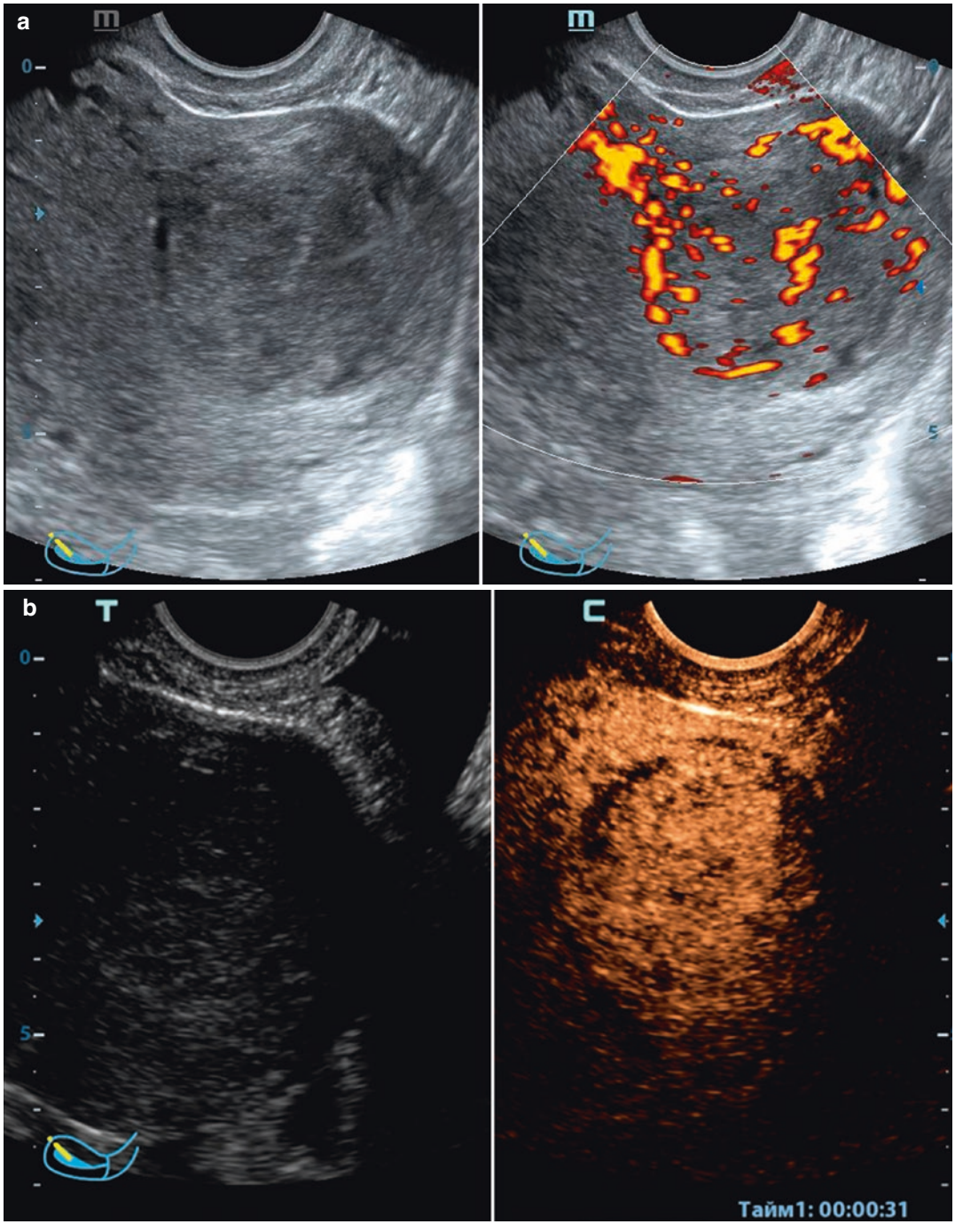

Fig. 12.5 Uterine fibroid. (**a**) Grayscale US and PDI. Intense vascularity of the fibroid. (**b**) CEUS image in the arterial phase demonstrates hyperenhancement of the lesion

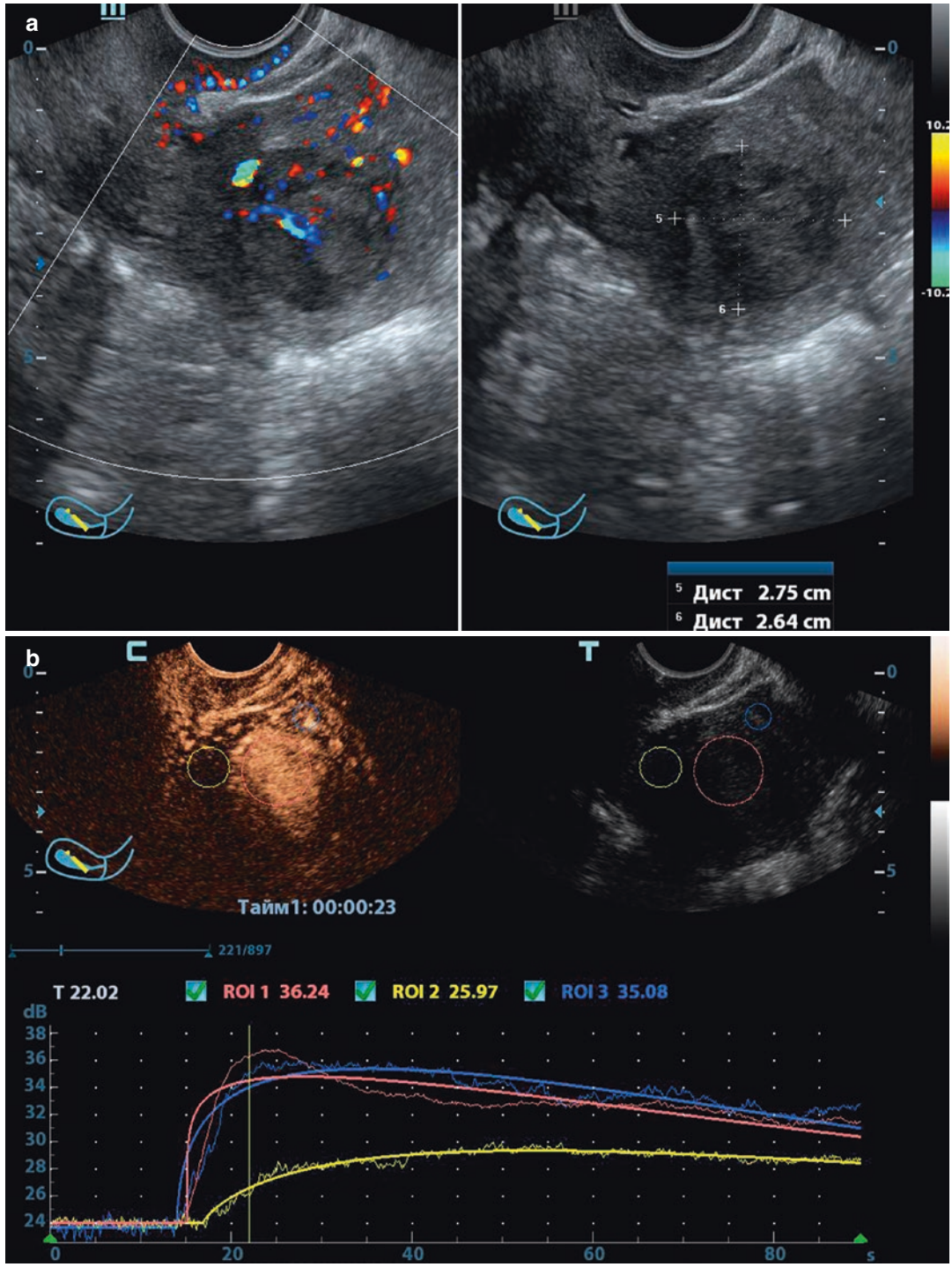

Fig. 12.6 Uterine fibroid. (**a**) Grayscale US and CDI. Moderate vascularity of the fibroid. (**b**) Quantitative analysis CEUS with TIC demonstrates hyperenhancement of the lesion (pink ROI)

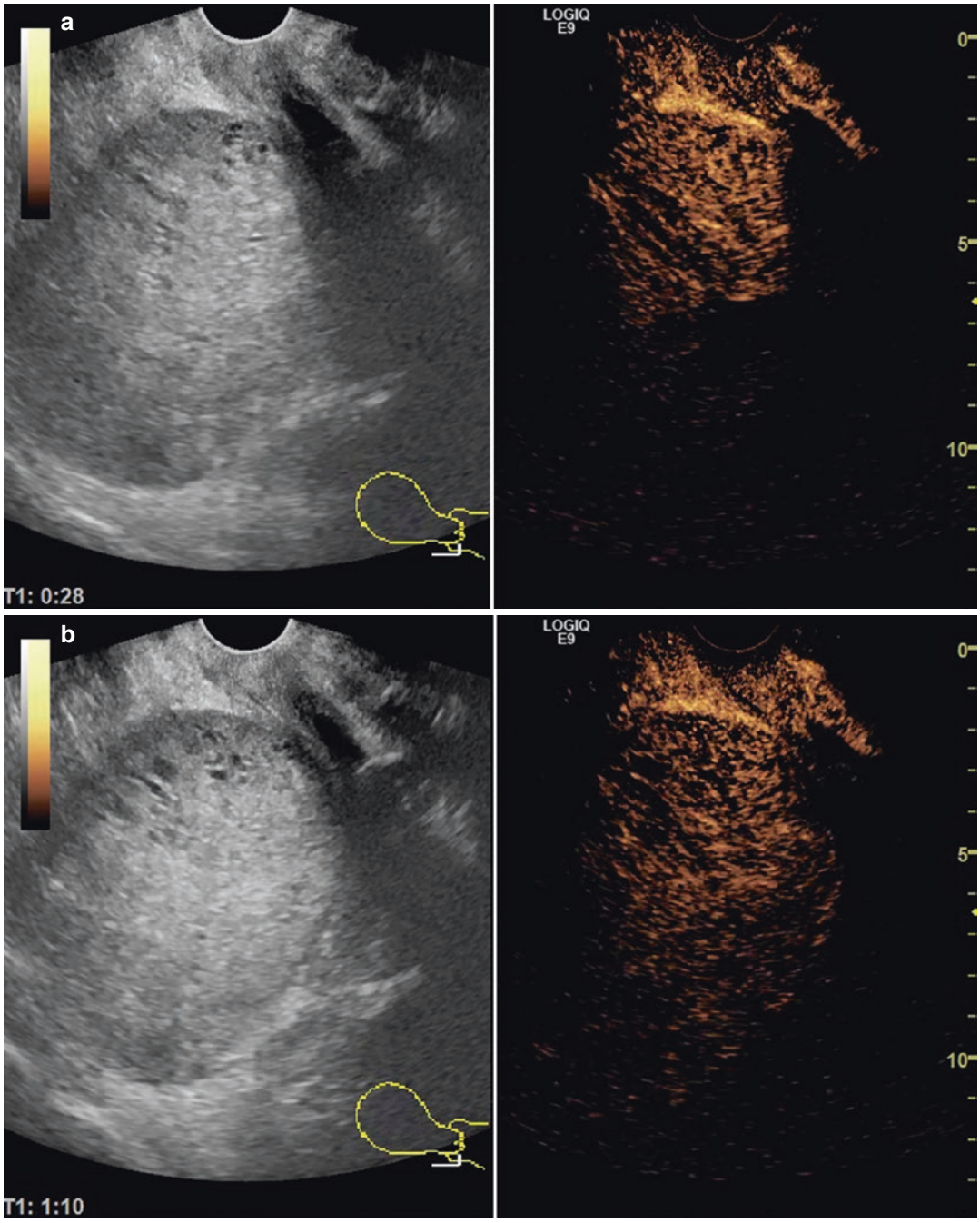

Fig. 12.7 Cervical cancer. (**a**) Arterial phase CEUS image. (**b**) Venous phase CEUS image

Table 12.2 Quantitative values of TIC in cervical cancer as compared with the reference zone [15]

Parameter	Peak intensity (%)	Rise time (s)	Time to peak intensity (s)	Mean transit time (s)
Cervical cancer	143.24 ± 54.54	9.36 ± 2.84	9.86 ± 3.00	100.95 ± 79.48
Reference area	100	17.49 ± 6.90	19.21 ± 7.97	121.12 ± 91.13

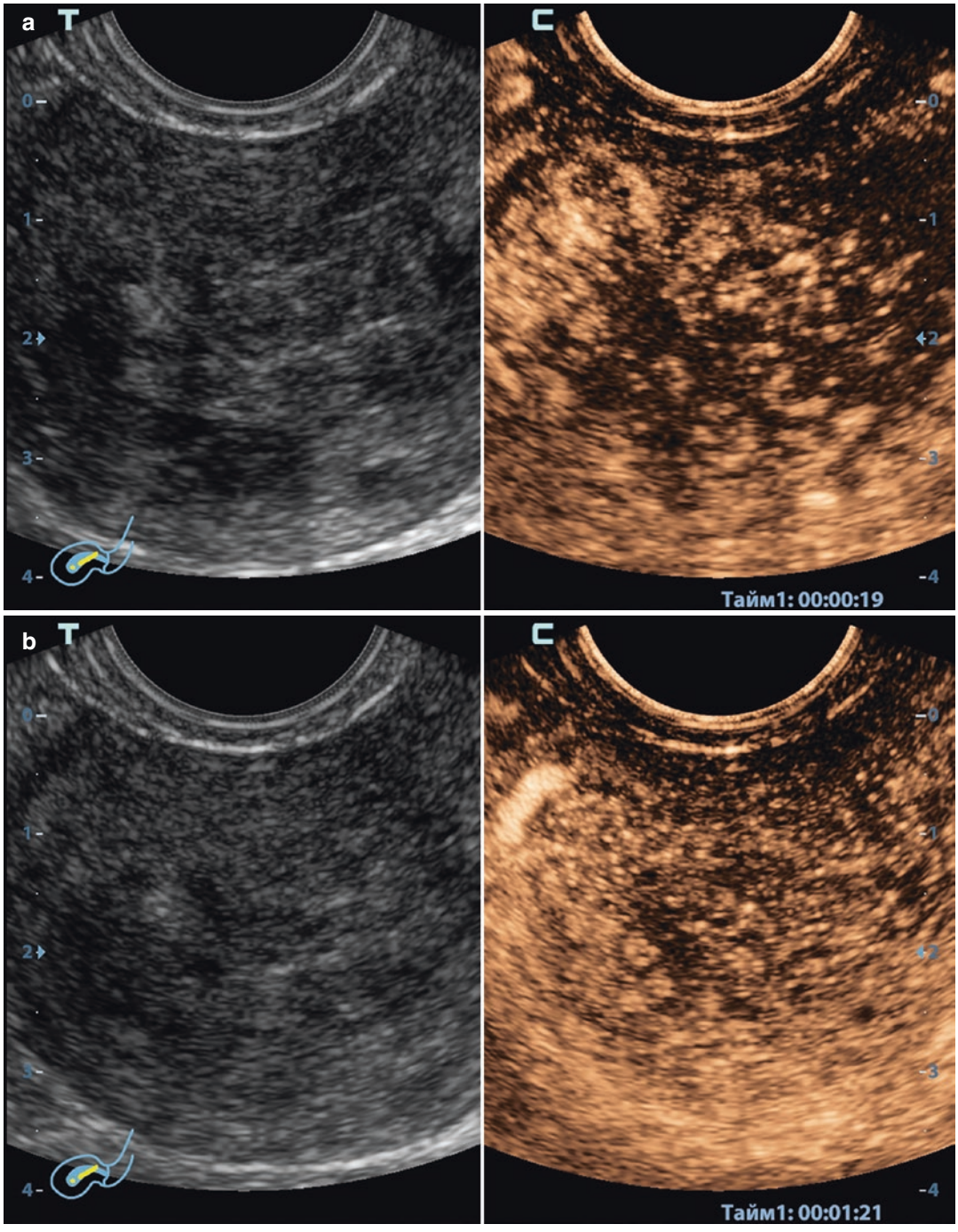

Fig. 12.8 Diffuse adenomyosis. (**a**) Arterial phase CEUS image. Irregular mild asymmetric enhancement of the myometrium. (**b**) Venous phase CEUS image. Diffuse contrast enhancement. (**c**) MRI, T1WI

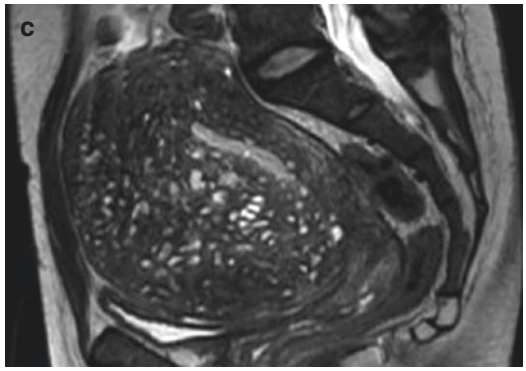

Fig. 12.8 (continued)

Another promising application of CEUS in gynecology is the evaluation of uterine artery embolization and ablation with high-intensity focused ultrasound (HIFU). With CEUS, it is considered that the areas without contrast enhancement are represented by necrotic tissue, whereas the enhancing areas—viable tissue. Therefore, CEUS immediately after the HIFU session detects the areas for additional ablation, which improves the treatment result. When comparing the ablation coefficient, measured as the ratio of non-enhanced fibroid volume to the total fibroid volume after HIFU treatment, a strong correlation between CEUS values with dynamic MRI was noted. It suggests CEUS as an alternative method for evaluation of the treatment effect [17]. Similar results were obtained for superselective embolization of the uterine arteries in patients with uterine fibroids [9].

12.2 Ovary

The ovaries are supplied with blood from the ovarian artery, which arises from the abdominal aorta. It sometimes may branch from the renal artery. It travels down with the ureter, passes in the suspensory ligament of the ovary to the upper part of the broad ligament of the uterus, and gives branches to the ovary and tube. The end section of the ovarian artery anastomoses with the uterine artery.

The ovary usually exhibits intense enhancement with CEUS, which is quite symmetrical with even and clear boundaries. The follicles demonstrate a persistent perfusion defect of a rounded shape (Fig. 12.9, Video 12.5).

Functional and paraovarian cysts are common findings with traditional echography in fertile women and typically cause no diagnostic difficulties. Some questions may arise if the cyst contains echogenic structures. In simple cysts, CEUS reveals no contrast enhancement within the cystic lumen, which excludes malignancy. Mild enhancement of the thin walls can be identified [18, 19] (Fig. 12.10, Video 12.6).

An endometriotic cyst is a manifestation of ovarian endometriosis. Irregular wall thickening and parietal echogenic component complicate its differentiation with cystadenoma and cystadenocarcinoma. Additionally, there is a risk of malignant transformation of endometrioma in postmenopausal women [4]. With CEUS, endometriotic cyst exhibits annular hyperenhancement of the walls in the arterial phase with slow washout in the venous phase and non-enhancing contents (Fig. 12.11, Video 12.7).

Borderline ovarian tumors comprise a number of lesions, which exhibit atypical epithelial proliferation without stromal invasion. They are usually represented by serous or mucinous variants. Endometrioid, Brenner, and clear cell variants are rare. With CEUS, they are characterized by hyperenhancement of the solid component with prolonged washout, which does not exclude their malignancy. Therefore, the diagnosis usually implicates histopathology [10, 18] (Fig. 12.12).

Ovarian cancer is an important problem in oncogynecology. Evaluation of neoangiogenesis and the density of microvessels in the tumor is important for assessing the prognosis. The sensitivity and specificity of CEUS in the differential diagnosis of benign and malignant ovarian tumors were 89–96% and 91–97%, respectively [18, 19]. Malignant tumors exhibit earlier heterogeneous hyperenhancement (Fig. 12.13 and Video 12.8).

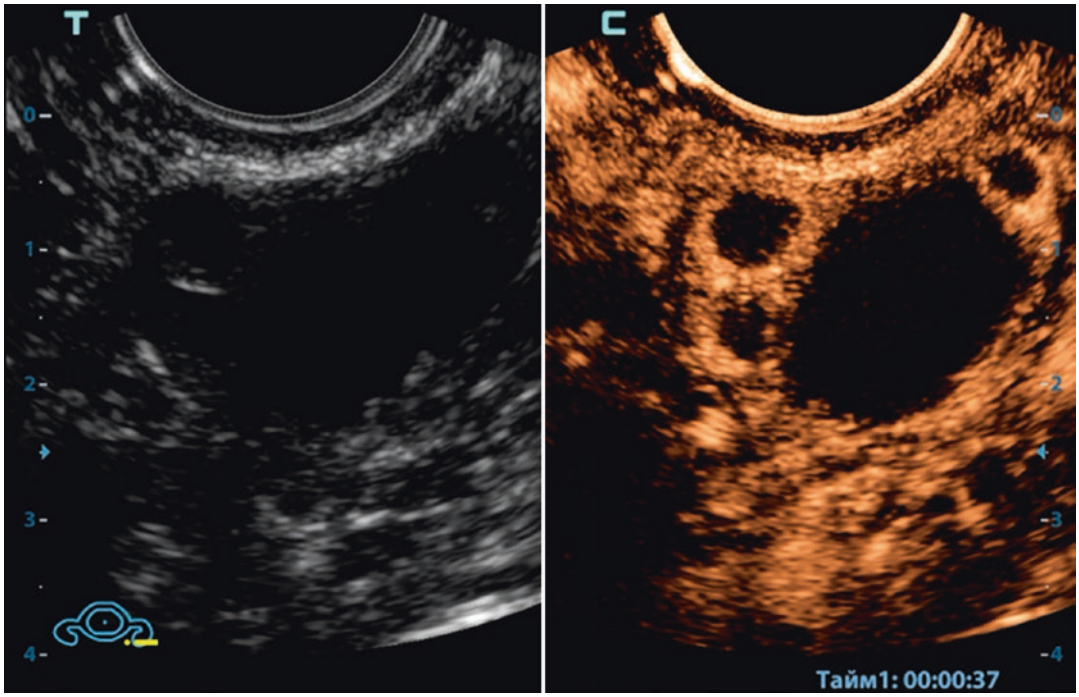

Fig. 12.9 Normal ovary. The arterial phase CEUS image. Enhancement of the ovarian stroma with non-enhancing follicles. Note a larger dominant follicle

Benign tumors demonstrate synchronous or late homogeneous arterial isoenhancement. Both benign and malignant lesions are hypoenhanced in the venous phase. In the study [20], which quantitatively analyzed CEUS with UCA Definity, malignant lesions had a longer half washout time (139.9 ± 43.6 vs. 46.3 ± 19.7 s) when compared with enhancing benign lesions. Greater peak enhancement (23.3 ± 2.8 vs. 12.3 ± 3.9 dB) and AUC (2012.9 ± 532.9 vs. 523.8 ± 318 s^{-1}) quantitatively confirmed intense perfusion of ovarian malignancies. Ovarian germ cell tumors also demonstrate heterogeneous hyperenhancement with penetrating vessels [10].

CEUS with the study of ovaries can confirm the ovarian torsion and assess its severity. Incomplete ovarian torsion is characterized by low enhancement of the ovarian tissue. The absence of enhancement indicates a complete ovarian torsion. The volume of enhanced areas within the ovary is related to its viability [10].

Currently, single reseachers attempt to integrate CEUS in GI-RADS (gynecological imaging reporting and data system) for evaluation of the ovarian lesions [21].

Despite a certain potential, the place of CEUS in the diagnostic flowchart in gynecological patients is currently not specified. The EFSUMB Guidelines and Recommendations for the Clinical Practice of Contrast-Enhanced Ultrasound (CEUS) in Non-Hepatic Applications [22] indicate that there are no recommended gynecological clinical indications for the use of CEUS, despite the finding that the absence of any enhancement in adnexal masses corresponds to benign lesions. However, according to the guidelines, intra-cavity administration of UCA can be used to determine tubal patency.

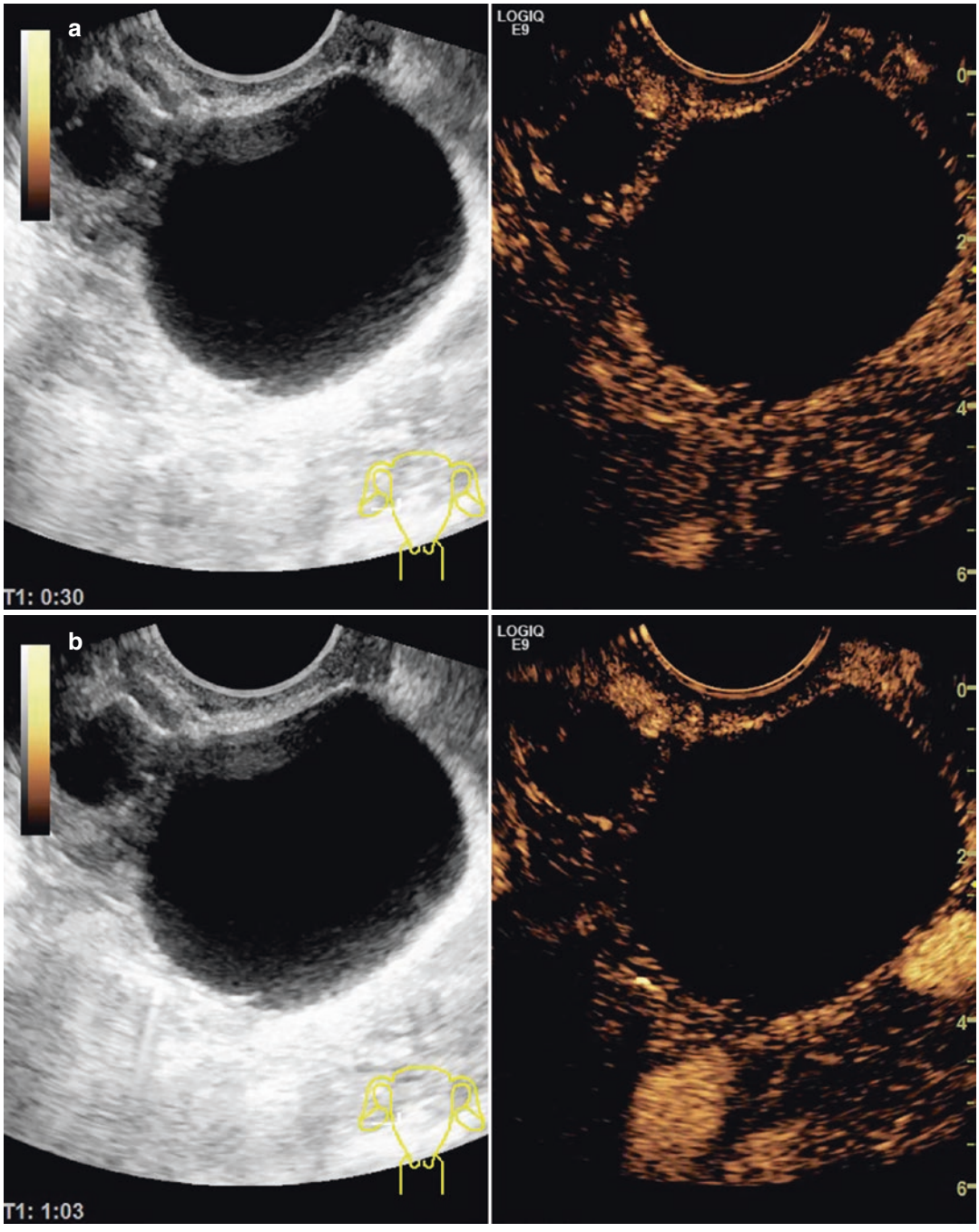

Fig. 12.10 Ovarian serous cystadenoma. CEUS images demonstrate a perfusion defect. (**a**) The arterial phase. (**b**) The venous phase

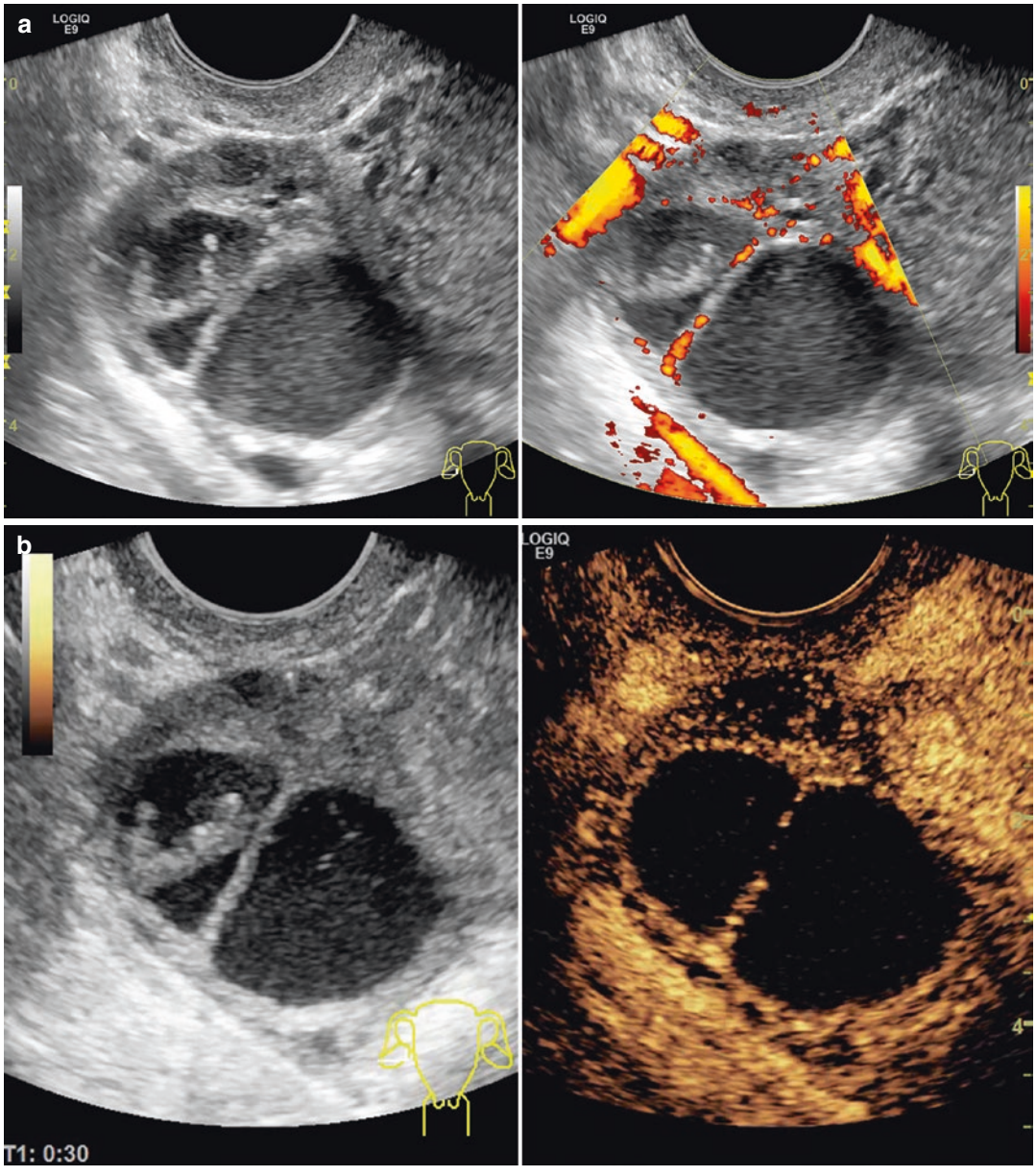

Fig. 12.11 Endometriotic cysts of the ovary. (**a**) Grayscale and PDI. (**b**) The arterial phase CEUS image demonstrates the enhancement of the cystic walls, even boundaries, and the avascularity of the inner contents. (**c**) Example 2 of an endometriotic cyst. (**d**) Example 3 of an endometriotic cyst

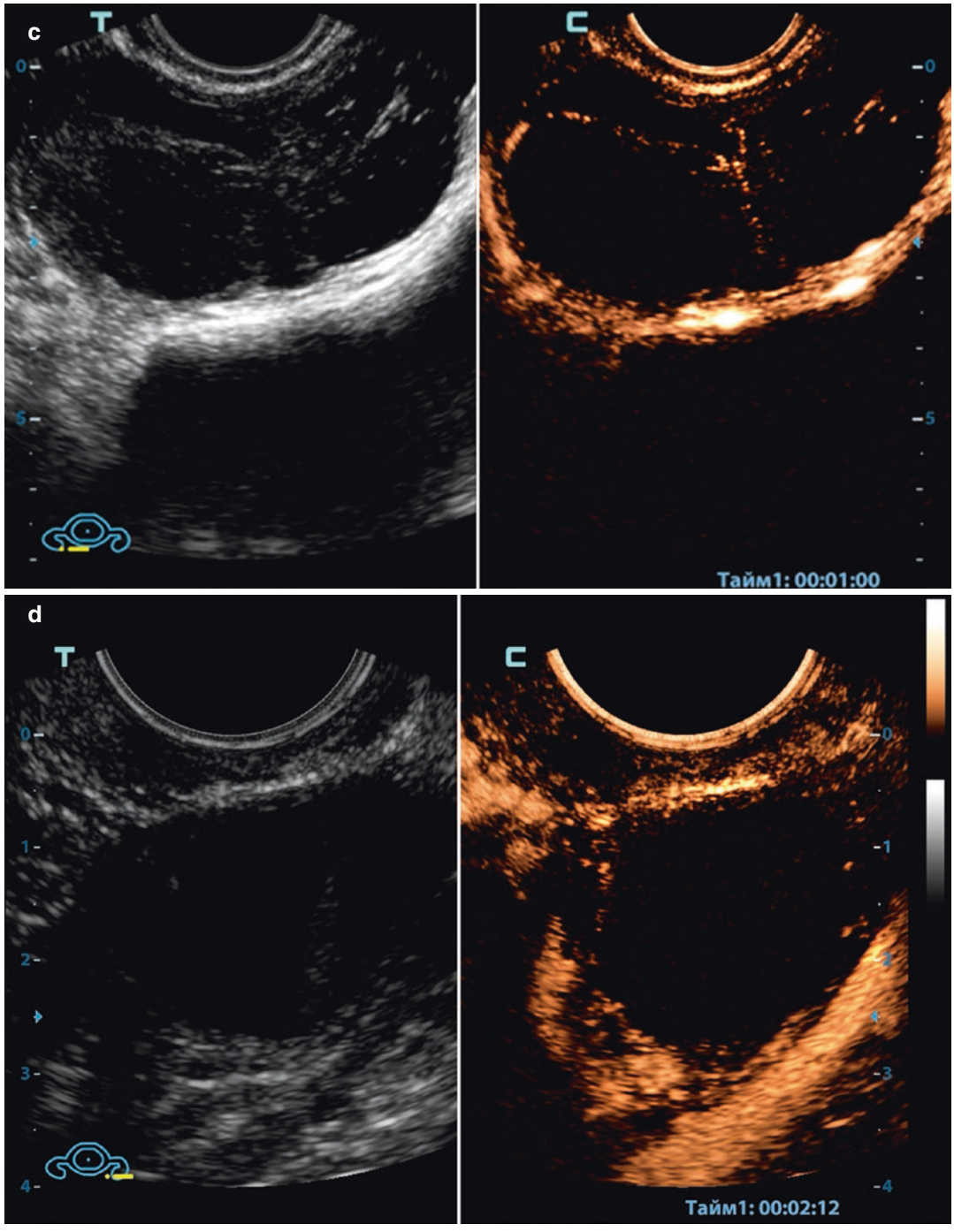

Fig. 12.11 (continued)

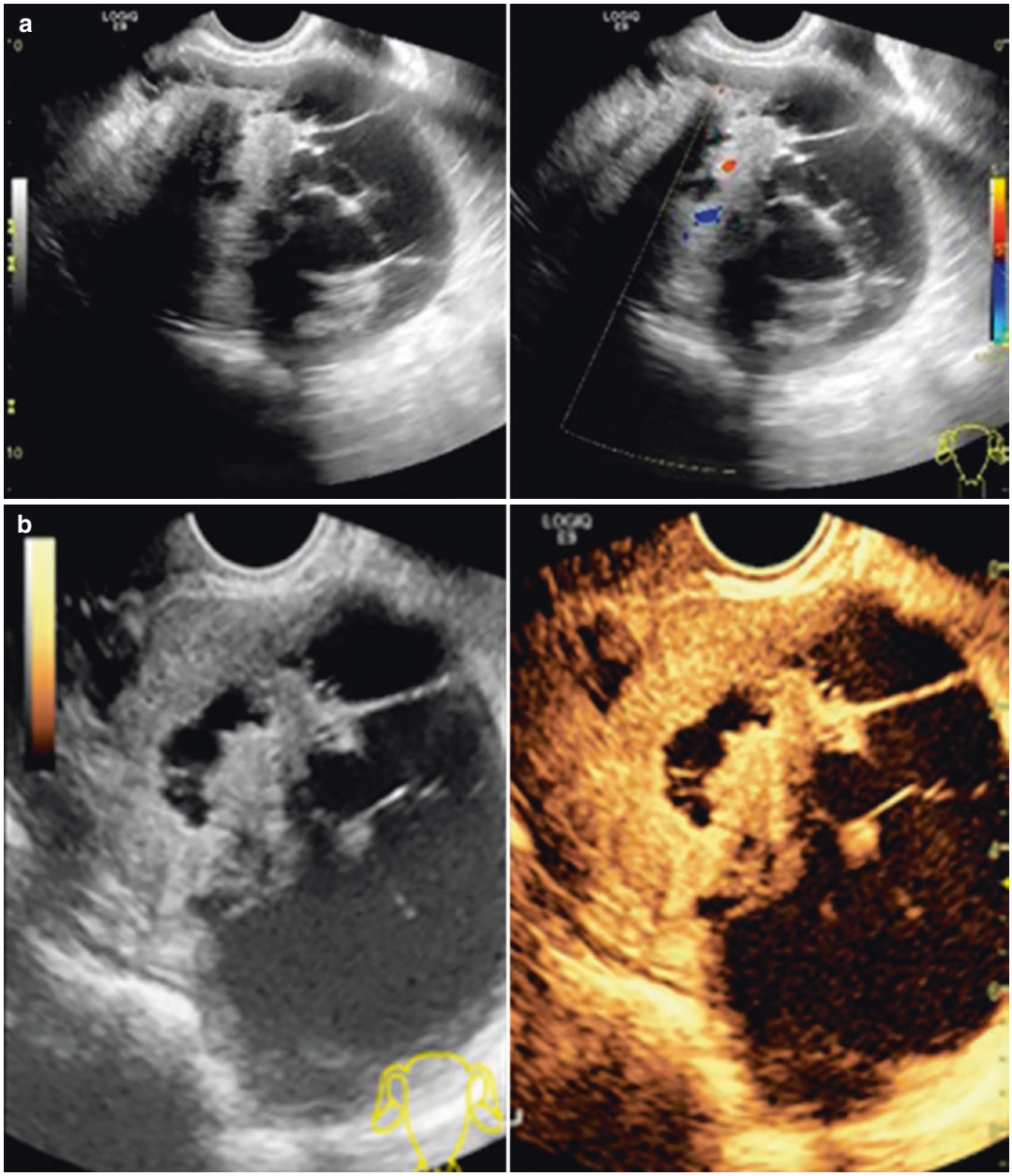

Fig. 12.12 Borderline ovarian tumor. (**a**) Grayscale and CDI. (**b**) The arterial phase CEUS image demonstrates the hyperenhancement of the solid component and regular boundaries of the lesion

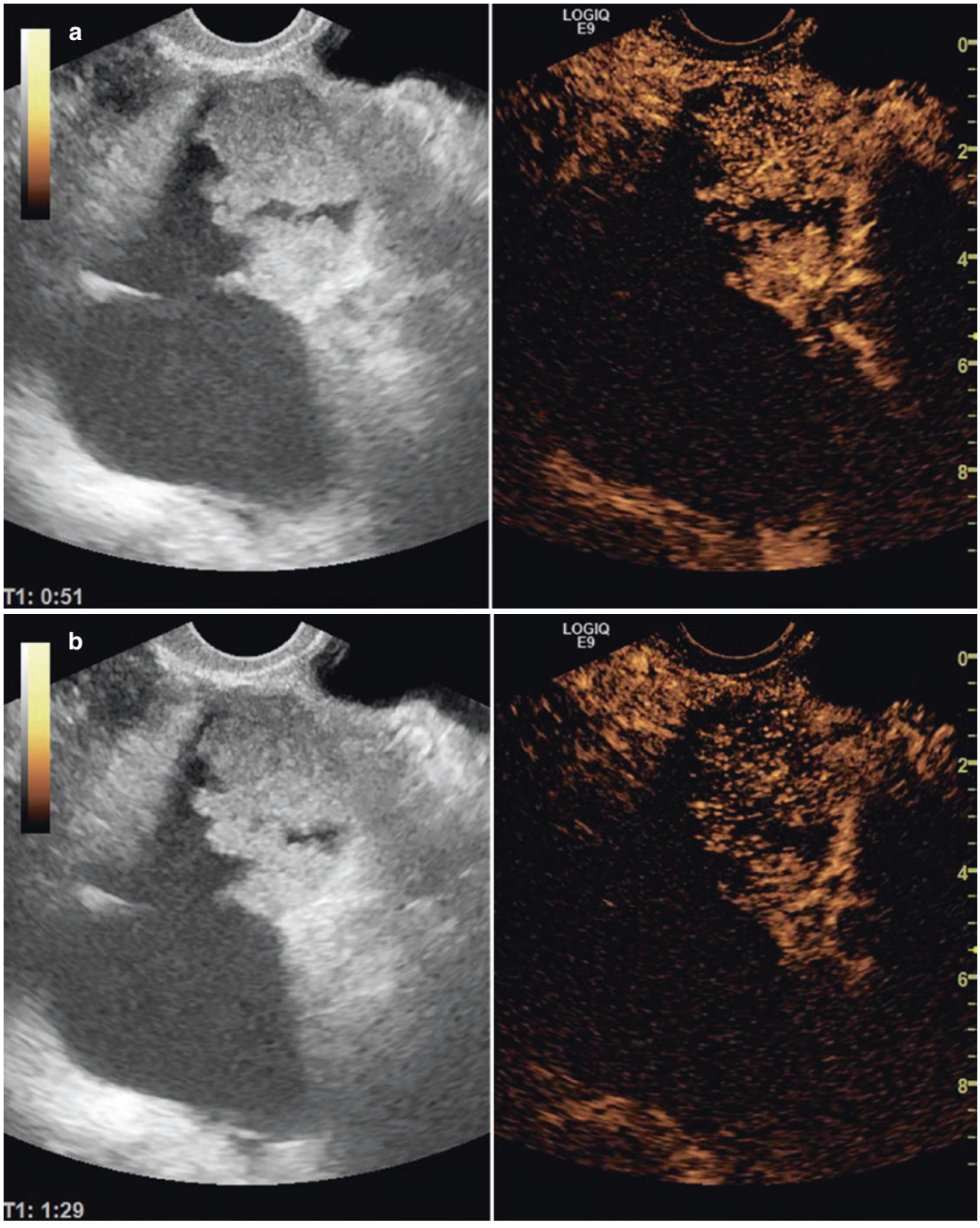

Fig. 12.13 Ovarian cancer. Irregular shape and enhancement of the solid component. (**a**) The arterial phase CEUS image. (**b**) The venous phase CEUS image

12.3 Hystero-Salpingo-Contrast Sonography

Female infertility is often a consequence of tubal and peritoneal factors, which account for 30–50% of cases [23–25]. Fallopian tube patency and the uterine cavity may be accurately assessed with imaging methods. One technology is multiparametric echography, which has an optional UCA application [26–28].

Hystero-salpingo-contrast sonography (HyCoSy) is a method of ultrasound imaging based on the introduction of a liquid contrast medium into the uterine cavity under the control of transvaginal echography, which permits the real-time diagnosis of structural abnormalities in the uterine cavity, evaluation of the anatomical and functional state of the fallopian tubes and paraovarian space.

For HyCoSy, both anechoic (saline) and echo-positive (e.g. SonoVue®) contrast agents can be used.

There are the following indications for HyCoSy:

- assessment of the tubal patency in the diagnosis of infertility,
- habitual miscarriage,
- abnormal uterine bleeding,
- the suspicion of endometrial polyps, submucous fibroid, or intrauterine adhesions,
- assessment of the scar on the uterus after cesarean section,
- poor imaging of the uterine cavity with transvaginal US or detection of local or diffuse thickening of the endometrium,
- congenital abnormalities of the uterus.

There are the following contraindications to HyCoSy:

- progressive pregnancy,
- malignant lesions of the reproductive system,
- inflammatory diseases of the pelvic organs, inclusive of salpingitis and hydrosalpinx.

Before HyCoSy, the case history is clarified and the transvaginal US of the pelvic organs is performed. Voluntary informed consent from the patient is necessary.

HyCoSy in fertile women is performed in the proliferative phase of the menstrual cycle (7–11 days). In patients with irregular menstrual cycles, the procedure should be performed only after a negative beta hCG blood pregnancy test. The patient is recommended to take an oral antispasmodic drug 15–30 min before the study to eliminate possible tubal spasms.

The HyCoSy procedure, like the standard CEUS, consists of several stages, as follows:

1. Preparatory stage
   - interview the patient, revise case history, and obtain informed consent for the procedure,
   - position the patient such a way to ensure convenient manipulations,
   - perform preliminary conventional US and determine the target area,
   - introduce and fix a HSG catheter,
   - pre-setup US equipment to contrast mode and make necessary adjustments,
   - prepare the UCA and make it ready for intravenous administration.
2. HyCoSy performance
   - introduce UCA into the uterine cavity through the catheter,
   - ensure simultaneous CEUS study with constant cine loop recording,
   - finish the procedure and cine loop recording once the required clinical information has been obtained.
3. Post-processing stage
   - revise the cine loop for further clarification if necessary, conduct quantitative analysis,
   - discuss the study results and make a report,
   - define further recommendations and consult the patient on the study result.

HyCoSy is performed in the conditions of the manipulation room and demands an US scanner with a transvaginal probe and a contrast option.

The patient is in a supine position with her legs bent at the knee and hip joints. The procedure may follow several stages. A two-stage

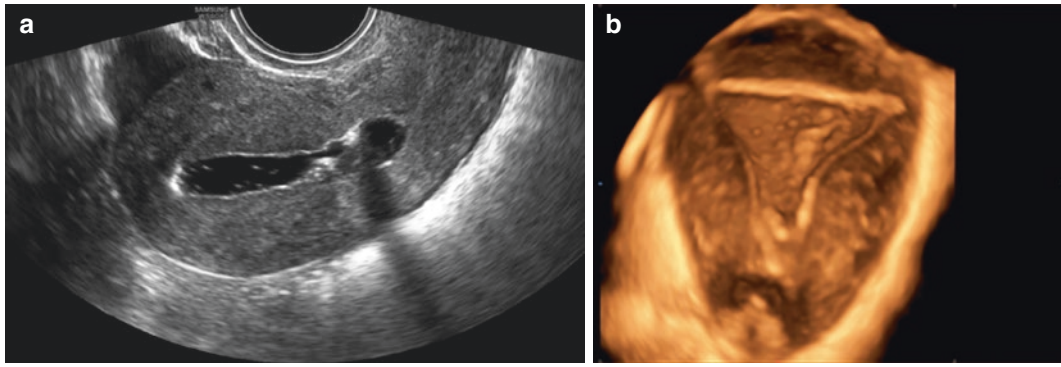

Fig. 12.14 HyCoSy with saline. Normal uterine cavity. (**a**) Grayscale US image. (**b**) 3D volume reconstruction image of the uterine cavity

HyCoSy procedure has been suggested [29, 30], which utilizes sequential use of two types of US media. Anechoic saline is used first to assess the condition of the uterine cavity and tubes followed by echopositive SonoVue® in ambiguous cases.

HyCoSy passes the following steps:

1. overview the pelvic organs with the transvaginal US,
2. install a disposable Cusco's speculum, expose the cervix, prepare the vagina and cervix with an antiseptic solution,
3. install a soft 5–7 Fr balloon HSG catheter through the cervix into the uterine cavity and inflate the balloon of the catheter with 1.5–2 mL sterile saline to secure the catheter,
4. introduce echonegative contrast agent (sterile saline) into the uterine cavity in a volume that allows for a 1.0 cm divergence of the anterior and posterior uterine walls to reliably outline the uterine cavity (Fig. 12.14).
5. The tubal patency with anechoic contrast is evaluated according to the following criteria:
   - accumulation of the contrast medium and air bubbles in the periovarian space,
   - turbulent fluid movement in the projection of the fimbrial part of the fallopian tube,
   - appearance of free fluid in the recto-uterine pouch indicates the free patency of the fallopian tube.

After the first stage is completed, prepare SonoVue® the standard way by adding 5 ml of saline to the vial with a dry substance. The technology of dilution of the SonoVue® lyophilisate is the same as for its intravenous use. Take 0.5 ml of the ready suspension into a syringe and additionally fill it with 0.9% normal saline up to 5.0 ml. The obtained fluid is introduced into the uterine cavity at the second stage of the study.

Normally, the uterine cavity is triangular with the apex pointing to the cervix. The base of the triangle corresponds to the uterine fundus. It may have a slightly concave or convex contour. With a tight filling, the uterine cavity boundaries are smooth and clear. UCA is uniformly distributed within the cavity without filling defects. In general, the shape of the uterine cavity does not depend on the position of the uterus and its contractions. The size depends on many aspects, such as the age, history of childbirth, etc. The cervical canal often has a fusiform shape and a width of about 3–4 mm.

The fallopian tubes originate at the lateral parts of the fundus of the uterus. They normally look like winding structures 2–6 mm in width and 10–12 cm long, located along with the upper parts of the broad ligaments of the uterus. Routine echography hardly identifies normal fallopian tubes. They are better imaged on the background of free fluid in the pelvis.

However, HyCoSy image of the fallopian tubes differs from the same in routine echogra-

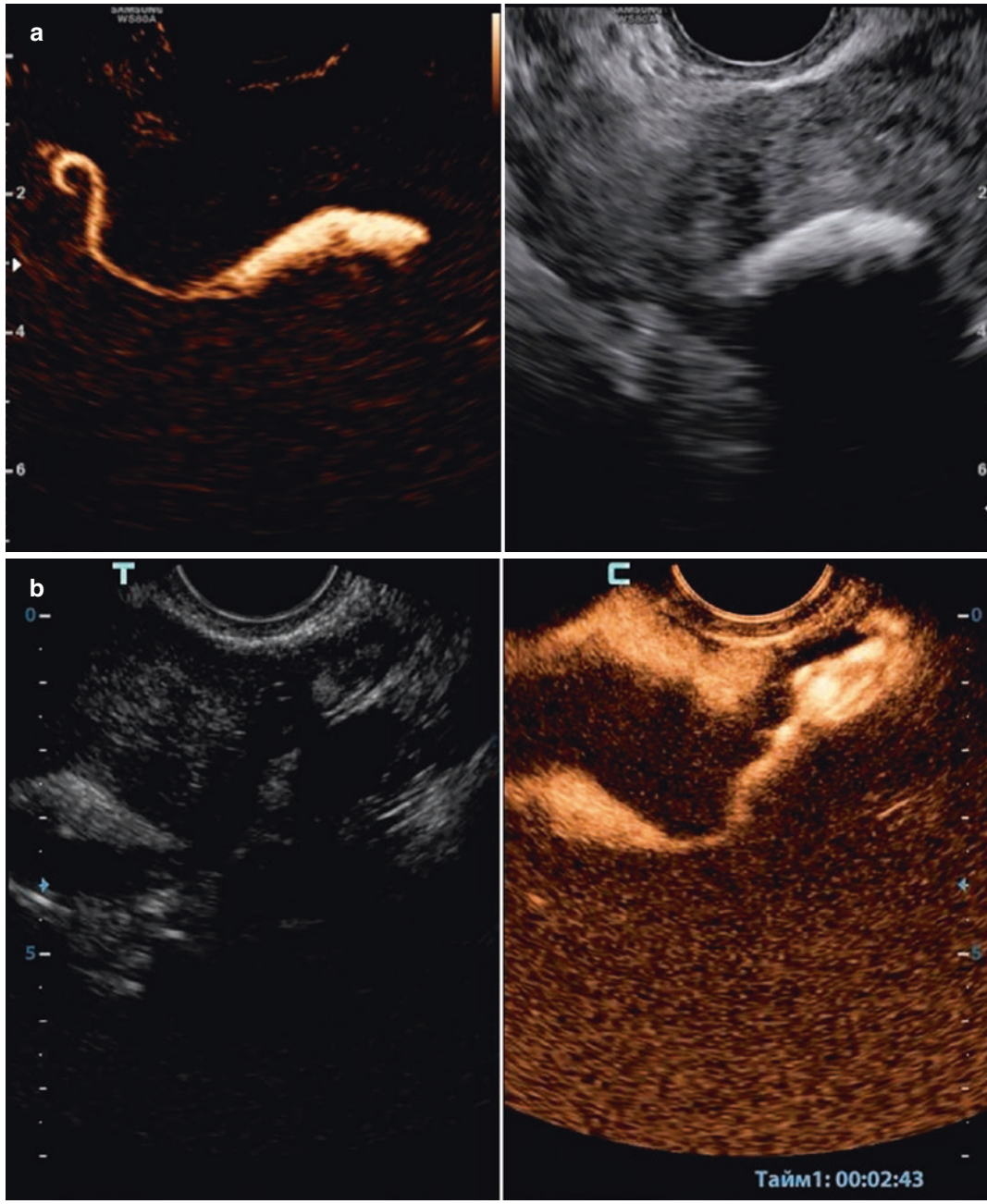

Fig. 12.15 HyCoSy images. Normal fallopian tubes. (**a**) Patient A CEUS image. (**b**) Patient B CEUS image

phy. SonoVue® depicts the lumen and is visualized as a hyperintense substance, which moves from the uterine cavity within the fallopian tube (Fig. 12.15, Videos 12.9 and 12.10).

The length of the first (interstitial) tubal segment is below 12 mm. The isthmic part is the longest and thinnest. With the enhancement, its width is about 1 mm. It starts from the interstitial segment and passes into the ampullary. The ampullary segment is the widest one, up to 10–12 mm. It approaches the ovary and ends with the infundibulum and fimbriae.

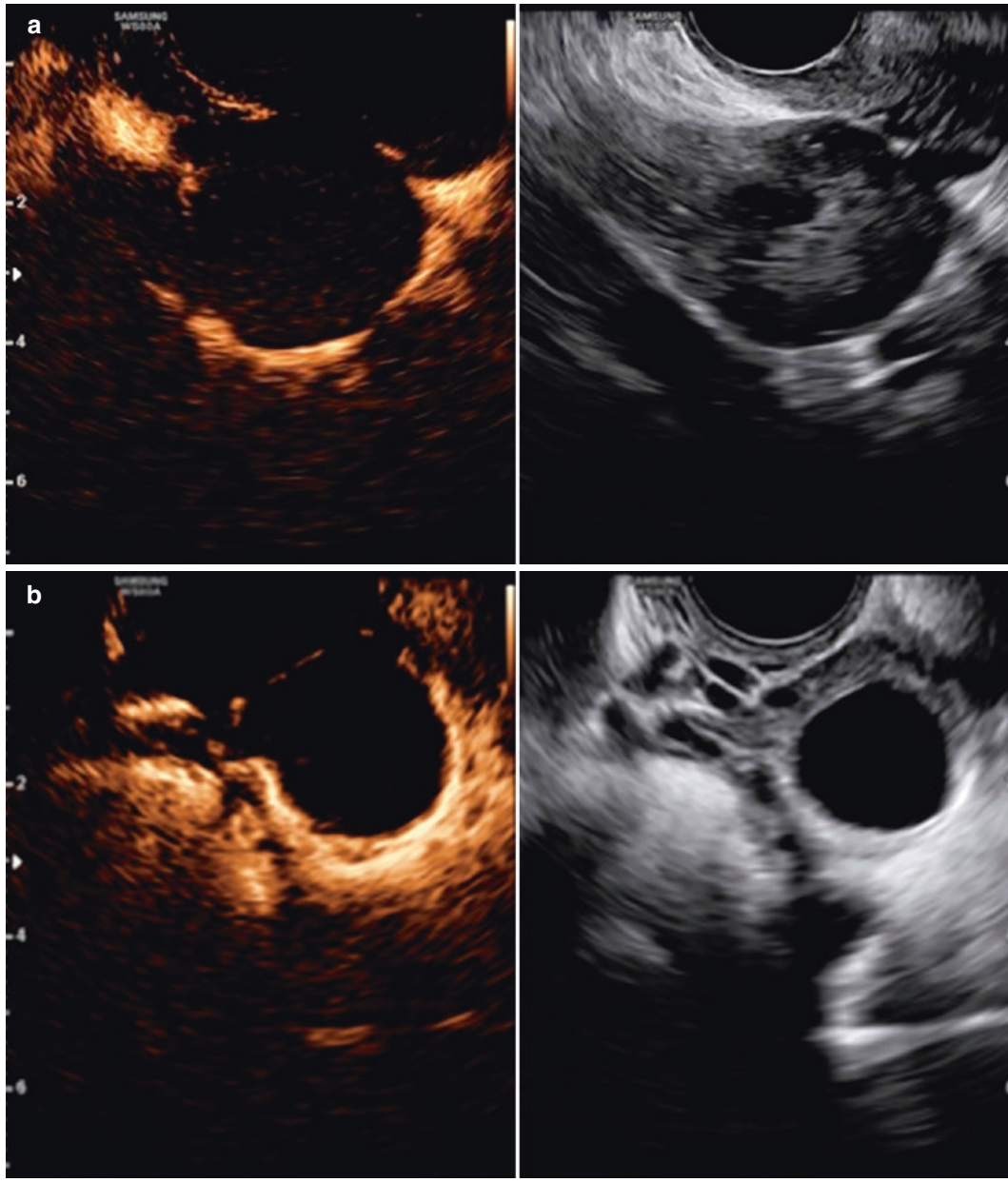

Fig. 12.16 HyCoSy images. Normal tubal patency with the contrast agent identified around the ovary. (**a**) Patient A. (**b**) Patient B

Normal fallopian tubes are well visualized with HyCoSy. The passage of SonoVue® through the fallopian tubes and the appearance of hyperintense substance in paraovarian and rectouterine spaces indicate free tubal patency (Fig. 12.16).

The introduction of a diluted SonoVue® leads to the same reliable enhancement of the tubal lumen as with higher concentrations. Fallopian tubes are often tortuous, and it is impossible to visualize their entire length in a single two-dimensional image. Three-dimensional recon-

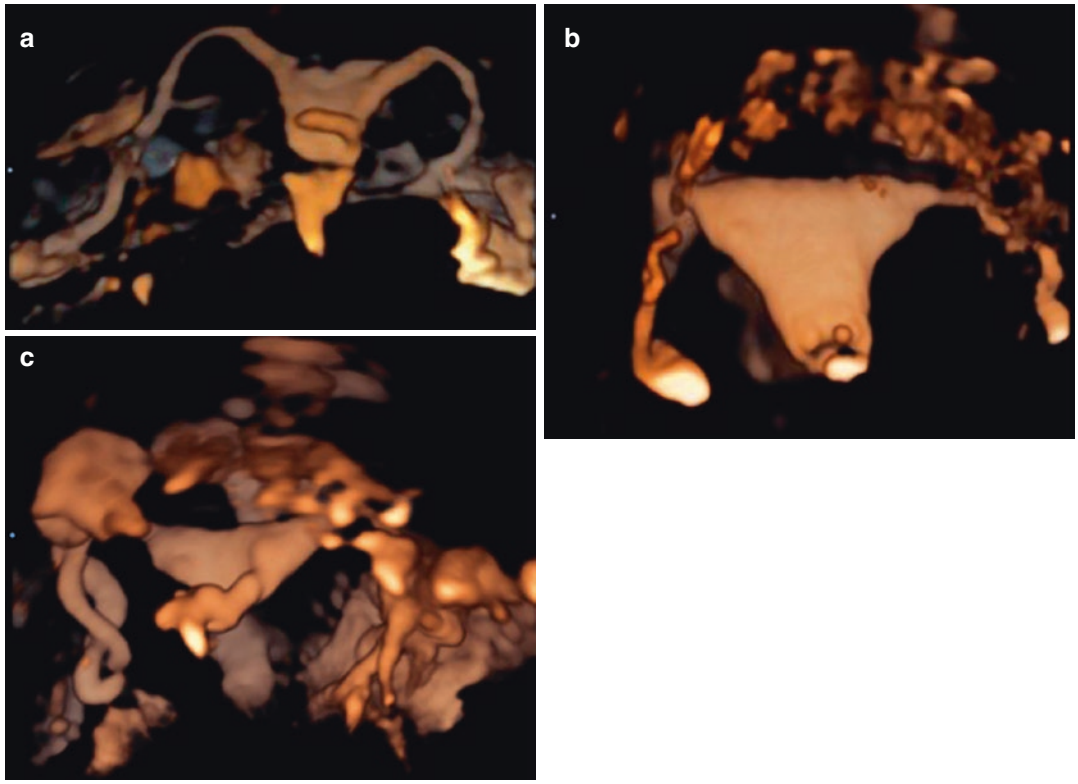

Fig. 12.17 HyCoSy images. Normal tubal patency. (**a**–**c**) Different examples in 3D-contrast mode

struction significantly improves visual perception (Fig. 12.17).

Once the required clinical information has been obtained, the catheter is removed from the uterine cavity, and the HyCoSy procedure is considered complete.

During and after HyCoSy, a cine loop is being recorded, which enables post-processing, delayed reassessment, transfer, and digital archiving. The last step assumes a description of the study and the creation of the report.

Inflammatory disease or traumatic injury of pelvic organs may be accompanied by edema and adhesions, which involve the fallopian tubes. Those lead to tube blockage and/or dilatation with fluid accumulation. Infection in the fallopian tube results in salpingitis and the adhesive process [25]. A pronounced inflammatory process leads to fimbrial adhesions, atrophy of the ciliated epithelium, an increase in the number of secretory cells and ends up with impaired fallopian tube motility [27]. The combination of both the accumulation of fluid in a closed space and the increased activity of secretory cells leads to the progression of the inflammatory process with the formation of the sactosalpinx [24]. The adhesions with fibrous tissue between the visceral and parietal peritoneum of the pelvis affect the anatomical and functional state of the internal genitalia, which is accompanied by chronic pelvic pain syndrome, dyspareunia, dysmenorrhea, and impaired function of neighboring organs [26, 31, 32].

Tubal obstruction is diagnosed with HyCoSy if the UCA fails to pass through the lumen and does not appear in the recto-uterine pouch and/or near ovaries. It was reported that 42–95% of proximal fallopian tubal obstructions are pseudo-obstructions induced by cramps, valvelike action, and mucous plug blockage [1, 33–36]. The distal obstruction is associated with the adhesion of the fimbriae. Inflammatory processes in the uterine tube induce the death of some fimbriae. The rest

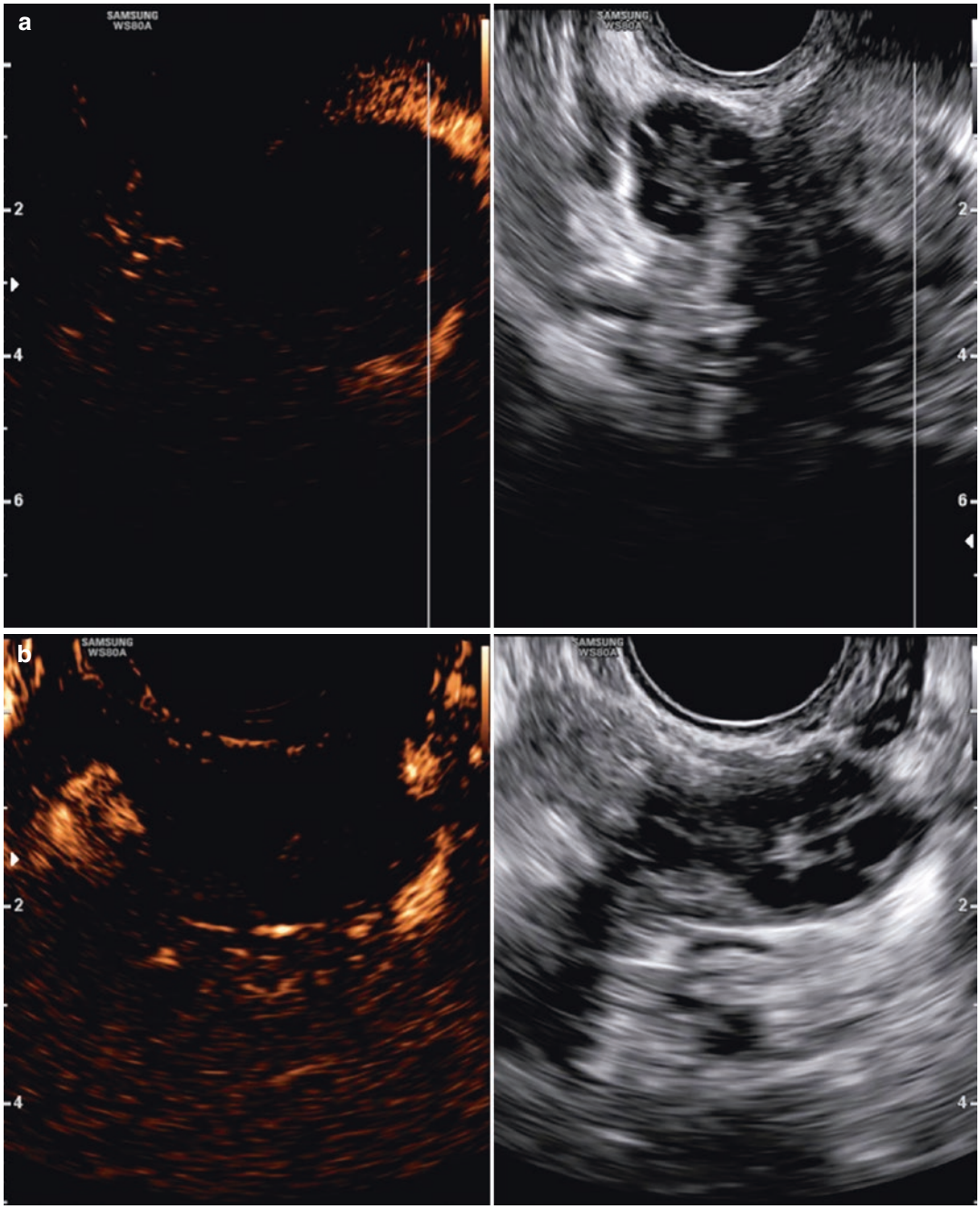

Fig. 12.18 HyCoSy. Ultrasound contrast medium in the periovarian space. The UCA is bounded around the ovary due to tubal fimbriae adhesions. (**a**, **b**) Different examples

remain tightly fixed together. As a result, they become hardly mobile and unable to function properly. The pattern of the UCA distribution in the periovarian space gives an idea of the presence or absence of adhesion in the fimbrial part of the fallopian tube (Figs. 12.18 and 12.19).

During HyCoSy, a hydrosalpinx may arise at one or both sides. It looks like an elongated tubular structure filled with homogeneous anechoic

fluid with multiple small hyperechoic folds of the mucosa (Fig. 12.20).

Endometrial pathology is a frequently diagnosed situation in the uterine cavity. It manifests with abnormal uterine bleeding, infertility, repeated IVF failure, etc. The US permits precise assessment of endometrium regarding its shape, margins, echostructure, thickness, and endometrial-myometrial interface.

Normally, the central hyperechoic endometrial line is smooth and regular. Non-linear, twisty, intermittent structure or vague imaging is considered abnormal. The anteroposterior size of central endometrial echo is measured in longitudinal uterine scans with simultaneous imaging of the cervical canal. The maximum value is considered. In fertile women, the thickness, configuration, and echostructure of the endometrium depend on the menstrual cycle phase. The thickness of the endometrium reaches its maximum in the secretory phase and accounts for 10–15 mm. In postmenopausal women, within the first 5 years, the thickness of the endometrium is 7–9 mm; beyond 5 years—it should not exceed 4–5 mm. However, transvaginal echography does not always provide the required data on the condition of the endometrium and uterine cavity. In these cases, HyCoSy may be of benefit.

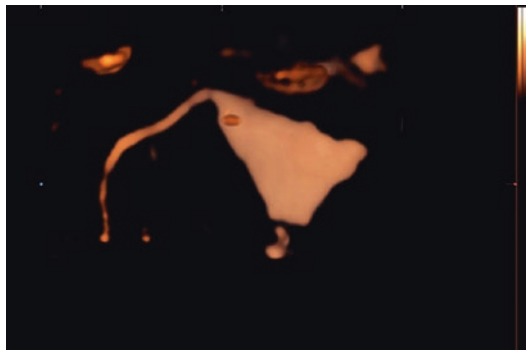

Fig. 12.19 HyCoSy. 3D-contrast mode. Patent right fallopian tube. Proximal blockade of the left tube

The instillation of UCA into the uterine cavity unfolds the normal endometrium, which permits the diagnosis of various pathologies and congenital anomalies. The advantage of HyCoSy over transvaginal US is the imaging of the basal and functional endometrial layers and endometrial-myometrial interface.

Endometrial polyp is a lesion that protrudes above the surface of the endometrium into the uterine cavity. It has a vascular pedicle and exhibits localized hyperplasia of endometrial glandular epithelium and stromal cells. The presence of a pedicle, which consists of fibrous and smooth muscle tissues, is an important feature.

The US with the introduction of anechoic UCA into the uterine cavity identifies a polyp as an echogenic intracavitary lesion with smooth margins, sessile or pedunculated, surrounded by fluid. The polyps are generally benign but incidentally may harbor atypia or carcinoma. The incidence of malignant and borderline types of endometrial pathology (endometrial polyps with complex hyperplasia and atypia) is higher in postmenopausal women.

The lesions below 5 mm in size, multiple or two adjacent polyps, and lesions in tubal ostia

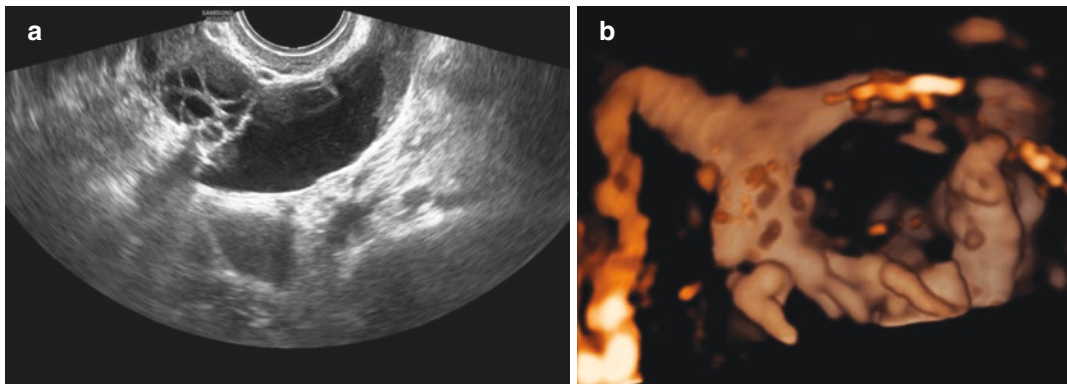

Fig. 12.20 HyCoSy. Hydrosalpinx formed during the procedure. (**a**) 2D grayscale US image. (**b**) 3D-contrast mode

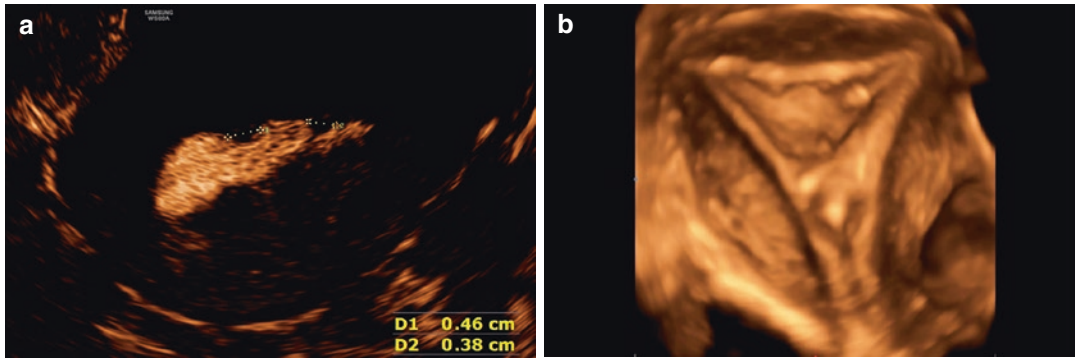

Fig. 12.21 Endometrial polyps. (**a**) 2D HyCoSy image. (**b**) 3D HyCoSy image

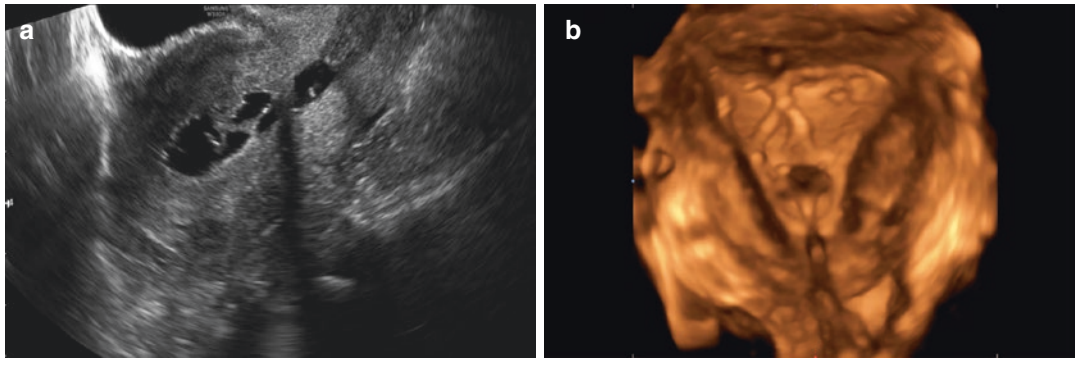

Fig. 12.22 Intrauterine synechiae. (**a**) 2D HyCoSy image. (**b**) 3D HyCoSy image

or uterine isthmus are not quite accurately imaged with 2D echography. Desquamated epithelium and blood clots may also lead to false-positive reports. The 3D study facilitates the diagnosis in areas that are difficult to visualize (Fig. 12.21).

Uterine synechiae (also called Ascherman syndrome) are adhesions between different areas of the uterine mucosa that lead to partial or complete obliteration of the uterine cavity. Intrauterine synechiae consist of fibrous tissue, sometimes with a glandular component. They are a consequence of infections, inflammations, intrauterine interventions (such as abortions or diagnostic dilation and curettage of the uterine cavity), or prolonged use of intrauterine contraceptives.

Ultrasound criteria for intrauterine synechiae are as follows:

- mismatch of the central endometrial echo to the menstrual cycle phase,
- discontinuous contours of the endometrium, the central endometrial echo of the hourglass shape,
- the structure of central endometrial echo with high echogenic areas,
- single intracavitary linear inclusions of increased echogenicity of various lengths with a thickness of 2–4 mm, fixed to the basal layer of the endometrium.

HyCoSy may encounter various problems while filling in the uterine cavity with UCA in

patients with intrauterine synechiae, such as the listed below:

- failure to move the catheter through the internal os,
- no passage of UCA into the uterine cavity when the balloon is inflated in the cervical canal,
- decrease in the UCA administration rate. The lowest rate may correspond to complete obliteration of the uterine cavity.

HyCoSy in 2D mode enables the detection of the irregular narrowing or an hourglass-like expansion of the cavity in uterine synechiae. Three-dimensional HyCoSy provides simultaneous three mutually perpendicular sections to enhance the study. The frontal plane is very practical to determine the topography of multiple multidirectional synechiae, the patency of the interstitial parts of the fallopian tubes, and identify the cause of various filling defects in the uterine cavity (Fig. 12.22). The combination of different scanning modes helps to identify thin spiderweb-like synechiae of 1–2 mm thick, including those with a course parallel to the axis of the uterine cavity.

Uterine leiomyoma (fibroid) is a benign hormone-dependent tumor composed of smooth muscle cells of the myometrium. HyCoSy helps to identify the lesions, which cause deformation of the uterine cavity.

Submucous fibroids tend to have a broad base and clear margins. They are hypo- or isoechoic to the myometrium as opposed to the polyps, which are isoechoic to the endometrium and more echogenic than myoma. Also, the echogenic endometrium covers the surface of the submucous fibroid. With CDI, blood flow in myoma is usually identified as several distributed color foci. Alternatively, polyps are characterized by a single central feeding vessel.

HyCoSy delineates the contours of the lesion, the width of its base, or the exact location of the pedicle. The introduction of UCA enables the assessment of the basal contour in the areas adjacent to the myoma (Fig. 12.23).

Congenital anomalies of the uterus confer the disorders of the anatomical structure with incomplete organogenesis, abnormal size, shape, proportions, symmetry, topography, etc. Abnormalities of the internal genitalia occur in 1–3% of the female population and often cause infertility.

For patients with uterine anomalies, HyCoSy is a less invasive and cheaper method as compared to hysteroscopy or MRI. The combination of different US modes has a sensitivity and specificity near 100% for the diagnosis of the saddle uterus and larger Müllerian duct anomalies. Coronary scanning planes better illustrate the findings.

Common variants of the uterus shape are arcuate and T-shaped uterus. The arcuate uterus is characterized by the thickened fundus (the fundal indentation has an obtuse angle and the depth of smaller than 15 mm) and a single uterine cavity. The arcuate uterus is often reported normal with the standard US. However, 3D reconstruction more reliably identifies this anomaly (Fig. 12.24).

T-shaped uterus demonstrates the change in the shape of the uterine cavity often in a combination with the decrease in its size (Fig. 12.25). It is usually caused by intrauterine exposure to diethylstilbestrol (DES). Patients with a T-shaped uterus have a high risk of spontaneous abortions, preterm labor, or ectopic pregnancies.

A unicornuate uterus is a congenital anomaly that results from the violation of the development of one Müllerian duct. This anomaly is a rare entity with an incidence of 1:10,000. Depending on the rudimentary horn condition the following subtypes are identified:

- No rudimentary horn (Fig. 12.26).
- Rudimentary horn with no uterine cavity (Fig. 12.27).
- Rudimentary horn with a noncommunicating or communicating cavity to the normal side.

A non-functional rudimentary horn has a rounded or oval shape and echogenicity of the myometrium. It is often visualized as a lesion adjacent to the lateral uterine wall near the internal os. Occasionally, it may be mistaken for a subserous leiomyoma.

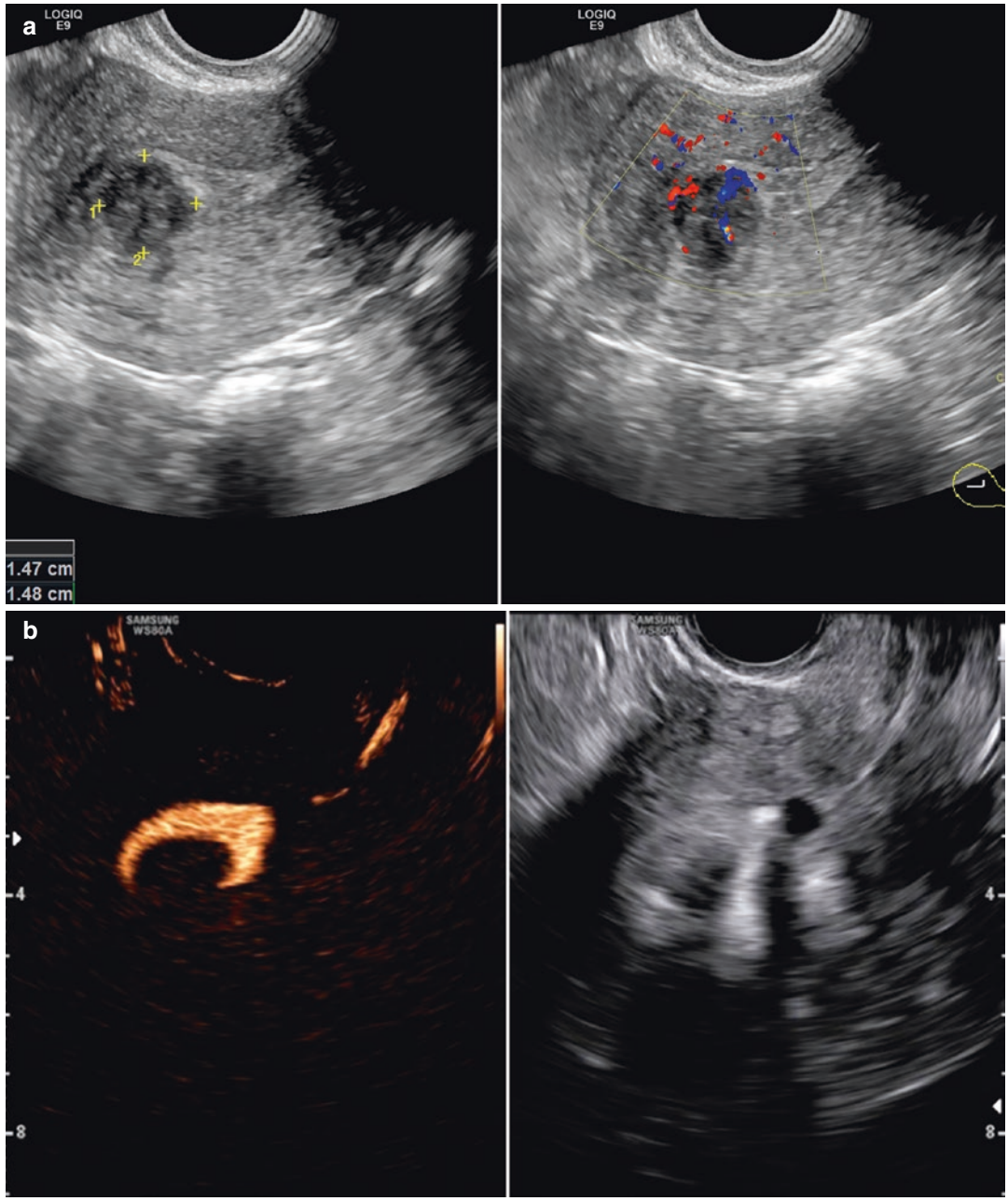

Fig. 12.23 Submucosal uterine fibroid. (**a**) CDI. (**b**) HyCoSy image

Septate uterus is characterized by the existence of two equal endometrial cavities separated by a septum (Fig. 12.28). The superior segment of the septum is myometrial. The inferior fibrous segment of the septum is visualized as a thin structure with an anterior-posterior orientation. Each cavity connects to the fallopian tube. The intrauterine septum can have a different length. In the partial septate uterus, a septum partly divides the uterine cavity above the level of the internal cervical os. In a complete septate uterus, the septum fully divides the cavity up to the level

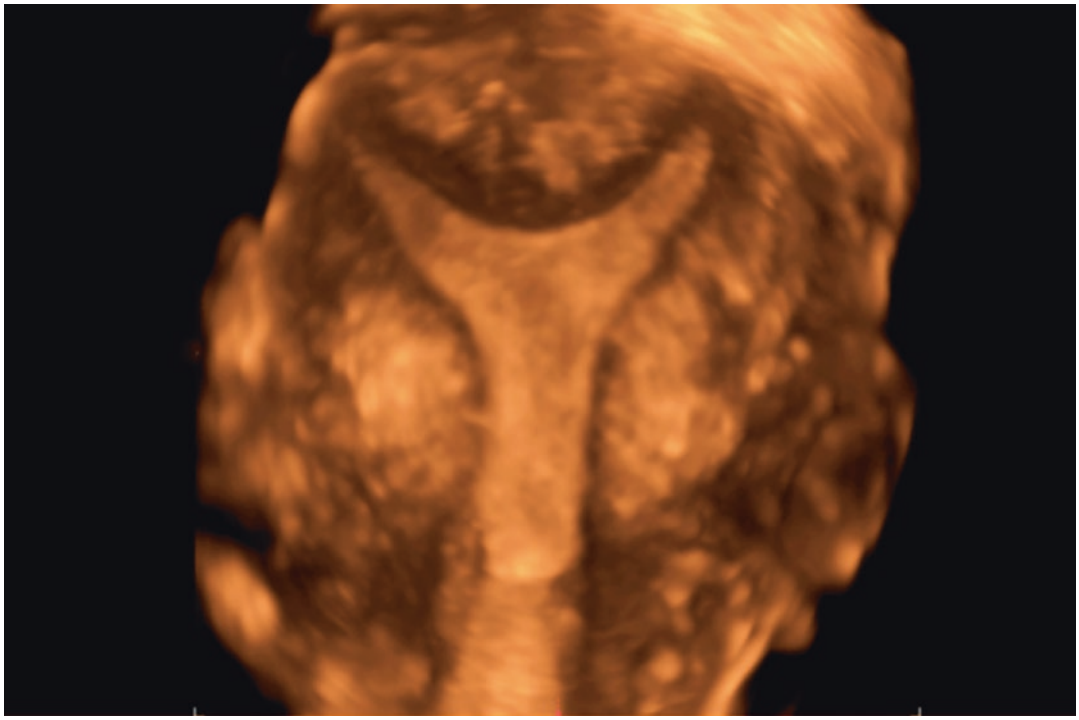

Fig. 12.24 Arcuate uterus. 3D HyCoSy image

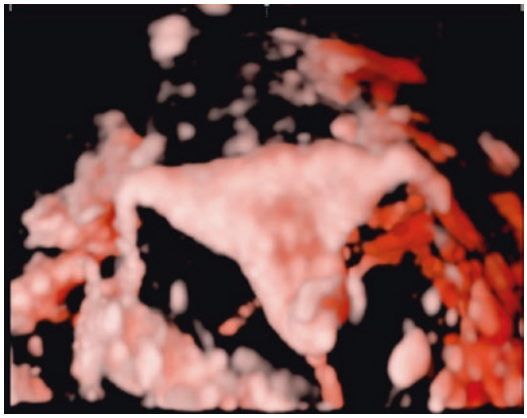

Fig. 12.25 T-shaped uterus. 3D HyCoSy image

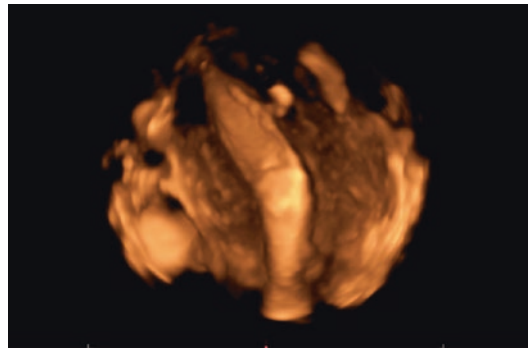

Fig. 12.26 Unicornuate uterus. 3D HyCoSy image. The uterus is narrow and deviated from the midline to the healthy side. The uterine cavity is asymmetric. Additionally, contralateral uterine adnexa and kidney are absent

of the internal os. Intrauterine septum can manifest by algodismenorrhea, uterine bleeding, infertility, or miscarriage.

Uterine scar arises after surgeries, inclusive of cesarean section. Assessment of its condition is an issue for women, who plans a pregnancy. The C-section scar is visualized as a UCA filled defect, which resulted from inadequate myometrial repair.

In most cases, the uterine scar is not accompanied by any clinical symptoms. However, it may cause prolonged menstrual discharge, postmenstrual bleeding, dyspareunia, chronic pelvic pain,

or secondary infertility. Besides, subsequent pregnancy implantation in the scar area is possible.

There are various diagnostic methods for the assessment of scar competence, such as standard US, MRI, and hysteroscopy. They have different diagnostic values, pros, and cons. The standard protocols of MRI and US are designed to identify patients with a high risk for scar failure. However, these methods do not always permit the assessment of myometrial elasticity in the scar that is crucial for deciding on metroplasty of the lower uterine segment. Hysteroscopy is feasible for determining the scar condition but fails to measure the thickness of the intact myometrium. Intrauterine administration of SonoVue® depicts the contours of the uterine cavity, identifies the C-section scar defect, and detects possible dehiscence (Fig. 12.29, 12.30, and 12.31).

When performing HyCoSy, some technical difficulties may arise due to preexisting features, as follows:

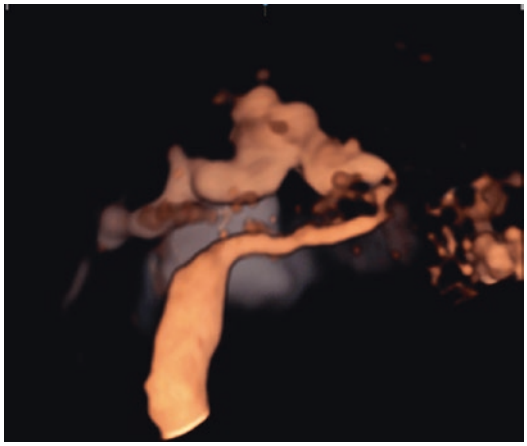

Fig. 12.27 Unicornuate uterus with a rudimentary horn with no uterine cavity. 3D HyCoSy image. The main horn is narrow

Fig. 12.28 Partial septate uterus. 3D HyCoSy image

- cervical stenosis, which may be a consequence of coagulation, cervical conization, or in postmenopausal patients
- excessively anteflexed or retroflexed uterus. Uterine traction with a tenaculum may be needed to insert the catheter

The most common complaint of patients during HyCoSy is a feeling of discomfort or pain in the lower abdomen. In this regard, it is recommended to introduce the contrast medium at a moderate pace continuously to ensure optimal stretching of the uterine cavity. Rapid filling of

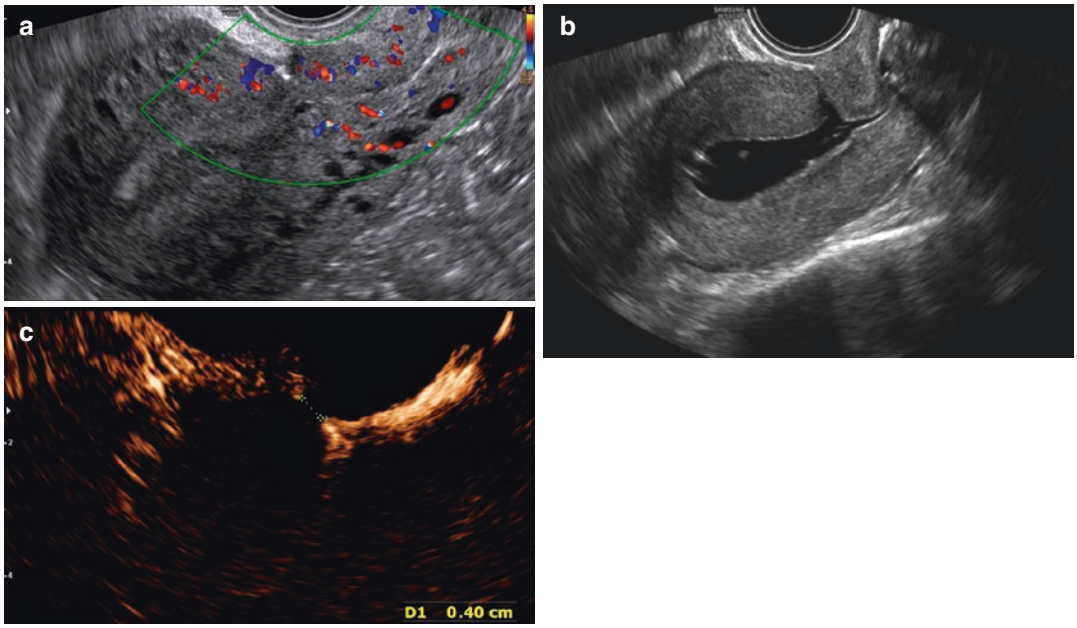

Fig. 12.29 Cesarean section uterine scar. (**a**) CDI. (**b**) 2D HyCoSy image. (**c**) 3D HyCoSy. (**d**) Multisliced 3D HyCoSy longitudinal image. (**e**) Multisliced 3D HyCoSy transverse image. UCA is not determined outside the uterine cavity

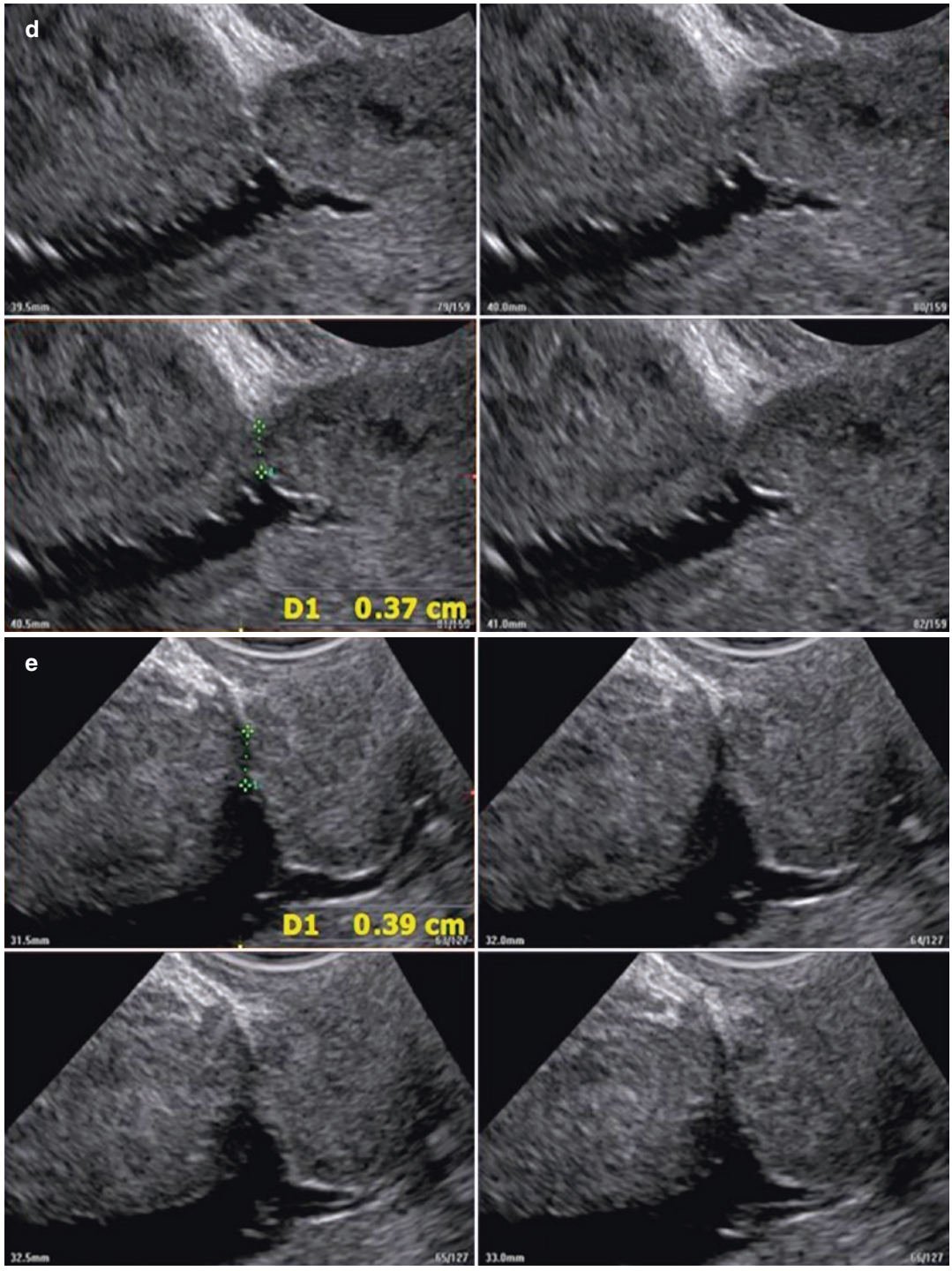

Fig. 12.29 (continued)

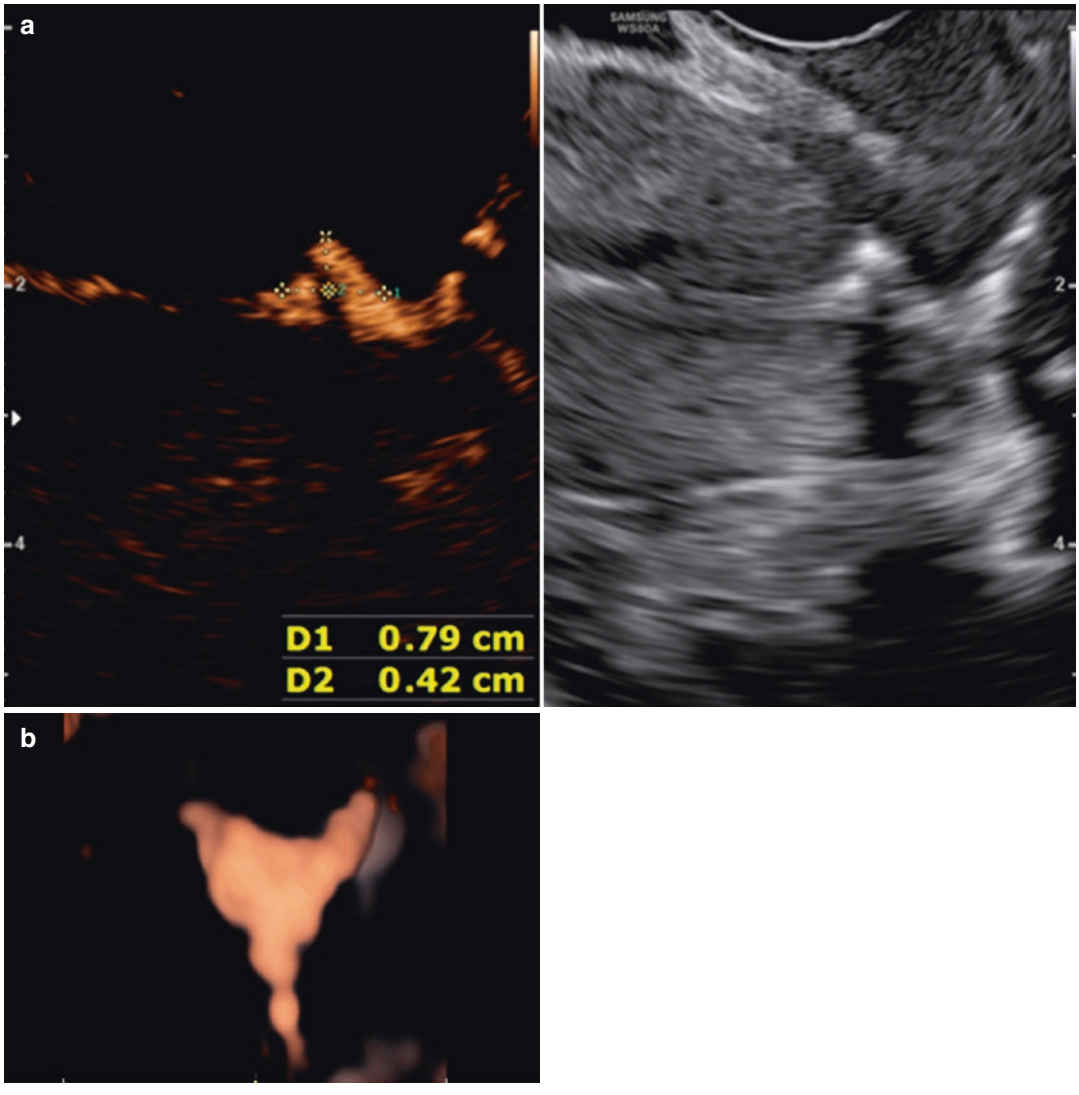

Fig. 12.30 Competent cesarean section uterine scar with a slight isthmocele. Contrast is not detected outside the uterine cavity. (**a**) 2D HyCoSy image. (**b**) 3D HyCoSy image

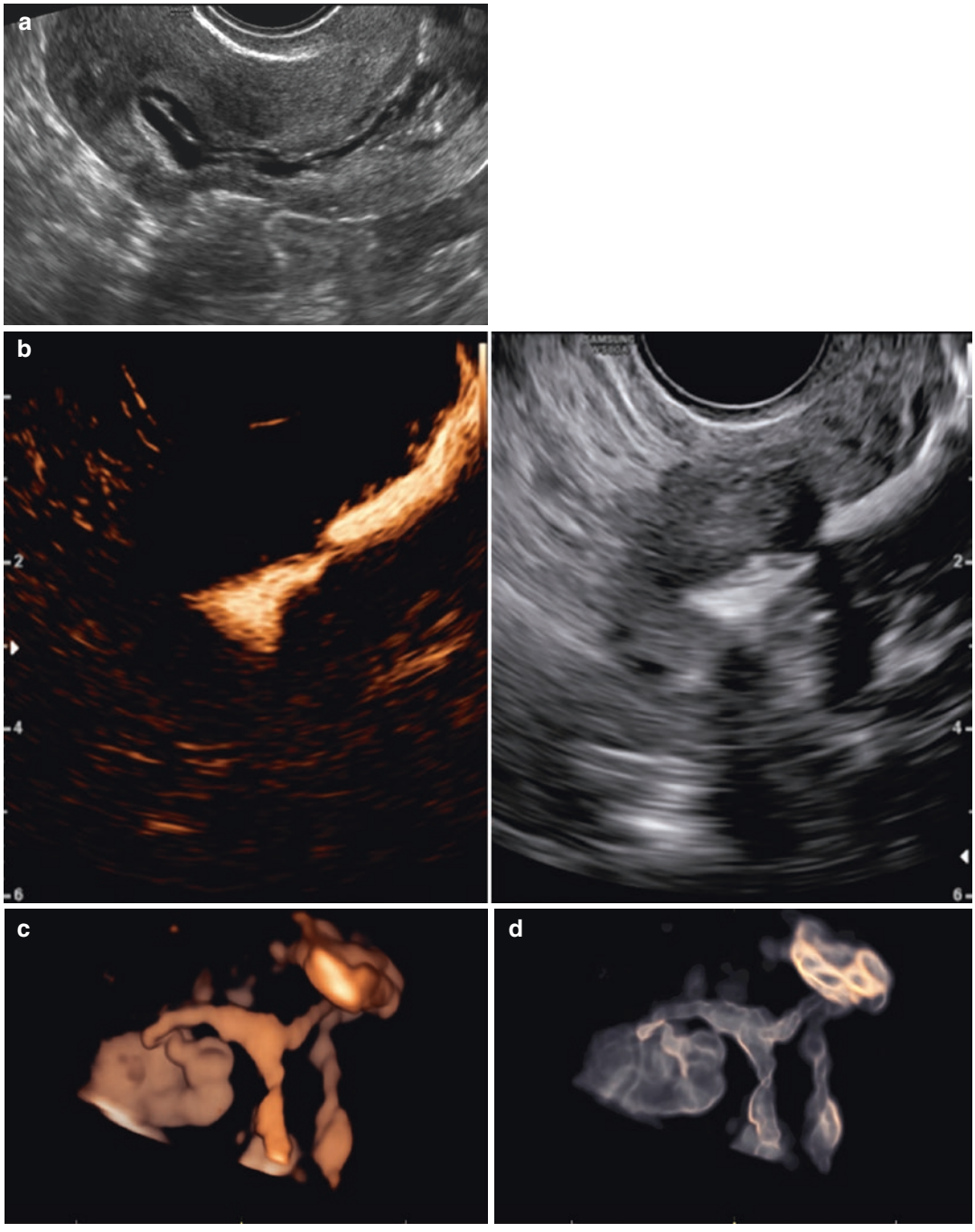

Fig. 12.31 Uterine scar of the posterior wall after myomectomy. The contour of the uterine cavity posterior wall is irregular and thin after myomectomy and excision of the fistula. Intrauterine adhesions are determined. (**a**) 2D HyCoSy image with saline. (**b**) 2D HyCoSy image with SonoVue®. (**c**) 3D HyCoSy. (**d**) 3D HyCoSy surface reconstruction

the uterine cavity can cause significant pain and, which may require antispasmodics or discontinuation of the procedure. Patients may also feel hot, report nausea or other vasovagal reactions, or faint. These manifestations also lead to the suspension of the HyCoSy procedure.

A rare complication of this procedure is iatrogenic hydrosalpinx, which occurs when the fallopian tube is blocked.

UCAs are highly effective and also have a high safety level. They are generally well-tolerated by patients, including in HyCoSy [27, 28, 37, 38]. HyCoSy is a safe, effective, and technologically simple method for the diagnosis of tubal-peritoneal infertility factor, pathology of the uterine cavity, abnormalities of the uterus, etc. It can be used as a first-line modality for the diagnosis of infertility to reduce the number of hysteroscopies.

12.4 CEUS of Pelvic Veins

Currently, the main diagnostic method in phlebology is echography with Doppler imaging. CEUS is used rarely, although it permits the precise study of pelvic veins. It significantly enhances the value of the US [39].

The varicose disease of pelvic veins implicates the ovarian veins and pelvic venous plexuses [40]. The valvular insufficiency of the ovarian veins causes the primary form of the disease. The secondary form occurs in obstructive diseases, typically in aorto-mesenteric compression of the left renal vein, which is also called Nutcracker syndrome. One type of surgery to relieve venous hypertension in this syndrome is a gonado-iliac bypass between a gonadal vein and the ipsilateral external iliac vein. A bypass is necessary if the pressure gradient is higher than 3 mmHg [40, 41]. Postoperative monitoring of such patients is an important issue. The bypass function is poorly identified with a conventional ultrasound; CT or phlebography have their well-known disadvantages and are not always economically appropriate. CEUS is a well-tolerated method, which is highly effective and applicable in an outpatient setting.

Indications for CEUS of the pelvic veins confer the following purposes:

- examination of the ovarian veins,
- follow-up after gonado-iliac bypass surgery,
- diameter of the venous bypass smaller than 0.4 cm,
- doubtful estimation of the bypass functionality with CE-CT or phlebography,
- detection of thrombus in pelvic veins.

CEUS is carried out on a device in low mechanical index contrast mode with multifrequency convex (2.5–5.5 MHz) and transvaginal (4–11 MHz) transducers. The study starts with unenhanced sonography. It reviews the diameter, patency, and flow velocity values of the inferior vena cava, iliac, left renal, ovarian, pelvic veins, etc. [42]. Ultrasound is performed in grayscale, color Doppler, and pulsed-wave modes. Since blood flow velocity in veins is very low, it is difficult to assess the functionality of the gonado-iliac venous bypass, especially if it has a small diameter. Transvaginal US also experiences problems with the identification of hypoechoic thrombus, especially early after surgery.

Contrast enhancement should answer the questions that appeared during the unenhanced US. CEUS of the ovarian vein, bypass, or pelvic venous plexus is carried out with intravenous administration of an UCA. To visualize an ovarian vein or venous bypass, position the probe on the anterior abdominal wall in the left or right hypogastrium. The pelvic venous plexus is assessed with a transvaginal probe.

Qualitative and quantitative characteristics of the ovarian vein and venous bypass CEUS are evaluated. Visual assessment of qualitative characteristics, such as the intensity of contrast enhancement and distribution of the UCA within the venous lumen, is described with the following terms: hyperenhancing, hypoenhancing, and persistent enhancement.

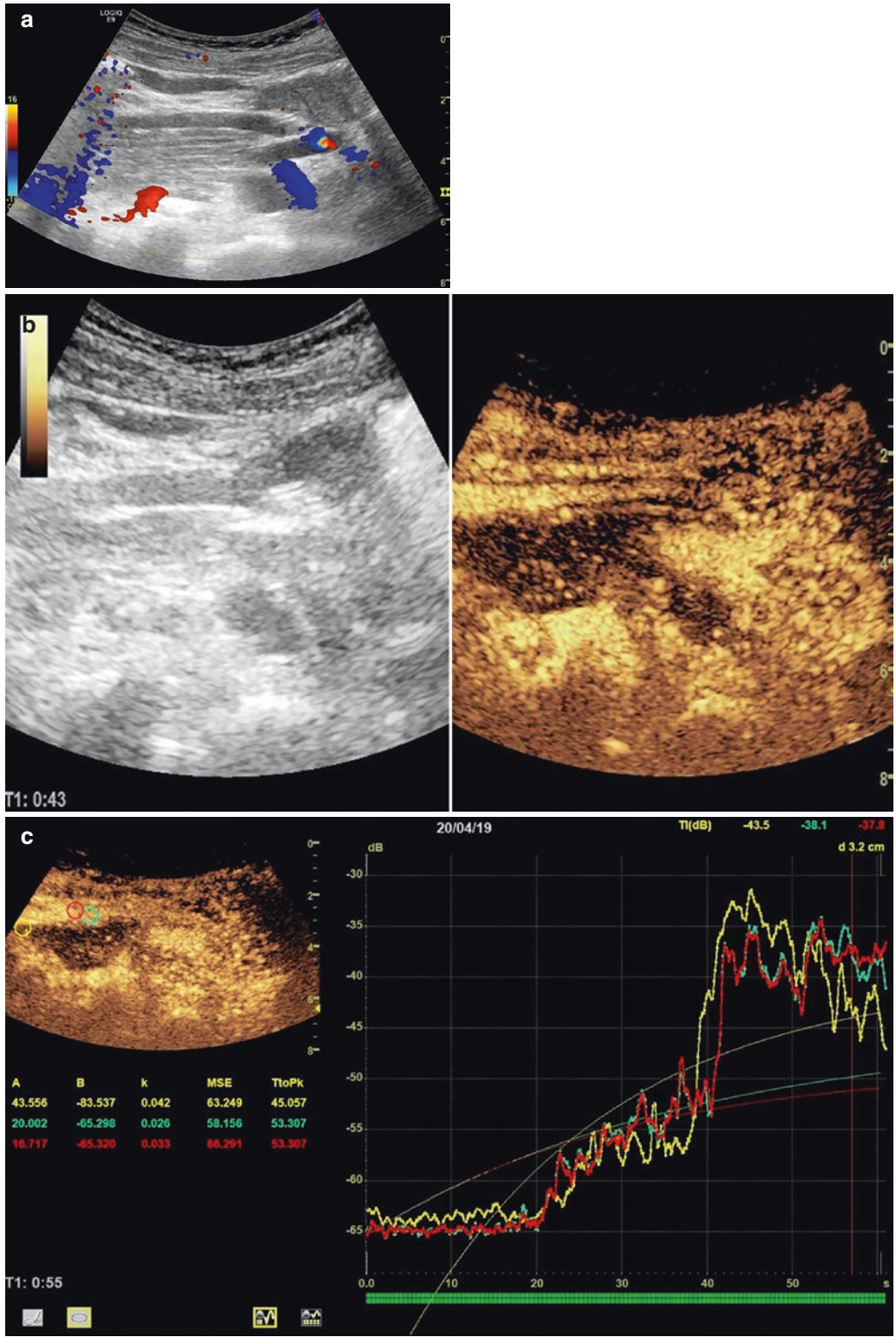

Fig. 12.32 Gonado-iliac bypass. (**a**) CDI fails to assess the bypass patency; no color is registered in the vein lumen. (**b**) CEUS image. Hyperenhanced venous bypass. (**c**) TIC in the bypass

Quantitative analysis is carried out with the scanner software at the post-processing stage. The region of interest is positioned on the distal part of the vein or bypass. The TIC shape and the numeric data are assessed with special attention to the time to peak value.

CEUS facilitates monitoring the gonadoiliac bypass after surgery [43] (Fig. 12.32). It is necessary if Doppler sonography fails to provide reliable data. The transducer is positioned still on the anterior abdominal wall in the left hypogastric area over the examined vessel. A cine loop record is started with the UCA introduction and lasts for up to 1.5 min. Normal bypass becomes hyperenhanced. The quantitative parameters confirm the bypass patency by the normal values of arrival time and time to peak intensity.

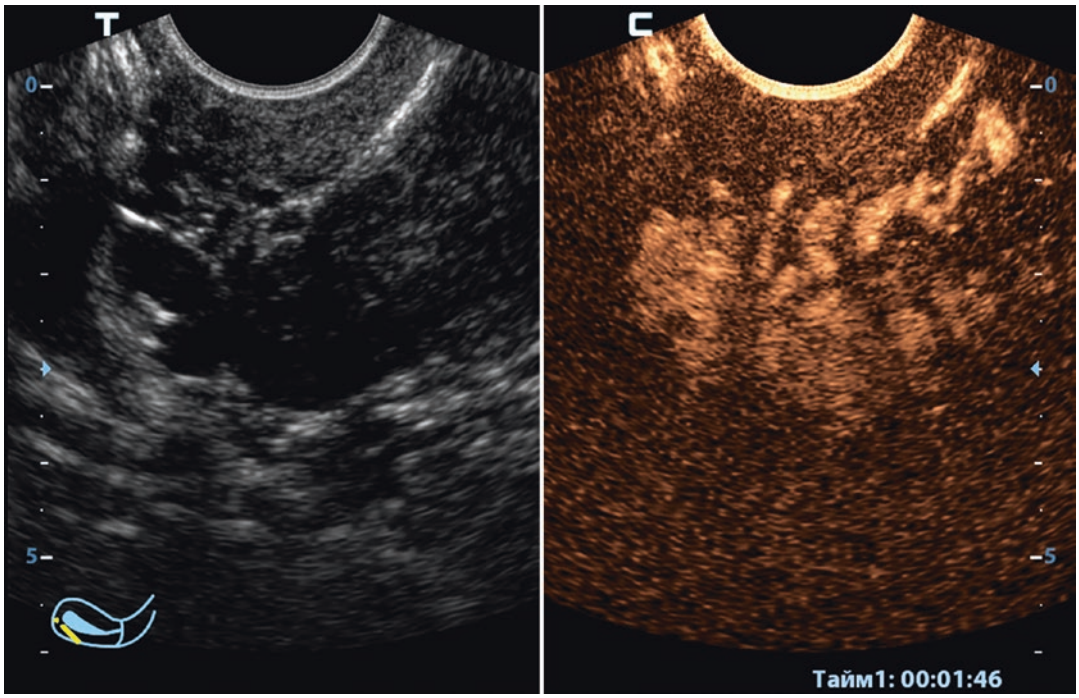

Fig. 12.33 Varicose pelvic veins. CEUS image demonstrate dilated tortuous varicose veins with the enhanced lumen and no thrombus

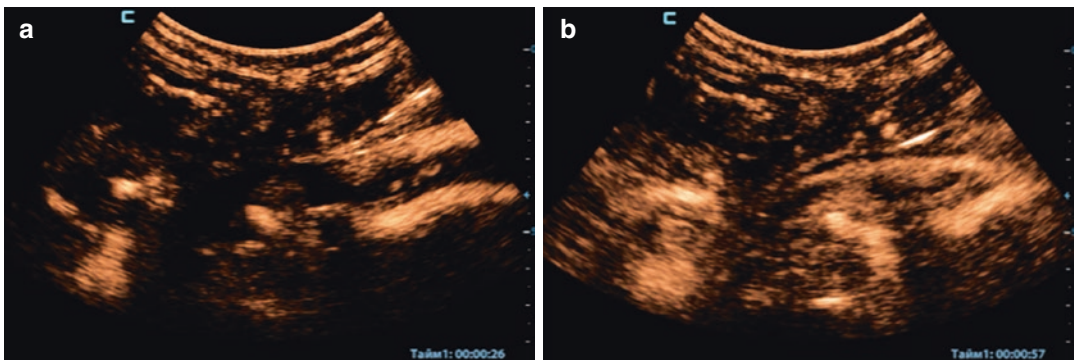

Fig. 12.34 Pelvic veins thrombosis. CEUS images. (**a**) Partially enhanced varicose pelvic vein. (**b**) Recanalization of the same vein in 3 months

The pelvic veins are typically studied for patency. After surgical treatment, especially with the increase in lower abdominal pain in the early postoperative period, pelvic venous thrombosis should be excluded. If Doppler US fails to do it, transvaginal CEUS is feasible. Qualitative parameters are most valuable. Patent veins are filled with UCA without enhancement defects (Fig. 12.33, Video 12.11).

CEUS can be successfully applied for the specification of the size and attachment details of blood clots within the lumen of the veins of any location, and depiction of venous recanalization in post-thrombotic syndrome (Fig. 12.34).

CEUS is a valuable complement to the Doppler ultrasound study of pelvic veins. This method has some advantages over radiation diagnostic methods, since it does not require special training, hospitalization, and is efficient in an outpatient setting.

References

1. Bulanov MN. Ul'trazvukovaya ginekologiya: kurs lekcij v trekh tomah [Ultrasound gynecology: a course of lectures in three volumes], vol. 2. Moscow: Vidar-M; 2010.
2. Prives MG, Lysenkov NK, Bushkovich VI. Anatomiya cheloveka [Human anatomy]. 12th ed. Saint Petersburg: Hyppokrat; 2017.
3. Proskuryakova OV, Zykin BI. Dopplerekhografiya matki [Dopplerography of the uterus]. In: Zykin BI, Medvedev MV, editors. Dopplerografiya v ginekologii: Enciklopediya ul'trazvukovoj diagnostiki v akusherstve i ginekologii [Doppler ultrasound in gynecology: an encyclopedia of ultrasonic diagnostics in obstetrics and gynecology]. Moscow: Real'noe vremya; 2000. p. 35–45.
4. Ozerskaya IA. Ekhografiya v ginekologii [Echography in gynecology]. Moscow: Vidar-M; 2013.
5. Liu Y, Xu Y, Cheng W, Liu X. Quantitative contrast-enhanced ultrasonography for the differential diagnosis of endometrial hyperplasia and endometrial neoplasms. Oncol Lett. 2016;12(5):3763–70. https://doi.org/10.3892/ol.2016.5206.
6. Pop CM, Mihu D, Badea R. Role of contrast-enhanced ultrasound (CEUS) in the diagnosis of endometrial pathology. Clujul Med. 2015;88(4):433–7. https://doi.org/10.15386/cjmed-499.
7. Wei JJ, Zhang XM, Chiriboga L, Yee H, Perle MA, Mittal K. Spatial differences in biologic activity of large uterine leiomyomas. Fertil Steril. 2006;85:179–87.
8. Martini C, Lacelli F, Grillo G, Gandolfo N, Orlandi D, Serafini G. Evaluation of pseudocapsule of uterine myomas with contrast enhanced ultrasound (CEUS). ECR. 2014;2014:376. https://doi.org/10.1594/ecr2014/C-0376.
9. Sconfienza LM, Lacelli F, Gandolfo N, Gazzo P, Perrone N, Serafini G. Contrast-enhanced ultrasound (CEUS) assessment of superselective uterine fibroid embolization (SUFE): preliminary experience. J Ultrasound. 2008;11(4):158–61. https://doi.org/10.1016/j.jus.2008.09.005.
10. Lyshchik A, editor. Specialty imaging: fundamentals of CEUS. 1st ed. Philadelphia: Elsevier; 2019. p. 214–40.
11. Zhang XL, Zheng RQ, Yang YB, Huang DM, Song Q, Mao YJ, et al. The use of contrast-enhanced ultrasound in uterine leiomyomas. Chin Med J. 2010;123(21):3095–9.
12. Stoelinga B, Dooper AMC, Juffermans LJM, et al. Use of contrast-enhanced ultrasound in the assessment of uterine fibroids: a feasibility study. Ultrasound Med Biol. 2018;44(8):1901–9. https://doi.org/10.1016/j.ultrasmedbio.2018.03.030.
13. Tjalma W, Van Marck E, Weyler J, Dirix L, Van Daele A, Goovaerts G, et al. Quantification and prognostic relevance of angiogenic parameters in invasive cervical cancer. Br J Cancer. 1998;78(2):170–4. https://doi.org/10.1038/bjc.1998.460.
14. Cooper RA, West CM, Wilks DP, Logue JP, Davidson SE, Roberts SA, Hunter RD. Tumour vascularity is a significant prognostic factor for cervix carcinoma treated with radiotherapy: independence from tumour radiosensitivity. Br J Cancer. 1999;81(2):354–8. https://doi.org/10.1038/sj.bjc.6690700.
15. Zheng W, Xiong YH, Han J, Guo ZX, Li YH, Li AH, Pei XQ. Contrast-enhanced ultrasonography of cervical carcinoma: perfusion pattern and relationship with tumour angiogenesis. Br J Radiol. 2016;89(1065):20150887. https://doi.org/10.1259/bjr.20150887.
16. Pomortsev AV, Grushevskaya YV, Makukhina TB. Controversial issues of radiologic diagnosis of adenomyosis in reproductive losses. Kuban Sci Med Bull. 2019;26(2):173–90. https://doi.org/10.25207/1608-6228-2019-26-2-173-190.
17. Wang Y, Wang W, Ye H. Contrast-enhanced ultrasonography assessment of therapeutic efficacy for ultrasound-guided high-intensity focused ultrasound ablation of uterine fibroids: comparison with contrast-enhanced magnetic resonance. J Med Ultrasound. 2014;22(1):22–8. https://doi.org/10.1016/j.jmu.2013.10.007.
18. Zhang X, Mao Y, Zheng R, Zheng Z, Huang Z, Huang D, et al. The contribution of qualitative CEUS to the determination of malignancy in adnexal masses, indeterminate on conventional US - a multicenter study. PLoS One. 2014;9(4):e93843. https://doi.org/10.1371/journal.pone.0093843.

19. Qiao JJ, Yu J, Yu Z, Li N, Song C, Li M. Contrast-enhanced ultrasonography in differential diagnosis of benign and malignant ovarian tumors. PLoS One. 2015;10(3):e0118872. https://doi.org/10.1371/journal.pone.0118872.
20. Fleischer AC, Lyshchik A, Jones HW Jr, Crispens M, Loveless M, Andreotti RF, et al. Contrast-enhanced transvaginal sonography of benign versus malignant ovarian masses: preliminary findings. J Ultrasound Med. 2008;27(7):1011–8. https://doi.org/10.7863/jum.2008.27.7.1011.
21. Wang X, Yang S, Lv G, Liao J, Wu S, Zhang W. Combination of GI-RADS and 3D-CEUS for differential diagnosis of ovarian masses. Rev Assoc Med Bras. 2019;65(7):959–64. https://doi.org/10.1590/1806-9282.65.7.959.
22. Sidhu PS, Cantisani V, Dietrich CF, Gilja OH, Saftoiu A, Bartels E, et al. The EFSUMB guidelines and recommendations for the clinical practice of contrast-enhanced ultrasound (CEUS) in non-Hepatic applications: update 2017. Ultraschall Med. 2018;39(2):e2–e44. https://doi.org/10.1055/a-0586-1107.
23. Graziano A, Lo Monte G, Soave I, Caserta D, Moscarini M, Marci R. Sonohysterosalpingography: a suitable choice in infertility workup. J Med Ultrason. 2013;40:225–9. https://doi.org/10.1007/s10396-012-0417-0.
24. Serov VA, Suhih GT. Akusherstvo i ginekologiya. Klinicheskie rekomendacii [Obstetrics and gynecology. Clinical recommendations]. GEOTAR-Media: Moscow; 2014.
25. Savel'eva GM, Suhih GT, Manuhin IB. Ginekologiya. Nacional'noe rukovodstvo [Gynecology. National guidelines]. GEOTAR-Media: Moscow; 2013.
26. Norton M, Scoutt L, Feldstein VA. Callen's ultrasonography in obstetrics and gynecology. 6th ed. London: Elsevier; 2017.
27. Sencha AN, Bychenko VG, Fedotkina EP, et al. Ekhogisterosal'pingografiya s primeneniem kontrastnogo preparata "SonoVue" – effektivnaya tekhnologiya ocenki prohodimosti matochnyh trub [Echohysterosalpingography with the use of SonoVue contrast agent – an effective technology for assessing the patency of the fallopian tubes]. Akush Ginekol. 2018;6:63–9.
28. Fedotkina EP, Sencha AN. Ekhogisterosal'pingografiya s primeneniem kontrastnogo preparata "SonoVue" [Echohysterosalpingography with the use of contrast agent SonoVue]. SonoAce Ultrasound. 2018;31:17–27.
29. Bychenko VG, Sencha AN. Gisterosal'pingografiya. Atlas ot A do Ya [Hysterosalpingography. Atlas from A to Z]. Moscow: MEDpress-inform; 2020.
30. Sencha AN, Fedotkina EP, Sheshko PL, Pavlovich SV. Metodika provedeniya ekhogisterosal'pingografii s primeneniem ekhokontrastnogo preparata SonoVue [Method of conducting echohisterosalpingography using SonoVue echocontrast preparation]. Russian Patent 2,697,370; 2019.
31. Chernov VI, Nosov VV, Vesnina ZV, Lishmanov YB. Gisterosal'pingoscintigrafiya v diagnostike neprohodimosti matochnyh trub [Hysterosalpingography in the diagnosis of obstruction of the fallopian tubes]. Radiologiya-praktika. 2005;2:19–23.
32. Ayida G, Kennedy S, Barlow D, Chamberlain P. A comparison of patient tolerance of hysterosalpingo-contrast sonography (HyCoSy) with Echovist-200 and X-ray hysterosalpingography for outpatient investigation of infertile women. Ultrasound Obstet Gynecol. 1996;7(3):201–4. https://doi.org/10.1046/j.1469-0705.1996.07030201.x.
33. Wang W, Zhou Q, Gong Y, Li Y, Huang Y, Chen Z. Assessment of fallopian tube fimbria patency with 4-dimensional hysterosalpingo-contrast sonography in infertile women. J Ultrasound Med. 2017;36(10):2061–9. https://doi.org/10.1002/jum.14244.
34. Demidov VN. Primenenie ekhografii v ginekologii [Application of echography in gynecology]. Moscow: Binom; 2017.
35. Medvedev MV, Ozerskaya IA. Ul'trazvukovoe issledovanie matochnyh trub. Klinicheskoe rukovodstvo po ul'trazvukovoj diagnostike [Ultrasound examination of the fallopian tubes. Clinical guide to ultrasound diagnostics], vol. 3. Moscow: Vidar; 1997. p. 175–200.
36. Hegazy AA. Hysterosalpingography might disturb the functional anatomy of Fallopian tube. Acad Anat Int. 2018;4(1):1–3.
37. Savelli L, Pollastri P, Guerrini M, Villa G, Manuzzi L, Mabrouk M, et al. Tolerability, side effects, and complications of hysterosalpingocontrast sonography (HyCoSy). Fertil Steril. 2009;92(4):1481–6. https://doi.org/10.1016/j.fertnstert.2008.07.1777.
38. Weskott HP. Contrast-enhanced ultrasound. 2nd ed. London: Uni-Med Science; 2013.
39. Smith A, Parker P, Byass O, Chiu K. Contrast sonovenography - Is this the answer to complex deep vein thrombosis imaging? Ultrasound. 2016;24(1):17–22. https://doi.org/10.1177/1742271X15625432.
40. Kalinin R, et al. Diagnostics and treatment of chronic venous disease: guidelines of Russian phlebological association. Phlebologiya. 2018;12(3):146–240. https://doi.org/10.17116/flebo20187031146.
41. Gulleroglu K, Gulleroglu B, Baskin E. Nutcracker syndrome. World J Nephrol. 2014;3(4):277–81. https://doi.org/10.5527/wjn.v3.i4.277.
42. Fomina EE, Ahmetzyanov RV, Tuhbatullin MG. Metodologiya ul'trazvukovogo issledovaniya pri varikoznoj bolezni ven taza [Methodology of ultrasound examination in pelvic varicose veins]. Prakt Med. 2016;9(101):53–8.
43. Fomina EE, Tuhbatullin MG, Ahmetzyanov RV. Sposob ul'trazvukovogo issledovaniya s kontrastnym usileniem venoznogo anastomoza malogo taza [Method of ultrasound examination with contrast enhancement of venous anastomosis in small pelvis]. Russian patent RU 2712104 C1, 24 Jan 2020.

Thyroid and Parathyroid Glands

13

Ekaterina A. Sencha and Alexander N. Sencha

The thyroid gland is supplied with blood by paired superior and inferior thyroid arteries, which originate from the external carotid arteries and the thyrocervical trunks (which in turn are the branches of the subclavian arteries). In 6–8% of cases, the unpaired thyroid ima artery, which departs from the brachiocephalic trunk contributes to the blood supply to the gland.

In the first publications on CEUS of focal thyroid lesions, Levovist (Schering, Germany) was used. This UCA is a gas microbubble suspension stabilized with galactose and palmitic acid [1–3]. Its microbubbles were able to pass pulmonary capillaries but their lifetime was limited to less than 2 min.

Currently, the second-generation UCAs (e.g., SonoVue®) permit imaging of tissue perfusion with vessel caliber below 40 μm and increase study duration up to 3–8 min [4].

Many authors report that 2.4 ml of SonoVue® is enough for thyroid CEUS [5–13]; however, it is not a final consensus. The dose in various publications [14–19] ranges from 1.2 to 4.8 ml.

In our opinion, the SonoVue® dose of 2.4 ml is optimal for the thyroid gland. It ensures detailed perfusion assessment in all vascular phases [20–24]. The arterial phase starts from the moment of UCA inflow and lasts up to 30–45 s. It is associated with the increase in contrast enhancement. It is followed by the venous phase, which demonstrates the plateau of enhancement with the subsequent decrease to the noise level.

The EFSUMB Guidelines and Recommendations for the Clinical Practice of CEUS in Non-Hepatic Applications (2017) presented a separate section on the thyroid gland [25]. It considers that CEUS for the characterization of thyroid nodules is an active research field and at present cannot be recommended for clinical use. However, substantial experience of CEUS and several meta-analyses suggest that contrast enhancement increases the diagnostic accuracy of routine ultrasound and can help in the identification of areas for fine-needle aspiration biopsy [6–8, 11, 26–32].

The indications for thyroid CEUS confer the following aims [20–24, 33, 34]:

- to clarify thyroid nodules microvascularity, especially in suspicion of thyroid cancer. Those include nodules with suspicious US signs identified for the first time and in nod-

Supplementary Information The online version contains supplementary material available at [https://doi.org/10.1007/978-3-030-91764-7_13].

E. A. Sencha (✉)
Ultrasound Diagnostics Department, Federal State Budget Institution "Medical Diagnostic Center No. 9" of the Ministry of Defence of the Russian Federation, Moscow, Russian Federation

A. N. Sencha
Department of Visual and Functional Diagnostics, Federal State Budget Institution "National Medical Research Center for Obstetrics, Gynecology and Perinatology n.a. V.I.Kulakov", Moscow, Russian Federation

A. N. Sencha, Y. N. Patrunov (eds.), *Contrast-Enhanced Ultrasound*,
https://doi.org/10.1007/978-3-030-91764-7_13

ules with the fast growth and changes in echostructure within 6–12 months of follow-up
- to characterize complex cystic lesions with multiple chambers, especially with hypervascular solid component
- to clarify cases with the inconsistency of US data with clinical signs, controversial interpretation, contradictory data of several diagnostic methods

Along with general contraindications, thyroid CEUS considers the below-listed limitations [20–24, 33–36]:

- suboptimal general US imaging quality, such as deep or superficial location or special scanning conditions
- the small size of the target area

The normal thyroid gland with CEUS demonstrates intense, fast, and symmetrical enhancement of the parenchyma in the arterial phase followed by slow regular washout (Fig. 13.1).

The main task of the thyroid CEUS is the differential diagnosis of benign and malignant lesions based on the assessment of qualitative and quantitative parameters of inflow, distribution, wash-out, and their ratio to the normal thyroid parenchyma. Thyroid CEUS with SonoVue® in the diagnosis of thyroid carcinoma published within the past 10 years demonstrates highly variable values. The sensitivity ranges from 68.0 to 97.6% and specificity from 57.0 to 98.7% (Table 13.1).

The meta-analyses of the studies on CEUS-based differential diagnosis of thyroid lesions indicate its high diagnostic accuracy (Table 13.2).

Contrast enhancement permits the increase in specificity and diagnostic accuracy of conventional sonography by 8% [29]. The majority of publications on the thyroid CEUS [10, 18, 19, 29] report on performing the qualitative analysis with visual assessment of the enhancement pattern and UCA kinetics in thyroid malignancies.

The first publications on CEUS of malignant lesions [46] noted that malignant nodules show

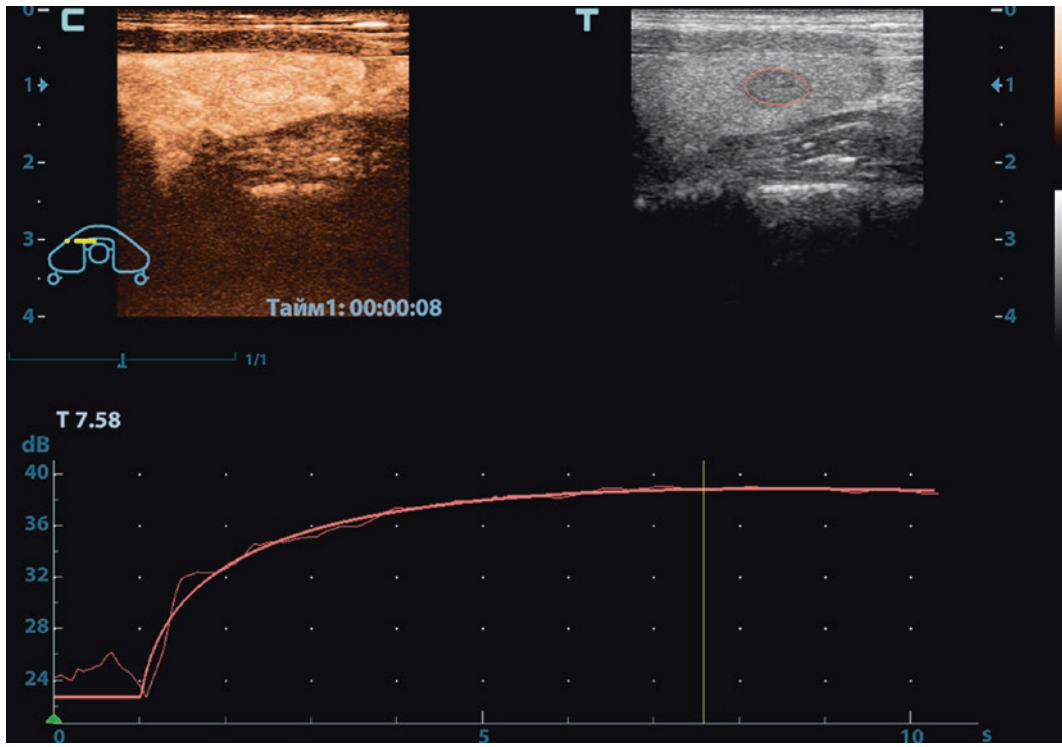

Fig. 13.1 Normal thyroid gland. Homogeneous isoenhancement of normal thyroid parenchyma in the arterial phase. CEUS image with 2.4 ml SonoVue®

Table 13.1 The diagnostic value of CEUS in thyroid cancer

Author	Year	Sensitivity (%)	Specificity (%)	PPV (%)	NPV (%)	Accuracy (%)	AUC (95% CI)
Nemec et al. [7]	2010	76.9	84.8	66.7	90.3	82.6	–
Li et al. [8]	2013	82.9	81.4	67.5	88.9	82.6	–
Giusti et al. [17]	2013	68.0	67.0	76.0	–	64.0	–
Pan et al. [37]	2013	86.7	95.8	–	–	91.0	–
Cantisani et al. [16]	2013	79.0	91.0	83.0	89.0	–	–
Ma et al. [38]	2014	–	–	–	–	–	0.910
Deng et al. [10]	2014	82.1	84.9	71.9	91.0	84.0	–
Jiang et al. [11]	2015	89.8	91.8	93.1	91.0	88.0	0.908 (0.847–0.969)
Schleder et al. [39]	2015	81.0	92.0	97.0	63.0	–	–
Li et al. [12]	2015	88.0	80.0	–	–	85.0	–
Sui et al. [40]	2016	81.8	90.7	93.1	90.7	85.3	0.883 (0.810 ± 0.956)
Prieditis et al. [32]	2016	82.0	57.0	–	70.0	–	–
Chen et al. [41]	2016	87.5	86.3	90.3	86.8	82.6	–
Zhang et al. [42]	2017	77.3	93.9	79.5	93.5	90.0	–
Rakitina et al. [29]	2017	94.1	87.5	97.0	77.8	92.8	–
Zhang et al. [13]	2017	97.6	98.7	97.6	98.7	98.3	–
Tian et al. [43]	2018	86.7	91.3	–	–	–	0.862 (0.813-0.924)
Sencha et al. [24]	2018	64.9	85.0				
Xu et al. [44]	2019	85.7	83.3	88.4	79.7	–	0.867 (0.830–0.905)

Table 13.2 The diagnostic value of CEUS on the data of meta-analyses

Author	Year	Number of studies	Number of thyroid lesions	Number of thyroid malignancies	Overall sensitivity (%) (CI)	Overall specificity (%) (CI)	PPV (%) (CI)	NPV (%) (CI)	AUC
Yu et al. [26]	2014	7	597	257	0.853 (0.80–0.89)	0.876 (0.84–0.91)	5.822 (3.51–9.66)	0.195 (0.13–0.30)	0.916
Sun et al. [27]	2015	25	1154	424	0.880 (0.85–0.91)	0.900 (0.88–0.92)	8.690 (5.76–13.09)	0.150 (0.12–0.19)	0.946
Ma et al. [45]	2015	13	1127		0.900 (0.88–0.93)	0.860 (0.83–0.89)	7.400 (3.63–15.08)	0.160 (0.09–0.28)	0.940
Liu et al. [28]	2018	33	3808	1840	0.880 (0.85–0.91)	0.880 (0.83–0.91)	7.100 (5.2–9.8)	0.130 (0.10–0.18)	0.940

increased vascularization. The authors skipped the grading and the specification of the UCA distribution. With the accumulation of knowledge, the descriptive part of the qualitative CEUS has expanded, but it is more of a recommendation than a standardized one [47].

Regarding the qualitative characteristics of CEUS, it is important to note that benign lesions are characterized by several types of enhancement. Peripheral rim-shaped enhancement is highly specific for benign lesions [15, 32, 38, 48]. Distinct margins and uniform character of

Table 13.3 The diagnostic value of the "heterogeneous enhancement" parameter of CEUS in the diagnosis of thyroid carcinoma

Author	Year	Sensitivity (%)	Specificity (%)	PPV (%)	NPV (%)	Accuracy (%)
Zhang et al. [15]	2010	88.2	92.5	91.8	89.1	90.4
Ma et al. [38]	2014	90.4	91.0	–	–	–
Yuan et al. [52]	2015	78.4	85.4	82.9	81.4	–
Deng et al. [53]	2015	73.1	75.3	74.8	–	
Wu et al. [19]	2016	50.6	90.7	77.6	74.3	75.1
Prieditis et al. [32]	2016	88.0	34.0	56.0	78.0	62.0
Ma et al. [54]	2017	83.5	82.9	88.0	78.3	83.7
Ballal et al. [48]	2017	92.5	93.2	95.2	88.2	92.4
Zhang et al. [14]	2017	40.5	92.3	73.9	74.2	74.2
Zhao et al. [55]	2018	82.0	74.0	82.0	74.0	78.7

Table 13.4 The diagnostic value of the "hypoenhancement" parameter of CEUS in the diagnosis of thyroid carcinoma

Author	Year	Sensitivity (%)	Specificity (%)	PPV (%)	NPV (%)	Accuracy (%)
Deng et al. [10]	2013	82.1	84.9	71.9	91.0	84.0
Ma et al. [38]	2014	66.0	82.1	–	–	–
Yuan et al. [52]	2015	78.4	95.1	93.6	83.0	–
Zhao et al. [18]	2015	97.6	85.7	93.0	94.7	93.5
Deng et al. [53]	2015	73.1	80.2	–	–	78.8
Wu et al. [19]	2016	41.6	95.7	86.1	72.0	74.7
Prieditis et al. [32]	2016	82.0	56.0	64.0	77.0	69.0
Ma et al. [54]	2017	78.5	55.4	71.3	64.6	68.9
Ballal et al. [48]	2017	82.4	96.9	97.8	76.8	89.3
Zhang et al. [14]	2017	40.5	92.3	73.9	74.2	74.2
Zhao et al. [55]	2018	56.7	73.3	75.5	53.9	63.5

enhancement are also considered benign features [29, 40, 49].

Heterogeneous arrival and distribution of UCA in the lesion along with its hypoenhancement are specific qualitative characteristics for thyroid carcinoma [18, 32, 41, 42, 48, 50, 51]. The diagnostic values of these qualitative parameters range in various studies and are presented in Tables 13.3 and 13.4.

Additional qualitative features of malignant lesions are irregular shape and indistinct boundaries of contrast enhancement [49, 50, 52, 54].

In recent studies, modern statistical analysis methods, such as ROC analysis [30, 38, 40, 43, 44, 53, 56], and construction of multimodal diagnostic models [31, 50, 54, 55] have been used for more effective evaluation of diagnostic parameters and prognosis.

Our study demonstrated a reliable difference in the uniformity of enhancement and UCA washout rate between the groups of malignant and benign thyroid masses [24]. Pseudonodules in autoimmune thyroid demonstrate uniform contrast enhancement and the UCA wash-in rate comparable to the surrounding thyroid parenchyma. It distinguishes autoimmune thyroid disease from all other groups and permits using the qualitative CEUS data for the differential diagnosis (Fig. 13.2).

The combined group of thyroid malignancies demonstrates a fast wash-out rate, which differentiates it from the group of benign lesions. However, binary logistic regression with ROC curves construction in the groups of benign and malignant thyroid masses demonstrates a low diagnostic value of individual qualitative enhancement parameters (Figs. 13.3, 13.4, 13.5, and 13.6, Video 13.1).

Quantitative perfusion analysis software uses raw data to construct time-intensity curves (TIC),

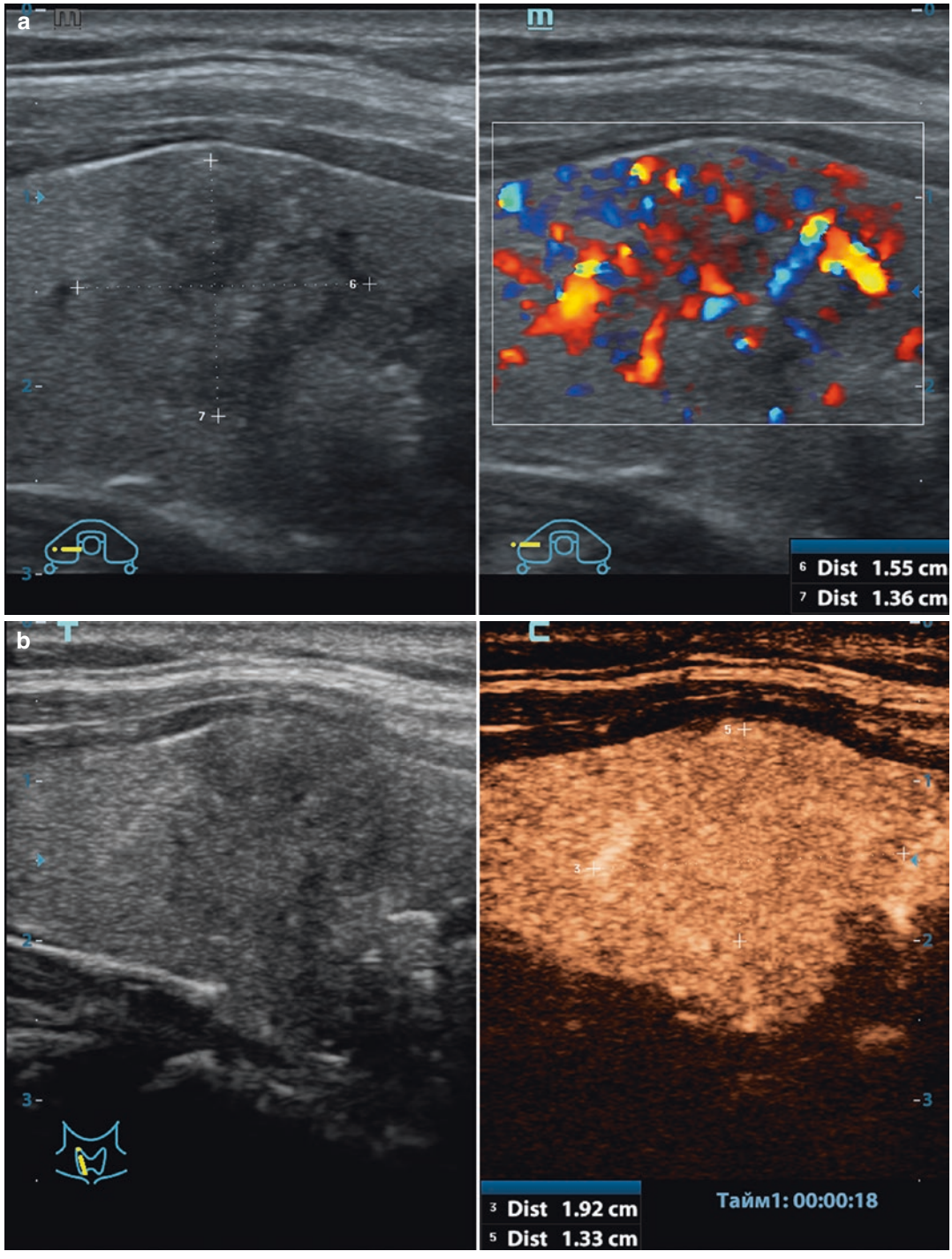

Fig. 13.2 Autoimmune thyroid disease with pseudonodules. (**a**) Grayscale and color Doppler image (**b**). The arterial phase CEUS image. The thyroid lesion and parenchyma exhibit identical homogeneous hyperenhancement

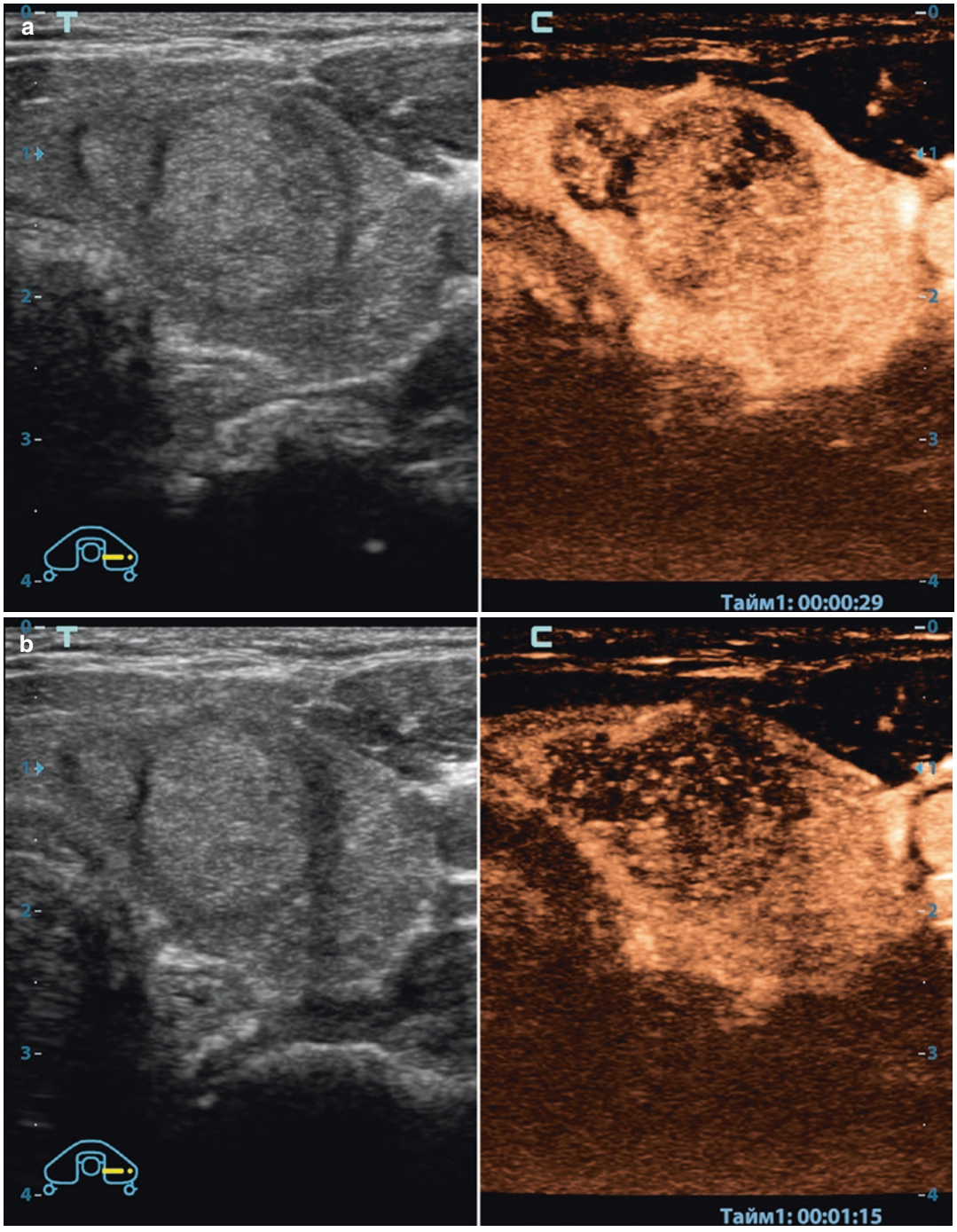

Fig. 13.3 Thyroid carcinoma. Irregular contrast enhancement of the lesion. CEUS images. (**a**) The arterial phase. (**b**) The venous phase

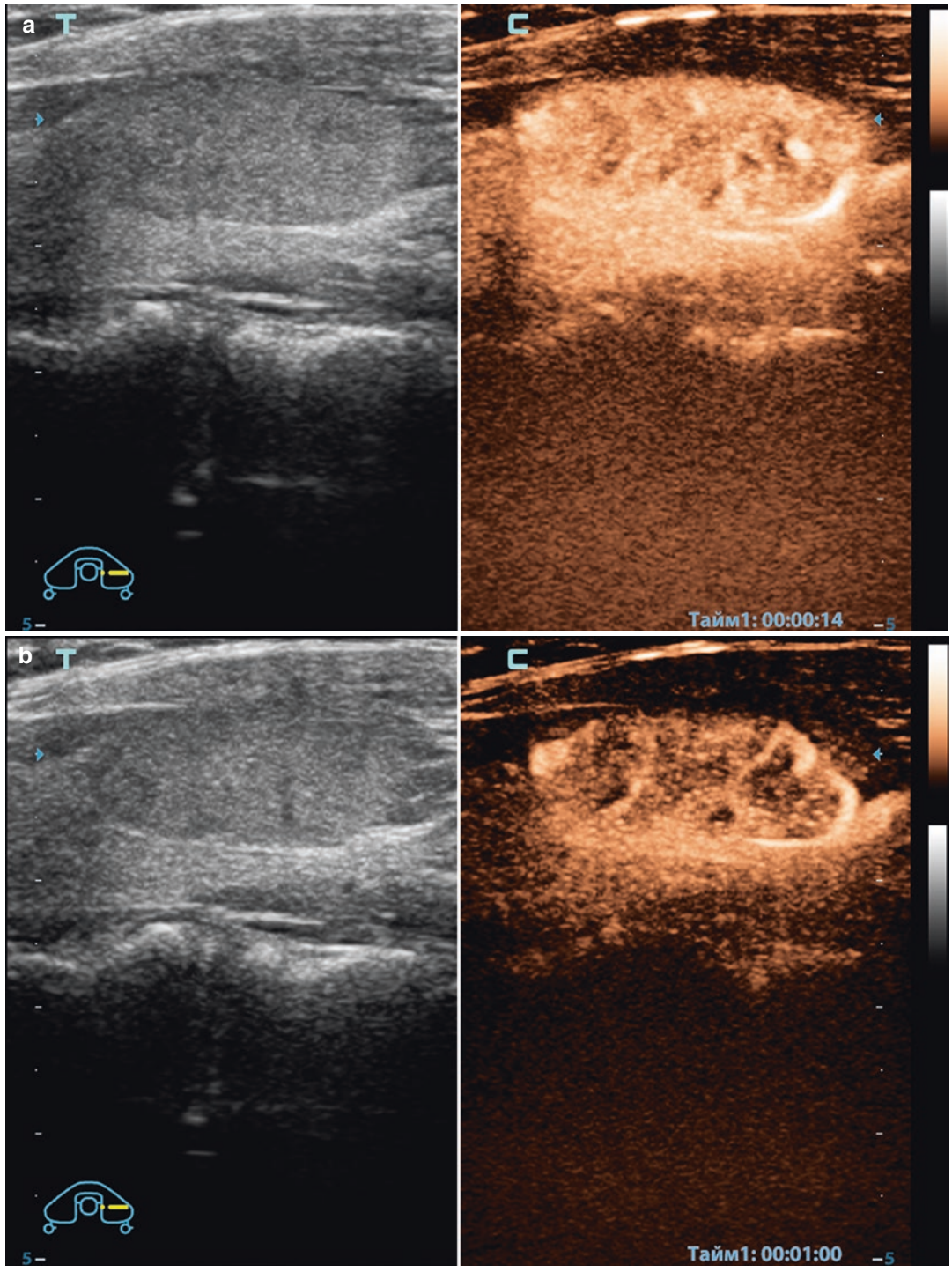

Fig. 13.4 Follicular thyroid adenoma. CEUS images. (**a**) The arterial phase. The lesion demonstrates clear boundaries, hyperenhancement with fast wash-in. (**b**) The venous phase. The wash-out rate of the lesion and the surrounding parenchyma is identical

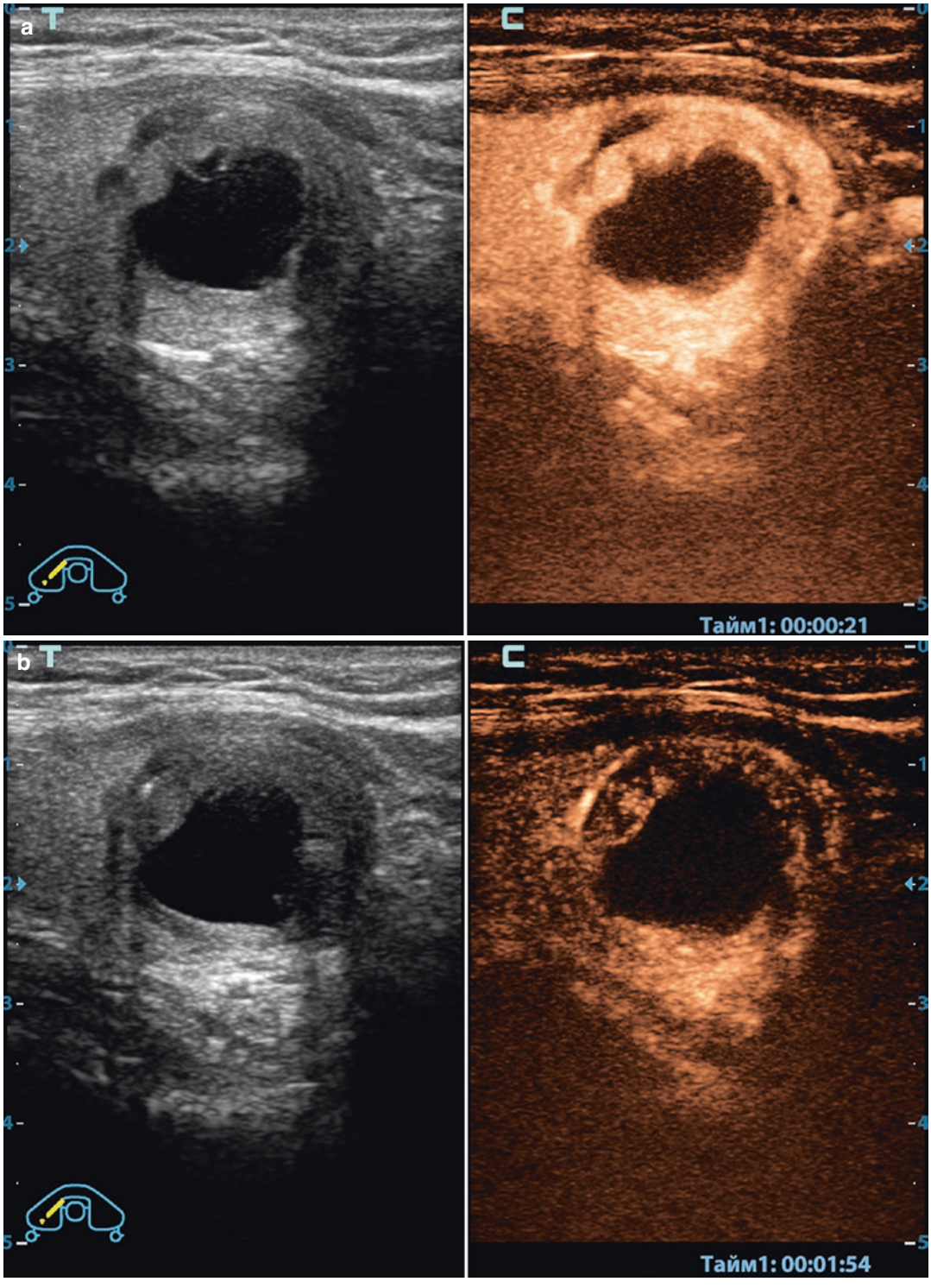

Fig. 13.5 Complex cystic lesion, thyroid carcinoma. CEUS images. (**a**) The arterial phase. (**b**) The venous phase

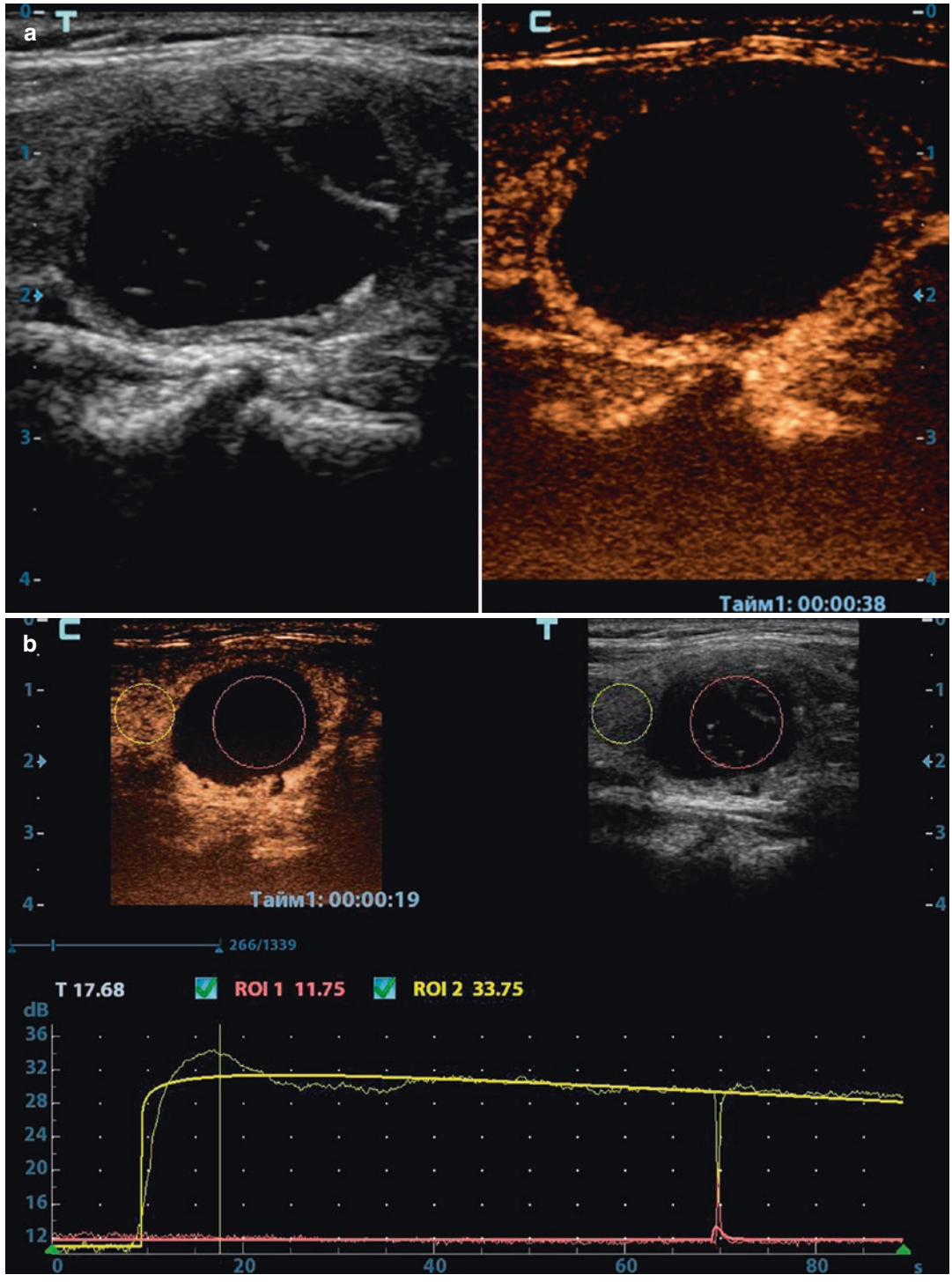

Fig. 13.6 Simple thyroid cyst with a single nonenhancing septum. (**a**) CEUS image. The early venous phase. (**b**) Quantitative analysis demonstrates the perfusion defect in the fluid component (pink ROI). The enhancement of the thyroid parenchyma is supplied for reference (yellow ROI)

permits more accurate and objective estimation of enhancement data, and increases intra- and interobserver agreement [20, 26, 31, 47, 51].

Many authors note that dynamic CEUS with subsequent TIC analysis enables a better understanding of the pathophysiology of neoangiogenesis in various thyroid pathologies and expands the prospects of the method in the differential diagnosis of thyroid lesions [9, 33, 51, 57–60]. TIC analysis is reported as efficient in oncology for objective evaluation of the tumor response to treatment [33].

The technology of three-dimensional visualization of CEUS with the algorithms for assessing the spatial location of small blood vessels in thyroid lesions is not widely available. It is analyzed in individual publications [46, 61], which point to its prospects for the differential diagnosis.

Although TIC analysis in thyroidology became popular over the past 5 years, the data of publications are still contradictory.

The first attempts to differentiate between carcinoma and follicular adenoma based on TIC characteristics were made by Spiezia et al. [1] with the first-generation UCA Levovist. Malignant thyroid lesion, as compared with colloid nodule and adenoma, demonstrated earlier contrast enhancement (8.1 ± 1.4 s vs. 19.6 ± 2.2 s, and 16.1 ± 2.8 s, respectively). However, there were no reliable differences in the initial, peak, and final contrast intensity between benign and malignant lesions.

The subsequent study by Argalia et al. [2] was limited to a visual assessment of the UCA kinetic without determining quantitative parameters. Most of the thyroid lesions were hyperenhancing. All nodules exhibited similar rapid distribution of UCA. However, most benign lesions had uniform monophase TIC, while thyroid carcinoma was characterized by an uneven polyphasic curve.

The first to provide quantitative parameters of perfusion was Bartolotta et al. [5]. Levovist exposure was calculated in certain time intervals for normal thyroid parenchyma and thyroid nodules. Based on the obtained overlapping results of the peak intensities of the studied lesions, the authors concluded that the method is not applicable for differential diagnosis in thyroid masses.

Similar contradictory data were obtained in the studies with the second-generation UCAs [14, 49]. The authors noted that time to peak (TTP) enhancement and wash-out time do not reliably differ in benign and malignant thyroid masses and suggested that there are no specific contrast enhancement features in thyroid lesions.

The study [7] presented a detailed quantitative analysis in thyroid CEUS. In addition to such values of benign and malignant lesions as the peak intensity (21.1± 4.0 dB and 22.8 ± 4.1 dB, respectively) and TTP (22.0 ± 6.9 s and 27.3 ± 11.1 s, respectively), the ratio of absolute intensity to base intensity in different time intervals of the TIC was estimated. The last parameter demonstrated good diagnostic value. The test "intensity ratio >2.35 in 20 s after peak intensity—thyroid carcinoma" demonstrated the sensitivity of 76.9% and accuracy of 82.6%.

CEUS quantification indices were also studied [17]. The area under the curve for the peak intensity index was 0.830, for the TTP intensity index 0.860. In malignant lesions, peak intensity index <0.99 demonstrated the sensitivity of 37.7% and specificity of 75.5%; TTP intensity index >0.98–56.6% and 75.5%, respectively.

The study [11] considered maximum peak intensity and TTP intensity. In papillary cancer, the maximum peak intensity value was 84 ± 9 units and TTP intensity 17 ± 1 s and in benign tumors 121 ± 17 and 14 ± 1 s, respectively. However, the difference was statistically significant only in the maximum peak intensity value parameter ($p < 0.05$). In another study, the authors report a statistically significant difference in the peak intensity values between malignant and benign lesions (41.40 ± 14.10% and 85.58 ± 10.76, respectively) [30]. The area under the curve was 0.908 ± 0.031 (95%CI 0.847–0.969).

The study [59] demonstrated that thyroid carcinomas ($N = 20$) had complete wash-out in the late phase, which was not typical for benign lesions and registered in 10% of adenomas. The authors noted one enhancement feature. The TTP enhancement between the central aspects of carcinoma and the surrounding parenchyma was different ($p < 0.05$), as well as TTP enhancement between the borderline zone and the surrounding tissues ($p = 0.01$). CEUS with TIC analysis per-

mitted dynamic assessment of the thyroid microvascularization, which is useful for the differentiation of benign and malignant nodules.

Relative values of perfusion for malignant lesions are different from benign lesions [60]. Carcinomas are characterized by low relative peak intensity, later relative rise time and TTP, gentler maximum slope coefficient of wash-in, and smaller area under the rising and falling curves, earlier relative mean transit time (MTT).

Low values of the maximum peak intensity were reported for malignant neoplasms as compared with benign lesions (42 ± 4.8 vs. 54 ± 5.4, respectively) with no reliable difference in TTP (19.21 ± 1.3 s vs. 17.77 ± 6.6, respectively) [48].

The quantitative parameter "peak intensity" and the qualitative characteristic "enhancement pattern" are reliably different between the groups of malignant and benign thyroid lesions [18]. The sensitivity, specificity, PPV, NPV, and accuracy of heterogeneous enhancement were 97.6%, 85.7%, 93.0%, 94.7%, and 93.5%, respectively. The sensitivity, specificity, PPV, NPV, and accuracy of low intensity at peak time were 85.4%, 52.4%, 77.8%, 64.7%, and 74.2%, respectively.

In our study, we obtained reliable differences between benign and malignant lesions in the values of the peak intensity of the nodule and parenchyma, DT/2 of the nodule, DT/2 index, descending velocity (DV) of the nodule, DV index, DV difference ($p < 0.05$). The most valuable for the diagnosis of thyroid cancer were the DT/2 index, DV index, and DV difference. The test "DT/2 index >1.028—thyroid cancer" was characterized by the sensitivity of 86.1%, the specificity of 85.2%, PPV of 87.7%, NPV of 83.4%, and AUC of 0.872. The test "DV index ≤0.895—thyroid cancer" was characterized by the sensitivity of 66.7%, the specificity of 95.1%, PPV of 94.3%, NPV of 70.0%, and AUC of 0.840. The test "DV difference ≤-0.020 dB/s—thyroid cancer" exhibited the sensitivity of 66.7%, specificity of 95.1%, PPV of 94.3%, NPV of 70.0%, and AUC of 0.842 (Figs. 13.7 and 13.8).

CEUS is a promising non-invasive method for the differential diagnosis of benign and malignant thyroid nodules and may complement fine-needle aspiration biopsy. Quantitative analysis of enhancement can help to improve the specificity and accuracy of sonography [62–64]. Thyroid CEUS is beneficial in the nodules with calcification and exhibits the sensitivity of 90%, the specificity of 92%, PPV of 88%, NPV of 93%, and accuracy of 91%, as compared to standard sonography (the sensitivity of 50%, the specificity of 77%, PPV of 59%, NPV of 69%, and accuracy of 66%) [30].

For *parathyroid gland* abnormalities, CEUS is a new method, which depicts perfusion.

It is thought to improve the differential diagnosis of the diseases of the parathyroid glands and other neck organs. It may appear especially valuable in parathyroid lesions or hyperplasia, which appear avascular with CDI and PDI and demand differentiation from the thyroid lesions and other neck masses [65]. CEUS can be proposed in selected patients in whom unenhanced color Doppler provides uncertain findings. The contrast agent helps in visualizing typical signs of the parathyroid lesions, such as "vascular pole" and "mixed pattern."

The lesions of parathyroid glands exhibit different contrast enhancement patterns. Their enhancement intensity is usually compared with the normal thyroid parenchyma. Parathyroid adenoma often demonstrates hyperenhancement, while normal parathyroid glands, if identified, are hypoenhanced (Fig. 13.9).

However, the fact of increased perfusion of a parathyroid lesion as compared with other masses is remarkable. Further determination of the vascular pattern in parathyroid hyperplasia or adenoma does not influence the conclusion and further management (Figs. 13.10 and 13.11, Video 13.2).

CEUS permits differentiation of parathyroid adenoma in 99% of cases, as compared with 70% with conventional echography [66]. The sensitivity of the method in the differentiation of abnormal parathyroid glands is 89.3–98.4% [64, 65, 67]. CEUS is also beneficial for the differentiation of abnormal parathyroid glands in concomitant thyroid nodules, after thyroid surgery, and in neck tumors [60, 61, 63]. Parathyroid adenoma is characterized by the time of complete washout of 30–60 s as opposed to the same of thyroid nodules of 120–180 s [66].

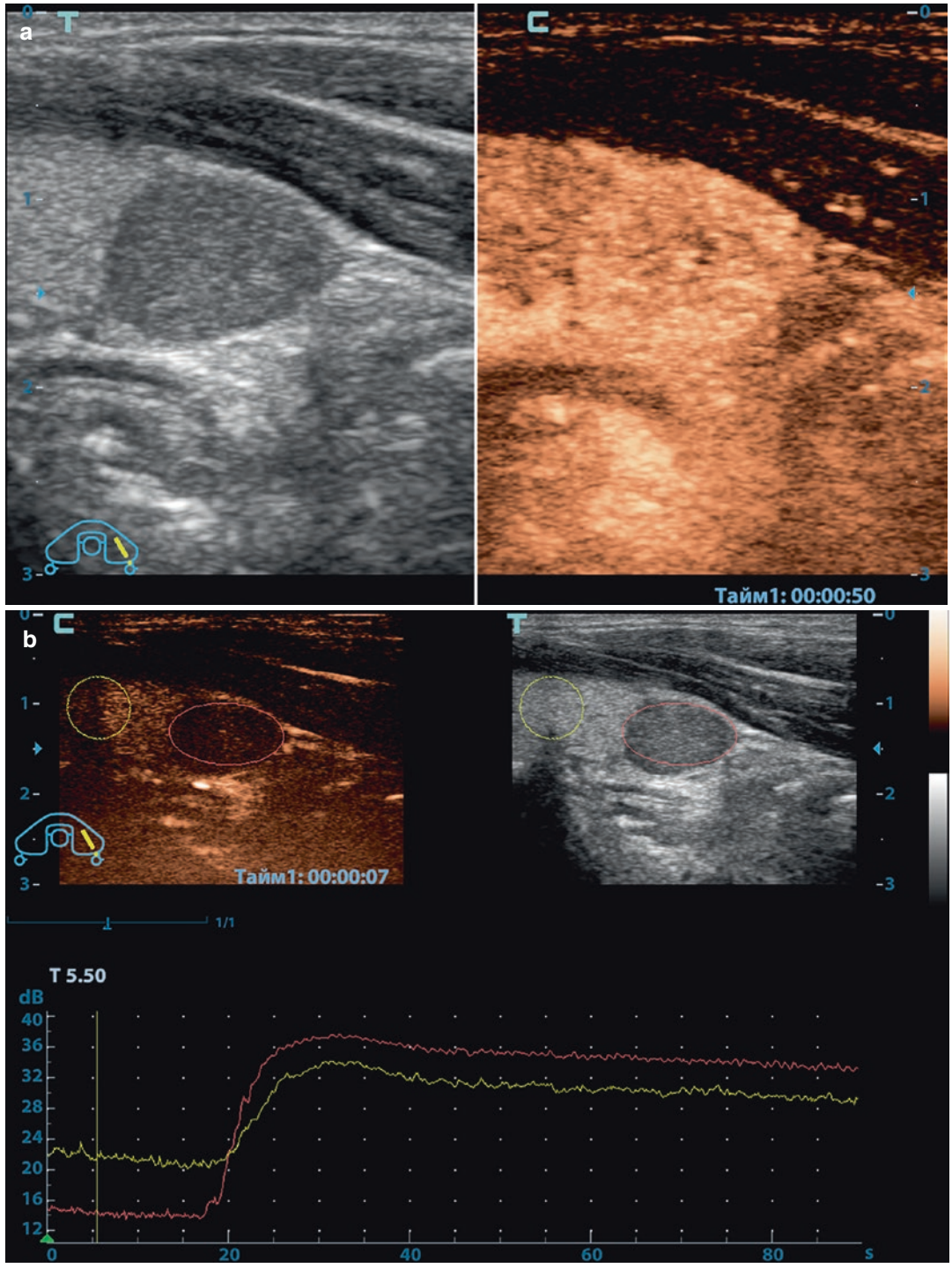

Fig. 13.7 Follicular thyroid carcinoma. (**a**) CEUS image in the venous phase. (**b**) The analysis of quantitative characteristics of contrast enhancement. TICs for carcinoma (pink ROI) and intact thyroid parenchyma (yellow ROI)

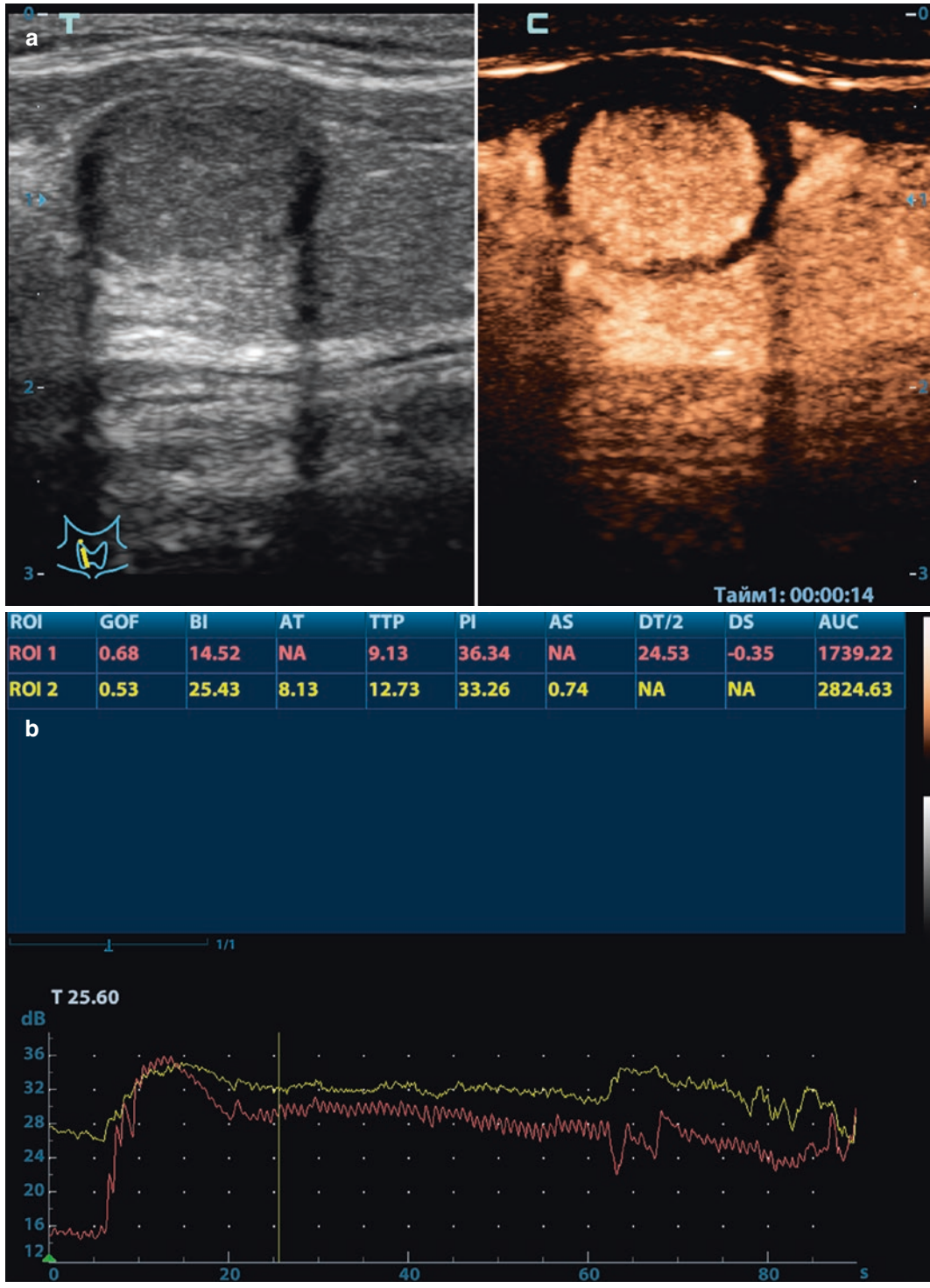

Fig. 13.8 Follicular thyroid adenoma. (**a**) CEUS image in the arterial phase. (**b**) The analysis of quantitative characteristics of contrast enhancement with TIC construction

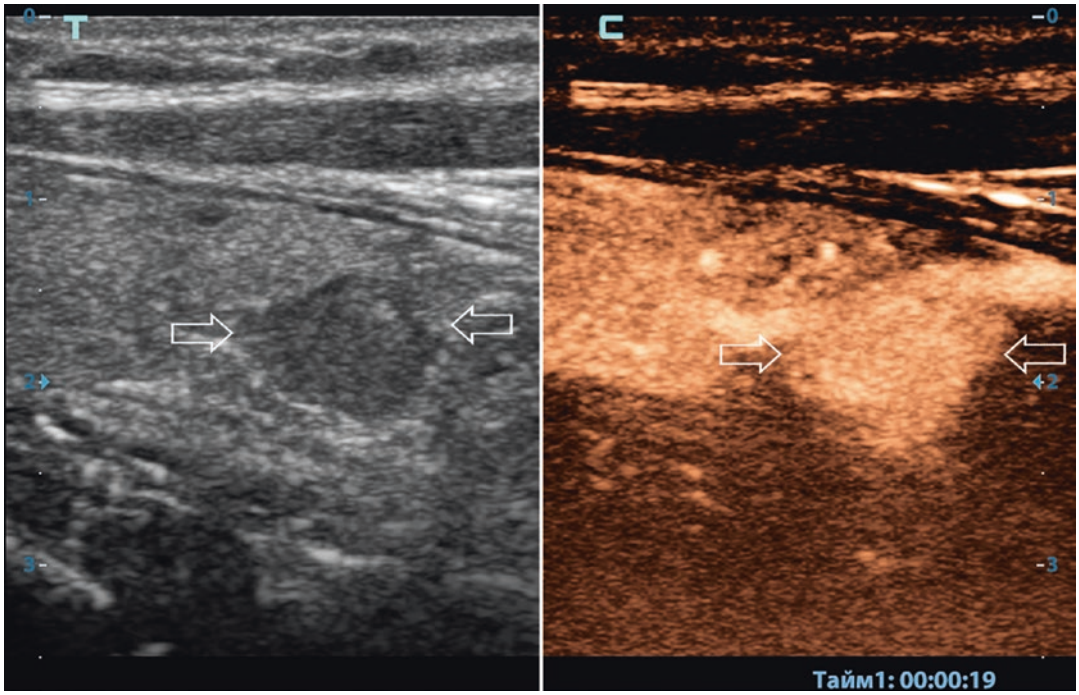

Fig. 13.9 Parathyroid adenoma. CEUS image shows diffuse mild arterial phase hyperenhancement of a parathyroid adenoma (between arrows)

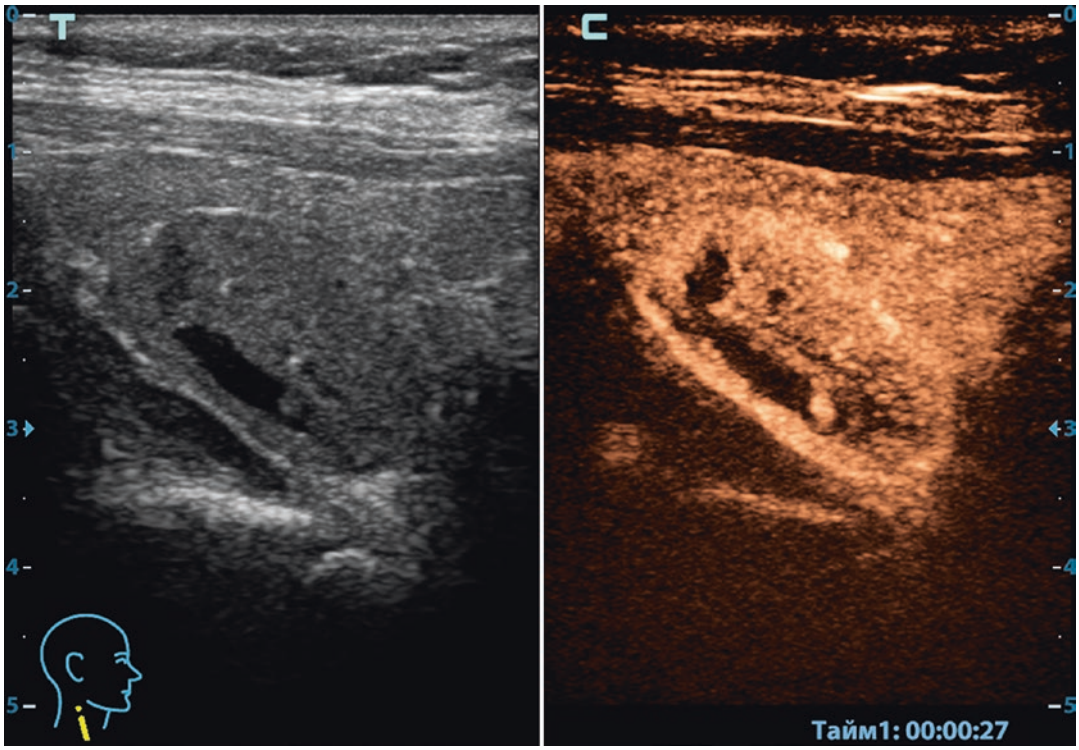

Fig. 13.10 Parathyroid adenoma. CEUS image demonstrates heterogeneous hyperenhancement of the adenoma in the arterial phase with perfusion defects due to cystic degeneration

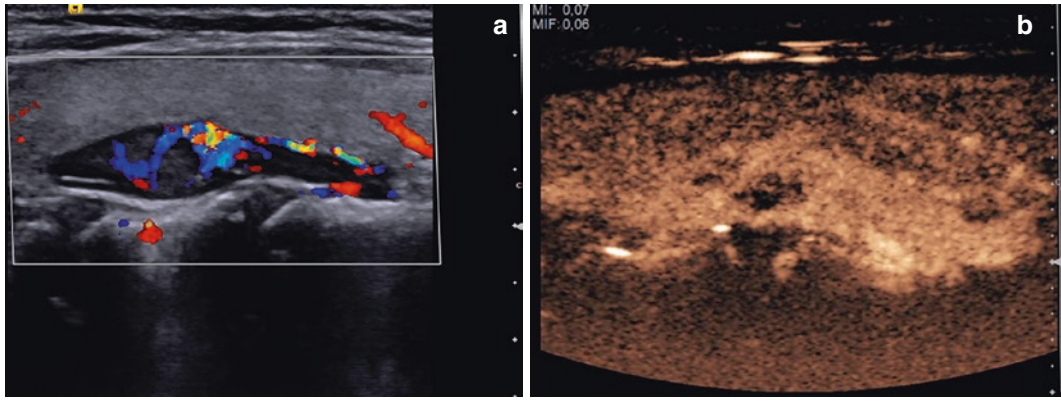

Fig. 13.11 Parathyroid adenoma. (**a**) Typical appearance of the superior parathyroid gland adenoma along the posterior aspect of the thyroid lobe with branching vessels with CDI. (**b**) CEUS image demonstrates hyperenhancement of the adenoma in the arterial phase with small perfusion defects

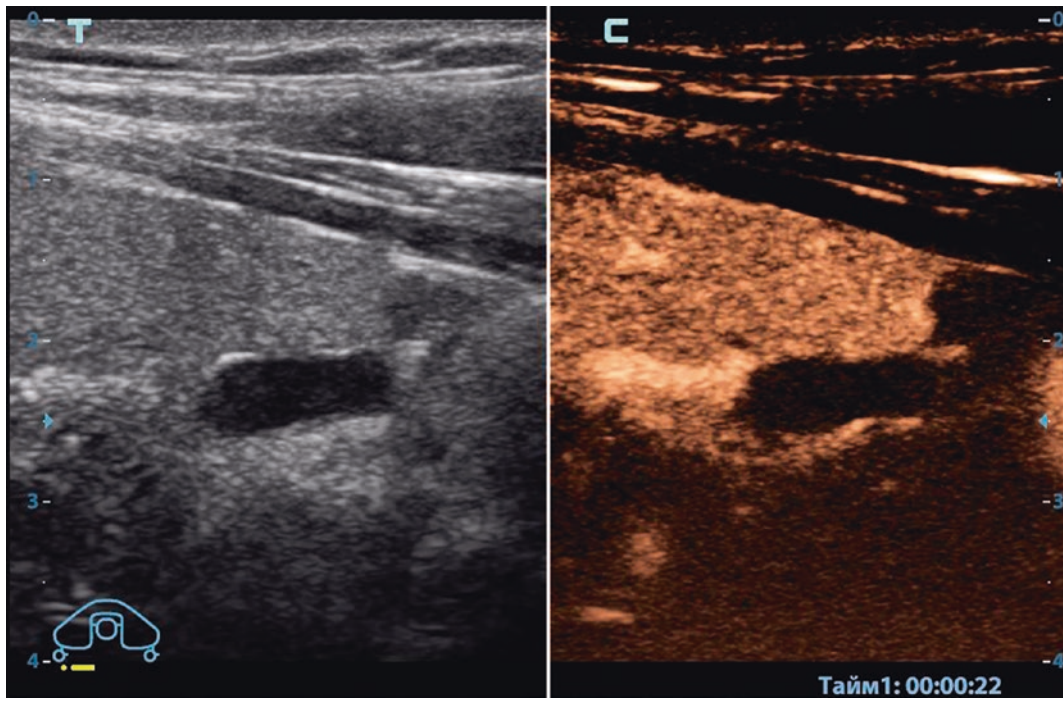

Fig. 13.12 Parathyroid cyst. The arterial phase CEUS image demonstrates no lesion enhancement

Parathyroid cyst demand differentiation from cystic thyroid lesion, lateral neck cyst, neck lymph node metastasis, etc. All parathyroid cysts with CEUS demonstrate a perfusion defect, which is typical for all fluid-containing cavities. However, the capsule of a parathyroid cyst is thin and does not enhance (Fig. 13.12).

Quantitative assessment of the perfusion within the lesion is expected to supply more reliable and reproducible data.

CEUS of the thyroid and parathyroid glands is a promising non-invasive diagnostic method. However, further studies are necessary to specify its place in the diagnostic flowchart in different abnormalities.

References

1. Spiezia S, Farina R, Cerbone G, Assanti AP, Iovino V, Siciliani M, et al. Analysis of color Doppler signal intensity variation after levovist injection: a new approach to the diagnosis of thyroid nodules. J Ultrasound Med. 2001;20(3):223–31. https://doi.org/10.7863/jum.2001.20.3.223.
2. Argalia G, De Bernardis S, Mariani D, Abbattista T, Taccaliti A, Ricciardelli L, et al. Ultrasonographic contrast agent: evaluation of time-intensity curves in the characterisation of solitary thyroid nodules. Radiol Med. 2002;103(4):407–13.
3. Appetecchia M, Bacaro D, Brigida R, Milardi D, Bianchi A, Solivetti F. Second generation ultrasonographic contrast agents in the diagnosis of neoplastic thyroid nodules. J Exp Clin Cancer Res. 2006;25(3):325–30.
4. SonoVue® product monograph. Dynamic contrast enhancement in real time. https://products.braccoimaging.com/sites/braccoimaging.com/files/technica_sheet_pdf/se-en-2016-04-30-monograph-sonovue.pdf. Accessed 26 Feb 2021.
5. Bartolotta TV, Midiri M, Galia M, Runza G, Attard M, Savoia G, et al. Qualitative and quantitative evaluation of solitary thyroid nodules with contrast-enhanced ultrasound: initial results. Eur Radiol. 2006;16(10):2234–41. https://doi.org/10.1007/s00330-006-0229-y.
6. Ferrari FS, Megliola A, Scorzelli A, Guarino E, Pacini F. Ultrasound examination using contrast agent and elastosonography in the evaluation of single thyroid nodules: preliminary results. J Ultrasound. 2008;11(2):47–54. https://doi.org/10.1016/j.jus.2008.03.004.
7. Nemec U, Nemec SF, Novotny C, Weber M, Czerny C, Krestan CR. Quantitative evaluation of contrast-enhanced ultrasound after intravenous administration of a microbubble contrast agent for differentiation of benign and malignant thyroid nodules: assessment of diagnostic accuracy. Eur Radiol. 2012;22(6):1357–65. https://doi.org/10.1007/s00330-012-2385-6.
8. Li F, Luo H. Comparative study of thyroid puncture biopsy guided by contrast-enhanced ultrasonography and conventional ultrasound. Exp Ther Med. 2013;5(5):1381–4. https://doi.org/10.3892/etm.2013.1016.
9. Zhou Q, Jiang J, Shang X, Zhang HL, Ma WQ, Xu YB, et al. Correlation of contrast-enhanced ultrasonographic features with microvessel density in papillary thyroid carcinomas. Asian Pac J Cancer Prev. 2014;15(17):7449–52. https://doi.org/10.7314/apjcp.2014.15.17.7449.
10. Deng J, Zhou P, Tian SM, Zhang L, Li JL, Qian Y. Comparison of diagnostic efficacy of contrast-enhanced ultrasound, acoustic radiation force impulse imaging, and their combined use in differentiating focal solid thyroid nodules. PLoS One. 2014;9(3):e90674. https://doi.org/10.1371/journal.pone.0090674.
11. Jiang J, Huang L, Zhang H, Ma W, Shang X, Zhou Q, et al. Contrast-enhanced sonography of thyroid nodules. J Clin Ultrasound. 2015;43(3):153–6. https://doi.org/10.1002/jcu.22240.
12. Li F, Zhang J, Wang Y, Liu L. Clinical value of elasticity imaging and contrast-enhanced ultrasound in the diagnosis of papillary thyroid microcarcinoma. Oncol Lett. 2015;10(3):1371–7. https://doi.org/10.3892/ol.2015.3387.
13. Zhang Y, Zhou P, Tian SM, Zhao YF, Li JL, Li L. Usefulness of combined use of contrast-enhanced ultrasound and TI-RADS classification for the differentiation of benign from malignant lesions of thyroid nodules. Eur Radiol. 2017;27(4):1527–36. https://doi.org/10.1007/s00330-016-4508-y.
14. Friedrich-Rust M, Sperber A, Holzer K, Diener J, Grünwald F, Badenhoop K, et al. Real-time elastography and contrast-enhanced ultrasound for the assessment of thyroid nodules. Exp Clin Endocrinol Diabetes. 2010;118(9):602–9. https://doi.org/10.1055/s-0029-1237701.
15. Zhang B, Jiang YX, Liu JB, Yang M, Dai Q, Zhu QL, Gao P. Utility of contrast-enhanced ultrasound for evaluation of thyroid nodules. Thyroid. 2010;20(1):51–7. https://doi.org/10.1089/thy.2009.0045.
16. Cantisani V, Consorti F, Guerrisi A, Guerrisi I, Ricci P, Di Segni M, et al. Prospective comparative evaluation of quantitative-elastosonography (Q-elastography) and contrast-enhanced ultrasound for the evaluation of thyroid nodules: preliminary experience. Eur J Radiol. 2013;82(11):1892–8. https://doi.org/10.1016/j.ejrad.2013.07.005.
17. Giusti M, Orlandi D, Melle G, Massa B, Silvestri E, Minuto F, Turtulici G. Is there a real diagnostic impact of elastosonography and contrast-enhanced ultrasonography in the management of thyroid nodules? J Zhejiang Univ Sci B. 2013;14(3):195–206. https://doi.org/10.1631/jzus.B1200106.
18. Zhao RN, Zhang B, Yang X, Jiang YX, Lai XJ, Zhu SL, Zhang XY. Diagnostic value of contrast-enhanced ultrasound of thyroid nodules coexisting with Hashimoto's thyroiditis. Zhongguo Yi Xue Ke Xue Yuan Xue Bao. 2015;37(1):66–70. https://doi.org/10.3881/j.issn.1000-503X.2015.01.012.
19. Wu Q, Wang Y, Li Y, Hu B, He ZY. Diagnostic value of contrast-enhanced ultrasound in solid thyroid nodules with and without enhancement. Endocrine. 2016;53(2):480–8. https://doi.org/10.1007/s12020-015-0850-0.
20. Sencha AN, Mogutov MS, Patrunov YN, Penyaeva EI, Kashmanova AV, Sencha EA. Ul'trazvukovoe issledovanie s ispol'zovaniem kontrastnyh preparatov [Ultrasound examination with contrast agents]. Moscow: Vidar-M; 2015.
21. Sencha AN, Mogutov MS, Penyaeva EI, Patrunov YN, Kashmanova AV, Sencha EA. Ul'trazvukovoe issle-

dovanie s kontrastnym usileniem v differencial'noj diagnostike uzlovyh obrazovanij shchitovidnoj zhelezy [Ultrasound examination with contrast enhancement in the differential diagnosis of thyroid nodules]. Ultrasound Funct Diagn. 2015;4:158–9.
22. Sencha AN, Mogutov MS, Patrunov YN, Penyaeva EI, Kashmanova AV, Sencha EA. Value of contrast enhanced ultrasound in thyroid cancer diagnosis. Ultrasound Funct Diagn. 2015;6:10–26.
23. Sencha EA. Contrast-enhanced ultrasound in thyroid nodules diagnosis. REJR. 2017;7(3):44–52. https://doi.org/10.21569/2222-7415-2017-7-3-44-52.
24. Sencha EA, Sencha AN, Penyaeva EI, Patrunov YN, Mitkova MD, Mitkov VV. Quantitative contrast-enhanced ultrasound in differential diagnosis of benign and malignant thyroid nodules. Ultrasound Funct Diagn. 2018;2:12–26.
25. Sidhu PS, Cantisani V, Dietrich CF, Gilja OH, Saftoiu A, Bartels E, et al. The EFSUMB guidelines and recommendations for the clinical practice of contrast-enhanced ultrasound (CEUS) in non-Hepatic applications: update 2017. Ultraschall Med. 2018;39(2):e2–e44. https://doi.org/10.1055/a-0586-1107.
26. Yu D, Han Y, Chen T. Contrast-enhanced ultrasound for differentiation of benign and malignant thyroid lesions: meta-analysis. Otolaryngol Head Neck Surg. 2014;151(6):909–15. https://doi.org/10.1177/0194599814555838.
27. Sun B, Lang L, Zhu X, Jiang F, Hong Y, He L. Accuracy of contrast-enhanced ultrasound in the identification of thyroid nodules: a meta-analysis. Int J Clin Exp Med. 2015;8(8):12882–9.
28. Liu Q, Cheng J, Li J, Gao X, Li H. The diagnostic accuracy of contrast-enhanced ultrasound for the differentiation of benign and malignant thyroid nodules: a PRISMA compliant meta-analysis. Medicine. 2018;97(49):e13325. https://doi.org/10.1097/MD.0000000000013325.
29. Rakitina DA, Belyaev AM, Radzhabova ZA, Kostromina EV, Kotov MA, Nazhmudinov RA. Znachimost' metoda ul'trazvukovogo issledovaniya shchitovidnoj zhelezy s kontrastnym usileniem v differencial'noj diagnostike ochagovyh uzlovyh obrazovanij [The significance of the method of ultrasound examination of the thyroid gland with contrast enhancement in the differential diagnosis of focal nodular lesions]. Opuholi golovy i shei. 2017;7:12–5.
30. Jiang J, Shang X, Wang H, Xu YB, Gao Y, Zhou Q. Diagnostic value of contrast-enhanced ultrasound in thyroid nodules with calcification. Kaohsiung J Med Sci. 2015;31(3):138–44. https://doi.org/10.1016/j.kjms.2014.12.001.
31. Liang XN, Guo RJ, Li S, Zheng ZM, Liang HD. Binary logistic regression analysis of solid thyroid nodules imaged by high-frequency ultrasonography, acoustic radiation force impulse, and contrast-enhanced ultrasonography. Eur Rev Med Pharmacol Sci. 2014;18(23):3601–10.
32. Prieditis P, Radzina M, Strumfa I, Narbuts Z, Ozolins A, Vanags A, Gardovskis J. Diagnostic value of contrast-enhanced ultrasound evaluation of malignant and benign solitary thyroid nodules. Proc Latvian Acad Sci. 2016;70(1):1–6. https://doi.org/10.1515/prolas-2016-0001.
33. Dietrich CF, Averkiou M, Nielsen MB, Barr RG, Burns PN, Calliada F, et al. How to perform contrast-enhanced ultrasound (CEUS). Ultrasound Int Open. 2018;4(1):E2–E15. https://doi.org/10.1055/s-0043-123931.
34. Sencha EA, Sencha AN, Penyaeva EI, Patrunov YN, Mit'kova MD, Mit'kov VV. Ul'trazvukovoe issledovanie s kontrastnym usileniem v differencial'noj diagnostike ochagovyh obrazovanij shchitovidnoj zhelezy [Ultrasound examination with contrast enhancement in the differential diagnosis of focal thyroid lesions]. Ultrasound Funct Diagn. 2019;3:S80.
35. Piskunowicz M, Kosiak W, Batko T. Intravenous application of second-generation ultrasound contrast agents in children: a review of the literature. Ultraschall Med. 2012;33(2):135–40. https://doi.org/10.1055/s-0031-1281936.
36. Feoktistova EV, Belyakova LA, Varfolomeeva SR. Contrast-enhanced ultrasound (CEUS) in pediatric oncology (literature review). Ultrasound Funct Diagn. 2016;5:22–32.
37. Pan J, Qin W, Deng B, Ma J, Wang H. Clinical value of combined contrast-enhanced ultrasonography with core-needle biopsy in diagnosis of thyroid nodules. Lingnan Mod Clin Surg. 2013;13(5):424–6. https://doi.org/10.3969/j.issn.1009-976X.2013.05.016.
38. Ma JJ, Ding H, Xu BH, Xu C, Song LJ, Huang BJ, Wang WP. Diagnostic performances of various gray-scale, color Doppler, and contrast-enhanced ultrasonography findings in predicting malignant thyroid nodules. Thyroid. 2014;24(2):355–63. https://doi.org/10.1089/thy.2013.0150.
39. Schleder S, Janke M, Agha A, Schacherer D, Hornung M, Schlitt HJ, et al. Preoperative differentiation of thyroid adenomas and thyroid carcinomas using high resolution contrast-enhanced ultrasound (CEUS). Clin Hemorheol Microcirc. 2015;61(1):13–22. https://doi.org/10.3233/CH-141848.
40. Sui X, Liu HJ, Jia HL, Fang QM. Contrast-enhanced ultrasound and real-time elastography in the differential diagnosis of malignant and benign thyroid nodules. Exp Ther Med. 2016;12(2):783–91. https://doi.org/10.3892/etm.2016.3344.
41. Chen M, Zhang KQ, Xu YF, Zhang SM, Cao Y, Sun WQ. Shear wave elastography and contrast-enhanced ultrasonography in the diagnosis of thyroid malignant nodules. Mol Clin Oncol. 2016;5(6):724–30. https://doi.org/10.3892/mco.2016.1053.
42. Zhang Y, Zhang MB, Luo YK, Li J, Wang ZL, Tang J. The value of peripheral enhancement pattern for diagnosing thyroid cancer using contrast-enhanced ultrasound. Int J Endocrinol. 2018;2018:1625958. https://doi.org/10.1155/2018/1625958.

43. Tian Q, Zhu H, Li H. Significance of contrast-enhanced ultrasonography in differential diagnosis of thyroid nodules. Medicine. 2018;97(40):e12688. https://doi.org/10.1097/MD.0000000000012688.
44. Xu Y, Qi X, Zhao X, Ren W, Ding W. Clinical diagnostic value of contrast-enhanced ultrasound and TI-RADS classification for benign and malignant thyroid tumors: one comparative cohort study. Medicine. 2019;98(4):e14051. https://doi.org/10.1097/MD.0000000000014051.
45. Ma X, Zhang B, Ling W, Liu R, Jia H, Zhu F, et al. Contrast-enhanced sonography for the identification of benign and malignant thyroid nodules: systematic review and meta-analysis. J Clin Ultrasound. 2016;44(4):199–209. https://doi.org/10.1002/jcu.22311.
46. Carraro R, Molinari F, Deandrea M, Garberoglio R, Suri JS. Characterization of thyroid nodules by 3-D contrast-enhanced ultrasound imaging. Annu Int Conf IEEE Eng Med Biol Soc. 2008;2008:2229–32. https://doi.org/10.1109/IEMBS.2008.4649639.
47. Claudon M, Dietrich CF, Choi BI, Cosgrove DO, Kudo M, Nolsøe CP, et al. Guidelines and good clinical practice recommendations for contrast enhanced ultrasound (CEUS) in the liver–update 2012: a WFUMB-EFSUMB initiative in cooperation with representatives of AFSUMB, AIUM, ASUM, FLAUS and ICUS. Ultraschall Med. 2013;34(1):11–29. https://doi.org/10.1055/s-0032-1325499.
48. Ballal S, Yadav MP, Gupta AK, Jana M, Deo SS. Comparison of conventional ultrasound, Doppler, elastography and contrast enhanced ultrasonography parameters with histopathology findings in the differential diagnosis of benign and malignant thyroid nodules. Thyroid Disorders Ther. 2016;6:213. https://doi.org/10.4172/2167-7948.1000213.
49. Gong H, Li C, Ye X. Diagnostic value of contrast-enhanced ultrasonography in differentiating benign thyroid nodules from malignant. Jiangsu Med J. 2014;18:2126–8.
50. Hong YR, Yan CX, Mo GQ, Luo ZY, Zhang Y, Wang Y, Huang PT. Conventional US, elastography, and contrast enhanced US features of papillary thyroid microcarcinoma predict central compartment lymph node metastases. Sci Rep. 2015;5:7748. https://doi.org/10.1038/srep07748.
51. Hu Y, Li P, Jiang S, Li F. Quantitative analysis of suspicious thyroid nodules by contrast-enhanced ultrasonography. Int J Clin Exp Med. 2015;8(7):11786–93.
52. Yuan Z, Quan J, Yunxiao Z, Jian C, Zhu H. Contrast-enhanced ultrasound in the diagnosis of solitary thyroid nodules. J Cancer Res Ther. 2015;11(1):41–5. https://doi.org/10.4103/0973-1482.147382.
53. Deng Y, He Y, Yang H, Fang Q, Chu T, Guo L. Value of thyroid imaging reporting and data system combined with contrast enhanced ultrasound in differential diagnosis of benign and malignant thyroid nodules. Guangxi Med J. 2015;8:1079–81.
54. Ma HJ, Yang JC, Leng ZP, Chang Y, Kang H, Teng LH. Preoperative prediction of papillary thyroid microcarcinoma via multiparameter ultrasound. Acta Radiol. 2017;58(11):1303–11. https://doi.org/10.1177/0284185117692167.
55. Zhao RN, Zhang B, Jiang YX, Yang X, Lai XJ, Zhu SL, Zhang XY. Ultrasonographic multimodality diagnostic model of thyroid nodules. Ultrason Imaging. 2019;41(2):63–77. https://doi.org/10.1177/0161734618815070.
56. Martynova E. Ispol'zovanie UZI, elastografii, kontrastno-usilennogo UZI dlya ocenki riska zlokachestvennosti uzlovyh obrazovanij shchitovidnoj zhelezy s neopredelennoj citologiej [The use of ultrasound, elastography, contrast-enhanced ultrasound to assess the risk of malignancy of thyroid nodules with indeterminate cytology]. Aktual'naya Endokrinol. 2015;1:4–8.
57. Greis C. Quantitative evaluation of microvascular blood flow by contrast-enhanced ultrasound (CEUS). Clin Hemorheol Microcirc. 2011;49(1-4):137–49. https://doi.org/10.3233/CH-2011-1464.
58. Gauthier TP, Averkiou MA, Leen EL. Perfusion quantification using dynamic contrast-enhanced ultrasound: the impact of dynamic range and gain on time-intensity curves. Ultrasonics. 2011;51(1):102–6. https://doi.org/10.1016/j.ultras.2010.06.004.
59. Wendl CM, Janke M, Jung W, Stroszczysnski C, Jung EM. Contrast-enhanced ultrasound with perfusion analysis for the identification of malignant and benign tumours of the thyroid gland. Clin Hemorheol Microcirc. 2015;63(2):113–21. https://doi.org/10.3233/CH-151966.
60. Gu F, Han L, Yang X, Liu H, Li X, Guo K, et al. Value of time-intensity curve analysis of contrast-enhanced ultrasound in the differential diagnosis of thyroid nodules. Eur J Radiol. 2018;105:182–7. https://doi.org/10.1016/j.ejrad.2018.05.013.
61. Molinari F, Mantovani A, Deandrea M, Limone P, Garberoglio R, Suri JS. Characterization of single thyroid nodules by contrast-enhanced 3-D ultrasound. Ultrasound Med Biol. 2010;36(10):1616–25. https://doi.org/10.1016/j.ultrasmedbio.2010.07.011.
62. Sencha AN. Ul'trazvukovoe shchitovidnoj zhelezy. Shag za shagom. Ot prostogo k slozhnomu [Ultrasound of the thyroid gland. Step by step. From simple to complex]. Moscow: MEDpress; 2019.
63. Sencha AN, Patrunov YN. Thyroid ultrasound. From simple to complex. Berlin: Springer; 2019.
64. Sencha AN. UZI okoloshchitovidnyh i slyunnyh zhelez. Ot prostogo k slozhnomu [Ultrasound of the parathyroid and salivary glands. From simple to complex]. Moscow: MEDpress-inform; 2020.
65. Mazzeo S, Caramella D, Marcocci C, Lonzi S, Cambi L, Miccoli P, et al. Contrast-enhanced color

Doppler ultrasonography in suspected parathyroid lesions. Acta Radiol. 2000;41(5):412–6. https://doi.org/10.1080/028418500127345820.

66. Agha A, Jung EM, Janke M, Hornung M, Georgieva M, Schlitt HJ, et al. Preoperative diagnosis of thyroid adenomas using high resolution contrast-enhanced ultrasound (CEUS). Clin Hemorheol Microcirc. 2013;55(4):403–9. https://doi.org/10.3233/CH-131777.
67. Uller W, Jung EM, Hornung M, Ross C, Jung W, Schlitt HJ, et al. Evaluation of the microvascularization of pathologic parathyroid glands in patients with primary hyperparathyroidism using conventional ultrasound and contrast-enhanced ultrasound. Clin Hemorheol Microcirc. 2011;48(1):95–103. https://doi.org/10.3233/CH-2011-1402.

Breast

14

Alexander N. Sencha, Ekaterina A. Sencha, and Liubov A. Timofeyeva

Breast blood supply comes from numerous branches of the internal thoracic, lateral thoracic, and intercostal arteries. The deep veins accompany the same-name arteries, the superficial veins form a subcutaneous network, which predominantly drains to the axillary vein.

The use of UCAs for the differential diagnosis of breast pathology based on perfusion features stimulated both scientific research and clinical practice. High diagnostic accuracy in the specification of neoangiogenesis of breast tumors is reported in many publications [1–5]. Although the assessment of breast lesions seems more complex as compared with liver lesions, CEUS is capable to supply additional diagnostic data [1, 5]. However, numerous studies on CEUS in breast carcinoma return ambiguous results [3, 6–8].

Breast CEUS may be indicated in the following situations:

- solid breast lesions of moderate or decreased echogenicity with signs of malignancy (BI-RADS 4) before biopsy
- solid breast lesions of moderate or decreased echogenicity with signs of malignancy (BI-RADS 4) without atypia with fine needle biopsy and cytology
- complex cysts (BI-RADS 3-4) with a solid component
- lesions with dubious or controversial features by the data of different diagnostic methods (BI-RADS 3-4)
- breast lesions that rapidly change their ultrasound characteristics, such as size, echogenicity, uniformity, vascularization, or elasticity (BI-RADS 3-4)
- breast lesions on the background of implants
- recurrent breast tumors
- accessory breast tissue
- breast lesions with no suspicion for malignancy in the presence of metastatic axillary lymph nodes

Supplementary Information The online version contains supplementary material available at [https://doi.org/10.1007/978-3-030-91764-7_14].

A. N. Sencha (✉)
Department of Visual and Functional Diagnostics, Federal State Budget Institution "National Medical Research Center for Obstetrics, Gynecology and Perinatology n.a. V.I.Kulakov", Moscow, Russian Federation

E. A. Sencha
Ultrasound Diagnostics Department, Federal State Budget Institution "Medical Diagnostic Center No. 9" of the Ministry of Defence of the Russian Federation, Moscow, Russian Federation

L. A. Timofeyeva
Department of Propaedeutics of Internal Diseases with Radiation Diagnostics Course, I. N. Ulianov Chuvash State University, Cheboksary, Chuvash Republic, Russian Federation

A. N. Sencha, Y. N. Patrunov (eds.), *Contrast-Enhanced Ultrasound*,
https://doi.org/10.1007/978-3-030-91764-7_14

The CEUS technology in breast abnormalities is identical to the same in other organs. The patient is in a supine position. The intravenous administration of a contrast agent, SonoVue® in particular, is performed by the instruction manual. The contrast enhancement is observed in real-time, and a continuous cine loop should be recorded throughout the study for further analysis.

As a rule, 2.4–5.0 ml of SonoVue® is administered intravenously by bolus injection. The best results in the study of breast lesions are achieved with the UCA dose of 4.8 ml followed by 5 ml saline flush [9].

Normal breast parenchyma exhibits not intense, not fast, relatively symmetric enhancement without perfusion defects or local hypervascularization in the arterial phase. Wash-out is slow and rather symmetric (Fig. 14.1, Video 14.1).

The differentiation of breast lesions with CEUS is based on the identification and specification of the organ and lesion microvasculature and the detection of neoangiogenesis within the tumor, which is characteristic of a malignant neoplasm. UCAs significantly improve imaging of the vascular pattern of the tumor. The number of visualized vessels increases from 36% to 95% [10]. The diagnostic accuracy of CEUS is higher than Doppler imaging mainly due to a more accurate assessment of vascular architectonics [11].

The study [10] used blood vessels as a criterion for malignancy and revealed an increase in sensitivity from 36% to 95% but the decrease in specificity from 86% to 79% due to hypervascularity of some benign neoplasms. There is some difference in microvessel distribution between breast carcinoma and fibroadenoma [12]. The higher is the tumor differentiation, the more regular is the vascular distribution [13]. These results suggest the absence of vascularization differences between low-grade tumors and some benign tumors.

The study [14] indicates that CEUS can reduce the number of biopsies. The authors suggested this method as an alternative to MRI, especially in the first 18 months after surgery, when postoperative scars and granulations may have a pronounced capillary network. Unfortunately, most CEUS data do not correlate with the histopathologically determined density of microvessels [9]. Since the breast is a superficial organ, the biopsy is considered a safe "gold standard" procedure.

CE-MRI is associated with the contrast media passage from the tumor microvessels to the extravascular space. Alternatively, SonoVue® microbubbles always remain in the vessel lumen. Therefore, with CEUS, the perfusion area and contrast enhancement curves strictly correspond to neoangiogenesis and do not depend on the state of extravascular space of the tumor.

CEUS is one imaging technique that allows long-term real-time dynamic observation of all vascular phases. As opposed to the study of parenchymatous organs, breast CEUS has no limitation of the unfavorable ratio between the rapid enhancement of the tumor and parenchyma. It allows clear long-term imaging of the nodule.

CEUS complements other methods with vascularization data, which concerns both solid and cystic lesions. Its high accuracy in the assessment of neoangiogenesis permits monitoring residues and detects tumor recurrence after treatment [1, 7, 9, 10, 15, 16].

The study is difficult to apply to small-sized lesions, which are poorly detected with grayscale sonography [9]. The limited field of view does not permit simultaneous imaging of the entire breast. There are still few publications on breast CEUS. It is not considered to replace conventional ultrasound and biopsy.

Simple breast cysts are benign and typically do not cause any diagnostic difficulties with the echography. After administration of the contrast agent, they demonstrate no contrast enhancement (Fig. 14.2).

CEUS is usually unnecessary for the diagnosis of breast cysts. Individual cases of complicated cysts with the echogenic component that mimic solid lesion may benefit from CEUS [1, 7, 9, 10, 16]. In these patients, it verifies the avascularity of the lesion.

Complex cysts with vascularized septa, papillary growths, or solid components must be differentiated from breast neoplasms. CEUS can identify a tumor with heterogeneous contrast

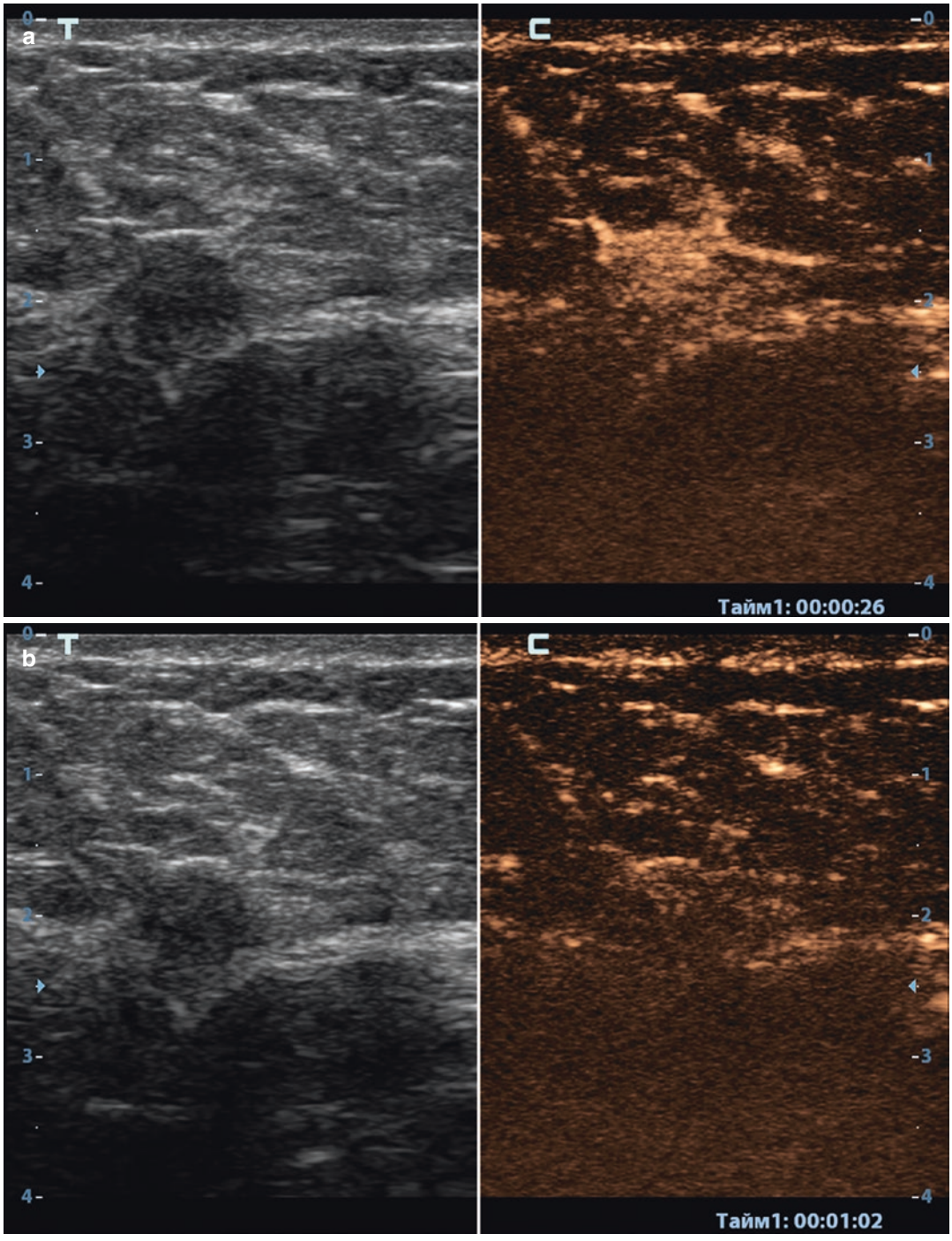

Fig. 14.1 Normal breast. CEUS demonstrates poor regular enhancement. (**a**) The arterial phase CEUS image (**b**) The venous phase CEUS image

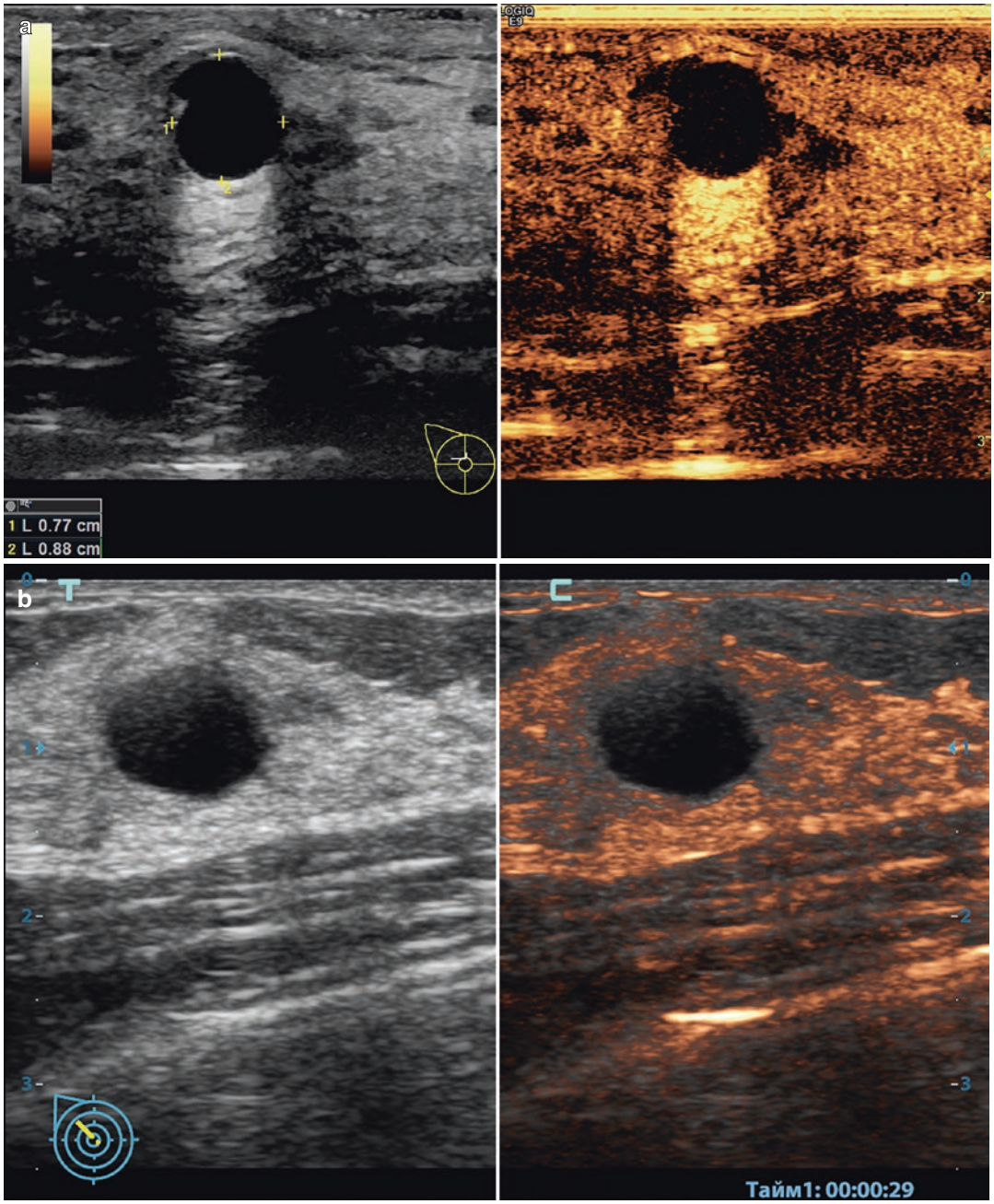

Fig. 14.2 Simple breast cyst. Breast CEUS images. (**a**) No contrast enhancement of the cyst in the arterial phase. (**b**) Another typical cyst with no contrast enhancement. (**c**) TIC demonstrates no enhancement within the cyst (blue ROI)

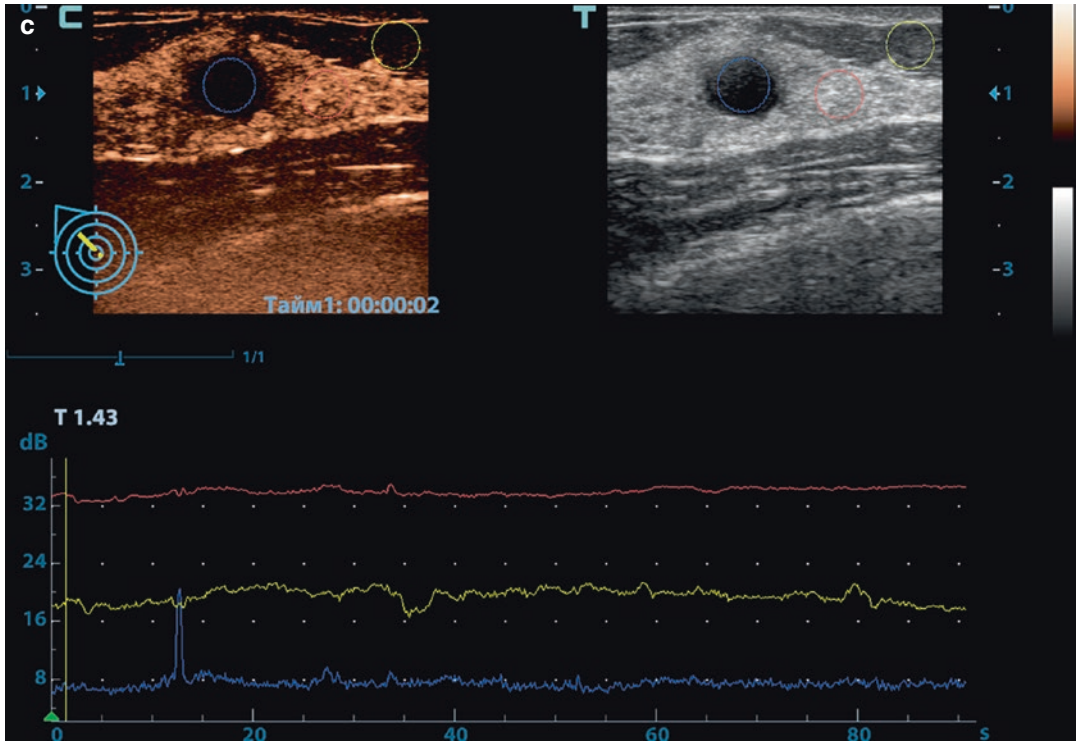

Fig. 14.2 (continued)

enhancement on the periphery of the cystic lesion and guide the targeted biopsy (Fig. 14.3, Video 14.2).

Breast fibroadenoma and many other benign breast tumors usually have a poor vascular network with color Doppler. The vessels are mainly located on the periphery of the lesion with sporadic regular branching. In some cases, a feeding or draining vessel directed to the lesion center may be identified.

The characteristic CEUS feature of breast fibroadenoma is peripheral enhancement. The combination of peripheral contrast enhancement and prolonged wash-out is observed in 80% of histopathologically verified fibroadenomas (Fig. 14.4, Videos 14.3 and 14.4).

Breast fibroadenoma is characterized by a longer TTP enhancement (≥30 s) and slower wash-out rate (70–150 s) [9]. These quantitative indicators have significantly higher values in fibroadenoma as compared to breast malignancies. In some cases, a fibroadenoma may exhibit intense heterogeneous contrast enhancement (Fig. 14.5, Videos 14.5 and 14.6). These fibroadenomas with Doppler imaging also demonstrate intranodular blood flow with wide centrally directed vessels.

In men with nodular gynecomastia, 60% of lesions demonstrate no contrast enhancement with CEUS. The rest lesions exhibit peripheral enhancement, which is in concordance with their benign nature (Fig. 14.6).

Breast malignancies are considered vascularized tumors. However, the capabilities of color and power Doppler imaging to visualize the vascular network in the tumor are limited due to low sensitivity to slow blood flow.

With CEUS, breast malignant lesions in both women and men typically demonstrate heterogeneous intense contrast enhancement in the arterial phase [17–21] (Figs. 14.7 and 14.8, Videos 14.7, 14.8, and 14.9). This pattern is observed in 2/3 of cases [1, 4, 16]. Irregular intense contrast enhancement depicts the abnormal branching of the vessels, randomly and atypically located arterioles and venules, and the arteriovenous shunts,

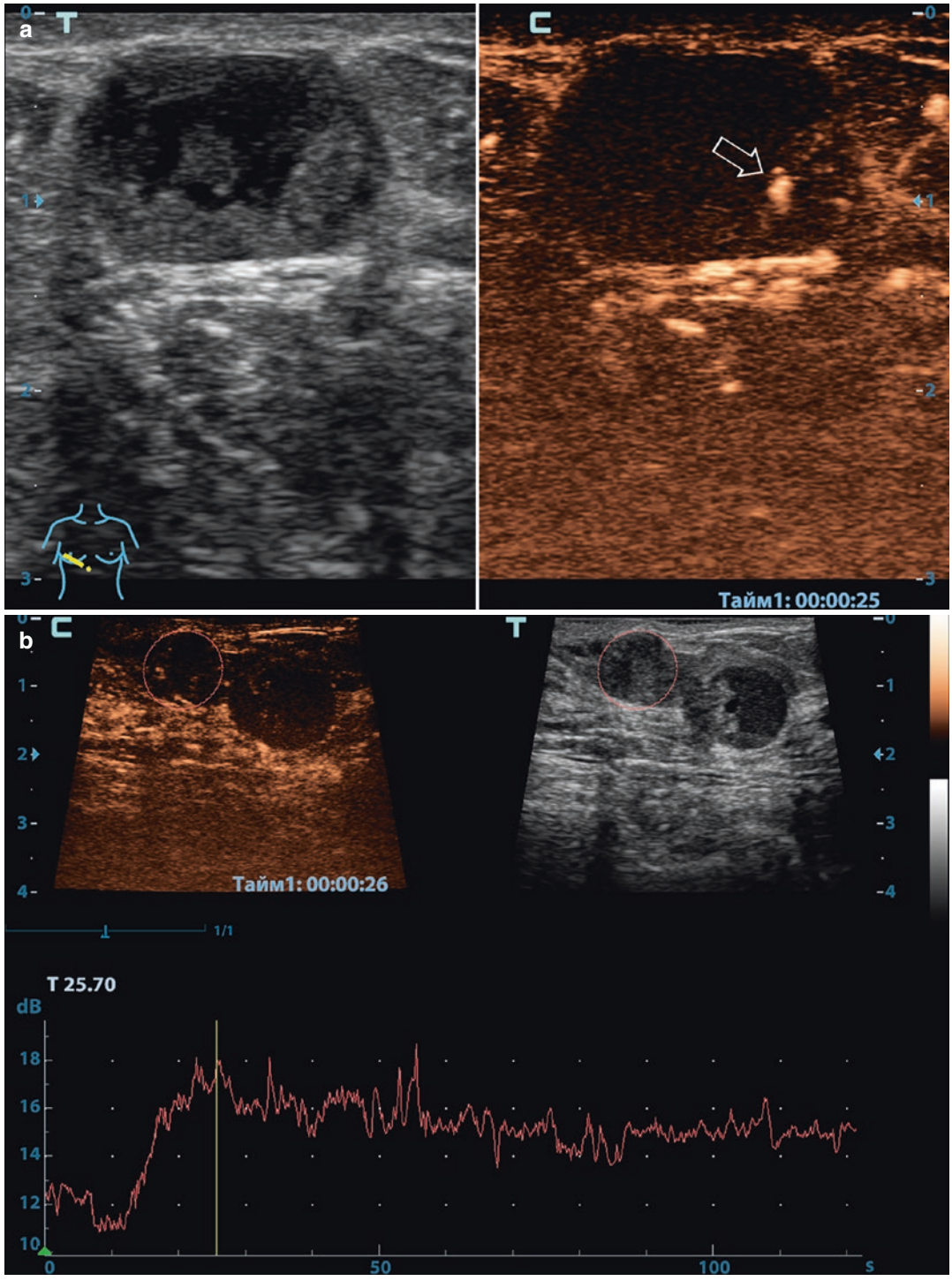

Fig. 14.3 Complex breast cystic lesions. (**a**) Patient A. CEUS image demonstrates enhancing solid components along the wall. (**b**) TIC quantitatively verifies enhancement of the cystic lesion. (**c**) Patient B. CEUS image demonstrates mild enhancement in the cyst. (**d**) Quantitative analysis of the cyst in (**c**) demonstrates enhancement in the cyst (yellow ROI) as compared with other structures

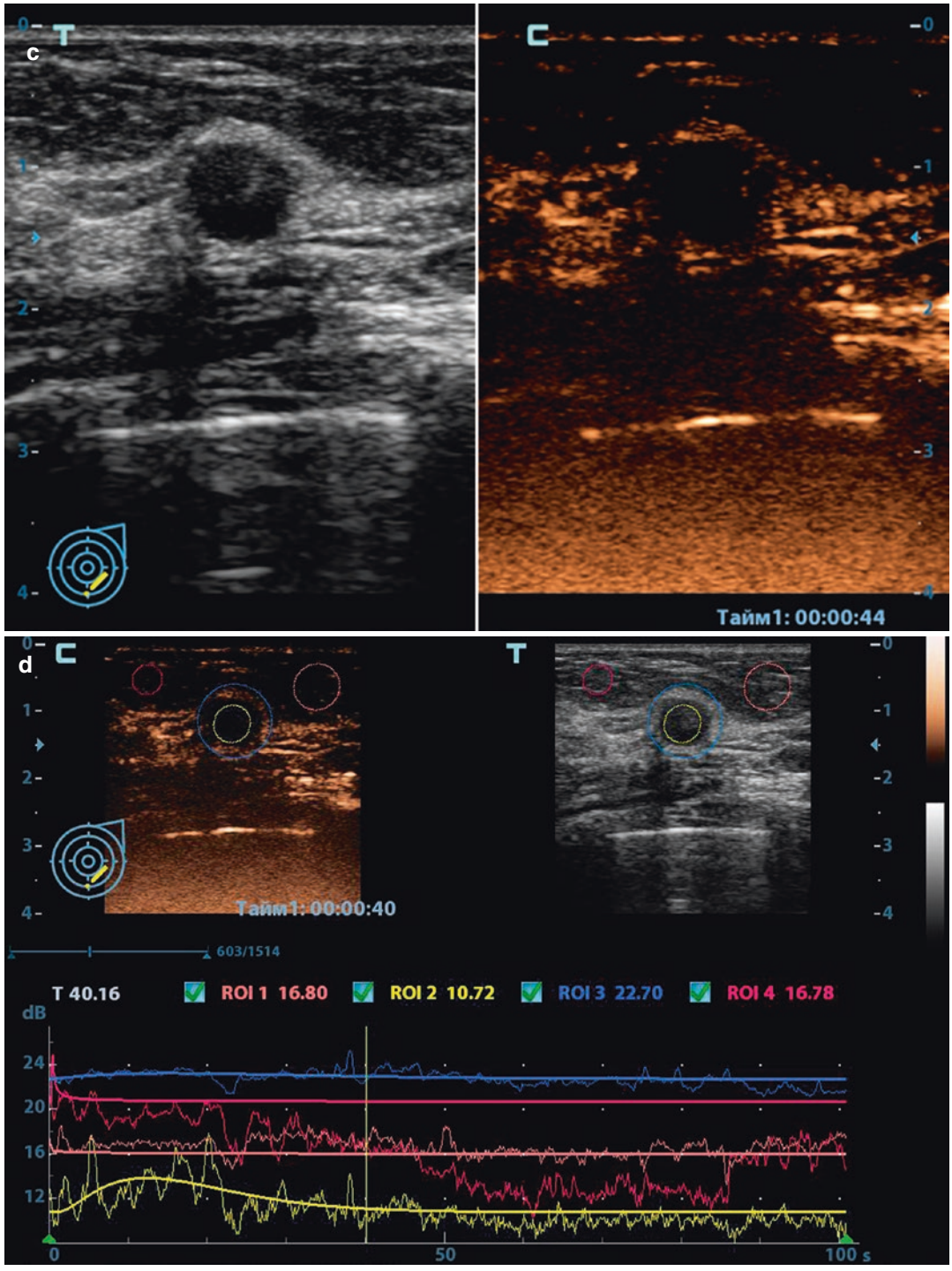

Fig. 14.3 (continued)

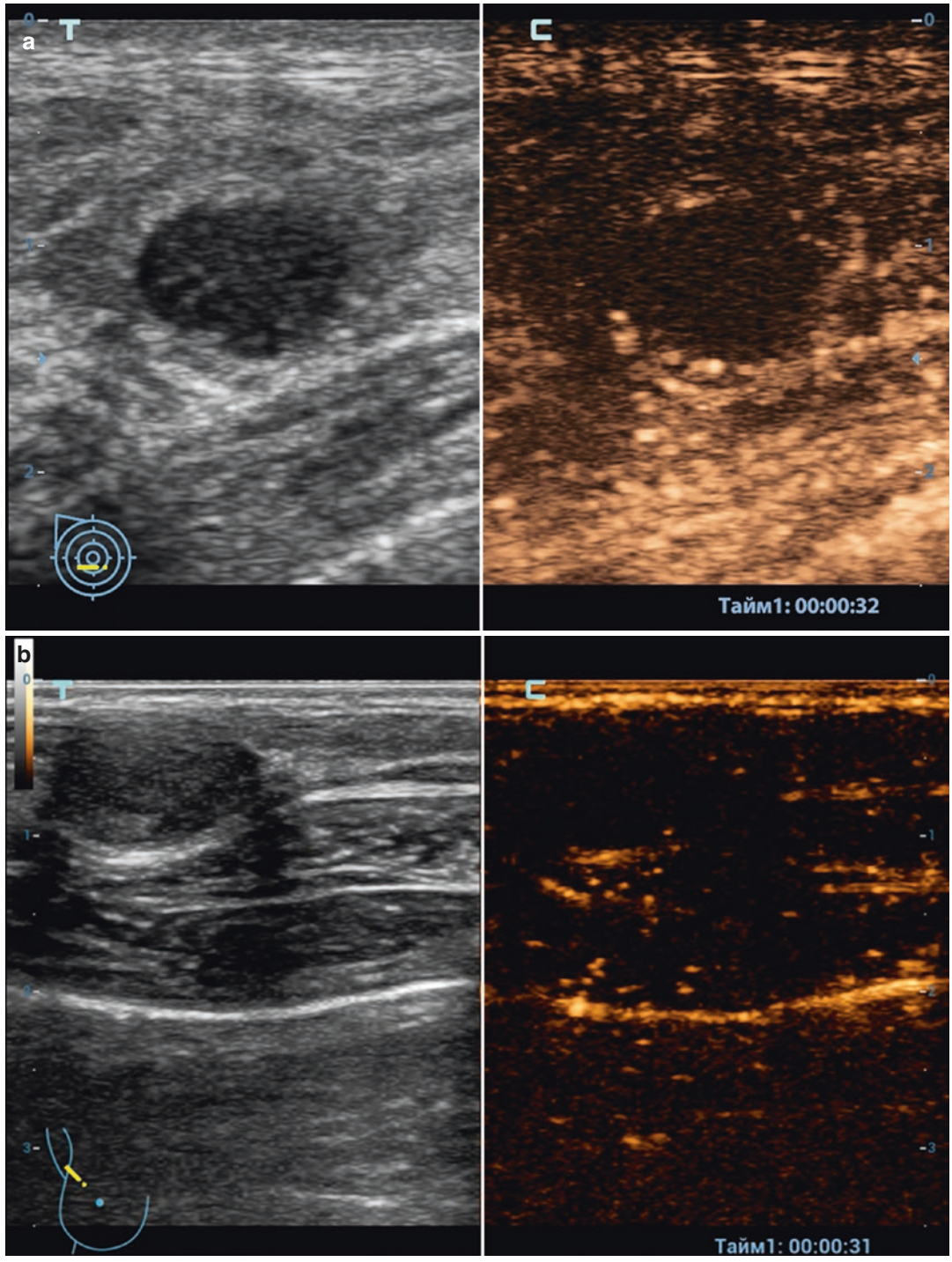

Fig. 14.4 Breast fibroadenoma. CEUS. (**a**) Patient A. The arterial phase CEUS image demonstrates peripheral enhancement. (**b**) Patient B. Poor enhancement of the lesion in the arterial phase. (**c**) Patient C. Poor enhancement in the arterial phase. (**d**) Quantitative analysis of TIC for (**c**) demonstrates mild enhancement and slow washout of the lesion (pink and yellow ROIs) as compared with other structures

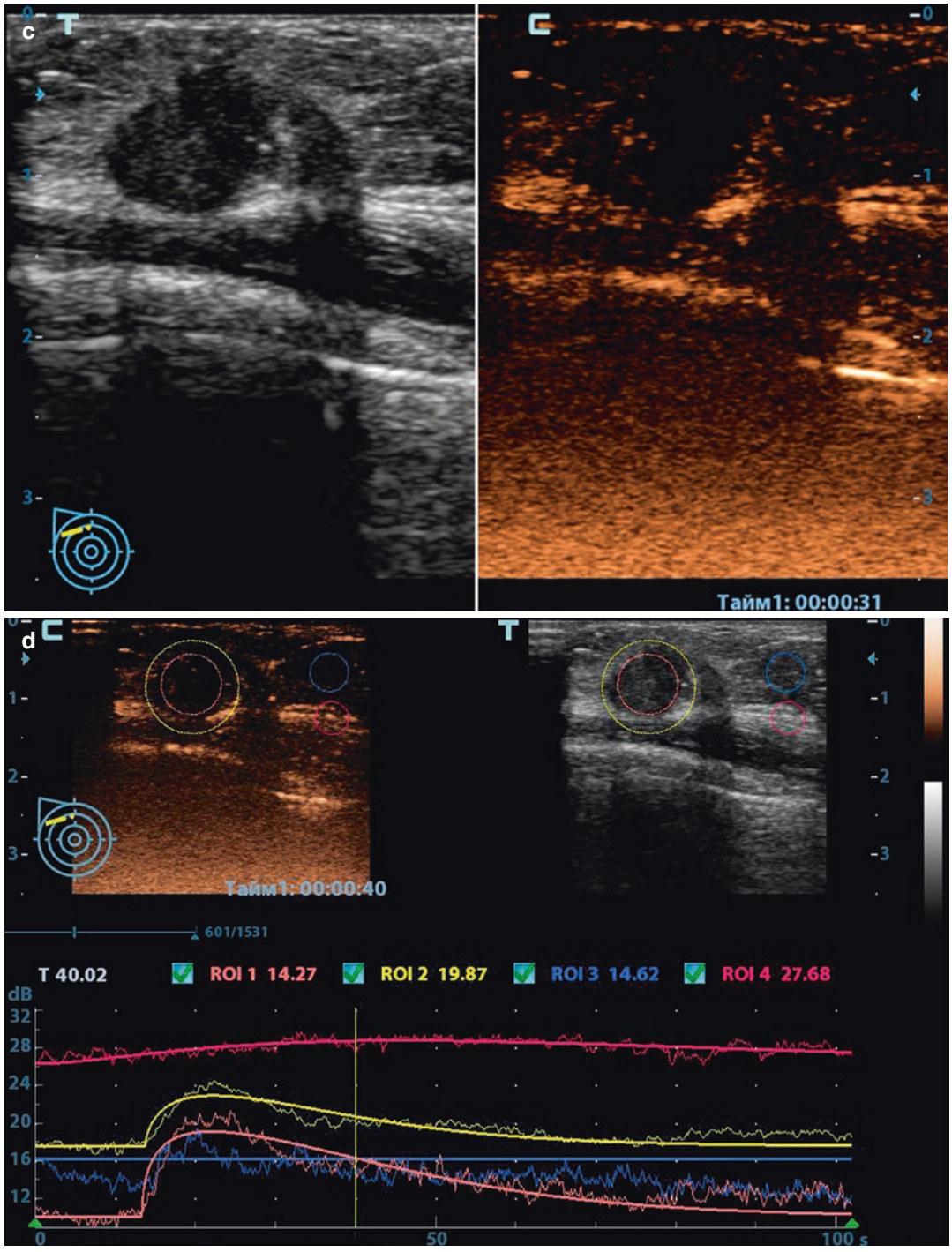

Fig. 14.4 (continued)

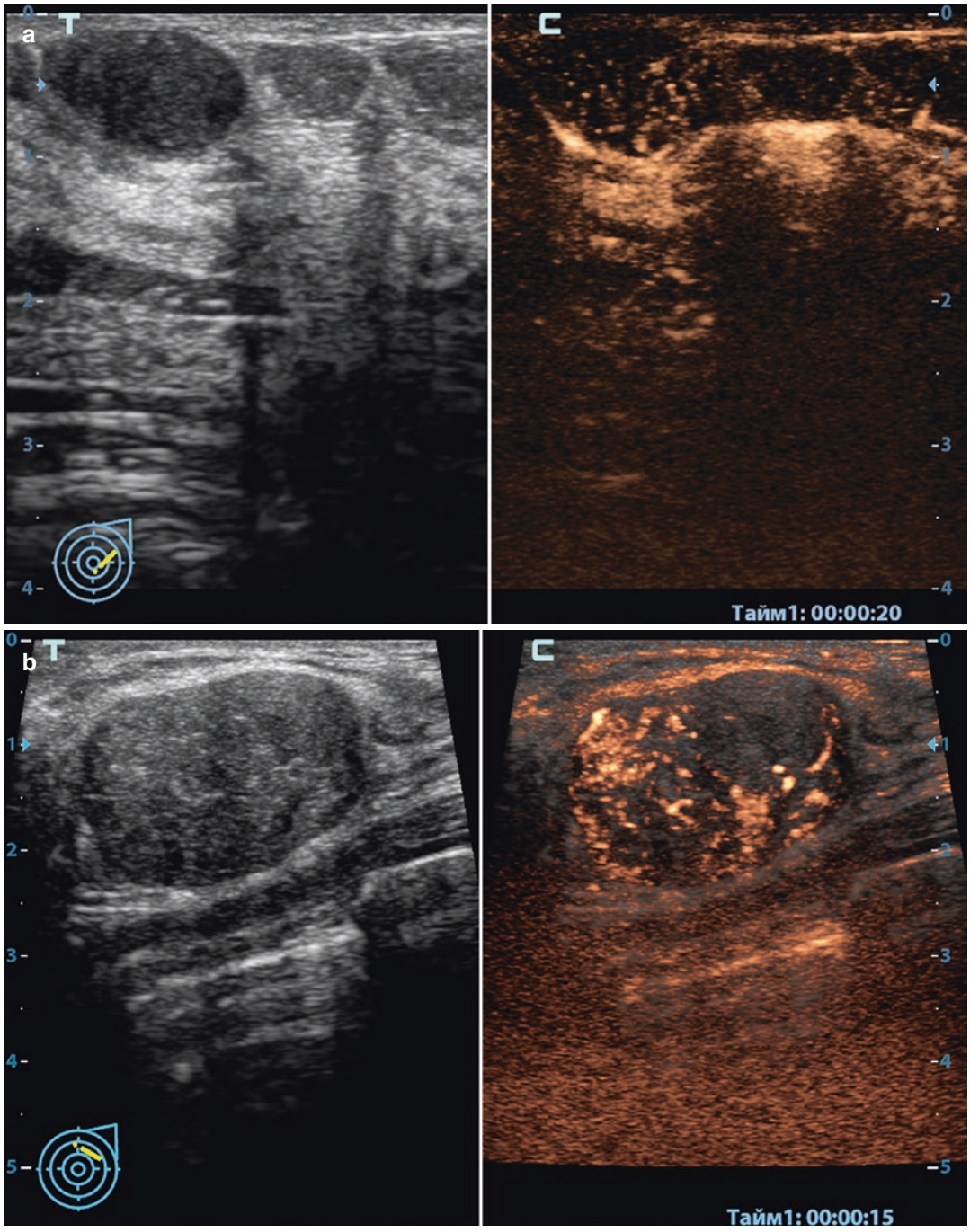

Fig. 14.5 Breast fibroadenoma. (**a**) Patient A. The arterial phase CEUS image demonstrates moderate peripheral and central enhancement. (**b**) Patient B. The arterial phase CEUS image demonstrates pronounced heterogeneous contrast enhancement in the arterial phase

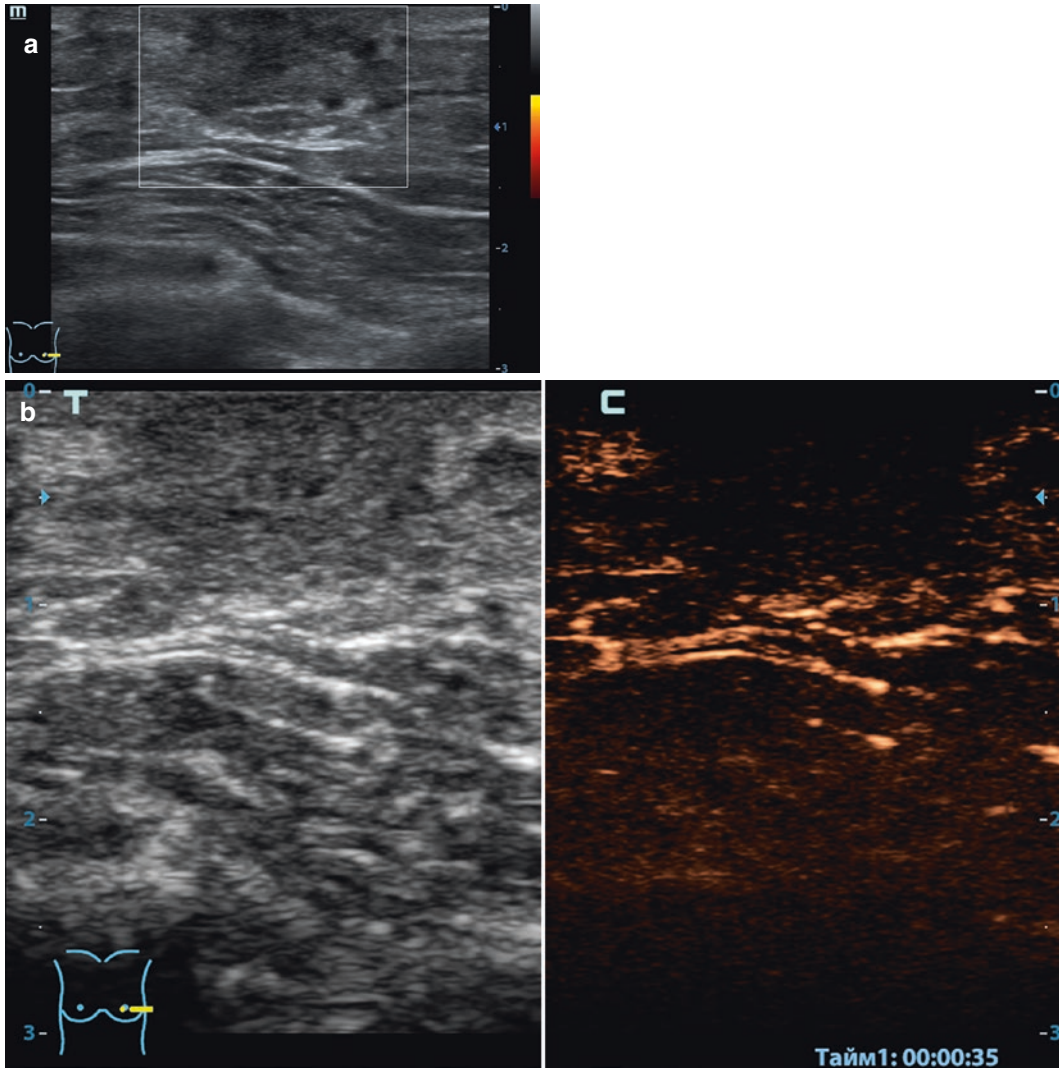

Fig. 14.6 Gynecomastia. (**a**) PDI reveals no vascularity. (**b**) The early venous phase CEUS image demonstrates no contrast enhancement of the lesion

which work for rapid wash-out of UCA from the tumor.

Fifteen percent of breast carcinomas have a marginal accumulation of UCA in a separate peripheral area of the tumor. This may be due to the hypoperfused areas within the tumor central part, which is associated with fibrosis and degeneration. In any case, the area of contrast enhancement is suspicious of malignancy, and a targeted biopsy of this area with ultrasound guidance is highly efficient.

Most breast malignant tumors have vascular features specific for rapidly growing neoplasms, such as irregular vessel course and caliber with spirals and dilatations, arteriovenous shunts, abnormal branching, and the inconsistency of the vascular wall (Figs. 14.9 and 14.10). The correlation between vascular disorganization and the anaplasia grade is very strong [7].

Abnormal vessels with the altered course, structure, and caliber end up with a mosaic pattern with CEUS, the detection of which corre-

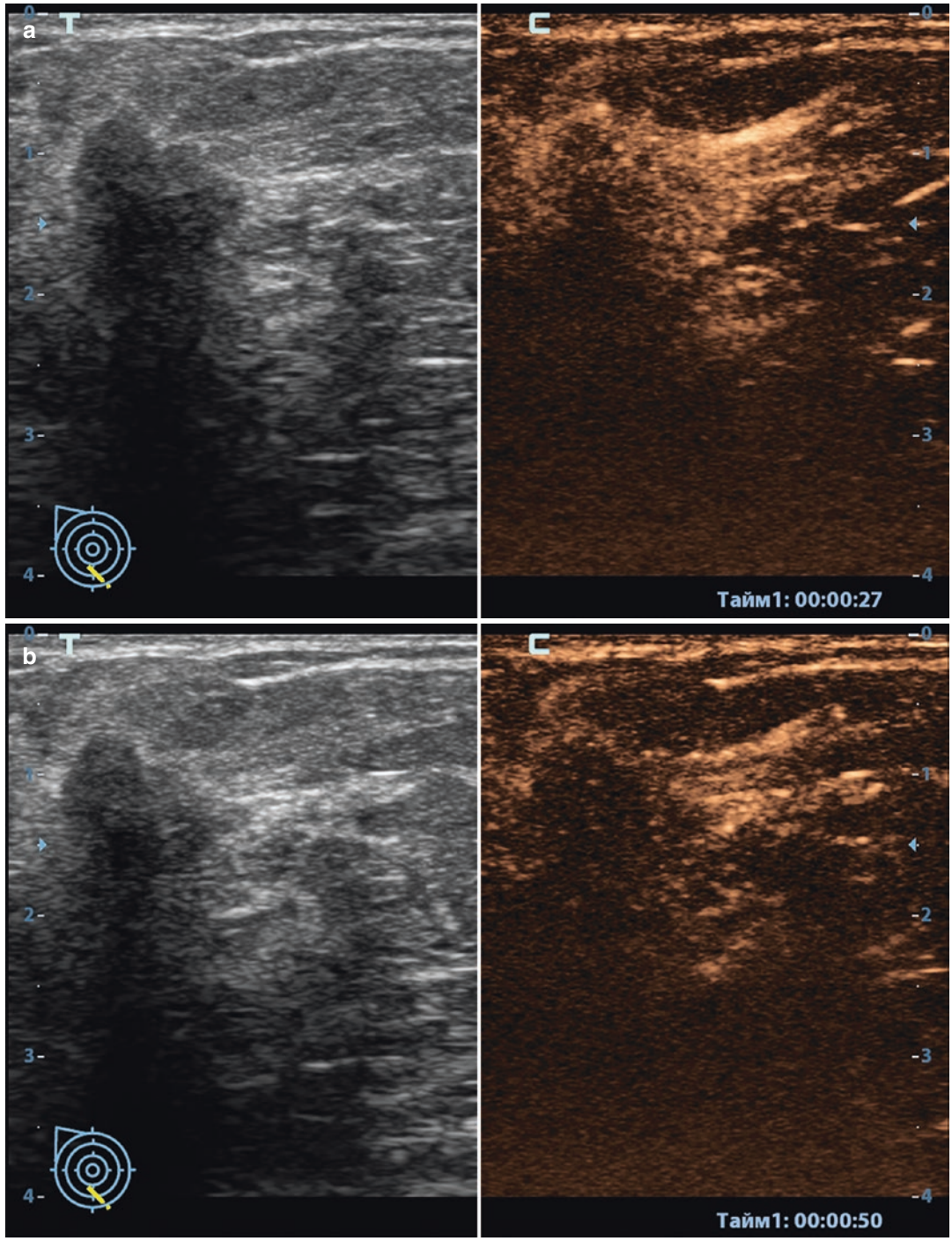

Fig. 14.7 Breast carcinoma in a woman. CEUS. (**a**) Patient A. Heterogeneous intense arterial phase enhancement. (**b**) Patient A. Rapid wash-out in the venous phase. (**c**) Patient B. Heterogeneous intense arterial phase enhancement. (**d**) Patient B. Very rapid wash-out, which starts at the end of arterial phase. (**e**) Patient C. Poor central enhancement in all vascular phases

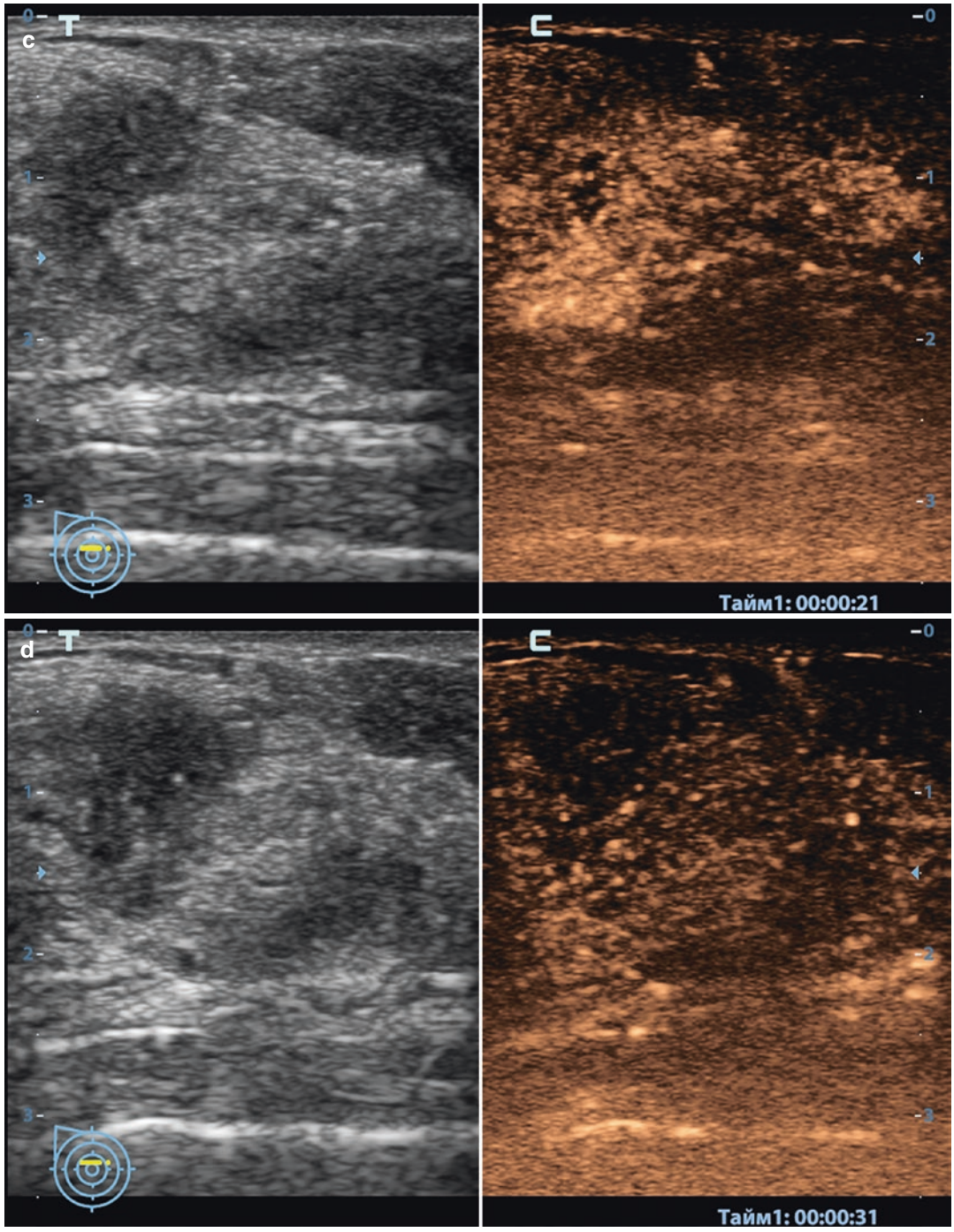

Fig. 14.7 (continued)

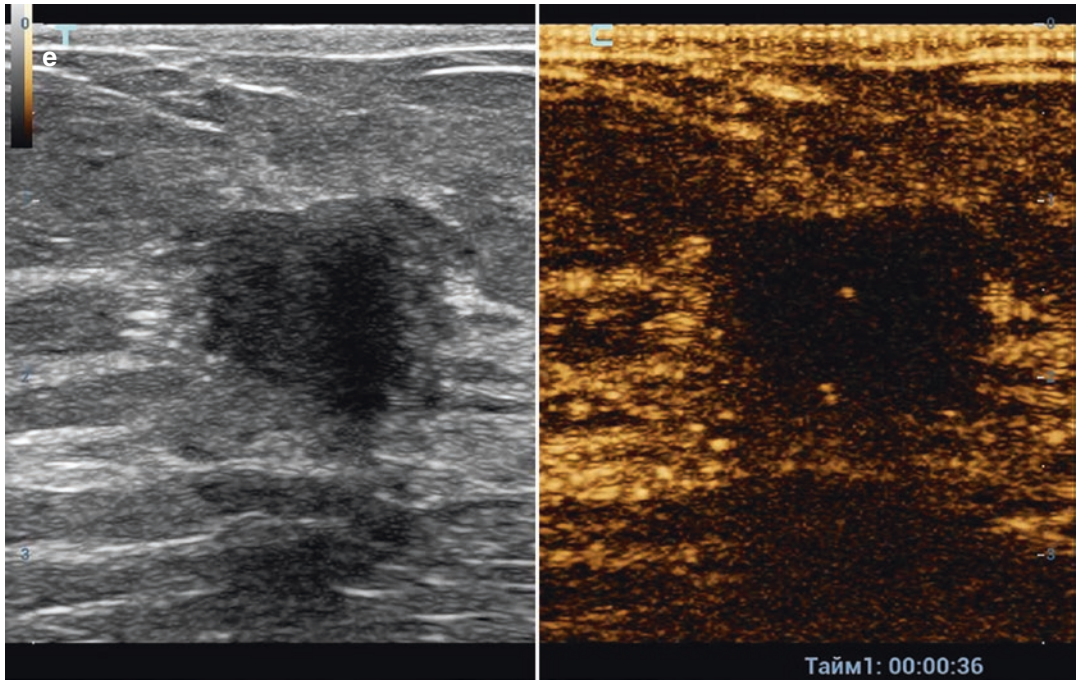

Fig. 14.7 (continued)

lates with the risk of breast malignancy. Alternatively, fibroadenoma usually has a poor, predominantly peripheral vascularity with uniform vascular branching [22]. However, about 10% of all benign breast masses, including inflammatory process, immature fibroadenoma, and the phylloid tumor may have a more or less prominent mosaic vascular pattern. Conversely, according to pathologists, peripheral enhancement has also been found in invasive breast cancer, which was associated with fibrosis and necrosis in the central aspects. Additionally, blood perfusion in some ductal carcinoma may be very low due to fibrosis and narrowing of vessel caliber.

Quantitative CEUS analysis showed that the rise time, TTP, and MTT values in benign lesions were higher than in malignant lesions (RT 16.52 ± 4.15 s vs. 13.86 ± 3.36 s; TTP 19.86 ± 4.87 s vs. 16.52 ± 4.85 s; DT/2 80.55 ± 18.65 s vs. 65.16 ± 20.28 s, respectively) [23] (Fig. 14.11).

The study [24] analyzed the value of quantitative CEUS indices in determining the main immunohistochemical parameters of breast carcinoma. TTP statistically significantly correlated with tumor grade, progesterone receptor status, and axillary lymph node status. The wash-out ratio was significantly associated with tumor estrogen and progesterone receptor status.

In clinical practice, the inconsistency of the sonographically measured tumor size with the pathology findings is a common entity. Underestimation of the lesion size may result in wrong staging and inappropriate management of breast carcinoma.

One meta-analysis [18] compared the performance of CEUS and the conventional US for the differential diagnosis of benign and malignant breast tumors. The accuracy of CEUS was higher with the sensitivity of 0.93 (95% CI 0.91–0.95) and the specificity of 0.86 (95% CI 0.84–0.88). Additionally, CEUS in both cases, as a single modality or in combination with the general US, demonstrated better values of the AUC than the conventional US.

CEUS demonstrates higher accuracy in determining the true size of the tumor as compared with grayscale US [25]. This may result from vascular invasion and peritumoral tissue

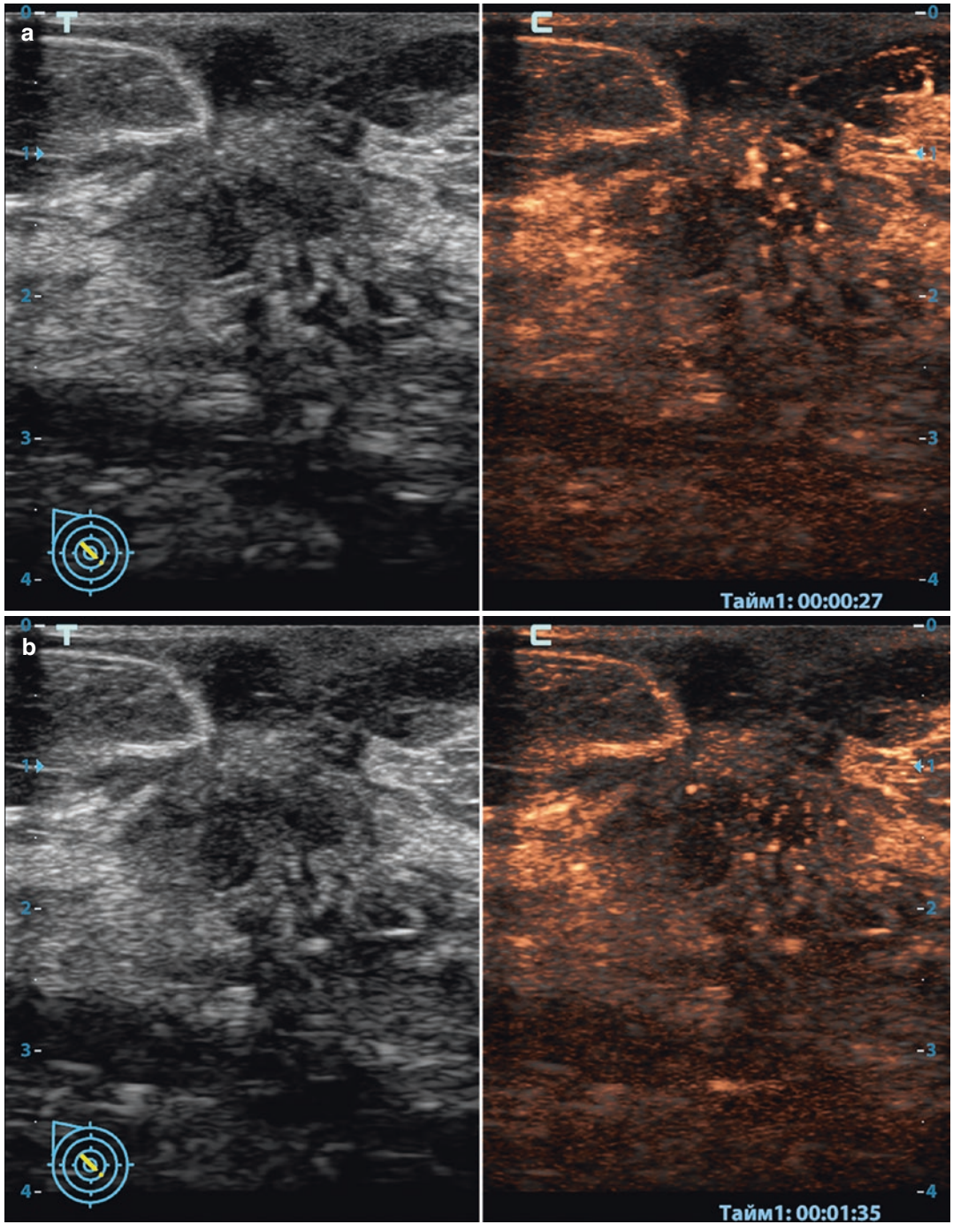

Fig. 14.8 Breast carcinoma in a man. CEUS images (**a**) Chaotic heterogeneous enhancement in the arterial phase. (**b**) Wash-out in the venous phase

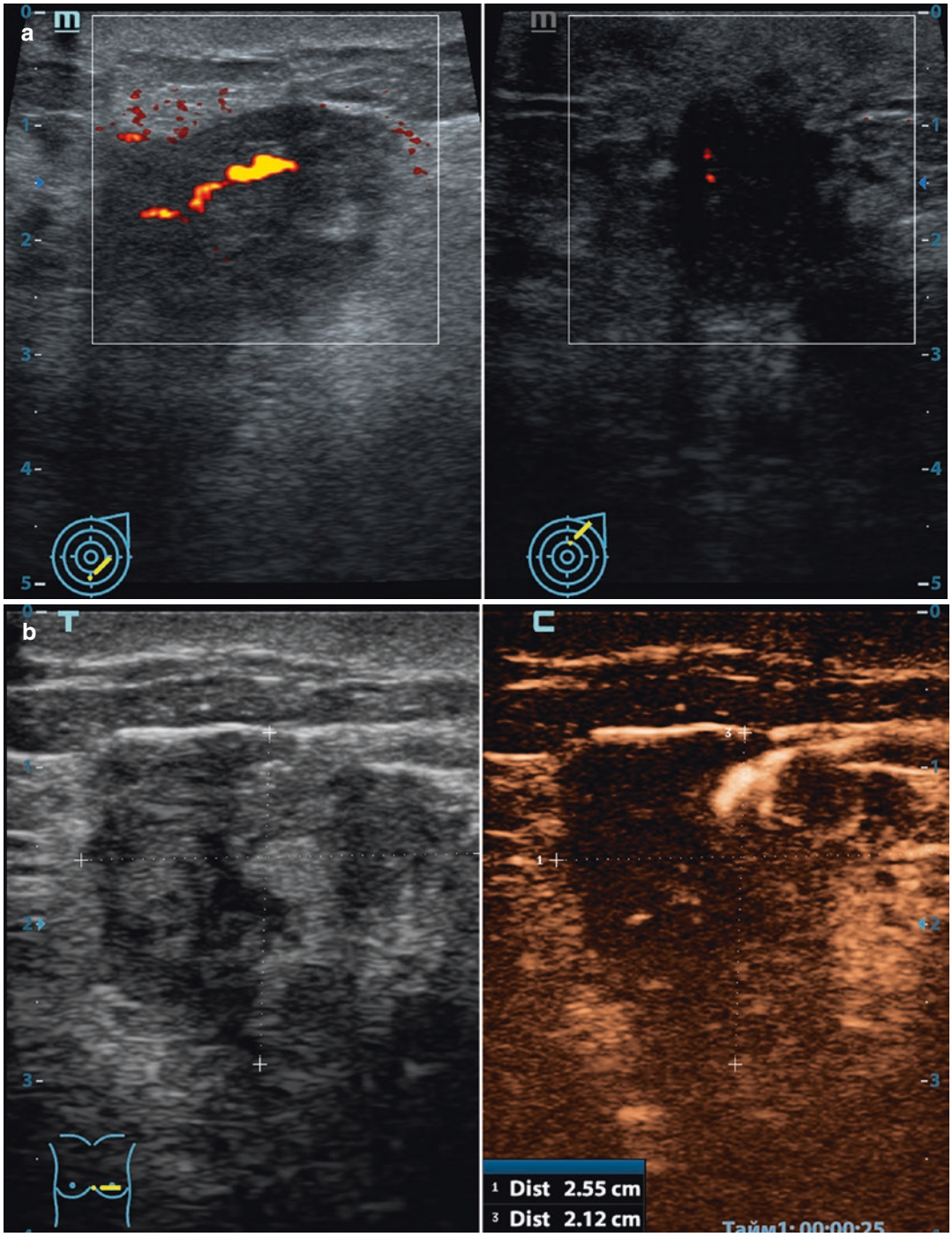

Fig. 14.9 Breast carcinoma. (**a**) PDI depicts irregular vessels within the tumor. (**b**) The arterial phase CEUS demonstrates heterogeneous contrast enhancement and a feeding vessel

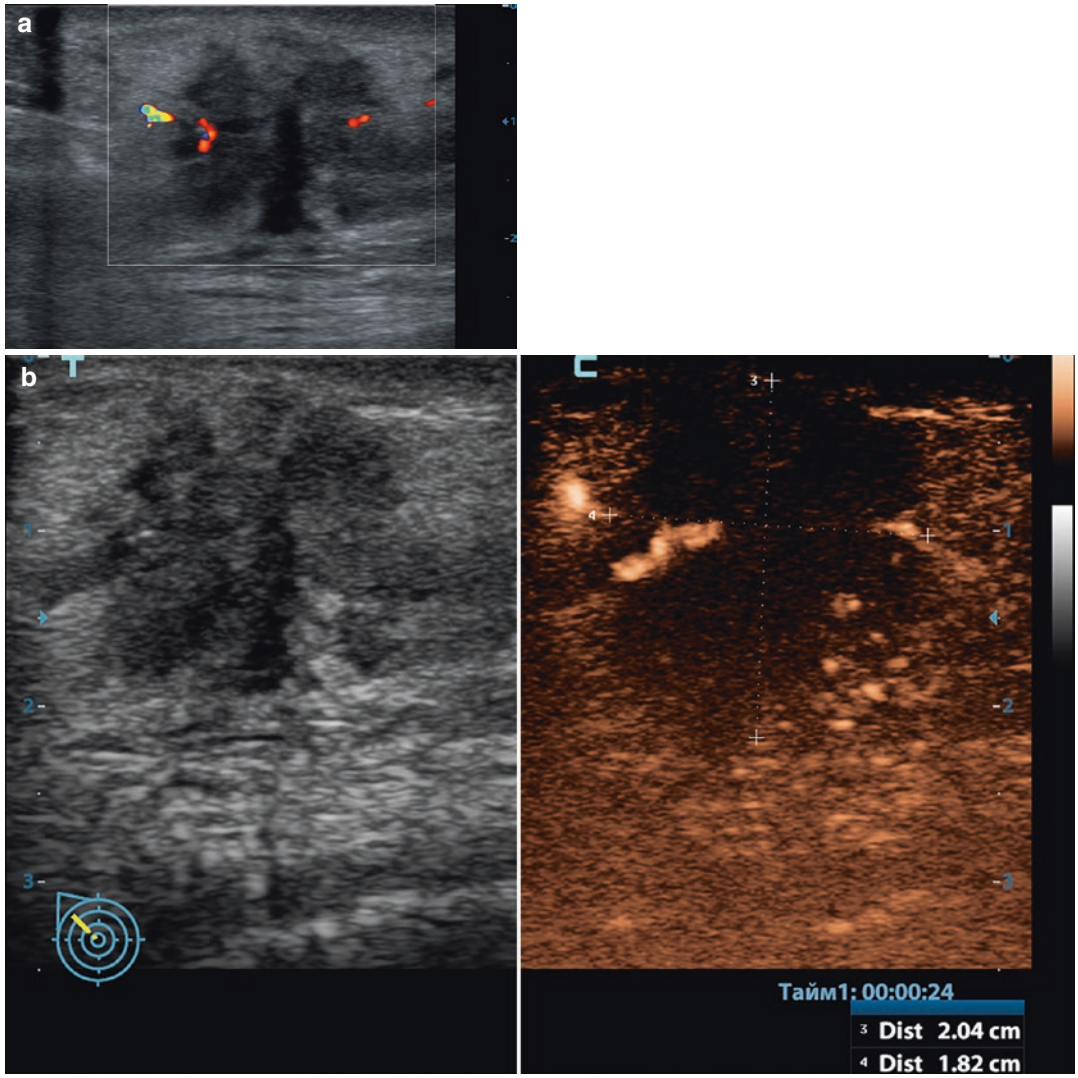

Fig. 14.10 Breast carcinoma. (**a**) CDI detects vessels with chaotic distribution throughout the tumor. (**b**) The arterial phase CEUS demonstrates heterogeneous contrast enhancement

enhancement. This new criterion for differential diagnosis can contribute to the BI-RADS classification [26].

There are attempts to establish a 5-point scoring system to simplify breast CEUS analysis, which displayed high diagnostic accuracy, as follows [27]:

1. No enhancement in the lesion, with a clear borderline separating the lesion from the surrounding tissue.
2. Iso- and synchronous enhancement with the surrounding tissue, without a clear outline in the contrast-enhanced image.
3. Earlier enhancement compared with the surrounding tissue, homogeneous or heterogeneous, with a clear margin (sometimes with ring-like enhancement). The scope of the lesion is almost identical to that shown in the 2D image. The shape of the lesion is regular: round or oval.
4. Earlier enhancement than the surrounding tissue, usually heterogeneous. The scope of the lesion in the contrast-enhanced image is larger than in the corresponding 2D image, but the lesion still displays a clear margin, with/without a perfusion defect in the lesions and

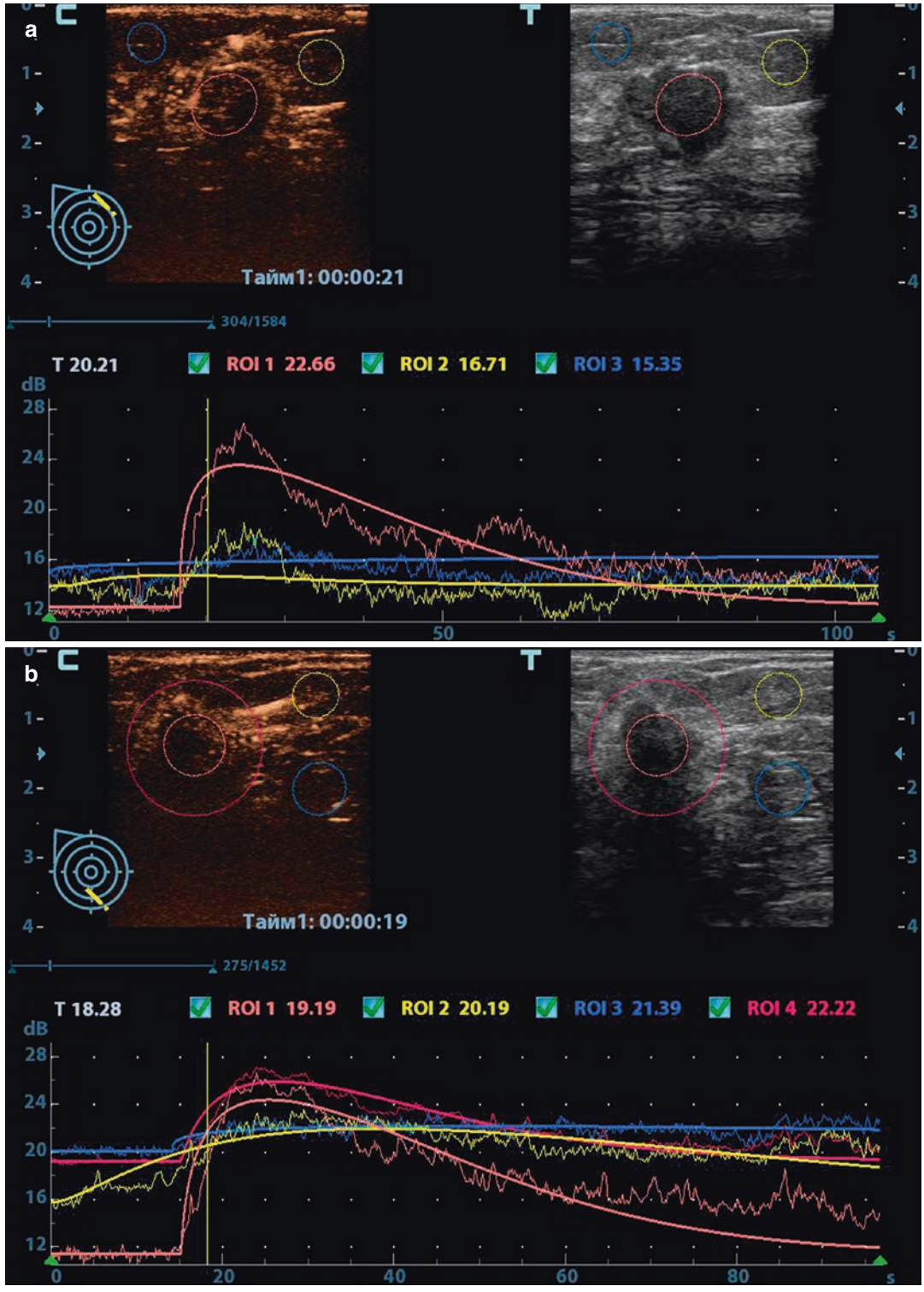

Fig. 14.11 Breast carcinoma. (**a**) TIC demonstrates contrast enhancement in the tumor (pink ROI) as compared with other tissue (yellow and blue ROIs). (**b**) TIC demonstrates contrast enhancement in the tumor (pink ROI), tumor with peritumoral tissue (red ROI) as compared with other tissue (yellow and blue ROIs)

without crab claw-like enhancement. The shape of the lesion is always irregular.

5. Heterogeneously enhanced, with a larger scope (compared with that of 2D image), earlier enhancement, and with/without perfusion defect, particularly with a typical crab claw-like enhancement and an unclear margin. The shape of the lesion is always irregular.

Some studies [4, 6] demonstrated a good correlation of CEUS data with breast MRI. The combined use of these methods exhibited high sensitivity (91% and 100%), specificity (73% and 64%), and accuracy (86% and 91%), which indicates sufficient reliability of CEUS quantification for the differential diagnosis of breast tumors [4, 6, 28]. Quantitative and qualitative CEUS data in the presented studies were based on vascular features obtained within the lesions, but considering the impact of the malignant tumor on the surrounding tissues evaluation of the data obtained from peritumoral tissues seems reasonable [2, 29, 30].

Malignant tumors are characterized by infiltrative growth, the boundaries are indistinct due to invasion of the surrounding tissues. On the contrary, benign tumors usually do not infiltrate the neighboring tissue, and the border between the tumor and peritumoral tissue is clearly defined.

The study [31] compared the accuracy of tumor size measurements in different modalities. It reported that the lesion size measured with US was significantly different from the same lesion size with pathology (the difference was up to 8 mm), which was especially prominent in lobular cancer. In the study [32], which conferred 6543 breast carcinoma patients, the average size of the tumor with US was 18.3 mm, while with pathology 20.8 mm. Probably, the US is limited only to tumor measurements and does not take into account the invasive growth and peritumoral tissue condition. Peritumoral tissue contains important diagnostic information, inclusive of neoangiogenesis, that facilitates differentiation between malignant and benign lesions. Moreover, the study demonstrated that the combination of both peritumoral parenchyma and the lesion characteristics works better for the differential diagnosis of breast carcinoma.

The risk of malignancy in the lesions of BI-RADS4 category ranges from 3% to 94%, which leads to a large number of unwanted biopsies. Identification of reliable differential features could alter the indications for this intervention.

Multimode US significantly improves the accuracy of the diagnosis in BIRADS4 category breast tumors. The study [33] reports that the sensitivity and specificity of grayscale US in BIRADS4 lesions were 88.6% and 75.7%, respectively. If complemented with CEUS, the specificity increased to 94.6%. The combination of grayscale US with share-wave elastography demonstrated the sensitivity and specificity of 88.6% and 90.5%, respectively. The maximum sensitivity of 97.7% and specificity of 93.2% were observed in a combination of grayscale US, elastography, and CEUS.

CEUS has higher sensitivity and specificity (67.6% and 90.6%) in breast carcinoma detection as compared with compression elastography (61.8% and 87.5%) [8].

In subcentimetric breast tumors, the specificity of grayscale US was 17.4%, elastography 56.2%, and CEUS 86.0% with sensitivity of 100%, 92.2%, 93.2%, respectively [27]. The AUC for the grayscale US was 0.867, for its combination with elastography 0.882, for combination with CEUS 0.953, and in a combination of all three modalities accounted for 0.924. Accordingly, CEUS increases the accuracy of general US in the diagnosis of breast nodules of less than 1 cm in size [27].

According to the American Cancer Society and, the annual diagnostic breast expenditures are estimated at US$7.91 billion, which assumes the need for higher specificity methods to achieve accurate diagnosis with a smaller number of diagnostic procedures. In the USA, US$3.05 billion a year is spent on diagnostic mammography (the mean cost of 1 study is US$349), US$0.92 billion a year on diagnostic ultrasound (the mean cost is US$132), and US$3.07 billion a year on biopsies (the mean cost is US$1938). Following initial diagnostic procedures, 49.4% had second procedures, 20.1% followed with third proce-

dures, and 10.0% had a fourth procedure. A biopsy is performed in 10.3% to verify the detected breast changes. According to the National Cancer Institute, 71% of biopsies (US$2.18 billion annually) are false-positive, which could have been avoided if a more precise method with better specificity had been utilized. Besides the economic component, the negative psychological impact on the woman who is subject to a biopsy procedure and has to wait for the pathology conclusion.

Quantitative multiparametric US with two different triple assessment modalities (B-mode, share-wave elastography, CEUS, or Doppler) shows the best diagnostic performance for breast cancer diagnosis. It significantly reduced the number of false-positive findings up to 46.9% [34].

In patients with non-mass breast carcinoma, all US modalities were highly sensitive (90–97.5%), but the specificity was different [35]. Grayscale US exhibited the specificity of 29%, with Doppler 41.9%, with strain elastography 58.1%, with CEUS 58.1%, and multimode method increased specificity to 77.4%. The accuracy of these methods was 69.0%, 70.4%, 80.2%, 76.1%, and 87.3%, respectively.

Data from a similar study [20] were published in 2020, and they also demonstrated the efficacy of CEUS in the differential diagnosis of non-mass breast lesions. Microcalcification, enhancement time, enhancement intensity, lesion scope, and peripheral blood vessels were significantly different between benign and malignant lesions. CEUS increased the sensitivity of US from 0.82 to 0.87, the specificity from 0.74 to 0.92, and accuracy from 0.76 to 0.9.

Summing up, CEUS facilitates an objective non-invasive assessment of blood flow and perfusion, which contributes to the detection and differential diagnosis of breast lesions [10, 15, 16, 25, 35–41]. Difficulties in CEUS interpretation may occur in minimally vascular breast lesions, such as adenosis, fibrous changes, scars, and some types of fibroadenoma. The quantitative values of enhancement depend on the way of UCA introduction (bolus, infusion, etc.), the patient's age (tumor perfusion is lower in patients above 60 years), the size, histological type, and structure of the tumor (e.g., invasive tumors demonstrate fast wash-out due to arteriovenous shunts). Biopsy and histopathology are still the final methods for verification in patients with breast lesions.

References

1. Sencha AN. Ul'trazvukovoe issledovanie molochnyh zhelez. SHag za shagom. Ot prostogo k slozhnomu [Ultrasound examination of the mammary glands. Step by step. From simple to complex]. 2nd ed. Moscow: MEDpress-inform; 2019.
2. Sencha AN, Bikeev YV, Rodionov VV, et al. Ul'trazvukovoe issledovanie s kontrastirovaniem v differencial'noj diagnostike uzlovyh obrazovanij molochnoj zhelezy [Ultrasound examination with contrast enhancement in the differential diagnosis of breast lesions]. Akush Ginekol. 2019;11:167–74.
3. Balleyguier C, Opolon P, Mathieu MC, Athanasiou A, Garbay JR, Delaloge S, Dromain C. New potential and applications of contrast-enhanced ultrasound of the breast: own investigations and review of the literature. Eur J Radiol. 2009;69(1):14–23. https://doi.org/10.1016/j.ejrad.2008.07.037.
4. Ricci P, Cantisani V, Ballesio L, Pagliara E, Sallusti E, Drudi FM, et al. Benign and malignant breast lesions: efficacy of real time contrast-enhanced ultrasound vs. magnetic resonance imaging. Ultraschall Med. 2007;28(1):57–62. https://doi.org/10.1055/s-2006-927226.
5. Zhao H, Xu R, Ouyang Q, Chen L, Dong B, Huihua Y. Contrast-enhanced ultrasound is helpful in the differentiation of malignant and benign breast lesions. Eur J Radiol. 2010;73(2):288–93. https://doi.org/10.1016/j.ejrad.2009.05.043.
6. Caproni N, Marchisio F, Pecchi A, Canossi B, Battista R, D'Alimonte P, Torricelli P. Contrast-enhanced ultrasound in the characterisation of breast masses: utility of quantitative analysis in comparison with MRI. Eur Radiol. 2010;20(6):1384–95. https://doi.org/10.1007/s00330-009-1690-1.
7. Liu H, Jiang YX, Liu JB, Zhu QL, Sun Q. Evaluation of breast lesions with contrast-enhanced ultrasound using the microvascular imaging technique: initial observations. Breast. 2008;17(5):532–9. https://doi.org/10.1016/j.breast.2008.04.004.
8. Sorelli PG, Cosgrove DO, Svensson WE, Zaman N, Satchithananda K, Barrett NK, Lim AK. Can contrast-enhanced sonography distinguish benign from malignant breast masses? J Clin Ultrasound. 2010;38(4):177–81. https://doi.org/10.1002/jcu.20671.
9. Rizzatto G, Chersevani R. Role of contrast ultrasound in breast lesions and sentinel lymph nodes. In:

Lencioni R, editor. Enhancing the role of ultrasound with contrast agents. Milano: Springer; 2006. p. 225–35. https://doi.org/10.1007/88-470-0476-4_18.
10. Moon WK, Im JG, Noh DY, Han MC. Nonpalpable breast lesions: evaluation with power Doppler US and a microbubble contrast agent-initial experience. Radiology. 2000;217(1):240–6. https://doi.org/10.1148/radiology.217.1.r00oc03240.
11. Schroeder RJ, Bostanjoglo M, Rademaker J, Maeurer J, Felix R. Role of power Doppler techniques and ultrasound contrast enhancement in the differential diagnosis of focal breast lesions. Eur Radiol. 2003;13(1):68–79. https://doi.org/10.1007/s00330-002-1413-3.
12. Weind KL, Maier CF, Rutt BK, Moussa M. Invasive carcinomas and fibroadenomas of the breast: comparison of microvessel distributions–implications for imaging modalities. Radiology. 1998;208(2):477–83. https://doi.org/10.1148/radiology.208.2.9680579.
13. Ellis RL. Differentiation of benign versus malignant breast disease. Radiology. 1999;210(3):878–80. https://doi.org/10.1148/radiology.210.3.r99mr30878.
14. Winehouse J, Douek M, Lees W. ROC curve analysis in the evaluation of contrast-enhanced color Doppler US. Radiology. 1999;212(3):911–2. https://doi.org/10.1148/radiology.212.3.r99jl38911.
15. Jung EM, Jungius KP, Rupp N, Gallegos M, Ritter G, Lenhart M, Clevert DA, Kubale R. Contrast enhanced harmonic ultrasound for differentiating breast tumors - first results. Clin Hemorheol Microcirc. 2005;33(2):109–20.
16. Sencha A, Patrunov Y, Sencha E, Penyaeva E, Rodionov V. Multiparametric examination: basic and innovative methods of ultrasound in diagnosis of breast cancer. In: Sukhikh GT, Sencha AN, editors. Multiparametric ultrasound diagnosis of breast diseases. Berlin: Springer; 2018. p. 115–92.
17. Huang R, Jiang L, Xu Y, Gong Y, Ran H, Wang Z, Sun Y. Comparative diagnostic accuracy of contrast-enhanced ultrasound and shear wave elastography in differentiating benign and malignant lesions: a network meta-analysis. Front Oncol. 2019;9:102. https://doi.org/10.3389/fonc.2019.00102.
18. Li Q, Hu M, Chen Z, Li C, Zhang X, Song Y, Xiang F. Meta-analysis: contrast-enhanced ultrasound versus conventional ultrasound for differentiation of benign and malignant breast lesions. Ultrasound Med Biol. 2018;44(5):919–29. https://doi.org/10.1016/j.ultrasmedbio.2018.01.022.
19. Vraka I, Panourgias E, Sifakis E, Koureas A, Galanis P, Dellaportas D, et al. Correlation between contrast-enhanced ultrasound characteristics (qualitative and quantitative) and pathological prognostic factors in breast cancer. In Vivo. 2018;32(4):945–54. https://doi.org/10.21873/invivo.11333.
20. Xu P, Yang M, Liu Y, Li YP, Zhang H, Shao GR. Breast non-mass-like lesions on contrast-enhanced ultrasonography: feature analysis, breast image reporting and data system classification assessment. World J Clin Cases. 2020;8(4):700–12. https://doi.org/10.12998/wjcc.v8.i4.700.
21. Zhao L, Zhang L, Zheng S, Zhao C, Wang H, Liu C, Chu X. Using the area ratio to differentiate between benign and malignant breast lesions: ultrasound strain elastography versus contrast enhanced. J Med Imaging Health Inform. 2019;9(4):744–9. https://doi.org/10.1166/jmihi.2019.2597.
22. Rizzatto GJ. Towards a more sophisticated use of breast ultrasound. Eur Radiol. 2001;11(12):2425–35. https://doi.org/10.1007/s00330-001-1165-5.
23. Yuan Z, Quan J, Yunxiao Z, Jian C, Zhu H, Liping G. Diagnostic value of contrast-enhanced ultrasound parametric imaging in breast tumors. J Breast Cancer. 2013;16(2):208–13. https://doi.org/10.4048/jbc.2013.16.2.208.
24. Szabó BK, Saracco A, Tánczos E, Aspelin P, Leifland K, Wilczek B, Axelsson R. Correlation of contrast-enhanced ultrasound kinetics with prognostic factors in invasive breast cancer. Eur Radiol. 2013;23(12):3228–36. https://doi.org/10.1007/s00330-013-2960-5.
25. van Esser S, Veldhuis WB, van Hillegersberg R, van Diest PJ, Stapper G, ElOuamari M, et al. Accuracy of contrast-enhanced breast ultrasound for pre-operative tumor size assessment in patients diagnosed with invasive ductal carcinoma of the breast. Cancer Imaging. 2007;7(1):63–8. https://doi.org/10.1102/1470-7330.2007.0012.
26. Luo J, Chen JD, Chen Q, Yue LX, Zhou G, Lan C, et al. Contrast-enhanced ultrasound improved performance of breast imaging reporting and data system evaluation of critical breast lesions. World J Radiol. 2016;8(6):610–7. https://doi.org/10.4329/wjr.v8.i6.610.
27. Xiao X, Ou B, Yang H, Wu H, Luo B. Breast contrast-enhanced ultrasound: is a scoring system feasible? A preliminary study in China. PLoS One. 2014;9(8):e105517. https://doi.org/10.1371/journal.pone.0105517.
28. Szabó BK, Aspelin P, Wiberg MK, Boné B. Dynamic MR imaging of the breast. Analysis of kinetic and morphologic diagnostic criteria. Acta Radiol. 2003;44(4):379–86. https://doi.org/10.1034/j.1600-0455.2003.00084.x.
29. Sencha AN, Bikeev YV, Rodionov VV, Shubin LB. Innovacii ul'trazvukovoj diagnostiki opuholej molochnoj zhelezy [Innovations in ultrasound diagnostics of breast tumors]. Medicinskij Opponent. 2019;3:89–92.
30. Klimonda Z, Karwat P, Dobruch-Sobczak K, Piotrzkowska-Wróblewska H, Litniewski J. Breast-lesions characterization using quantitative ultrasound features of peritumoral tissue. Sci Rep. 2019;9(1):7963. https://doi.org/10.1038/s41598-019-44376-z.
31. Gruber IV, Rueckert M, Kagan KO, Staebler A, Siegmann KC, Hartkopf A, et al. Measurement of tumour size with mammography, sonography and magnetic resonance imaging as compared to histological tumour size in primary breast cancer. BMC Cancer. 2013;13:328. https://doi.org/10.1186/1471-2407-13-328.

32. Stein RG, Wollschläger D, Kreienberg R, Janni W, Wischnewsky M, Diessner J, et al. The impact of breast cancer biological subtyping on tumor size assessment by ultrasound and mammography - a retrospective multicenter cohort study of 6543 primary breast cancer patients. BMC Cancer. 2016;16:459. https://doi.org/10.1186/s12885-016-2426-7.
33. Liu G, Zhang MK, He Y, Liu Y, Li XR, Wang ZL. BI-RADS 4 breast lesions: could multi-mode ultrasound be helpful for their diagnosis? Gland Surg. 2019;8(3):258–70. https://doi.org/10.21037/gs.2019.05.01.
34. Kapetas P, Clauser P, Woitek R, Wengert GJ, Lazar M, Pinker K, et al. Quantitative multiparametric breast ultrasound: application of contrast-enhanced ultrasound and elastography leads to an improved differentiation of benign and malignant lesions. Investig Radiol. 2019;54(5):257–64. https://doi.org/10.1097/RLI.0000000000000543.
35. Zhang W, Xiao X, Xu X, Liang M, Wu H, Ruan J, Luo B. Non-mass breast lesions on ultrasound: feature exploration and multimode ultrasonic diagnosis. Ultrasound Med Biol. 2018;44(8):1703–11. https://doi.org/10.1016/j.ultrasmedbio.2018.05.005.
36. Bikeev YV, Sencha AN, Rodionov VV, et al. Kachestvennyj analiz ul'trazvukovogo issledovaniya s primeneniem kontrastnogo preparata v differencial'noj diagnostike uzlovyh obrazovanij molochnoj zhelezy [Qualitative analysis of ultrasound examination with the use of a contrast agent in the differential diagnosis of breast nodules]. Medicinskaya Vizualizaciya. 2019;1:87–96.
37. Gauthier TP, Averkiou MA, Leen EL. Perfusion quantification using dynamic contrast-enhanced ultrasound: the impact of dynamic range and gain on time-intensity curves. Ultrasonics. 2011;51(1):102–6. https://doi.org/10.1016/j.ultras.2010.06.004.
38. Ozdemir A, Ozdemir H, Maral I, Konuş O, Yücel S, Işik S. Differential diagnosis of solid breast lesions: contribution of Doppler studies to mammography and gray scale imaging. J Ultrasound Med. 2001;20(10):1091–101.; quiz 1102. https://doi.org/10.7863/jum.2001.20.10.1091.
39. Park AY, Kwon M, Woo OH, Cho KR, Park EK, Cha SH, et al. A prospective study on the value of ultrasound microflow assessment to distinguish malignant from benign solid breast masses: association between ultrasound parameters and histologic microvessel densities. Korean J Radiol. 2019;20(5):759–72. https://doi.org/10.3348/kjr.2018.0515.
40. Piscaglia F, Nolsøe C, Dietrich CF, Cosgrove DO, Gilja OH, Bachmann Nielsen M, et al. The EFSUMB guidelines and recommendations on the clinical practice of contrast enhanced ultrasound (CEUS): update 2011 on non-hepatic applications. Ultraschall Med. 2012;33(1):33–59. https://doi.org/10.1055/s-0031-1281676.
41. Sardanelli F, Podo F, Santoro F, Manoukian S, Bergonzi S, Trecate G, et al. Multicenter surveillance of women at high genetic breast cancer risk using mammography, ultrasonography, and contrast-enhanced magnetic resonance imaging (the high breast cancer risk Italian 1 study): final results. Investig Radiol. 2011;46(2):94–105. https://doi.org/10.1097/RLI.0b013e3181f3fcdf.

Salivary Glands

15

Alexander N. Sencha and Ella I. Peniaeva

Humans have three paired major salivary glands (parotid, submandibular, and sublingual). Each gland has an individual blood supply. The parotid glands are supplied by the branches of the superficial temporal artery, the venous blood drains to the retromandibular veins. The submandibular glands obtain the blood from the facial artery with the venous outflow to the same-name veins. The sublingual glands get their blood supply via the branches of the lingual and facial arteries, venous blood drains to the lingual veins.

High-resolution sonography with intraductal and/or intravenous contrast enhancement is increasingly used to expand the possibility of ultrasound and improve its diagnostic efficiency [1–5]. Additionally, CEUS quantification permits more efficient, reliable, and reproducible data.

As a rule, there is no need to use CEUS in the norm, inflammatory, or degenerative changes of salivary glands. However, this method is efficient in the differential diagnosis of tumors. Focal lesions of salivary glands exhibit different patterns of contrast enhancement, which serve as a valuable diagnostic sign.

The salivary gland CEUS implicates a single intravenous injection of 2.4–4.8 ml of SonoVue®. Normally, the filling with UCA of the normal salivary gland parenchyma is intensive, regular, and symmetric with mild wash-out (Fig. 15.1).

Time-intensity curve parameters of salivary gland CEUS can be used for non-invasive monitoring of treatment in chronic sialadenitis with sialolithiasis and identification of tumor vascularization [6].

Salivary gland cyst typically has specific ultrasound signs, such as anechoic uniform contents with grayscale US and avascular with Doppler imaging. A simple cyst of a salivary gland, as well as of any other location, with CEUS demonstrates a characteristic perfusion defect with no contrast enhancement in all vascular phases (Fig. 15.2).

CEUS is often used to assess the microvascularization of salivary gland neoplasms. The parotid gland develops 70–90% of all salivary gland tumors, 8–10% arise in the submandibular and sublingual glands, and 4.9–22% in small glands [1, 7, 8].

Supplementary Information The online version contains supplementary material available at [https://doi.org/10.1007/978-3-030-91764-7_15].

A. N. Sencha (✉)
Department of Visual and Functional Diagnostics, Federal State Budget Institution "National Medical Research Center for Obstetrics, Gynecology and Perinatology n.a. V.I.Kulakov", Moscow, Russian Federation

E. I. Peniaeva
Department of Ultrasound Diagnostics, Center for Radiological Diagnostics, Private Healthcare Institution "Clinical Hospital "RZD-Medicina" of Yaroslavl City", Yaroslavl, Russian Federation

A. N. Sencha, Y. N. Patrunov (eds.), *Contrast-Enhanced Ultrasound*,
https://doi.org/10.1007/978-3-030-91764-7_15

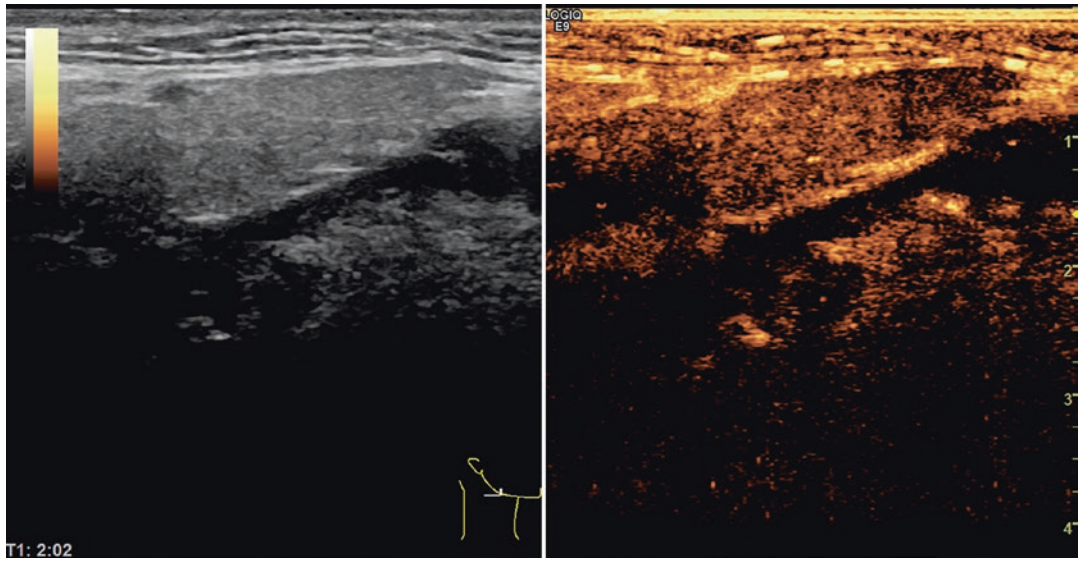

Fig. 15.1 Normal submandibular salivary gland. The venous phase CEUS image. Regular enhancement of the parenchyma

Benign tumors of the salivary glands are most often represented by the pleomorphic adenoma. General sonography with CDI reveals clear boundaries, some circumscribing vessels, and poor blood flow within the neoplasm. With CEUS, pleomorphic adenoma is usually hypoenhanced [9] (Fig. 15.3, Video 15.1). Although some other types of tumors like Warthin's tumor (cystadenolymphoma) may appear hyperenhanced [9].

Perfusion quantification demonstrates hypovascularity of pleomorphic adenoma with low perfusion indices and hypervascularity of adenolymphoma. The study [10] analyzed TICs in various salivary gland tumors and reported that the mean transit time (MTT) and AUC values in benign lesions (14.6 ± 1.24 s and 400.63 ± 53.85, respectively) were lower than the same in malignant tumors. However, cystadenolymphoma exhibited a higher AUC value (515.4 ± 71.26 vs. 285.82 ± 36.44, respectively) and the maximum signal increase (22.74 ± 2.69 dB/s vs. 14.32 ± 2.66 dB/s) than pleomorphic adenoma.

The special aim of CEUS is the detection and differential diagnosis of malignant tumors. Malignancies are observed in 3.6–30% of salivary gland lesions and predominantly affect the parotid glands [1, 11]. The use of UCAs is based on the identification of enhanced vascularity and neoangiogenesis. Most salivary gland malignancies are characterized by chaotic vascular branching, irregular course and caliber of the vessels, arteriovenous shunts, the inconsistency of the vascular wall, and sometimes multiple afferent vessels [1–4, 9] (Fig. 15.4).

Different histological types of salivary gland neoplasms have different qualitative and quantitative characteristics of contrast enhancement. CEUS can be an independent quantitative method for the evaluation of malignant and benign tumors of the parotid gland [10]. The salivary gland's malignancies have indistinct contours and are typically hypervascular. With a quantitative assessment, they are highly perfused [9]. TIC demonstrates the MTT for malignant neoplasms of 17.94 ± 1.62 s, which is significantly higher

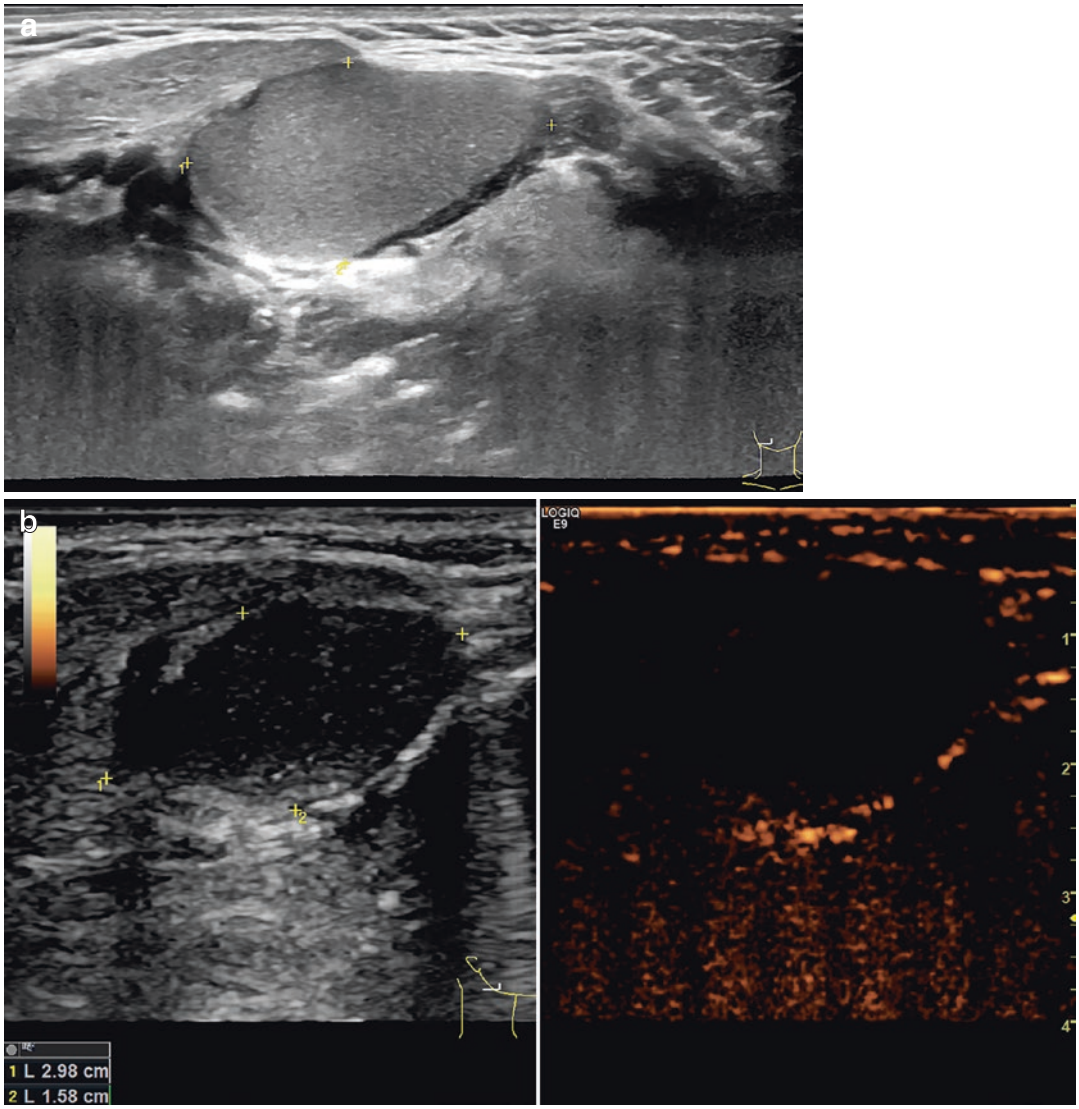

Fig. 15.2 A simple salivary gland cyst. (**a**) Grayscale US image. (**b**) CEUS demonstrates a perfusion defect

than in benign lesions. The AUC value for malignant tumors is also significantly higher (584.9 ± 143.0).

Contrast enhancement enables detailed imaging of the vascular tree of the salivary gland tumors, which exceeds standard Doppler modes [4, 6, 10, 12–14].

CEUS in salivary glands has significant prospects. Further studies and accumulation of practical experience are still necessary.

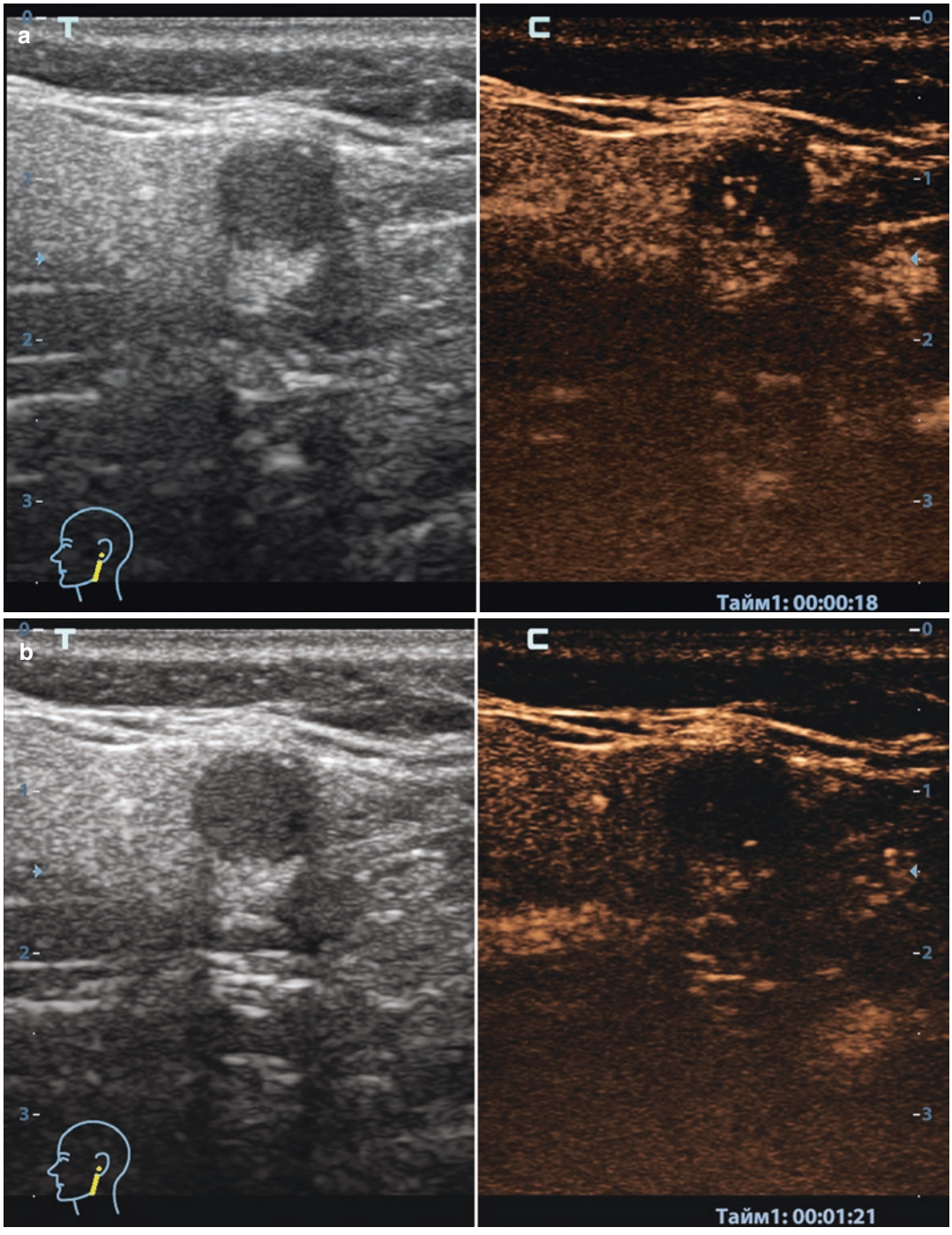

Fig. 15.3 Pleomorphic adenoma of the parotid gland. CEUS images. (**a**) Patient A. The arterial phase CEUS demonstrates hypoenhancement of the lesion. (**b**) Patient A. The venous phase CEUS demonstrates slow wash-out. (**c**) Patient B. Moderate enhancement in the venous phase. (**d**) Patient B. The TIC quantifies slow wash-in and wash-out of the lesion

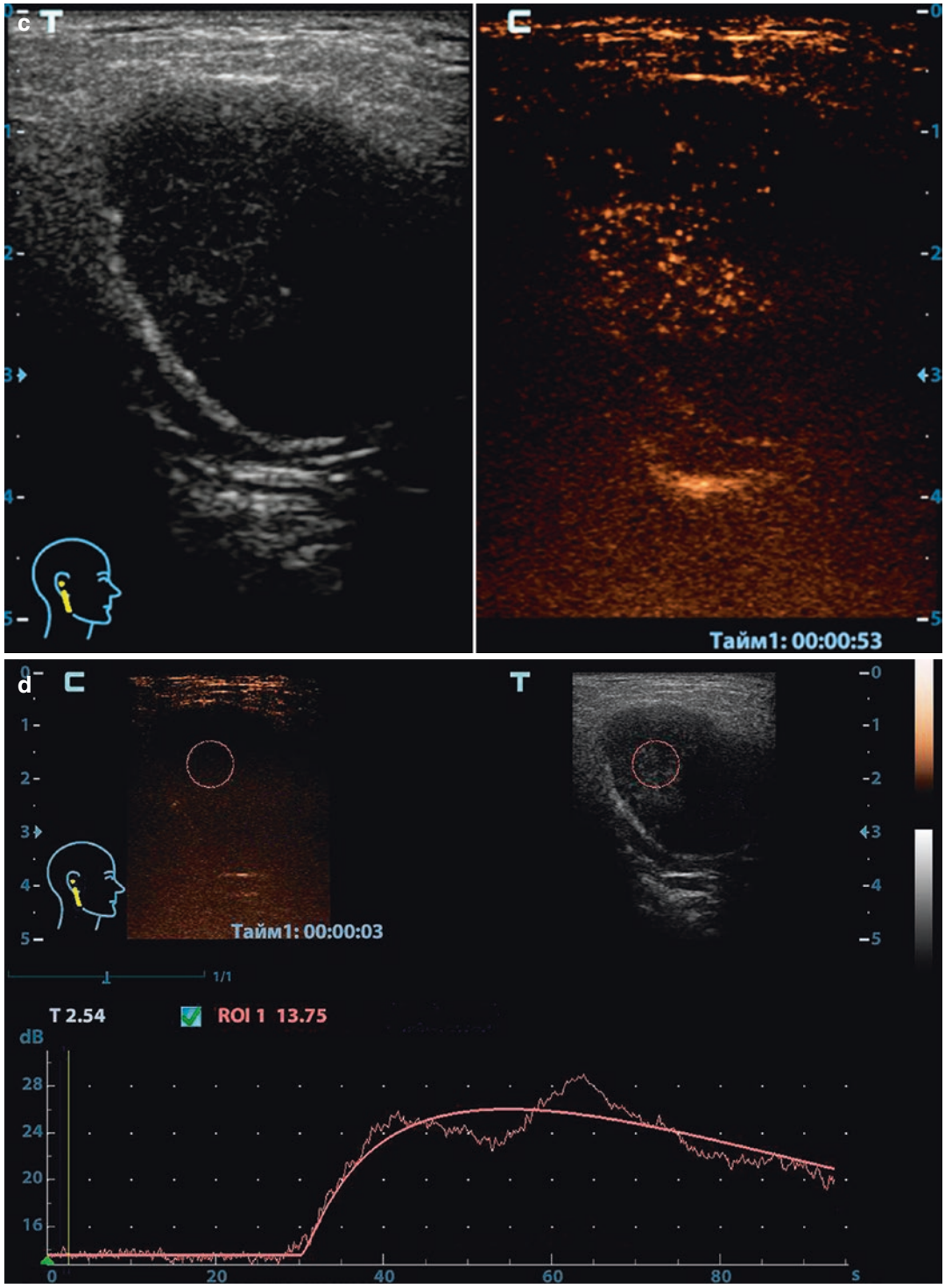

Fig. 15.3 (continued)

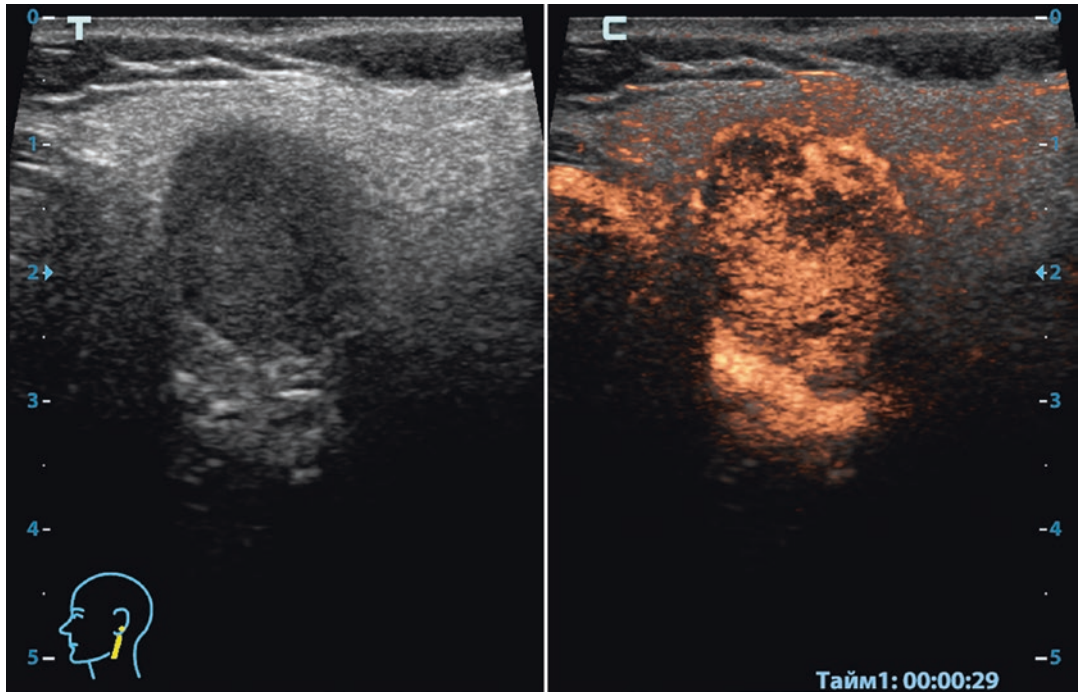

Fig. 15.4 Parotid gland adenocarcinoma. CEUS image with SonoVue® demonstrates irregular hyperenhancement of the tumor in the arterial phase

References

1. Afanas'ev VV. Slyunnye zhelezy. Bolezni i travmy [Salivary glands. Illnesses and injuries]. Moscow: Geotar-Media; 2019.
2. Sencha AN. Ul'trazvukovaya diagnostika. Poverhnostno-raspolozhennye organy [Ultrasound diagnostics. Surface-located organs]. Moscow: Vidar; 2015.
3. Sencha AN. Ul'trazvukovoe issledovanie okoloshchitovidnyh i slyunnyh zhelez. Ot prostogo k slozhnomu [Ultrasound examination of the parathyroid and salivary glands. From simple to complex]. Moscow: MEDpress-inform; 2020.
4. Sencha AN, Mogutov MS, Patrunov YN, Peniaeva EI, Kashmanova AV, Sencha EA. Ul'trazvukovoe issledovanie s ispol'zovaniem kontrastnyh preparatov [Ultrasound examination with contrast agents]. Moscow: Vidar; 2015.
5. Shchipskij AV, Afanas'ev VV. Diagnostika hronicheskih zabolevanij slyunnyh zhelez s pomoshch'yu differencial'no-diagnosticheskogo algoritma [Diagnosis of chronic diseases of the salivary glands using a differential diagnostic algorithm]. Moscow: GOU VUNMC MZ RF; 2001.
6. Strieth S, Siedek V, Rytvina M, Gürkov R, Berghaus A, Clevert DA. Dynamic contrast-enhanced ultrasound for differential diagnosis of submandibular gland disease. Eur Arch Otorhinolaryngol. 2014;271(1):163–9. https://doi.org/10.1007/s00405-013-2523-z.
7. Bykova AA, Kondrashin SA, Agapov VS, Zaderenko IA. Kompleksnaya sonografiya v diagnostike i lechenii opuholej bol'shih slyunnyh zhelez [Complex sonography in the diagnosis and treatment of tumors of the large salivary glands]. Sibirskij onkologicheskij zhurnal. 2002;3:128–32.
8. Sedova YS, Sinyukova GT. Sovremennye vozmozhnosti ul'trazvukovogo issledovaniya v diagnostike opuholej slyunnyh zhelez [Modern possibilities of ultrasound research in the diagnosis of salivary gland tumors]. Ul'trazvukovaya i funkcional'naya diagnostika. 2010;6:117–24.
9. Gou JM, Chen Q, Zhou Q, Liu YX. Quantitative diagnosis of salivary gland tumors with contrast-enhanced ultrasound–a preliminary study. Oral Surg Oral Med Oral Pathol Oral Radiol. 2013;116(6):784–90. https://doi.org/10.1016/j.oooo.2013.09.013.
10. Klotz LV, Gürkov R, Eichhorn ME, Siedek V, Krause E, Jauch KW, et al. Perfusion characteristics of parotid gland tumors evaluated by contrast-enhanced ultrasound. Eur J Radiol. 2013;82(12):2227–32. https://doi.org/10.1016/j.ejrad.2013.08.033.
11. Ihrler S. Speicheldrüsenpathologie: Ausgewählte Themen zu speziellen Problembereichen [Pathology of the salivary glands: selected topics in particular

problem areas]. Pathologe. 2009;30(6):423. https://doi.org/10.1007/s00292-009-1201-9.
12. Alyas F, Lewis K, Williams M, Moody AB, Wong KT, Ahuja AT, Howlett DC. Diseases of the submandibular gland as demonstrated using high resolution ultrasound. Br J Radiol. 2005;78(928):362–9. https://doi.org/10.1259/bjr/93120352.
13. Inohara H, Akahani S, Yamamoto Y, Hattori K, Tomiyama Y, Tomita Y, et al. The role of fine-needle aspiration cytology and magnetic resonance imaging in the management of parotid mass lesions. Acta Otolaryngol. 2008;128(10):1152–8. https://doi.org/10.1080/00016480701827533.
14. Iro H, Zenk J, Escudier MP, Nahlieli O, Capaccio P, Katz P, et al. Outcome of minimally invasive management of salivary calculi in 4,691 patients. Laryngoscope. 2009;119(2):263–8. https://doi.org/10.1002/lary.20008.

Scrotum and Testicles

16

Alexander N. Sencha, Yury N. Patrunov, and Ella I. Peniaeva

A traditional US study is highly sensitive in the identification of scrotal lesions. However, its capability to differentiate them is limited [1]. Therefore, there are attempts to increase its value with microbubble injection [2–8]. UCA administration increases the sensitivity of US from 76% to 96% and the specificity from 45% to 100% [8]. CEUS also surpasses the diagnostic value of various types of elastography [9]. The diagnostic values of ultrasound methods in the diagnosis of testicular lesions are presented in Table 16.1 [9]:

According to the EFSUMB guidelines and recommendations for the clinical practice of CEUS in non-hepatic applications (2017) [10], it is advised in the following conditions:

- distinguish vascularized from non-vascularized focal testicular lesions, helping to exclude malignancy
- discriminate non-viable regions in testicular trauma
- identify segmental infarction
- identify abscess formation and infarction in severe epididymo-orchitis

Testicular CEUS is technically similar to the same study in the majority of superficial organs. An increase in the SonoVue® dose to 2.4–4.8 mL is required. The contrast enhancement of normal testicles typically occurs no earlier than 20 s after the UCA injection. The arteries enhance first, followed within seconds by complete parenchymal enhancement. The scrotal wall tends to enhance to a lesser degree than the contents. There is no accumulation of UCA in the parenchyma of the testicles and the enhancement fades within 3 min [10] (Fig. 16.1). The arterial phase contrast enhancement depicts regular capsular and centripetal arteries. Any other pattern should be paid special attention to and considered abnormal.

The conventional US detects scrotal tumors with sensitivity near 100% but the differentiation between benign and malignant lesions remains a problem. It is believed that avascular masses are benign, whereas vascularization of the tumor is associated with the risk of malignancy [11–13]. However, the meta-analysis [13] demonstrated

Supplementary Information The online version contains supplementary material available at [https://doi.org/10.1007/978-3-030-91764-7_16].

A. N. Sencha (✉)
Department of Visual and Functional Diagnostics, Federal State Budget Institution "National Medical Research Center for Obstetrics, Gynecology and Perinatology n.a. V.I.Kulakov", Moscow, Russian Federation

Y. N. Patrunov · E. I. Peniaeva
Department of Ultrasound Diagnostics of the Center for Radiological Diagnostics, Private Healthcare Institution "Clinical Hospital "RZD-Medicina" of Yaroslavl City", Yaroslavl, Russian Federation

A. N. Sencha, Y. N. Patrunov (eds.), *Contrast-Enhanced Ultrasound*,
https://doi.org/10.1007/978-3-030-91764-7_16

Table 16.1 The diagnostic values of ultrasound methods in the diagnosis of testicular lesions

Modality	Sensitivity	Specificity	Accuracy	PPV	NPV
Grayscale	100%	43%	88%	87%	100%
CDI	81%	86%	82%	96%	55%
CEUS	93%	85%	91%	96%	73%
Real-time elastography, elasticity score	98%	25%	85%	85%	75%
Real-time elastography, difference of elasticity score	98%	50%	89%	90%	83%
Real-time elastography, strain ratio	90%	45%	81%	86%	56%

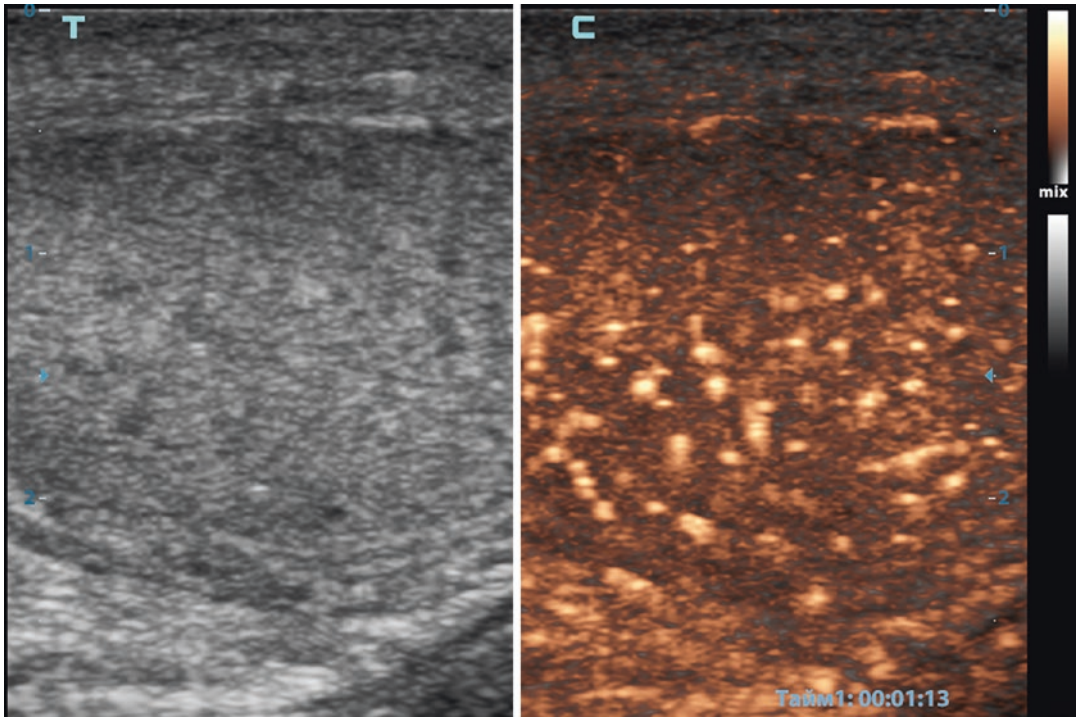

Fig. 16.1 Normal testicle. Venous phase CEUS image. Moderate relatively homogeneous enhancement of the testicular parenchyma

that a significant number of the hypoechogenic lesions, which were avascular with CDI and PDI, were malignant. CEUS demonstrates lesion perfusion and is more sensitive in low-velocity blood flow. Lesion avascularity with CEUS reliably identifies epidermoid and simple cysts from testicular tumors.

A simple testicular cyst does not cause any difficulties in a typical ultrasound grayscale image. Differentiation with rare cystic tumors is necessary if the cyst exhibits dense or irregularly thickened walls or echogenic contents. With CEUS, simple cysts do not enhance in all vascular phases and are represented by perfusion defects with clear smooth boundaries. In cystic tumors, the walls and intraluminal solid components demonstrate contrast enhancement [5].

Despite the characteristic ultrasound signs of epidermoid cysts, such as the "onion rings" pattern and pronounced central or peripheral calcification with acoustic shadowing, the principal feature for their differentiation from malignant neoplasms is the absence of vascularization [14, 15]. Epidermoid cyst always remains nonenhanced with CEUS. In most cases, peripheral rim-like hyperenhancement is present that is associated with the increased density of blood vessels in the compressed adjacent testicular

parenchyma. A small-sized epidermoid cyst may lack the peripheral hyperenhancing rim [7].

There are many other benign testicular and scrotal lesions, such as testicular adrenal rests, rete tubular ectasia, sarcoidosis, papillary cystadenoma of the epididymis, leiomyoma, lipoma, paratesticular fibrous pseudotumor, etc., which are rare and insufficiently studied with CEUS.

Tubular ectasia of the rete testis arises as a result of the obstruction of the efferent ducts. CEUS reveals the normal vascular pattern of the testis and no enhancement within the characteristic cystic or tubular structures [16].

Testicular adrenal rest tumors arise due to the increased adrenocorticotropic hormone (ACTH). During fetal development, adrenal cell migration in gonads may be impaired with some cell groups trapped within testicular parenchyma. They may enlarge in the corresponding circumstances and remain asymptomatic. The lesions are usually multiple and bilateral. CEUS determines the hyperenhancement of these masses in the arterial phase and isoenhancement in the venous phase. The vessels that pass through the lesions do not branch, which is a characteristic feature.

Extratesticular scrotal lesions are mainly considered benign. As in cases of testicular masses, CEUS enables specification of their vascularity but no characteristic enhancement patterns are reported yet [17].

Malignant tumors of the testicles are diagnosed in up to 1% of all malignant tumors in males. From 90% to 95% of them are represented by germ cell tumors [12]. With CEUS, malignant tumors are characterized by complete or partial contrast enhancement. Intersecting vessels are typical for primary testicular tumors. In infiltrative lesions, such as lymphoma, plasmacytoma, and granulocytic sarcoma, the linear vessels without branching may be observed [3].

Seminoma is the most common germ cell tumor. Its hypervascularity is usually registered with CDI and PDI. The advantage of CEUS is the precise display of the tumor perfusion, which also works for small-sized lesions. Seminoma demonstrates rapid hyperenhancement with a loss of the characteristic linear vascular pattern of the testicular parenchyma. Wash-out of the contrast within the lesion may be rapid, but with the persistence of abnormal "crossing" vessels [3].

Non-seminomatous germ cell tumors are represented by mixed tumors that contain two or more germ cell components in various combinations. The tumor may have a different sonographic image, which depends on the prevailing component. CDI may not identify increased vascularity that mimics a benign lesion. With CEUS, the chaotic movements of microbubbles within the mass indicate abnormal vascularization and the malignant nature of the lesion [3].

Embryonal carcinoma with CEUS may have various image patterns ranging from hyperenhancing lesion in the early arterial phase with rapid wash-out to a significantly hypoenhanced mass [18] (Fig. 16.2 and Video 16.1). Testicular choriocarcinoma additionally may have a nonenhancing hemorrhagic component [19].

Yolk sac tumors do not exhibit any principal difference in contrast enhancement from other germ cell tumors. The chaotic distribution of vessels within the lesion is also characteristic.

Sex cord gonadal stromal tumors are the second most common neoplasm of the testicles after the germ cell tumors, although they are usually benign. They originate from Leydig cells and/or Sertoli cells. These tumors typically demonstrate arterial phase hyperenhancement, but as opposed to germ cell tumors, the enhancement persists for a long time.

Testicular lymphoma regardless of primary or secondary involvement in both focal lesion and diffuse infiltration exhibits hyperenhancement with a preserved vascular pattern. Hence, CEUS does not provide any additional information. It is similar to orchitis, and the differential diagnosis requires correlations with clinical data [18, 20].

Metastatic lesions in the testicles do not show any specific enhancement features and appear similar to the primary testicular tumors.

Currently, the specific patterns of contrast enhancement in individual histological types of malignant testicular tumors are not recognized. Any tumor, which demonstrates contrast enhancement with CEUS, should be considered potentially malignant, especially in the cases of rapid wash-out [10, 21].

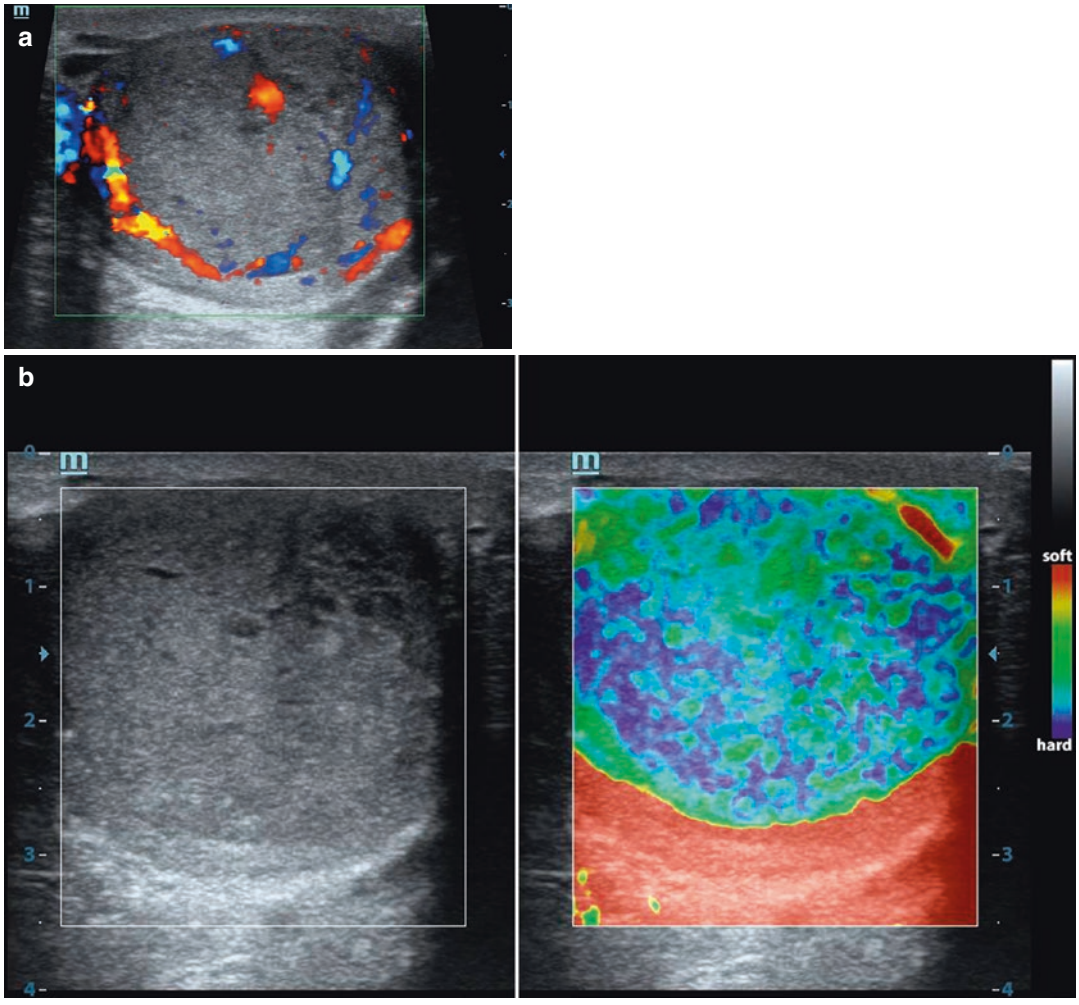

Fig. 16.2 Embryonal carcinoma of the testis. (**a**) CDI depicts irregular vascularity of the testicular mass. (**b**) Ultrasound compression elastography demonstrates the heterogeneous hard pattern of the testicular lesion. (**c**) Arterial phase CEUS image demonstrates twisted arteries in the tumor. (**d**) Venous phase CEUS image reveals heterogeneous enhancement with abnormal vessels

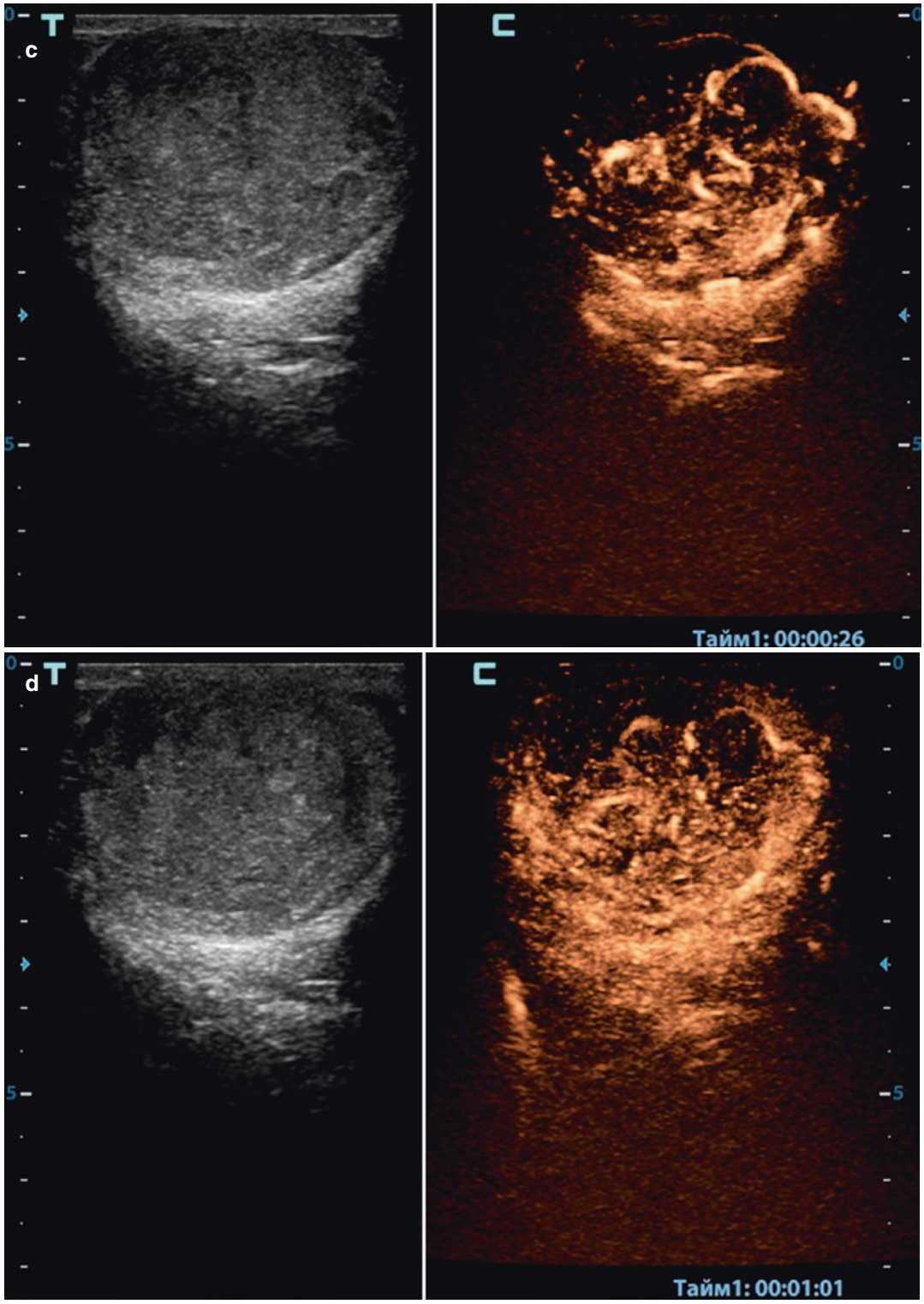

Fig. 16.2 (continued)

Table 16.2 Quantitative features of CEUS in malignant and benign tumors, non-neoplastic lesions, and normal testicular parenchyma

Parameter	Malignant tumors	All benign lesions	*p*	All tumors	Non-neoplastic lesions	*p*	Parenchyma
WIT, s	5.9 (4.6–7.8)	8.1 (6.7–12.6)	0.001	6.9 (5.2–8.6)	9.5 (7.7–17.24)	0.002	8.1 (5.9–12.0)
TTP, s	31.7 (27–35.8)	38.8 (31.2–45.7)	0.005	33.3 (29.0–40.4)	43.4 (32.6–51.9)	0.009	38.2 (31.4–44.4)
MTT, s	8.8 (6.8–11.4)	11.4 (9.4–17.8)	0.001	10.2 (7.7–12.4)	13.1 (10.8–24.4)	0.004	12.1 (8.9–17.1)
WOT, s	18.8	26.5 (19.9–36.5)	0.001	20.6 (15.9–25.2)	34.3 (24.1–46.6)	0.001	23.1 (16.8–35.5)
PI, dB	3.5 (2.0–5.2)	4.0 (1.4–5.4)	0.799	4.0 (2.3–5.4)	1.6 (0.6–4.2)	0.002	2.3 (1.5–3.3)
Az	140 (84–223)	177 (77–263)	0.260	180 (99–261)	102 (30–215)	0.026	104 (67–169)
AS, dB/s	0.49 (0.3–0.8)	0.4 (0.1–0.7)	0.162	0.5 (0.3–0.8)	0.1 (0.05–0.3)	0.001	0.2 (0.1–0.4)

WIT wash-in time, *TTP* time to the peak enhancement, *MTT* mean transit time, *WOT* wash-out time, *PI* peak intensity, *Az* area under the curve, *AS* ascending slope

Rare publications on quantitative analysis of CEUS indicate its prospects for the differential diagnosis of testicular lesions. The study [21] reported that testicular tumors are characterized by faster wash-in, peak intensity, and wash-out, as compared with non-neoplastic lesions. Additionally, malignant tumors exhibit faster wash-in and wash-out with no difference in peak intensity (Table 16.2). However, yet a small number of publications and the lack of standardization do not permit any recommendations.

Non-neoplastic diseases of the scrotum also benefit from CEUS. Testicular torsion is rarely reported to be examined with microbubble injection [6, 22–24]. This is probably because testicular torsion is primarily found in children and adolescents, and UCAs were not licensed for pediatric patients, and in many countries were used off-label. Depending on the severity of the spermatic cord twisting, the arterial blood supply to the testicle is significantly reduced or blocked. An animal model demonstrated that the arterial inflow stops only in cases of greater than 450° twist [25]. Considering the high sensitivity and specificity of modern CDI and PDI (86–100% and 98–100%, respectively) in the diagnosis of the testicular torsion, CEUS does not provide any additional clinically significant information, but reliably confirms testicular avascularity [2]. However, CEUS may be useful in small-sized testicles when Doppler imaging fails to provide the necessary quality of blood flow detection. CEUS confirms the decrease or absence of the vascular supply to the testicle, which corresponds to hypo- or nonenhancement as compared with the normal testicle [6] (see Chap. 20).

Acute segmental testicular infarction is wall diagnosed with normal ultrasound if a typical wedge-shaped lesion in a combination with the significant decrease or absence of vascularity with CDI and PDI is detected [19]. But in an atypical appearance with a rounded lesion shape, the differential diagnosis with a hypovascular tumor is necessary. CEUS demonstrates one or more ischemic lobules separated by normal testicular vessels in the acute phase [2]. The subacute segmental infarction is characterized by the annular contrast enhancement around the ischemic zone, which is associated with reactive hyperemia and decreases with time [2]. In a month, a hyperenhancing rim is absent, and spots of contrast enhancement within the lesion may appear [2].

In orchiepididymitis, the diagnosis is based on clinical data reinforced with sonography, which detects hypervascularization with CDI and PDI. The increase in venous flow is usually associated with testicular inflammation. CEUS confirms the obtained US data in uncomplicated orchitis and provides valuable diagnostic information regarding complications, such as abscess, venous infarction, spermatic vein thrombosis, hemorrhage, etc. CEUS increases the sensitivity in the detection of thrombosis in funiculitis and

identification of postinflammatory ischemic changes in the testicular parenchyma [19].

Venous infarction of the testis is a result of a segmental or diffuse failure of venous outflow due to inflammation, which leads to necrosis and abscess. It also may be a consequence of hypercoagulation or testicular trauma. Traditional echography hardly differentiates arterial infarction, tumor, and venous infarction with abscess. The study [26] reported that nonenhancing focal lesions of a rounded shape centrally located within the testicle were characteristic of a venous infarction with abscess. Irregular margins and peripheral rim-like hyperenhancement typically accompany both venous infarction and testicular abscess. CEUS is also beneficial for the assessment of the real abscess size [6].

Scrotal trauma accompanies about 1% of all body trauma. Blunt trauma is the most common mechanism of injury often due to sporting activities. Penetrating injuries are rare. Scrotal trauma usually confers bruise, hematoma, hematocele, testicular rupture, etc. The first line imaging method is US with CDI and PDI. The key point is the identification of the tunica albuginea continuity or defects. Besides, the volume of viable testicular tissue is important, which determines the surgery type [27]. In most cases, CEUS defines traumatic changes with better accuracy. It precisely reveals the nature and volume of the damage. CEUS clearly defines the ruptured areas represented by nonenhancing lesions of irregular linear shape and hematomas, which appear hypoenhanced or nonenhanced depending on the severity of the injury [8] (Figs. 16.3 and 16.4).

CEUS surpasses traditional echography in the evaluation of both focal testicular lesions and traumatic damage. It reliably demonstrates the perfusion of scrotal organs in real-time. An especially important aspect is the identification of avascular lesions [27–30]. CEUS data in some cases can be a significant argument for the tactics of "watchful observation" or puncture biopsy, which permits to avoid unwanted orchiectomy.

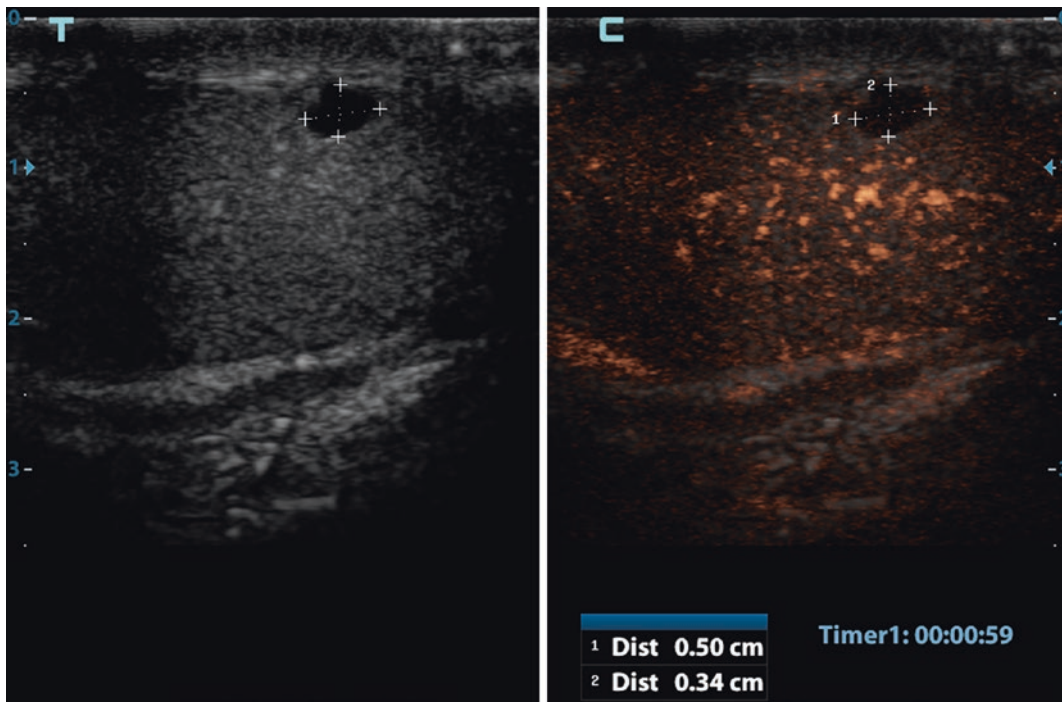

Fig. 16.3 Post-traumatic cyst in the parenchyma of the testis. CEUS image identifies the perfusion defect

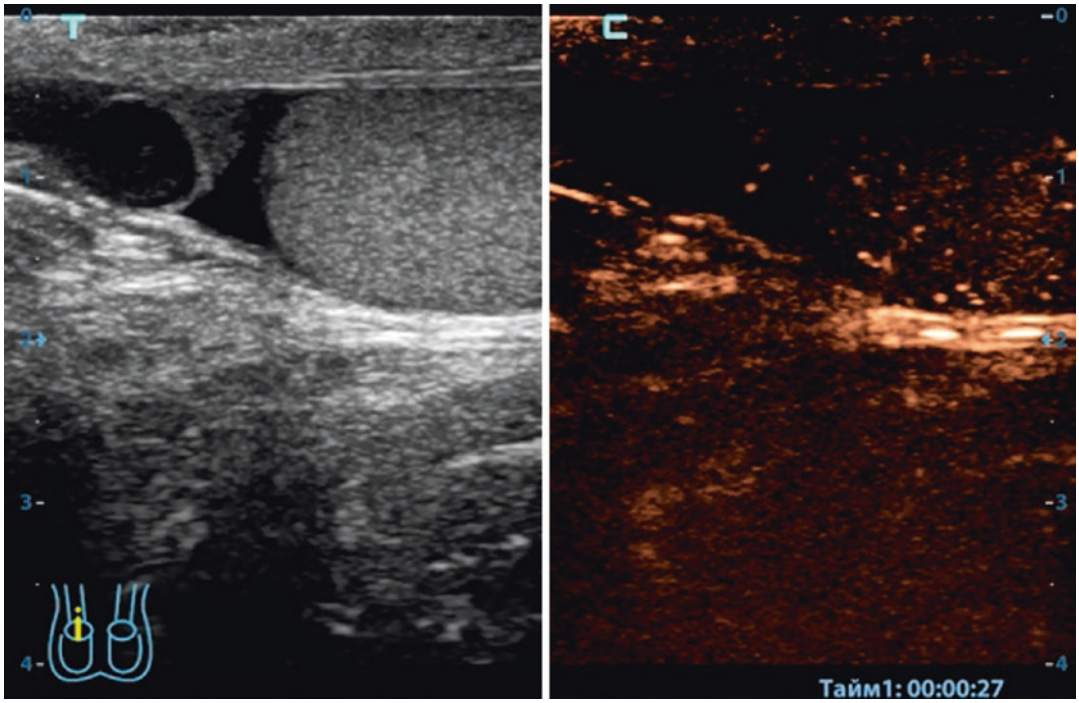

Fig. 16.4 Testicular appendage cyst. CEUS image identifies the perfusion defect

References

1. Müller T, Gozzi C, Akkad T, Pallwein L, Bartsch G, Steiner H. Management of incidental impalpable intratesticular masses of < or = 5 mm in diameter. BJU Int. 2006;98(5):1001–4. https://doi.org/10.1111/j.1464-410X.2006.06485.x.
2. Bertolotto M, Derchi LE, Sidhu PS, Serafini G, Valentino M, Grenier N, Cova MA. Acute segmental testicular infarction at contrast-enhanced ultrasound: early features and changes during follow-up. AJR Am J Roentgenol. 2011;196(4):834–41. https://doi.org/10.2214/AJR.10.4821.
3. Huang DY, Sidhu PS. Focal testicular lesions: colour Doppler ultrasound, contrast-enhanced ultrasound and tissue elastography as adjuvants to the diagnosis. Br J Radiol. 2012;85(1):S41–53. https://doi.org/10.1259/bjr/30029741. Special Issue.
4. Hedayati V, Sellars ME, Sharma DM, Sidhu PS. Contrast-enhanced ultrasound in testicular trauma: role in directing exploration, debridement and organ salvage. Br J Radiol. 2012;85(1011):e65–8. https://doi.org/10.1259/bjr/95600238.
5. Lock G, Schmidt C, Helmich F, Stolle E, Dieckmann KP. Early experience with contrast-enhanced ultrasound in the diagnosis of testicular masses: a feasibility study. Urology. 2011;77(5):1049–53. https://doi.org/10.1016/j.urology.2010.12.035.
6. Moschouris H, Stamatiou K, Lampropoulou E, Kalikis D, Matsaidonis D. Imaging of the acute scrotum: is there a place for contrast-enhanced ultrasonography? Int Braz J Urol. 2009;35(6):692–702. https://doi.org/10.1590/s1677-55382009000600008; discussion 702–5.
7. Patel K, Sellars ME, Clarke JL, Sidhu PS. Features of testicular epidermoid cysts on contrast-enhanced sonography and real-time tissue elastography. J Ultrasound Med. 2012;31(1):115–22. https://doi.org/10.7863/jum.2012.31.1.115.
8. Valentino M, Bertolotto M, Derchi L, Bertaccini A, Pavlica P, Martorana G, Barozzi L. Role of contrast enhanced ultrasound in acute scrotal diseases. Eur Radiol. 2011;21(9):1831–40. https://doi.org/10.1007/s00330-010-2039-5.
9. Schröder C, Lock G, Schmidt C, Löning T, Dieckmann KP. Real-time elastography and contrast-enhanced ultrasonography in the evaluation of testicular masses: a comparative prospective study. Ultrasound Med Biol. 2016;42(8):1807–15. https://doi.org/10.1016/j.ultrasmedbio.2016.03.026.
10. Sidhu PS, Cantisani V, Dietrich CF, Gilja OH, Saftoiu A, Bartels E, et al. The EFSUMB guidelines and recommendations for the clinical practice of contrast-enhanced ultrasound (CEUS) in non-hepatic applications: update 2017 (long version). Ultraschall Med. 2018;39(2):e2–e44. https://doi.org/10.1055/a-0586-1107.

11. Baxter GM, Sidhu PS. Ultrasound of urogenital system. Stuttgart: Thieme; 2004.
12. Ministerstva Zdravookhraneniya Rossiyskoy Federatsii. Germinogennye Opuholi u Muzhchin. Klinicheskie rekomendacii [Germinogenic tumors in men: clinical recommendations]. Moscow: Ministerstva Zdravookhraneniya Rossiyskoy Federatsii; 2018. Russian. http://www.oncology.ru/association/clinical-guidelines/2018/germinogennye_opukholi_u_muzhchin_pr2018.pdf. Accessed 21 Feb 2021.
13. Ma W, Sarasohn D, Zheng J, Vargas HA, Bach A. Causes of avascular hypoechoic testicular lesions detected at scrotal ultrasound: can they be considered benign? AJR Am J Roentgenol. 2017;209(1):110–5. https://doi.org/10.2214/AJR.16.17333.
14. Mitkov VV, editor. Prakticheskoe rukovodstvo po ul'trazvukovoj diagnostike [Practical guide to ultrasound diagnostics]. 2nd ed. Moscow: Vidar; 2011. p. 501–23. Russian.
15. Langer JE, Ramchandani P, Siegelman ES, Banner MP. Epidermoid cysts of the testicle: sonographic and MR imaging features. AJR Am J Roentgenol. 1999;173(5):1295–9. https://doi.org/10.2214/ajr.173.5.10541108.
16. Fang C, Huang D, Sidhu PS. Scrotum: benign lesions. In: Lyshchik A, editor. Specialty imaging: fundamentals of CEUS. 1st ed. Philadelphia, PA: Elsevier; 2019. p. 254–72.
17. Rafailidis V, Robbie H, Konstantatou E, Huang DY, Deganello A, Sellars ME, Cantisani V, Isidori AM, Sidhu PS. Sonographic imaging of extratesticular focal lesions: comparison of grey-scale, colour Doppler and contrast-enhanced ultrasound. Ultrasound. 2016;24(1):23–33. https://doi.org/10.1177/1742271X15626195.
18. Jaffer OS, Sidhu PS. Contrast-enhanced ultrasonography of the testes. Ultrasound Clin. 2013;8(4):509–23.
19. Valentino M, Bertolotto M, Martino P, Barozzi L, Pavlica P. Incidentally detection of non-palpable testicular nodules at scrotal ultrasound: what is new? Arch Ital Urol Androl. 2014;86(4):378–82. https://doi.org/10.4081/aiua.2014.4.378.
20. Kachramanoglou C, Rafailidis V, Philippidou M, Bertolotto M, Huang DY, Deganello A, et al. multiparametric sonography of hematologic malignancies of the testis: grayscale, color Doppler, and contrast-enhanced ultrasound and strain elastographic appearances with histologic correlation. J Ultrasound Med. 2017;36(2):409–20. https://doi.org/10.7863/ultra.16.02013.
21. Isidori AM, Pozza C, Gianfrilli D, Giannetta E, Lemma A, Pofi R, et al. Differential diagnosis of nonpalpable testicular lesions: qualitative and quantitative contrast-enhanced US of benign and malignant testicular tumors. Radiology. 2014;273(2):606–18. https://doi.org/10.1148/radiol.14132718.
22. Kitami M. Ultrasonography of pediatric urogenital emergencies: review of classic and new techniques. Ultrasonography. 2017;36(3):222–38. https://doi.org/10.14366/usg.17011.
23. Syed A, Pranay P, Chua N, Naleem A, Mahmood I, Khan S. A case of testicular torsion demonstrated on contrast enhances ultrasound. Russ Electron J Radiol. 2017;7(4):161–3. https://doi.org/10.21569/2222-7415-2017-7-4-161-163.
24. Yusuf GT, Sidhu PS. A review of ultrasound imaging in scrotal emergencies. J Ultrasound. 2013;16(4):171–8. https://doi.org/10.1007/s40477-013-0033-x.
25. Lee FT Jr, Winter DB, Madsen FA, Zagzebski JA, Pozniak MA, Chosy SG, Scanlan KA. Conventional color Doppler velocity sonography versus color Doppler energy sonography for the diagnosis of acute experimental torsion of the spermatic cord. AJR Am J Roentgenol. 1996;167(3):785–90. https://doi.org/10.2214/ajr.167.3.8751701.
26. Lung PF, Jaffer OS, Sellars ME, Sriprasad S, Kooiman GG, Sidhu PS. Contrast-enhanced ultrasound in the evaluation of focal testicular complications secondary to epididymitis. AJR Am J Roentgenol. 2012;199(3):W345–54. https://doi.org/10.2214/AJR.11.7997.
27. Trinci M, Cirimele V, Ferrari R, Ianniello S, Galluzzo M, Miele V. Diagnostic value of contrast-enhanced ultrasound (CEUS) and comparison with color Doppler ultrasound and magnetic resonance in a case of scrotal trauma. J Ultrasound. 2020;23(2):189–94. https://doi.org/10.1007/s40477-019-00389-y.
28. Badea R, Lucan C, Suciu M, Vasile T, Gersak M. Contrast enhanced harmonic ultrasonography for the evaluation of acute scrotal pathology. A pictorial essay. Med Ultrason. 2016;18(1):110–5. https://doi.org/10.11152/mu.2013.2066.181.esy.
29. Dahiya N, Patel MD, Menias CO. Ultrasonography of the scrotum: extratesticular. Ultrasound Clin. 2014;9(3):457–69. https://doi.org/10.1016/j.cult.2014.03.002.
30. Lobianco R, Regine R, De Siero M, Catalano O, Caiazzo C, Ragozzino A. Contrast-enhanced sonography in blunt scrotal trauma. J Ultrasound. 2011;14(4):188–95. https://doi.org/10.1016/j.jus.2011.09.003.

Lymph Nodes

17

Alexander N. Sencha, Ekaterina A. Sencha, Ella I. Peniaeva, and Yury N. Patrunov

Sonography is the most common and widely available imaging modality for the diagnosis of lymph node (LN) abnormalities. The grayscale US evaluates the size, shape, and structure. Vascularization is one feature for the differentiation of reactive and malignant LN. The possibilities of CDI and PDI in the identification of microvascularity and detection of vessels with slow blood flow are limited. Some publications [1] indicate the prospects of CEUS in the diagnosis of benign and malignant LN changes due to the ability to assess LN perfusion. The sensitivity, specificity, and accuracy of CEUS in the detection of malignant LNs reach 98%, 99%, and 99%, respectively [2].

Doppler techniques permit specification of the vascular anatomy of the LN, while CEUS comprehensively assesses the LN perfusion, which is especially important in the cases of local thickening of the LN cortex [3].

In CEUS of LN, the choice of a transducer, scanning plane, and access is based on the same principles as in traditional echography. UCA is introduced according to the standard technique in a dose of 2.4 or 4.8 mL depending on the equipment and the probe frequency. The higher is the transducer frequency, the higher the UCA dose is required [4].

Normal LN typically has a single hilum and vascular pedicle with an artery, veins, and efferent lymphatic vessels. The artery enters the LN through the hilum, arterioles pass within trabeculae, branch as approaching the capsule. Within the cortex, networks of arterioles, capillaries, and venules occur near subcapsular and trabecular sinuses and around nodules. The draining veins pass out of the hilum. In conventional sonography, the detection of LN vessels depends on the capabilities of the scanner. Normally, it detects the vessels in the LN hilum [3, 5, 6]. In most inflammatory processes, the typical LN vascular pattern remains intact [3].

The changes in the vascular pattern in LN malignancies result from the mass effect of desmoplastic reaction and necrosis, neoplastic infil-

Supplementary Information The online version contains supplementary material available at [https://doi.org/10.1007/978-3-030-91764-7_17].

A. N. Sencha (✉)
Department of Visual and Functional Diagnostics, Federal State Budget Institution "National Medical Research Center for Obstetrics, Gynecology and Perinatology n.a. V.I.Kulakov", Moscow, Russian Federation

E. A. Sencha
Ultrasound Diagnostics Department, Federal State Budget Institution "Medical Diagnostic Center No. 9" of the Ministry of Defence of the Russian Federation, Moscow, Russian Federation

E. I. Peniaeva · Y. N. Patrunov
Department of Ultrasound Diagnostics of the Center for Radiological Diagnostics, Private Healthcare Institution "Clinical Hospital "RZD-Medicina" of Yaroslavl City", Yaroslavl, Russian Federation

A. N. Sencha, Y. N. Patrunov (eds.), *Contrast-Enhanced Ultrasound*,
https://doi.org/10.1007/978-3-030-91764-7_17

tration with associated peripheral hypervascularity, the appearance of tortuous, aberrant, and paracapsular vessels, which penetrate the capsule. However, at the early stages and the metastases of well-differentiated carcinomas, the initial vascular pattern may remain normal with hypervascularization due to local inflammatory immune response [3].

CEUS can register all vascular changes in the LN. The introduction of microbubbles and CDI/PDI modes facilitates the depiction of the LN vascular arrangement. It enables the registration of the regular vascular pattern with branching from the hilum to the capsule, which is typical for reactive LNs.

With CEUS, different types of lymphadenopathy are characterized by different patterns of contrast enhancement.

Normal and reactive lymph nodes exhibit a normal vascular pattern in the early arterial phase (Fig. 17.1, Video 17.1). The contrast enhancement starts 10–15 s after the UCA introduction from the hilar area followed by the intense uniform centrifugal filling of the LN. This enhancement pattern is characteristic of 70–80% of histologically intact LNs [7, 8]. Reactive hyperplasia may demonstrate uniform hyperenhancement of the cortex, which demands the differential diagnosis with lymphoma [9]. Heterogeneity of contrast enhancement can be registered if necrotic areas arise on the background of granulomatous inflammation [10].

Malignant lymph nodes with CEUS are diagnosed with high sensitivity, specificity, positive-predictive value, and low negative predictive value. This conclusion arises from the meta-analysis [11] based on 16 studies comprising 1563 LN lesions. CEUS was advised for use in clinical practice as an excellent diagnostic tool for the diagnosis of LN malignancies.

Lymph nodes are often affected by metastasis. Neck LNs metastases are diagnosed with an obscure primary tumor in 3–8% of cases, thyroid cancer in 9–90%, and breast cancer in 19–80% [5]. The tumor cells in metastatic LN cause distortion and destruction of regular vascular anatomy. Tumor infiltration of the cortex is combined with neoangiogenesis and an increase in capsular vessels. It leads to peripheral hypervascularization with tortuous and aberrant vessels that supply the LN periphery and tumor foci.

With CEUS, metastatic LN in most cases (82.5%) demonstrates heterogeneous contrast enhancement with diffuse or centripetal filling with UCA from the periphery to the hilum [12, 13]. The enhancement of capsular vessels begins in 10–15 s after UCA injection followed by the enhancement of aberrant and disorganized vessels within the LN, while the hilum may remain unenhanced. In 15–25 s, there appears heterogeneous enhancement of the cortex with local hypovascular zones associated with metastatic foci or avascular necrotic areas. In 40–60 s, the wash-out starts and hypoenhanced foci could not be further visualized. As opposed to benign LN, this heterogeneous centripetal or mixed enhancement pattern is characteristic of metastatic LN (Figs. 17.2, 17.3, and 17.4, Video 17.2).

The analysis of quantitative data of enhancement in benign and metastatic LNs [14] demonstrated that benign lymph nodes exhibited higher derived peak intensity than metastatic ones (17.72 ± 5.43% vs. 11.76 ± 4.88%, respectively) and higher values of regional blood volume (849.8 ± 467.1 vs. 458.3 ± 283.3, respectively).

The second malignancy that affects LNs is lymphoma. It is typically divided into non-Hodgkin lymphoma and Hodgkin lymphoma. The most common histological type of non-Hodgkin lymphoma is diffuse large B cell lymphoma, and the most common indolent non-Hodgkin lymphoma is follicular lymphoma. Hodgkin lymphoma, large B cell lymphoma, and follicular lymphoma account for up to 80% of all lymphomas in adults [4].

With CEUS, the diagnosis of lymphoma is a challenge due to the variability of enhancement patterns, some of which can also correspond to reactive or metastatic LNs. In the majority of cases (70–83%), lymphoma is characterized by rapid homogeneous hyperenhancement. Heterogeneous contrast enhancement is registered in only 17%, which is rare and differentiates lymphoma from metastatic LNs [4, 12]. Additionally, lymphoma often exhibits the specific “snowstorm” pattern with diffuse dotted

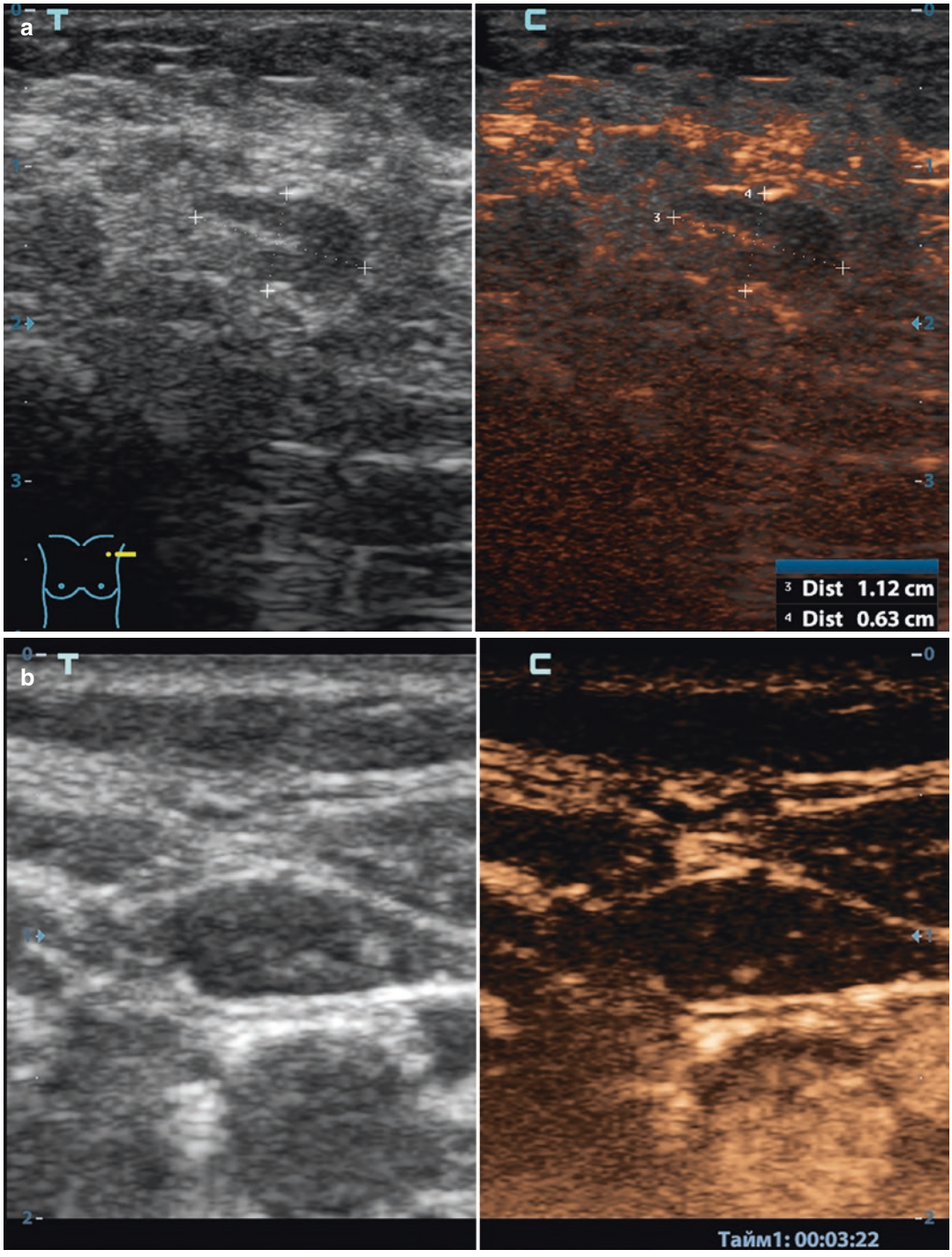

Fig. 17.1 Normal axillary lymph nodes. (**a**) Arterial phase CEUS image with a hypoenhancing lymph node. (**b**) Late phase CEUS demonstrates poor enhancement

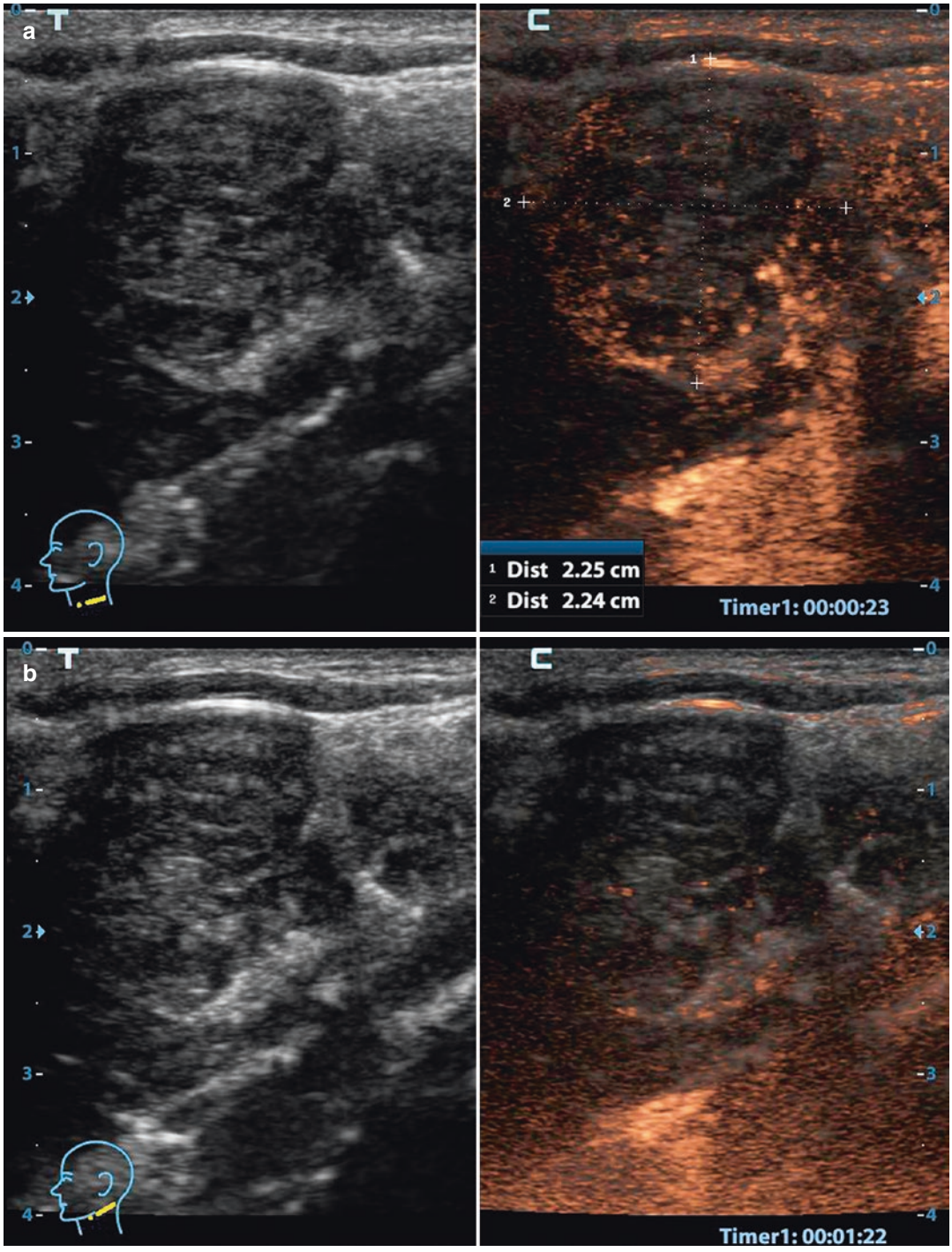

Fig. 17.2 Metastatic LN. CEUS images. (**a**) Chaotic enhancement of the LN with hypovascular areas in the arterial phase. (**b**) Hypoenhancement in the venous phase

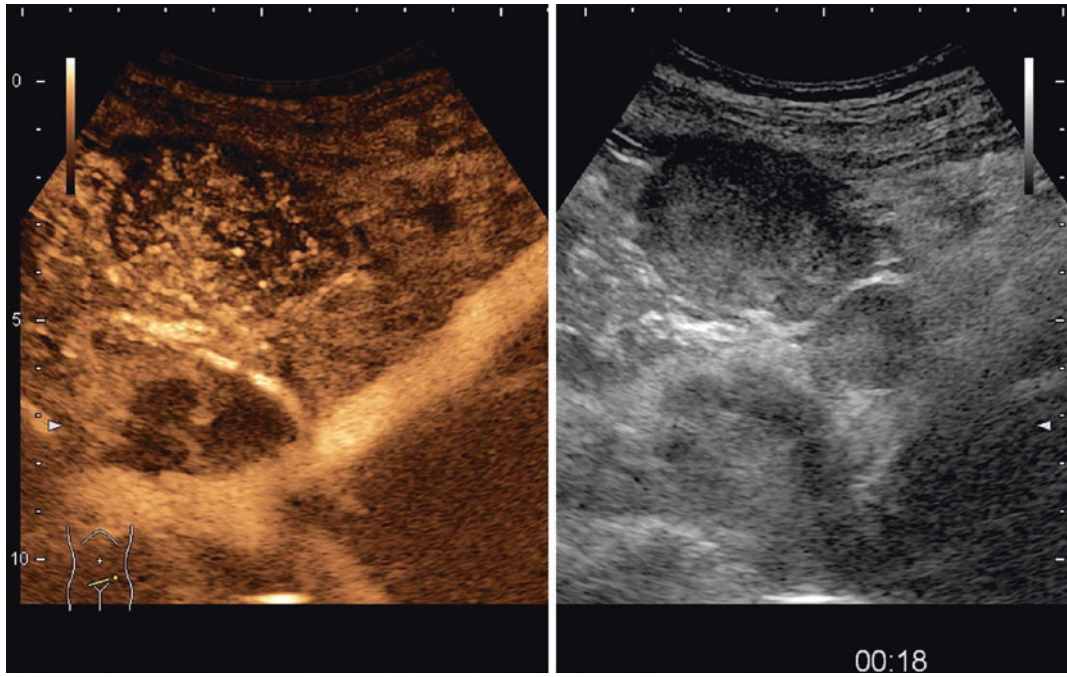

Fig. 17.3 Metastatic iliac LN. CEUS image. Chaotic heterogeneous hyperenhancement in the arterial phase

enhancement in the early arterial phase (Fig. 17.5, Video 17.3).

The accuracy of CEUS in the diagnosis of lymphoma is 83.57%, which exceeds the accuracy of CE-CT (80.71%) but is lower than PET-CT (88.57%) [4].

Reliable differences between the TIC parameters of lymphoma and metastatic LNs were reported [12]. Lymphoma exhibited smaller peak intensity and area under the curve (PI of 8.78 ± 2.53 dB and AUC of 652.62 ± 249.60) than metastatic LNs (PI of 10.51 ± 2.98 dB and AUC of 784.09 ± 340.24).

Quantitative analysis of CEUS enables evaluation of the response to treatment of lymphoma and metastatic LNs [15]. The difference in the contrast enhancement of the neck LNs with nasopharynx cancer metastases before and after radiation therapy was reported [16]. In patients with complete response, peak intensity (PI) was reliably higher than in patients with partial response (34.24 ± 3.78% vs. 25.62 ± 2.30%). The ratio of PI before treatment to PI during treatment (PI Ratio) was significantly higher in the full response group than in the partial response group (0.81 ± 0.01 vs. 0.66 ± 0.01; $p = 0.001$). The sensitivity and specificity of in-treatment PI in predicting the therapeutic response were 94.3% and 88.2%, and the corresponding values of the PI Ratio were 92.5% and 83.8%, respectively.

Quantitative CEUS in lymphoma patients before and after the first three cycles of chemotherapy demonstrates the reliable difference in the area under the curve (AUC), peak intensity (PI), and change of peak intensity (I) between the groups of good responders and non-responders, which are summarized in Table 17.1 [15].

They demonstrated that the effectiveness of the therapeutic response can be predicted by the CEUS parameter ΔI (AUC—0.889). The values of ΔAUC and ΔPI have the highest diagnostic performance of ineffectiveness (AUC 0.925 and 0.832, respectively).

Besides, in LNs with focal cortical thickening, CEUS may be used to guide a biopsy needle to the zone of abnormal perfusion and decrease the number of false-negative samples.

Detection of sentinel lymph nodes is a specific feature of CEUS. Sentinel LN is the first regional lymph node, which drains the primary

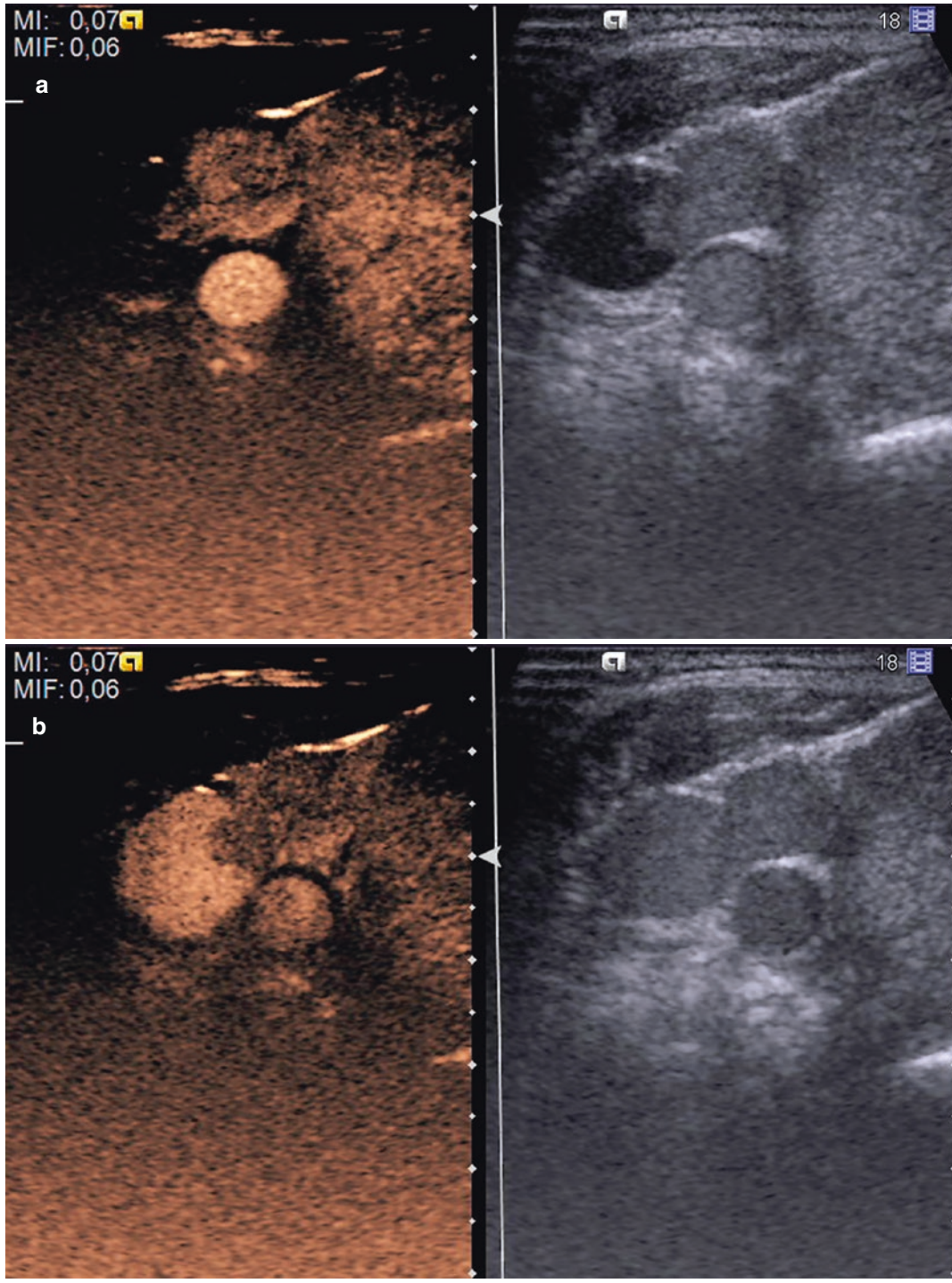

Fig. 17.4 Metastatic jugular and axillary LNs. CEUS images. (**a**) Early arterial phase CEUS demonstrates heterogeneous hyperenhancement of the right jugular LN. (**b**) Late arterial phase CEUS depicts the same LN, which invades the enhanced jugular vein. (**c**) Homogeneously enhanced axillary LN in the arterial phase CEUS image. (**d**) Poor heterogeneous enhancement of the axillary LNs

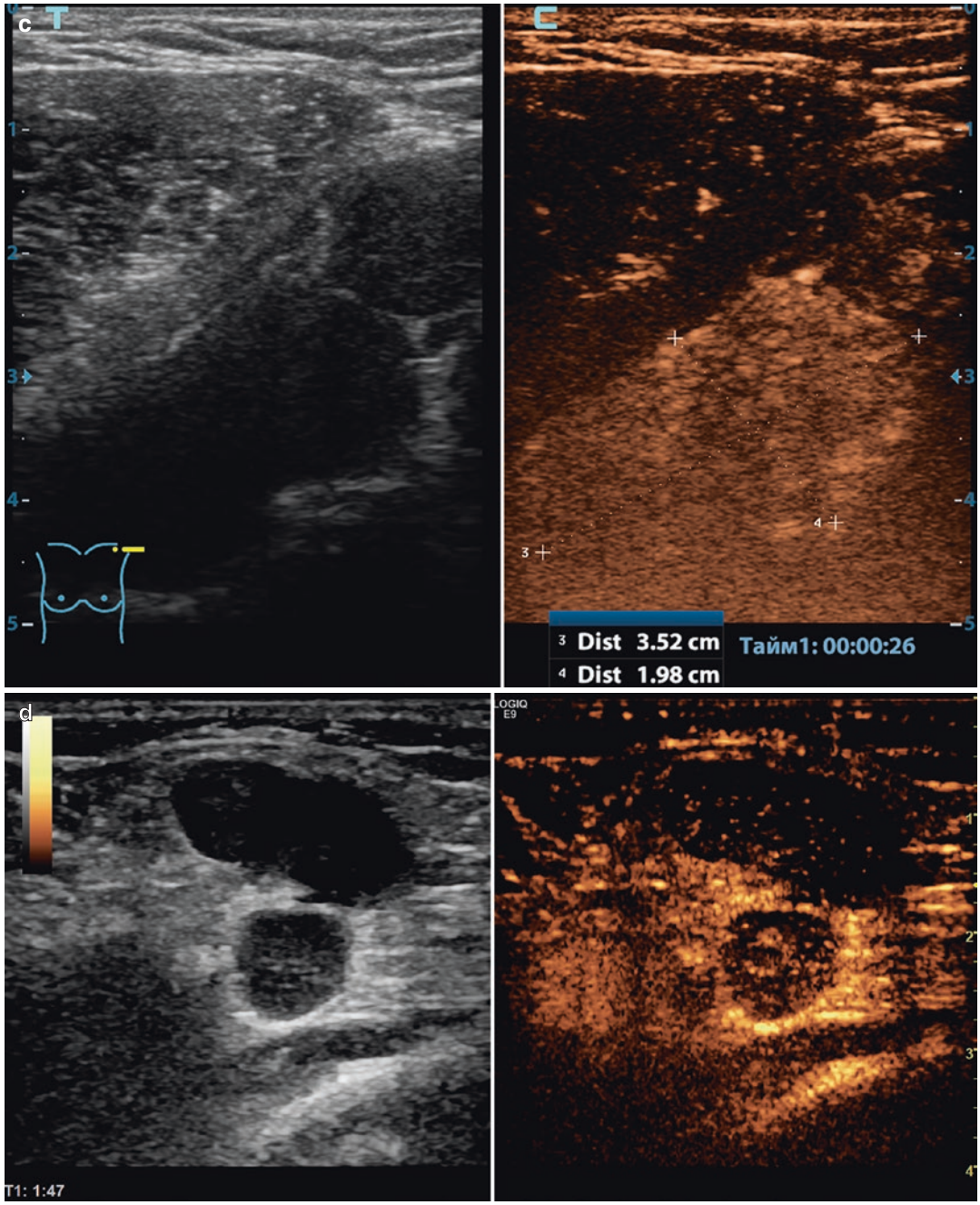

Fig. 17.4 (continued)

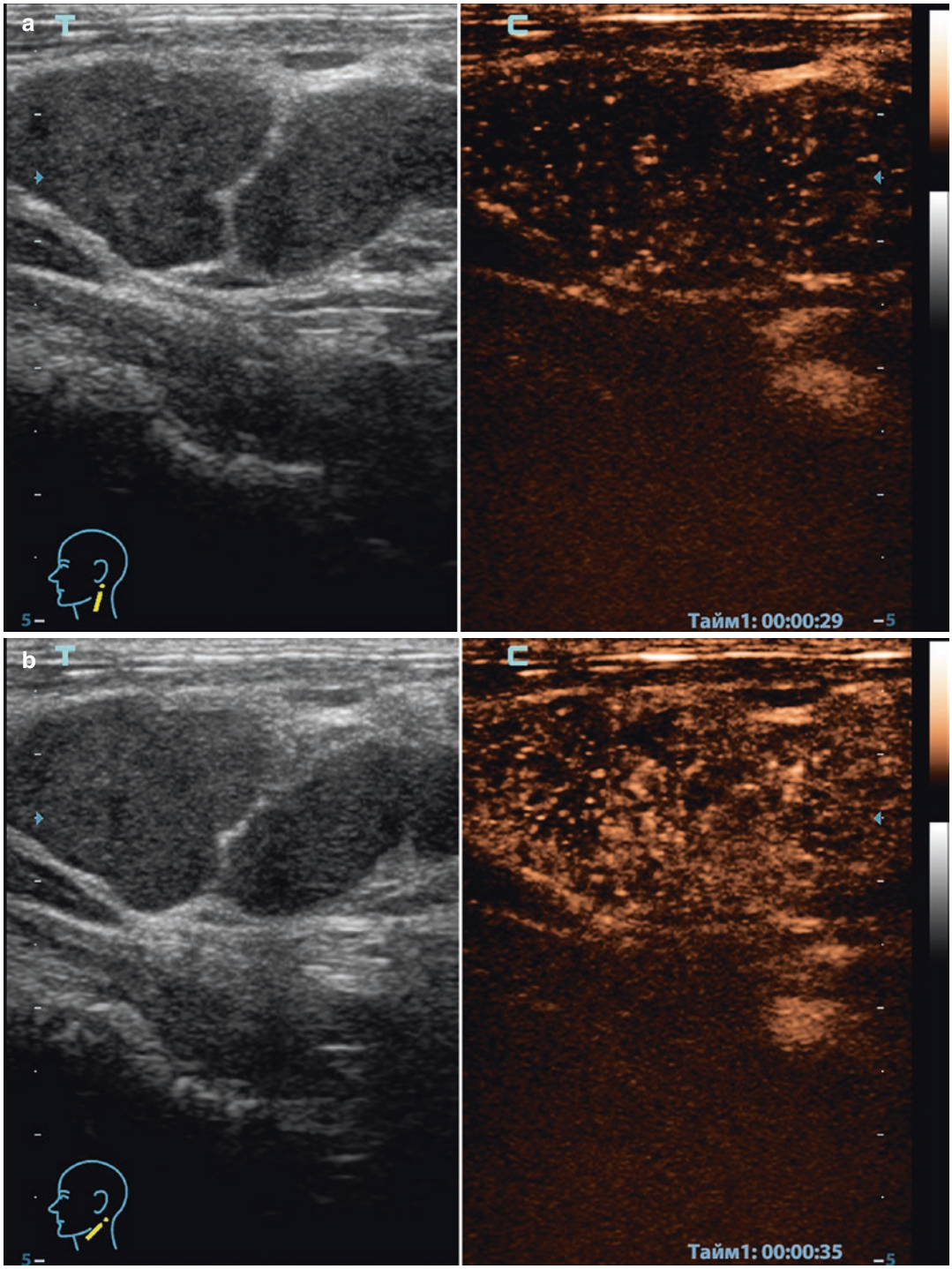

Fig. 17.5 Neck LNs in Hodgkin lymphoma. CEUS images. (**a**) The uniform dotted enhancement of the increased LN in the arterial phase. (**b**) Heterogeneous enhancement in the early venous phase

Table 17.1 The values of TIC in the study of patients with lymphoma before and after therapy in groups with full response and no response to therapy

	Responders		Non-responders	
	Before therapy	After therapy	Before therapy	After therapy
AUC	574.5 ± 123.6	244.9 ± 120.8	484.9 ± 67.0	455.5 ± 135.1
ΔAUC	−329.5 ± 129.4		−29.4 ± 153.8	
PI	−35.3 ± 3.4	−40.5 ± 5.2	−35.9 ± 3.6	−34.3 ± 2.7
ΔPI	−5.38 ± 5.8		1.6 ± 3.9	
I	14.4 ± 4.2	7.7 ± 3.0	14.861 ± 6.213	13.1 ± 5.3
Δ*I*	6.6 ± 3.5		−1.7 ± 7.5	

AUC area under the curve, *PI* peak intensity
I—change of peak intensity, Δ marks the changes before treatment and after the first three cycles of chemotherapy

tumor and detains the tumor cells. The status of a sentinel LN is extremely important because it determines the tumor stage and management. The possibility to use CEUS for the detection of sentinel LN was first reported in 2004 in an animal model [17]. Up to now, the proposed method was used in many studies [2, 7, 18–22].

The method is often applied in patients with breast carcinoma. Subcutaneous administration of UCA is used.

This technique has high sensitivity in the detection of sentinel LN, but low specificity for its metastatic involvement in patients with breast carcinoma. Sentinel LN detection rate reaches 71–96%; the sensitivity, specificity, positive-predictive value, negative predictive value, and accuracy of predicting sentinel LN metastases by CEUS enhancement patterns account for 98–100%, 49–52%, 43%, 100%, and 65%, respectively [23, 24].

The SonoVue® microbubble suspension is prepared with 2 mL of sterile saline. After periareolar local infiltration anesthesia, UCA is administered subcutaneously and intradermally with several 0.2–0.5 mL injections in the periareolar area. After that, the injection area is gently massaged avoiding increased pressure. This stimulates the spreading of microbubbles to the lymphatic channels. Microbubble distribution in the ducts and their accumulation in LN can be registered with low MI sonography immediately after UCA injection (Figs. 17.6 and 17.7). Typically, the time of UCA passage from the injection site to the axillary LN ranges from 5 to 70 s, and UCA remains in the LN for up to 4 min. Enhanced lymph nodes could be detected by moving the probe along the enhanced lymph channels. The first or first group of enhanced lymph nodes are considered sentinel LNs. Massaging the injection site intensifies the image again [21].

UCA accumulation in a LN exhibits various patterns of contrast enhancement that have the corresponding prognostic value [20]. Heterogeneous enhancement may indicate metastatic nature, while uniform accumulation enhancement suggests normal LN. However, the enhancement patterns are not considered for differential diagnosis. The identification of sentinel LN aims to assist the targeted biopsy. In the absence of contrast enhancement of the ducts or LNs, another injection may be given. The sensitivity of this CEUS method in the detection of sentinel LNs is 92–98% as referred to intraoperative detection with blue dye [14, 21–25].

CEUS enables effective assessment of the state of regional lymph drainage in different locations. It facilitates the determination of tumor dissemination, staging, and management.

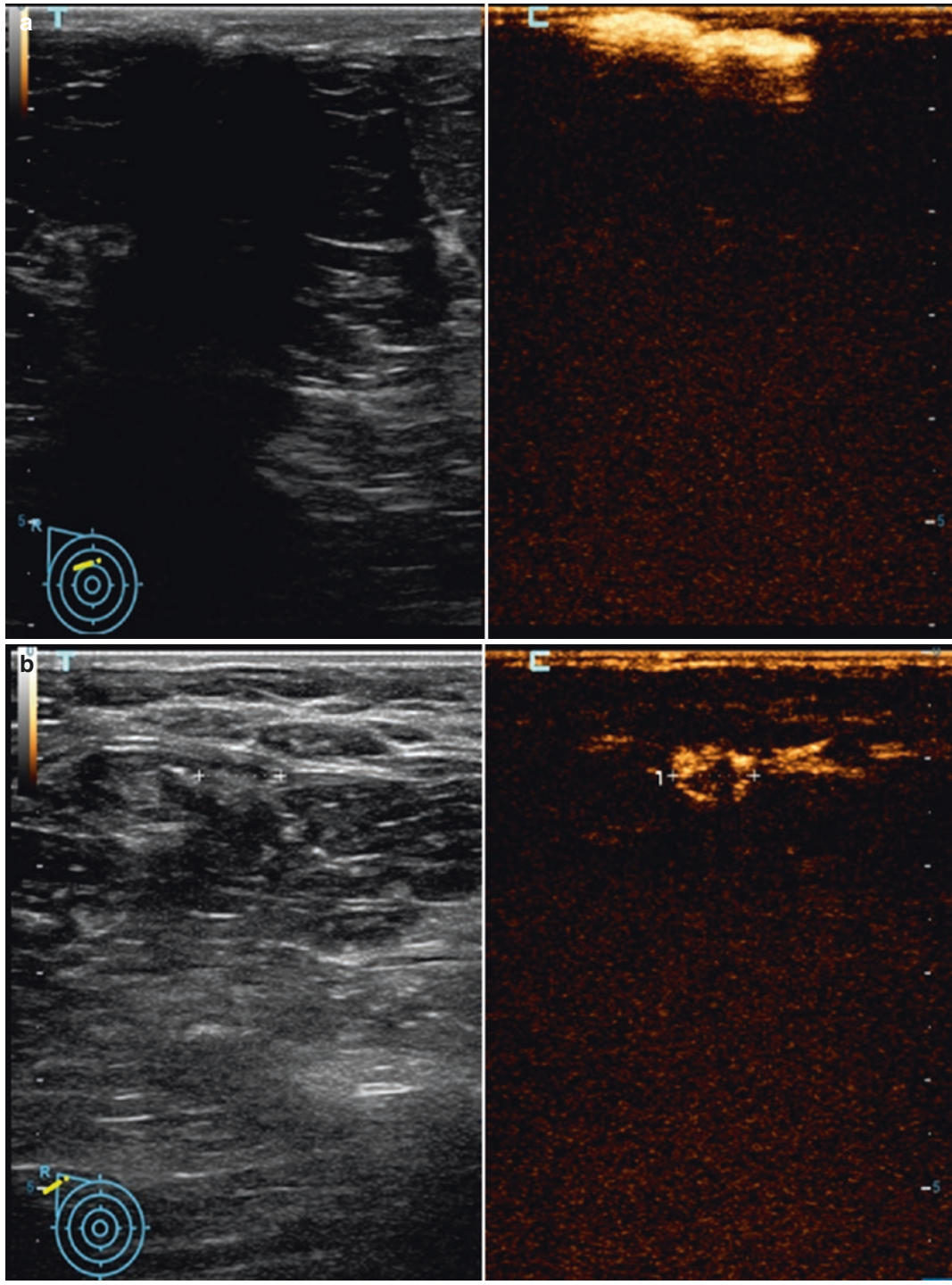

Fig. 17.6 CEUS of the regional lymph drainage area with peritumoral intradermal administration of SonoView in a patient with breast carcinoma. CEUS images. (**a**) UCA collection at the place of injection. (**b**) A small sentinel LN with irregular enhancement in the axillary area

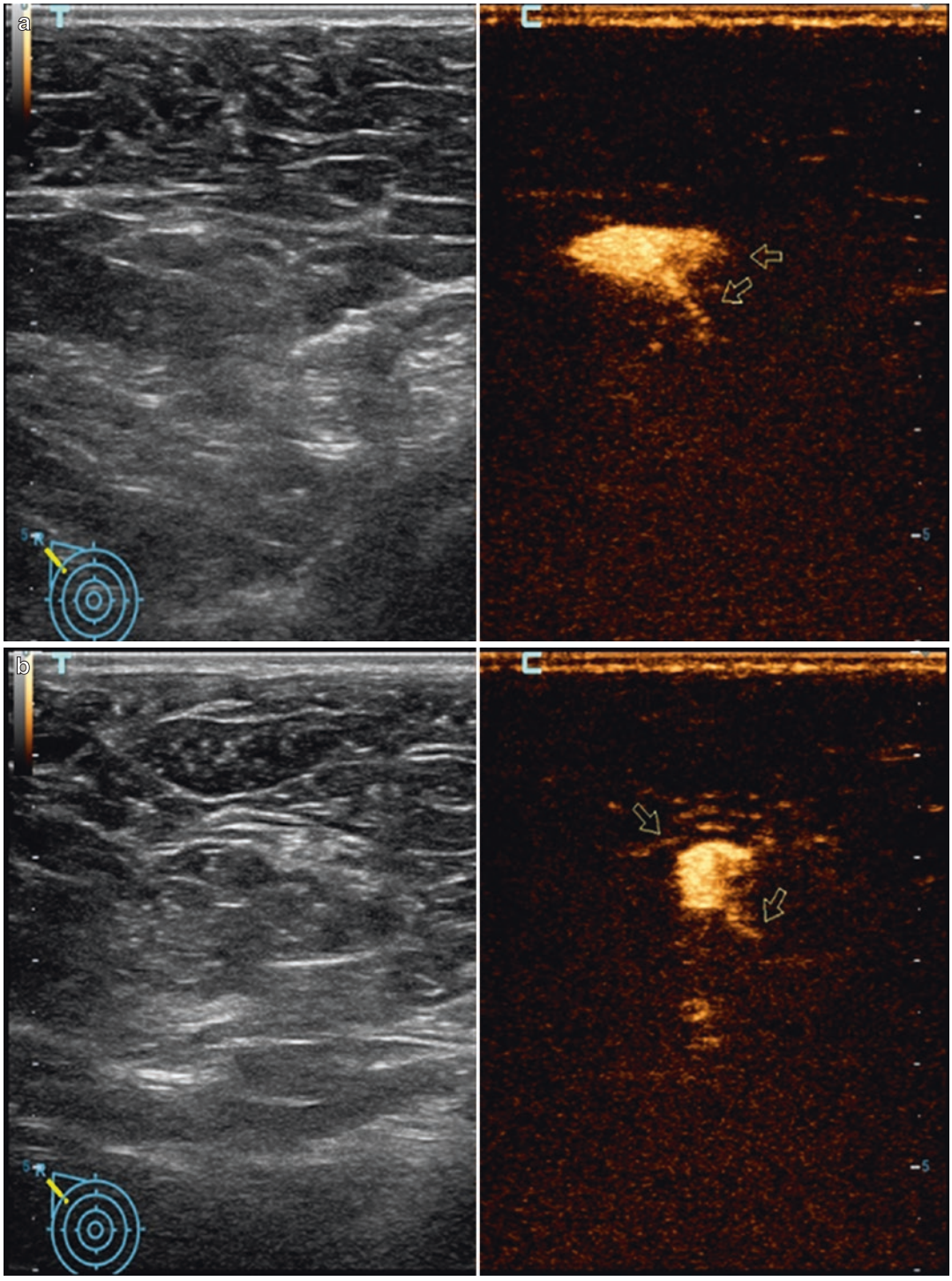

Fig. 17.7 CEUS of the regional lymph drainage area with peritumoral intradermal administration of SonoView in a patient with breast carcinoma. (**a**) Homogeneously hyperenhanced sentinel LN. (**b**) Heterogeneously hyperenhanced sentinel LN. Lymph nodes and ducts are marked with arrows

References

1. Sidhu PS, Cantisani V, Dietrich CF, Gilja OH, Saftoiu A, Bartels E, et al. The EFSUMB guidelines and recommendations for the clinical practice of contrast-enhanced ultrasound (CEUS) in non-hepatic applications: update 2017 (long version). Ultraschall Med. 2018;39(2):e2–e44. https://doi.org/10.1055/a-0586-1107.
2. Rubaltelli L, Beltrame V, Scagliori E, Bezzon E, Frigo AC, Rastrelli M, Stramare R. Potential use of contrast-enhanced ultrasound (CEUS) in the detection of metastatic superficial lymph nodes in melanoma patients. Ultraschall Med. 2014;35(1):67–71. https://doi.org/10.1055/s-0033-1335857.
3. Dietrich CF. The potential of contrast-enhanced ultrasonography to evaluate lymphadenopathy. Gastrointest Endosc. 2019;90(2):251–3. https://doi.org/10.1016/j.gie.2019.05.019.
4. Ma X, Ling W, Xia F, Zhang Y, Zhu C, He J. Application of contrast-enhanced ultrasound (CEUS) in lymphomatous lymph nodes: a comparison between PET/CT and contrast-enhanced CT. Contrast Media Mol Imaging. 2019;2019:5709698. https://doi.org/10.1155/2019/5709698.
5. Sencha AN, editor. Ul'trazvukovaya diagnostika. Poverhnostno-raspolozhennye organy [Ultrasound diagnostics. Surface-located organs]. Moscow: Vidar; 2015. Russian.
6. Trofimova EY. Ul'trazvukovoe issledovanie limfaticheskih uzlov [Ultrasound examination of the lymph nodes]. SonoAce Int. 2008;18:59–64. Russian.
7. Ouyang Q, Chen L, Zhao H, Xu R, Lin Q. Detecting metastasis of lymph nodes and predicting aggressiveness in patients with breast carcinomas. J Ultrasound Med. 2010;29(3):343–52. https://doi.org/10.7863/jum.2010.29.3.343.
8. Yu M, Liu Q, Song HP, Han ZH, Su HL, He GB, Zhou XD. Clinical application of contrast-enhanced ultrasonography in diagnosis of superficial lymphadenopathy. J Ultrasound Med. 2010;29(5):735–40. https://doi.org/10.7863/jum.2010.29.5.735.
9. Mei M, Ye L, Quan J, Huang P. Contrast-enhanced ultrasound for the differential diagnosis between benign and metastatic superficial lymph nodes: a meta-analysis. Cancer Manag Res. 2018;10:4987–97. https://doi.org/10.2147/CMAR.S174751.
10. Wescott HP, Lyshchik A. Lymph nodes. In: Lyshchik A, editor. Specialty imaging: fundamentals of CEUS. 1st ed. Philadelphia, PA: Elsevier; 2019. p. 296–302.
11. Jin Y, He YS, Zhang MM, Parajuly SS, Chen S, Zhao HN, Peng YL. Value of contrast-enhanced ultrasonography in the differential diagnosis of enlarged lymph nodes: a meta-analysis of diagnostic accuracy studies. Asian Pac J Cancer Prev. 2015;16(6):2361–8. https://doi.org/10.7314/apjcp.2015.16.6.2361.
12. Nie J, Ling W, Yang Q, Jin H, Ou X, Ma X. The value of CEUS in distinguishing cancerous lymph nodes from the primary lymphoma of the head and neck. Front Oncol. 2020;10:473. https://doi.org/10.3389/fonc.2020.00473.
13. Xiang D, Hong Y, Zhang B, Huang P, Li G, Wang P, Li Z. Contrast-enhanced ultrasound (CEUS) facilitated US in detecting lateral neck lymph node metastasis of thyroid cancer patients: diagnosis value and enhancement patterns of malignant lymph nodes. Eur Radiol. 2014;24(10):2513–9. https://doi.org/10.1007/s00330-014-3288-5.
14. Poanta L, Serban O, Pascu I, Pop S, Cosgarea M, Fodor D. The place of CEUS in distinguishing benign from malignant cervical lymph nodes: a prospective study. Med Ultrason. 2014;16(1):7–14. https://doi.org/10.11152/mu.2014.2066.161.lp1os2.
15. Xin L, Yan Z, Zhang X, Zang Y, Ding Z, Xue H, Zhao C. Parameters for contrast-enhanced ultrasound (CEUS) of enlarged superficial lymph nodes for the evaluation of therapeutic response in lymphoma: a preliminary study. Med Sci Monit. 2017;23:5430–8. https://doi.org/10.12659/msm.907293.
16. Ye Z, Huang P, Zhou X, Huang Q, Hu Q, Shui Y, Shen L, Lai E, Wei Q. Parametric contrast-enhanced ultrasound as an early predictor of radiation-based therapeutic response for lymph node metastases of nasopharyngeal carcinoma. Mol Clin Oncol. 2014;2(5):666–72. https://doi.org/10.3892/mco.2014.331.
17. Goldberg BB, Merton DA, Liu JB, Thakur M, Murphy GF, Needleman L, Tornes A, Forsberg F. Sentinel lymph nodes in a swine model with melanoma: contrast-enhanced lymphatic US. Radiology. 2004;230(3):727–34. https://doi.org/10.1148/radiol.2303021440.
18. Li J, Lu M, Cheng X, Hu Z, Li H, Wang H, et al. How pre-operative sentinel lymph node contrast-enhanced ultrasound helps intra-operative sentinel lymph node biopsy in breast cancer: initial experience. Ultrasound Med Biol. 2019;45(8):1865–73. https://doi.org/10.1016/j.ultrasmedbio.2019.04.006.
19. Nielsen Moody A, Bull J, Culpan AM, Munyombwe T, Sharma N, Whitaker M, Wolstenhulme S. Preoperative sentinel lymph node identification, biopsy and localisation using contrast enhanced ultrasound (CEUS) in patients with breast cancer: a systematic review and meta-analysis. Clin Radiol. 2017;72(11):959–71. https://doi.org/10.1016/j.crad.2017.06.121.
20. Sever AR, Mills P, Weeks J, Jones SE, Fish D, Jones PA, Mali W. Preoperative needle biopsy of sentinel lymph nodes using intradermal microbubbles and contrast-enhanced ultrasound in patients with breast cancer. AJR Am J Roentgenol. 2012;199(2):465–70. https://doi.org/10.2214/AJR.11.7702.
21. Xie F, Zhang D, Cheng L, Yu L, Yang L, Tong F, et al. Intradermal microbubbles and contrast-enhanced ultrasound (CEUS) is a feasible approach for sentinel lymph node identification in early-stage breast cancer. World J Surg Oncol. 2015;13:319. https://doi.org/10.1186/s12957-015-0736-x.
22. Zhong J, Sun DS, Wei W, Liu X, Liu J, Wu X, et al. Contrast-enhanced ultrasound-guided fine-

needle aspiration for sentinel lymph node biopsy in early-stage breast cancer. Ultrasound Med Biol. 2018;44(7):1371–8. https://doi.org/10.1016/j.ultrasmedbio.2018.03.005.

23. Zhao J, Zhang J, Zhu QL, Jiang YX, Sun Q, Zhou YD, et al. The value of contrast-enhanced ultrasound for sentinel lymph node identification and characterisation in pre-operative breast cancer patients: a prospective study. Eur Radiol. 2018;28(4):1654–61. https://doi.org/10.1007/s00330-017-5089-0.
24. Liu J, Liu X, He J, Gou B, Luo Y, Deng S, et al. Percutaneous contrast-enhanced ultrasound for localization and diagnosis of sentinel lymph node in early breast cancer. Sci Rep. 2019;9(1):135–45. https://doi.org/10.1038/s41598-019-49736-3.
25. Rodionov VV, Kometova VV, Sencha AN, et al. Biopsiya signal'nyh limfouzlov u bol'nyh rakom molochnoj zhelezy: sobstvennyj opyt [Signal lymph node biopsy in breast cancer patients: own experience]. Akusherstvo Ginekol. 2018;12:111–6. Russian.

Major Blood Vessels

18

Munir G. Tukhbatullin, Elena E. Fomina, Natalya I. Bayazova, and Marat Z. Khasanov

Modern ultrasound technologies permit accurate diagnosis of a wide range of vascular pathologies. However, Doppler imaging has some limitations, which may distort a true hemodynamic picture.

CEUS lacks many well-known disadvantages of color Doppler. It enables better delineation of the intima boundary and high-quality imaging of the vessel lumen regardless of the scanning angle and the severity of stenosis. It is also efficient in the identification of aneurysms and small areas of dissection.

Abdominal aortic aneurism incidence is 10–40 cases per 100,000 population per year [1]. More than 85% of aneurysms are asymptomatic. The traditional US is the first-line screening method and an accurate modality for the differential diagnosis of abdominal aortic aneurysm. It has a sensitivity of 95–98%. However, certain limitations result from the lack of direct signs of the abdominal aortic aneurysm rupture [2–4]. UCAs enable imaging of the aortic wall and extravasation of microbubbles beyond the aneurysm [5].

M. G. Tukhbatullin (✉) · E. E. Fomina
N. I. Bayazova
Department of Ultrasound Diagnosis, Kazan State Medical Academy, Kazan, Russian Federation
e-mail: munir.tuhbatullin@tatar.ru

M. Z. Khasanov
Department of Ultrasound Diagnostics, Republican Clinical Oncological Dispensary of the Ministry of Healthcare of the Republic of Tatarstan, Kazan, Russian Federation

CEUS is a simple and non-invasive modality that permits reliable monitoring of the patients after stent-graft aortic repair [6, 7]. It aims to detect endoleaks and other local complications. Endoleak is the persistent blood flow outside the lumen of an endoluminal graft but within the aneurysm sac or adjacent vascular segment being treated by the device used for endovascular aneurysm repair [8].

There are five below listed types of endoleaks, each with different causes and treatment options (Figs. 18.1, 18.2, 18.3, and 18.4):

- Type I endoleak occurs when there is a gap between the graft and the vessel wall at the superior or inferior "seal zone," which allows blood to flow along the side of the graft into the aneurysm.
- Type II endoleak results from the increased pressure within the side branches of the aorta, such as lumbar, inferior mesenteric, accessory renal, or other arteries, which force blood to leak back into the lower-pressure aneurysm sac.
- Type III endoleak results from a defect or misalignment between the components of the endograft.
- Type IV endoleak occurs soon due to the porosity of certain graft materials.
- Type V endoleak, known as endotension, has no evident cause.

A. N. Sencha, Y. N. Patrunov (eds.), *Contrast-Enhanced Ultrasound*,
https://doi.org/10.1007/978-3-030-91764-7_18

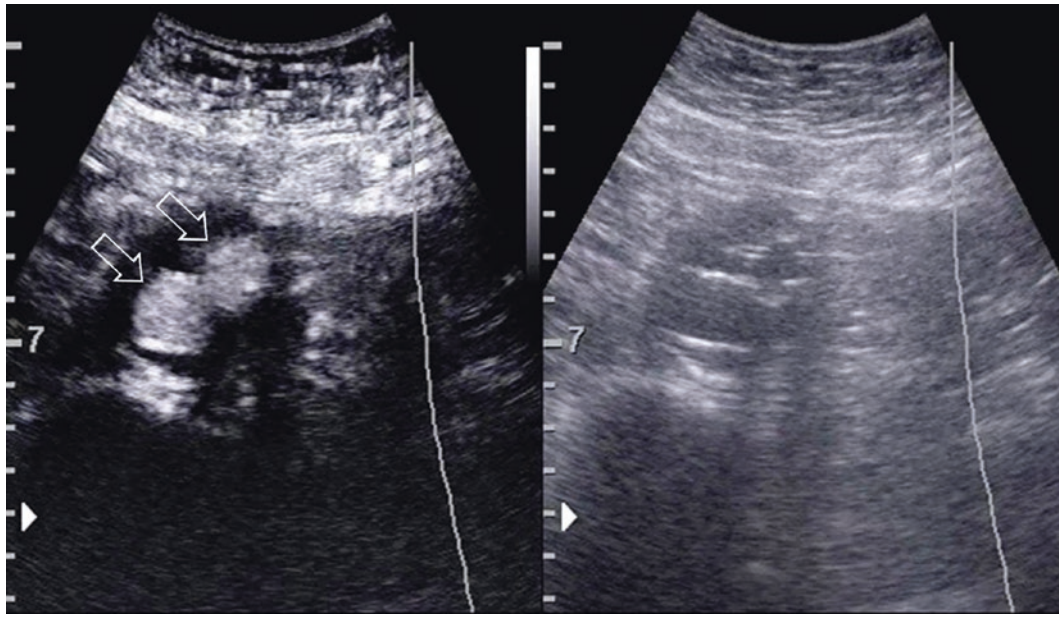

Fig. 18.1 Abdominal aorta after normal endovascular aortic aneurysm repair. The arterial phase transverse CEUS image. Two iliac stent-graft segments (arrows) with regularly enhanced lumen are identified. The aneurism sac has no enhancement

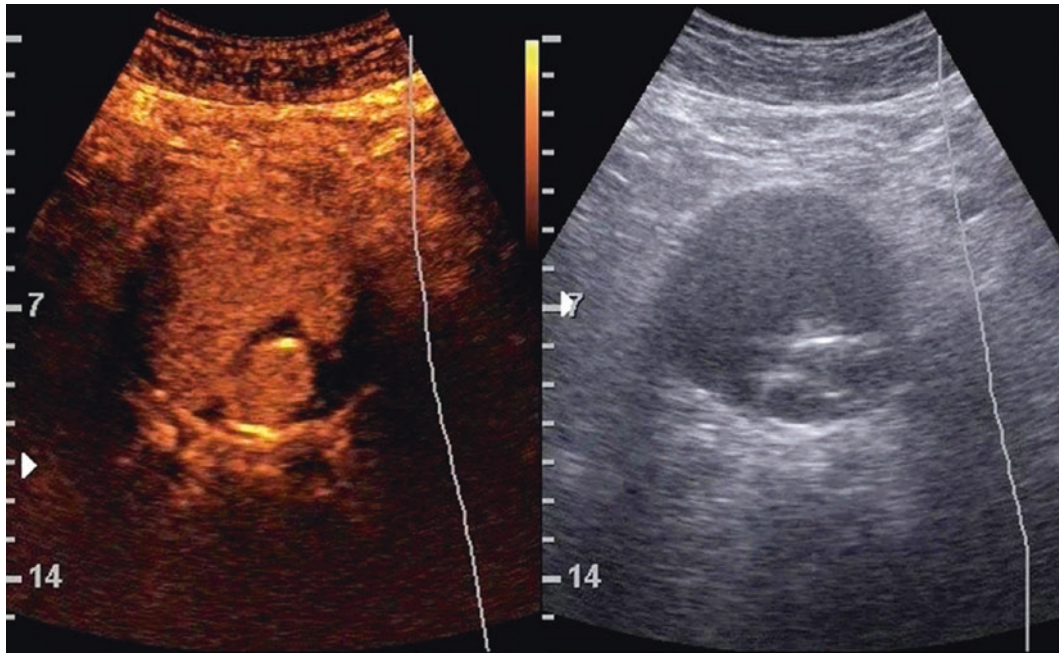

Fig. 18.2 Abdominal aorta after endovascular aortic aneurysm repair complicated with type Ia proximal endoleak. The arterial phase transverse CEUS image. The aortic aneurysm sac is enhanced along with the stent-graft lumen. Endoleak type Ia due to inadequate proximal seal

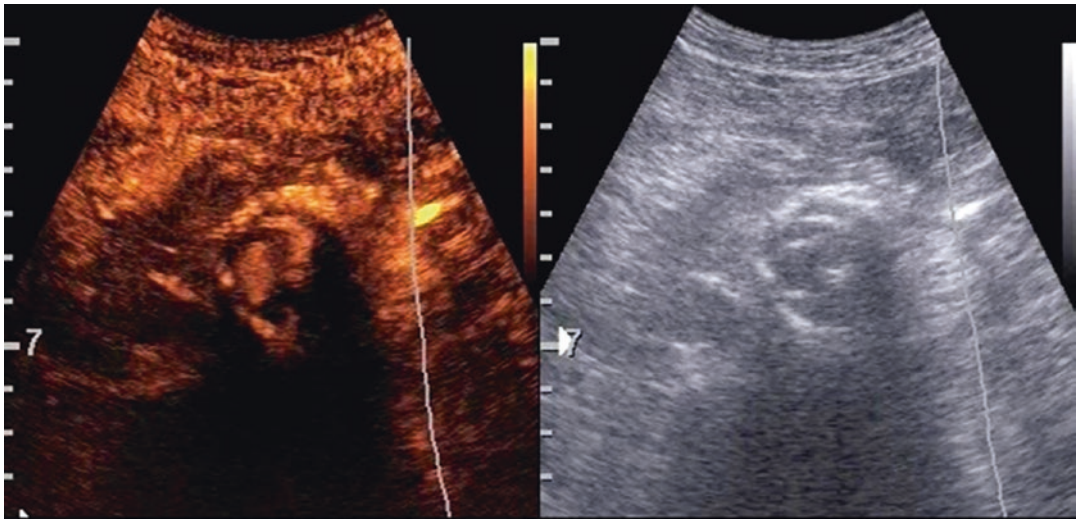

Fig. 18.3 Abdominal aorta after endovascular aortic aneurysm repair complicated with type II endoleak. The arterial phase transverse CEUS image. The lumbar artery is detected posteriorly to the stent-graft (type II endoleak). Perfused iliac segments of the stent-graft are also observed

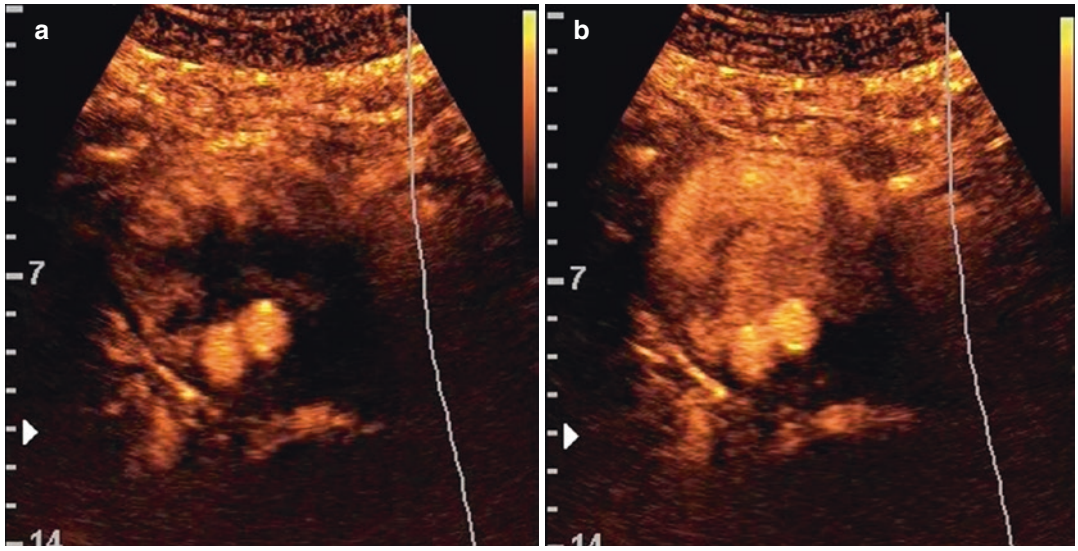

Fig. 18.4 Abdominal aorta after endovascular aortic aneurysm repair complicated with type II endoleak from the inferior mesenteric artery. Transverse CEUS image. (**a**) The early arterial phase. Contrast enhancement of the peripheral aspects of the aortic aneurysm sac ventrally from the perfused stent-graft. (**b**) Gradual enhancement aortic aneurysm sac in the late arterial phase

CEUS is also feasible to follow up the patients after various endovascular interventions, such as stenting the iliac arteries. It is capable to detect the complications when the imaging conditions are too poor for the conventional US with Doppler imaging and other imaging modalities are not applicable (Fig. 18.5).

One useful CEUS feature is the reliable differentiation of retroperitoneal cystic lesions from blood vessels (Fig. 18.6).

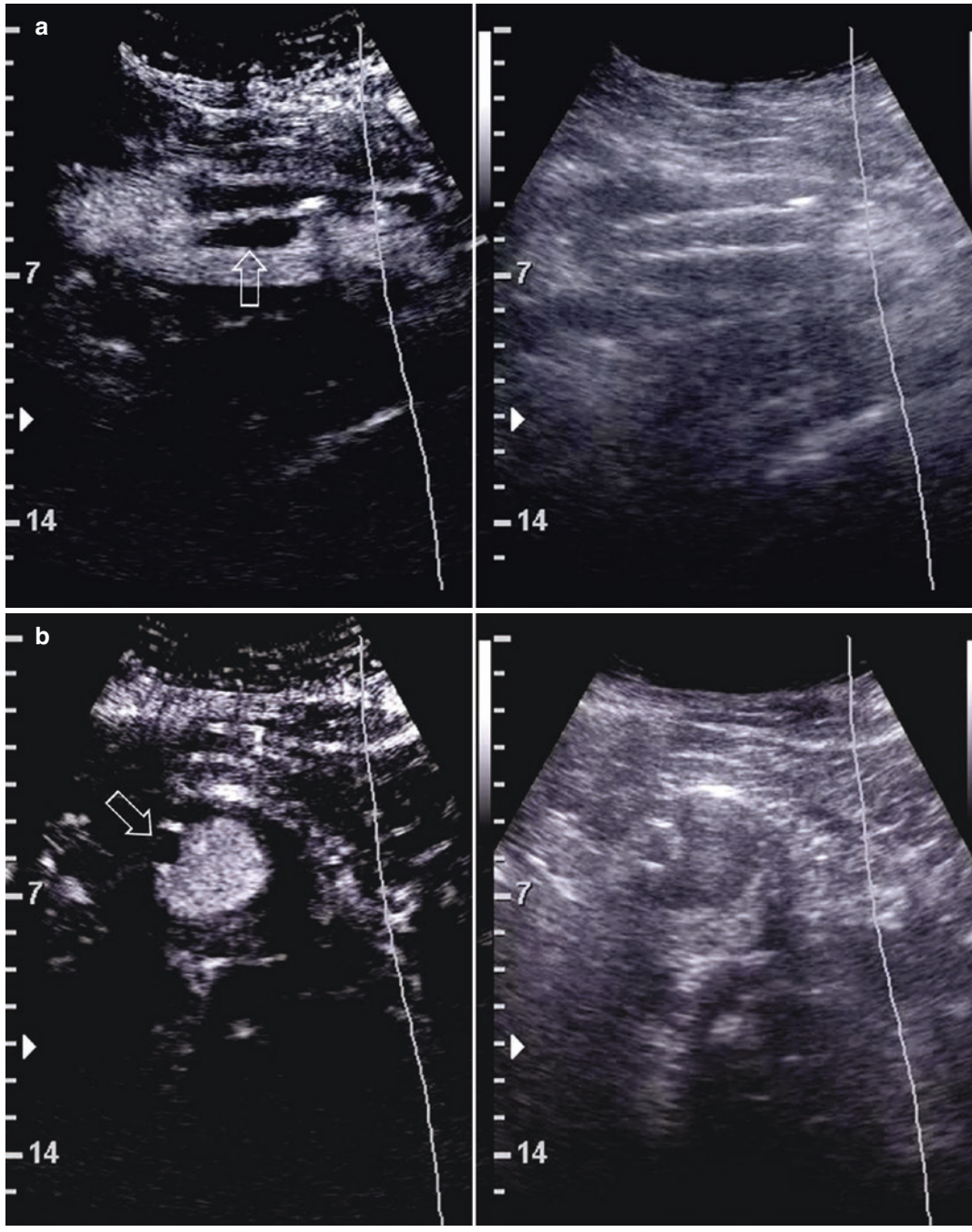

Fig. 18.5 The thrombosis of the stent in the aneurysm of the external iliac artery. The arterial phase CEUS images. (**a**) The aneurysm of the external iliac artery with nonocclusive thrombus and a partially occluded stent. The stent has an enhancement defect (arrow), the enhanced blood bypasses the occluded segment of the stent via the aneurysm sac. Scan along the iliac vessels. (**b**) The aneurysm sac with concentric thrombus and the enhanced central aspects. Occluded stent (arrow). Transverse image

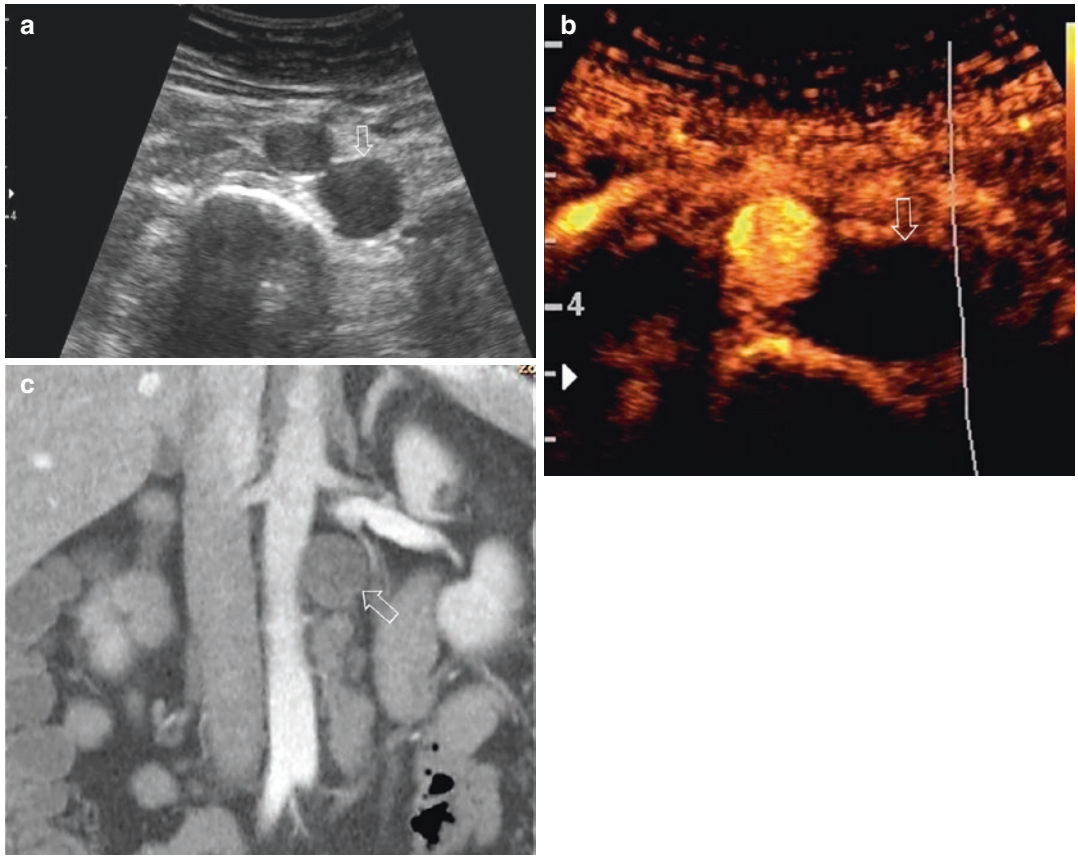

Fig. 18.6 The cyst of the retroperitoneal space. (**a**) Grayscale sonography. The anechoic lesion with clear smooth boundaries is detected adjacent to the abdominal aorta (arrow). (**b**). CEUS image, the arterial phase. The lesion is nonenhanced (arrow). (**c**) CE-CT identifies a nonenhancing retroperitoneal lesion of fluid density (arrow)

Visceral artery aneurysms are rare entities. One example is the gastroduodenal artery aneurism, which accounts for 3.5% of all aneurysms of visceral arteries [9]. False aneurysms are different from true ones and may result from trauma and other causes. However, some of them typically arise in patients with chronic pancreatitis. Chronic pancreatitis often develops cysts, which cannot resolve by themselves. Large-sized (>5 cm) pancreatic cyst compresses the surrounding structures and if affects the adjacent artery results in periarterial inflammation, necrosis of the wall, and the development of the fistula between the artery and cystic lumen [9–12] (Fig. 18.7).

Aneurysm of the internal carotid artery along with atherosclerotic plaques may cause a transient ischemic attack or acute ischemic stroke. The extracranial carotid artery aneurysm is quite rare and accounts for 1–2% of all abnormalities [13] (Fig. 18.8).

Atherosclerotic lesions of the carotid arteries are currently widely diagnosed with Doppler sonography. It precisely determines the degree and length of the stenosis, structure of atherosclerotic plaque, and the condition of its surface. The data obtained with duplex scanning comprise the basis for the classification of atherosclerotic plaques, which pays special attention to the signs of instability. High-grade stenosis and certain

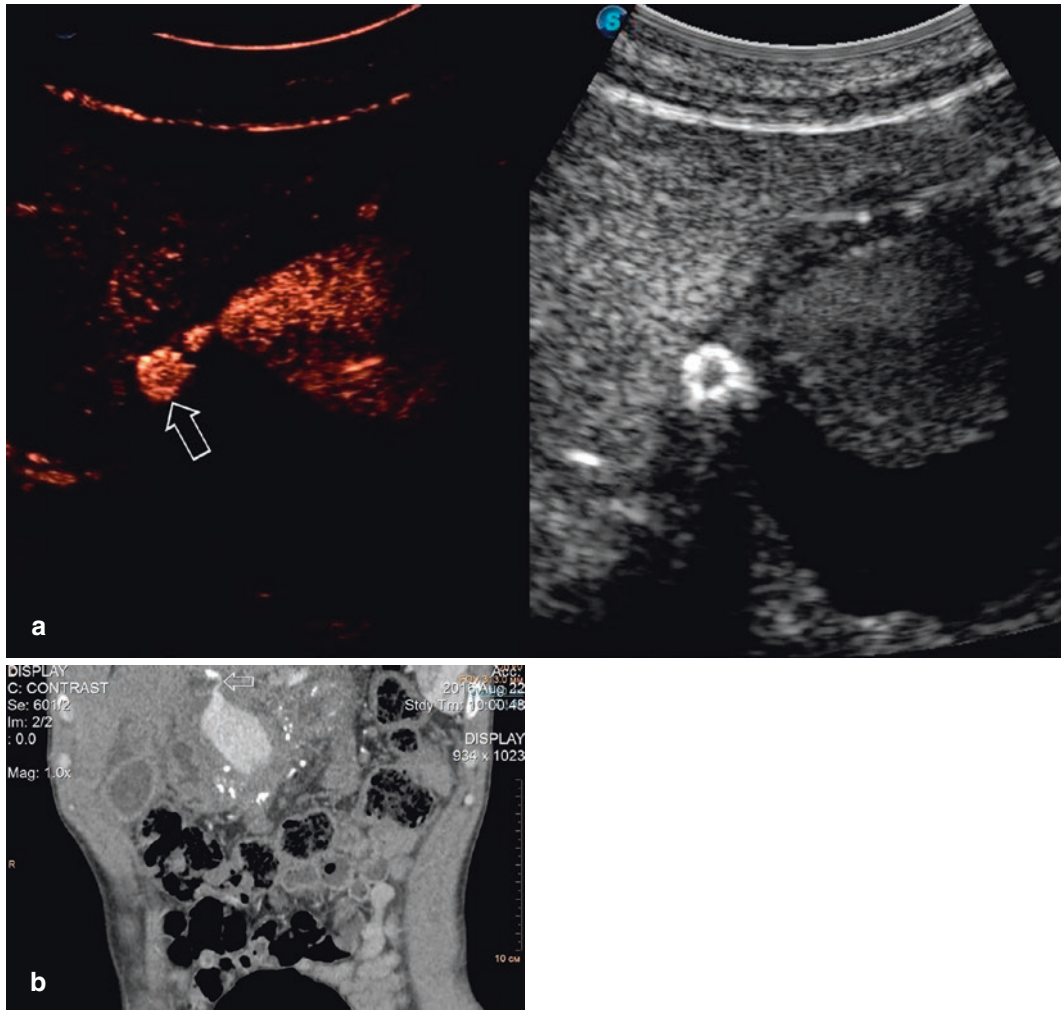

Fig. 18.7 A false aneurysm of the gastroduodenal artery in the pancreatic head cyst. The status after stenting of the common hepatic artery. (**a**) The arterial phase CEUS image demonstrates a gradual inflow of microbubbles into the false aneurysm sac, which is located in the otherwise nonenhanced pancreatic head cyst. The common hepatic artery stent (arrow) is enhanced. (**b**) CE-CT demonstrates the connection of the pseudoaneurysm with the gastroduodenal artery (arrow)

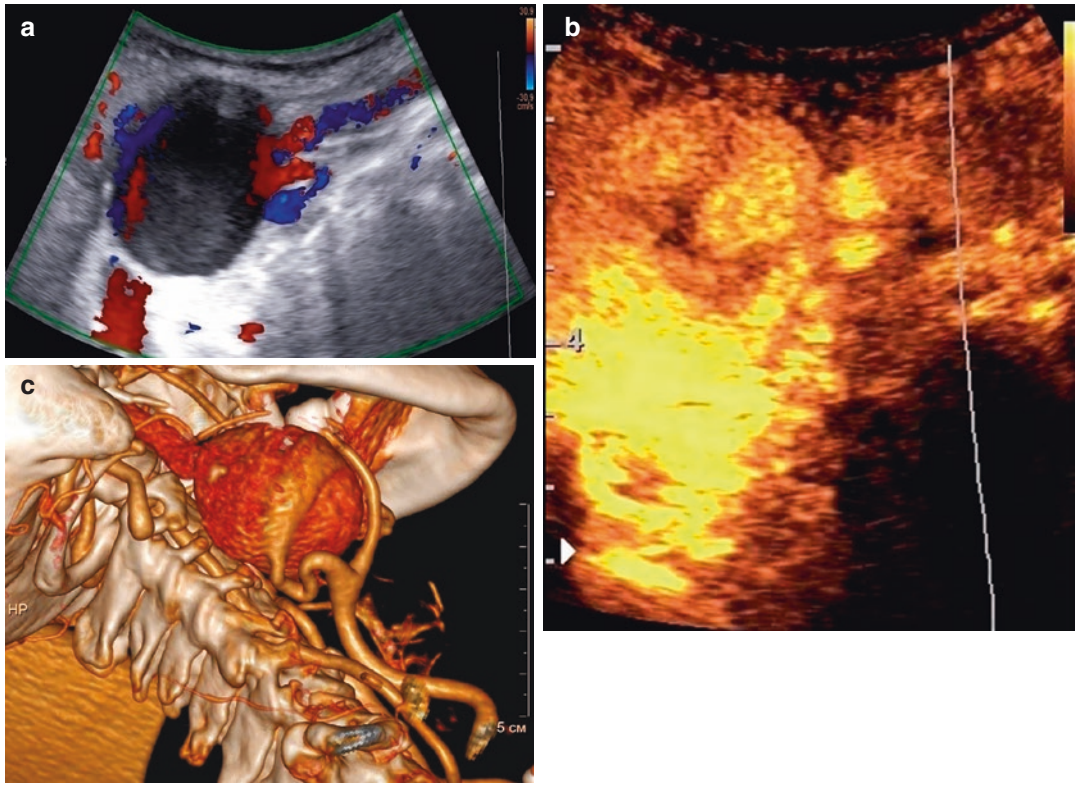

Fig. 18.8 False aneurysm of the right internal carotid artery. (**a**) Grayscale with CDI sonography reveals the artery kinking. (**b**). The arterial phase CEUS image demonstrates the enhancement of the aneurism sac. (**c**) Volumetric representation of CE-CT of the same lesion

plaque structure features, such as ulceration or large hypoechoic area under the surface, indicate the transition of the stable plaque to an unstable condition. Unstable atherosclerotic plaques are associated with a high risk of thrombosis and embolism of distal branches, which can lead to a stroke [14–17].

From the point of view of pathology, this transition is a consequence of the progressive inflammation of the vascular wall. It implicates the increase in the density of vasa vasorum and neovascularization of the atherosclerotic plaque [18, 19]. The clinical manifestation of the plaque is associated with prominent neovascularization.

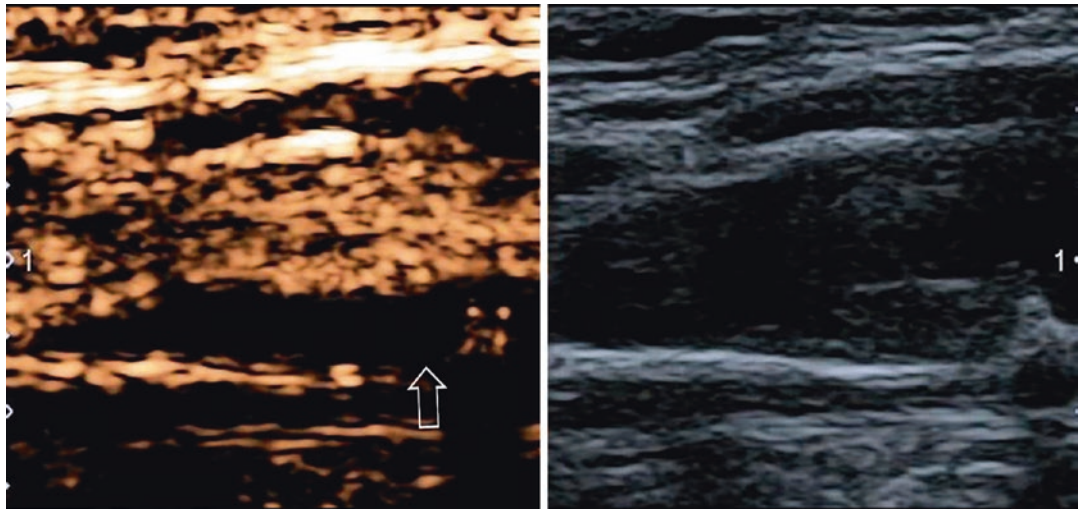

Fig. 18.9 Atherosclerotic plaque in the internal carotid artery. The arterial phase CEUS image demonstrates a regular cap and avascular structure of the plaque (arrow)

Currently, there is an opinion that vasa vasorum within the plaque is an independent predictor of hemorrhage and plaque rupture with possible embolism [17]. Therefore, neovascularization is considered in determining the indications and type of surgical intervention in addition to the grade of stenosis, the plaque composition features, and the state of the surface of the atherosclerotic plaque.

The use of UCAs provides new opportunities for the diagnosis of atherosclerotic lesions. It significantly improves the imaging of the vascular lumen regardless of the angle and scanning plane. CEUS enables the detection of local fibrous cap ulceration and increased neovascularization of the plaque. Besides, it is more accurate in the estimation of the degree and geometry of stenosis.

To assess the plaque neovascularization, the following grades may be used [20]:

- Grade 0: no appearance of neovascularization within the plaque (Fig. 18.9)
- Grade 1: the limited appearance of neovascularization within the plaque
- Grade 2: moderate neovascularization (Figs. 18.10 and 18.11)
- Grade 3: the presence of a pulsating arterial vessel within the plaque

Therefore, CEUS is a promising non-invasive method for the diagnosis of vascular pathologies, which facilitates risk assessment and the choice of management strategy.

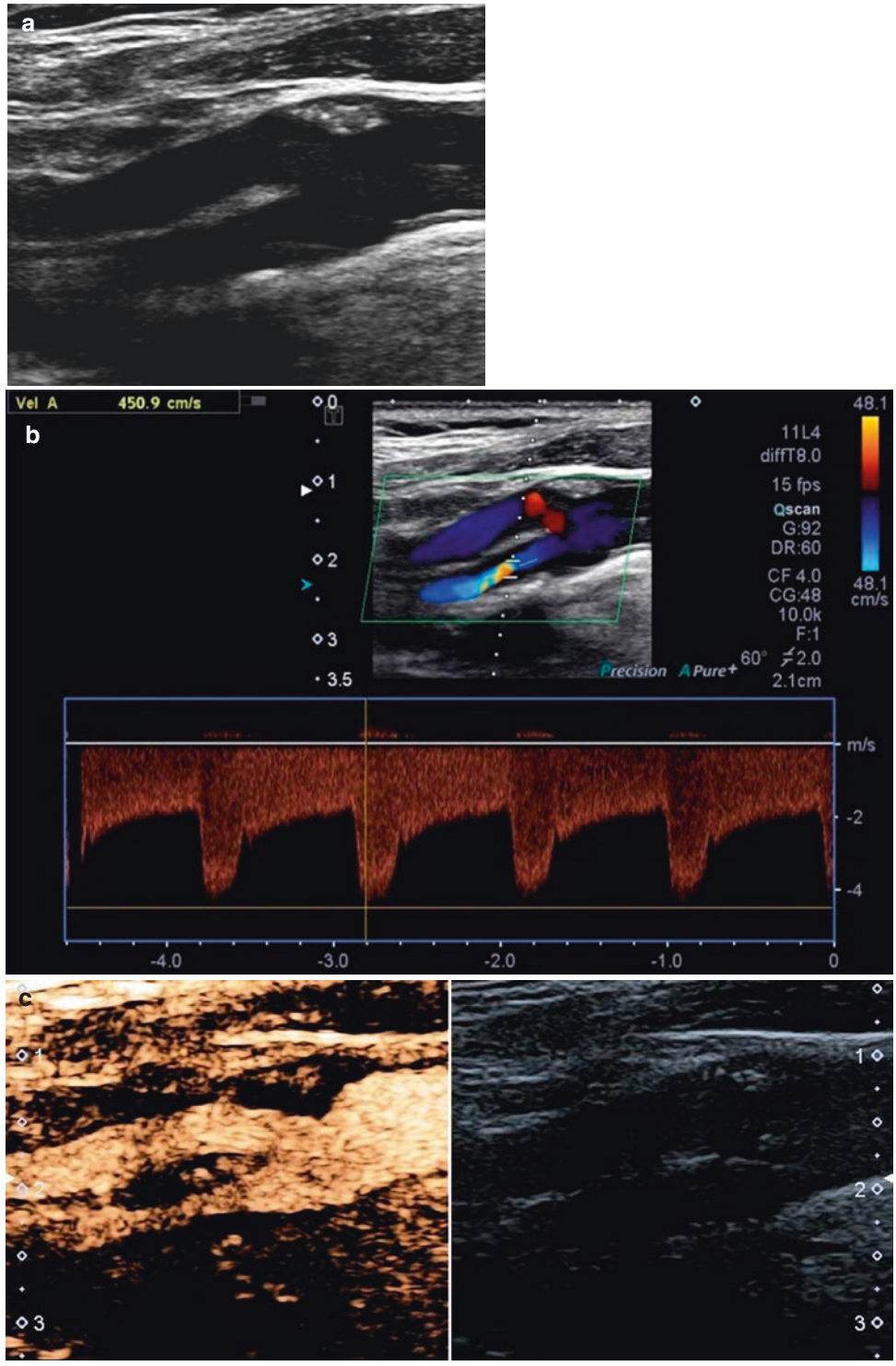

Fig. 18.10 Atherosclerotic plaque of carotid bifurcation with the transition to the external carotid artery and the proximal segment of the internal carotid artery. (**a**) Grayscale sonography. (**b**) CDI. (**c**) CEUS image demonstrates the enhancement of the arterial lumen with the improved delineation of the geometry and length of the stenotic area. Pronounced asymmetric accumulation of microbubbles within the plaque is identified

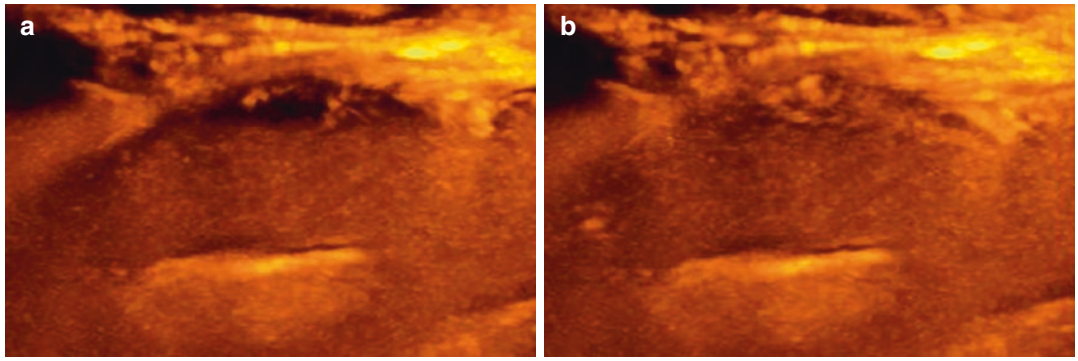

Fig. 18.11 Atherosclerotic plaque with prominent neovascularization. CEUS images demonstrate progressive inflow of UCA into the plaque. (**a**) Multiple neovessels are visualized within the plaque in the arterial phase. The filling begins from the arterial wall. (**b**) The plaque is enhanced in the venous phase with long persistence of the microbubbles

References

1. Gillum RF. Epidemiology of aortic aneurysm in the United States. J Clin Epidemiol. 1995;48(11):1289–98. https://doi.org/10.1016/0895-4356(95)00045-3.
2. Bode PJ, Edwards MJ, Kruit MC, van Vugt AB. Sonography in a clinical algorithm for early evaluation of 1671 patients with blunt abdominal trauma. AJR Am J Roentgenol. 1999;172(4):905–11. https://doi.org/10.2214/ajr.172.4.10587119.
3. Hendrickson RG, Dean AJ, Costantino TG. A novel use of ultrasound in pulseless electrical activity: the diagnosis of an acute abdominal aortic aneurysm rupture. J Emerg Med. 2001;21(2):141–4. https://doi.org/10.1016/s0736-4679(01)00362-6.
4. Miller J, Miller J. Small ruptured abdominal aneurysm diagnosed by emergency physician ultrasound. Am J Emerg Med. 1999;17(2):174–5. https://doi.org/10.1016/s0735-6757(99)90055-4.
5. Catalano O, Lobianco R, Cusati B, Siani A. Contrast-enhanced sonography for diagnosis of ruptured abdominal aortic aneurysm. AJR Am J Roentgenol. 2005;184(2):423–7. https://doi.org/10.2214/ajr.184.2.01840423.
6. White RA. Endograft surveillance: a priority for long-term device performance. J Endovasc Ther. 2000;7(6):522. https://doi.org/10.1177/152660280000700616.
7. Cuypers P, Buth J, Harris PL, Gevers E, Lahey R. Realistic expectations for patients with stent-graft treatment of abdominal aortic aneurysms. Results of a European multicentre registry. Eur J Vasc Endovasc Surg. 1999;17(6):507–16. https://doi.org/10.1053/ejvs.1999.0836.
8. White GH, Yu W, May J. Endoleak--a proposed new terminology to describe incomplete aneurysm exclusion by an endoluminal graft. J Endovasc Surg. 1996;3(1):124–5. https://doi.org/10.1583/1074-6218(1996)003<0124b:>2.0.CO;2.
9. Pokrovskij AV, editor. Klinicheskaya angiologiya. [Clinical angiology], vol. 2. Moscow: Medicina; 2004. p. 117–28. Russian.
10. Stepanova YA. Luchevye metody diagnostiki kistoznyh obrazovanij podzheludochnoj zhelezy i parapankreaticheskoj zony na etapah hirurgicheskogo lecheniya [Radiation methods of diagnostics of cystic lesions of the pancreas and parapancreatic zone at the stages of surgical treatment]. Dissertation. Moscow. 2009. Russian.
11. Buriev IM, Kornyak BS, Azimov RH, Panova NV. Redkoe oslozhnenie postnekroticheskoj kisty podzheludochnoj zhelezy (sluchaj iz praktiki) [A rare complication of a postnecrotic pancreatic cyst (a case from practice)]. Annaly Hirurgicheskoj Gepatol. 2000;1:77–80. Russian.
12. Ido K, Isobe K, Kimura K, Adachi M, Tsuruta R, Ono K, et al. Case of hemorrhagic pancreatic pseudocyst in which ultrasound imaging was useful. J Med Ultrason. 2004;31(1):41–5. https://doi.org/10.1007/s10396-003-0002-7.
13. Isaeva IV, Cygel'nikov SA, Teplickij EA, Ryazanova TV. Anevrizmy vnecherepnogo otdela vnutrennej sonnoj arterii. [Aneurysms of the extracranial part of the internal carotid artery]. Angiol Sosud Khir. 2007;13(1):143–51. Russian.
14. Gray-Weale AC, Graham JC, Burnett JR, Byrne K, Lusby RJ. Carotid artery atheroma: comparison of preoperative B-mode ultrasound appearance with carotid endarterectomy specimen pathology. J Cardiovasc Surg. 1988;29(6):676–81.
15. Kulikov VP. Ul'trazvukovaya diagnostika sosudistyh zabolevanij [Ultrasound diagnostics of vascular diseases]. Moscow: Strom; 2011. Russian.
16. Husain T, Abbott C, Scott J, Gough M. Macrophage accumulation within the cap of carotid atherosclerotic

plaques is associated with the onset of cerebral ischemic events. J Vasc Surg. 1999;30(2):269–76. https://doi.org/10.1016/S0741-5214(99)70137-0.
17. Kolodgie FD, Narula J, Yuan C, Burke AP, Finn AV, Virmani R. Elimination of neoangiogenesis for plaque stabilization: is there a role for local drug therapy? J Am Coll Cardiol. 2007;49(21):2093–101. https://doi.org/10.1016/j.jacc.2006.10.083.
18. Partovi S, Loebe M, Aschwanden M, Baldi T, Jäger KA, Feinstein SB, Staub D. Contrast-enhanced ultrasound for assessing carotid atherosclerotic plaque lesions. AJR Am J Roentgenol. 2012;198(1):W13–9. https://doi.org/10.2214/AJR.11.7312.
19. Chistiakov DA, Orekhov AN, Bobryshev YV. Contribution of neovascularization and intraplaque haemorrhage to atherosclerotic plaque progression and instability. Acta Physiol (Oxford). 2015;213(3):539–53.
20. Shah F, Balan P, Weinberg M, Reddy V, Neems R, Feinstein M, et al. Contrast-enhanced ultrasound imaging of atherosclerotic carotid plaque neovascularization: a new surrogate marker of atherosclerosis? Vasc Med. 2007;12(4):291–7. https://doi.org/10.1177/1358863X07083363.

CEUS for Minimally Invasive Procedures: Intracavitary CEUS

19

Yury N. Patrunov, Inna A. Apolikhina, Ella I. Peniaeva, Alexander N. Sencha, and Ayna S. Saidova

Ultrasound monitoring of interventional procedures with microbubble injection has many advantages over traditional US, CT, or MRI and assumes both intravenous and intraluminal UCA administration. Microbubble contrast media can be introduced into any physiological or pathological cavity of the body to estimate its composition, potential fistula, the position of the drainage system, patency of a hollow organ or duct (e.g., fallopian tubes, biliary system, or reflux detection), etc. [1–7]. CEUS is feasible for the identification of viable tumor tissue to guide biopsies and monitor ablative techniques, such as radiofrequency or thermal ablation [8–12].

The EFSUMB guidelines and recommendations for the clinical practice of CEUS in non-hepatic applications (2017) advise intravenous UCA injection to assist interventional procedures and achieve the following goals [13]:

- to delineate the abscess cavity or necrotic area for efficient drainage
- to avoid necrotic tissue or identify perfused tissue in the biopsy of tumors
- to identify biopsy targets inconspicuous on US
- to manage patients treated with ablation therapies

Intracavitary CEUS is useful for the following purposes, optionally supplemented by intravenous CEUS [13]:

- identification of needle or catheter position
- delineation of any cavity or duct
- improved tracking of a fistula

Intracavitary CEUS may contribute to many minimally invasive diagnostic or therapeutic modalities, such as listed below [13]:

Supplementary Information The online version contains supplementary material available at [https://doi.org/10.1007/978-3-030-91764-7_19].

Y. N. Patrunov (✉) · E. I. Peniaeva
Department of Ultrasound Diagnostics of the Center for Radiological Diagnostics, Private Healthcare Institution "Clinical Hospital "RZD-Medicina" of Yaroslavl City", Yaroslavl, Russian Federation

I. A. Apolikhina · A. S. Saidova
Department of Aesthetic Gynecology and Rehabilitation, Federal State Budget Institution "National Medical Research Center for Obstetrics, Gynecology and Perinatology n.a. V.I.Kulakov", Moscow, Russian Federation

A. N. Sencha
Department of Visual and Functional Diagnostics, Federal State Budget Institution "National Medical Research Center for Obstetrics, Gynecology and Perinatology n.a. V.I.Kulakov", Moscow, Russian Federation

A. N. Sencha, Y. N. Patrunov (eds.), *Contrast-Enhanced Ultrasound*,
https://doi.org/10.1007/978-3-030-91764-7_19

- diagnosis of vesicoureteral reflux
- imaging of tubal patency (contrast-enhanced hystero-salpingo-contrast sonography)
- percutaneous transhepatic cholangiography, endoscopic retrograde cholangiography
- detection of peritoneal-pleural communication (hepatic hydrothorax in cirrhotic patients)
- percutaneous nephrostomy
- sialography
- detection and classification of fistulas
- abscess drainage

Intracavitary CEUS demands a much smaller dose of UCA than for intravenous administration. On average, 0.1–1 mL of ready SonoVue® solution diluted in 40–50 mL of 0.9% normal saline is enough. Excess concentration causes posterior acoustic shadowing, which decreases the imaging quality. A distinctive feature of intraluminal UCA administration is the long persistence of the enhancement, which lasts up to 20–30 min [14].

Percutaneous drainage with US guidance is now standard therapy for patients with abscess or pathological fluid collections who do not have other indications for surgery. Conventional sonography reliably identifies anechogenic fluid, while its sensitivity significantly decreases if echogenic content, such as pus or blood, is present [14]. Intravenous UCA introduction effectively depicts the avascular content in the abscess regardless of its origin and facilitates optimal access route and installation of the drainage system [14–16] (Fig. 19.1, Video 19.1).

CEUS permits a more accurate control over the positioning of the drain due to precise allocation of the fluid and septa. CEUS differentiates the intact organ parenchyma from avascular collections, which allows avoiding its unintentional injury.

In patients with the preinstalled drainage catheter, intraluminal administration of UCA permits to control its location and patency, depicts the total volume of communicating cavities and possible fistula. The repeated studies help to evaluate the drainage efficacy while the cavities volume changes, especially in a complex abscess. One specific application of the intraluminal administration of UCA is the evaluation of pseudocyst or abscess in necrotizing pancreatitis (Fig. 19.2). However, CEUS is usually of limited value due to the overlying bowel. It is more effective for the drainage of large pseudocysts or collections near the anterolateral abdominal wall.

The possibility of repeated studies with portable US devices and real-time workflow in any patient's position at the point of care make CEUS a valuable monitoring tool during and after the drainage procedure [14, 17].

Percutaneous transhepatic CEUS-cholangiography appears necessary to specify the position of the drain in bile ducts, assess the severity and level of biliary obstruction, or detect biliary leakage [2, 18–20]. With the preinstalled catheter, CEUS-cholangiography may identify complications of transhepatic access, such as arterio-biliary fistula when along with the opacification of the biliary tree, microbubbles enter the blood pool and enhance the liver parenchyma [14].

Peritoneal-pleural communication in cirrhotic patients with hepatic hydrothorax is possible to detect with UCA introduction into the abdominal cavity early after thoracentesis. Propagation of microbubbles to the pleural cavity indicates direct connections between peritoneal and pleural cavities [9, 13].

Single publications report on intraluminal UCA administration via the percutaneous catheter drain in patients with complex or echogenic pleural effusion, incl. of empyema. It outlines the pleural cavity, detects local pleural adhesion and loculations, which benefits the decision on fibrinolytic therapy [9, 21, 22].

Percutaneous nephrostomy may be also assisted with CEUS. Some unsuccessful procedures are a consequence of poor US guidance if the renal collecting system is filled with echogenic content, such as blood clots and pus. Intravenous introduction of UCA depicts nonenhanced calyces and pelvis on the background of the otherwise enhanced kidney. During the nephrostomy, before the guidewire introduction, the collecting system may be filled with UCA via the entry needle to ensure the correct

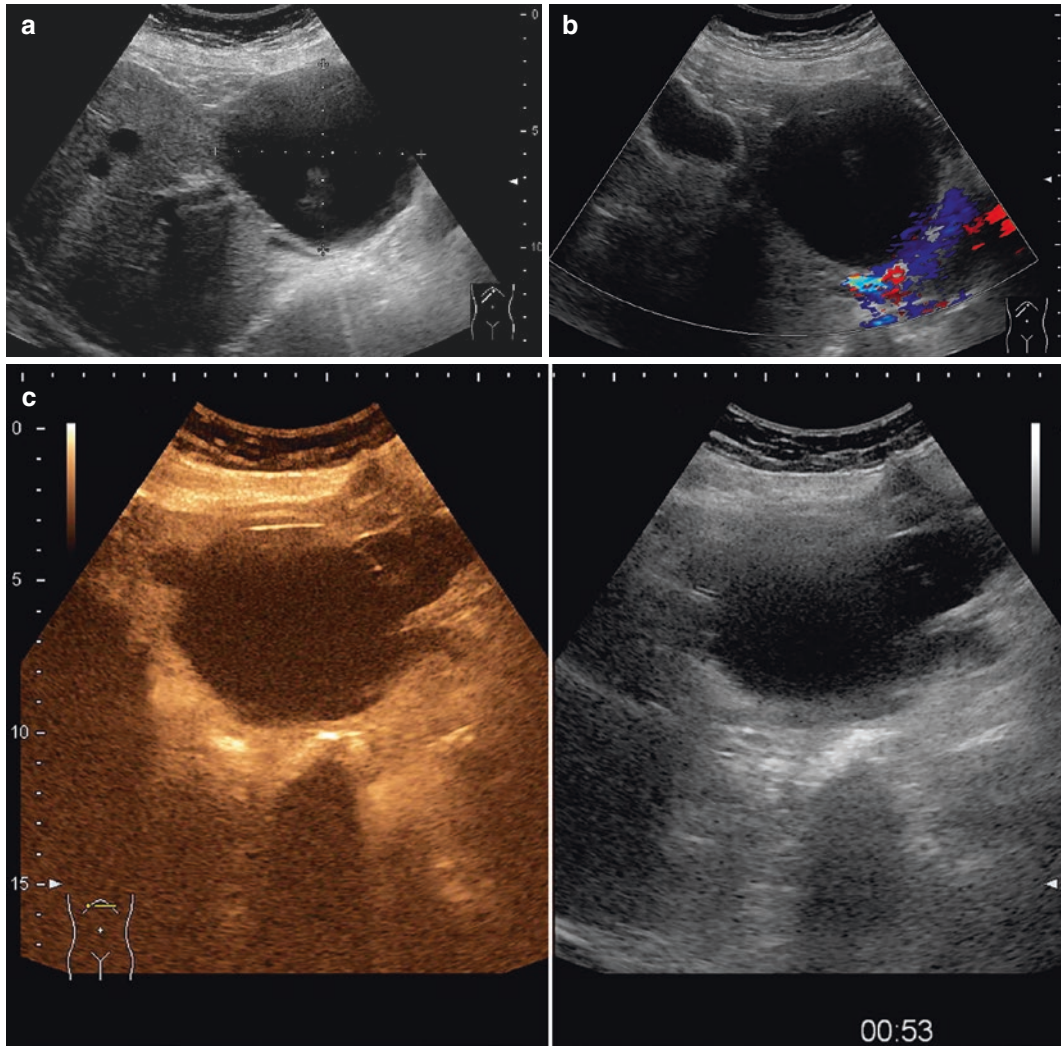

Fig. 19.1 Infected pancreatic pseudocyst. (**a**) Grayscale US image. (**b**) CDI fails to supply any information due to artifacts from the aortic pulsation. (**c**, **d**) CEUS with intravenous administration of SonoVue® demonstrated avascularity of the pseudocyst lumen with thin septations at the periphery. It excludes pseudoaneurysm and confirms a safe transgastric approach

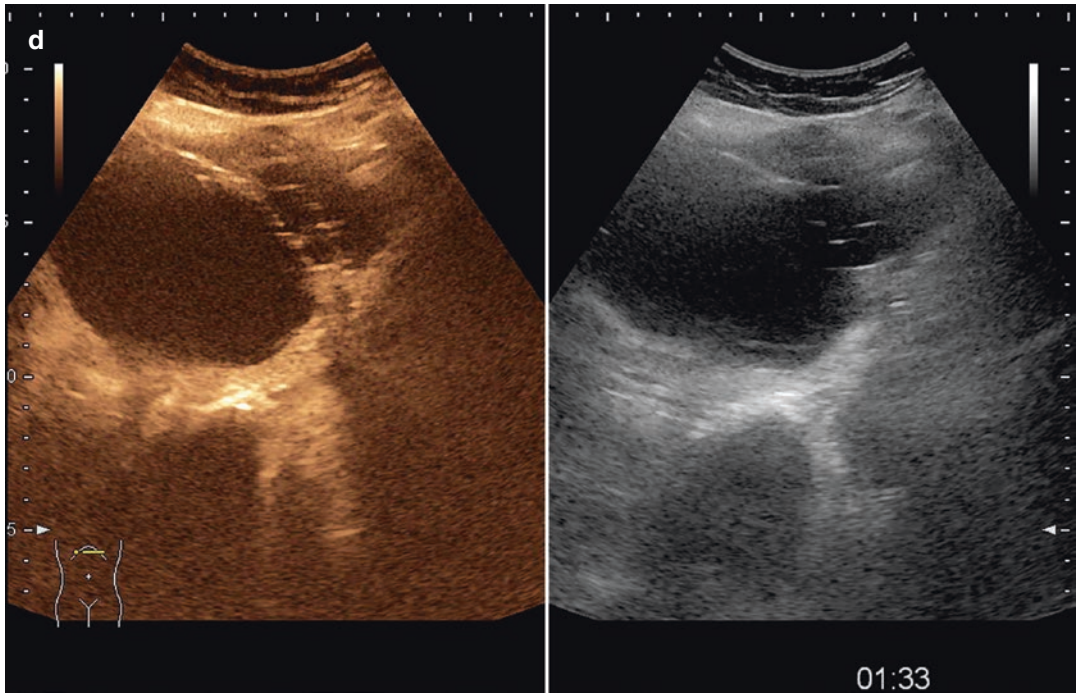

Fig. 19.1 (continued)

position of the needle tip that is the alternative to radiocontrast administration. Contrast enhancement of the calyces, pelvis, and ureter confirms the entry into the collecting system. It also permits to specify the obstruction site or confirm the ureter patency if the UCA descends to the bladder [14]. An additional advantage of UCAs is the opportunity to destroy microbubbles and reconduct the procedure in the case of needle tip dislocation. As compared to radiocontrast agents, the misadministered UCA after destruction does not prevent while resuming nephrostomy.

UCA can also be introduced through the nephrostomy catheter for dynamic CEUS urography or to assess its position and patency. The ureter, when filled up with UCA, can be better visualized, which is an alternative to classical X-ray urography in the point of care, children, and patients with contraindications to iodine-containing contrast media.

CEUS sialography is reported in sporadic publications [13] and implicates the injection of UCA into the salivary gland main duct to determine the obstruction. After the introduction of sialendoscopy to clinical practice, sialography is rarely applied for the diagnosis of obstructive diseases of major salivary glands.

There are individual publications on intraluminal UCA administration for the studies of the gastrointestinal tract to identify filling defects, diverticula, complications in IBD, duodenogastric reflux, etc.

The imaging of the patency of the fallopian tubes (HyCoSy) and contrast-enhanced voiding ultrasound are presented in Sect. 12.3 and Chap. 20, respectively.

Interventions with CEUS guidance often require two intravenous introductions of UCA in a standard dose. The first introduction permits the thorough study of the target organ, determines its composition, volume (for ablation), and relation to the surrounding structures followed by the choice of access route and puncture pathway [9–11]. The second injection, if necessary, aims to guide the needle introduction and positioning of

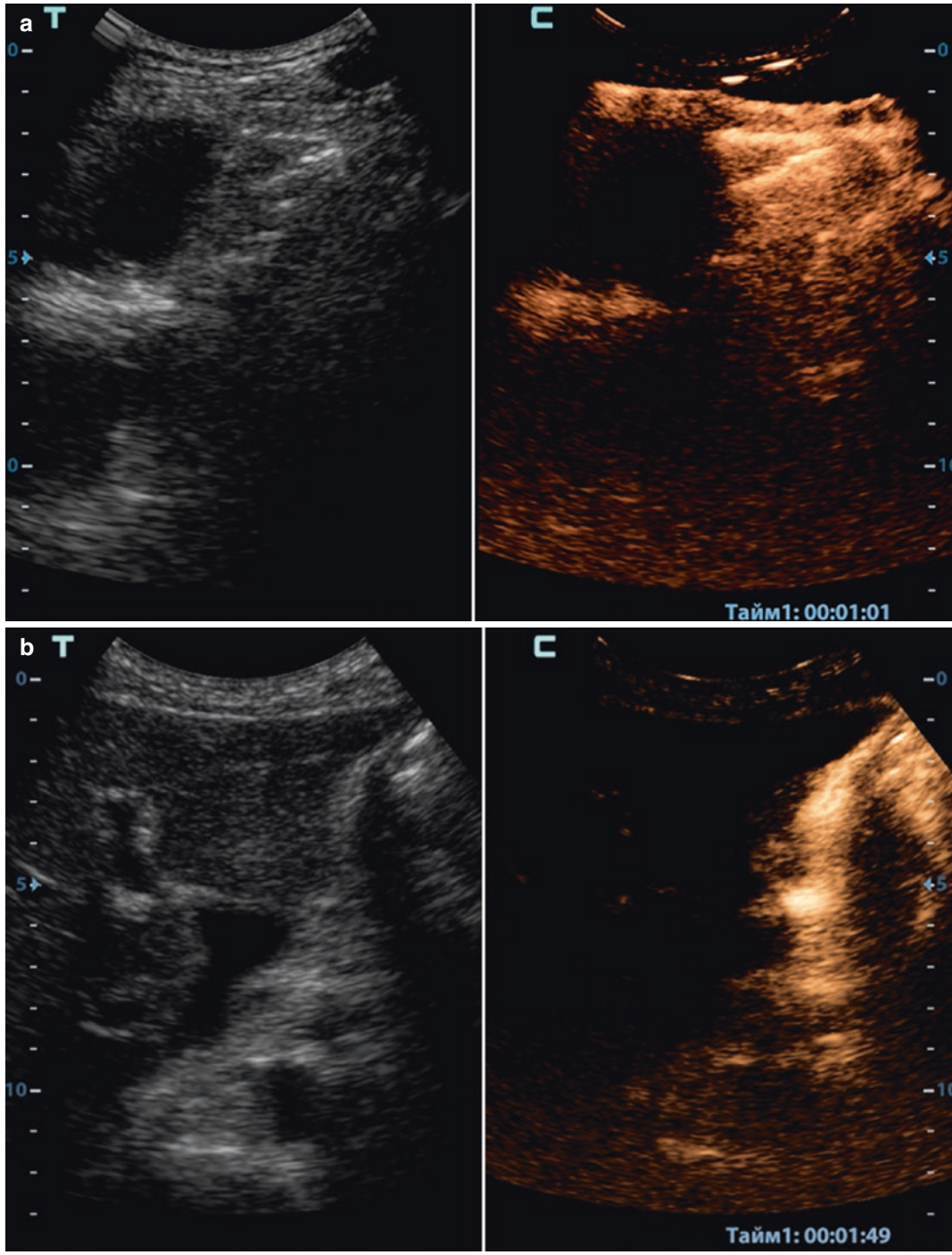

Fig. 19.2 Acute necrotizing pancreatitis and multiple drained pseudocysts. CEUS was performed with intraluminal administration of SonoVue® solution via the drainage catheter due to the suspicion of the drain dislocation. (**a**) The microbubbles appear outside the abscess cavity. The abscess cavity remains nonenhanced. (**b**) Microbubbles spread in the abdominal cavity

the needle tip or is used to assess the completeness of the ablation.

Biopsy in some cases returns nondiagnostic, unsatisfactory, or false-negative reports due to inadequate sampling [23]. Depiction of the boundaries between the target lesion and intact tissue with the conventional US may be a challenge regardless of its clear image with MRI or CE-CT. CEUS image is based on the perfusion features, so the differences in the microvascular pattern of the lesion and the surrounding intact parenchyma facilitate their delineation and successful biopsy. CEUS navigation is beneficial for the biopsy of the liver, pancreas, kidney, and other abdominal, retroperitoneal, and superficial lesions [24–27].

In tumors, it permits sampling from vascularized viable tissues and bypassing avascular necrotic areas [14, 28]. In patients with renal failure, CEUS navigation improves the identification of the target aspects on the background of thin hyperechogenic renal parenchyma, which is usually poorly differentiated from the surrounding tissues with grayscale sonography [14].

Interstitial ablative techniques , such as radiofrequency, thermal ablation, cryoablation are regarded as an alternative to surgery in individual patients with hepatocellular carcinoma, liver metastases, kidney tumors, etc. [29–32].

Treatment efficacy depends on the accurate positioning of the ablation probes in the target lesion and adequate assessment of the mass viability after the ablation. Therefore, it demands precise imaging before, during, and after the procedure. Evaluation of tissue perfusion is crucial for differentiation of necrotic zones from the viable residual tumor.

- Preablation CEUS enables evaluation of the lesions subject to treatment, considering their number, size, perfusion intensity, homogeneity of vascularization, the presence of feeding vessels to develop the best ablation strategy.
- During the procedure, if grayscale sonography fails to identify the target lesion or its parts, CEUS may improve the imaging quality based on perfusion features to adjust the ablation probe position.
- CEUS after the ablation permits immediate evaluation of its efficiency. A completely ablated target lesion demonstrates no contrast enhancement (Fig. 19.3, Videos 19.2, 19.3, and 19.4). Alternatively, in incomplete ablation, CEUS identifies residual viable tumor areas with persisting perfusion. If present, re-ablation of these areas is considered.

However, immediately after the ablation, CEUS hardly differentiates the surrounding hyperemia and the remaining gas bubbles within the ablated area from the residual tumor vascularization. The hyperenhanced rim, which is typical for hyperemia, persists in all vascular phases, as opposed to the perfusion of the residual tumor tissue. Hyperechogenic gas bubbles in the ablation site are visualized with the grayscale US before the introduction of UCA [33]. CEUS immediately after the ablation of hepatocellular carcinoma demonstrated the sensitivity of 88% as referenced to CE-CT in 2 weeks after ablation. However, it exhibited low specificity of only 40%, probably due to the above-mentioned interpretation difficulties [34]. In 1 month after ablation, CEUS was characterized by the sensitivity of 83–93% and specificity of 97–100% [35–37]. In these terms, CEUS appeared the most efficient method for the identification of the local tumor recurrence in the ablated nodule.

A quite interesting and new aspect of CEUS application is the assessment of the effect of the methods, which stimulate local perfusion to induce the reparation process. As opposed to the ablative techniques, which aim to rich complete avascularity of the target lesion, many methods of physical therapy enhance tissue vasculature. However, the prominence of this enhancement is a subjective entity. CEUS with intravenous UCA administration permits its objective assessment.

For example, the methods of laser therapy and carboxytherapy are successfully applied in esthetic medicine and for the treatment of genitourinary syndrome of menopause in women [38, 39]. CEUS permits visual control for these techniques to objectively assess the microvascular-

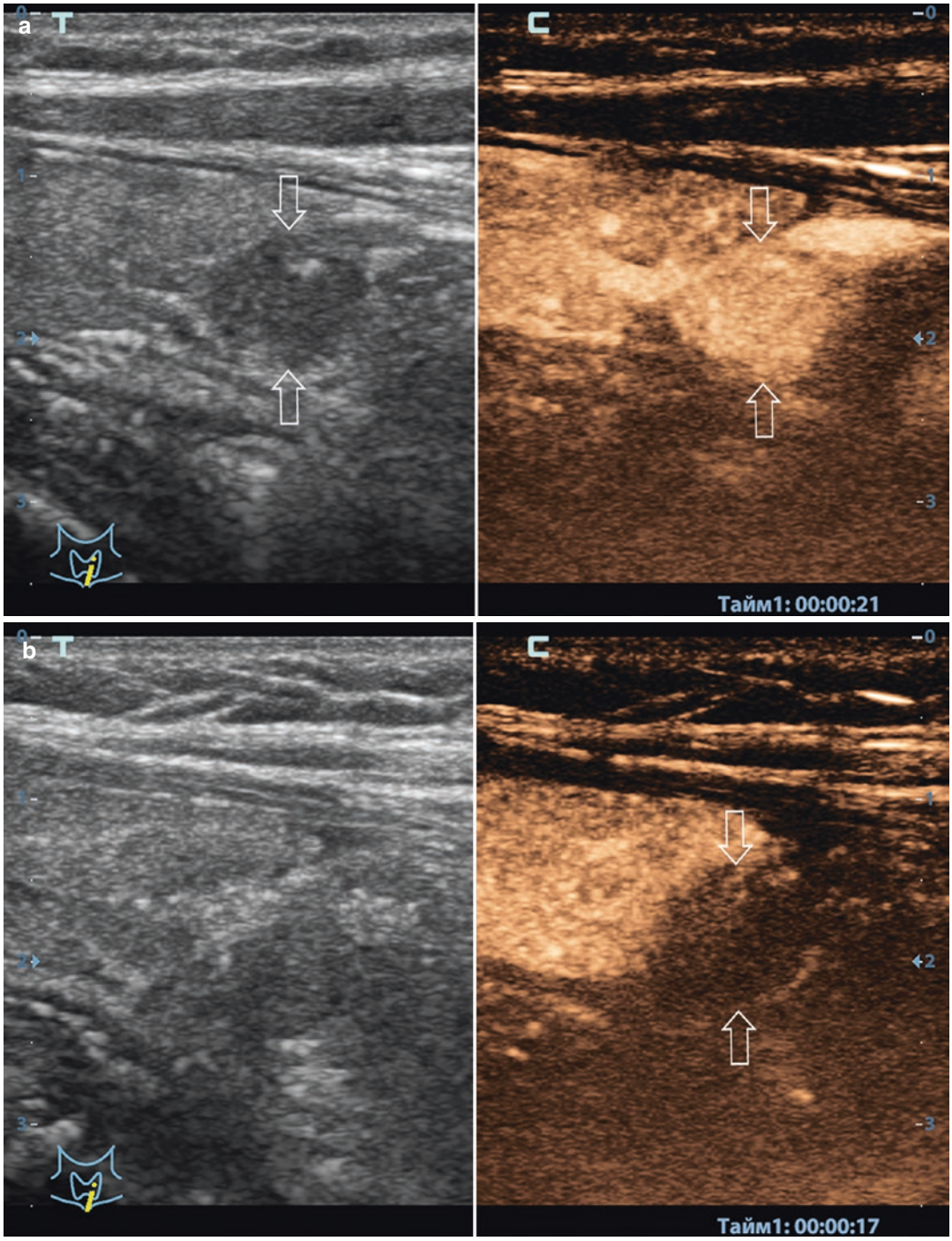

Fig. 19.3 CEUS in the percutaneous laser ablation of a parathyroid adenoma. (**a**) The parathyroid adenoma is located adjacent to the inferior segment of the left thyroid lobe. Before percutaneous laser ablation, it exhibits uniform hyperenhancement, which is similar to the enhancement pattern of the thyroid parenchyma. CEUS image, longitudinal scan. (**b**) CEUS in 10 min after the ablation of the parathyroid adenoma. A perfusion defect is observed in the place of the ablated adenoma near the inferior segment of the left thyroid lobe. CEUS image, longitudinal scan. (**c**) TIC demonstrates no contrast enhancement of the ablated parathyroid adenoma (pink ROI). The thyroid parenchyma enhancement is supplied for reference (yellow ROI)

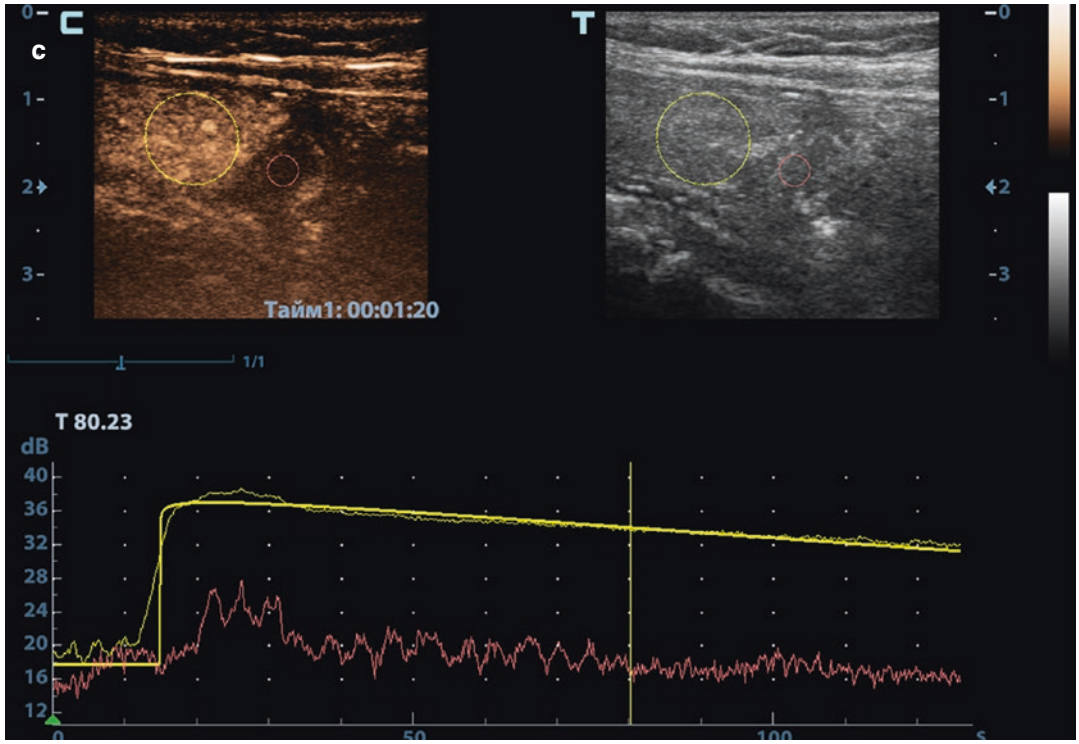

Fig. 19.3 (continued)

ization of soft tissues in the area of interest in the vulva. A qualitative assessment is usually based on visual registration of tissue enhancement in the area of interest. It implicates the intensity of enhancement and symmetric distribution of UCA with subsequent wash-out in the area of the labia majora, the clitoral hood, and the adjacent parts of the vulva before the procedure, within the first hour after the procedure, and 5–7 days after treatment (Fig. 19.4). Quantitative assessment of the change in contrast enhancement is typically based on the ratio of the time parameters and the intensity of enhancement in the corresponding terms.

In successful treatment, CEUS reveals the increase in the perfusion in the zone of interest. Activated arterial inflow and venous outflow result in improved tissue oxygenation and stimulation of the reparative process with the development of new microvessels and the generation of collagen [38].

Microbubble administration in minimally invasive modalities permits overcoming some limitations of conventional US to improve the guidance quality and increase the number of successful procedures. It is also efficient for the assessment of the therapies, which implicate influence on the tissue perfusion.

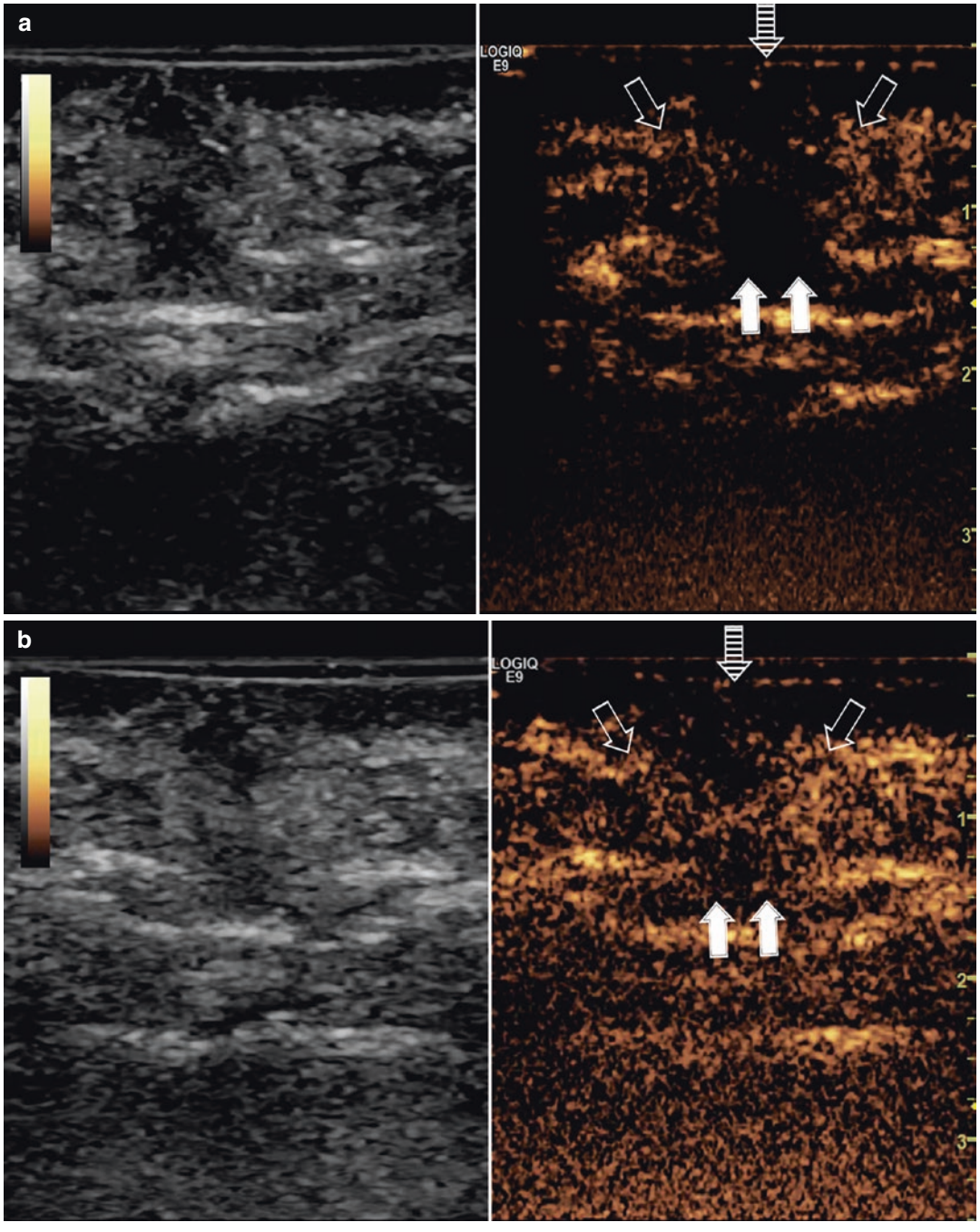

Fig. 19.4 CEUS of the perineum with carboxytherapy. (**a**) Peak enhancement before the procedure. (**b**) Peak enhancement 1 h after the procedure. Striped arrow: clitoral hood, empty arrows: labia majora, solid arrows: labia minora

References

1. Zhou L, Zhang X, Chen X, Liao L, Pan R, Zhou N, Di N. Value of three-dimensional hysterosalpingo-contrast sonography with SonoVue in the assessment of tubal patency. Ultrasound Obstet Gynecol. 2012;40(1):93–8. https://doi.org/10.1002/uog.11085.
2. Luyao Z, Xiaoyan X, Huixiong X, Zuo-Feng X, Guang-Jian L, Ming-de L. Percutaneous ultrasound-guided cholangiography using microbubbles to evaluate the dilated biliary tract: initial experience. Eur Radiol. 2012 Feb;22(2):371–8. https://doi.org/10.1007/s00330-011-2265-5.
3. Darge K. Voiding urosonography with ultrasound contrast agents for the diagnosis of vesicoureteric reflux in children. I Procedure. Pediatr Radiol. 2008;38(1):40–53. https://doi.org/10.1007/s00247-007-0529-7.
4. Cui XW, Ignee A, Maros T, Straub B, Wen JG, Dietrich CF. Feasibility and usefulness of intra-cavitary contrast-enhanced ultrasound in percutaneous nephrostomy. Ultrasound Med Biol. 2016;42(9):2180–8. https://doi.org/10.1016/j.ultrasmedbio.2016.04.015.
5. Cui XW, Ignee A, Baum U, Dietrich CF. Feasibility and usefulness of using swallow contrast-enhanced ultrasound to diagnose Zenker's diverticulum: preliminary results. Ultrasound Med Biol. 2015;41(4):975–81. https://doi.org/10.1016/j.ultrasmedbio.2014.12.003.
6. Ignee A, Schuessler G, Cui XW, Dietrich CF. Der endokavitäre Kontrastmittelultraschall--verschiedene Anwendungen, eine Übersicht über die Literatur und zukünftige Perspektiven [Intracavitary contrast medium ultrasound - different applications, a review of the literature ad future prospects]. Ultraschall Med. 2013;34(6):504–25. https://doi.org/10.1055/s--0033-1335546; quiz 526–8. German.
7. Ignee A, Cui X, Schuessler G, Dietrich CF. Percutaneous transhepatic cholangiography and drainage using extravascular contrast enhanced ultrasound. Z Gastroenterol. 2015;53(5):385–90. https://doi.org/10.1055/s-0034-1398796.
8. Dietrich CF, Averkiou M, Nielsen MB, Barr RG, Burns PN, Calliada F, et al. How to perform contrast-enhanced ultrasound (CEUS). Ultrasound Int Open. 2018;4(1):E2–E15. https://doi.org/10.1055/s-0043-123931.
9. Lorentzen T, Nolsøe CP, Ewertsen C, Nielsen MB, Leen E, Havre RF, et al. EFSUMB guidelines on interventional ultrasound (INVUS), Part I. General aspects (long version). Ultraschall Med. 2015;36(5):E1–14. https://doi.org/10.1055/s-0035-1553593.
10. Sidhu PS, Brabrand K, Cantisani V, Correas JM, Cui XW, D'Onofrio M, et al. EFSUMB guidelines on interventional ultrasound (INVUS), Part II. Diagnostic ultrasound-guided interventional procedures (long version). Ultraschall Med. 2015;36(6):E15–35. https://doi.org/10.1055/s-0035-1554036.
11. Dietrich CF, Lorentzen T, Appelbaum L, Buscarini E, Cantisani V, Correas JM, et al. EFSUMB guidelines on interventional ultrasound (INVUS), Part III - Abdominal treatment procedures (long version). Ultraschall Med. 2016;37(1):E1–E32. https://doi.org/10.1055/s-0035-1553917.
12. Meloni MF, Andreano A, Franza E, Passamonti M, Lazzaroni S. Contrast enhanced ultrasound: should it play a role in immediate evaluation of liver tumors following thermal ablation? Eur J Radiol. 2012;81(8):e897–902. https://doi.org/10.1016/j.ejrad.2012.05.002.
13. Sidhu PS, Cantisani V, Dietrich CF, Gilja OH, Saftoiu A, Bartels E, et al. The EFSUMB guidelines and recommendations for the clinical practice of contrast-enhanced ultrasound (CEUS) in non-hepatic applications: update 2017 (long version). Ultraschall Med. 2018;39(2):e2–e44. https://doi.org/10.1055/a-0586-1107.
14. Huang DY, Yusuf GT, Daneshi M, Husainy MA, Ramnarine R, Sellars ME, Sidhu PS. Contrast-enhanced US-guided interventions: improving success rate and avoiding complications using US contrast agents. Radiographics. 2017;37(2):652–64. https://doi.org/10.1148/rg.2017160123.
15. Bartolotta TV, Taibbi A, Midiri M, Lagalla R. Focal liver lesions: contrast-enhanced ultrasound. Abdom Imaging. 2009;34(2):193–209. https://doi.org/10.1007/s00261-008-9378-6.
16. Meloni MF, Andreano A, Laeseke PF, Lee FT Jr, Sironi S, Filice C, Ferraioli G. Contrast-enhanced ultrasonographic findings in a brucellar hepatic abscess. J Ultrasound Med. 2008;27(10):1511–5. https://doi.org/10.7863/jum.2008.27.10.1511.
17. Ignee A, Jenssen C, Cui XW, Schuessler G, Dietrich CF. Intracavitary contrast-enhanced ultrasound in abscess drainage--feasibility and clinical value. Scand J Gastroenterol. 2016;51(1):41–7. https://doi.org/10.3109/00365521.2015.1066423.
18. Daneshi M, Rajayogeswaran B, Peddu P, Sidhu PS. Demonstration of an occult biliary-arterial fistula using percutaneous contrast-enhanced ultrasound cholangiography in a transplanted liver. J Clin Ultrasound. 2014;42(2):108–11. https://doi.org/10.1002/jcu.22048.
19. Mao R, Xu EJ, Li K, Zheng RQ. Usefulness of contrast-enhanced ultrasound in the diagnosis of biliary leakage following T-tube removal. J Clin Ultrasound. 2010;38(1):38–40. https://doi.org/10.1002/jcu.20622.
20. Xu EJ, Zheng RQ, Su ZZ, Li K, Ren J, Guo HY. Intrabiliary contrast-enhanced ultrasound for evaluating biliary obstruction during percutaneous transhepatic biliary drainage: a preliminary study. Eur J Radiol. 2012;81(12):3846–50. https://doi.org/10.1016/j.ejrad.2012.06.025.
21. Görg C. Transcutaneous contrast-enhanced sonography of pleural-based pulmonary lesions. Eur J Radiol. 2007;64(2):213–21. https://doi.org/10.1016/j.ejrad.2007.06.037.
22. Linde HN, Holland A, Greene BH, Görg C. Kontrastunterstützte Sonografie (CEUS) bei Pneumonie: Darstellungsmuster und prognostische Bedeutung - eine retrospektive Studie bei n = 50

Patienten [Contrast-enhanced sonography (CEUS) in pneumonia: typical patterns and clinical value - a retrospective study on n = 50 patients]. Ultraschall Med. 2012;33(2):146–51. https://doi.org/10.1055/s--0031-1273280. German.
23. Sainani NI, Arellano RS, Shyn PB, Gervais DA, Mueller PR, Silverman SG. The challenging image-guided abdominal mass biopsy: established and emerging techniques 'if you can see it, you can biopsy it'. Abdom Imaging. 2013;38(4):672–96. https://doi.org/10.1007/s00261-013-9980-0.
24. Mao F, Dong Y, Ji Z, Cao J, Wang WP. Contrast-enhanced ultrasound guided biopsy of undetermined abdominal lesions: a multidisciplinary decision-making approach. Biomed Res Int. 2017;2017:8791259. https://doi.org/10.1155/2017/8791259.
25. Sparchez Z, Radu P, Kacso G, Eniu D, Hica S, Sparchez M. Contrast-enhanced ultrasound guided biopsy of superficial thoraco-abdominal and neck lesions. Initial experience in 20 patients. Med Ultrason. 2012;14(4):288–93.
26. Spârchez Z, Radu P, Zaharia T, Kacso G, Grigorescu I, Badea R. Contrast enhanced ultrasound guidance: a new tool to improve accuracy in percutaneous biopsies. Med Ultrason. 2010;12(2):133–8.
27. Yoon SH, Lee KH, Kim SY, Kim YH, Kim JH, Lee SH, Kim TK. Real-time contrast-enhanced ultrasound-guided biopsy of focal hepatic lesions not localised on B-mode ultrasound. Eur Radiol. 2010;20(8):2047–56. https://doi.org/10.1007/s00330-010-1757-z.
28. Wang J, Zhou D, Xie X, Shen P, Zeng Y. Utility of contrast-enhanced ultrasound with SonoVue in biopsy of small subpleural nodules. Int J Clin Exp Med. 2015;8(9):15991–8.
29. Bruix J, Hessheimer AJ, Forner A, Boix L, Vilana R, Llovet JM. New aspects of diagnosis and therapy of hepatocellular carcinoma. Oncogene. 2006;25(27):3848–56. https://doi.org/10.1038/sj.onc.1209548.
30. Dominguez-Escrig JL, Sahadevan K, Johnson P. Cryoablation for small renal masses. Adv Urol. 2008;2008:479495. https://doi.org/10.1155/2008/479495.
31. Gillams AR, Lees WR. Five-year survival in 309 patients with colorectal liver metastases treated with radiofrequency ablation. Eur Radiol. 2009;19(5):1206–13. https://doi.org/10.1007/s00330-008-1258-5.
32. Livraghi T, Goldberg SN, Lazzaroni S, Meloni F, Ierace T, Solbiati L, Gazelle GS. Hepatocellular carcinoma: radio-frequency ablation of medium and large lesions. Radiology. 2000;214(3):761–8. https://doi.org/10.1148/radiology.214.3.r00mr02761.
33. Chan AK, Hegarty C, Klass D, Yoshida E, Chung S, Liu DM, et al. The role of contrast-enhanced ultrasound in guiding radiofrequency ablation of hepatocellular carcinoma: a retrospective study. Can Assoc Radiol J. 2015;66(2):171–8. https://doi.org/10.1016/j.carj.2014.11.005.
34. Dill-Macky MJ, Asch M, Burns P, Wilson S. Radiofrequency ablation of hepatocellular carcinoma: predicting success using contrast-enhanced sonography. AJR Am J Roentgenol. 2006;186(5 Suppl):S287–95. https://doi.org/10.2214/AJR.04.1916.
35. Ricci P, Cantisani V, Drudi F, Pagliara E, Bezzi M, Meloni F, et al. Is contrast-enhanced US alternative to spiral CT in the assessment of treatment outcome of radiofrequency ablation in hepatocellular carcinoma? Ultraschall Med. 2009 Jun;30(3):252–8. https://doi.org/10.1055/s-2008-1027727.
36. Salvaggio G, Campisi A, Lo Greco V, Cannella I, Meloni MF, Caruso G. Evaluation of posttreatment response of hepatocellular carcinoma: comparison of ultrasonography with second-generation ultrasound contrast agent and multidetector CT. Abdom Imaging. 2010;35(4):447–53. https://doi.org/10.1007/s00261-009-9551-6.
37. Vilana R, Bianchi L, Varela M, Nicolau C, Sánchez M, Ayuso C, et al. Is microbubble-enhanced ultrasonography sufficient for assessment of response to percutaneous treatment in patients with early hepatocellular carcinoma? Eur Radiol. 2006;16(11):2454–62. https://doi.org/10.1007/s00330-006-0264-8.
38. Apolihina IA, Sencha AN, Saidova AS. Sovremenyj podhod k terapii genitourinarnogo menopauzal'nogo sindroma [A modern approach to the treatment of genitourinary syndrome of menopause]. Medicinskij Opponent. 2020;3:27–31. Russian.
39. Saidova AS, Sencha AN, Apolihina IA. Karboksiterapiya genitourinarnogo menopauzal'nogo sindroma [Carboxytherapy for genitourinary syndrome of menopause]. Akusherstvo Ginekol. 2020;5:113–21. https://doi.org/10.18565/aig.2020.5.113-21. Russian.

CEUS in Pediatric Practice

20

Alexander N. Sencha and Elena A. Zubareva

According to the manufacturer's instruction, SonoVue® is contraindicated in patients of the age below 18 years. The studies in pediatric practice utilized SonoVue® on the "off-label" basis. Nevertheless, extensive experience of CEUS in children under 18 years was obtained. It indicates the efficacy and safety of SonoVue® in pediatric patients for the diagnosis of diseases and injuries of the internal organs [1–8].

Off-label use of pharmaceutical preparations is possible if the potential benefits of its use exceed the potential risk of no treatment. The CEUS data in many cases can influence the subsequent diagnostic strategy and treatment. The accumulated experience enabled the European Federation of Societies for Ultrasound in Medicine and Biology to publish the official position of EFSUMB on the possibility of application of UCAs in pediatric practice [9]. In 2016, the SonoVue® under the trade name Lumason was approved for use in the USA to study the liver and vesicoureteral reflux in pediatric practice [10, 11].

Publications most often report on intravenous use of UCA in children for the assessment of focal liver lesions, tumor response to therapy, for the studies of pelvic and retroperitoneal organs, and in the trauma of parenchymal organs. Besides, intracavitary administration of UCA is possible, for example, contrast-enhanced voiding urosonography.

The main advantage of CEUS in pediatric patients is the lack of ionizing radiation and UCA nephrotoxicity, as compared with CE-CT [12]. It does not require sedation or general anesthesia necessary for many MRI studies to ensure the child's immobility.

CEUS procedure in pediatric practice requires the legal parental or guardian permission and in some cases requires the decision of the medical board or concilium of doctors. In assessing the possibility of conducting CEUS, it is necessary to focus on the official instruction on the UCA considering all other possible contraindications [9].

Adverse reactions to UCAs in children are rare and mainly represented by the change in taste, slight dizziness, tinnitus, headache, nausea, or skin itching. Retrospective assessment of the safety of UCAs in children based on the data of 29 studies with a total of 948 pediatric patients

Supplementary Information The online version contains supplementary material available at [https://doi.org/10.1007/978-3-030-91764-7_20].

A. N. Sencha (✉)
Department of Visual and Functional Diagnostics, Federal State Budget Institution "National Medical Research Center for Obstetrics, Gynecology and Perinatology n.a. V.I.Kulakov", Moscow, Russian Federation

E. A. Zubareva
Department of Ultrasound Diagnosis of the Postgraduate Education Division, Russian National Medical Research University n.a. N.I.Pirogov, Moscow, Russian Federation

A. N. Sencha, Y. N. Patrunov (eds.), *Contrast-Enhanced Ultrasound*,
https://doi.org/10.1007/978-3-030-91764-7_20

reported mild side effects in five of them and one case of severe anaphylactoid reaction, which completely resolved with therapy within 2 h [6, 13].

Intracavitary use of UCAs may also be accompanied by some rare adverse reactions, such as dysuria, abdominal pain, hematuria, perineal irritation, and urinary tract infection, which are more likely to be associated with bladder catheterization rather than with UCA administration [6, 14].

The CEUS procedure with bolus intravenous injection of UCA in children is similar to the same in adults and is described in detail in the relevant chapters. The dose of the UCA depends on the patient's age or weight. It can be calculated based on 0.1 mL of SonoVue® per year of life or following FDA recommendations 0.03 mL/kg, but not more than 2.4 mL [10]. The following options are also available: 0.6 mL of SonoVue® for children under 6 years of age, 1.2 mL for children aged 6–12 years, and 2.4 mL for children over 12 years of age; 0.1 mL for each year of age; 0.1 mL/kg for children below 24 kg; and a standard dose of 2.4 mL for children exceeding 24 kg [2, 15–17]. A useful technique to quiet down early childhood patients may be the study in the mother's hands during breastfeeding or feeding from a bottle.

CEUS in adults has been successfully used for many years to differentiate focal liver lesions (see Chap. 4) and is also expected to be widely used in pediatric practice. There are significant advantages of CEUS in the examination of children with hepatoblastoma and neuroblastoma, especially in the intensive care unit and in lesions not determined by CT [18].

Liver tumors in children implicate both the tumors of adults and the specific to childhood neoplasms. Two-thirds of liver tumors in children are malignant, of which two-thirds are hepatoblastoma. Other malignant neoplasms of the liver in children include sarcoma, germ-cell tumors, rhabdomyoma, and hepatocellular carcinoma. Benign liver tumors in children include vascular tumors, hamartoma, adenoma, and focal nodular hyperplasia [19–21].

Liver CEUS in pediatric patients uses the standard method with an individual dose of UCA. The features of contrast enhancement of benign and malignant liver tumors, which occur in both children and adults, were discussed in Chap. 4. This chapter presents the data specific to the pathology of childhood. The main differential diagnostic sign of a malignant liver lesion is the UCA washout, while benign lesions demonstrate persistent contrast enhancement [2, 22–24].

Infantile hemangioendothelioma (infantile hepatic hemangioma) is a vascular neoplasm. It is the most common benign tumor of the liver in infants. Almost one-third of these tumors are diagnosed within the first month of life and about 90% within the first 6 months [19]. Despite their benign character, they can lead to severe complications, such as congestive heart failure, Kasabach–Merritt syndrome, bleeding, and jaundice.

There are three subtypes of infantile hepatic hemangioma: focal, multifocal, and diffuse. This neoplasm most often demonstrates peripheral nodular contrast enhancement with centripetal filling in the portal venous phase without UCA washout [24, 25] (Fig. 20.1).

Hepatoblastoma is a malignant liver tumor that occurs on average at the age of 18 months. With CEUS, hyperenhancement of the lesion in the arterial phase with washout effect in the portal venous and late phases is reported, which is also characteristic of other types of malignant tumors, metastases, and hepatocellular carcinoma (Fig. 20.2).

Renal CEUS in pediatric practice has the same indications as in adults. It eliminates the risk of contrast-induced nephropathy due to iodine-containing radiocontrast media. The most popular application of UCA in pediatric urological practice is the study of vesicoureteral reflux.

Although the recommendations for the use of CEUS were developed for an adult practice, the indications and principles of assessing pathological changes can be extrapolated to pediatric patients. It is especially valuable in patients with contraindications to radiocontrast agents, CT, or MRI. Besides, CEUS of the kidneys in pediatric practice may be used in trauma, monitoring renal transplant, and evaluation of tumor response to therapy. The value of CEUS in the differential

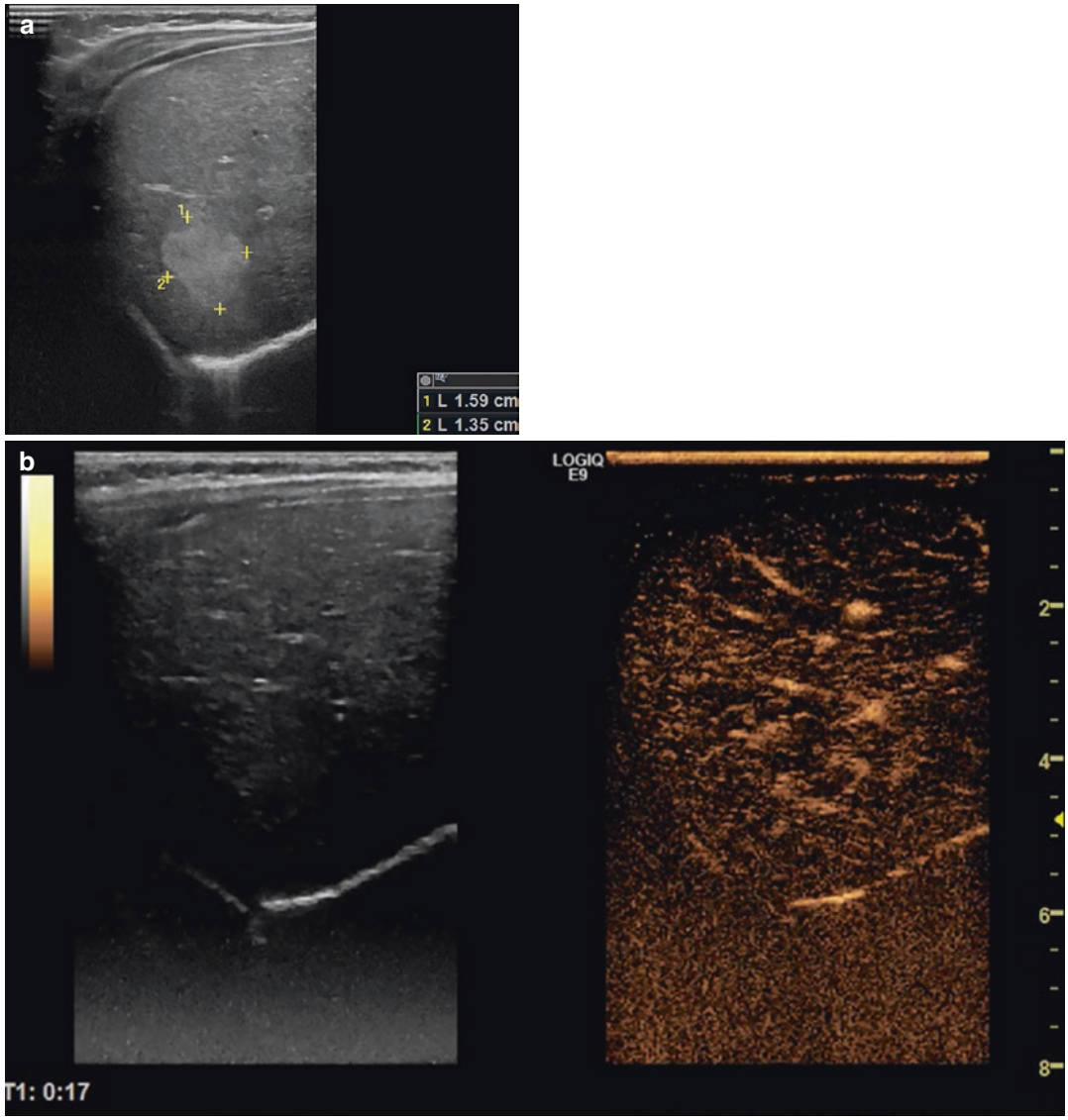

Fig. 20.1 Infantile hepatic hemangioma. The child's age is 6 months. (**a**) Grayscale US image. (**b**) CEUS image with SonoVue® 0.03 mL. Peripheral nodular contrast enhancement of the lesion in the arterial phase

diagnosis of kidney tumors is currently the subject for discussion. The reliable differential signs of Wilms tumor, which is the most common in children, are not reported. CEUS is not included in oncological examination protocols in children.

Fluid lesions of the adrenal glands, kidneys, and other organs demonstrate a persistent perfusion defect (Fig. 20.3).

Vesicoureteral reflux (VUR) is one most common urinary tract abnormality in children. It may be associated with reflux nephropathy; however, the correlations between these pathologies remain controversial [26]. VUR screening is important in children with prenatal hydronephrosis, recurrent or complicated urinary tract infections, and nephrosclerosis. Contrast-enhanced voiding urosonography (CEVUS) is widely

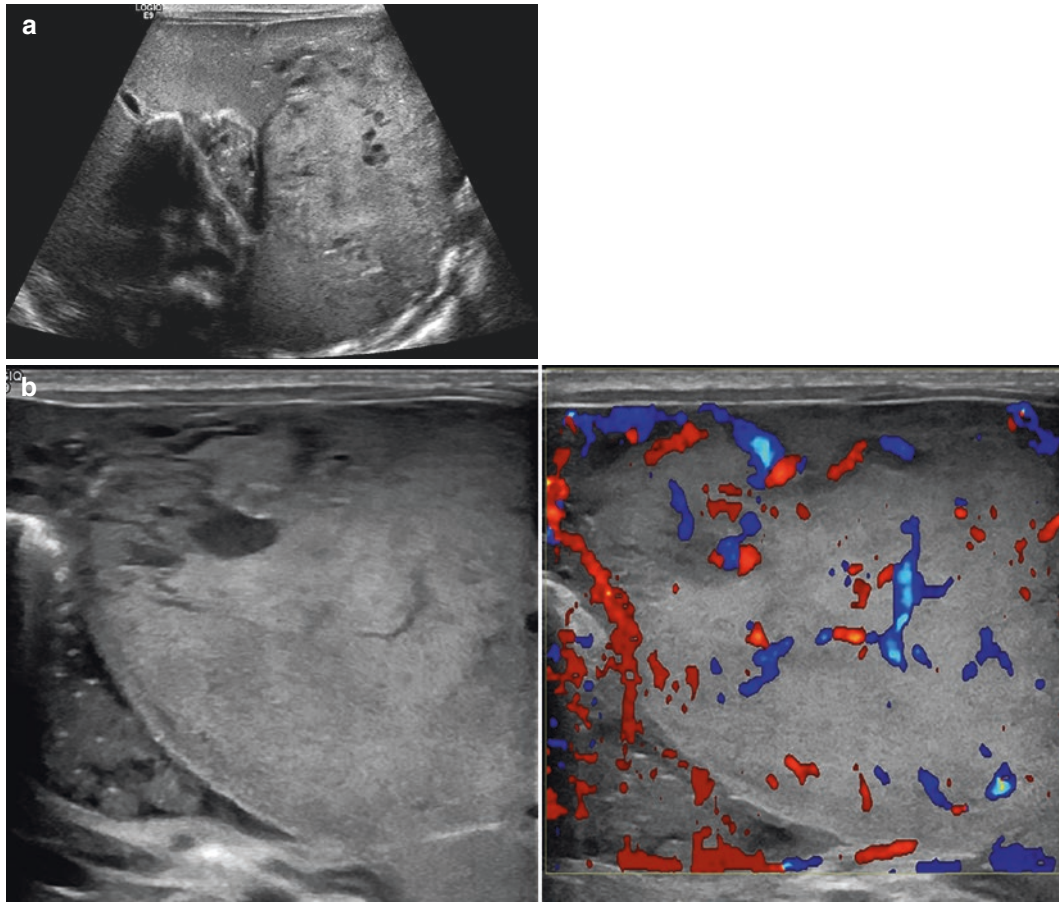

Fig. 20.2 Hepatoblastoma. The child's age is 2 months. (**a**) Grayscale US image. (**b**) CDI. (**c**) CEUS image with SonoVue® 0.03 mL. (**d**) Quantitative analysis of CEUS

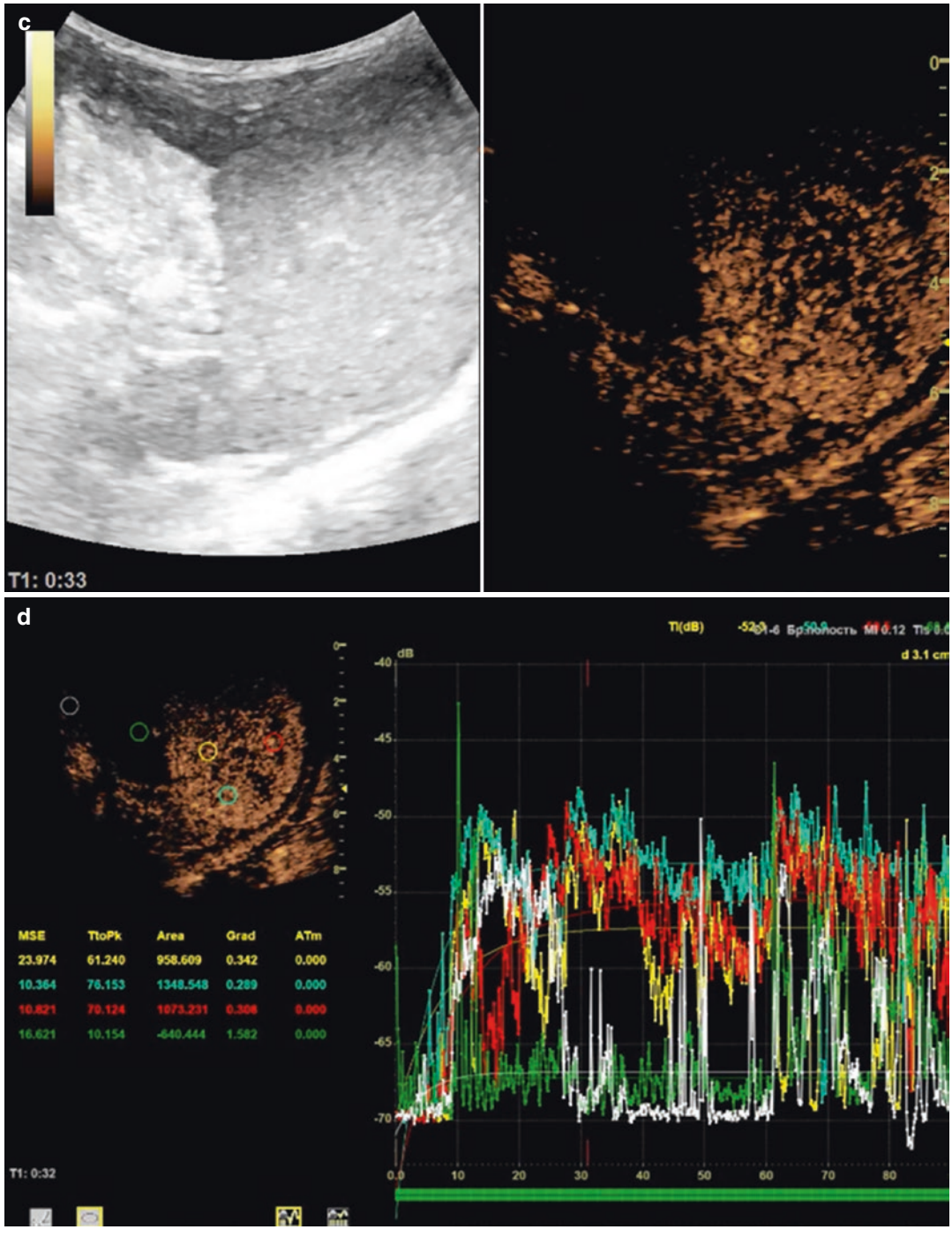

Fig. 20.2 (continued)

introduced to clinical practice [14, 27–30]. Other methods, such as X-ray retrograde urethrocystography and radionuclide cystography, are associated with radiation exposure and intermittent imaging. CEVUS has become the main screening method in children with suspected VUR. It demonstrates high diagnostic accuracy (the sensitivity of 80–100% and specificity of 77–97%), which is higher than traditional urosonography [9, 14, 27–31]. Modern CEVUS permits three-dimensional scanning with improved volumetric imaging. The real-time study may accompany endoscopic treatment that facilitates the immediate assessment of its efficacy [21, 32–35].

The study is performed in a supine position. A small amount of UCA is administered intravesically through a catheter. Scanning of the kidneys and retrovesical space is performed in real-time as the bladder fills and during voiding. Another option is to dilute the UCA in the saline and introduce it into the bladder cavity through a catheter with dropper infusion [9]. The detection of UCA in the ureter, renal pelvis, or calyces indicates the presence of VUR. Its grading is similar to X-ray urosonography. The study ends with scanning of the urethra during voiding by transperineal or transabdominal access.

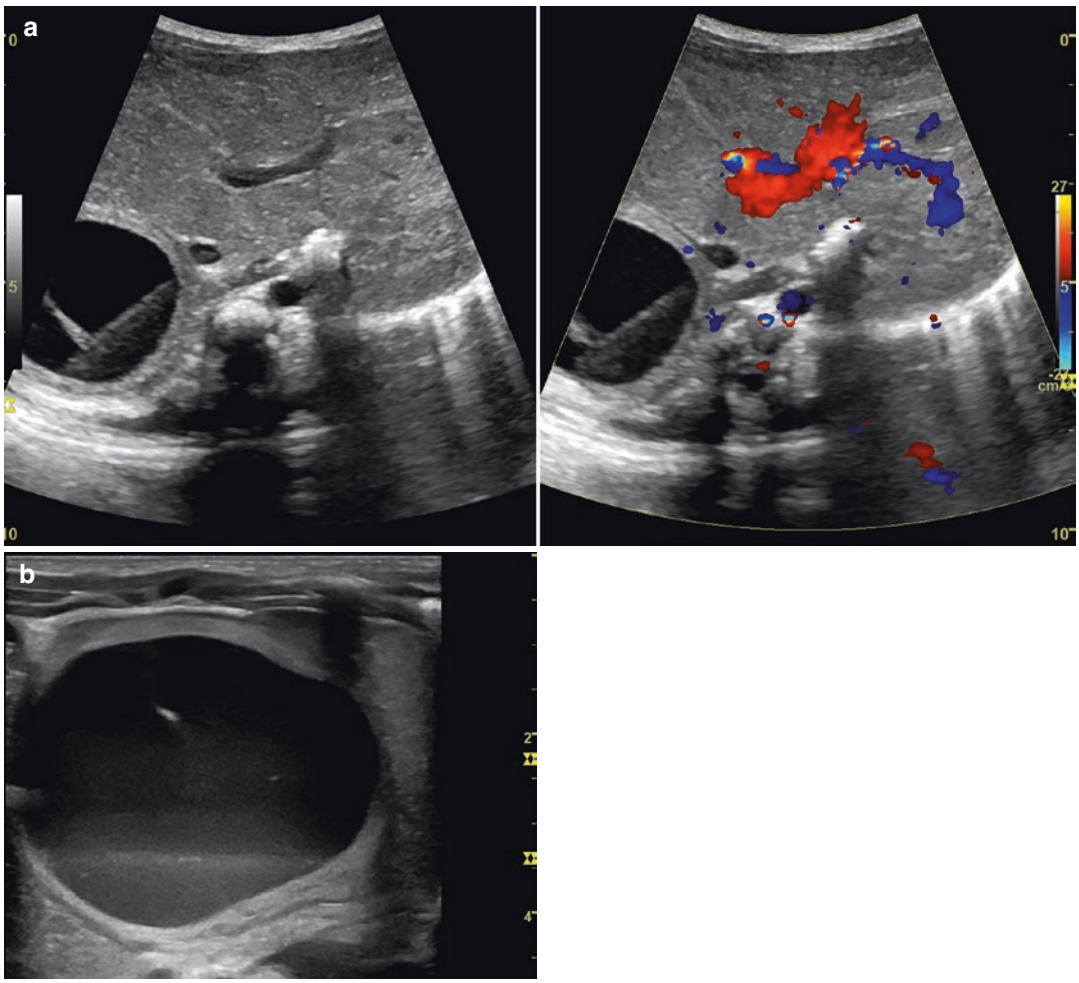

Fig. 20.3 The cyst of the right adrenal gland. The child's age is 4 months. (**a**) Grayscale US and CDI. (**b**) The grayscale US with linear array probe. (**c**) CEUS image with SonoVue® 0.03 mL reveals the enhancement defect in the lesion. Transverse scan. (**d**) CEUS image. Longitudinal scan

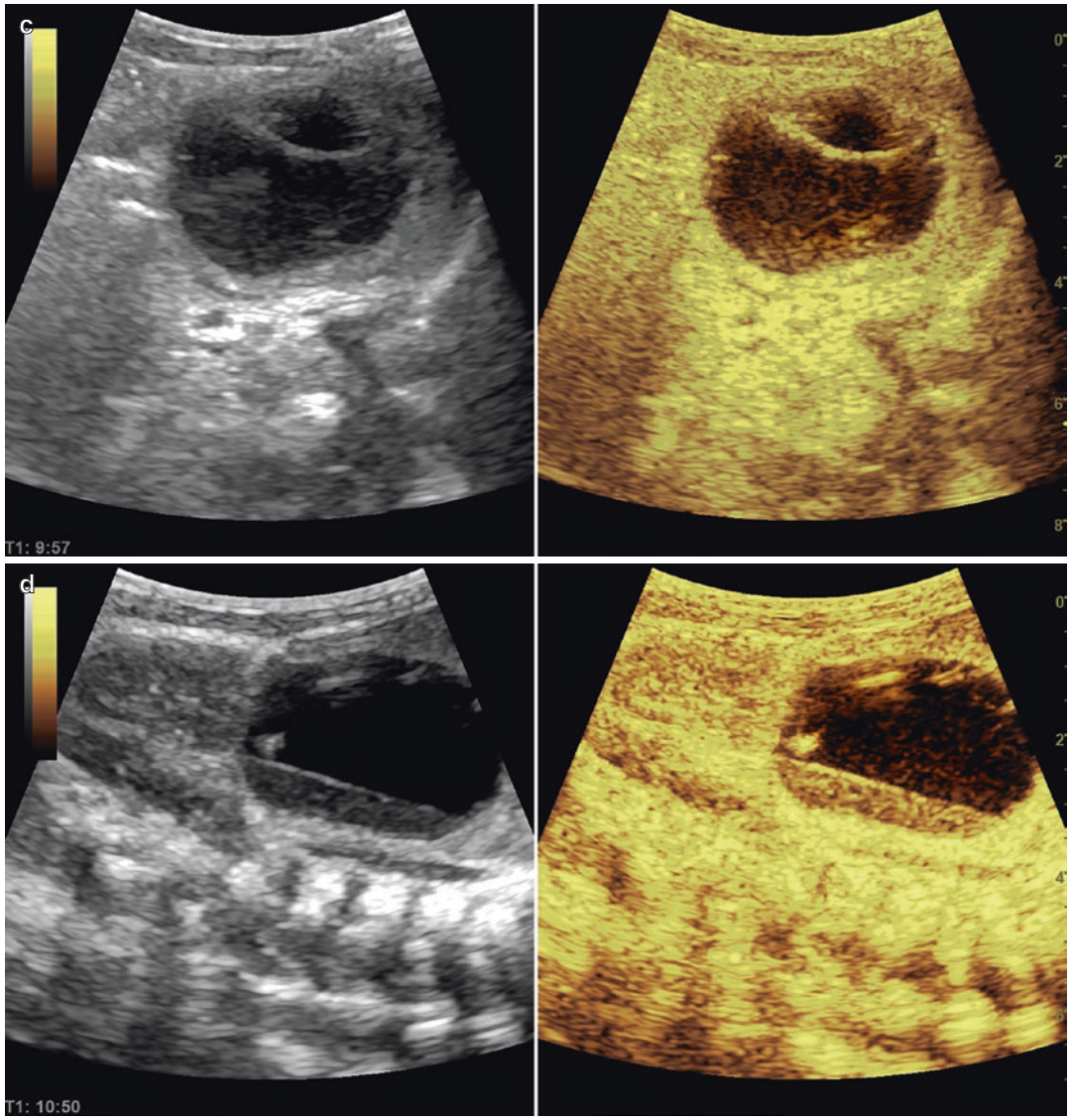

Fig. 20.3 (continued)

The reflux grading implicates the following scale (Fig. 20.4):

- Grade 1: reflux limited to the ureter
- Grade 2: reflux up to the renal pelvis
- Grade 3: mild dilatation of the ureter and pelvicalyceal system
- Grade 4: tortuous ureter with moderate dilatation, blunting of fornices but preserved papillary impressions
- Grade 5: tortuous ureter with severe dilatation of the ureter and pelvicalyceal system, loss of fornices and papillary impressions

CEUS of the spleen appears necessary in trauma, which can also serve as an indication for its use in pediatrics patients. It is feasible in the detection of splenic rupture and active bleeding. It has higher sensitivity than the grayscale US and Doppler imaging with the diagnostic accuracy comparable to CT [2, 9, 36].

Considering the difficulties in the diagnosis of splenic pathologies with imaging methods, CEUS can serve as a supplement for the differential diagnosis of focal splenic lesions (e.g., lymphoma, hemangioma, complex cyst, or abscess). A specific feature of focal splenic

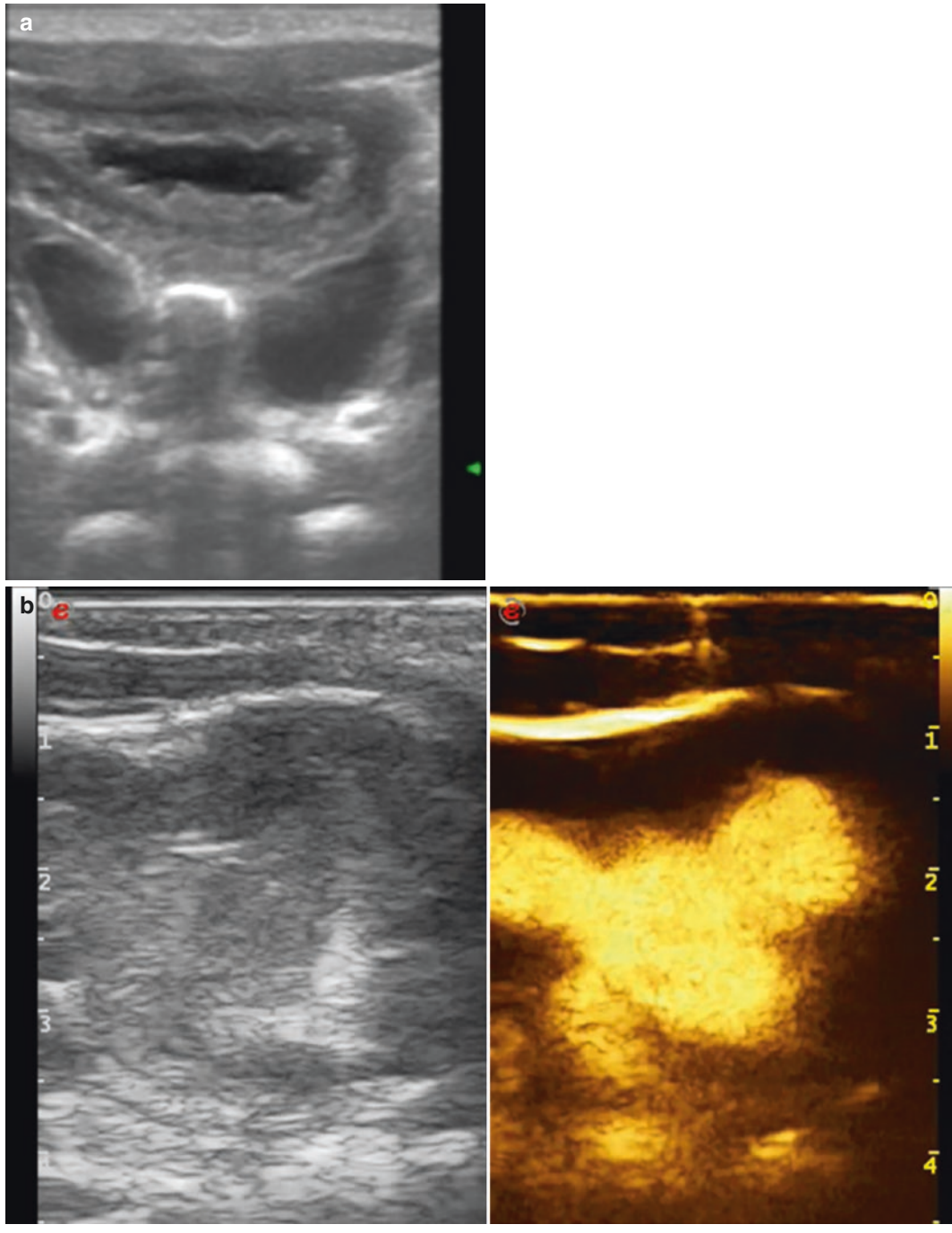

Fig. 20.4 CEVUS with SonoVue® 1.0 mL diluted in 10.0 mL of saline injected into the bladder through the urethra. The child's age is 6 days. (**a**) The beginning of the UCA injection into the bladder. Dilated terminal parts of both ureters. (**b**) VUR and the enhancement of one renal pelvis and calyces. (**c**). Absence of VUR and no enhancement of the collecting system of the contralateral kidney in the same patient

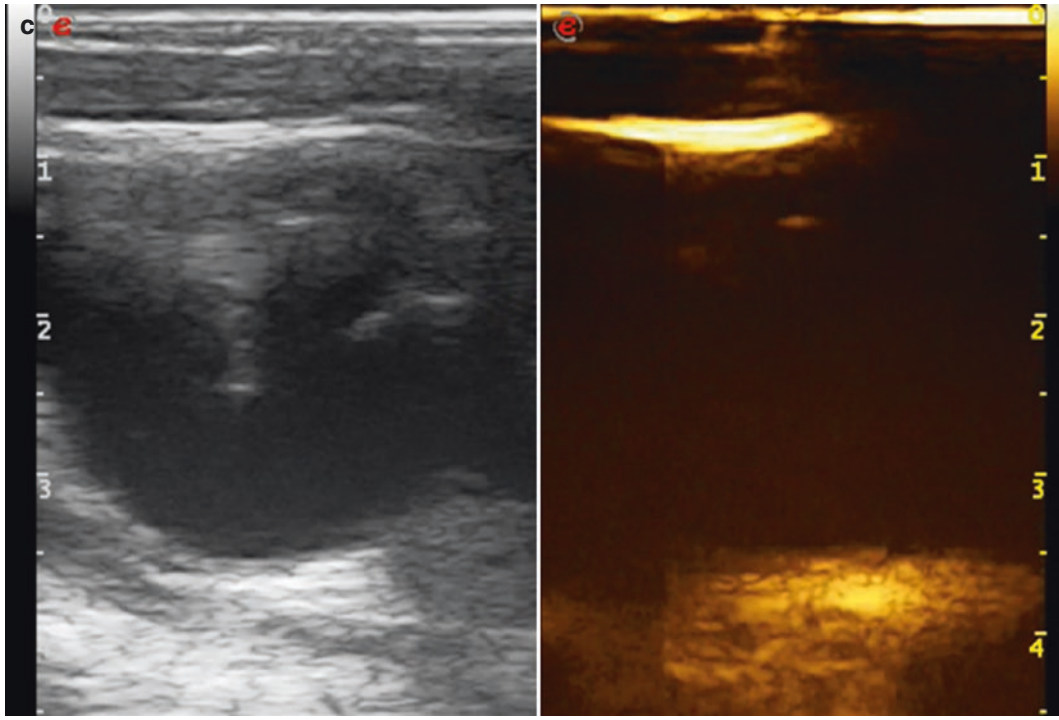

Fig. 20.4 (continued)

lesions in children is an increased number of congenital abnormalities, such as hamartoma or lymphangioma, which expand the differential diagnostic range [9].

The trauma of internal organs in pediatric patients has many specific features. A child's body is not a small copy of an adult and has anatomical and physiological points that contribute to traumatic injuries, such as the thin abdominal wall, a closer location of internal organs to the abdominal wall, and a lower position of the abdominal organs than in adults [15]. The FAST protocol, which is often used in internal injuries, is highly sensitive in the detection of free peritoneal fluid but has low sensitivity in the direct identification of the parenchymal organ damage [15].

In children, as in adults, CEUS is an efficient alternative or additional imaging method to the CT and can be used in the following situations [9, 37]:

- in hemodynamically stable patients with isolated blunt abdominal trauma
- in patients with ambiguous or negative CT and suspicious laboratory tests
- for monitoring conservative treatment of trauma

A special feature of CEUS for trauma patients is the double-fold introduction of UCA, which allows separate studies of the organs of the right and left sides of the abdominal cavity and retroperitoneal space—the right kidney, right adrenal gland, liver, and pancreas, followed by the left kidney, left adrenal gland, and spleen. It seems better to start scanning with the kidneys in the arterial phase and proceed with the study of the liver and spleen in the portal venous and late phases. CEUS is not inferior to CT in the diagnostic accuracy in the study of patients with blunt abdominal trauma and is capable to diagnose active bleeding [38]. The sensitivity of CEUS is

92.2% with specificity of 100% as compared with CT as a reference method [39]. CEUS determines the viability of the organ by detection of vessels and perfusion (Figs. 20.5 and 20.6, Videos 20.1 and 20.2).

Examination of the bowel benefits from CEUS in patients with inflammatory bowel diseases in adult patients (see Chap. 9). In pediatric practice, CEUS permits the determination of the disease activity, differential diagnosis of the active inflammatory process with chronic fibrotic changes, to assess the response to treatment. The data on the use of CEUS for the bowel study in pediatric patients is limited and typically published as the reports of clinical cases or in mixed studies.

CEUS in pediatric practice can be useful not only for the diagnostics of the focal liver, splenic,

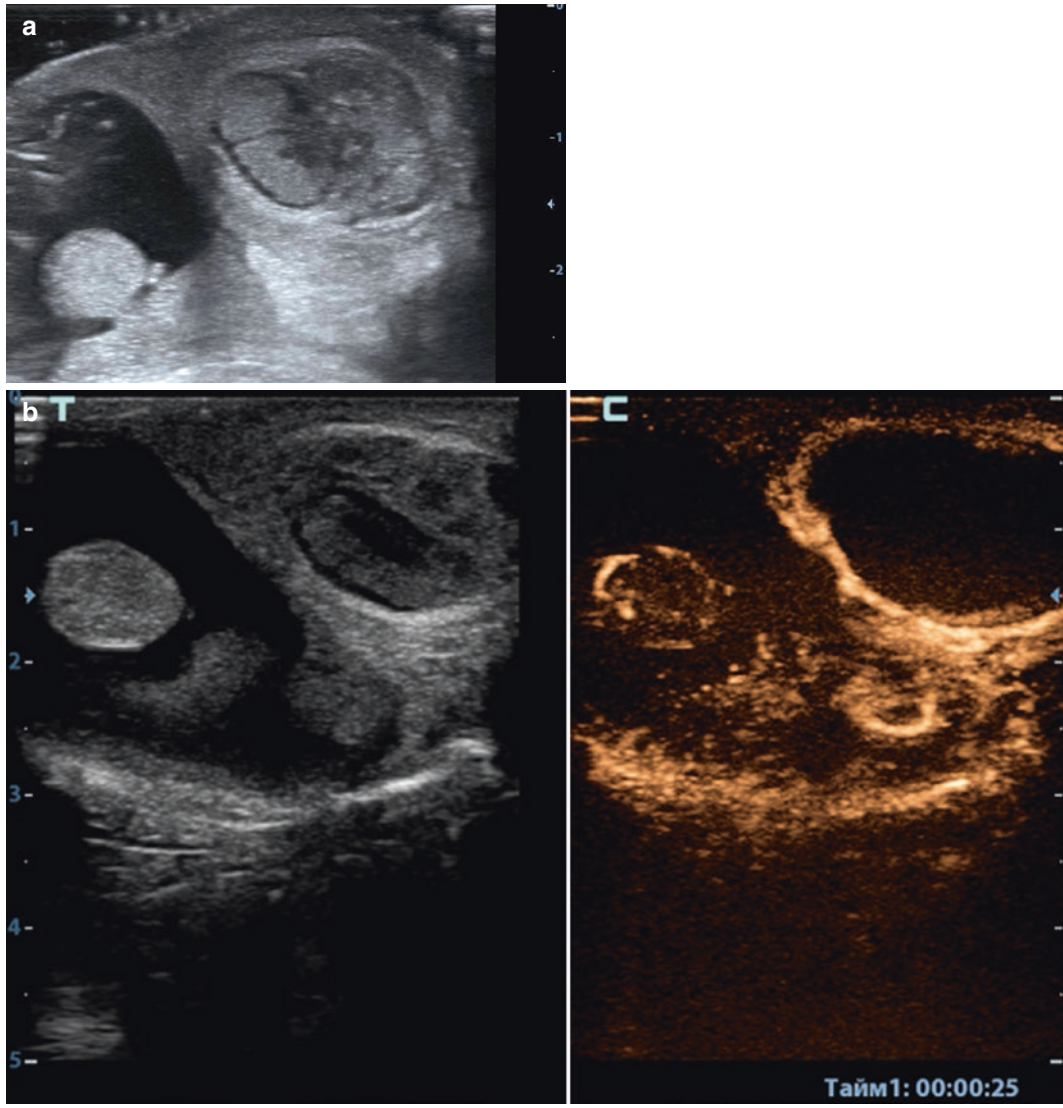

Fig. 20.5 Testicular torsion. The boy's age is 2 days. (**a**) Grayscale US image. (**b**) CEUS with SonoVue®, 0.03 mL intravenous bolus injection detects no enhancement of the testicle in the arterial phase. (**c**) The venous phase CEUS demonstrates the persistence of the perfusion defect. (**d**) Quantitative analysis of CEUS with TIC reveals no enhancement of the testicle (yellow ROI)

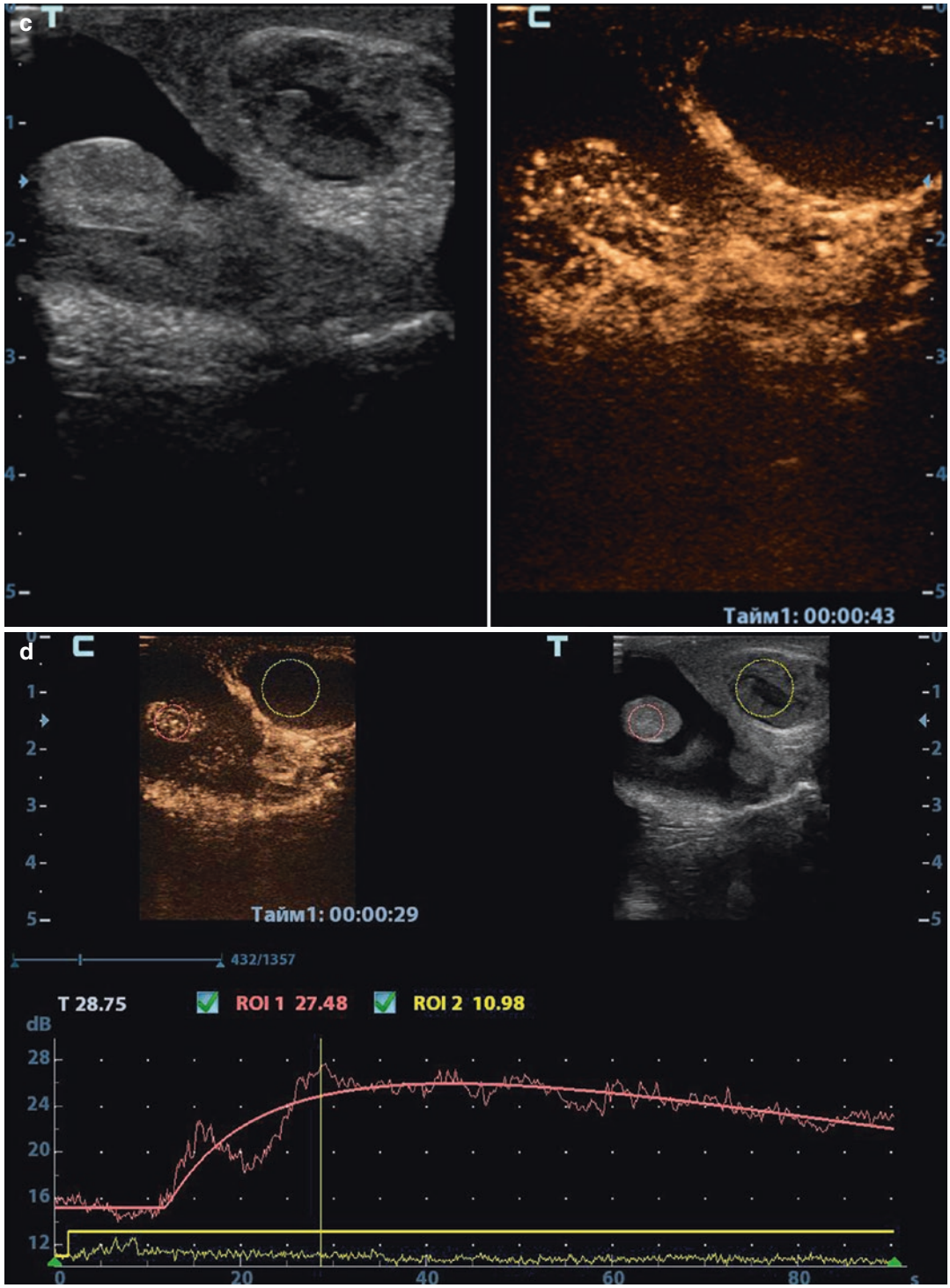

Fig. 20.5 (continued)

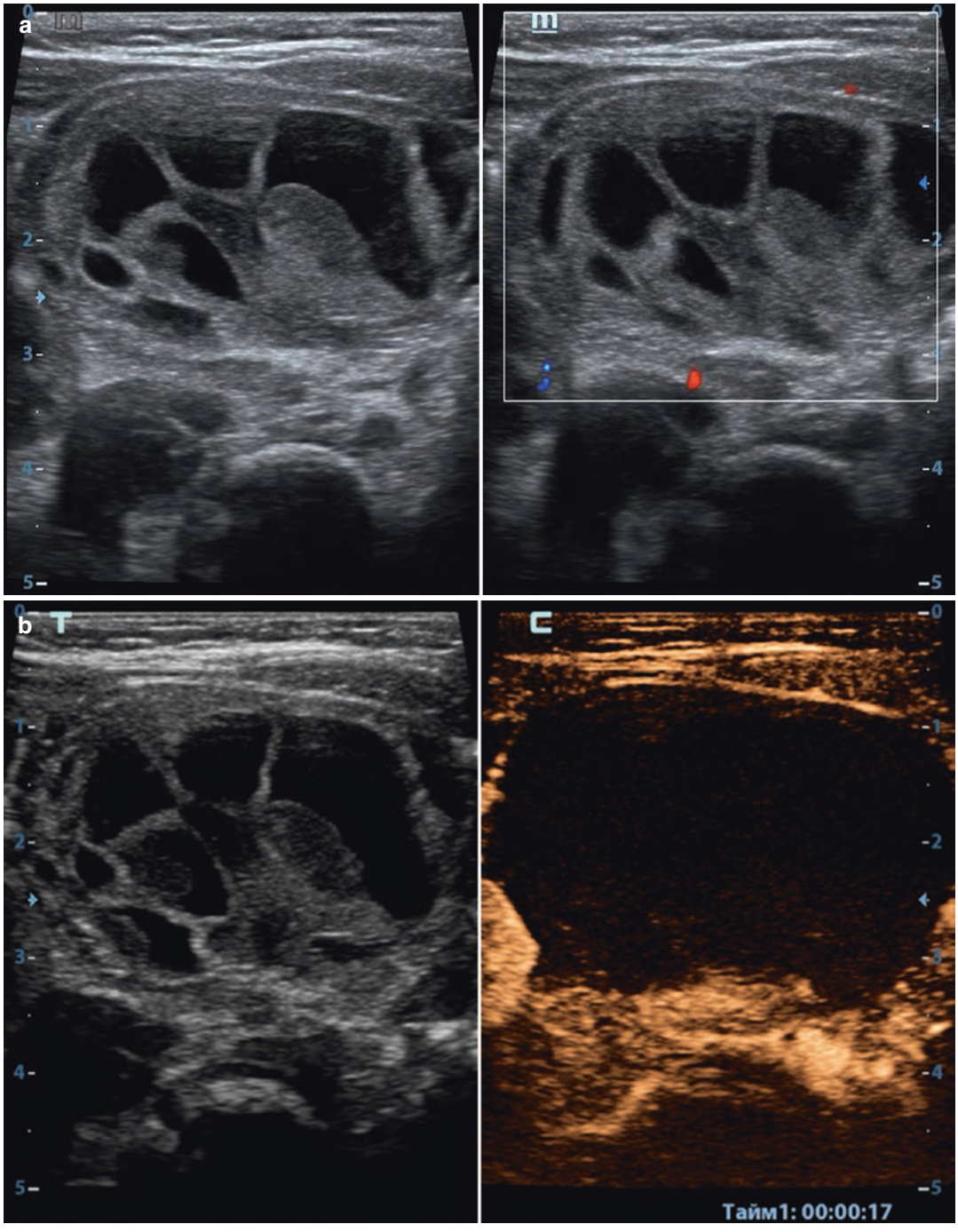

Fig. 20.6 Ovarian torsion. The girl's age is 3 months. (**a**) Grayscale US image and CDI. (**b**) CEUS with SonoVue®, 0.03 mL intravenous bolus injection detects no enhancement of the ovary in the arterial phase. (**c**) The venous phase CEUS demonstrates the persistence of the perfusion defect. (**d**) Quantitative analysis of CEUS with TIC reveals no enhancement of the ovary

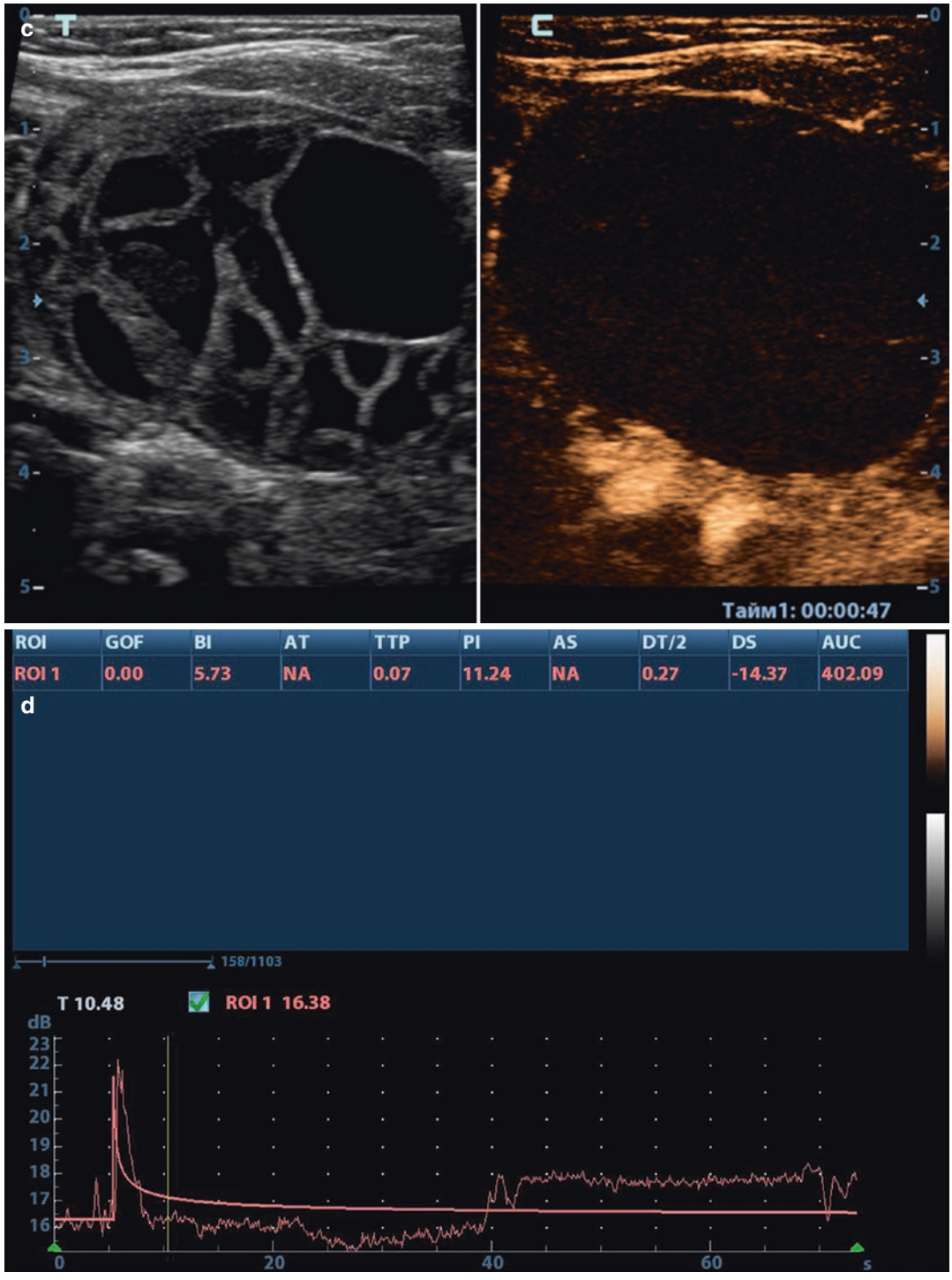

Fig. 20.6 (continued)

renal lesions, post-traumatic changes of internal organs, in the detection of VUR, but also in the assessment of transplant disorders, state of the chest, scrotum, intestine, during intraoperative, interventional studies, and exhibits prospects in oncology and neonatal examinations [2].

Considering the lack of official approval for the use of UCA in children and based on the obtained experience, we use the following principles in pediatric CEUS:

- The decision to use UCA for indications not listed in the official instruction (off-label) is made by the medical board or doctors' concilium.
- Parents should give a legal written voluntary informed consent for medical intervention and the use of UCA for indications not listed in the instruction (off-label).
- The study is conducted in the presence of the child's parent or guardian, an attending physician, and an intensive care unit doctor.

In our practice, we used CEUS in pediatric patients as an additional imaging method for the specification of focal lesions, ischemia, and VUR grade when the results of multiparametric sonography and other imaging methods were insufficient or conflicting.

The advantages of CEUS in pediatric echography are as follows:

- good tolerability of UCAs
- the ability to assess macro- and microcirculation of the organ, affected area, and surrounding structures with high temporal and spatial resolution, which is beyond the limits of the conventional US
- the ability to identify tumor perfusion features is crucial for differential diagnosis
- significant increase in the diagnostic value of sonography up to CT and MRI level
- no ionizing radiation, nephrotoxicity, and the need for sedation [40]

Modern CEUS technologies have many options to facilitate diagnosis in pediatric practice. Its efficacy prompts further research to improve the existing methods and provide even more reliable diagnostic signs.

References

1. Coleman JL, Navid F, Furman WL, McCarville MB. Safety of ultrasound contrast agents in the pediatric oncologic population: a single-institution experience. AJR Am J Roentgenol. 2014;202(5):966–70. https://doi.org/10.2214/AJR.13.12010.
2. Sidhu PS, Sellars ME, Deganello A, editors. Contrast-enhanced ultrasound in pediatric imaging. Berlin: Springer; 2021.
3. Darge K, Papadopoulou F, Ntoulia A, Bulas DI, Coley BD, Fordham LA, et al. Safety of contrast-enhanced ultrasound in children for non-cardiac applications: a review by the Society for Pediatric Radiology (SPR) and the International Contrast Ultrasound Society (ICUS). Pediatr Radiol. 2013;43(9):1063–73. https://doi.org/10.1007/s00247-013-2746-6.
4. Harkanyi Z. Potential applications of contrast-enhanced ultrasound in pediatric patients. Ultrasound Clin North Am. 2013;8:403–22.
5. Rosado E, Riccabona M. Off-label use of ultrasound contrast agents for intravenous applications in children: analysis of the existing literature. J Ultrasound Med. 2016;35(3):487–96. https://doi.org/10.7863/ultra.15.02030.
6. Riccabona M. Application of a second-generation US contrast agent in infants and children--a European questionnaire-based survey. Pediatr Radiol. 2012;42(12):1471–80. https://doi.org/10.1007/s00247-012-2472-5.
7. Riccabona M. Contrast media use in pediatrics: safety issues. In: Thompson HS, Webb JAW, editors. Contrast media: safety issues and ESUR guidelines. Berlin: Springer; 2014. p. 245–51.
8. Ntoulia A, Anupindi SA, Darge K, Back SJ. Applications of contrast-enhanced ultrasound in the pediatric abdomen. Abdom Radiol (NY). 2018;43(4):948–59. https://doi.org/10.1007/s00261-017-1315-0.
9. Sidhu PS, Cantisani V, Deganello A, Dietrich CF, Duran C, Franke D, et al. Role of contrast-enhanced ultrasound (CEUS) in paediatric practice: an EFSUMB position statement. Ultraschall Med. 2017;38(1):33–43. https://doi.org/10.1055/s-0042-110394.
10. Bracco. Lumason prescribing information. Revised December 2020. https://imaging.bracco.com/sites/braccoimaging.com/files/technica_sheet_pdf/us-en-2021-02-08-spc-lumason.pdf. Accessed 23 Feb 2021.
11. Food & Drug Administration. Approved drug product list. Silver Spring, MD: FDA; 2020. https://www.fda.gov/media/71502/download. Accessed 23 Feb 2021.
12. Mathews JD, Forsythe AV, Brady Z, Butler MW, Goergen SK, Byrnes GB, et al. Cancer risk in 680,000 people exposed to computed tomography scans in

childhood or adolescence: data linkage study of 11 million Australians. BMJ. 2013;346:f2360. https://doi.org/10.1136/bmj.f2360.
13. Piskunowicz M, Kosiak W, Batko T, Piankowski A, Połczyńska K, Adamkiewicz-Drożyńska E. Safety of intravenous application of second-generation ultrasound contrast agent in children: prospective analysis. Ultrasound Med Biol. 2015;41(4):1095–9. https://doi.org/10.1016/j.ultrasmedbio.2014.11.003.
14. Papadopoulou F, Ntoulia A, Siomou E, Darge K. Contrast-enhanced voiding urosonography with intravesical administration of a second-generation ultrasound contrast agent for diagnosis of vesicoureteral reflux: prospective evaluation of contrast safety in 1,010 children. Pediatr Radiol. 2014;44(6):719–28. https://doi.org/10.1007/s00247-013-2832-9.
15. Trinci M, Piccolo CL, Ferrari R, Galluzzo M, Ianniello S, Miele V. Contrast-enhanced ultrasound (CEUS) in pediatric blunt abdominal trauma. J Ultrasound. 2019;22(1):27–40. https://doi.org/10.1007/s40477-018-0346-x.
16. Stenzel M. Intravenous contrast-enhanced sonography in children and adolescents - a single center experience. J Ultrason. 2013;13(53):133–44. https://doi.org/10.15557/JoU.2013.0014.
17. Yusuf GT, Sellars ME, Deganello A, Cosgrove DO, Sidhu PS. Retrospective analysis of the safety and cost implications of pediatric contrast-enhanced ultrasound at a single center. AJR Am J Roentgenol. 2017;208(2):446–52. https://doi.org/10.2214/AJR.16.16700.
18. Frank D. Intravenous-contrast enhanced sonography (CEUS) in children: single center experience. Ultraschall Med. 2013;34:S32.
19. Chung EM, Cube R, Lewis RB, Conran RM. From the archives of the AFIP: pediatric liver masses: radiologic-pathologic correlation Part 1. Benign tumors. Radiographics. 2010;30(3):801–26. https://doi.org/10.1148/rg.303095173.
20. Chung EM, Lattin GE Jr, Cube R, Lewis RB, Marichal-Hernández C, Shawhan R, Conran RM. From the archives of the AFIP: pediatric liver masses: radiologic-pathologic correlation. Part 2. Malignant tumors. Radiographics. 2011;31(2):483–507. https://doi.org/10.1148/rg.312105201.
21. Dezsőfi A, McLin V, Hadzic N. Hepatic neoplasms in children: a focus on differential diagnosis. Clin Res Hepatol Gastroenterol. 2014;38(4):399–402. https://doi.org/10.1016/j.clinre.2014.05.001.
22. Claudon M, Dietrich CF, Choi BI, Cosgrove DO, Kudo M, Nolsøe CP, et al. Guidelines and good clinical practice recommendations for contrast enhanced ultrasound (CEUS) in the liver--update 2012: a WFUMB-EFSUMB initiative in cooperation with representatives of AFSUMB, AIUM, ASUM, FLAUS and ICUS. Ultraschall Med. 2013;34(1):11–29. https://doi.org/10.1055/s-0032-1325499.
23. McCarville MB, Coleman JL, Guo J, Li Y, Li X, Honnoll PJ, et al. Use of quantitative dynamic contrast-enhanced ultrasound to assess response to antiangiogenic therapy in children and adolescents with solid malignancies: a pilot study. AJR Am J Roentgenol. 2016;206(5):933–9. https://doi.org/10.2214/AJR.15.15789.
24. Jacob J, Deganello A, Sellars ME, Hadzic N, Sidhu PS. Contrast enhanced ultrasound (CEUS) characterization of grey-scale sonographic indeterminate focal liver lesions in pediatric practice. Ultraschall Med. 2013;34(6):529–40. https://doi.org/10.1055/s-0033-1355785.
25. Piorkowska MA, Dezman R, Sellars ME, Deganello A, Sidhu PS. Characterization of a hepatic haemangioma with contrast-enhanced ultrasound in an infant. Ultrasound. 2018;26(3):178–81. https://doi.org/10.1177/1742271X17733298.
26. Venhola M, Hannula A, Huttunen NP, Renko M, Pokka T, Uhari M. Occurrence of vesicoureteral reflux in children. Acta Paediatr. 2010;99(12):1875–8. https://doi.org/10.1111/j.1651-2227.2010.01909.x.
27. Kis E, Nyitrai A, Várkonyi I, Máttyus I, Cseprekál O, Reusz G, Szabó A. Voiding urosonography with second-generation contrast agent versus voiding cystourethrography. Pediatr Nephrol. 2010;25(11):2289–93. https://doi.org/10.1007/s00467-010-1618-7.
28. Ključevšek D, Battelino N, Tomažič M, Kersnik Levart T. A comparison of echo-enhanced voiding urosonography with X-ray voiding cystourethrography in the first year of life. Acta Paediatr. 2012;101(5):e235–9. https://doi.org/10.1111/j.1651-2227.2011.02588.x.
29. Papadopoulou F, Anthopoulou A, Siomou E, Efremidis S, Tsamboulas C, Darge K. Harmonic voiding urosonography with a second-generation contrast agent for the diagnosis of vesicoureteral reflux. Pediatr Radiol. 2009;39(3):239–44. https://doi.org/10.1007/s00247-008-1080-x.
30. Roić G, Roić AC, Palcić I, Grmoja T, Batos AT. Mikcijska urosonografija pojacana kontrastom (CEVUS) u dijagnostici vezikoureteralnog refluksa [Contrast enhanced voiding urosonography (CEVUS) in the diagnosis of vesicoureteral reflux]. Lijec Vjesn. 2016;138(1–2):39–46.
31. Zhang W, Cai B, Zhang X, Zhou J, Qiu L, Yi H. Contrast-enhanced voiding urosonography with intravesical administration of ultrasound contrast agent for the diagnosis of pediatric vesicoureteral reflux. Exp Ther Med. 2018;16(6):4546–52. https://doi.org/10.3892/etm.2018.6793.
32. Diamond DA, Mattoo TK. Endoscopic treatment of primary vesicoureteral reflux. N Engl J Med. 2012;366(13):1218–26. https://doi.org/10.1056/NEJMct1108922.
33. Wong LS, Tse KS, Fan TW, Kwok KY, Tsang TK, Fung HS, et al. Voiding urosonography with second-generation ultrasound contrast versus micturating cystourethrography in the diagnosis of vesicoureteric reflux. Eur J Pediatr. 2014;173(8):1095–101. https://doi.org/10.1007/s00431-014-2297-3.
34. Woźniak MM, Osemlak P, Pawelec A, Brodzisz A, Nachulewicz P, Wieczorek AP, Zajączkowska MM. Intraoperative contrast-enhanced urosonogra-

phy during endoscopic treatment of vesicoureteral reflux in children. Pediatr Radiol. 2014;44(9):1093–100. https://doi.org/10.1007/s00247-014-2963-7.

35. Woźniak MM, Wieczorek AP, Pawelec A, Brodzisz A, Zajączkowska MM, Borzęcka H, Nachulewicz P. Two-dimensional (2D), three-dimensional static (3D) and real-time (4D) contrast enhanced voiding urosonography (ceVUS) versus voiding cystourethrography (VCUG) in children with vesicoureteral reflux. Eur J Radiol. 2016;85(6):1238–45. https://doi.org/10.1016/j.ejrad.2015.11.006.
36. Sidhu PS, Cantisani V, Dietrich CF, Gilja OH, Saftoiu A, Bartels E, et al. The EFSUMB guidelines and recommendations for the clinical practice of contrast-enhanced ultrasound (CEUS) in non-hepatic applications: update 2017 (long version). Ultraschall Med. 2018;39(2):e2–e44. https://doi.org/10.1055/a-0586-1107.
37. Armstrong LB, Mooney DP, Paltiel H, Barnewolt C, Dionigi B, Arbuthnot M, et al. Contrast enhanced ultrasound for the evaluation of blunt pediatric abdominal trauma. J Pediatr Surg. 2018;53(3):548–52. https://doi.org/10.1016/j.jpedsurg.2017.03.042.
38. Menichini G, Sessa B, Trinci M, Galluzzo M, Miele V. Accuracy of contrast-enhanced ultrasound (CEUS) in the identification and characterization of traumatic solid organ lesions in children: a retrospective comparison with baseline US and CE-MDCT. Radiol Med. 2015;120(11):989–1001. https://doi.org/10.1007/s11547-015-0535-z.
39. Valentino M, Serra C, Pavlica P, Labate AM, Lima M, Baroncini S, Barozzi L. Blunt abdominal trauma: diagnostic performance of contrast-enhanced US in children--initial experience. Radiology. 2008;246(3):903–9. https://doi.org/10.1148/radiol.2463070652.
40. Torres A, Koskinen SK, Gjertsen H, Fischler B. Contrast-enhanced ultrasound using sulfur hexafluoride is safe in the pediatric setting. Acta Radiol. 2017;58(11):1395–9. https://doi.org/10.1177/0284185117690423.